

AFAPL - TR - 76 - 114  
VOLUME I

12 8

AD A 042980

GAS LUBRICATED FOIL BEARING DEVELOPMENT  
FOR ADVANCED TURBOMACHINES

AIRESEARCH MANUFACTURING COMPANY OF ARIZONA  
A DIVISION OF THE GARRET CORPORATION  
402 S. 36 STREET  
PHOENIX ARIZONA 85010

March 1977

TECHNICAL REPORT AFAPL-TR-76-114 ,  
VOLUME 1-TECHNICAL DISCUSSION

DDC  
AUG 1 1977  
RECEIVED

Final Report for Period 30 June 1973 - 30 November 1976

Approved for public release; distribution unlimited

AU NO. \_\_\_\_\_  
DDC FILE COPY

AIR FORCE AERO PROPULSION LABORATORY  
AIR FORCE WRIGHT AERONAUTICAL LABORATORIES  
AIR FORCE SYSTEMS COMMAND  
WRIGHT-PATTERSON AIR FORCE BASE, OHIO 45433


NOTICE

When Government drawings, specifications, or other data are used for any purpose other than in connection with a definitely related Government procurement operation, the United States Government thereby incurs no responsibility nor any obligation whatsoever; and the fact that the government may have formulated, furnished or in any way supplied the said drawings, specifications, or other data, is not to be regarded by implication or otherwise as in any manner licensing the holder or any other person or corporation, or conveying any rights or permission to manufacture, use, or sell any patented invention that may in any way be related thereto.


This technical report was submitted by the AiResearch Manufacturing Company of Arizona under Contract F33615-73-C-2058. The effort was administered by the Air Force Aero-Propulsion Laboratory, Air Force Wright Aeronautical Laboratories, Air Force Systems Command, Wright-Patterson AFB, Ohio under Project 3048, Task 304806 and Work Unit 30480666. Mr. E. Lake, Mr. H. Jones and Mr. R. Dayton administered the project for the Air Force. Funding support for this effort was also provided by the Eustis Directorate, US Army Air Mobility Research and Development Laboratory, Ft. Eustis, VA and the Naval Air Propulsion Test Center, Trenton, NJ. Mr. R. Furgurson and Mr. A. D'Orazio were the cognizant project engineers for the Army and Navy, respectively. Mr. W. Koepsel of AiResearch was technically responsible for the work.

This report has been reviewed by the Information Office (ASD/OIP) and is releasable to the National Technical Information Service (NTIS). At NTIS, it will be available to the general public, including foreign nations.

This technical report has been reviewed and is approved for publication.

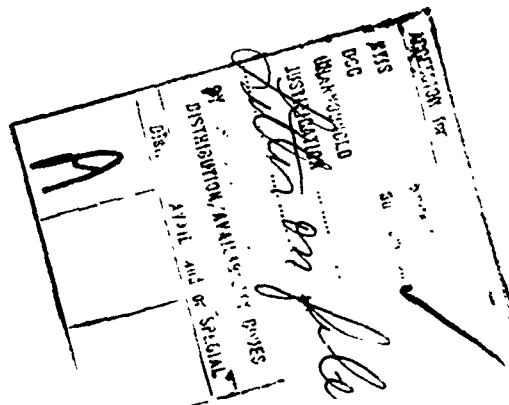
  
RONALD D. DAYTON  
Project Engineer

FOR THE COMMANDER

  
HOWARD F. JONES  
Chief, Lubrication Branch  
Fuels & Lubrication Division

Copies of this report should not be returned unless return is required by security consideration, contractual obligations, or notice on a specific document.

AIR FORCE - 14 JUL 77 - 225





Unclassified

SECURITY CLASSIFICATION OF THIS PAGE (When Data Entered)

REPORT DOCUMENTATION PAGE		READ INSTRUCTIONS BEFORE COMPLETING FORM	
18	1. REPORT NUMBER AFAPL-TR-76-114-Vol-1	2. GOVT ACCESSION NO.	3. RECIPIENT'S CATALOG NUMBER
19	4. TITLE (and Subtitle) GAS LUBRICATED FOIL BEARING DEVELOPMENT FOR ADVANCED TURBOMACHINES, Volume I	5. TYPE OF REPORT & PERIOD COVERED Final Report (Volume I) 30 Mar 73 to 30 Nov 76	6. PERFORMING ORG. REPORT NUMBER 76-312202
10	7. AUTHOR WARREN F. KOEPEL	8. CONTRACT OR GRANT NUMBER(s) F33615-73-C-2058	9. PROGRAM ELEMENT PROJECT TASK AREA & WORK UNIT NUMBERS 3048 06 66
	9. PERFORMING ORGANIZATION NAME AND ADDRESS AiResearch Manufacturing Co. of Arizona a Division of The Garrett Corporation, Phoenix, Arizona 85010	10. REPORT DATE March 1977	11. NUMBER OF PAGES 382
	11. CONTROLLING OFFICE NAME AND ADDRESS Air Force Aero Propulsion Laboratory/SF Air Force Systems Command Wright-Patterson AFB, Ohio	12. SECURITY CLASS (of this report) Unclassified	13. DECLASSIFICATION DOWNGRADING SCHEDULE
	14. MONITORING AGENCY NAME & ADDRESS (if different from Controlling Office) 387p	15. DISTRIBUTION STATEMENT (of this Report) Approved for public release; distribution unlimited	
17. DISTRIBUTION STATEMENT (of the abstract entered in Block 20, if different from Report)			
18. SUPPLEMENTARY NOTES			
19. KEY WORDS (Continue on reverse side if necessary and identify by block number) Foil Bearing                      Advanced Turbomachines Gas Lubricated Bearing Air Bearing			
20. ABSTRACT (Continue on reverse side if necessary and identify by block number) This document presents and discusses the design and development of gas lubricated foil journal and thrust bearings for the specific application in a 1000 to 3000 pound thrust propulsion engine. The design activity included the development of analytical tools for the thrust and journal bearings and their use during the bearing test phase, for the purpose of increasing bearing load capacity. A significant effort was spent toward materials and coating development for capabilities to 1200°F.			

404 796

JP

# TABLE OF CONTENTS

SECTION		PAGE
I	INTRODUCTION	1
1.1	Background	1
1.1.1	Advantages	3
1.1.2	Related Programs	4
1.2	Program Objectives	6
1.3	Program Approach	6
II	SUMMARY	10
2.1	Analytical	10
2.2	Materials Development	13
2.3	Bearing Development and Testing	16
III	DISCUSSION	19
3.1	Engine Characteristics	19
3.1.1	Power Section	21
3.1.2	Performance	22
3.1.3	Maneuver Load Analysis	22
3.1.4	Thrust Bearing Runner Stress Analysis	27
3.1.5	Rear Journal Bearing Runner	29
3.1.6	Forward Journal Bearing Runner Stress and Deflection Analysis	32
3.1.7	Critical Speed Analysis	35
3.1.8	Thermal Analysis	39
3.1.8.1	Journal Bearing Temperatures	42
3.1.8.2	Thrust Bearing Temperatures	50
3.2	Design	56
3.2.1	Baseline Bearing Design	56
3.2.1.1	Journal Bearing Baseline Design	57
3.2.1.2	Thrust Bearing Baseline Design	59
3.2.2	Thrust Bearing Test Rig Design	61
3.2.3	Journal Bearing Test Rig Design	63
3.3	Bearing Design Analytical Tools	72
3.3.1	Thrust Bearing Analytical Program	72
3.3.1.1	Elasticity Solution	74
3.3.1.2	Hydrodynamics Solution	76
3.3.1.3	Computational Results	81
3.3.2	Journal Bearing Analytical Program	89
3.3.2.1	Discussion of Geometry Subroutine	96
3.3.2.2	Elasticity Subroutine	98
3.3.2.3	Hydrodynamic Analyses	102
3.3.2.4	Comparison of Analytical and Experimental Data for Elasticity Solution	107
3.3.2.5	Foil Bearing Analytical Program Preliminary Results	114
3.4	Materials Development	114
3.4.1	Approach	119
3.4.2	Materials Survey	120
3.4.2.1	Alloys	120
3.4.2.2	Coatings	124
3.4.2.3	Fabrication and Process Considerations	127

# TABLE OF CONTENTS (Contd)

SECTION		PAGE
3.4.3	Materials Screening	131
3.4.3.1	Substrate Alloys	131
3.4.3.2	Coatings	137
3.4.3.3	Selection of Materials for Wear Rig Evaluation	152
3.4.3.4	Materials Screening Summary	154
3.4.4	Materials Wear Rig	155
3.4.4.1	Wear Rig Design	155
3.4.4.2	Fabrication of Wear Rig Foil Bearings	160
3.4.5	Materials	160
3.4.5.1	Test Approach	160
3.4.5.2	Wear Rig Performance Difficulty	164
3.4.5.3	Wear Rig Low Speed Test Results	164
3.4.5.4	Wear Rig High Speed Test Results	172
3.4.5.5	Metallurgical Evaluation of Wear Rig Materials	174
3.4.5.6	Friction Measurements	184
3.4.6	Materials Selection for Journal and Thrust Rigs	187
3.5	Bearing Development and Testing	188
3.5.1	Foil Journal Bearing Development Tests	188
3.5.1.1	General	188
3.5.1.2	Phase A - Journal Bearing Development Tests	189
3.5.1.3	Phase B - Journal Bearing Development Tests	207
3.5.1.4	Phase C - Journal Bearing Development Tests	216
3.5.2	Foil Thrust Bearing Development Tests	237
3.5.2.1	Baseline Bearing	237
3.5.2.2	Dual Spring Design	237
3.5.2.3	Partial Pad Stiffener	241
IV	CONCLUSIONS AND RECOMMENDATIONS	264
4.1	Analytical Program	264
4.1.1	Analytical Tools - Conclusions	264
4.1.2	Analytical Tools - Recommendations	264
4.1.2.1	Bearings	264
4.1.2.2	Foil Journal Bearing/Rotor Dynamic Analysis	265
4.1.3	Thermal Analysis Conclusions	265
4.1.4	Thermal Analysis Recommendations	265
4.2	Materials Development	266
4.2.1	Conclusions	266
4.2.2	Recommendations	267
4.3	Bearing Tests and Development Program	268
4.3.1	Thrust Bearing - Conclusions	268
4.3.1.1	Bearing Configuration	268
4.3.1.2	Foil Coatings	268
4.3.2	Thrust Bearing - Recommendations	270

# TABLE OF CONTENTS (Contd)

SECTION		PAGE
4.3.3	Journal Bearing - Conclusions	270
4.3.3.1	Bearing Configuration	270
4.3.3.2	Foil Coatings	273
4.3.4	Journal Bearing - Recommendations	273
4.4	Overall Conclusions and Recommendations	274
DRAWINGS	3605849	275
	3605850	277
	L-3621113	279
APPENDIX A		281
APPENDIX B		299
REFERENCES		371

# LIST OF ILLUSTRATIONS

FIGURE	TITLE	PAGE
1	The Gas Bearing Concept	2
2	The Self-Acting Compliant Foil Bearing Concept	5
3	Foil Bearing Applications	7
4	Flight Maneuver Load Diagrams	25
5	Thrust Runner Axial Displacement	28
6	Radial Displacement of the Rear Bearing Journal	30
7	Analytical Model of the Rear Bearing Journal of the TJE331-1029 Engine	31
8	Radial Displacement of the Forward Journal Runner	33
9	Magnified Displacement and Tangential Stress Distribution for Front Bearing Journal at 33,000 RPM	34
10	Critical Speed Versus Bearing Springrate for TJE331-1029	37
11	Mode Shapes of the First Four Criticals for the TJE331-P4 Foil Bearing Engine	38
12	Internal Airflow Schematic	41
13	Thermal Model Schematic Foil Bearing	43
14	Sample Results of Thermal Analysis on Turbine-End Journal Bearing	44
15	Baseline Journal Bearing Configuration Cooling Flow Characteristics	46
16	Baseline Journal Bearing Thermal Analysis. Power Loss = 1500 Watts	47
17	Baseline Journal Bearing Thermal Analysis. Seal Clearance = 0.008 Inch	48
18	Effect of Bearing Sway Space	49
19	Thermal Model Schematic Foil Bearing Type: Cantilevered-Leaf Thrust	51
20	Thermal Model Thrust Foils Schematic	52
21	Rim Impingement, Thrust Runner Cooling	53
22	Sample Results of Thermal Analysis	54
23	Sample Results of Thermal Analysis Thrust Bearing - Meridional View	55
24	Thrust Bearing Test Rig	62
25	Foil Thrust Bearing Rig Critical Speeds	64
26	Normalized Mode Shapes. Thrust Bearing Rig No Flywheel and Shortened Overhang Bearing Spring Rate = 10,000 lb/in.	65
27	Mass and Stiffness Model, Thrust Bearing Rig No Flywheel and Short Overhang	66
28	Thrust Bearing Test Rig	67
29	Journal Bearing Test Rig	68
30	Test Rig Parachute Loader	70
31	Journal Bearing Test Rig	71

# LIST OF ILLUSTRATIONS (Contd)

FIGURE	TITLE	PAGE
32	Elasto-Hydrodynamics Program Logic Diagram	73
33	Finite Element Grid	74
34	Thrust Foil Bearing Mathematical Model	75
35	Thrust Bearing Geometry	78
36	Experimental Correlation of Finite Difference Solution	79
37	Dependency of Turbulence Constant on Bearing Eccentricity	80
38	Baseline Bearing Film Thickness Isopleth (In./10,000)	82
39	Baseline Bearing Film Pressure Isopleth (psi)	83
40	Film Thickness at $R_M$ for Baseline Thrust Bearing	85
41	Baseline Bearing Friction Loss as Function of Bearing Load	86
42	Pressure Profile at $R_M$ for Baseline Thrust Bearing	87
43	Baseline Bearing Load as Function of Minimum Film Thickness	88
44	Dual Spring Foil Thrust Bearing Schematic	90
45	Film Thickness at $R_M$ for Dual Spring Thrust Bearing	91
46	Pressure Profile at $R_M$ for Dual Spring Thrust Bearing	92
47	Friction Loss as Function of Bearing Load for Dual Spring Thrust Bearing	93
48	Bearing Load as Function of Minimum Film Thickness for Dual Spring Thrust Bearing	94
49	Baseline Spring with Backup Stiffener	95
50	Elasto-Hydrodynamics Program Logic	97
51	Assembly Position	99
52	6, 12, and 16-Foils Configurations	100
53	Assembly and Stiffness Flow Chart	101
54	Foil Geometry Ccoordinate System	103
55	Foil Journal Bearing Geometry for Hydrodynamic Solution	105
56	Foil Journal Bearing Tangential and Radial Velocity Components	106
57	Geometry and Coordinate System for Elasticity Program	108
58	Sixteen-Foil Geometry Load Versus Eccentricity	110
59	Eight-Segment Journal Bearing (0.010)	111
60	Twelve-Segment Foil Effect of Load Direction	112
61	Twelve-Segment Foil Orthogonal Loading	113
62	Twelve-Segment Foil Effect of Length	115
63	Eight-Segment Foil Center Plane Pressure Distribution	116
64	Eight-Segment Foil Center Plane Pressure Distribution	117

# LIST OF ILLUSTRATIONS (Contd)

FIGURE	TITLE	PAGE
65	Materials Development Logic Diagram	121
66	Typical Coated Shaft and Foil Configurations	129
67	Influence of Thermal Exposure on the Microstructure of Three Alloys	133
68	Influence of Thermal Exposure on the Microstructure of Three Alloys	134
69	Kaman Sciences Corporation Ceramic Coated Samples. Foils at the Top Were Coated with DES Coating (Pure $\text{Cr}_2\text{O}_3$ ), Thickness: 0.5-Mil. Bottom Foils and Bar Were Coated with SCA Coating ( $\text{Cr}_2\text{O}_3\text{-Al}_2\text{O}_3\text{-SiO}_2$ ), Thickness: 2-Mils.	139
70	Sputter Coatings Applied to Inconel X-750 Foil ( $\text{B}_4\text{C}$ , $\text{Cr}_3\text{C}_2$ , $\text{Cr}_2\text{O}_3$ , $\text{Cr}_2\text{O}_3 + \text{Al}_2\text{O}_3$ , $\text{Cr}_2\text{O}_3$ One Side and Au on Reverse Side, and $\text{Si}_3\text{N}_4$ ).	140
71	Sputtered Coatings Applied to Inconel X-750 Foil ( $\text{TiB}_2$ , $\text{TiB}_2$ with Au Overcoat, $\text{TiB}_2$ with $\text{CaF}_2$ Overcoat, $\text{TiC}$ , $\text{TiN}$ , and Tribaloy T-400). Defect Patterns at Arrows Caused by Target Imprint Image Occurring During Sputtering	141
72	Influence of Thermal Exposure at $1200^\circ\text{F}$ on Weight of Several Coated Samples	143
73	Influence of Thermal Cycling on Weight of Several Coated Samples	144
74	Typical Appearance of Coatings After Long Term Exposure (800 Hours) and Thermal Cycling (100 Cycles) at $1200^\circ\text{F}$ . Coating Shown is Kaman SCA	145
75	(Ba,Ca) $\text{F}_2$ Coated Haynes 25 Alloy Foil	146
76	Typical SEM Appearances of Sputtered Coatings That Have Been Deformed. As-Received Coatings in (A) and (B) and the Same Coating After $1200^\circ\text{F}/260\text{-Hr}$ Exposure in Air (Deformed After Exposure). This Sample is Chromium Carbide Sputtered to Thickness of 1.5 Microns	150
77	Comparison of Cracking for Various Coatings on 0.006-In. Thick Inconel X-250 Foil Bent Around a 1/8-In. Diameter Mandrel. Highest Bars Indicate Best Ductility Coatings	151
78	Schematic of Foil Bearing Materials Wear Test Rig	156
79	Materials Wear Test Rig Installed in High-Temperature Oven	158
80	Materials Wear Test Rig Foil Bearing Section	159

# LIST OF ILLUSTRATIONS (Contd)

FIGURE	TITLE	PAGE
81	Torque Measurements (Vertical Axis) for Various Coating Combinations Tested in the Materials Wear Test Rig. (Numbers in Caption Block Refer to Test Number. The First Coating Listed was Applied to Shaft and the Second Coating Listed was Applied to Foils.)	167
82	Typical Appearance of Wear Rig Shaft and Foils After Testing. Center Two Bearing Groups Were Evaluated for Wear Appearance. B <sub>4</sub> C Coating on Foils and Tribaloy-400 Coated Shaft Segments (Test 27)	169
83	Foil Bearing Wear Categories	170
84	Coated Shaft (NiCo) and Foils (Sputtered Cr <sub>2</sub> O <sub>3</sub> +Al <sub>2</sub> O <sub>3</sub> ) After High Speed Test 38	175
85	Typical Appearance (SEM) of National Process Industries (Ba,Ca)F <sub>2</sub> Coating Surface	177
86	Typical Appearance (SEM) of NASA Fluoride Coating [(Ba,Ca)F <sub>2</sub> ·CaSiO <sub>3</sub> ·CaO] in Smooth and Rough Areas	179
87	Appearance of NASA CaSiO <sub>3</sub> Modified Fluoride Coating Before (a and b) and After (c and d) Thermal Exposure at 1200°F for 1300 Hours	180
88	Typical Appearance of Blisters on Surface of Plasma Sprayed Tribaloy 400 Wear Rig Shaft Segment	182
89	Appearance of Blister Area (a) and Area of Ti and Al Contamination (b)	183
90	Experimental Setup for Coefficient of Friction (C <sub>f</sub> ) Measurements (C <sub>f</sub> = F/W)	185
91	Theoretical Foil Journal Bearing Overlap Schematic	190
92	Foil Journal Bearings Overlap vs Unlapped Length	192
93	Shaft Excursion Characteristics	194
94	Mountain Ranges Obtained From the GTCP36-50 APU Rotor Dynamics Rig	195
95	Test Journal Bearing and Shaft	198
96	Foil Journal Bearing Strain Gauge Installation	200
97	8-Segment Bearing Static Cooling Flow Test	201
98	Journal Bearing Spring Rate Measurement Test Set-Up	203
99	Load/Deflection, 10-Segment Journal Bearing	204
100	16-Segment Bearing Design	206
101	Center 3 of 5 Plane Clearance Probes Used to Determine Shaft Bending in Configuration 18	210
102	Measured Shaft Bending at Speed	211



# LIST OF ILLUSTRATIONS (Contd)

FIGURE	TITLE	PAGE
103	Normalized Mode Shapes, TJE331 Foil Journal Bearing Rig - Bearing Spring Rate = 10,000 LB/IN.	213
104	Free-Free Shaft Excitation	214
105	Shaft Whirl Influence on Critical Speeds	215
106	Shaft Shortening Influence on Critical Speeds	217
107	Parachute Loader Final Configuration	219
108	Journal Bearing Test Rig Shaft After Bearing Failure at 6.5 psi and 33,000 rpm	220
109	12-Segment Journal Bearing Foils After Bearing Failure at 6.5 psi and 33,000 rpm	221
110	Run History, 12-Segment Teflon-S Journal Bearing	224
111	12-Segment Foil Journal Bearing Failure Development	225
112	Turbine-End Bearing and Shaft Before Disassembly	228
113	Shaft After Bearing Removal	229
114	Bearing Segments	230
115	Configuration 26 Foil Journal Bearing Test	231
116	Shaft Excursion Versus Speed (Configuration 27-10 Segment Bearing)	232
117	Configuration 28, Run 2-Start Cycles	234
118	Journal Bearing Test Rig Thrust Bearing Failure	236
119	Thrust Bearing	238
120	Thrust Bearing Load Pattern 304 Pounds Applied at 33,000 RPM	239
121	Dual Spring Foil Thrust Bearing Schematic	240
122	Dual Spring Thrust Bearing Deterioration	242
123	Baseline Spring With Partial Pad Stiffener	243
124	Foil Thrust Bearing Data Torque Versus Specific Torque	244
125	Constant Discharge Air Temperature Test	246
126	Failed Thrust Bearing, 40 Lb Load	248
127	Thrust Bearing Spring Heights Before and After Adjusting	251
128	Single Thrust Bearing Spring Yield Point	252
129	Bearing Assembly With Repositioned Locating Slots	254
130	Beryllium Copper Foils with Teflon-S Coating After 469-Lb Load	257
131	Test Results - Foil Thrust Bearing Configuration 30-High Temperature Test	259
132	Kaman DES on Inconel X-750 Foils After Full (200 Lbs) Engine Thrust Test at Operating Temperature	260
133	Foil Thrust Bearing Misalignment Test-Configuration 31	262

LIST OF ILLUSTRATIONS (Contd)

FIGURE	TITLE	PAGE
134	Dynamic Loading Test Results	263
135	Foil Thrust Bearing Geometry	271

# LIST OF TABLES

TABLE	TITLE	PAGE
1	FOIL BEARING APPLICATIONS	8
2	TJE331-1029 FOIL BEARING ENGINE BEARING OPERATING CONDITIONS	23
3	TJE331-1029 FOIL BEARING ENGINE BEARING OPERATING CONDITIONS (MINIMUM SEAL CLEARANCES	24
4	REQUIRED UNIT LOAD CAPACITY AND CALCULATED DEFLECTIONS OF FOIL BEARINGS WHEN SUBJECTED TO MIL-C-5007C CASE LOADS	26
5	TJE331-1029 ROTOR/BEARING CHARACTERISTICS	36
6	FOIL CANDIDATE ALLOYS AND PROPERTIES	123
7	COATING MATERIALS SELECTED FOR PROGRAM EVALUATION	126
8	COMPILATION OF TENSILE PROPERTIES FOR AIR FOILS	136
9	EVALUATION OF COATED FOIL SURFACES BY SCANNING ELECTRON MICROSCOPE	148
10	MATERIAL SELECTIONS FOR WEAR RIG TESTING	153
11	SPECIAL FABRICATION OF WEAR RIG BEARING COMPONENTS	161
12	TORQUE MEASUREMENTS FOR VARIOUS SHAFT COATINGS RUN AGAINST TEFLON-S COATED FOILS*	165
13	WEAR APPEARANCE OF COATED FOILS EVALUATED IN WEAR RIG TESTS	171
14	COATING PERFORMANCE FOR HIGH SPEED WEAR RIG TESTS	173
15	SUMMARY OF ELECTRON PROBE MICROANALYSIS OF NPI AND NASA FLUORIDE COATINGS	178
16	MEASURED SLIDING COEFFICIENT OF FRICTION	186
17	JOURNAL BEARING SPRING RATE SUMMARY	205
18	DEFLECTION CHARACTERISTICS OF THRUST BEARING SPRINGS	250
19	PERFORMANCE COMPARISONS - COMPLIANT FOIL THRUST BEARING GEOMETRIES	269

## SECTION I

### INTRODUCTION

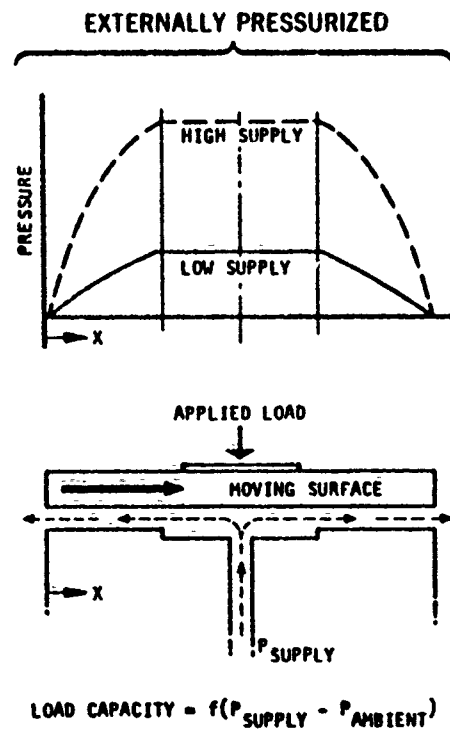
#### 1.1 Background

For many years, gas bearings have been a natural candidate for high-speed turbomachinery design because of the convenience and simplicity of using the process fluid, plant air, or ambient atmosphere as the lubricant. Consequently, a system concept that can capitalize on the advantages of a gas bearing has been the object of intensive research throughout the world.

Air bearings constitute one type of the more general class of process fluid film-lubricated bearings. The process fluid is the fluid most readily available as the lubricant. There are two general types of such fluid-film bearings in use today: the self-acting (hydrodynamic) type, and externally pressurized (hydrostatic) type. The self-acting bearing derives its load-carrying capacity from the pressure generated in the fluid film by the relative motion of two converging surfaces. The externally pressurized bearing relies on an external pressure as its source of load capacity. The type of bearing used in any particular application depends on the detailed requirements of the application. The self-acting bearing has the advantage of being independent of an external pressure source whereas the externally pressurized bearing has the advantage of increased load capacity, if sufficient pressure is available. The two concepts are shown in Figure 1.

Gas-lubricated foil bearings show potential for providing the advantages of simplicity, reduced maintenance, added reliability, reduced vulnerability, high-temperature operation, reduced weight, and cost savings to an advanced engine system.

## HYDROSTATIC



## HYDRODYNAMIC

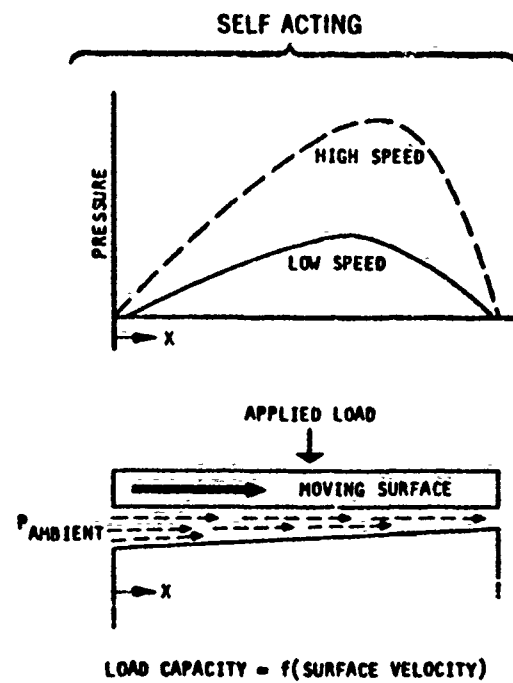


Figure 1. The Gas Bearing Concept.

### 1.1.1 Advantages

- (a) Simplicity - Simplicity of gas-lubricated bearings is effected by the absence of a complicated delivery and scavenge oil network, especially critical at the hot end bearing, where oil crosses the engine exhaust path upon entering and leaving the bearing cavity. In this area, extensive development is sometimes necessary to prevent high oil temperature during soakback, which often reduces engine reliability and time-between-overhaul.
- (b) Reduced Maintenance and Added Reliability - Foil bearing endurance capability has been proven by foil bearing-equipped cooling turbines used in the DC-10 environmental control system (ECS). Reliability also is being demonstrated in several military aircraft ECSs.

Foil bearings can achieve a longer life because there is no contact between bearing and shaft during normal operation. Wear-resistant coatings provide adequate wear protection for contact during starts and stops.

Eliminating the need for a viscous bearing lubricant reduces the load on the lubrication pump and enhances cold weather starting capability.

- (c) Reduced Vulnerability - Since the foil bearings do not require external engine hardware, such as oil lines and an oil heat exchanger, engine vulnerability is reduced.
- (d) High-Temperature Operation - Advancements in foil coating temperature tolerance were achieved during this program. Because air viscosity increases with

temperature, a hotter-running bearing provides higher load capacity, thus making high temperature operation desirable.

- (e) Reduced Weight - A weight saving is effected by the reduction in oil capacity required by a system incorporating foil bearings, assuming that an engine gearbox is still required. The reduced oil capacity, in turn, would reduce capacity requirements for the oil heat exchanger and the oil pump. Eliminating oil delivery and scavenge networks results in a less complex, more uniform, and lighter weight assembly. The weight saving, however, is compromised by the requirement for larger diameter journal bearings and the addition of a thrust runner on the rotor for the thrust bearing.
- (f) Cost Saving - The inherent simplicity of the foil bearing lends itself to rapid and easy fabrication. After an initial investment in tooling, foils can be stamped or rolled out at low cost. The greatest cost saving is realized by elimination of the oil network.

#### 1.1.2 Related Programs

The gas-lubricated foil bearings utilized for this program are of a design patented by The Garrett Corporation. The bearings were initially developed for experimental use in cooling turbines of the Boeing 727 air conditioning system. General design of these bearings is depicted in Figure 2.

Observing this successful application to the cooling turbines and recognizing the advantages foil bearings offer to advanced

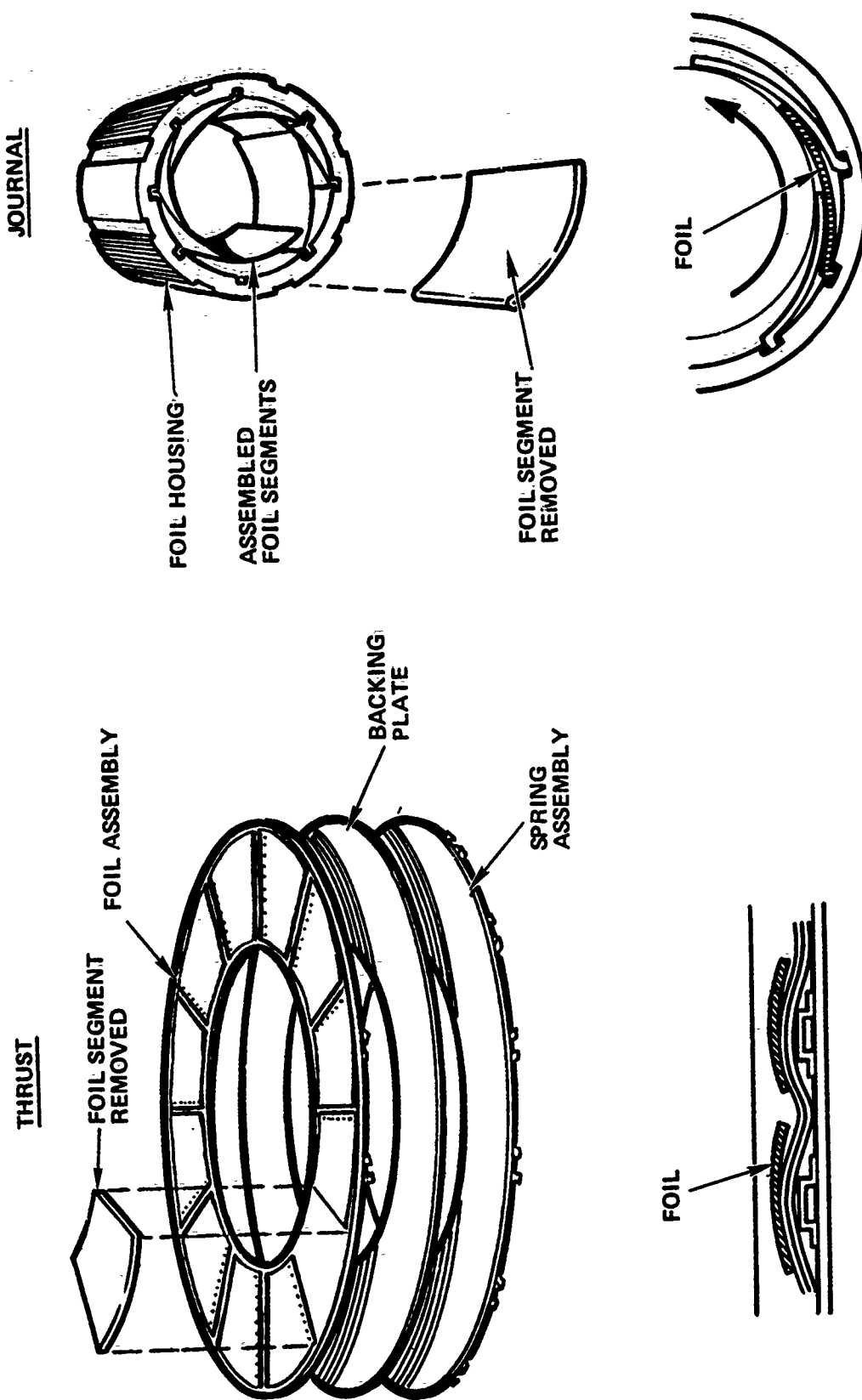


Figure 2. The Self Acting Compliant Foil Bearing Concept.



military engines, the U.S. Air Force sponsored a feasibility study of the application of gas-lubricated, compliant foil bearings to gas turbine engines. This initial program was completed and is described in Technical Report AFAPL-TR-72-41, dated June 1972.

During a follow-on program, a foil bearing demonstrator was designed and fabricated from an AiResearch Model JFS100-13A Jet Fuel Starter gas generator, which is used on the Air Force A7D light-attack aircraft. Modifications to the original production equipment included replacing the rolling element bearings with compliant foil gas bearings and replacing the power turbine module with an exhaust thrust nozzle. The resultant engine is a 95-pound static thrust turbojet engine, mounted on compliant foil-gas bearings totally free of oil and external air supply and operating at 72,000 rpm. The demonstrator was operated continuously for five hours and underwent 135 start/stop cycles. This activity was reported in Technical Report AFAPL-TR-73-56 dated June 1973. Other foil bearing application and demonstration vehicles are shown in Figure 3 and tabulated in Table 1.

### 1.2 Program Objectives

The program objective was to extend and demonstrate the state-of-the-art of gas lubricated compliant surface bearings to 1000 to 3000 pound thrust class full scale turbomachine requirements and constraints.

### 1.3 Program Approach

The program approach was as follows:

- (a) Establish the loads imposed on the journal and thrust bearings by the selected turbomachine rotor.

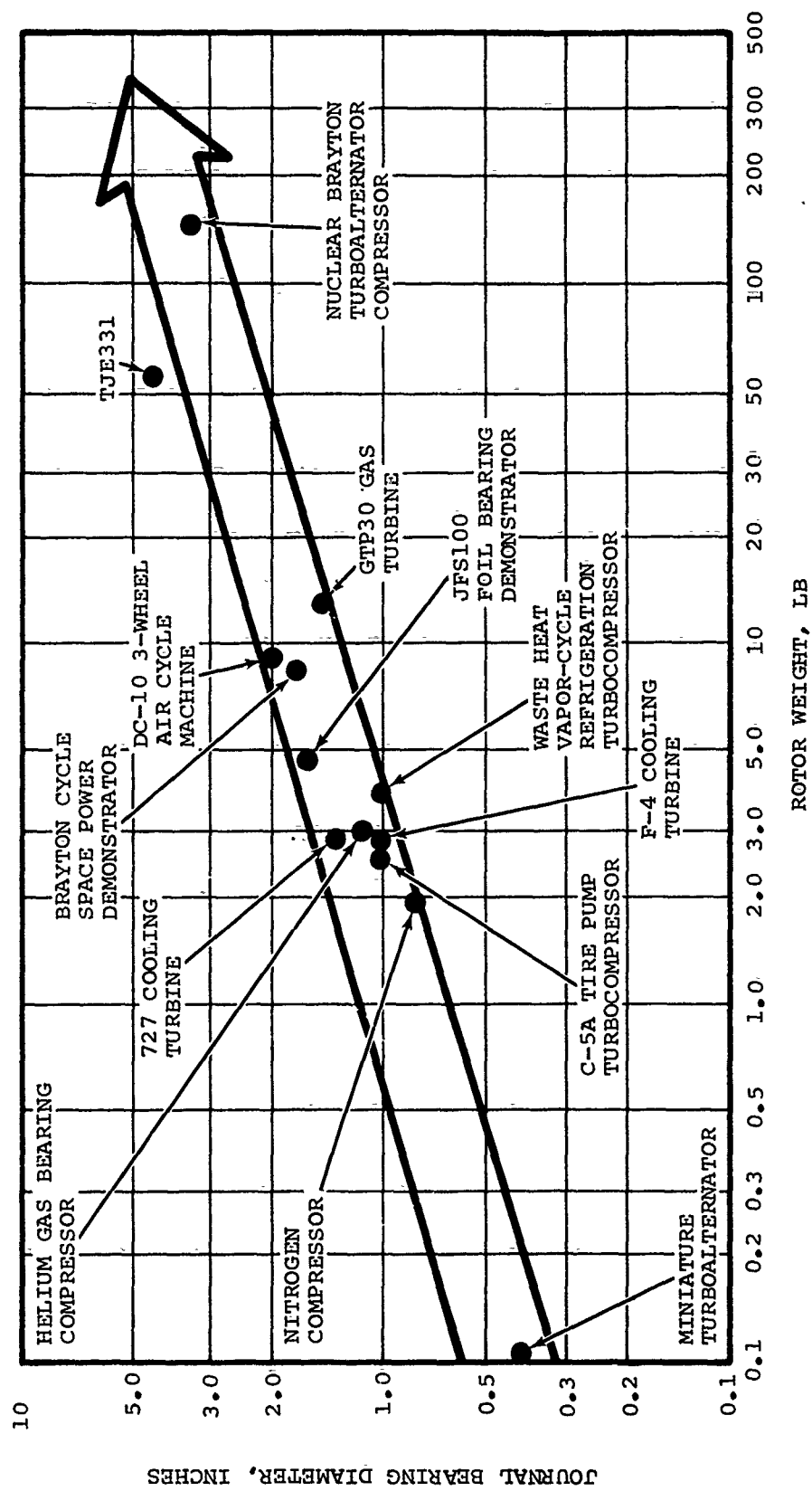


Figure 3. Foil Bearing Applications

TABLE 1  
FOIL BEARING APPLICATIONS

	Shaft Speed (Nom) K rpm	Rotor Weight lb	Rotor Polar Moment of Inertia in.lb.sec <sup>2</sup>	Journal Foil Bearings qty	Thrust Foil Bearings qty	Gas Temperature to Foils °F	Process Fluid Temperature °F
Miniature Turbo- alternator	350	0.222	--	2 (Conical)		-370	-380
Nitrogen Compressor	135	1.85	--	2	2	220	300
C5A Tire Pump Turbocompressor	96	2.6	--	2	2 Hydrost.	450	600
F-4 Cooling Turbine	74	2.85	--	2	2 Hydrost.	350	800
Helium Gas Bearing Compressor	85	3.0	--	2	2	150	300
727 Cooling Turbine	76	2.9	--	2	2	375	850
Waste Heat Vapor- cycle Refrigera- tion Turbo Compressor	52	3.8	--	2	2 Hydrost.	150	325
JFS100 Foil Bearing Demonstration	72	4.9	0.013	2	2	350	1500
Brayton Cycle Space Power Demonstra- tion	48	7.5	0.0098	2	2	N/A	1550
DC-10 3-Wheel, Air Cycle Machine	46	8.0	0.062	2	2	400	800
GTP30 Gas Turbine	38	13.5	--	2	2	N/A	1350
Nuclear Brayton TAC	24	152	1.746	2	2	350	1550

- (b) Apply existing and/or develop the analytical design tools required for bearing development and for the proper application of these bearings to the 1000- to 3000-pound thrust turbomachine.
- (c) Design, fabricate and develop a thrust bearing and a journal bearing test rig for baseline bearing testing and development to meet the selected turbomachine requirements, while subjected to the maneuvers of MIL-E-5007C.
- (d) Conduct a base material and coating selection and evaluation program to select materials that will meet temperature requirements of the thermal analysis. Candidate materials are to be evaluated in a high temperature wear test rig to determine fabrication suitability, wear and friction factor.
- (e) Conduct a bearing development program with the support of analytical tools. Development activities goal was to achieve the load capacity, high temperature operation, and other turbomachine application requirements.

## SECTION II

### SUMMARY

The program consisted of the following three major divisions of effort, each dependent on the others to achieve program goals:

- o Analytical
- o Materials Development
- o Bearing Development and Testing

Accomplishments within these areas are summarized in the following paragraphs.

#### 2.1 Analytical

The elasto-hydrodynamic thrust and journal foil bearing computer analytical programs developed during this program are a major first step in developing full analytical capability to predict foil bearing performance. These analytical tools permit evaluating foil bearing performance for a complete range of bearing parameters (foil thickness, number of foils, journal free form radius, foil overlap, etc.) The foil thrust bearing solution already has been demonstrated as a powerful design aid in assessing the baseline design load capacity as well as providing proper direction to increase load capacity. This has been established with excellent experimental correlation from the baseline configuration thrust bearing test, and the increased load capacity achieved by proper control of foil rigidity as analytically predicted. The journal bearing computer simulation has permitted evaluation of foil elasticity effects such as static stiffness and foil preload, which has proven to be a major factor in control of journal rig shaft dynamics and stability. Excellent correlation was achieved for the elasticity routine, which includes the nonlinear effects characterized by foil and boundary interactions.

Thus, a major obstacle has been overcome by predicting the nonlinear elasticity effects of foil journal bearings. The full elasto-hydrodynamic journal bearing computer solution has been executing at low eccentricities. However these low eccentricity values are characteristic of test results. Measured eccentricity values of 0.002 to 0.005 inches were obtained from the twelve-segment bearing (Figure 115). Further development and program improvement is required for the journal bearing program to be completely operational. It is expected that when operational, this design tool will be recognized as a major advancement in predicting foil bearing performance.

A maneuver load analysis was conducted on the TJE331-1029 engine to determine foil bearing load capacity requirements imposed by MIL-E-5007C maneuvers. Highest load capacity requirement for the journal bearings is 16 psi, due to a 3.5 radian/sec yaw rate maneuver, combined with a 1 g vertical load. Highest load capacity requirement for the thrust bearing is 37 psi, due to a combination of simultaneous maneuvers which include 10 g forward thrust, 2 g side load,  $\pm 14 \text{ rad/sec}^2$  pitch acceleration,  $\pm 6 \text{ rad/sec}^2$  yaw acceleration, and 200 lb forward aerodynamic thrust.

The front and rear bearing journals were designed to minimize the distortion band to 0.0006 inch from a true cylindrical shape. Even though centrifugal growth reduces the clearance space between the journal and foil bearing, the true cylindrical shape of the journal is maintained. Both journals are made from Inconel 718 to allow potential bearing operating temperatures in excess of 1000°F. Structural reliability is very good because stresses in the journals are relatively low.

The thrust runner was designed to maintain the bearing surface flat within a 0.0006 inch band. Unlike the journals centrifugal effects will not cause distortion in the bearing runners.

Additional distortion may occur due to temperature differences on the runner surfaces. The thrust runner is also Inconel 718 to allow for high temperature operation. Stresses in the thrust runner are relatively low.

A rotor dynamics analysis has indicated the first 3 critical speeds occur at 4000 rpm, 8000 rpm, and 52,000 rpm, respectively, for foil bearing spring rates of 10,000 lb/in. The two lower criticals are rigid body modes that increase with increasing bearing spring rates but the third mode remains insensitive to bearing spring rates. However, even at spring rates of 75,000 lb/in, a large operating window exists between the second and third criticals.

A thermal analysis was performed on both the thrust and journal foil bearings. An existing thermal analysis program was used, which had the capability of analyzing the foil bearing with the variable characteristics of sway space, number of foils, power loss within the bearing, cooling airflows, and material characteristics. After devising a cooling airflow schematic and modeling the bearing characteristics the bearing element temperatures were determined.

Results of the analysis clearly showed trends in journal bearing operating temperatures as a result of changing any variable. Increasing operating altitude conditions resulted in higher indicated bearing temperature. The analysis at 50,000 ft altitude shows bearing temperatures that are too high, but until actual foil temperatures are measured to substantiate the analysis, the figures should be used only to indicate operating temperature trends. The analysis done at 25,000 ft altitude indicates a safe operating condition for the journal foil bearing.

The thrust bearing thermal analysis indicates higher operating temperatures than the journal bearing, mainly because of reduced pressure drop across the bearing available for effective

cooling. A sea level operating condition indicates a thrust runner operating temperature of 1000°F under a 370 lbs thrust load. Since this analysis was completed, the rotor aerodynamic thrust load has been reduced to 200 lbs by thrust piston design techniques within the engine.

## 2.2 Materials Development

Lubricative and wear resistant coatings for foil bearings are required during the low speed range prior to hydrodynamic separation of the foil and shaft. Therefore, the objective of materials development activities was to establish appropriate bearing surface coatings that were capable of performing at 1200°F in air. In addition to coatings, it was necessary to specify alloys for substrates (rotating shafts and bearing foils) that were compatible with coatings and capable of extended service at temperatures to 1200°F. Specific material development goals were as follows:

- (a) Identify and evaluate candidate foil coating materials for temperature capability to 1200°F.
- (b) Evaluate foil alloys that show promise of minimum loss in strength and elastic modulus from room temperature through the maximum operating temperature (1200°F).
- (c) Select appropriate coatings and alloys with the best combination of properties for operation in bearing test rigs.
- (d) Demonstrate survivability under simulated engine operating conditions.



These goals were accomplished in a two-phase effort; the first, a materials screening activity to select candidate alloys and coatings, and the second involving wear rig evaluations of the candidate materials. Upon completion of these activities, the best alloys and coatings were identified and appropriate materials selected for use in the full scale thrust and journal bearing rigs.

Materials screening was performed by subjecting candidate alloys and coatings to a variety of metallurgical examinations to establish strength properties, long term oxidation resistance, coating ductibility, surface finish capability and coating bond quality. Inconel 718 was selected as the shaft alloy and Inconel X-750 as the foil alloy for wear rig evaluations. Sixteen coatings were chosen for further evaluation in wear rig tests.

A materials wear test rig was used to evaluate coatings for friction and wear behavior over the temperature range 70° - 1000°F (sliding friction would account for an additional temperature rise to near the 1200°F objective). Coated shafts and foils were subjected to low speed (157 rpm, constant bearing contact) and high speed (>11,000 rpm, foil lift-off attained) shaft rotating tests at several temperatures (room to 1200°F). Drag torque measurements indicated relative friction behavior between coatings, and visual and microscopic evaluations defined relative wear characteristics.

Based on these evaluations and materials screening data the following materials (in order of preference) were established for high temperature foil bearing components:

<u>Shaft Alloys</u>	<u>Foil Alloys</u>
o Inconel 718	o Inconel X-750
o Haynes 25	o Inconel 718
o Inconel X-750	o Haynes 25
	o 446 Stainless Steel

#### Shaft or Foil Coatings

- o  $B_4C$
- o  $TiB_2$
- o  $Cr_2O_3$
- o  $TiC$
- o Kaman DES or SCA ( $Cr_2O_3$  compositions)
- o NiCo (Nickel-Cobalt)
- o Tribaloy-400

The above coatings were determined to be the best, but not all were practical for bearing fabrication due to lack of manufacturing reliability or experience. Therefore, the following coatings were selected for use in foil bearing rigs:

#### Shaft or Runner

Kaman SCA  
Tribaloy-400 (oxidized)  
Haynes 25 (oxidized)  
NiCo (oxidized)

#### Foil Coatings

Kaman DES  
NiCo

Results of materials development work also indicated the following:

- (a) Conventional bonded carbide coatings did not perform adequately in oxidation resistance or frictional characteristics.
- (b) High cobalt-containing materials (Haynes 25, Tribaloy-400 and NiCo) performed well, generally when surface oxide layers were present (pre-heat treated to form oxide or used at temperatures above 800°F).

- (c) The use of a gold overplate on several coatings provided only moderate decreases in friction and was not necessarily helpful on rotating parts (dependent upon the substrate coating).
- (d) The baseline Teflon-S coating displayed a friction coefficient near the middle of coatings evaluated, indicating most of the coatings evaluated in the program were capable of matching Teflon performance in this respect over a wide temperature range (70-1200°F). None of the program coatings were, however, able to approach the durability and wear resistance of the Teflon at room temperature.
- (e) Data suggest placement of the metallic or softer coatings on rotating components and hard coatings on stationary components.

Future improvements in application processes, thickness, ease of repair, and reliability will encourage the use of other promising coatings such as  $B_4C$ ,  $TiB_2$ ,  $Cr_2O_3$ ,  $TiC$ ,  $Si_3N_4$  and  $(Ba,Ca)F_2$  compositions.

Most of the above coatings are acceptable for 1200°F, or higher, operation and all are capable of at least 1000°F operation for extended periods. The possibilities for singular or multiple combinations of these coatings is extremely encouraging for low friction and wear applications both at room and elevated temperatures.

### 2.3 Bearing Development and Testing

Design and fabrication of baseline bearings and suitable test rigs was required as a preliminary to bearing development. Baseline thrust and journal bearing designs were based on the

successful DC-10 environmental control system (ECS) cooling turbine foil bearings. The bearings were scaled to the required size and then adjusted by known empirical parameters and experience judgements.

Separate thrust and journal bearing development test rigs were designed and fabricated for full size bearing development. The rigs were designed to perform all test conditions required by the test plan.

The thrust bearing baseline design was tested to a capacity limit of 15 psi, which is 25 percent higher than estimated. Bearing capacity improvement followed the dual spring concept, which evolved from the elasto-hydrodynamic analysis. Although fabrication and testing this concept failed to prove its validity, the elasticity requirement of the analysis was attained, using partial pad stiffeners. Thrust bearing capacity was increased to 27.5 psi at a steady-state condition. Since these high bearing capacities are only required for short term transient maneuvers, the bearing was tested by incrementally increasing the load for short durations. This technique permitted the bearing to carry 33.8 psi before failure, which is 91 percent of the 37.2 psi goal. Cause of failure at this limit was not found to be a bearing capacity limit but a yielding of the pad spring. Stress calculations of the spring indicated possible yielding at this load level. Design, fabrication, and testing of a spring to solve the problem earlier in the program resulted in other problems with the spring. Further effort is required in this area before 100 percent of the goal can be achieved.

Journal bearing development on the test rig presented a problem that initially was not understood. Test rig operation could not exceed 80 percent of design speed without bearing failure, regardless of the bearing configuration installed in the test rig. Extensive instrumentation of the rig revealed that

the test shaft was bending up to 0.012 inch. The first bending critical speed of the shaft was calculated to be 43,999 rpm, but severe bending was experienced at 25,000 rpm. Shortening the shaft 6 inches increased the bending critical speed sufficiently to permit operation to 34,000 rpm with a minimum of shaft bending. All testing to this point indicated that the 12-segment journal foil was the most stable operating bearing, therefore the most development time was spent on that configuration. The highest demonstrated load capacity was 6.5 psi at 33,000 rpm, while a modification to that bearing developed an extrapolated (for speed correction) load capacity of 7.1 psi. A further extrapolation for operation at engine operating pressure shows a capacity of 8.6 psi, which is only 50 percent of goal. However, since load capacity can be increased with fewer bearing segments, a ten-segment bearing was designed and fabricated to get closer to the load capacity goal. This configuration also was fabricated of materials and coatings for the high temperature test. As tested, this configuration appeared very sensitive to the backward precession mode of shaft whirl and the operational speed had to be limited to 22,000 rpm. In spite of this limitation the bearing was subjected to operation at engine operating cooling air temperatures up to 500°F. Also, 50 starts and stops were successfully accomplished, for the purpose of evaluating the selected coating in a high temperature environment. The test showed the high temperature coating could meet program requirements but had a peculiar characteristic of varying break-away torque, which should be investigated in future programs. The Kaman DES foil coating ( $\text{Cr}_2\text{O}_3$ ) and the Tribaloy-400 (Cobalt base wear alloy) are compatible coatings acceptable for journal bearing operation to 1200°F.

## SECTION III

### DISCUSSION

#### 3.1 Engine Characteristics

The ETJ341-P1 engine was selected as the vehicle for the application of foil bearings. Specific advantages achieved by selecting this turbomachine are as follows:

- (a) The selected configuration is a high technology turbomachine, representative of that required for future remotely piloted vehicle (RPV) applications. Also, the final demonstration of the bearing system in the turbomachine would provide a firm basis for a near-term flight test of the same machine in several potential flight test vehicles.
- (b) The selected turbomachine has an excellent operational and production potential. Factors that support this are:
  - o The selected turbomachine is of an advanced technology design. Low-cost engine design studies, performed by AiResearch<sup>1</sup> under contract to the Air Force, showed that turbomachinery design configurations similar to that proposed for use in this program, will be required for future applications, i.e., all-axial aerodynamic components.
  - o The turbine inlet temperatures are representative of the state of the art (1700° to 1900°F) for this type of application.

<sup>1</sup>Six, L.D., F.W. Lewis, and C.S. Stone, Low Cost, Limited Life Turbine Engine Analysis, AFAPL-TR-71-102, January 19, 1972

- o Although the technology level of this engine is high, relative program and production costs are low.
- (c) The selected turbomachine has a low rotor weight and inertia ( $I_p$ ), with a relatively long bearing span, which results in moderate maneuver bearing loads.
- (d) The selected turbomachine has simple structural design, which allows easy removal of bearings for inspection or replacement and provides access to bearing instrumentation
- (e) The rotating group provides flexibility with regard to bearing placement, i.e., inboard or outboard of the aerodynamic components.
- (f) The potential of variable bearing span allows for minimizing misalignment and deleterious thermal conditions.
- (g) The rotor weight, unbalanced rotor forces, and g loadings permit minimizing load per unit area requirements.
- (h) The bearing size permits accurate measurement of all bearing performance criteria as related to configuration, materials, details of geometry, environment and control thereof, as a function of test condition.
- (i) The high temperature imposed on the hot end of the rotating group allows for a step-by-step examination of the many effects of high temperature, including bearing performance, materials, life, thermal gradients, and soakback during shutdown.

### 3.1.1 Power Section

To adapt the ETJ341-P1 for use as the foil bearing demonstrator required modification of the rotor assembly interface and tie-bolt arrangement to minimize bearing surface distortion. This distortion can result from centrifugal loading, tie-bolt clamping force, and temperature gradients. As a result, the following features were incorporated, as shown in Drawing L3621113.

- o The rotor clamping load path does not include the bearing journals.
- o Center supported journals.
- o Journals supported with thermally compliant tubular shaft member.
- o Tapered drum journal design to provide uniform centrifugal growth.
- o Curvic couplings to ensure excellent concentricity and normality of all rotating elements, especially the bearing surfaces.

While accomplishing these modifications, it was possible to retain, unchanged, the outer shell of the engine, compressor and turbine aerodynamic blading, combustor, and inner and outer tail-cones. The last three compressor disks were unchanged, and the turbine wheel was machined from the same casting as the ETJ341-P1. The first two compressor disks were modified to adapt to the new tie-bolt/bearing system.

The modified engine was reidentified as the TJE331-1029.



### 3.1.2 Performance

To make the life of the ETJ341-P1 baseline turbomachine more compatible with overall program goals, the rated thrust was reduced from 800 lb to 700 lb. This change extended engine life from 0.7 hours to more than 50 hours.

A complete cycle analysis on the TJE331-1029 was performed for various altitudes, vehicle air speeds, and standard day variations. The analysis resulted in a listing of the air pressures and temperatures of each bearing inlet and the pressure of the cavity into which the cooling air is dumped. The added temperature rise of the cooling air as a result of the bearing power loss was then calculated, arriving at the conditions listed in Tables 2 and 3. The conditions of bearing cooling air were then used as a basis for the thermal analysis reported in Paragraph 3.1.8.

### 3.1.3 Maneuver Load Analysis

The MIL-E-5007C Specification flight maneuver load diagrams are shown in Figure 4. Bearing loads were calculated for maneuvers defined by each corner of the diagram and labeled for easy reference to Table 4. Table 4 lists the average bearing load capacity required of the bearing by the maneuver condition. Only the ten most highly loaded conditions are reported.

In addition to the diagrams, MIL-E-5007C indicates the rotor bearings must be capable of carrying a 3.5 rad/sec yaw rate combined with a 1 (g) vertical load. This is the highest maneuver load condition imposed on the journal bearings. The journal bearings must generate an average load capacity of 16 psi to survive this maneuver. The most severe load condition for the thrust bearing is case number 35, Figure 4, which may occur from an arrested landing. These specified maneuvers and an additional 200 lb aerodynamic thrust require a thrust bearing load capacity of 37 psi.

TABLE 2

## TJE331-1029 FOIL BEARING ENGINE BEARING OPERATING CONDITIONS

Engine Operating Conditions		Cold Day S/L M = 0.8	Hot Day S/L M = 0.8	Std. Day S/L Static	Std Day 25,000 M = 0.85	Hot Day 50,000 M = 0.9
Front Journal Foil Bearing	Inlet press., psia	110.94	82.41	73.3	44.17	11.65
	Inlet temp., °F	332	564	452	405	366
	Outlet press., psia	59.46	45.02	38.98	23.18	5.53
	Outlet temp., °F	446	745	643	744	800
Rear Journal Foil Bearing	Inlet press., psia	111.16	82.64	73.43	44.23	11.63
	Inlet temp., °F	332	564	452	405	366
	Outlet press., psia	72.8	53.97	47.8	28.53	6.77
	Outlet temp., °F	461	768	670	790	800
Middle Thrust Foil Bearing	Inlet press., psia	110.35	82.44	72.94	43.92	11.57
	Inlet temp., °F	332	564	452	405	366
	Outlet press, front-side, psia	102.27	78.24	67.41	40.47	10.73
	Outlet temp., front-side, °F	400	693	565	595	800
	Outlet press, rear side, psia	109.3	81.74	72.29	43.4	11.4
	Outlet temp, rear side, °F	437	758	623	693	800

NOTES: 1. All outlet temperatures were estimated based on an assumed bearing power loss.  
2. All labyrinth seal clearances are 0.009 in.

TABLE 3  
TJE331-1029 FOIL BEARING ENGINE BEARING OPERATING CONDITIONS  
(MINIMUM SEAL CLEARANCES)

Engine Operating Conditions		Cold Day S/L M = 0.8	Hot Day S/L M = 0.8	Std. Day S/L Static	Std. Day 25,000 M = 0.85	Hot Day 50,000 M = 0.9
Front Journal Foil Bearing	Inlet press, psia	111.65	82.87	73.74	44.39	11.65
	Inlet temp., °F	332	564	452	405	366
	Outlet press, psia	84.34	61.86	55.02	33.07	7.63
	Outlet temp., °F*	482	802	707	855	800
Rear Journal Foil Bearing	Inlet press, psia	111.57	82.86	73.69	44.37	11.65
	Inlet temp., °F	332	564	452	405	366
	Outlet press, psia	76.56	56.57	50.21	30.0	7.05
	Outlet temp., °F*	466	777	679	805	800
Middle Thrust Foil Bearing	Inlet press, psia	110.1	82.33	72.77	43.82	11.56
	Inlet temp., °F	332	564	452	405	366
	Outlet press, front-side, psia	102.3	78.28	67.45	40.5	10.73
	Outlet temp, front-side, °F*	402	698	569	602	800
	Outlet press, rear-side, psia	108.5	81.3	71.58	43.1	11.31
	Outlet temp, rear-side, °F*	445	773	636	717	800

- NOTES: 1. \*Outlet temperatures were estimated based on an assumed power loss for the bearings.
2. All Labyrinth seal clearances are 0.003 inches except turbine end seal which is 0.008 inches.

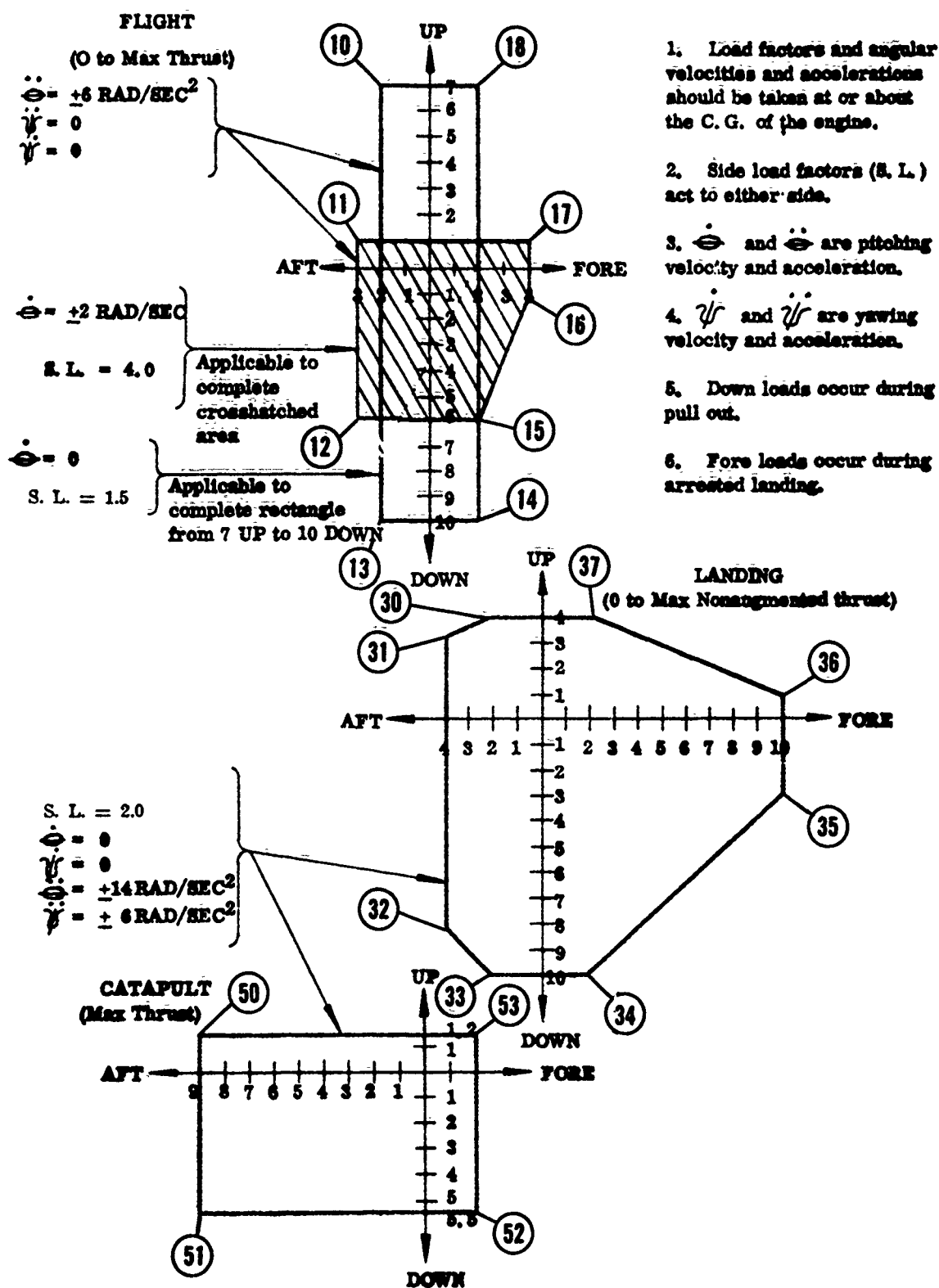


Figure 4. Flight Maneuver Load Diagrams

TABLE 4

REQUIRED UNIT LOAD CAPACITY AND CALCULATED DEFLECTIONS OF FOIL  
BEARINGS WHEN SUBJECTED TO MIL-E-5007C CASE  
LOADS FROM FIGURE 4.

Case Load From MIL-E-5007C Figure 4	Compressor Journal Bearing		Turbine Journal Bearing		Thrust Bearing	
	Deflection X-Forward Y-Side Z-Down	Unit Loading psi	Deflection X-Forward Y-Side Z-Down	Unit Loading psi	Deflection X-Forward Y-Side Z-Down	Peak Unit Loading psi
3.5 rad/ sec and 1-g down	0.006 0.000 0.011	16.37	0.006 0.000 -0.010	14.48	0.006 0.000 -0.005	29.28
11	0.002 -0.007 0.001	6.22	0.002 0.010 0.001	13.72	0.002 0.006 0.001	18.43
12	0.002 -0.007 0.004	7.34	0.002 0.009 0.005	15.54	0.002 0.006 0.005	17.28
14	0.007 0.001 0.008	6.59	0.007 0.001 -0.010	12.32	0.007 0.001 0.009	16.93
15	0.007 -0.007 0.004	7.34	0.007 0.009 0.005	15.54	0.007 0.006 0.005	29.87
16	0.009 -0.007 0.001	6.22	0.009 0.010 0.001	13.72	0.009 0.006 0.001	36.05
17	0.009 -0.007 -0.001	6.22	0.009 0.010 -0.001	13.72	0.009 0.006 -0.001	36.05
33	0.004 0.002 0.008	6.65	0.004 0.002 0.010	12.43	0.004 0.002 0.009	6.90
34	0.007 0.002 0.008	6.65	0.007 0.002 0.010	12.43	0.007 0.002 0.009	16.96
35	0.011 0.002 0.003	2.40	0.011 0.003 0.005	4.36	0.011 0.003 0.005	37.19
36	0.011 0.002 -0.001	1.49	0.011 0.004 -0.002	2.70	0.011 0.003 -0.002	36.57

It is apparent that the maneuver loads imposed on the thrust and journal bearings are of a transient, not steady-state, nature. This parameter is important to realistic bearing design and development because the short term load capacity of foil (or other) bearings is greater than the long term capacity.

#### 3.1.4 Thrust Bearing Runner Stress Analysis

The thrust bearing runner was analyzed to investigate distortion and stress resulting from loads imposed by MIL-E-5007C maneuvers. The most severe load specified for the thrust bearing (case 35 in Figure 4) results from a combination of maneuvers listed for case 35 and 200 lb forward aerodynamic thrust on the rotor.

Inconel 718 was the material selected for the runner because its high temperature capability would allow potential bearing temperatures beyond 1000°F.

Results of the thrust runner displacement analysis, when subjected to maximum axial bearing loads and centrifugal effects at 33,000 rpm, are shown in Figure 5. Total maximum axial distortion (excluding axial displacement) is 0.00052 inch. This distortion must be compensated by the bearings compliancy to maintain full load capacity when it is most needed. The equivalent stress distribution also is presented in Figure 5. Equivalent stress is calculated using distortion energy theory of failure. Stresses are sufficiently low in the bore to allow an excess of  $10^6$  starts at 1000°F. Stresses in the runner just under the pressure equalization holes, reach 60 ksi. At 1000°F 0.1% creep life is calculated to be greater than  $2 \times 10^5$  hrs. With these large safety factors on life from a fatigue and creep consideration, no problems are anticipated with the structural integrity of the thrust runner.

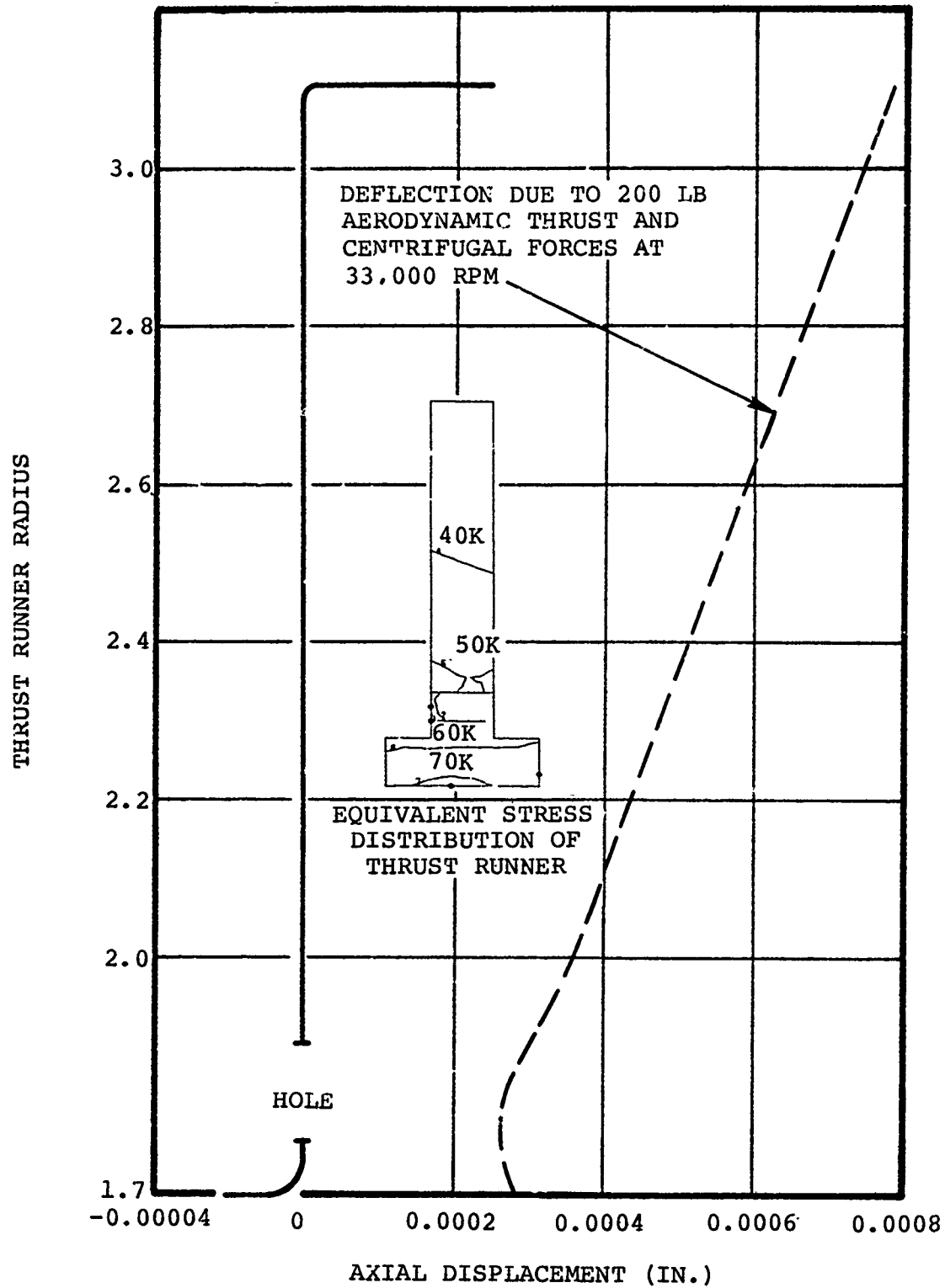


Figure 5. Thrust Runner Axial Displacement

### 3.1.5 Rear Journal Bearing Runner

A stress and deflection analysis was conducted on the rear bearing journal of the TJE331-1029. Deflections were calculated for an axial tie-bolt load in combination with centrifugal effects. No temperature effects were included in the analysis, as this analysis was performed concurrently with the thermal analysis. A review of the thermal condition indicated no further analysis was necessary as thermal gradients were not expected to contribute to significant distortion of the journals.

The calculated distortion of the bearing journal is shown in Figure 6. The two cases shown include (1) centrifugal effects alone, and (2) centrifugal effects in combination with the tie-bolt load. Since the tie-bolt load is taken through the journal, a wave-like distortion results, as shown. The radial displacement at the center of the runner is reduced because of the attachment of the tie-bolt bumper. This bumper has a cylindrical section to minimize the effect of restraining radial deflection, and hence reduce distortion of the journal surface. The remaining two "dips" in the surface displacement result from journal attachment to the rotor, again reducing radial displacement at these locations. The two hoops at the ends of the journal inhibit end displacement and maintain total distortion of the journal surface within a 0.0006 inch band. Average radial displacement is approximately 3 mils.

Figure 7 shows magnified displacement characteristics and an isopleth of tangential stresses for the rear bearing journal at 33,000 rpm and 25,000 lb tie-bolt load. The analysis was conducted for a uniform 70°F temperature.

Peak tangential stresses in the journal hub at the turbine end reach 120 ksi in compression. This stress is highly localized and does not undergo extensive cycle duty since it is caused



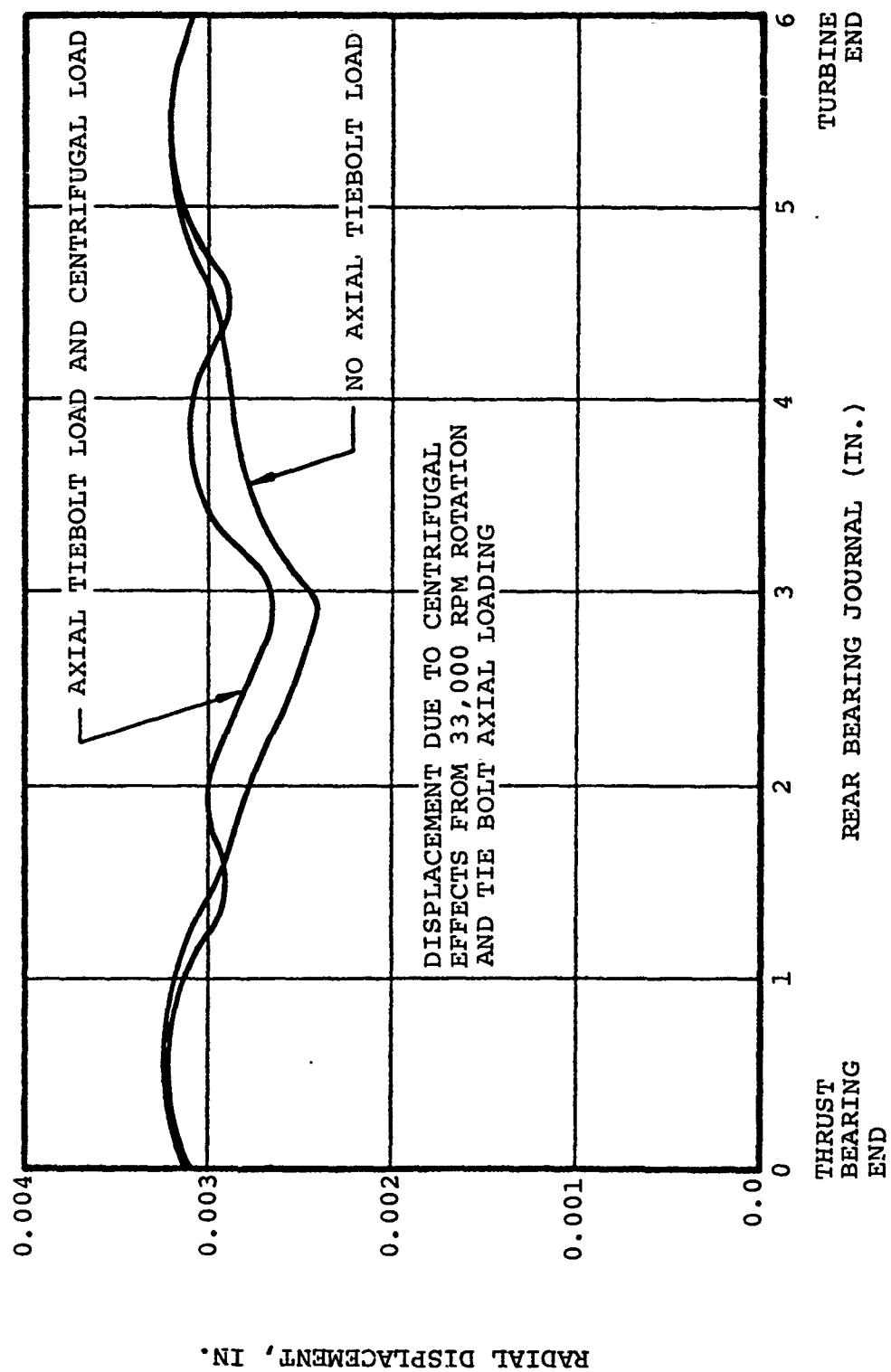


Figure 6. Radial Displacement of the Rear Bearing Journal

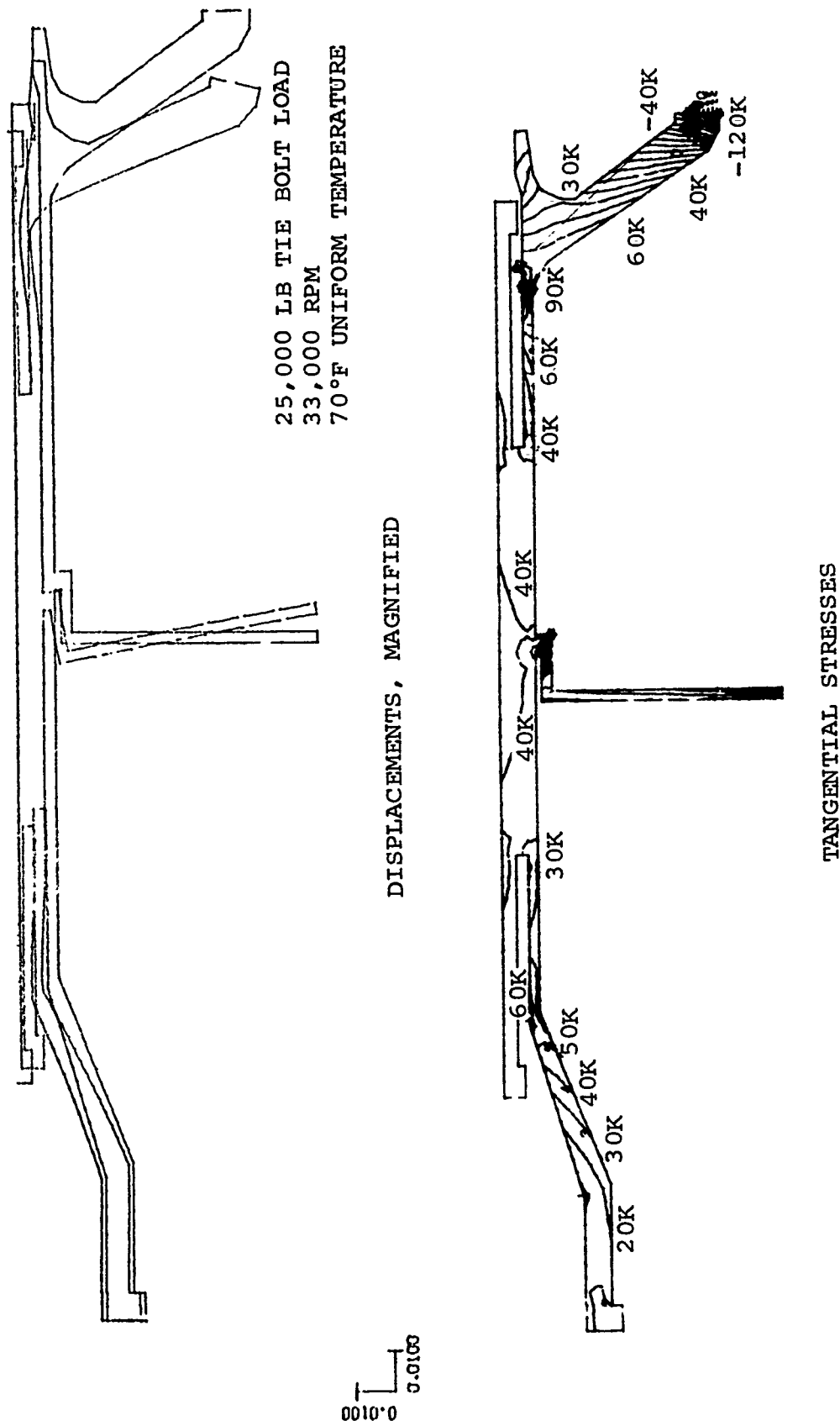


Figure 7. Analytical Model of the Rear Bearing Journal of the TJE331-1029 Engine.

primarily by the tie-bolt load. Axial and radial stresses were low relative to the tangential stresses. Hence the equivalent stresses closely follow tangential stresses.

Since peak stresses are substantially below the 148,000 psi yield strength of Inconel 718 at 1000°F, no problems are anticipated with operation of the rear bearing journal.

### 3.1.6 Forward Journal Bearing Runner Stress and Deflection Analysis

An analysis similar to the one conducted on the rear bearing journal was conducted on the forward journal. The journal was designed to be as free as possible from influence from the rotor. This is accomplished by the long thin cylinder that attaches the journal to the main rotor and isolates the journal from thermal and centrifugal deflections that may occur in the rotor. With this isolation, the journal can rotate like a free body, unaffected by rotor behavior.

The calculated displacement of the journal surface, which contacts the foils of the air bearing, is shown in Figure 8. This displacement, which amounts to about 3 mils radially, results from centrifugal effects. Effects due to a temperature profile are not included. The decreased displacement at the center is a result of attachment between the journal and rotor. The ring required for attachment inhibits radial growth. Centrifugal effects tend to cause the ends of the journal to flower but small hoops at the ends of the journal restrain radial deflection and force the journal surface to remain within an 0.0006 inch distortion band. Unlike the rear journal, the forward journal does not carry the tie-bolt load.

Figure 9 shows a magnified displacement curve and the tangential stress distribution for the journal. Both radial and axial stresses were presented. As with the rear journal bearing,

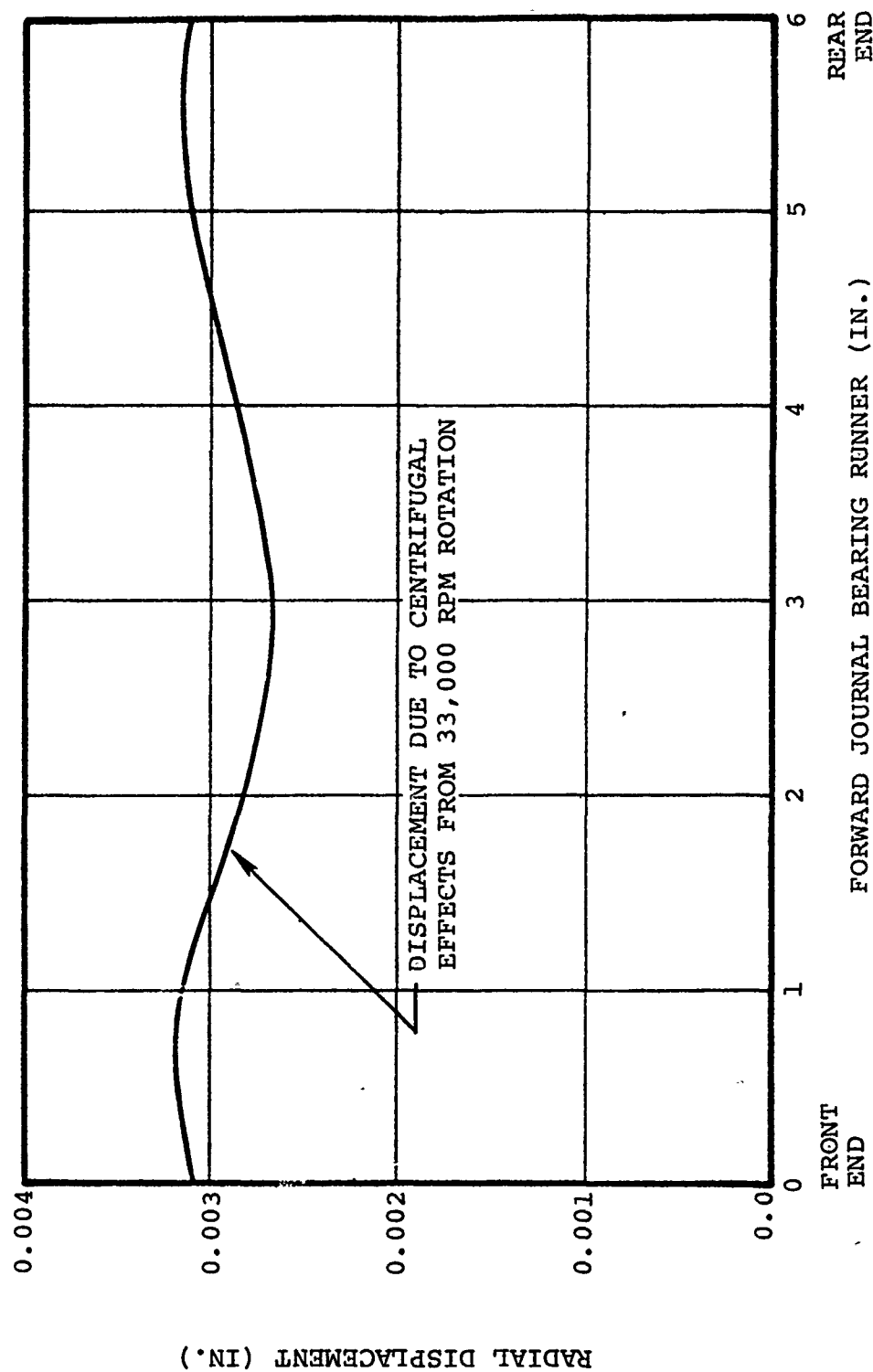
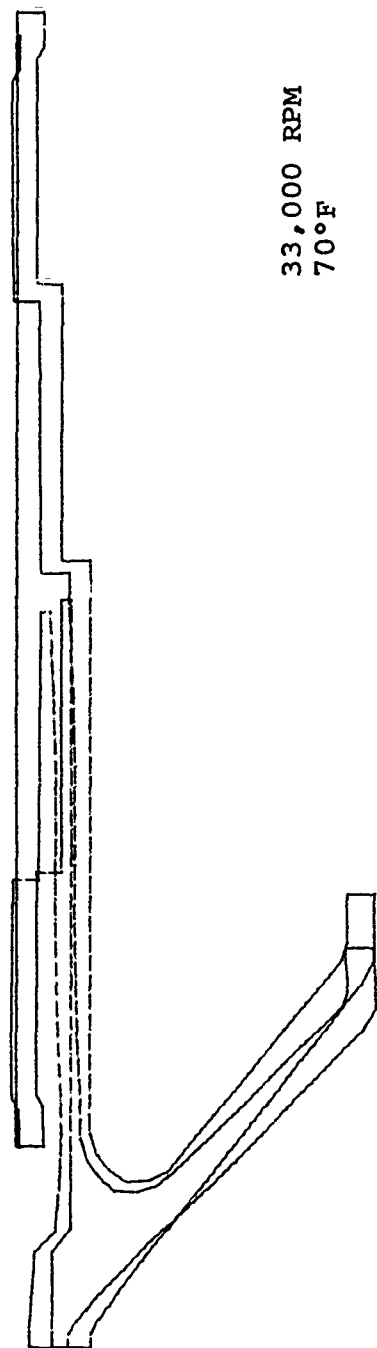
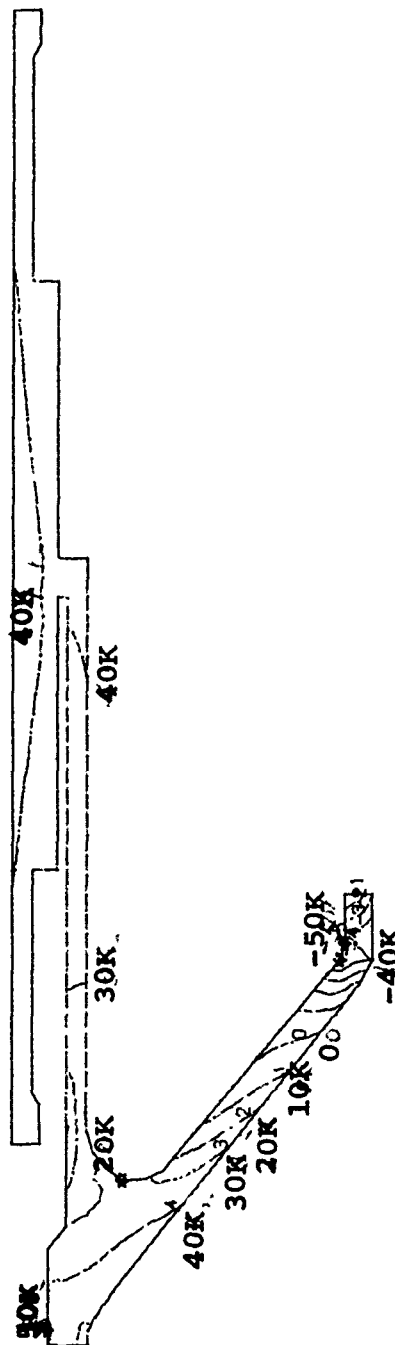


Figure 8. Radial Displacement of the Forward Bearing Journal



0.0050  
0.0050

# DISPLACEMENTS, MAGNIFIED



# TANGENTIAL STRESSES

Figure 9. Magnified Displacements and Tangential Stress Distribution for Front Bearing Journal at 33,000 RPM.

equivalent stresses closely follow tangential stresses. To accommodate potentially high temperature operation for this bearing, Inconel 718 was also chosen as the runner material. Stresses are low in relation to the strength of Inconel 718 and no problems with journal structural integrity are anticipated with this design.

### 3.1.7 Critical Speed Analysis

A rotor dynamics analysis was conducted for the foil bearing engine. The analysis was conducted using engine rotor properties listed in Table 5.

Critical speed characteristics of the engine are shown in Figure 10. In an effort to cover a wide range of foil bearing designs, critical speeds are shown as a function of spring rate. A large operating window between the rigid body criticals and the bending critical indicates the engine can be operated successfully regardless of the bearing spring rates. Results of bearing tests indicate journal bearing spring rates near 10,000 lb/in. Hence the first three critical speeds are anticipated to be at 4000, 8000, and 52,000 rpm respectively.

Figure 11 shows normal mode shapes of the first four critical speeds for journal bearing spring rates of 75,000 lb/in. Little difference in mode shapes are anticipated with spring rate reductions to 10,000 lb/in. The first two critical speeds are rigid body modes with little main rotor bending. The third plot shows tie-bolt excursion and slight bending of the main rotor. The major bending critical is the fourth plot which shows major main rotor bending but retains the high tie-bolt excursions. The tie-bolt excitation could be stopped with the addition of an extra tie-bolt bumper. However, the excitation occurs sufficiently beyond operating speeds that the design is considered safe.

TABLE 5

## TJE331-1029 ROTOR/BEARING CHARACTERISTICS

Rotor Material	Inconel 718
Rotor Weight	50.5 LB
Polar Moment of Inertia	0.776 IN.-LB-SEC <sup>2</sup>
Thrust Bearing Outer Diameter	6.15 IN.
Thrust Bearing Inner Diameter	3.50 IN.
Thrust Bearing Projected Area	20.09 IN. <sup>2</sup>
Journal Bearing Diameter	4.5 IN.
Journal Bearing Length	6.0 IN.
Journal Bearing Projected Area	27.0 IN. <sup>2</sup>
Journal Bearing Span	21.0 IN.

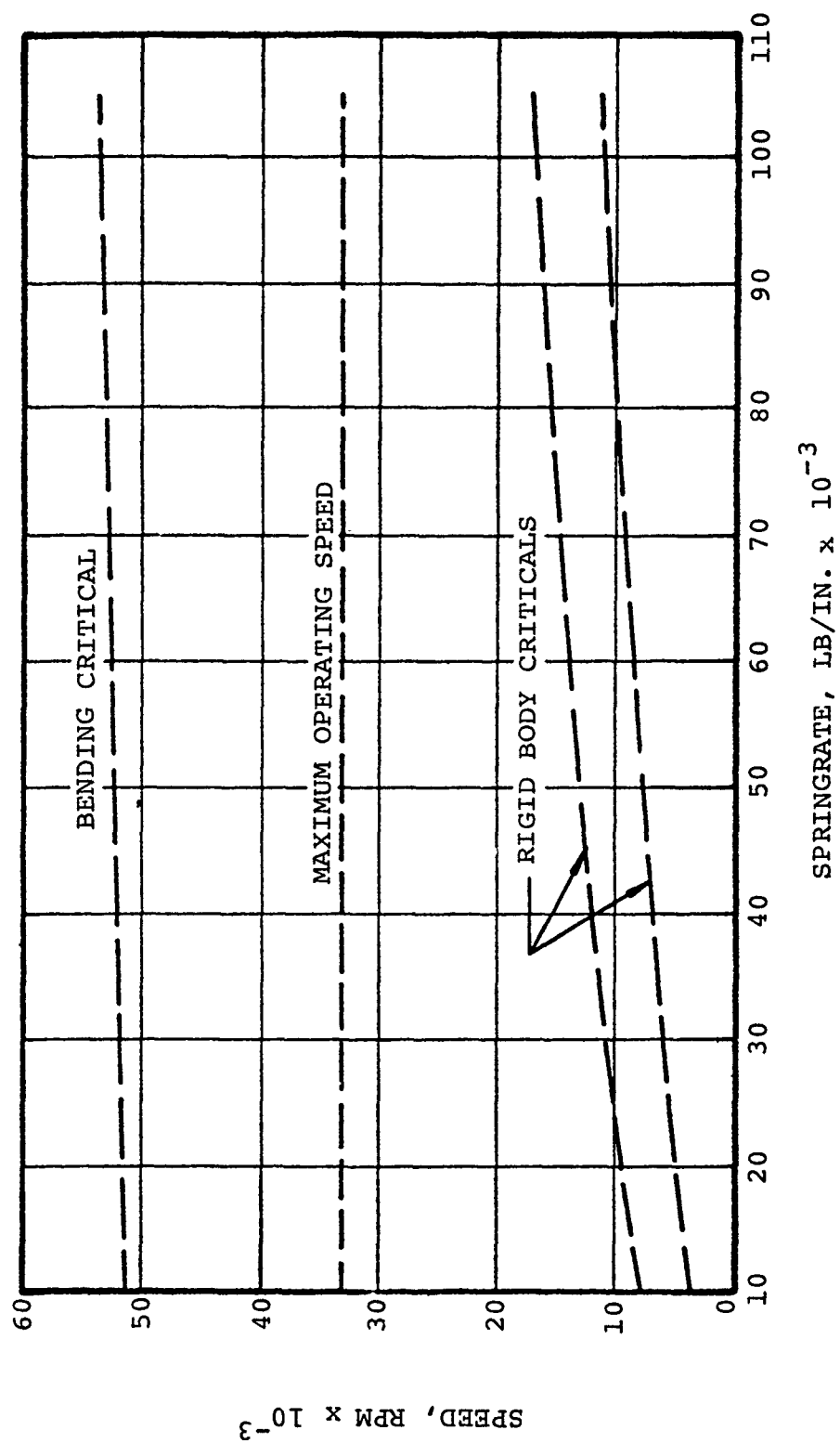


Figure 10. Critical Speed Versus Bearing Springrate for TJE331-1029



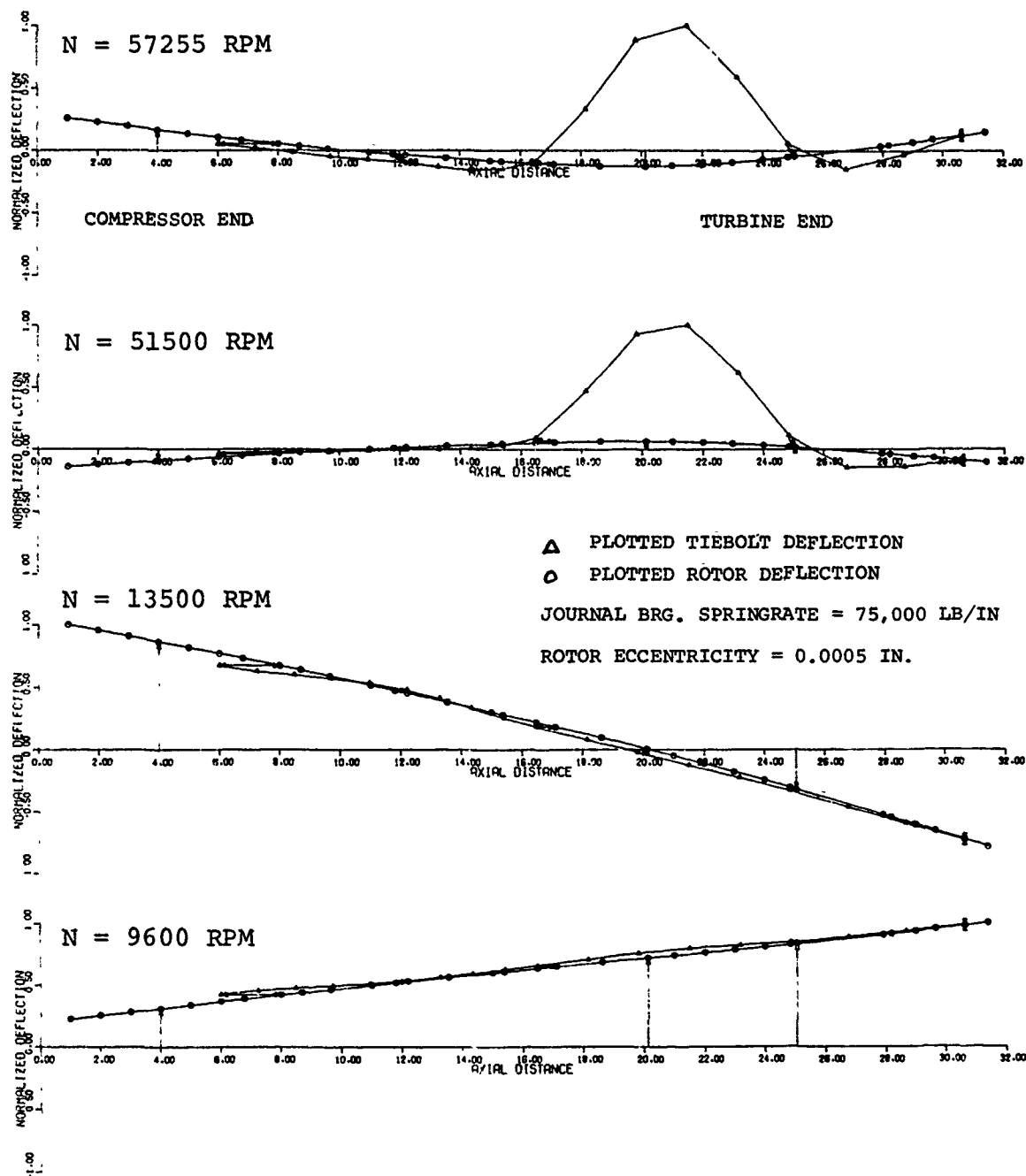


Figure 11. Mode Shapes of the First Four Criticals for the TJE331-1029 Foil Bearing Engine

### 3.1.8 Thermal Analysis

Bearing cooling is important in gas-lubricated foil bearings to keep the foil base metal and coating from exceeding its operating temperature limit because of self-generated heat (power loss). The cooling scheme utilized in this program passes compressor discharge air directly over the foils by imposing a pressure difference across the bearing. In general, cooling air flow is controlled by orifices and seals in the overall cooling circuit so that internal details of the bearing design are somewhat independent of cooling requirements.

Detailed heat transfer analysis was performed on both thrust and journal bearings. Steady-state temperature solutions are reported herein for the two bearings in baseline configurations. Analytical models of each bearing were constructed and solved using the general thermal analyzer code developed at AiResearch over the years. The code uses a finite difference model and a solution technique of relaxation over multiple iterations. It is capable of three-dimensional conduction, convection, and radiation as well as internal heat sources and cooling flow circuitry.

It was found early in the modeling of the bearings that the amount of thermal data (number of nodes) required for three-dimensional conduction in the foils made it difficult to accommodate bearing design changes. Therefore, auxiliary codes were written to generate thermal model input data automatically for the particular types of bearings involved. With these additional tools, it is relatively easy to specify various geometry, operating conditions, and material and fluid properties. Design changes are made by specifying recognizable geometric parameters such as foil thickness, number of foils, sway space, etc. instead of an entire system of conduction lengths and areas as used by the thermal analyzer code. Specific descriptions of the two foil bearing thermal models are given in Paragraphs 3.1.8.1 and 3.1.8.2.

The operating condition used as a reference point in the thermal analysis is "Hot day, Sea level, Mach 0.8". This is one of five engine operating conditions analyzed. Having defined the pressures and temperatures at points of communication with the interior (bearing cavities, rotor cavities, etc.), a complete flow circuit model of the internal flow system was set up. By a trial and error process, the internal flow system was designed so that the bearings are adequately pressurized on both inlet and discharge sides, while permitting adequate cooling flow to each, based on expected power loss and cooling effectiveness values. This process determined internal orifice sizes and seal locations. Since labyrinth seal clearances are never exactly known, results were obtained for both minimum and maximum expected running clearances. The results are tabulated in Table 2 for minimum seal clearances (0.0003 in. radial) and in Table 3 for maximum clearances (0.009 in. radial). A scheme for reducing rotor thrust was also worked into the design by pressurizing the cavity forward of the front journal bearing.

The final internal flow circuit is shown schematically in Figure 12. Compressor discharge air is supplied to all three bearings from a common collection point on the outer wall of the final diffuser. An external line carries air to the forward end of the front journal bearing via one of the bearing carrier struts. The aft end is pressurized by means of a 4-stage stepped labyrinth seal and a pressure controlling orifice which carries spent cooling air to the rotor interior. The forward end of the aft journal bearing is pressured as shown, with the aft end pressurized by the spent air passing through a labyrinth seal. In each case, the cooling flow is controlled by the sum of flow resistance of the bearing and the downstream orifice or seal. In the case of the thrust bearing, cooling air is metered at the inlet since internal flow resistance is negligible. The inlet is at the OD where metered air is impinged on the rim of the thrust runner, from where it flows inward behind the foil plates on both sides. Spent air is again metered through the curvic coupling V-seals

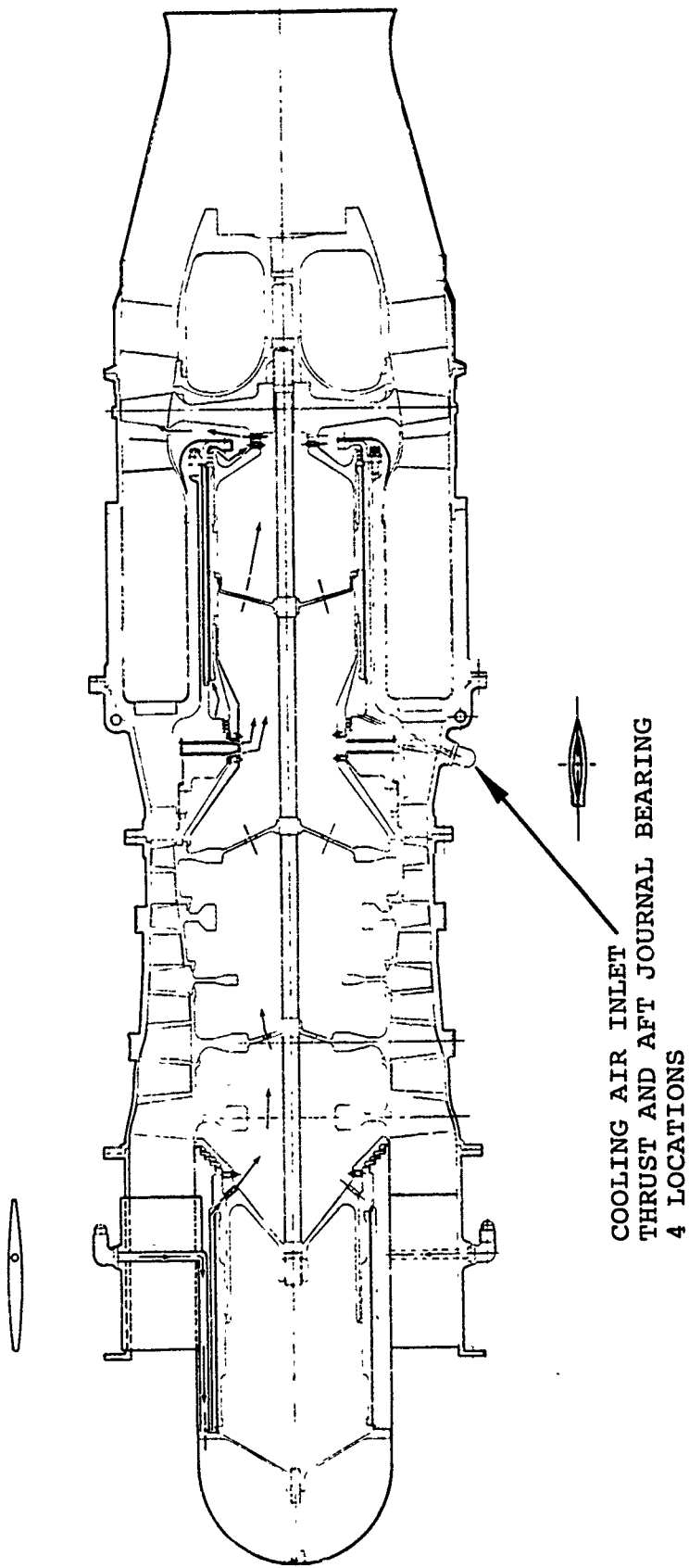


Figure 12. Internal Airflow Schematic.

since the thrust bearing pressure is established by communication with the static pressure upstream of the final diffuser. Spent air from all three bearings is ultimately discharged to the turbine rotor cavity from where it re-enters the main flow path upstream of the turbine rotor.

#### 3.1.8.1 Journal Bearing Temperatures

The generalized journal bearing thermal schematic is shown in Figure 13. It is applicable to any pinned-leaf type journal bearing. Labeled dimensions are those used as input data in the automatic thermal model generator. Each numbered thermal node shown in the schematic is the first of a series of five nodes distributed along the bearing length. Cooling flow passes through the bearing film and through the clearance space (between foils and housing) axially in the direction of increasing node numbers. Internal heat generation in the bearing film is distributed uniformly along the bearing length.

The bearing film is treated as isothermal at any axial station, which implies a concentric (unloaded) bearing, although the power loss (heat generation) representative of a loaded bearing may be input. As such, the computed temperature results may be considered to apply to the foils at 90 degree positions from the applied load. The highest foil temperatures occur on the loaded side of the bearing because of increased frictional heating and reduced flow area there. However, this analytical model has not been extended to the point of predicting eccentricity effects. Foil-to-foil temperature variations are believed to be minor because the computed peak foil temperatures reported herein are not much higher than the journal surface temperature, and the latter is obviously symmetrical due to high speed rotation.

Foil temperature results are presented in Figure 14 for operating conditions applicable to the baseline configuration, turbine-end journal bearing. These conditions correspond to hot day, sea



# BEARING COOLING ANALYSIS NOTES

1. BASELINE CONFIGURATION, CONCENTRIC
2. ADIABATIC BEARING (ISOLATED FROM ENVIRONMENT)
3. POWER LOSS = 1500 WATTS
4. INLET AIR = 564°F, 83 PSIA
5. EXIT AIR = 666°F, 56.5 PSIA
6. AIR FLOW RATE = .0536 LBM/SEC
7. SPEED = 33,198 RPM
8. FOIL CONTACT RESISTANCE = .0005 - .003  
HR FT<sup>2</sup> °F/BTU
9. MINIMUM FILM THICKNESS = 0.001 IN.

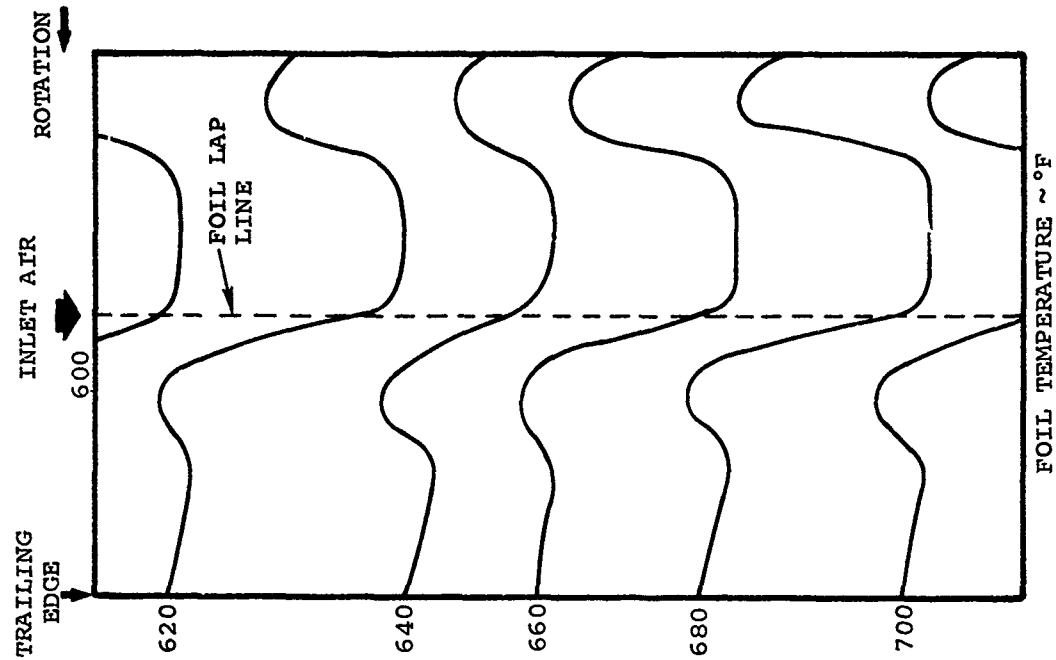


Figure 14. Sample Results of Thermal Analysis on Turbine-End Journal Bearing.

level, Mach 0.8 and a downstream labyrinth seal running clearance of 0.008 inch. A power loss of 1500 watts, as predicted analytically, was used. Assumed airflow, speed, foil contact resistance and minimum film thickness are also listed on Figure 14. In addition to the reference point, a parametric study was made to determine the effects of altitude, downstream pressure, power loss, and sway space.

Figure 15 shows the effect of pressure ratio across the bearing on the cooling airflow function (based on exit conditions) at three different altitude conditions. Seal clearances required to achieve a given pressure ratio are shown by dashed lines. The flow function for the 50,000 feet condition was found to be relatively low because of low flow Reynolds numbers and high friction factors.

Figure 16 shows the effect of pressure ratio across the bearing (and therefore cooling flow rate) on maximum foil temperatures (hot spot) and on maximum temperature differences within a foil. In this figure, the power loss was held constant at 1500 watts for sea level and 25,000 feet conditions and at 1000 watts for the 50,000 feet condition. This clearly indicates a need for more cooling airflow at high altitudes, which, if provided by increasing the flow area will result in unrequired cooling flow at the lower altitudes. To prevent the resulting loss in engine performance a barometric valve can be employed to correct the cooling air flow to the bearings.

Power loss effects on foil temperatures are shown in Figure 17. The downstream seal clearance was held constant at 0.008 inch (radial), so the bearing pressure ratio and cooling airflow can be obtained from Figure 15.

Finally, the effect of increasing the bearing sway space is shown in Figure 18. This is the only deviation from the baseline



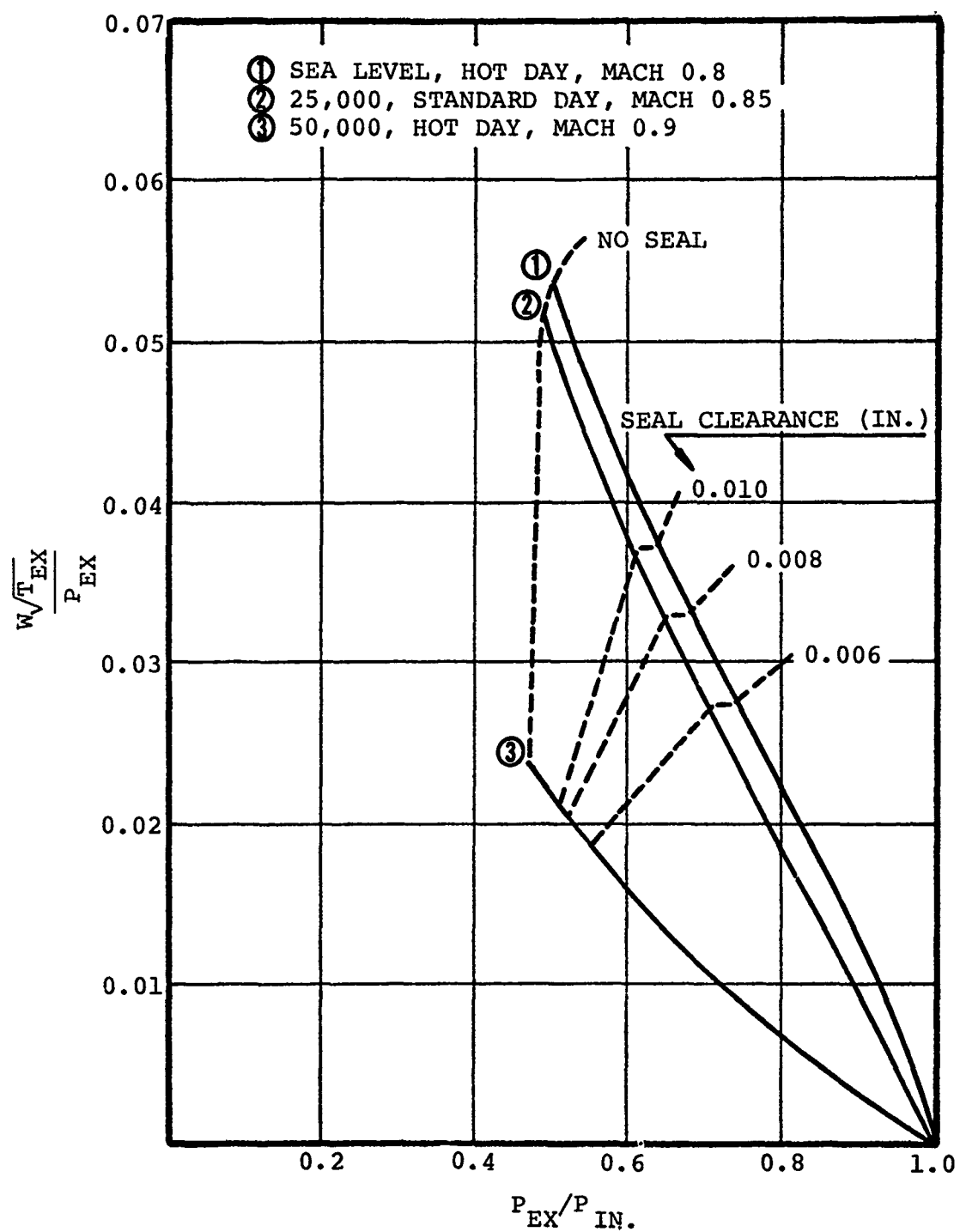


Figure 15. Baseline Journal Bearing Configuration Cooling Flow Characteristics.

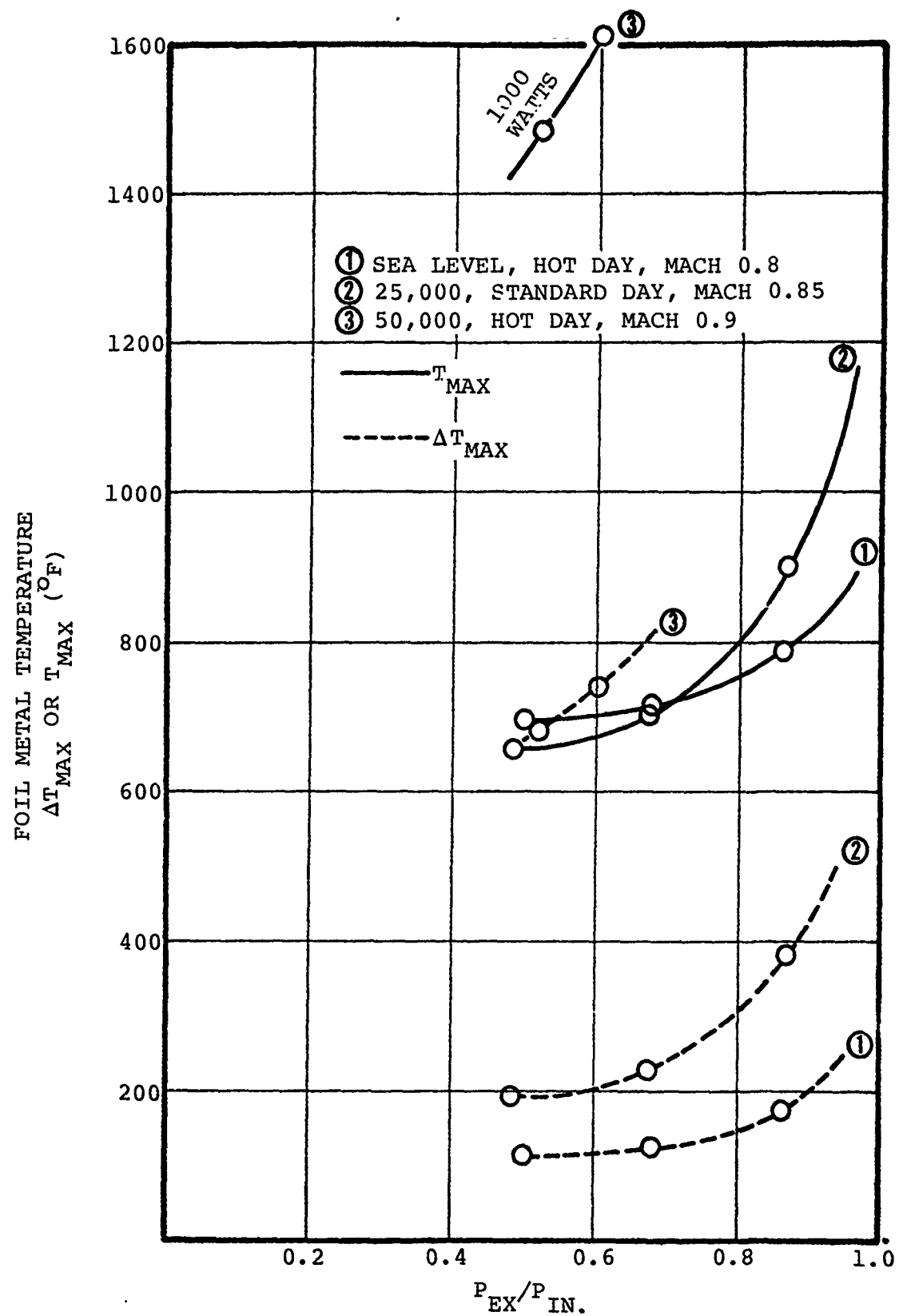


Figure 16. Baseline Journal Bearing Thermal Analysis.  
 Power Loss = 1500 Watts

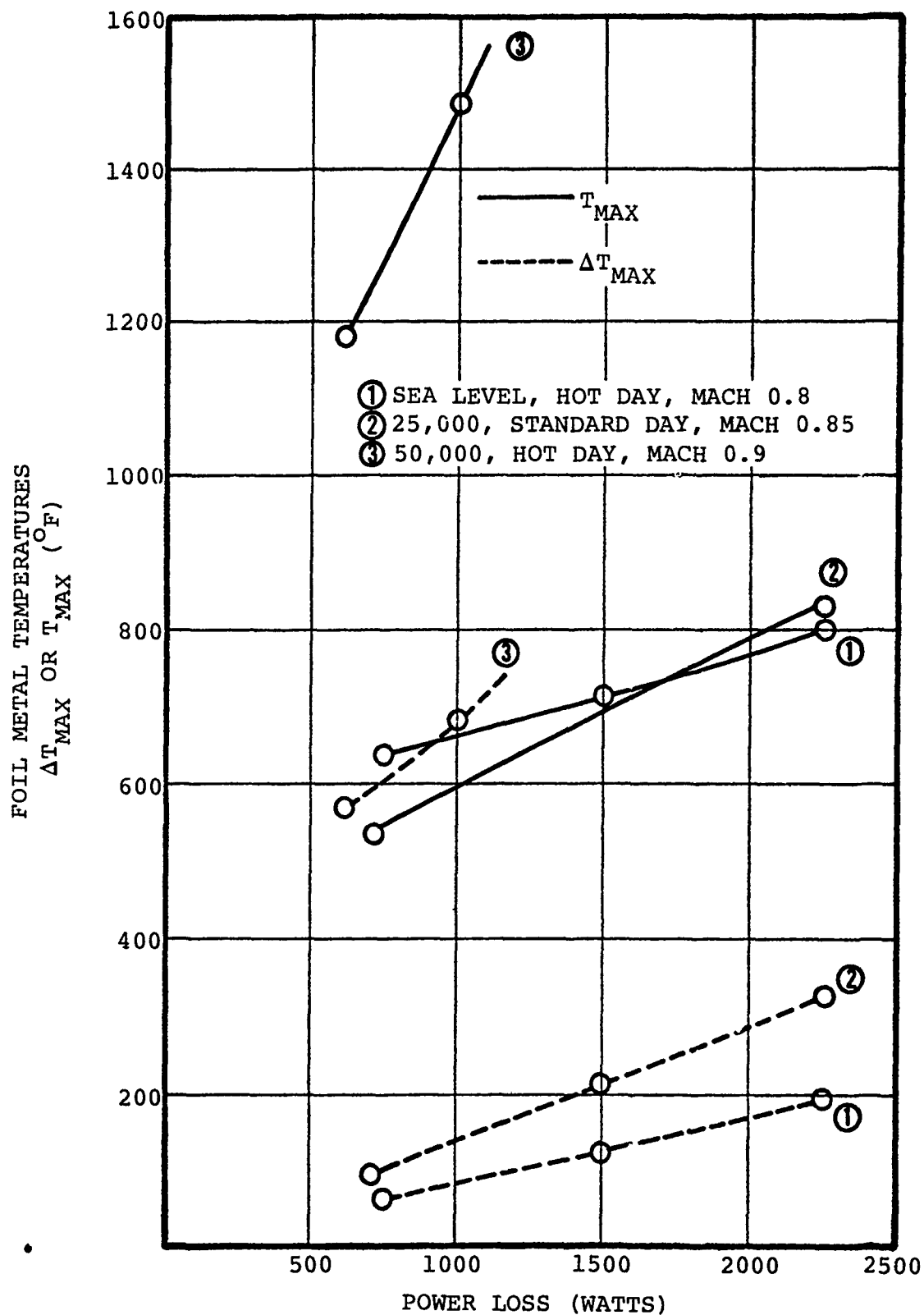


Figure 17. Baseline Journal Bearing Thermal Analysis.  
Seal Clearance = 0.008 Inch

FOIL METAL TEMPERATURE  
 $\Delta T_{MAX}$  OR  $T_{MAX}$  ( $^{\circ}F$ )

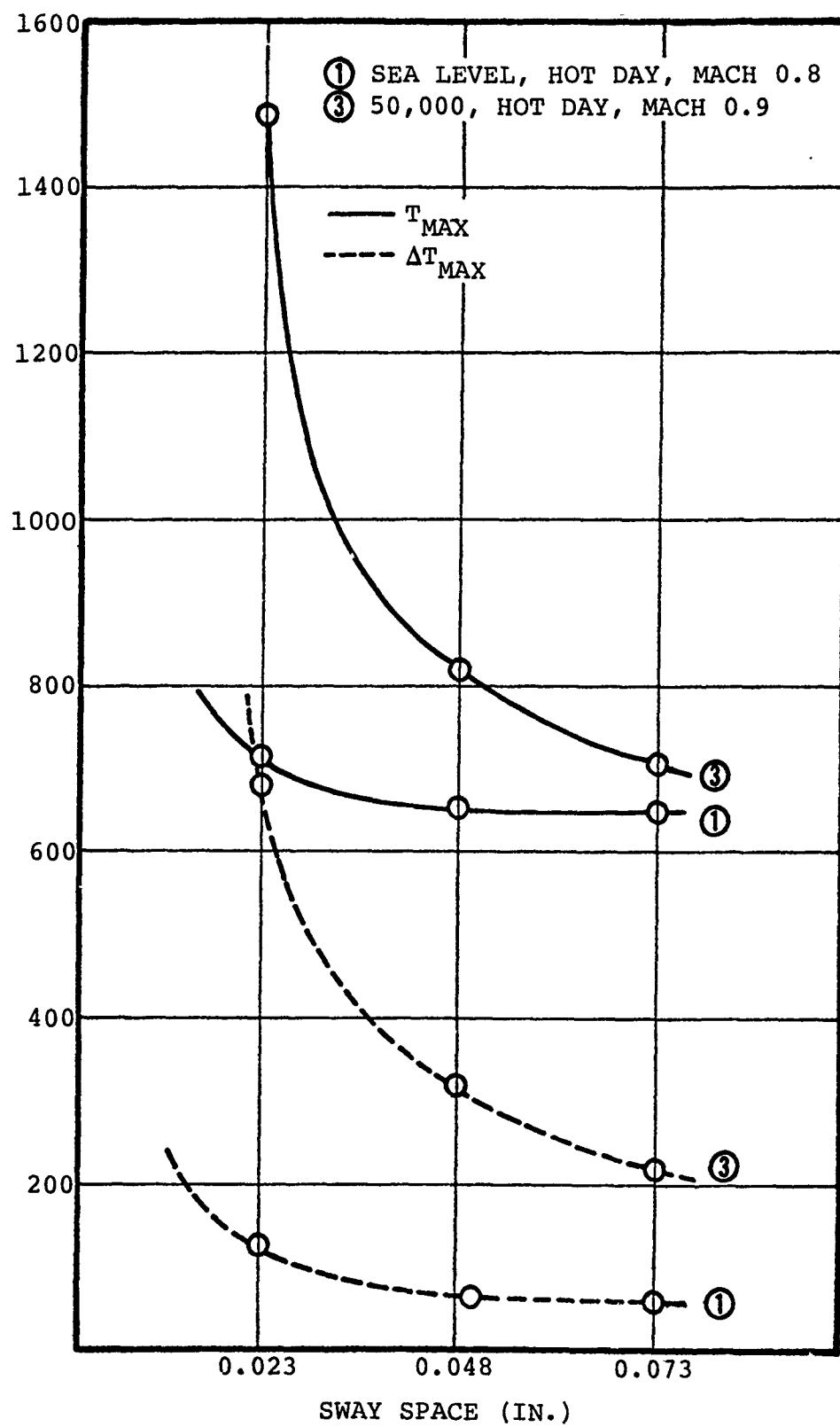


Figure 18. Effect of Bearing Sway Space.

configuration and the results are rather dramatic at the high altitude condition. Here, the seal clearance is held constant at 0.008 inch and the power loss is 1500 watts at sea level and 1000 watts at 50,000 feet.

The purpose in reporting these results is only to show trends for use in seeking a satisfactory cooling scheme. They do not represent a final cooled bearing design. Indications are that increasing bearing sway space area in a manner that does not affect bearing performance, such as bearing carrier grooving, is a possible approach to a satisfactory cooling system design without increasing the bearing cooling flow rate.

#### 3.1.8.2 Thrust Bearing Temperatures

The generalized thrust bearing thermal schematic is shown in Figures 19 and 20. Figure 19 is an overall meridional view including thrust runner and housing and Figure 20 is an axial view of one of the foil sectors on the loaded side. The modeling concept is similar to the journal bearing modeling discussed above, while the configuration and the cooling scheme differ.

The cooling scheme employed in the thrust bearing baseline configuration consists of cooling air jets impinging on the thrust runner rim, followed by radially inward flow behind the thrust plates on both sides. The jets are introduced at an angle in the rotation direction to depress the inlet total temperature relative to the thrust runner. A sketch of this concept is shown in Figure 21.

A steady-state temperature solution was obtained for the thrust bearing operating under hot day, sea level, Mach 0.8 conditions. Results are shown in Figures 22 and 23 as isothermal diagrams (the notes on Figure 22 are applicable to each figure). Figure 22 represents one of 13 identical sectors, looking at a thrust pad where peak temperatures occur. Figure 23 shows the axisymmetrical temperatures in the overall bearing.

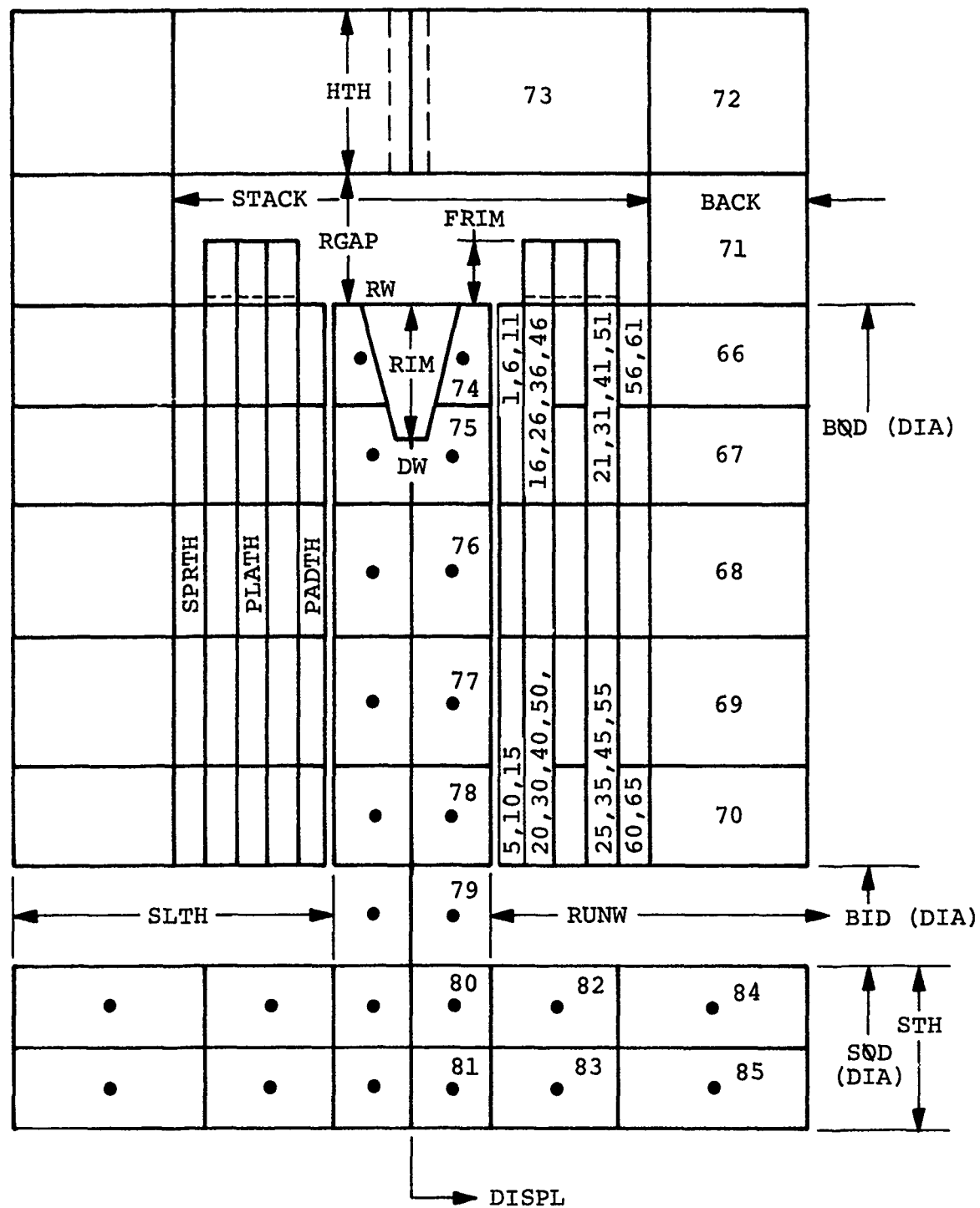


Figure 19. Thermal Model Schematic Foil Bearing  
Type: Cantilevered-Leaf Thrust

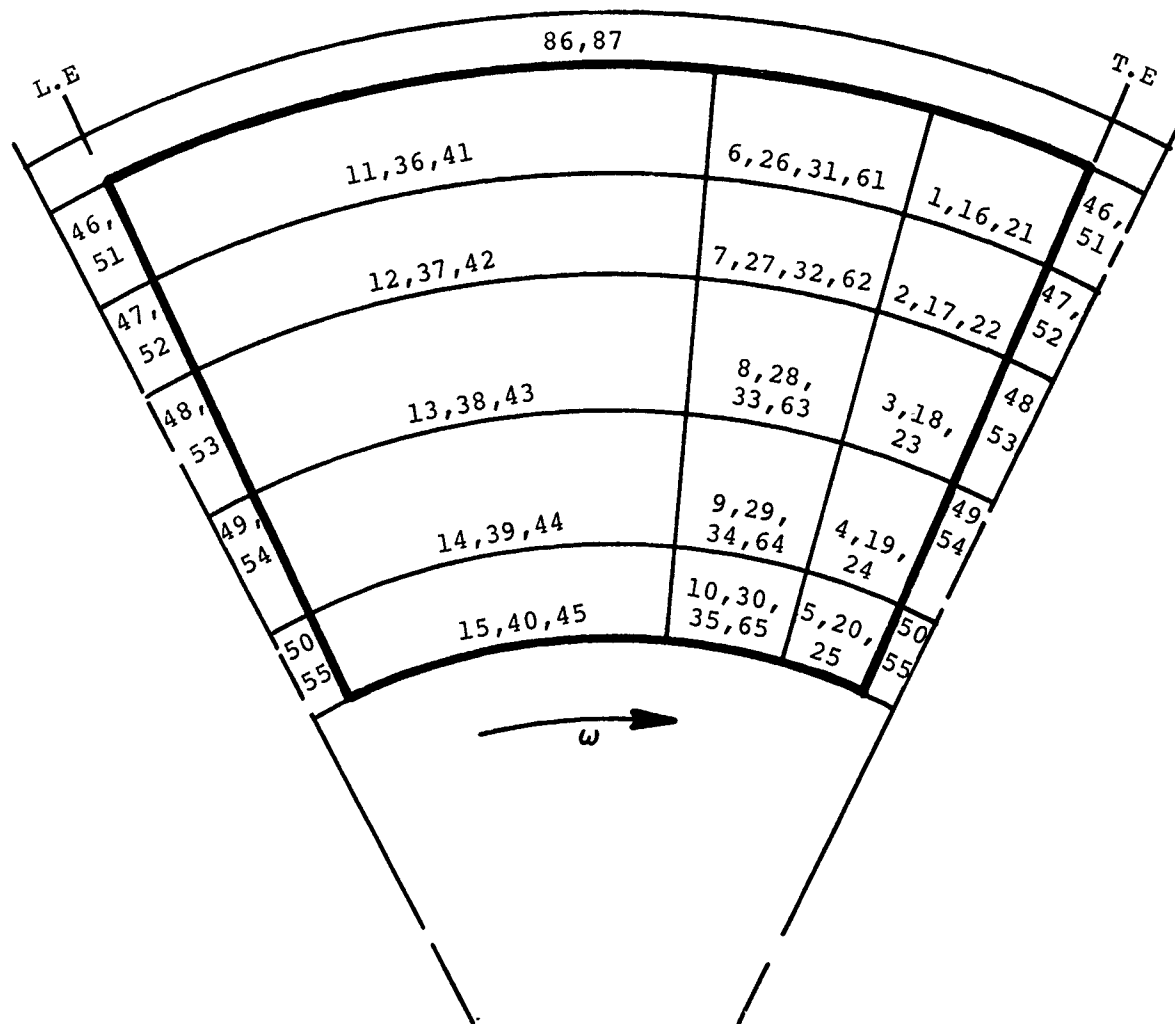


Figure 20. Thermal Model Thrust Foils Schematic.

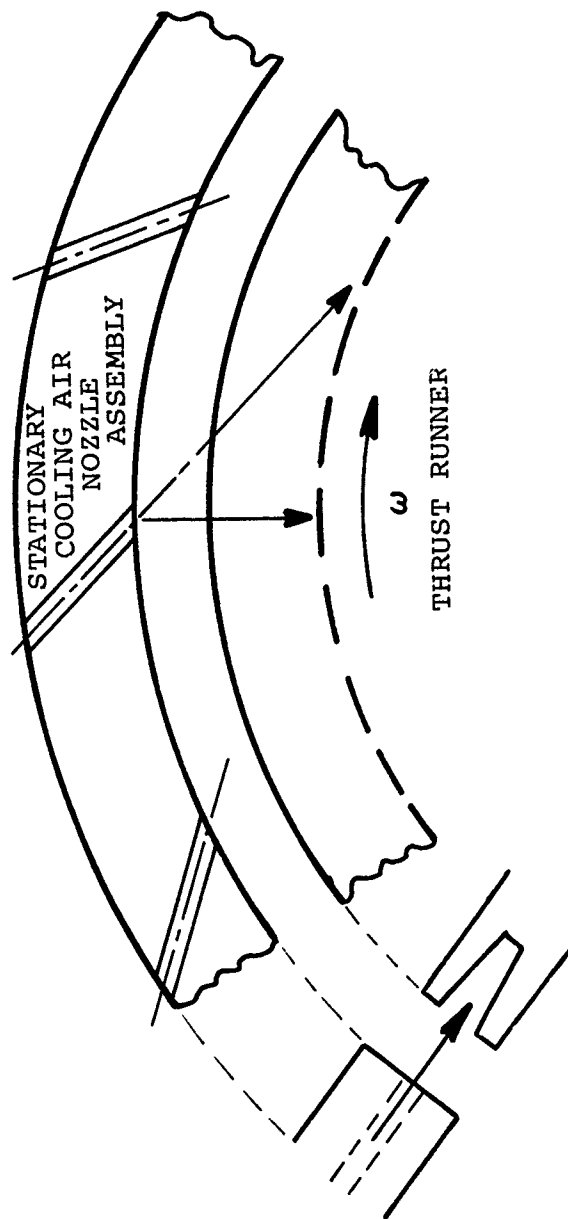
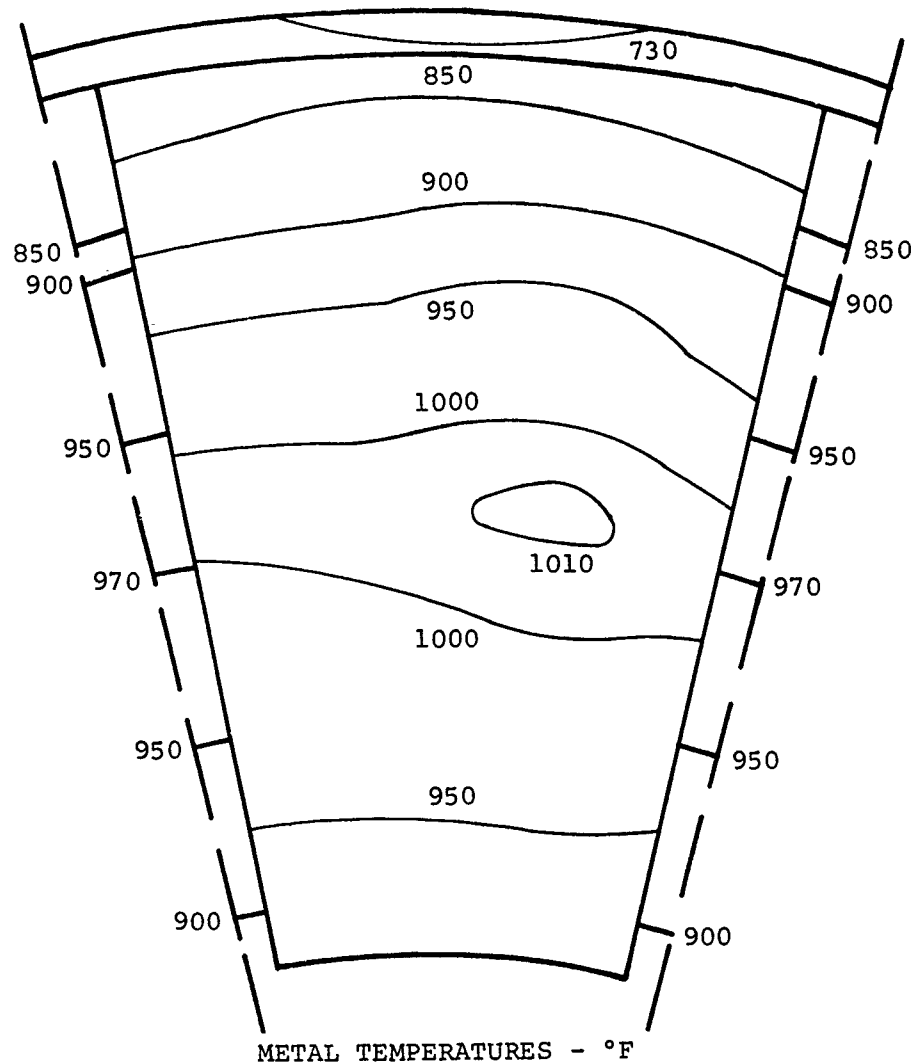


Figure 21. Rim Impingement, Thrust Runner Cooling.





METAL TEMPERATURES - °F

NOTES:

- |                                 |  |
|---------------------------------|--|
| 1. 6.15 OD, 3.52 ID             | 6. INLET AIR = 564°F, 83.5 PSIA        |
| 2. 33,198 RPM                   | 7. EXIT AIR = 653°F, 78.3 PSIA         |
| 3. NET THRUST = 370 LB          | 8. FLOW RATE = 0.1365 LB/SEC           |
| 4. FRICTIONAL LOSS = 2870 WATTS | (0.96 PERCENT)                         |
| 5. WINDAGE LOSS = 410 WATTS     | 9. FOIL CONTACT RESISTANCE =           |
|                                 | 0.0005-0.002 HR-FT <sup>2</sup> °F/BTU |

Figure 22. Sample Results of Thermal Analysis Thrust Bearing - Foil Sector View

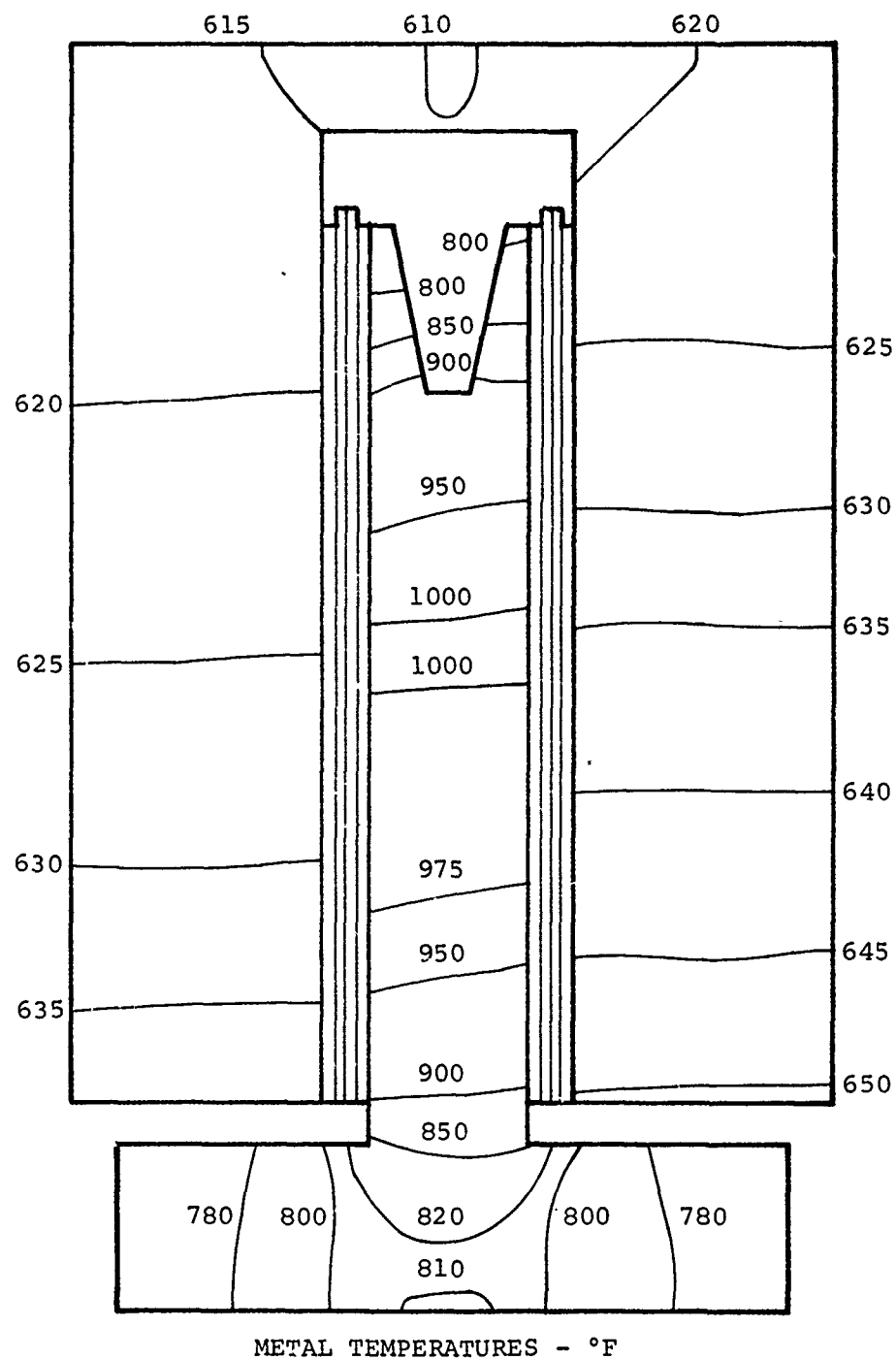


Figure 23. Sample Results of Thermal Analysis Thrust Bearing - Meridional View

After examining model data and resulting metal temperatures, and checking the energy balance, it was concluded that these results are valid, and therefore represent the best effort at predicting operating temperatures. Temperatures may be affected by: (1) heat rejection to the bearing surroundings, (2) net thrust load lower than 370 pounds, and (3) lower power loss characteristic due to a slight reduction in bearing size, such that the present results are on the high side. The effects of (2) and (3) could be quite significant and should be examined further as a next step. However, these effects would not change bearing cooling effectiveness, which, for this case is:

$$\epsilon_c = \frac{t_{ex} - t_{in}}{t_{hot} - t_{in}} = \frac{653 - 564}{1015 - 564} = 0.20$$

This value, depicting performance of the cooling scheme employed (rim impingement), is very low compared to that predicted for journal bearings. The problem is related to low air pressure drop across the bearing used in this case, resulting in low jet velocities for rim impingement. However, it is possible that the cooling scheme is simply inadequate for a bearing of this size and power loss density. In view of the parametric study on the turbine-end journal bearing, which shows the 50,000 foot condition to be most severe for cooling, it is expected that internal cooling passages in rotating parts of all bearings will be required to achieve high altitude operation capability.

### 3.2 Design

#### 3.2.1 Baseline Bearing Design

The TJE331-1029 engine configuration limited the thrust and journal bearing size. Since MIL-E-5007 maneuvers impose high loads on foil bearings (Figure 4) the foil bearings were designed

with as large a projected area as possible. This resulted in 27 square inches of projected journal bearing area and 20.09 square inches of projected thrust bearing area.

The baseline (initial) bearings designed, fabricated and tested in this program were based on the successful DC-10 configuration.

#### 3.2.1.1 Journal Bearing Baseline Design

The first configuration of journal bearings were made by scaling the well-proved DC-10 cooling turbine journal bearings. Modifications were made where experience indicated they would be beneficial.

DC-10 bearing has the following configuration:

Diameter	2.0 inch
Length	2.0 inch
Number of foils	8
Foil thickness (uncoated)	0.006 inch
Preformed radius	1.5 inch
Overlap	47 percent
Calculated diametrical sway	10.5 mils

The maximum diameter of the TJE331-1029 journal bearings is 4.5 inches. Hence, all linear dimensions (except length) are scaled by:

$$\frac{4.5}{2.0} = 2.25$$

The length was fixed by load capacity considerations. Calculated dimensions for the bearings were as follows:

Diameter	4.5 inch
Length	6.0 inch

Number of foils	8
Foil thickness (uncoated)	13.5 mils
Preformed radius	3.37 inch
Overlap	47 percent
Calculated diametrical sway	23.6 mils

During the DC-10 cooling turbine development program, several preformed radius bearings were tested in the laboratory. Tests showed that a 1.2 inch preformed radius showed somewhat better performance than 1.5 inch. However, the 1.5 inch preformed radius bearing had the successful service record. So an average value of 1.35 inch was selected as the baseline preformed radius for the large bearings. Hence,

$$\begin{aligned} \text{Preformed radius of the TJE331 bearings} &= 1.35 \times 2.25 = \\ 3.03 &\approx 3.00 \text{ inch} \end{aligned}$$

It was felt that 13.5 mil foil thickness was too stiff to maintain the compliancy for six inch long bearings. Hence, the thickness was reduced to 10 mils. However, to maintain the same radial stiffness, necessary reduction in the sway space was made.

On the basis of test data collected up to that time, it was felt that stiffness varied directly with the foil thickness ratio to the power 1.3. Hence, by using 10 mil foils instead of 13.5, the stiffness reduces approximately by:

$$\left( \frac{10}{13.5} \right)^{1.3} = 0.68$$

This was compensated by reducing the sway space. It was observed that the stiffness varied inversely with the sway space. Hence, new sway space was calculated as:

$$\frac{S}{23.6} = 0.68$$

$$S = (23.6) (0.68) = 16 \text{ mils}$$

Based on these calculations, dimensions of the first cut journal bearings were as follows:

Diameter	4.5 inch
Length	6.0 inch
Number of foils	8
Foil Thickness (uncoated)	10 mils
Preformed radius	3.0 inch
Overlap	47 percent
Calculated sway	16 mils

### 3.2.1.2 Thrust Bearing Baseline Design

Similar to journal bearings, the thrust bearings were also designed by scaling the well-proven DC-10 cooling turbine thrust bearings. The DC-10 thrust bearing configuration is as follows:

Outside diameter	4.23 inches
Inside diameter	2.34 inches
Number of pads	12
Pad thickness (uncoated)	6 mils
Pad plate thickness	7 mils
Stiffener thickness	8-1/2 mils
Spring plate thickness	7 mils
Thickness of spring stock	10 mils

From other considerations, the TJE331-1029 thrust bearing outside and inside diameters were established at 6.15 and 3.50 inches, respectively.

$$\text{Area of DC-10 thrust bearings} = \frac{\pi}{4} (4.23^2 - 2.34^2) = 9.77 \text{ sq in.}$$

$$\text{Area of TJE331 thrust bearings} = \frac{\pi}{4} (6.15^2 - 3.50^2) = 20.08 \text{ sq in.}$$

$$\text{Scale factor} = \sqrt{\frac{20.08}{9.77}} = 1.43$$

Hence, TJE331 thrust bearings calculated dimensions are:

Number of pads	12
Pad thickness	8.56 mils
Pad plate thickness	10.0 mils
Stiffener thickness	12.1 mils
Spring plate	10.0 mils
Thickness of spring stock	14.3 mils

The number of thrust bearing pads was increased from 12 to 13 for the purpose of having a prime number of pads. From several tests of DC-10 size, it was concluded that pad thickness was not a crucial factor in bearing performance on the rig. However, from the compliance point of view, it was decided to keep the pad thickness 6 mils instead of 8.5 mils as calculated. From a manufacturing point of view, to maintain flatness when the pads are welded, it is better to keep the pad plate slightly thicker. Hence, the pad plate thickness was established at 12 mils; and to maintain the same total stiffness, the middle stiffener thickness was established at 10 mils. From further DC-10 thrust bearings rig tests, it was determined that it would be better to make the spring plate slightly heavier. Hence, a 12-mil spring plate was chosen. The final dimensions as selected were as follows:

Outside diameter	6.15 inches
Inside diameter	3.50 inches
Number of pads	13
Pad thickness	6 mils
Pad plate thickness	12 mils
Stiffener stickness	10 mils
Spring plate thickness	12 mils
Spring stock	14 mils

### 3.2.2 Thrust Bearing Test Rig Design

A test rig was designed and fabricated for full scale thrust bearing testing and development. This required the rig to be capable of testing a 6.15-inch diameter bearing with the bearing runner spinning at 33,000 rpm (plus overspeed capability) while being subjected to an axial thrust load of 780 pounds. The design resulting from these requirements is shown in Drawing 3605849.

The thrust bearing test rig shaft assembly consists of four major elements, the drive turbine, supporting journal bearings, the hydrostatic thrust runner, and the test bearing thrust runner. The drive turbine and drive turbine nozzle assembly and inlet scroll are production components of the air cycle turbine used in the DC-10 Aircraft ECS. The tandem journal bearings are two-inch diameter, eight-segment foil bearings from the same system. The hydrostatic thrust runner, which is merely a rotating disk, opposes the thrust that the rotating assembly applies to the test bearing. The air supply, with its distribution hole pattern, is within the adjacent stationary disk. The test bearing thrust runner is at the end of the rotating group. The test rig operates with a vertical centerline and is shown schematically in Figure 24.

The test bearing and thrust runner are housed in a chamber so the air supplied to the bearing can be pressure- and temperature-controlled. The load is applied to the test thrust bearing by a pneumatic piston that is floating hydrostatically. The approach permits the bearing drag torque to be measured by a strain-gaged lever that resists rotation of the torque table on which the foil thrust bearing assembly is mounted.

The initial test rig design included a flywheel to simulate engine rotational energy. Although the critical speed analysis



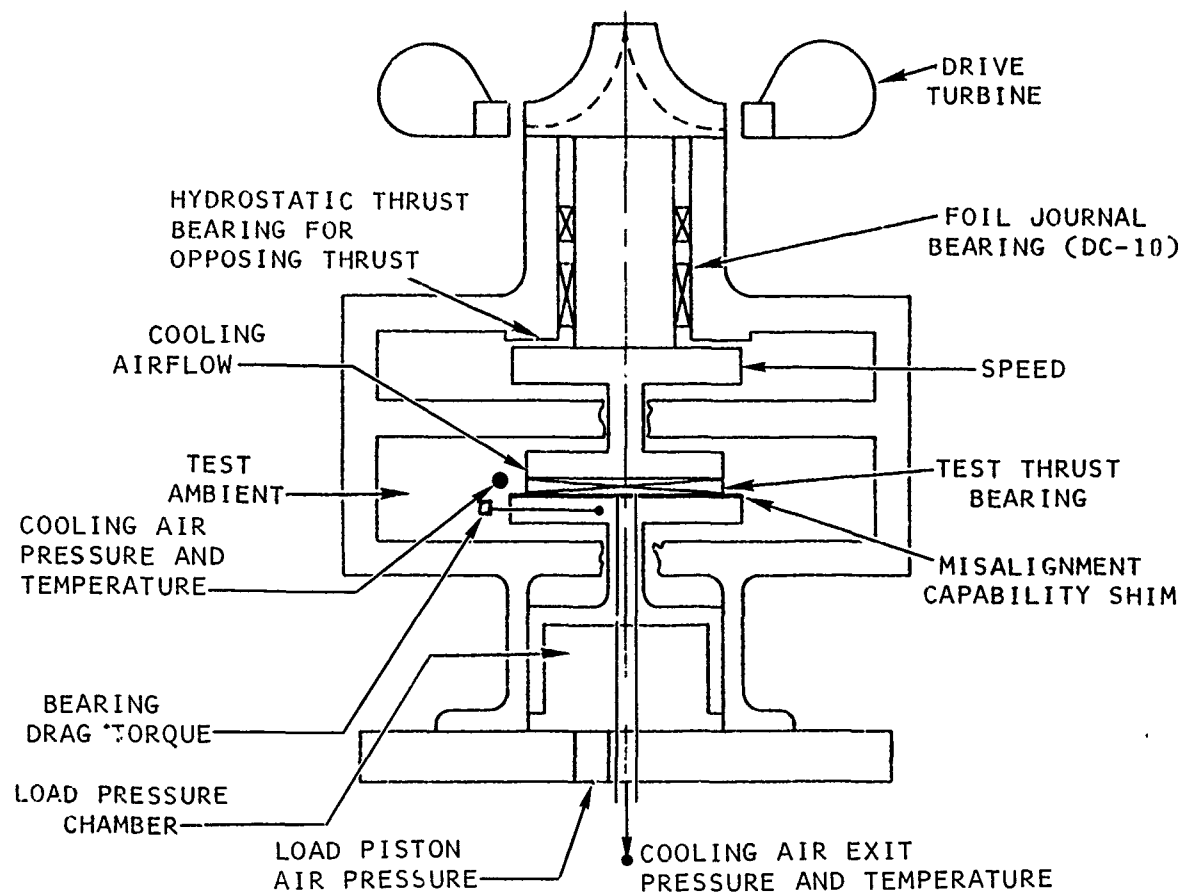


Figure 24. Thrust Bearing Test Rig.

(Figures 25, 26, and 27) indicated no significant difference with or without the flywheel, the severity of the first critical required removal of the flywheel with the resulting 2.2 inches shorter shaft system. Figure 28 illustrates the rig as set up for initial checkout runs.

Test rig instrumentation included: rotation speed, cooling air flow to the test bearing ambient compartment, test bearing cavity ambient pressure and temperature, test bearing cooling air exit temperature and pressure, test bearing drag torque, test bearing load chamber air pressure, and orthogonal shaft motion probes.

The resulting thrust bearing test rig proved to be a very versatile tool for bearing development and presented no problem once the critical speed condition was changed. The test bearing thrust runner was easily changed in the event of a failure.

### 3.2.3 Journal Bearing Test Rig Design

A test rig was designed and built for full scale journal bearing testing and development. This required that the test rig be capable of testing a journal bearing 4.5 inches in diameter and 6 inches long (L/D 1.33). The journal (shaft) is required to spin at 33,000 rpm (plus overspeed capability) and subject the bearing to a radial load of 442 pounds. The test rig also was designed to subject the bearing to altitude simulation, operating temperatures to engine conditions, and misalignment. A schematic of the resulting test rig design is shown in Figure 29. The design layout is shown in Drawing 3605850.

The test rig rotating assembly is supported by two foil journal bearings. A parachute loader located between the journal bearings is used to apply radial loads to the shaft. A thrust bearing located outboard of one journal bearing axially positions the shaft, which is driven by an air turbine outboard of the thrust bearing.



AIRESEARCH MANUFACTURING COMPANY OF ARIZONA  
A DIVISION OF THE GARRETT CORPORATION  
PHOENIX, ARIZONA

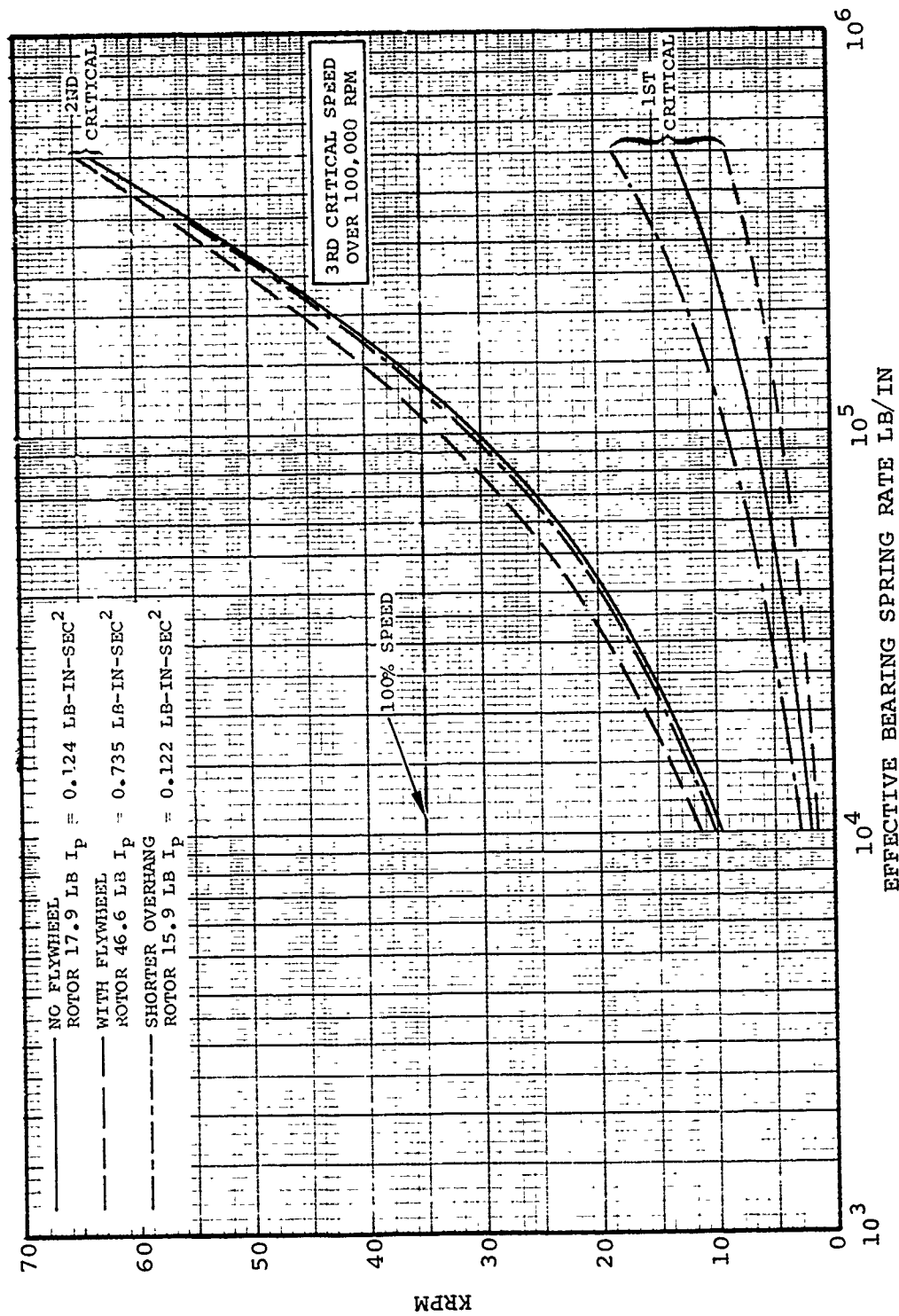


Figure 25. Foil Thrust Bearing Rig Critical Speeds.

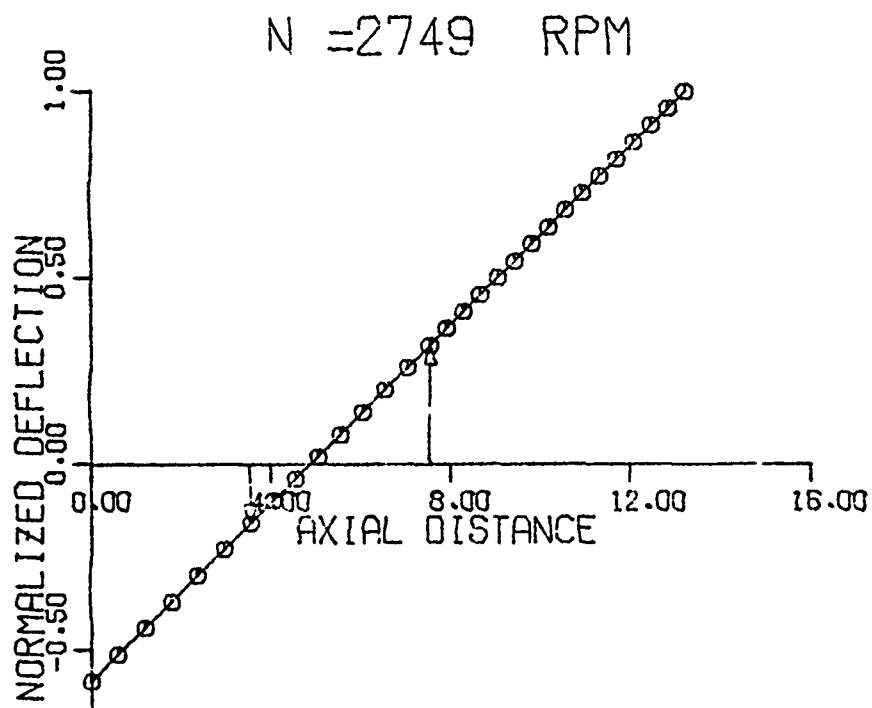
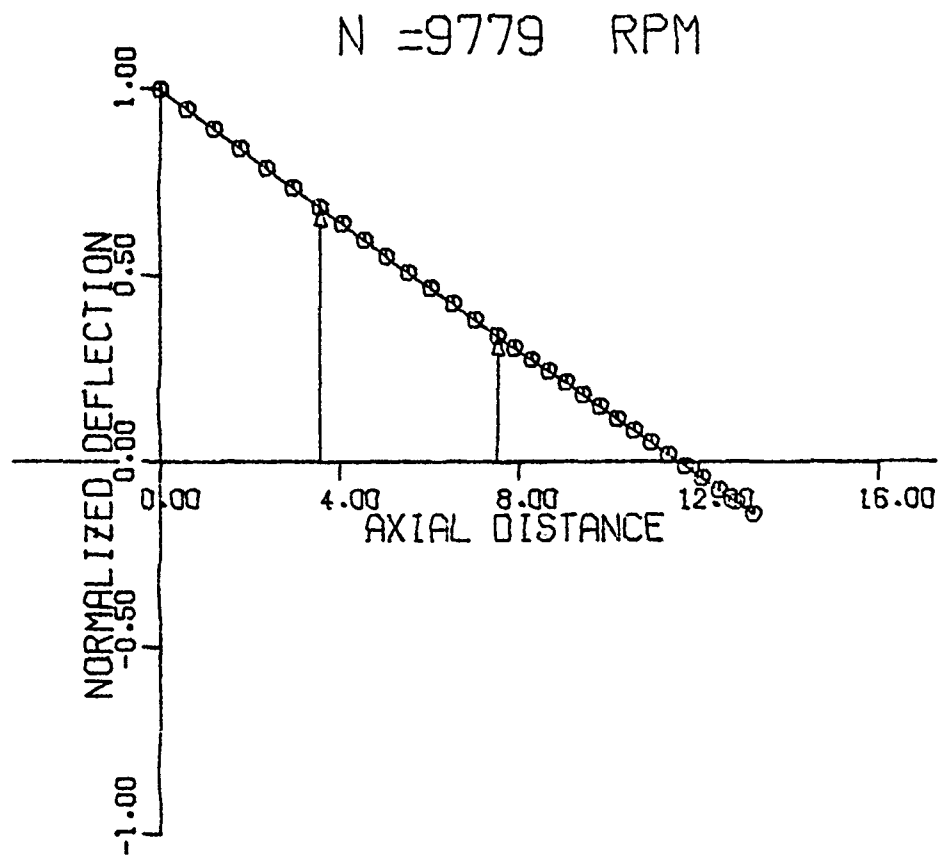


Figure 26. Normalized Mode Shapes. Thrust Bearing Rig no Flywheel and Shortened Overhang Bearing Spring Rate = 10,000 lb/in.

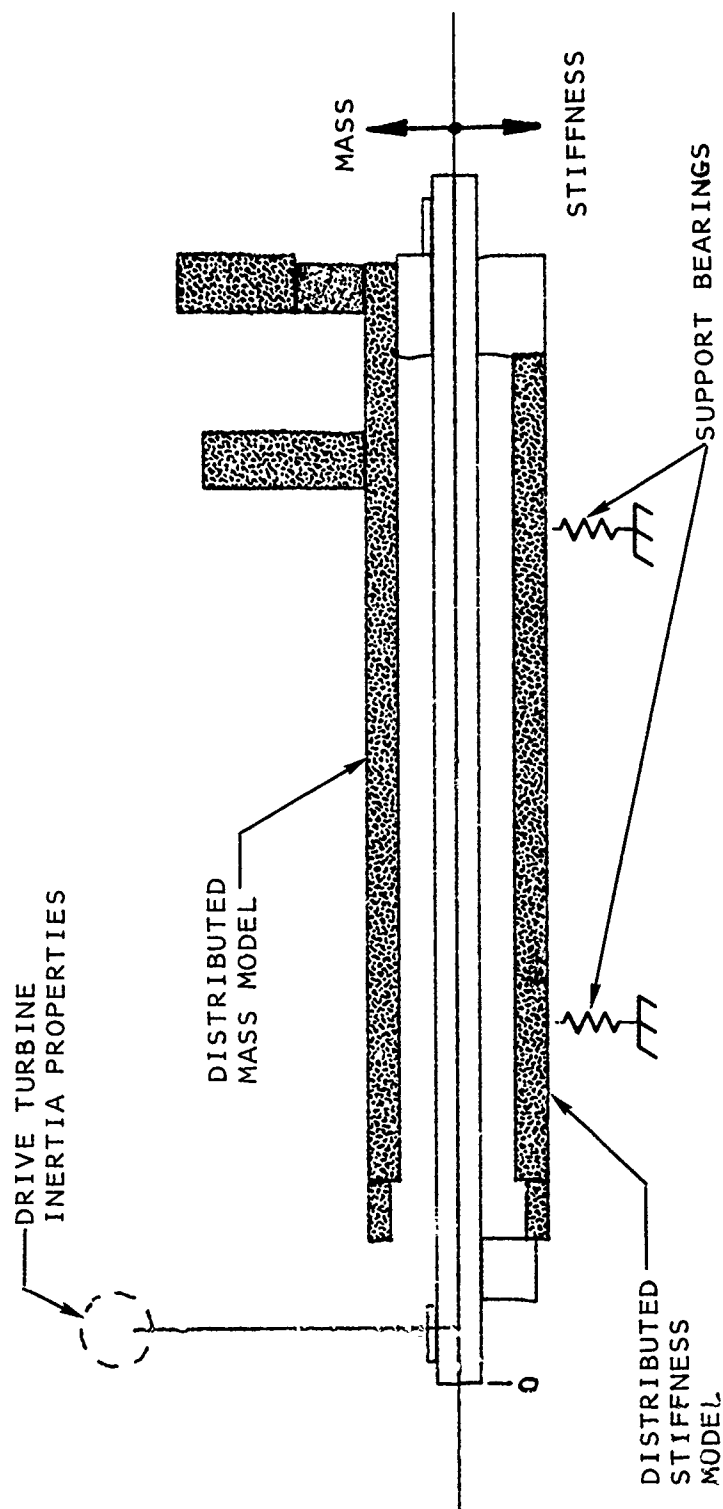


Figure 27. Mass and Stiffness Model, Thrust Bearing Rig No Flywheel and Short Overhang.

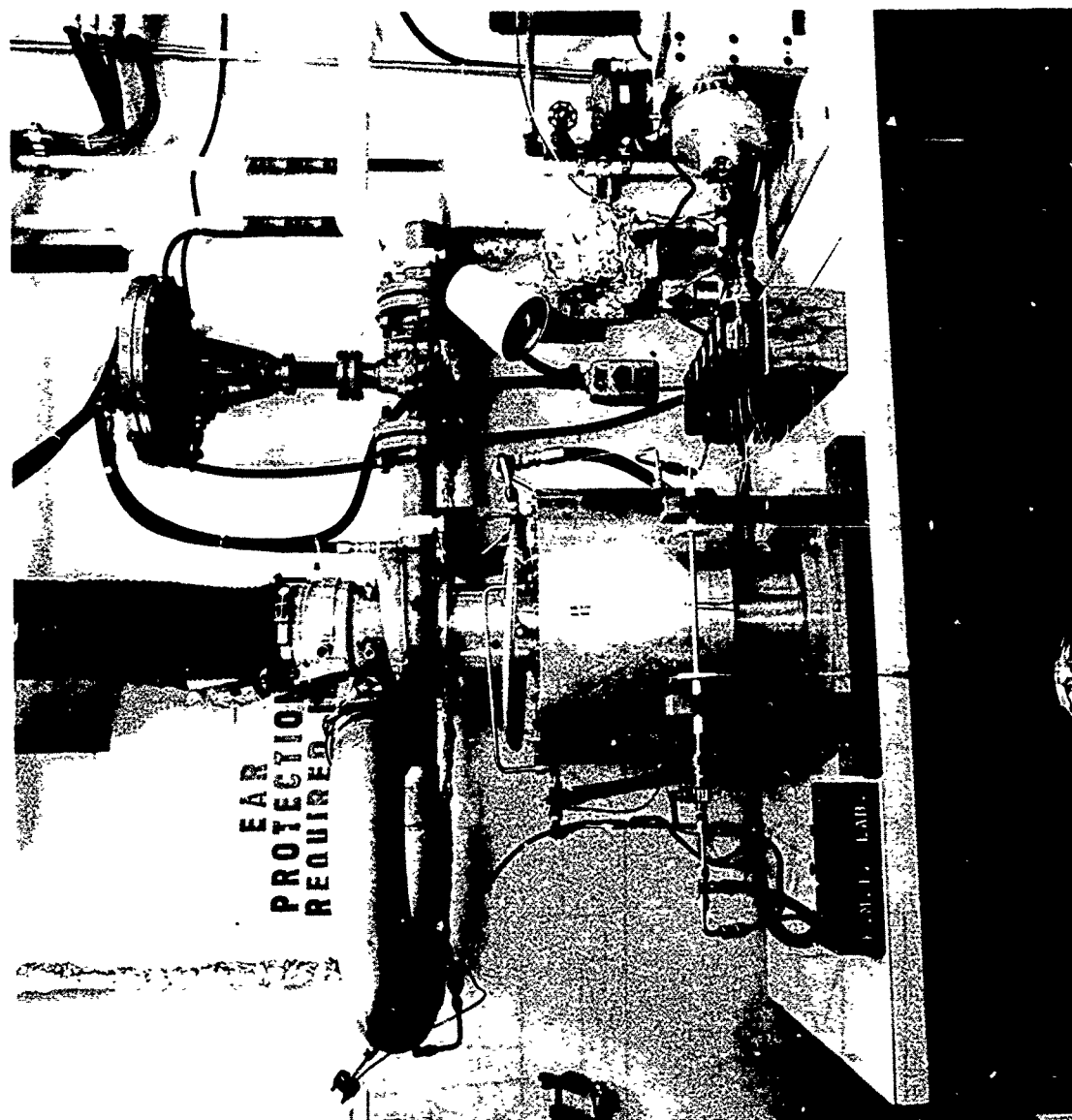


Figure 28. Thrust Bearing Test Rig.

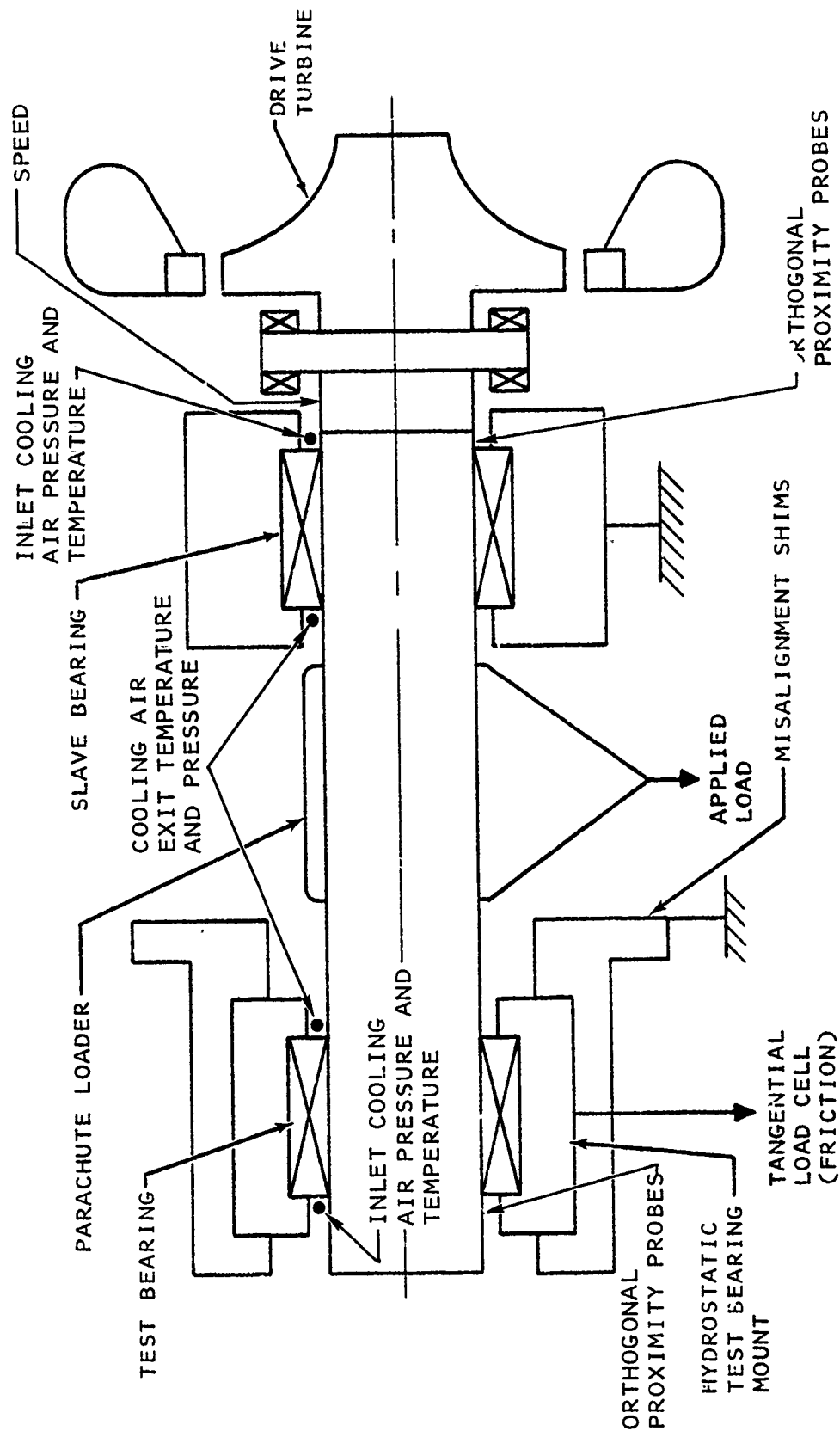


Figure 29. Journal Bearing Test Rig.

The parachute loader consists of a hydrostatic (air) bearing between the shaft and a thin sheet metal half wrap-around band (Figure 30). The shaft is hollow, with holes under the parachute loader to supply high pressure cooling air.

The drive turbine is a production air cooling turbine, modified for shaft attachment with an associated nozzle and air inlet scroll.

The thrust bearing used for shaft axial position control, is the baseline thrust bearing of this program, assembled in a double-acting configuration.

The journal bearing at the drive turbine end is considered to be the slave bearing but is identical to the test bearing at the other end. The test bearing is mounted in a hydrostatically floating carrier so the bearing frictional drag can be measured with a strain-gaged lever.

Six separate controlled air systems provided to the rig include: drive turbine air, thrust bearing cooling air, slave bearing cooling air, test bearing cooling air (pressure and temperature control), test bearing mount hydrostatic air, and parachute loader air.

Basic instrumentation for the test rig includes orthogonal proximity probes for measuring shaft motion, (one at the outboard edge of the test bearing and the other between the slave bearing and the thrust bearing) speed pickup, inlet and exit air pressure and temperature measurement for the slave and test journal bearing, parachute loader load and bearing drag torque. The journal bearing test rig is shown in Figure 31 during its initial checkout runs.



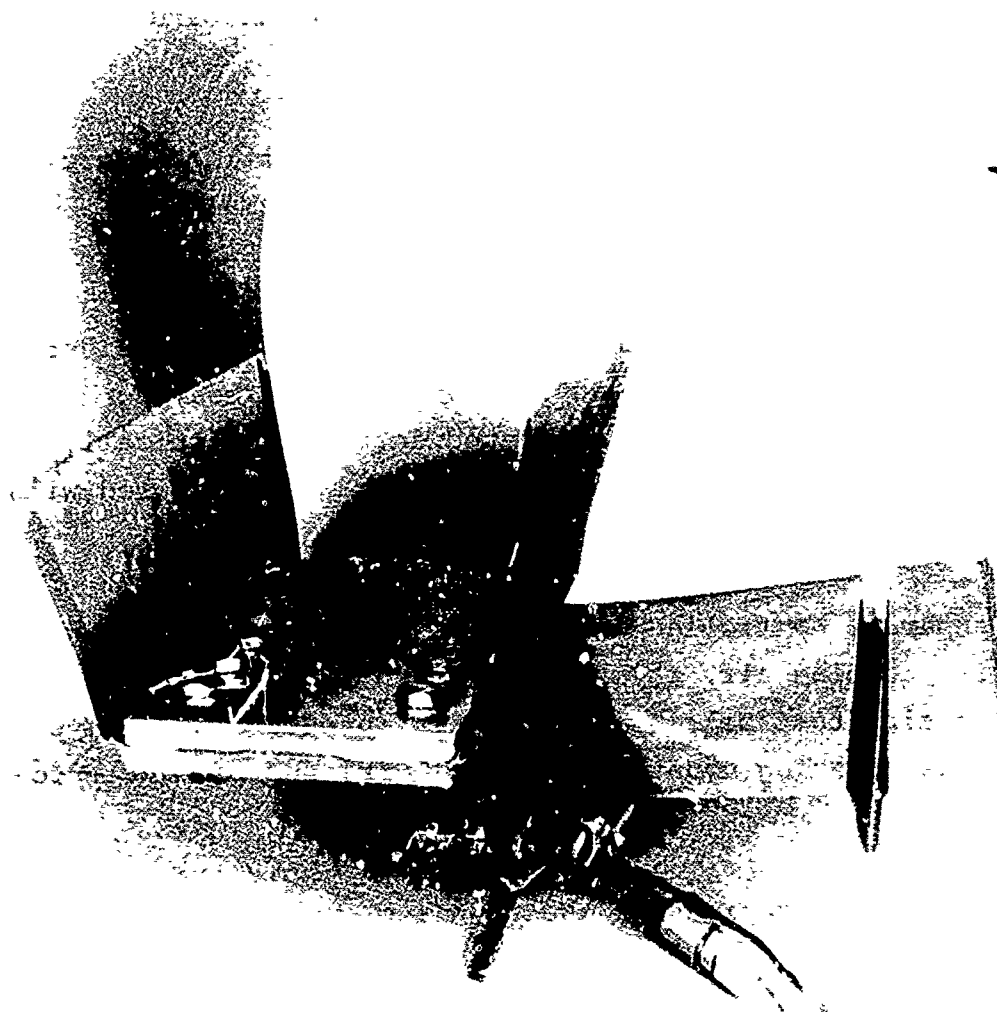


Figure 30. Test Rig Parachute Loader.

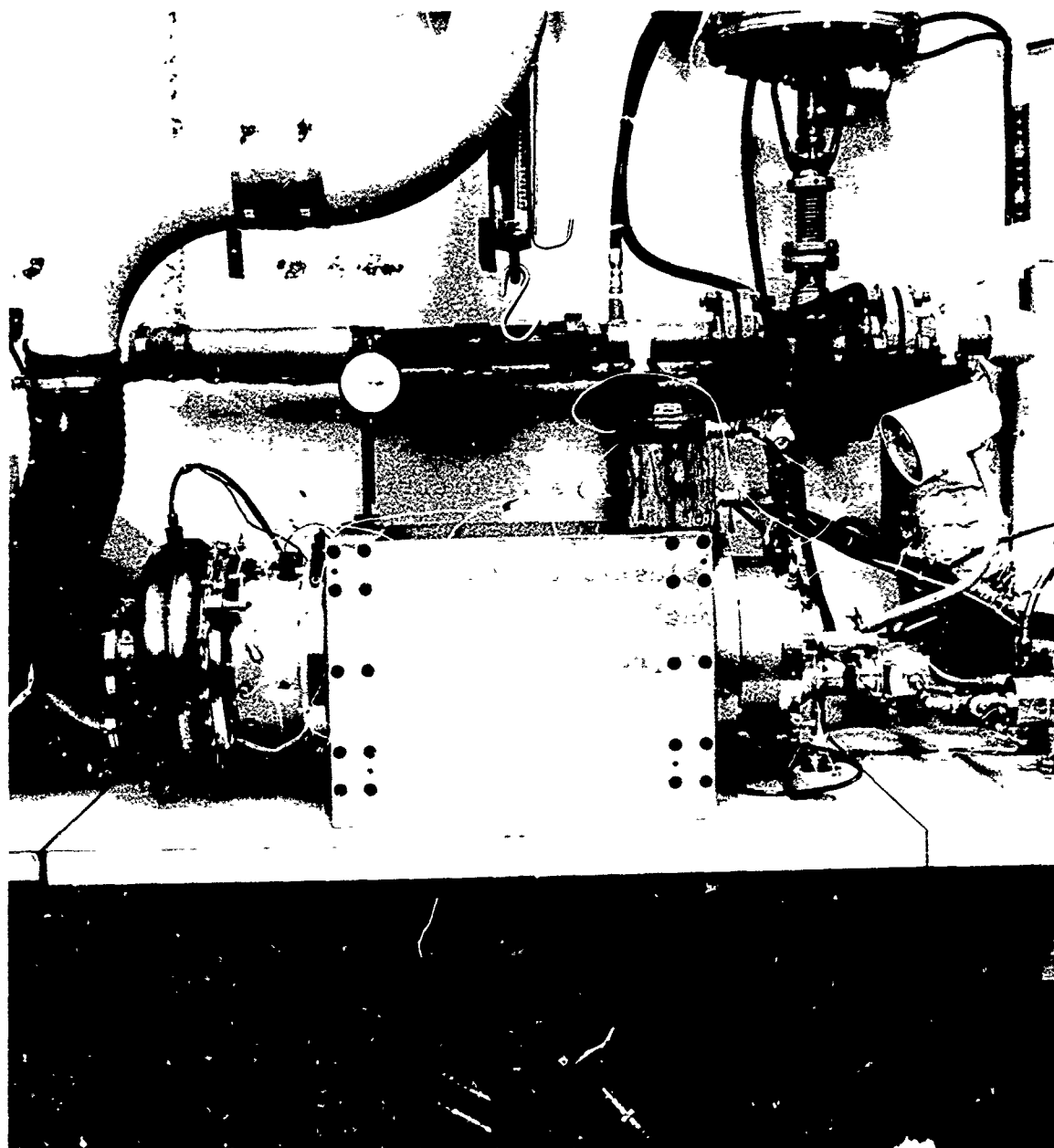


Figure 31. Journal Bearing Test Rig.

### 3.3 Bearing Design Analytical Tools

#### 3.3.1 Thrust Bearing Analytical Program

The Thrust Foil Bearing Analytic Solution consists of a finite difference hydrodynamic analysis and a finite element elasticity routine, which exchange information to obtain a converged solution. As shown in the program logic diagram, Figure 32, the program commences by requiring a definition of the bearing geometry and initial film thickness. The starting film thickness is a user input requirement. The closer the initial film is to the converged solution, the more rapid the convergence of the elastohydrodynamics solution. Once the initial film and input parameters are defined, the program proceeds to the hydrodynamic analysis to determine a fluid pressure distribution and the resulting loads to be applied to the finite element elasticity routine. With these loads, the elasticity solution provides the foil deflections and consequently, the elasticity film distribution ( $h_e$ ). With ( $h_e$ ) and the hydrodynamic film ( $h_H$ ) defined, a relaxation of the form:

$$h_H^{(i)} = \alpha h_e^{(i-1)} + (1 - \alpha) h_H^{(i-1)}$$

Where:

(i) is the iteration index

$\alpha$  is the relaxation parameter

permits redefinition of a new hydrodynamic film and the cycle continues. When the film distribution used in the hydrodynamics ( $h_H^{i-1}$ ) is the same as that predicted by the elasticity routine ( $h_e^{i-1}$ ) then convergence is achieved as:

$$h_H^{(i)} \approx h_e^{(i-1)} \approx h_H^{(i-1)}$$

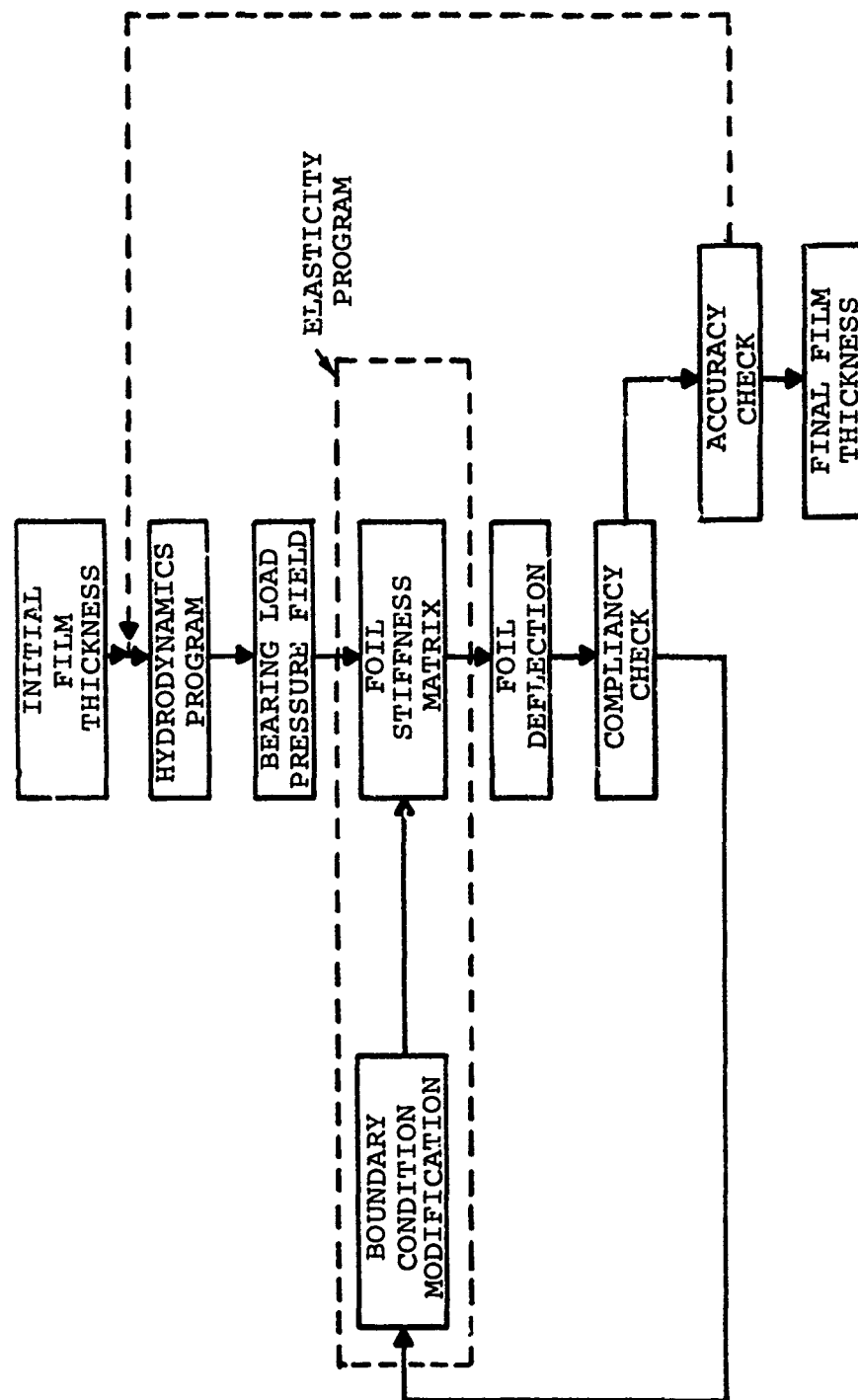


Figure 32. Elasto-Hydrodynamics Program Logic Diagram.

### 3.3.1.1 Elasticity Solution

The elasticity solution is a three-dimensional triangular-plate finite element representation of the foil with provisions for assigning spring stiffness at prescribed nodal locations. This linear elasticity solution contains provisions for evaluating thermal effects, including that due to thermal gradients across the plate thickness. The elasticity routine accepts the pressure distribution, as determined by the hydrodynamic finite difference solution. The pressure loading is then integrated for nodal loads, which provide foil deformations for the linear elasticity solution. Special boundary conditions such as symmetry are directly provided by proper conditioning of the finite element elasticity matrix. A schematic of a typical thrust bearing model, illustrating the finite difference and finite element grids is shown in Figure 34.

The finite element grid consist of triangular shell elements. As shown in Figure 33 below, three cartesian components of translation and rotations at each of the three mid-thickness vertex are provided.

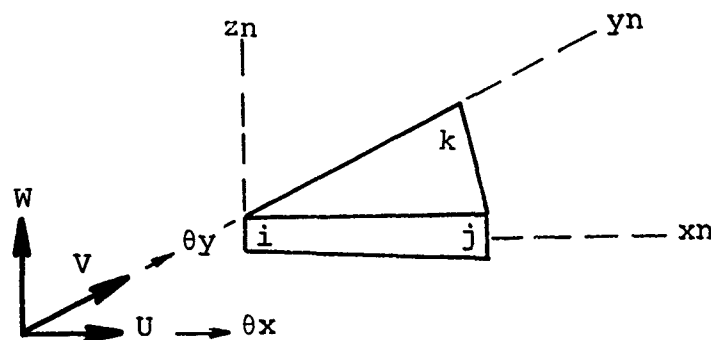


Figure 33. Finite Element Grid

The local coordinate system shown in Figure 33 is utilized in the computations but foil elasticity deflections are reported by the program in a global coordinate system.

----- FINITE ELEMENT GRID  
 ——— FINITE DIFFERENCE GRID

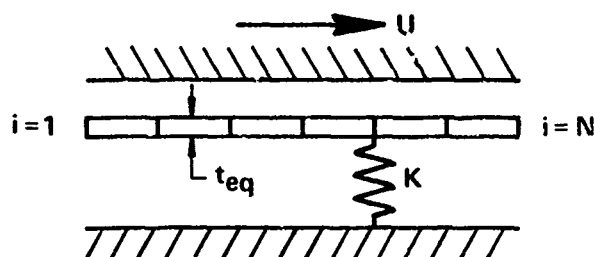
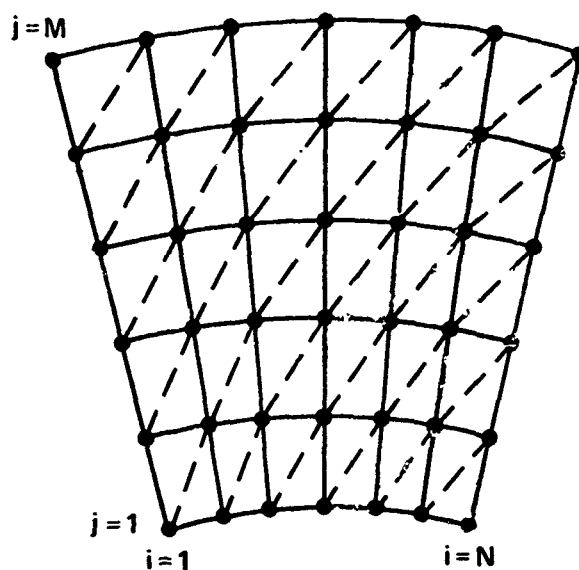


Figure 34. Thrust Foil Bearing Mathematical Model.

### 3.3.1.2 Hydrodynamics Solution

The thrust foil bearing subroutine termed the hydrodynamics program of Figure 32 is a finite difference solution to the Reynolds equation. Based upon the assumptions that:

- (a) The axial clearance between bearing surfaces is much smaller than other bearing dimensions.
- (b) The flow may be laminar or turbulent.
- (c) Both bearing surfaces are wet.
- (d) The velocity gradients across the fluid film are much larger than other velocity gradients.
- (e) Body forces, pressures, viscosity and density are invariant across the lubricant film.
- (f) The working fluid may be compressible or incompressible.
- (g)  $\rho = P/RT$  (Isothermal conditions).

The Reynold's equation can be expressed in a cartesian frame as:

$$\begin{aligned} \frac{\partial}{\partial x} \left[ \frac{P}{k_z} \frac{h^3}{\mu} \left( \frac{\partial P}{\partial x} - \bar{X} \right) \right] + \frac{\partial}{\partial z} \left[ \frac{P}{k_z} \frac{h^3}{\mu} \left( \frac{\partial P}{\partial z} - \bar{Z} \right) \right] \\ = 6 \left[ P (U_0 - U_1) \frac{\partial h}{\partial x} + Ph \frac{\partial}{\partial x} (U_0 + U_1) \right. \\ \left. + h (U_0 + U_1) \frac{\partial P}{\partial x} + 2P (V_1 - V_0) \right] \end{aligned}$$

Where subscripts (o) and (1) refer to velocity components at the surfaces indicated on Figure 35 and:

$P$  = the pressure

$\rho$  = the density

$\bar{X}, \bar{Z}$  = body forces

$U_o, V_o, U_1, V_1$  = velocity components

$h$  = film thickness

$\mu$  = viscosity

and the turbulence constants  $k_x$  and  $k_z$  are given by:

$$k_x = 12 + 0.53 (k^2 R_e)^{0.725}$$

$$k_z = 12 + 0.296 (k^2 R_e)^{0.65}$$

Where  $R_e$  is the local Reynolds Number and Kappa ( $k$ ) is the Prandtl's mixing length, which has been experimentally determined to be dependent upon the eccentricity ratio for plain journal bearings as shown in Figure 36 with analytic correlation per Figure 37.

Transformed to cylindrical coordinates, and accounting for the velocity terms, the Reynold's equation becomes:

$$\begin{aligned} & \frac{\partial}{r \partial \theta} \left[ \frac{P}{k_x} \frac{h^3}{\mu} \left( \frac{\partial}{r \partial \theta} - \bar{\theta} \right) \right] + \frac{\partial P}{\partial r} \left[ \frac{P}{k_z} \frac{h^3}{\mu} \left( \frac{\partial P}{\partial r} - \bar{R} \right) \right] \\ & = 6 \left( \frac{P U_o}{r} \frac{\partial h}{\partial \theta} + \frac{h U_o}{r} \frac{\partial P}{\partial \theta} + 2 P V_1 \right) \end{aligned}$$



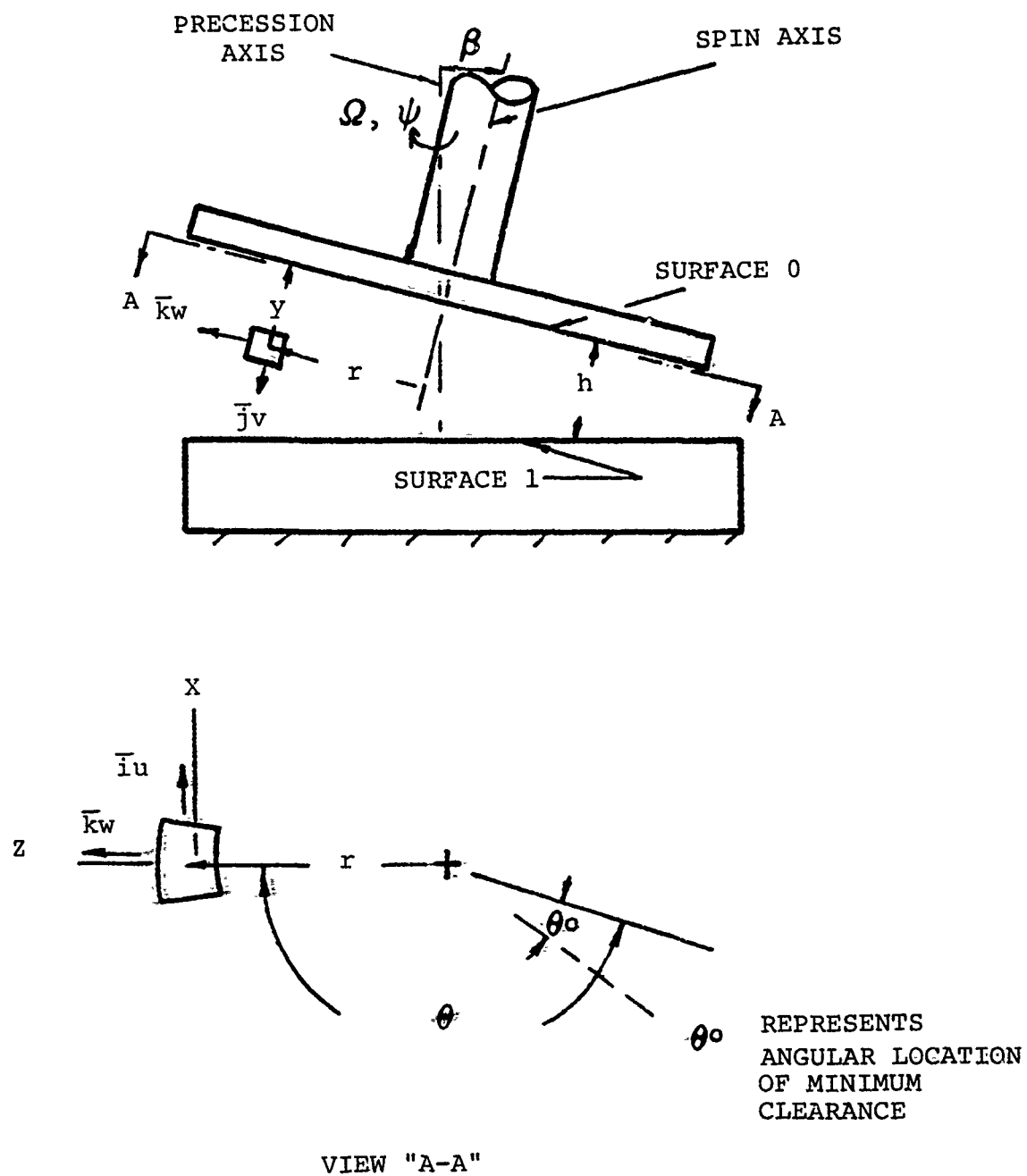


Figure 35. Thrust Bearing Geometry.

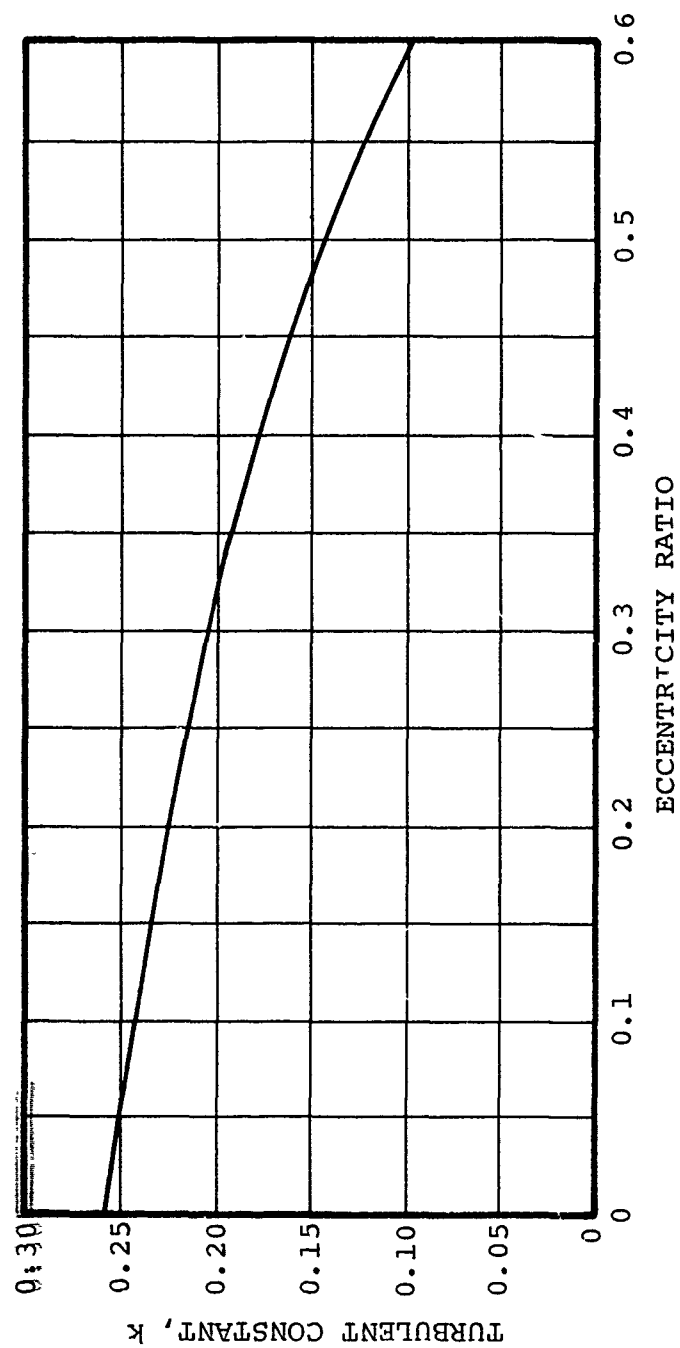


Figure 36. Experimental Correlation of Finite Difference Solution.

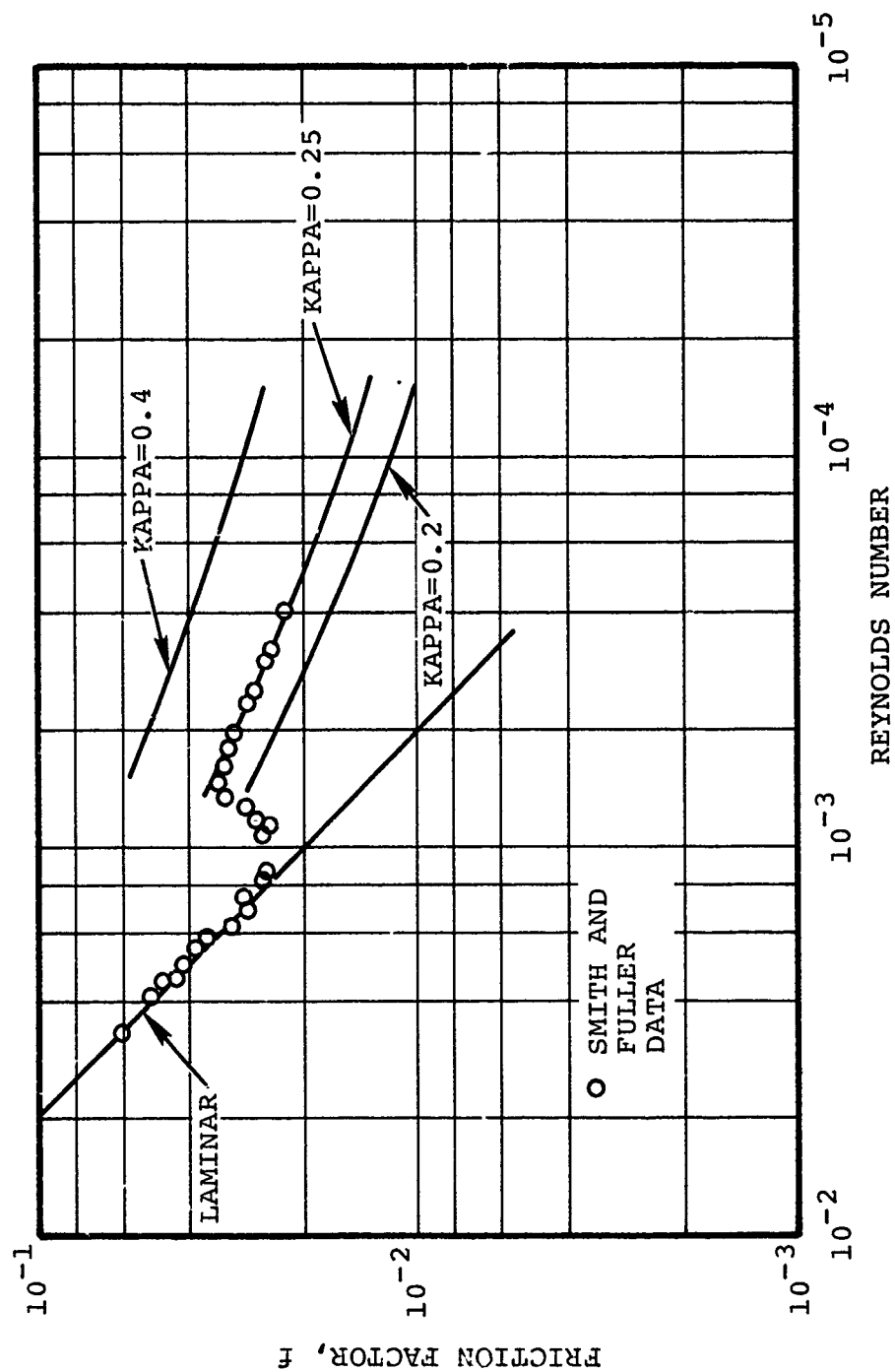


Figure 37. Dependency of Turbulence Constant on Bearing Eccentricity.

where:

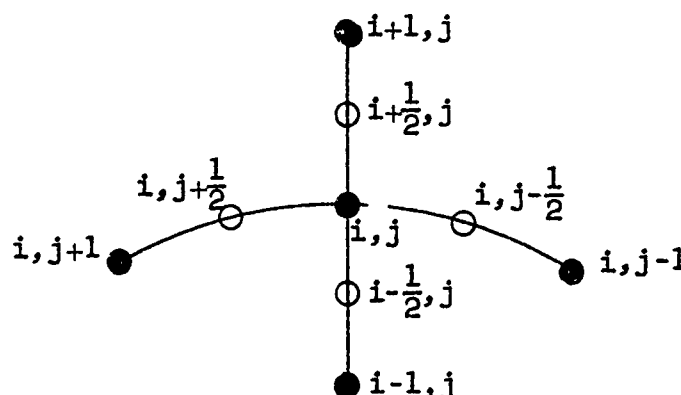
$$\dot{V}_1 = \frac{\partial h}{\partial t} - r \dot{\beta} \cos(\theta - \theta_0) - r \dot{\psi} \beta \sin(\theta - \theta_0)$$

$$U_0 = r\Omega$$

$\theta_0$  is the angular location of minimum film clearance

• indicates derivative with respect to time.

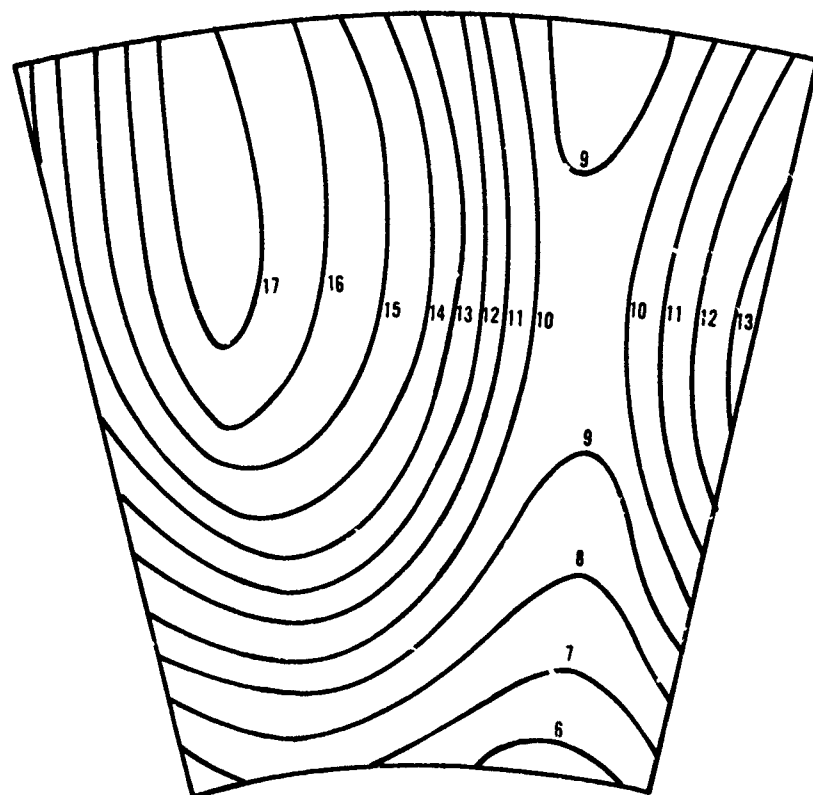
The Reynolds equation is written and solved in finite difference form to provide an expression for pressure at the point (i,j).



Pressure distribution within the bearing is obtained by an iteration technique. The program includes the option of considering fluid inertia. Mean values of the fluid inertia terms  $\rho \frac{Du}{Dt}$  and  $\rho \frac{Dw}{Dt}$  are computed utilizing pressure distributions at intermediate stages of iteration and incorporated in subsequent iterations until the designated accuracy requirement is satisfied.

### 3.3.1.3 Computational Results

The baseline foil thrust bearing, as specified below was first analyzed using this newly developed elasto-hydrodynamics computer program. Figures 38 and 39 show typical computer results



OD = 6.15 IN.  
ID = 3.50 IN.  
N = 33,000 RPM  
Pa = 15 PSI

LOAD  
CAPACITY = 100 LBS (5 PSI)

Figure 38. Baseline Bearing Film Thickness Isopleth  
(In./10,000)

of film thickness and film pressure distribution in isopleth form for one thrust bearing sector at a bearing load of 100 pounds (5 psi).

Outside Diameter (OD)	6.15 In.
Inside Diameter (ID)	3.5 In.
Thickness of Foil ( $T_1$ )	0.006 In.
Thickness of Foil Pad Plate ( $T_2$ )	0.010 In.
Thickness of Stiffener ( $T_3$ )	0.012 In.
Thickness of Spring Pad ( $T_4$ )	0.012 In.
Number of Sectors (N)	13

Figure 40 shows film thickness results and runner positions at the mean radius ( $R = R_m$ ) for various bearing loading conditions. The effects of foil bearing compliance are also shown on Figure 40 by the shape of the film. Since the film shape becomes extremely steep at higher loading conditions (Figure 40), higher friction losses are expected. The bearing friction loss versus bearing load, as predicted by the analytical program is shown in Figure 41. Gas film pressure profiles along the mean radius line ( $R = R_m$ ) for various bearing loading conditions are shown in Figure 42. The minimum film thickness, usually located near the bearing inside diameter (see Figure 39), is shown against the bearing load in Figure 43. Bearing load capacity is predicted by using a minimum film thickness of 0.0001 inch. The baseline bearing was predicted to fail at a bearing load of 280 pounds by the analytical study.

The baseline thrust bearing was tested in the test rig. The bearing carried a load of 304 pounds. The rubbing pattern shown in that test clearly indicates that rubbing was initiated at the regions of minimum film thickness as predicted by the analytical results.

The baseline bearing failure, at a 304 pound load is a result of incorrect film shape at higher bearing loading conditions, as shown in Figure 40. A good film shape can increase the bearing

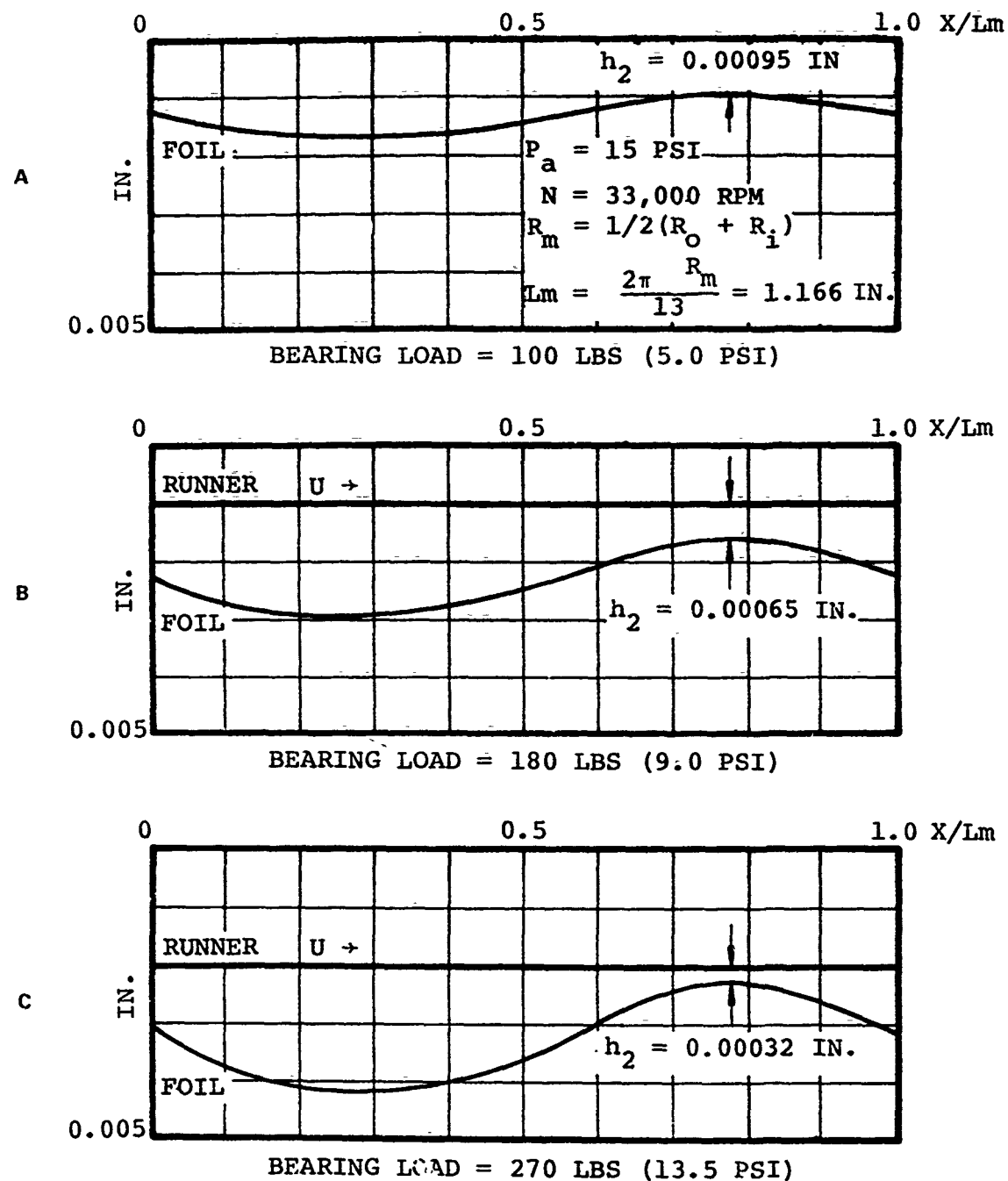


Figure 40. Film Thickness at  $R_m$  for Baseline Thrust Bearing

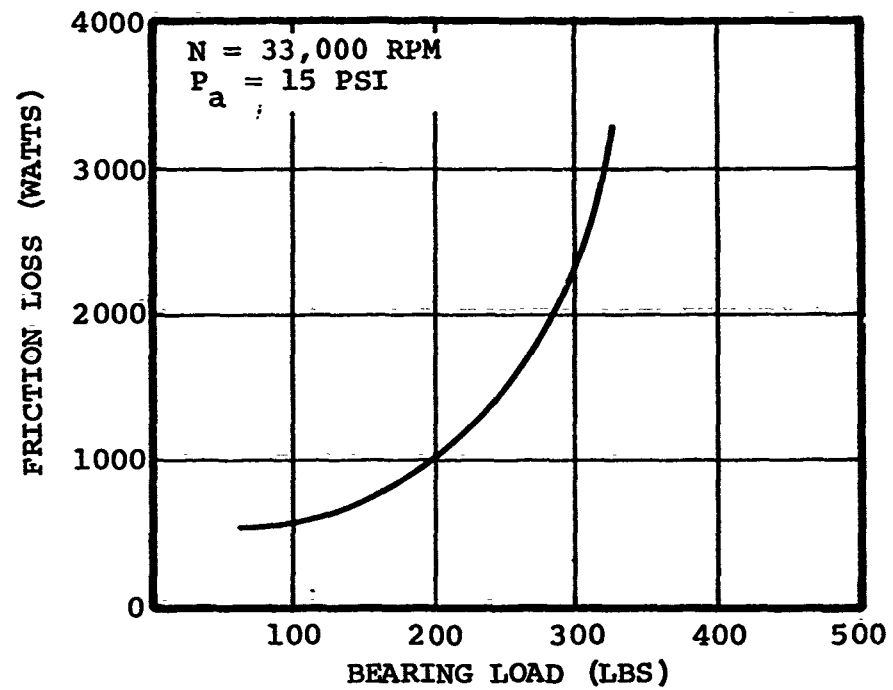


Figure 41. Baseline Bearing Friction Loss as Function of Bearing Load



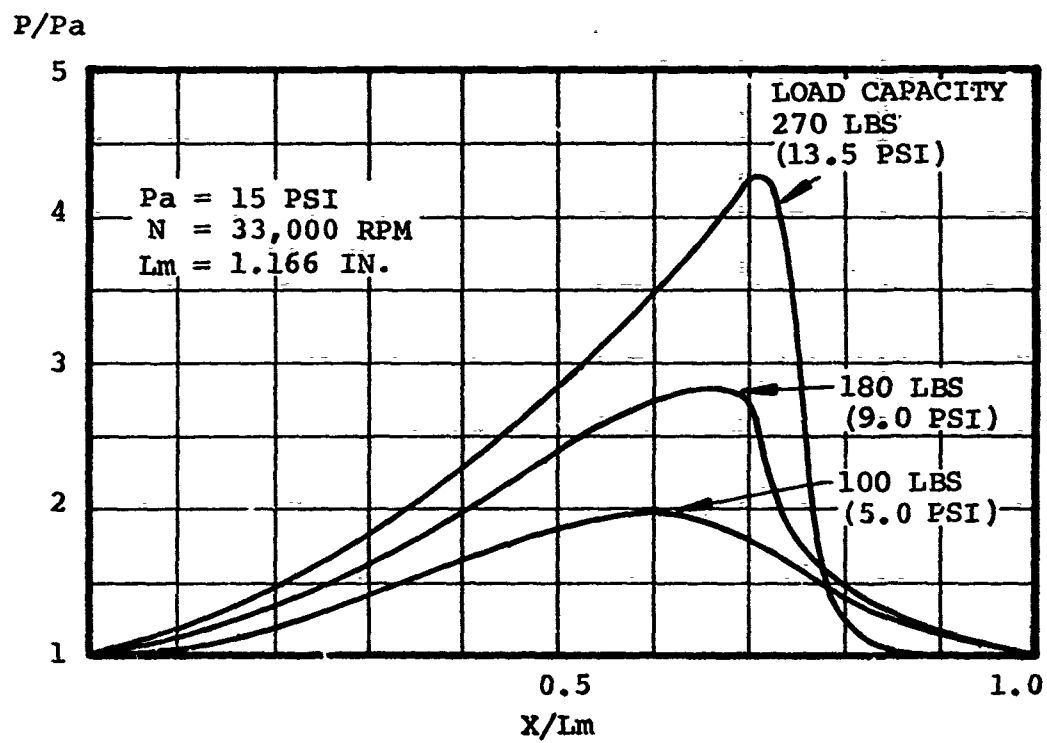


Figure 42. Pressure Profile at  $R_M$  for Baseline Thrust Bearing

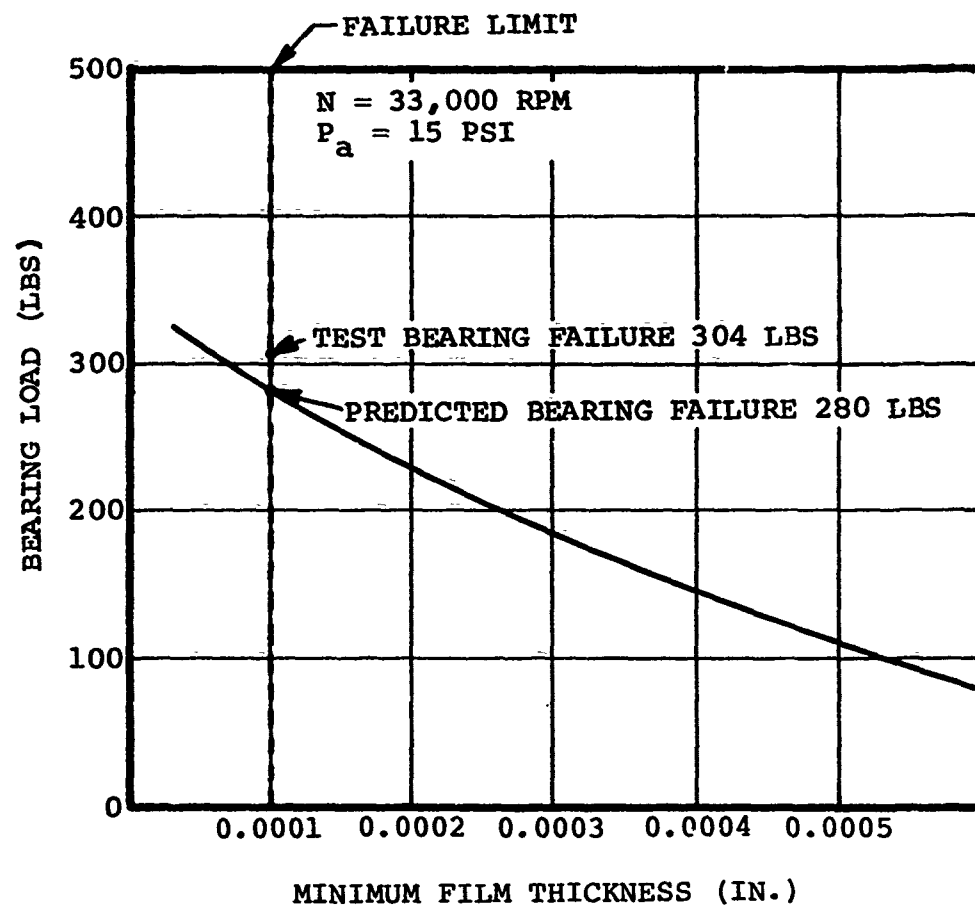


Figure 43. Baseline Bearing Load as Function of Minimum Film Thickness

load and decrease friction loss, thus improving these major bearing characteristics. Therefore, an analytical study focused on controlling the film shape was initiated to aid in optimizing the bearing design.

The "Dual Spring" spring assembly shown schematically in Figure 44 is the new design concept resulting from the analytical study. The gas film thickness distribution in the dual spring foil thrust bearing can be optimized varying the spring ratio,  $r = k_2/k_1$ , and the stiffening segment thickness "t" (Figure 44).

The analytical results for the dual spring foil thrust bearing having the same dimensions as the baseline bearing are shown in Figures 44 through 48. Figure 45 shows the film thickness results and runner positions at the mean radius ( $R = R_m$ ). Figure 46 shows the pressure profiles. Figure 47 shows friction losses versus bearing load. The bearing load capacity versus minimum film thickness curve is shown in Figure 48. Results of a single spring baseline bearing were also plotted in Figures 47 and 48 for comparison. As indicated in Figure 48, the dual spring thrust bearing was expected to develop significant improvement in load capacity.

Subsequent testing of the dual spring design did not provide the load capacity predicted. This was due to the sensitivity of this design to manufacturing tolerances, etc. However, the analytic computer program did indicate that, by proper control of the foil and stiffener elasticity, increased load capacity could be achieved. This was experimentally demonstrated by the partial pad stiffener design (Figure 49), which achieved a load capacity of 540 pounds.

### 3.3.2 Journal Bearing Analytic Program

The foil journal bearing computer elasto-hydrodynamic analysis parallels the thrust bearing computer analysis program. A

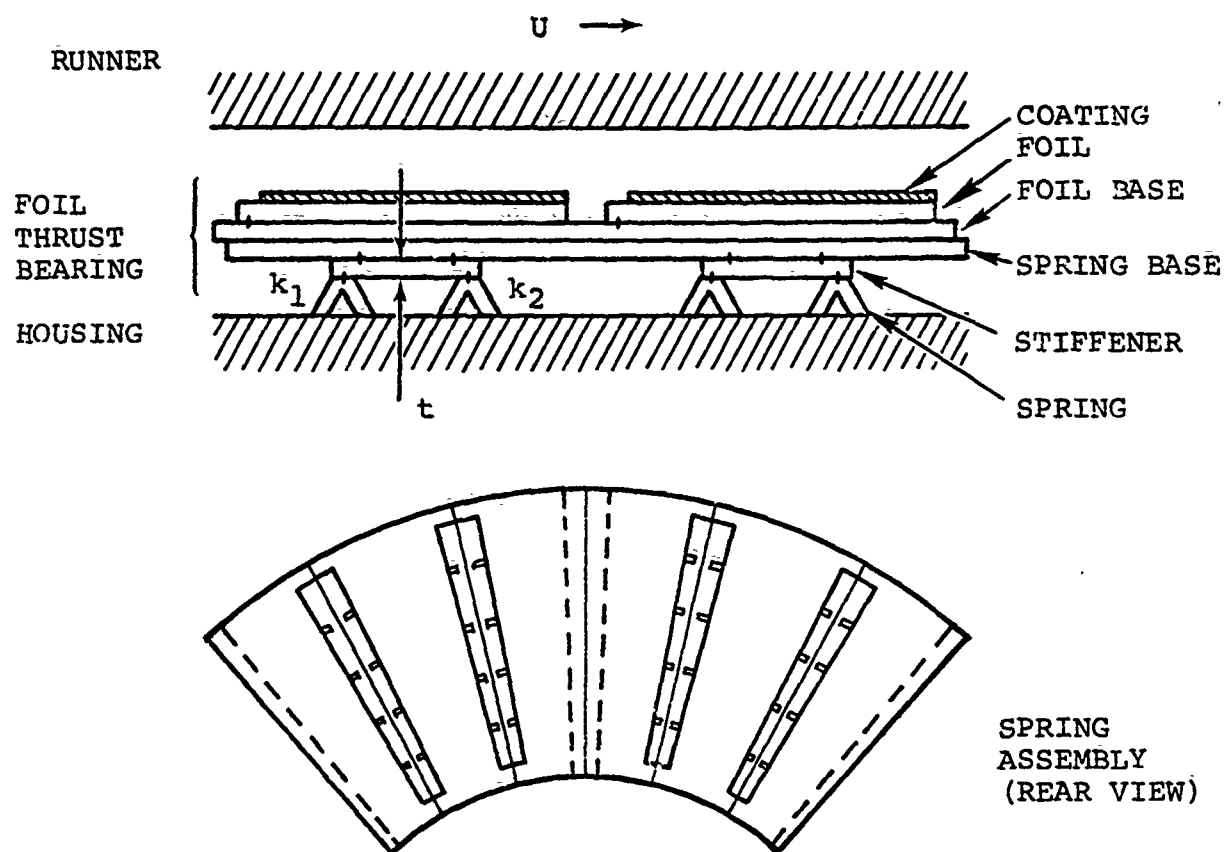


Figure 44. Dual Spring Foil Thrust Bearing Schematic.

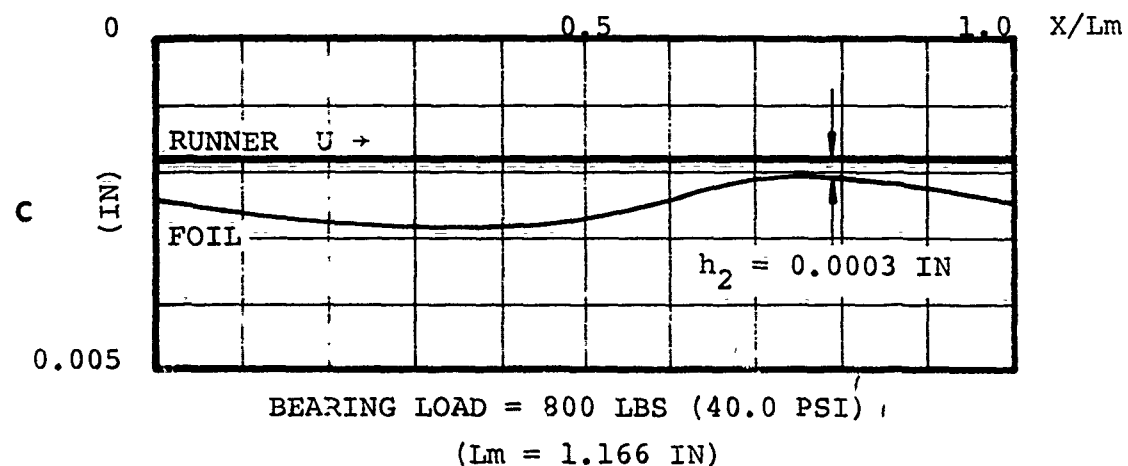
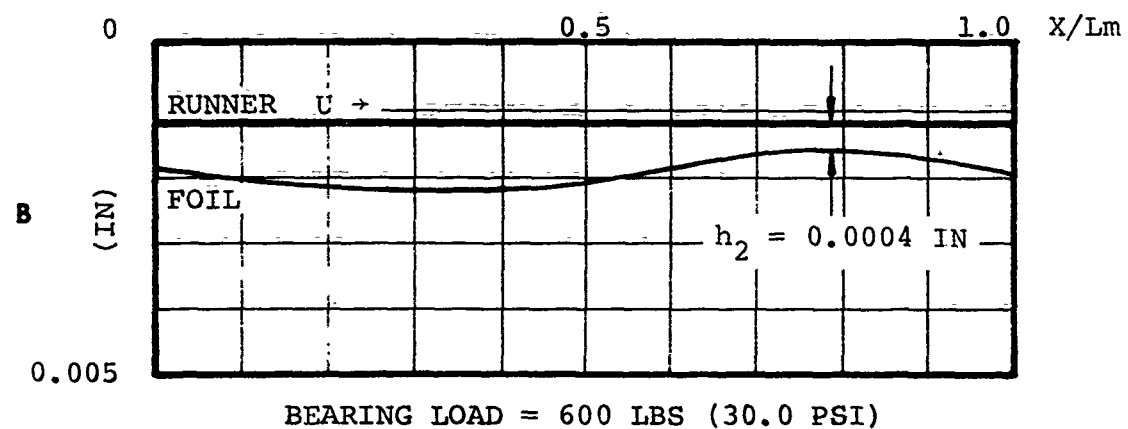
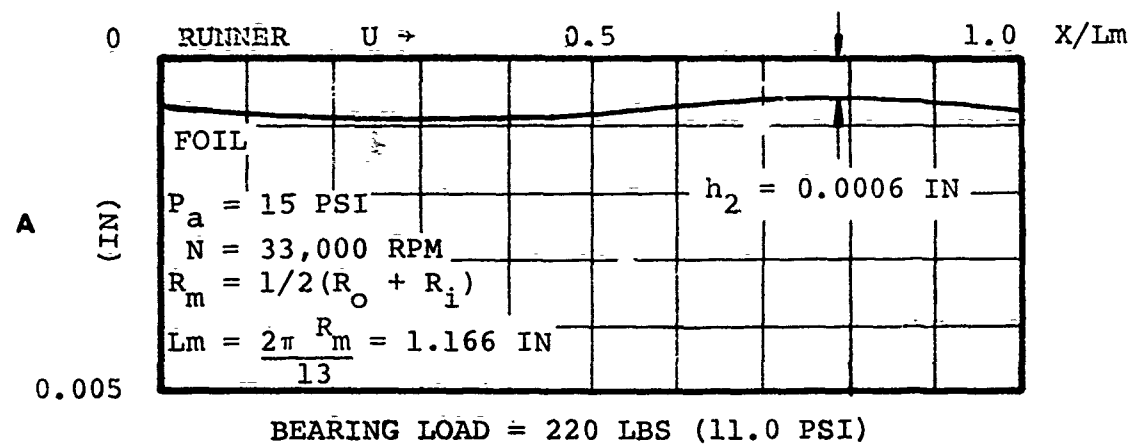


Figure 45. Film Thickness at  $R_m$  for Dual Spring Thrust Bearing

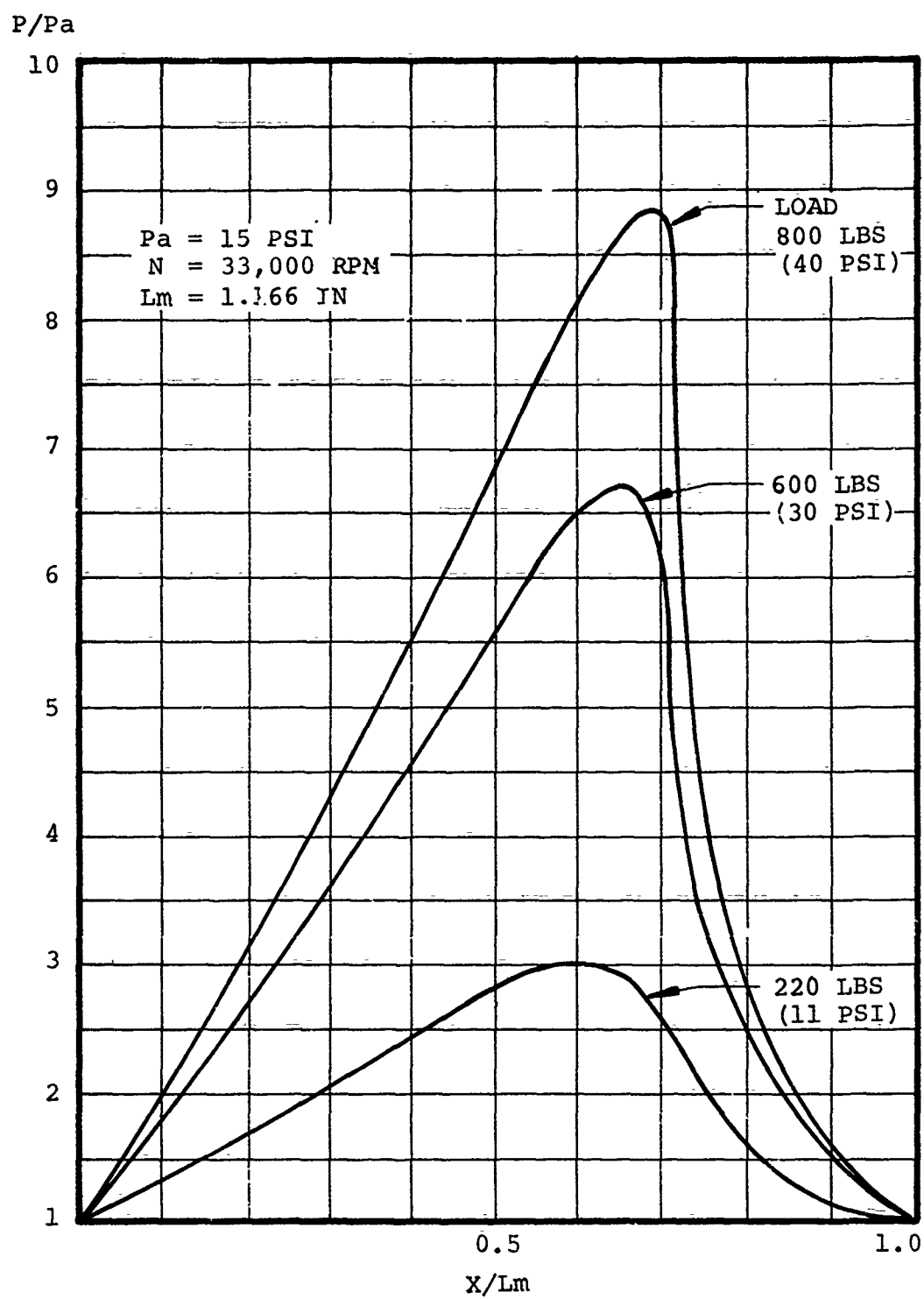


Figure 46. Pressure Profile at  $R_m$  for Dual Spring Thrust Bearing

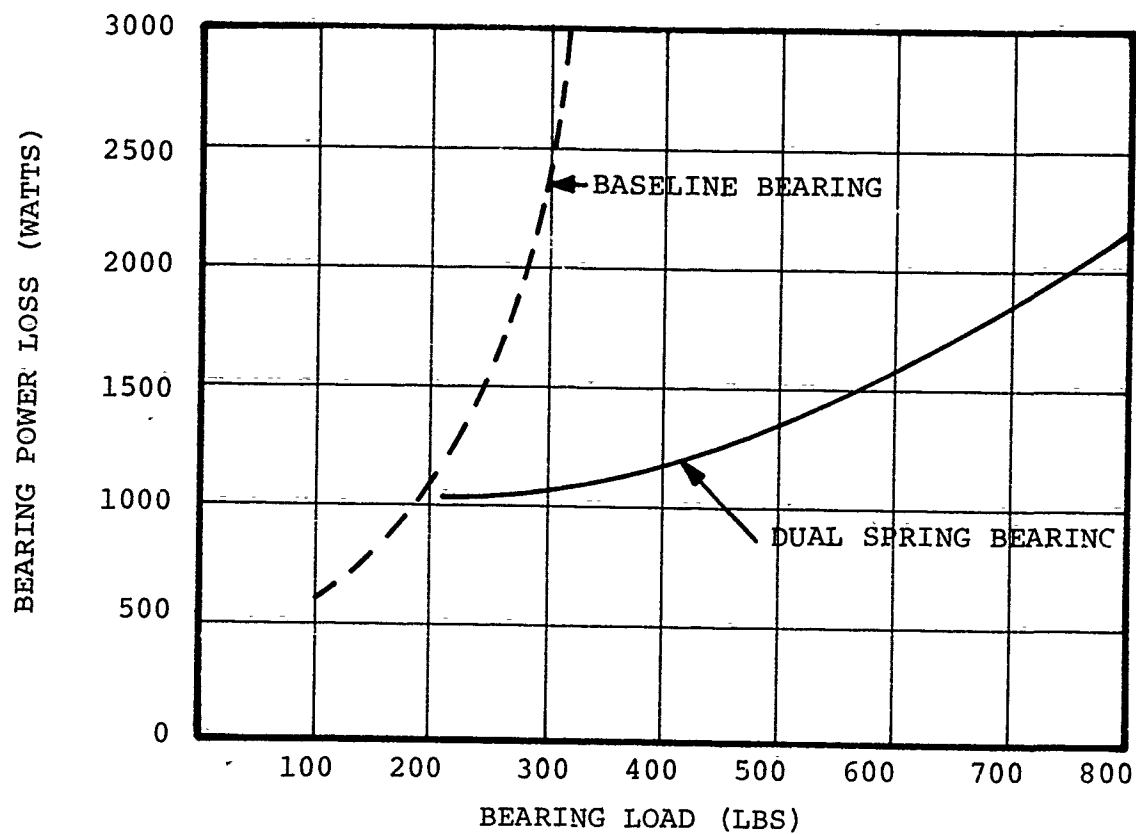


Figure 47. Friction Loss as Function of Bearing Load for Dual Spring Thrust Bearing

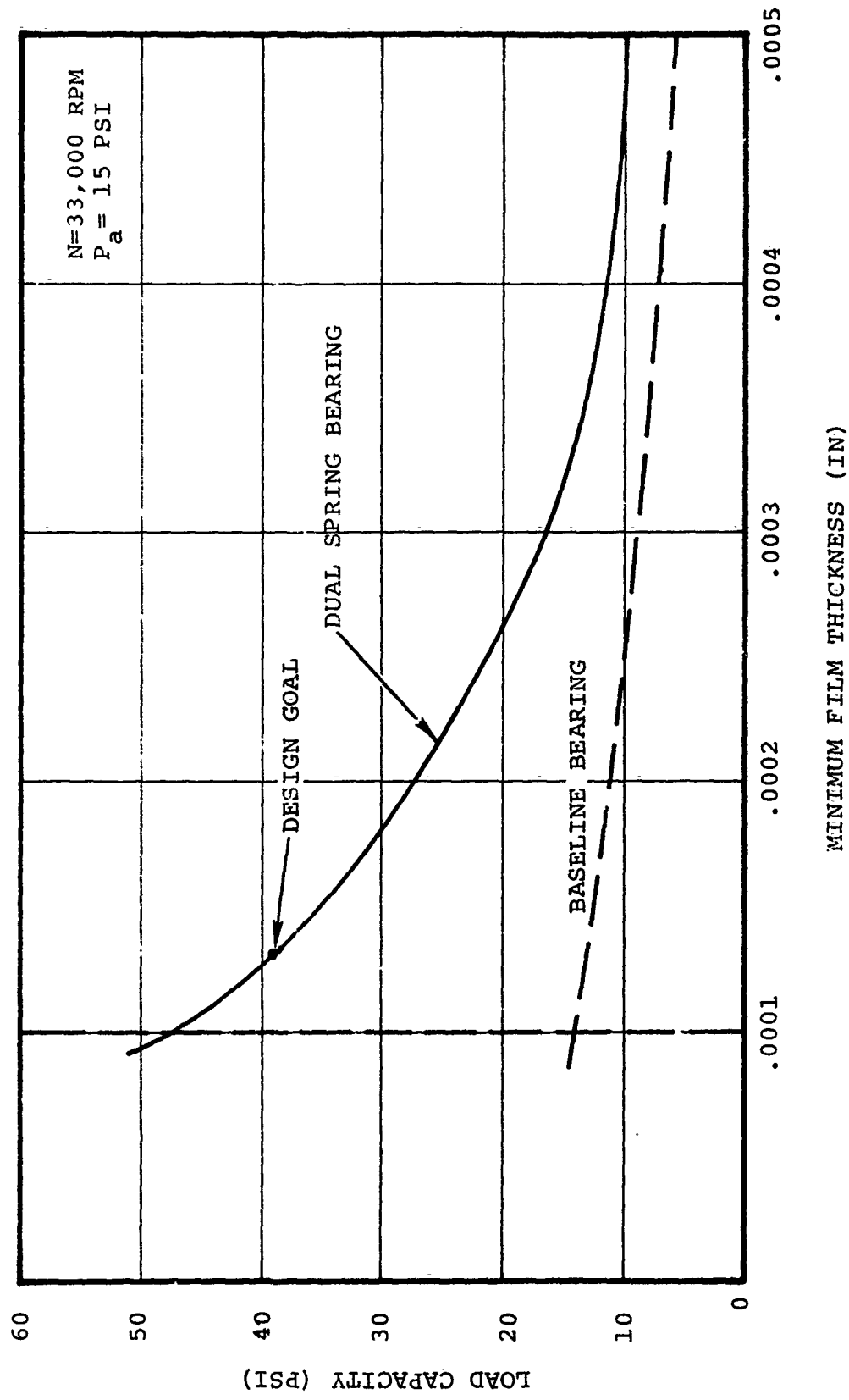


Figure 48. Bearing Load as Function of Minimum Film Thickness for Dual Spring Thrust Bearing



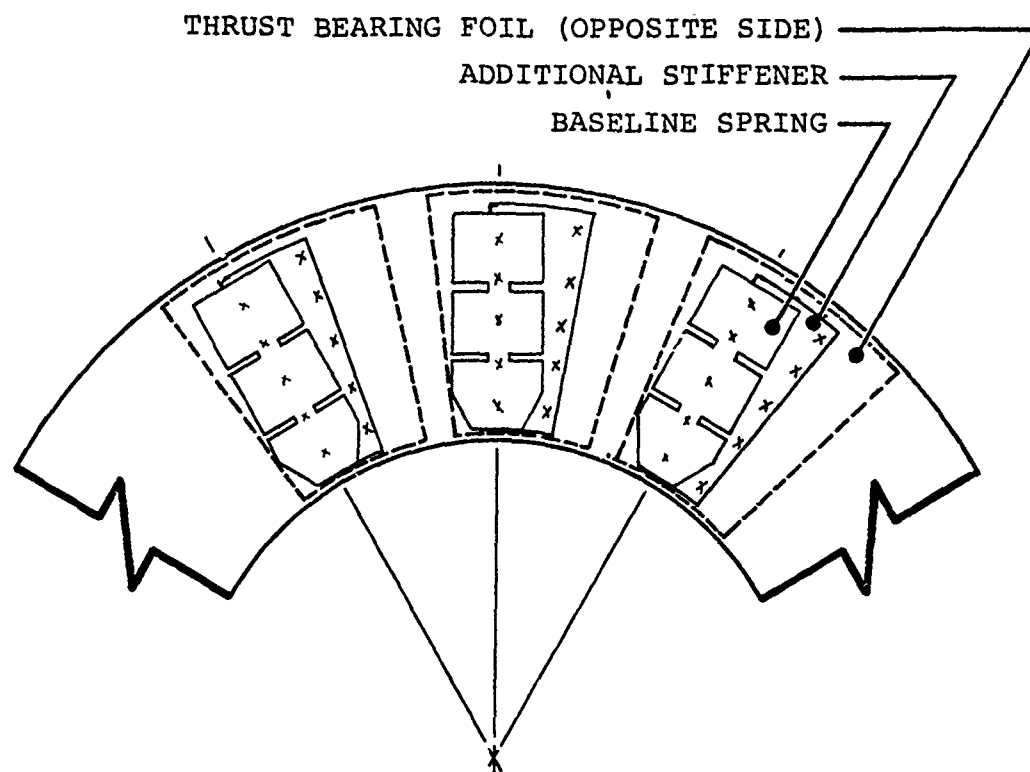


Figure 49. Baseline Spring with Backup Stiffener.

separate hydrodynamics subroutine and elasticity subroutine exchange the appropriate information on loads and foil deformations until convergence is achieved. Convergence is attained when the hydrodynamic film thickness used to obtain the pressure distribution and resulting foil loading is the same film thickness (within a reasonable error) predicted by the elasticity program when the hydrodynamic loads are imposed on the foils. The Foil Journal Bearing Program flow chart is provided in Figure 50. This logic chart differs from that previously presented for the thrust bearing program in two respects. First, a geometry routine has been added to the Journal Bearing Program to predict the assembly configuration. Second, the elasticity solution is nonlinear. These differences result from a fundamental but significant feature of journal bearing geometry, which is that journal foil segments are not independent elastic members but are in contact with each other. Thus, each foil encounters loading due to the hydrodynamics of the bearing as well as traction loads and kinematic constraints from foil interaction. In simple terms, foils may: (1) be in contact with each other, (2) be in contact with each other and constrained by the bearing housing, (3) be in contact with boundaries and not in contact with other foils, or (4) be in contact neither with other foils nor boundaries. These conditions must be correctly assessed by the elasticity program, thereby requiring a difficult nonlinear iterative elasticity subroutine to be programmed. This has been successfully achieved.

#### 3.3.2.1 Discussion of Geometry Subroutine

As all foil displacements must be referenced from prescribed datum, it is first necessary to determine this reference configuration. For the foil thrust bearing this datum is the free foil geometry. For the journal bearing, the configuration of the foils may differ in the assembled state from the free form state due to foil interaction loading. Generally, the fewer the number of segments, the more likely that the assembly configuration deviates

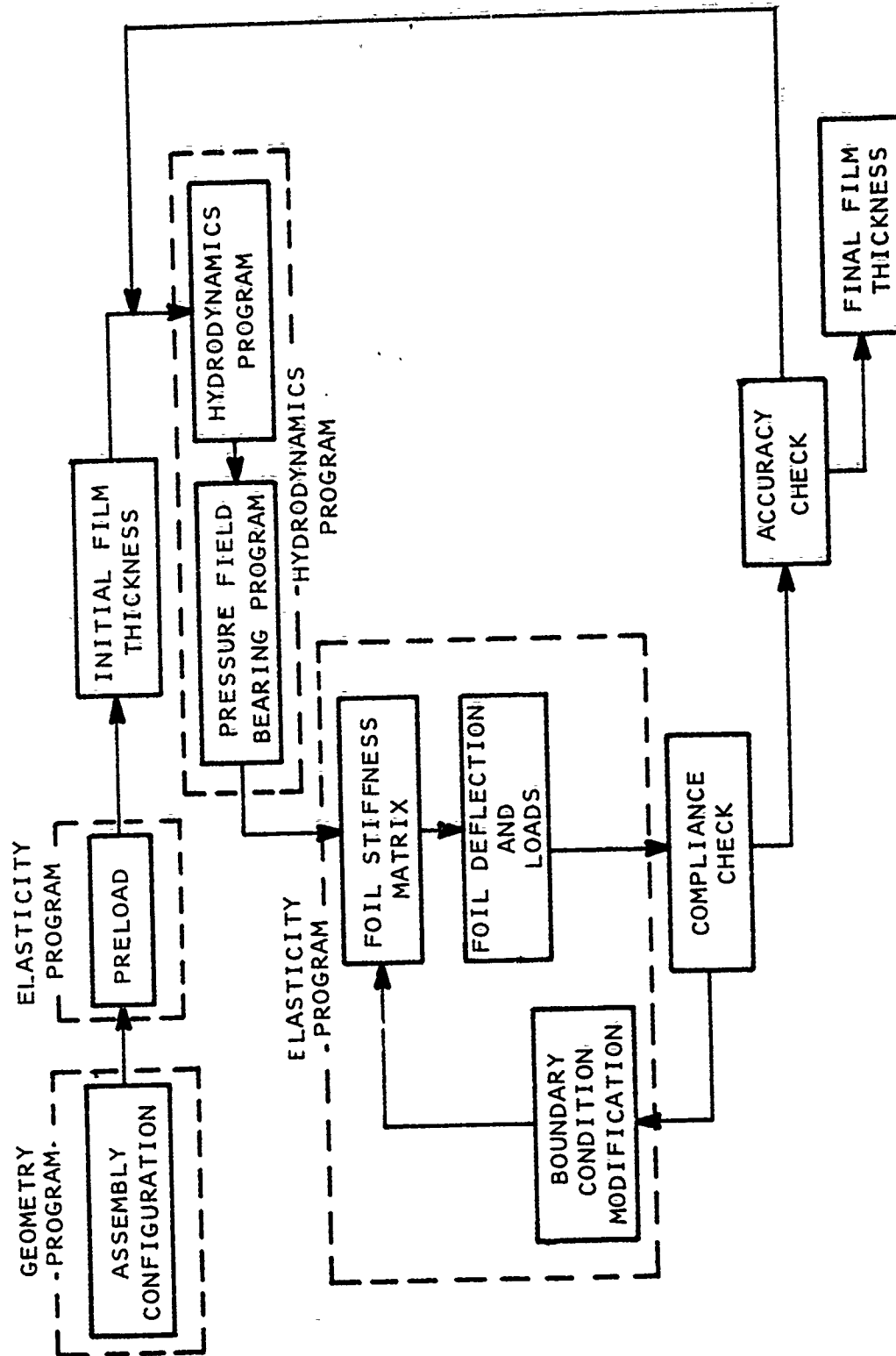


Figure 50. Elasto-Hydrodynamics Program Logic.

from the free foil state. The assembly subroutine has been programmed to determine the assembled configuration of the foil journal bearing prior to shaft insertion. This geometry subroutine has been programmed to search for an acceptable constant curvature position at assembly. Given the free foil radius (RFF), the length of the foil (FL), the base material thickness ( $t_f$ ), the non-structural coating thickness ( $t_c$ ), and the bearing radius ( $R_B$ ), the assembly subroutine seeks a foil radius  $R_O$  (Figure 51) where  $R' = R + t_f + t_c$ . The assembly routine reports  $R_O$ , as well as  $R_N$  (the radius to each node from the geometric center of the bearing) from which all foil deformations are measured. Figure 52 presents some typical Calcomp computer plots generated by the assembly routine for 6-, 12- and 16-segment foils.

#### 3.3.2.2 Elasticity Subroutine

Figure 53 presents the details of the assembly/elasticity solution. As noted, the elasticity solution commences by obtaining the symmetric "preload" position of the foils. This is the configuration when the shaft is inserted in a zero "g" position. The program proceeds from there to obtain the foil configuration when the hydrodynamic loads are applied. Program checks provide for:

- (a) Constraint or release of nodes on adjacent foils and/or contact with boundaries
- (b) Constraint or release of nodes in contact with the shaft
- (c) Constraint or release of nodes on the bearing housing

Nodal constraint is provided when displacements indicate a violation of kinematic boundaries. Release of nodes occurs when traction loads produced by constraint are no longer physically realizable.

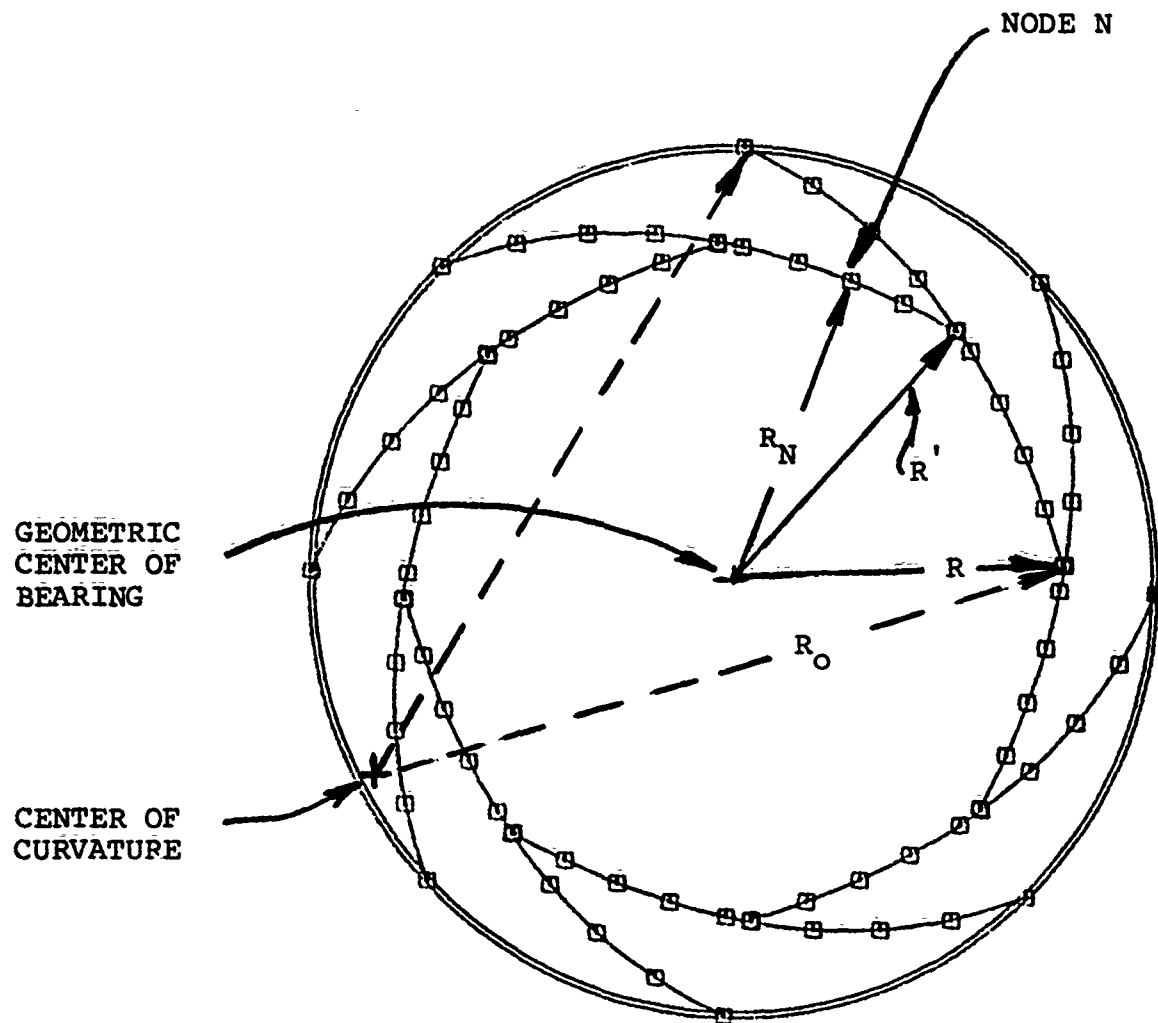
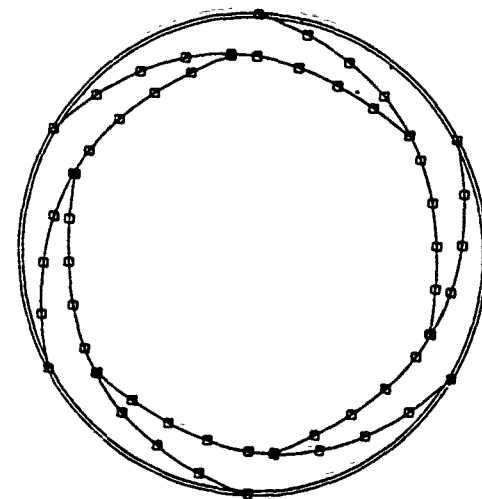
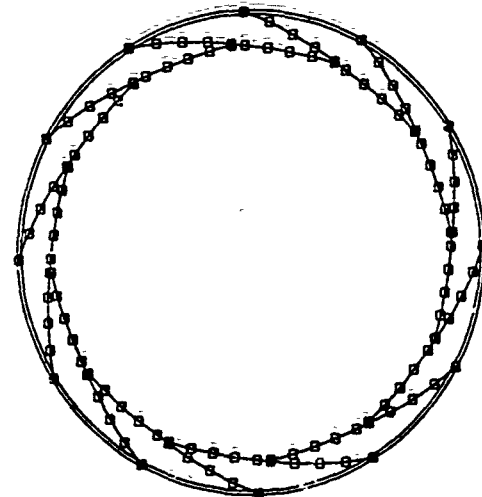


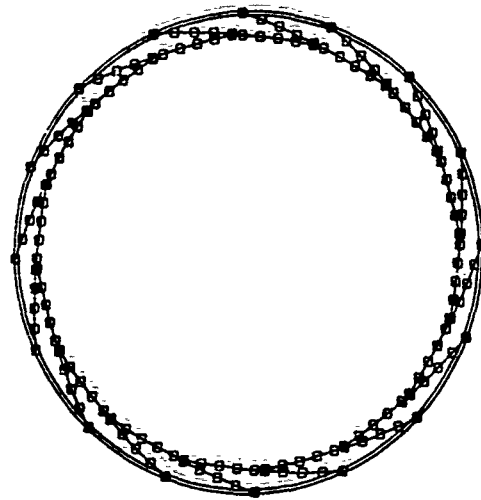
Figure 51. Assembly Position.



6-FOIL ASSEMBLY  
POSITION



12-FOIL ASSEMBLY  
POSITION



16-FOIL ASSEMBLY  
POSITION

Figure 52. 6, 12, and 16-Foils Configurations.

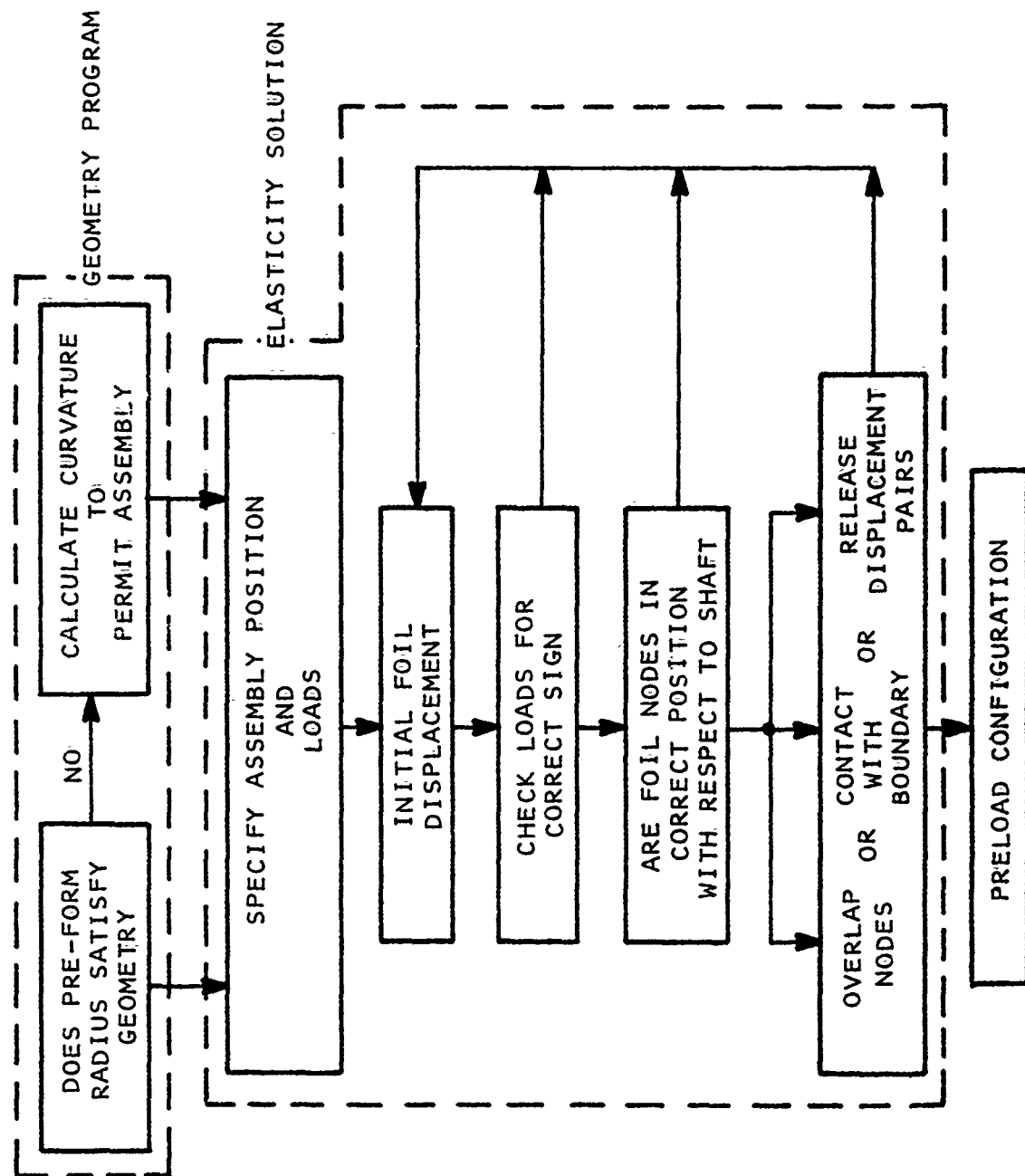


Figure 53. Assembly and Stiffness Flow Chart.

The foil elasticity is analytically represented as a series of short curved elements with a coordinate system and sign convention (Figure 54).

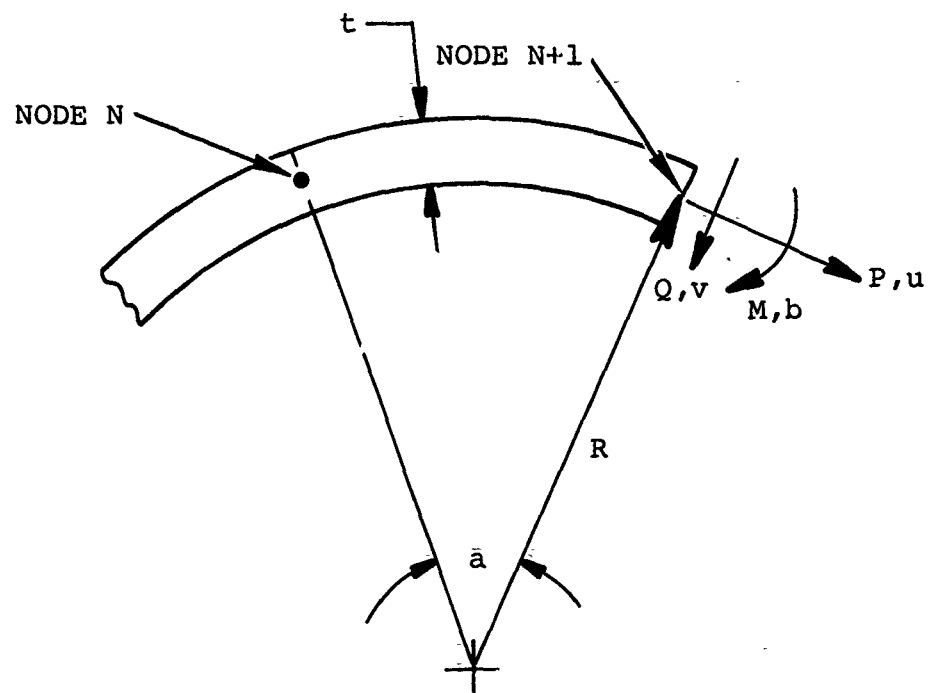
By application of Castigliano's second theorem, the element and system stiffness matrices may be determined. The stiffness equation solution is provided by a straight-forward displacement matrix approach. The fixity of the foil to the bearing housing is assumed to be a "pinned joint". The difficulty in the solution is encountered when the foils are loaded. The foils begin to contact each other and encounter kinematic constraints of the journal and bearing housing. It is apparent that this provides a highly nonlinear stiffness characteristic of foil journal bearings. To deal with these problems the elasticity program generates a constraint matrix. This constraint matrix is used in a transformation of the governing equations to deflate (reduction of degrees of freedom due to constraints) the set of equations. By proper partitioning of this reduced set and by back transformation, the solution to the constrained equation is determined. This permits the nonlinear stiffness characteristics to be simulated.

### 3.3.2.3 Hydrodynamic Analyses

The journal foil bearing subroutine termed the "Hydrodynamics Program" (Figure 50) is a finite difference solution to the Reynolds equation, based upon the assumptions that:

- (a) The film clearance between the shaft and foil is small compared to the radius and length of the bearing.
- (b) The flow may be laminar or turbulent depending upon the local Reynolds number.





$R$  = Radius of curvature  
 $P$  = Tangential load  
 $M$  = Bending moment  
 $Q$  = Shear load  
 $a$  = Angle which subtends the element  
 $u$  = Tangential displacement  
 $v$  = Flexure displacement  
 $b$  = Rotation  
 $t$  = Thickness

Figure 54. Foil Geometry Coordinate System.

- (c) Wet surfaces - no slip at bearing surfaces is permitted.
- (d) The working fluid may be compressible or incompressible.
- (e) The velocity gradients across the fluid film are larger than other velocity gradients.
- (f) Axial and circumferential flows are permitted.  
Program solution for finite length bearings.
- (g) Body forces, viscosity and density may vary with position in the axial and tangential directions.
- (h) Nonsynchronous and squeeze film loading permitted.

Figure 55 illustrates the foil journal bearing geometry for the hydrodynamics solution. Figure 56 illustrates the tangential and radial velocity components  $U$  and  $V$ , respectively. With this geometry defined, the compressible Reynolds equation can be expressed as:

$$\frac{\partial}{\partial x} \left[ \frac{P}{k_x} \frac{h^3}{\mu} \left( \frac{\partial P}{\partial x} - \bar{X} \right) \right] + \frac{\partial}{\partial z} \left[ \frac{P}{k_z} \frac{h^3}{\mu} \left( \frac{\partial P}{\partial z} - \bar{Z} \right) \right] =$$

$$6 \left( P(U_0 - U_1) \frac{\partial h}{\partial x} + Ph \frac{\partial}{\partial x} (U_0 + U_1) + h (U_0 + U_1) \frac{\partial P}{\partial x} \right)$$

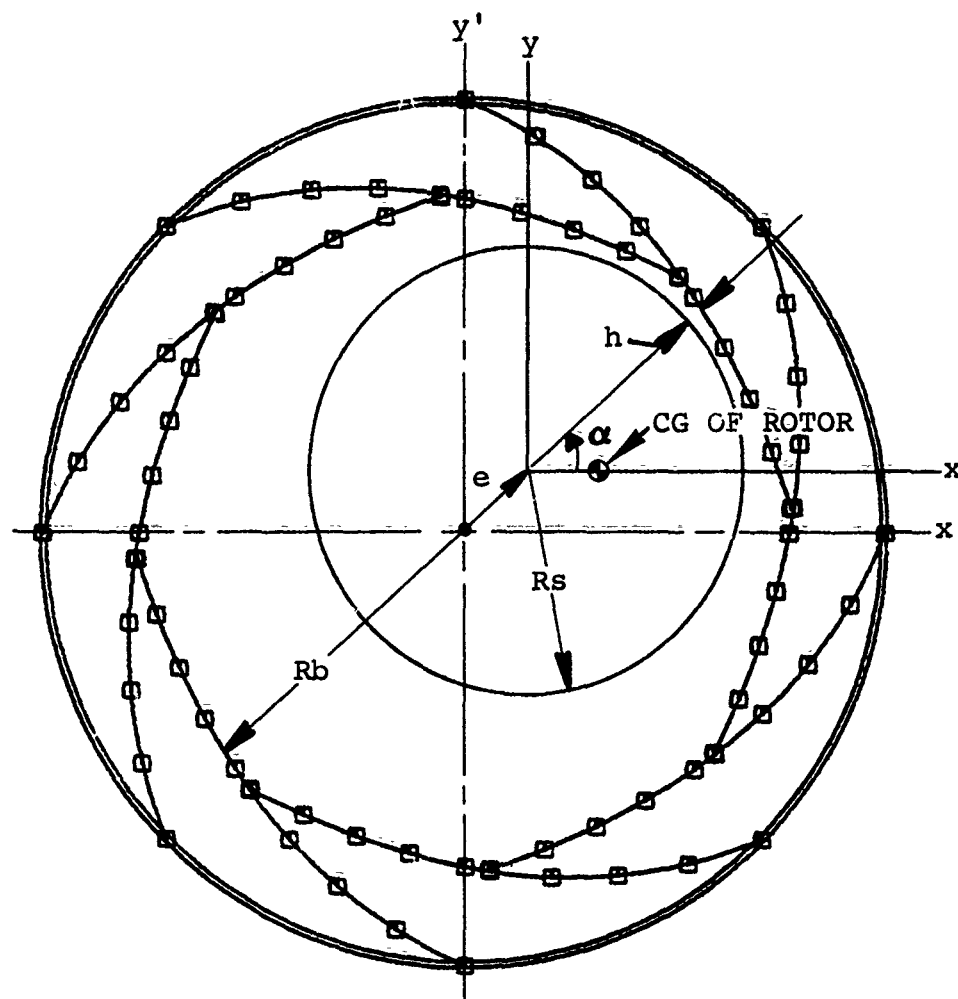
where:

$P$  = hydrodynamic pressure

$\rho$  = Density =  $P/RT$  (Isothermal conditions)

$\bar{X}$ ,  $\bar{Z}$  = body forces

$U_0$ ,  $V_0$  = velocity components at shaft surface



$x', y'$     FIXED FRAME AXES  
 $x, y$       WHIRL FRAME AXES

Figure 55. Foil Journal Bearing Geometry for Hydrodynamic Solution.

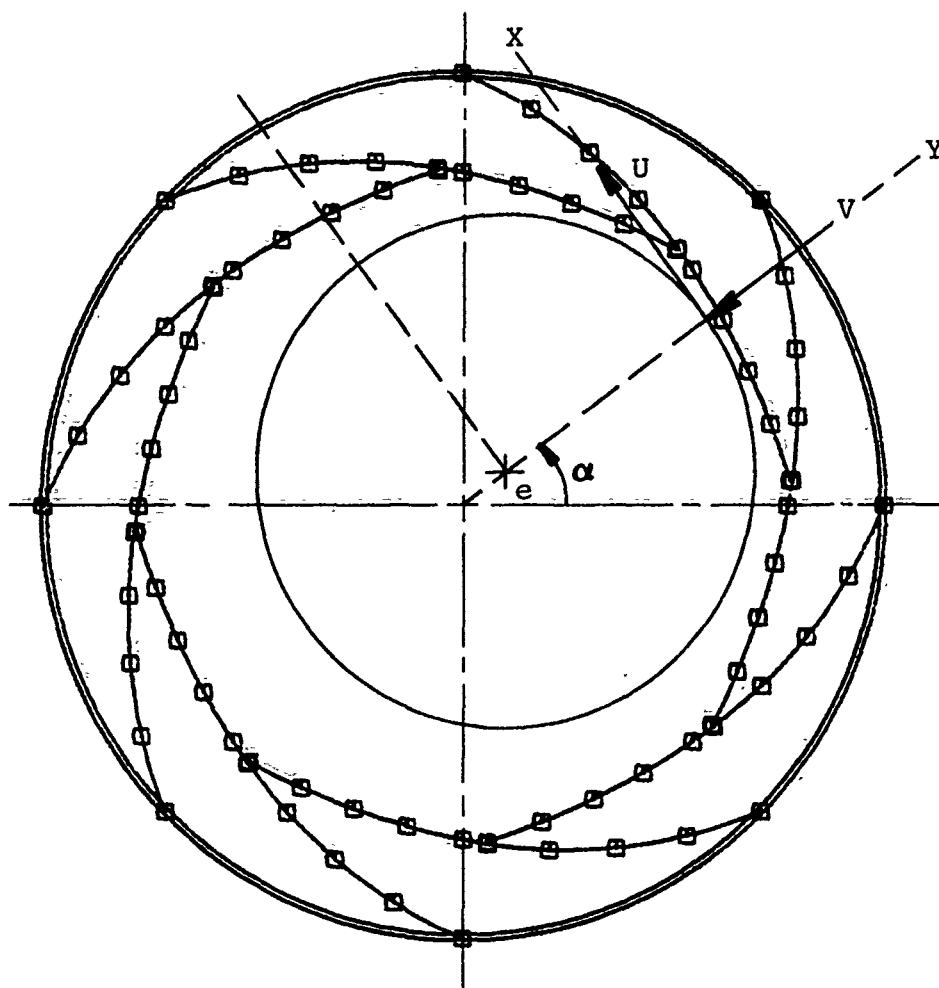


Figure 56. Foil Journal Bearing Tangential and Radial Velocity Components.

$U_1, V_1$  = velocity components at foil surface

$h$  = film thickness

$\mu$  = viscosity

and the turbulence constants  $K_x$  and  $K_z$  are given by:

$$K_x = 12 + 0.53(K^2 R_e)^{0.725}$$

$$K_z = 12 + 0.296 (K^2 R_e)^{0.65}$$

where  $R_e$  is the local Reynolds Number and  $K$  is the Prandtl's mixing length as indicated previously in Figures 36 and 37.

#### 3.3.2.4 Comparison of Analytical and Experimental Data for Elasticity Solution

Numerous test cases have been evaluated to demonstrate the program's capability in recognizing proper release, kinematic constraints, and foil overlap in duplicating experimental static stiffness data. A thorough examination of the elasticity program and correlation with experimental data has demonstrated the adequacy of this portion of the elasto-hydrodynamics journal bearing program. Some of these results are presented below:

- o Figure 57 illustrates a typical foil geometry and the coordinate system utilized in this study. Note that the positive direction of eccentricity ( $e$ ) has been established in the direction of the positive Y axis. Accordingly, a negative value of ( $F_y$ ) on the journal opposes a positive value of eccentricity. Further, a positive value of ( $F_x$ ) encourages forward precession (whirl), whereas a negative value of ( $F_x$ ) opposes forward whirl. The angle ( $\Psi$ ) is a geometric parameter and is a user input option to control the displacement vector (eccentricity) direction with respect to foil geometry.

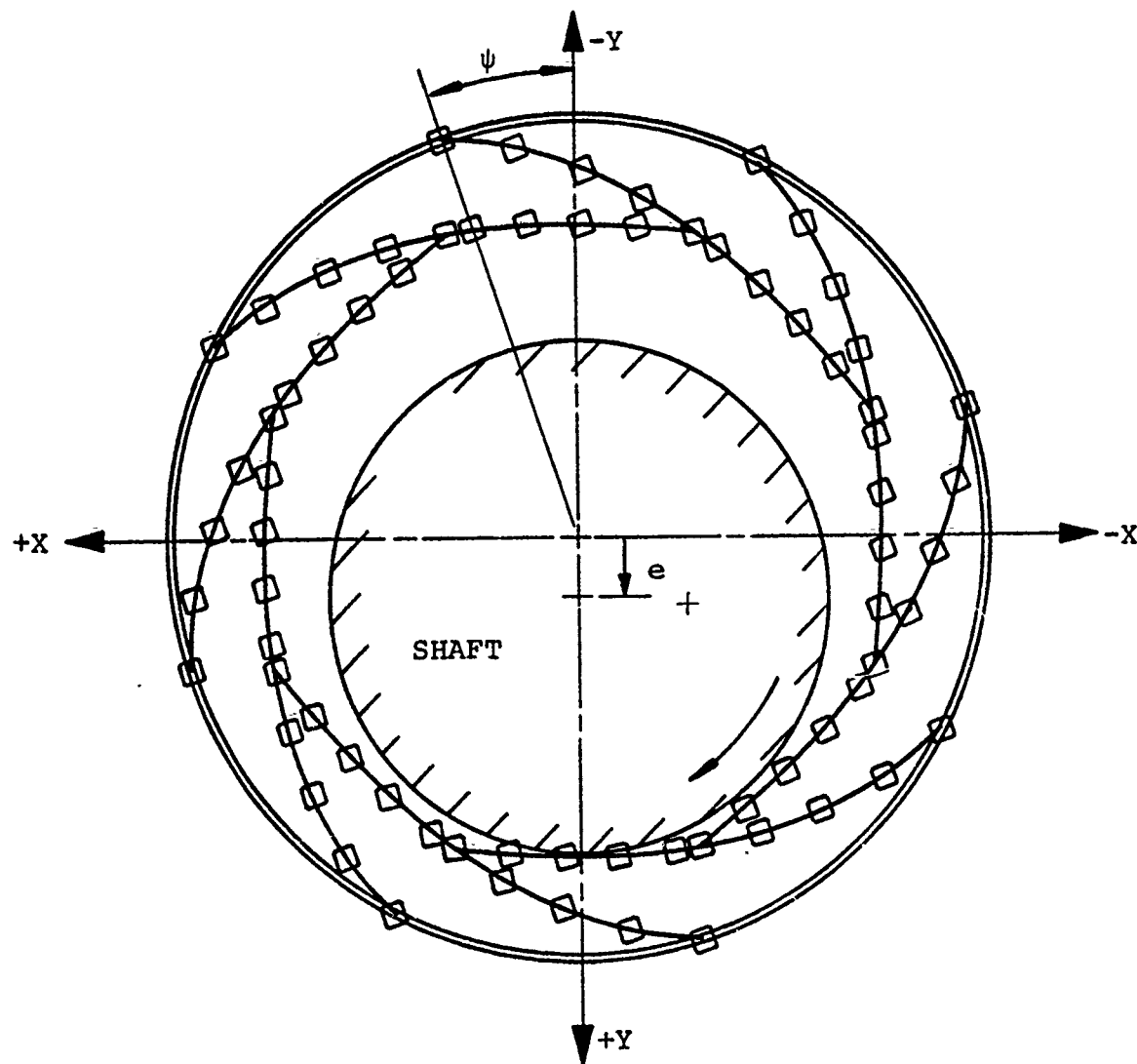


Figure 57. Geometry and Coordinate System for Elasticity Program

- o Figure 58 shows a comparison of experimental data and analytic data for a 0.0085-in. thick 16-segment foil coated with 0.001 in. of Teflon-S. As shown, excellent correlation was achieved.
- o Figure 59 is a comparison of analytic and experimental data for a 0.010-in. thick uncoated 8-segment foil. Two curves are present; one for the displacement vector (eccentricity) directed toward the trailing edge (T.E.) of a foil, the other with the eccentricity directed midway between two trailing edges of adjacent foils. It is interesting that both experimental and analytic data demonstrate the "stiffer" curve is produced when loading is directed midway between the trailing edges of two adjacent foils.
- o Figure 60 presents the data obtained for a 0.012-in. thick 12-segment foil coated with 0.001 in. of Teflon-S. Two curves for the experimental and analytic study are presented similar to those of Figure 59 for the 8-segment foil. It is noteworthy that, unlike Figure 59, the experimental curves for loading over the trailing edge and loading between adjacent foils cross at approximately 0.005-in. eccentricity. This same characteristic is duplicated at an eccentricity of 0.006 in. for the analytic data.
- o Figure 61 presents the loading obtained analytically, which represents the resultant orthogonal load  $F_x$  (see Figure 57), for the 12-segment foil studied in Figure 60. The magnitude of this load is small in comparison to the load resisting eccentricity ( $F_y$ ) of Figure 60. It is interesting to note the apparent symmetry when the loading direction is altered.

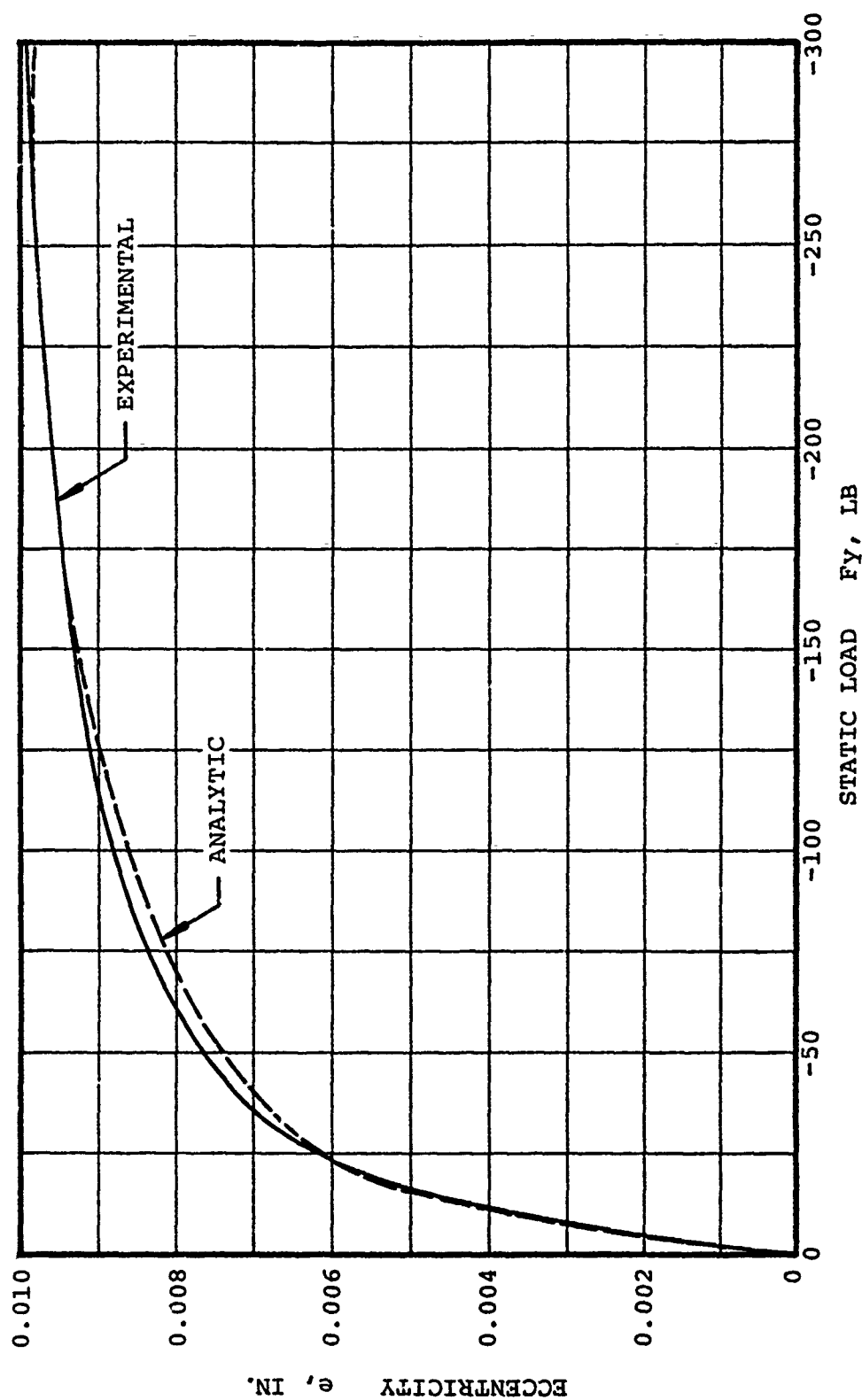


Figure 58. Sixteen-Foil Geometry Load Versus Eccentricity



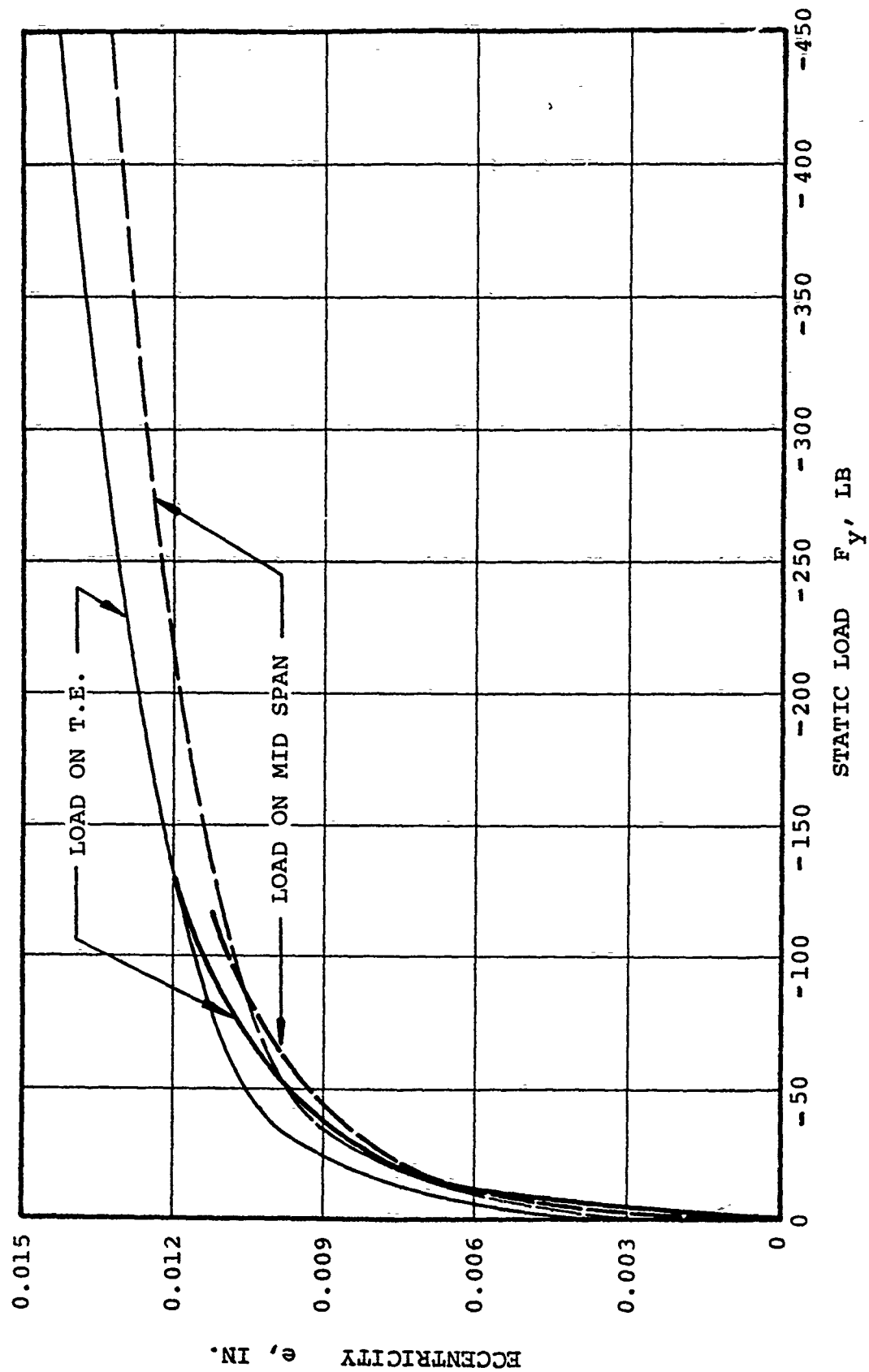


Figure 59. Eight-Segment Journal Bearing (0.010)

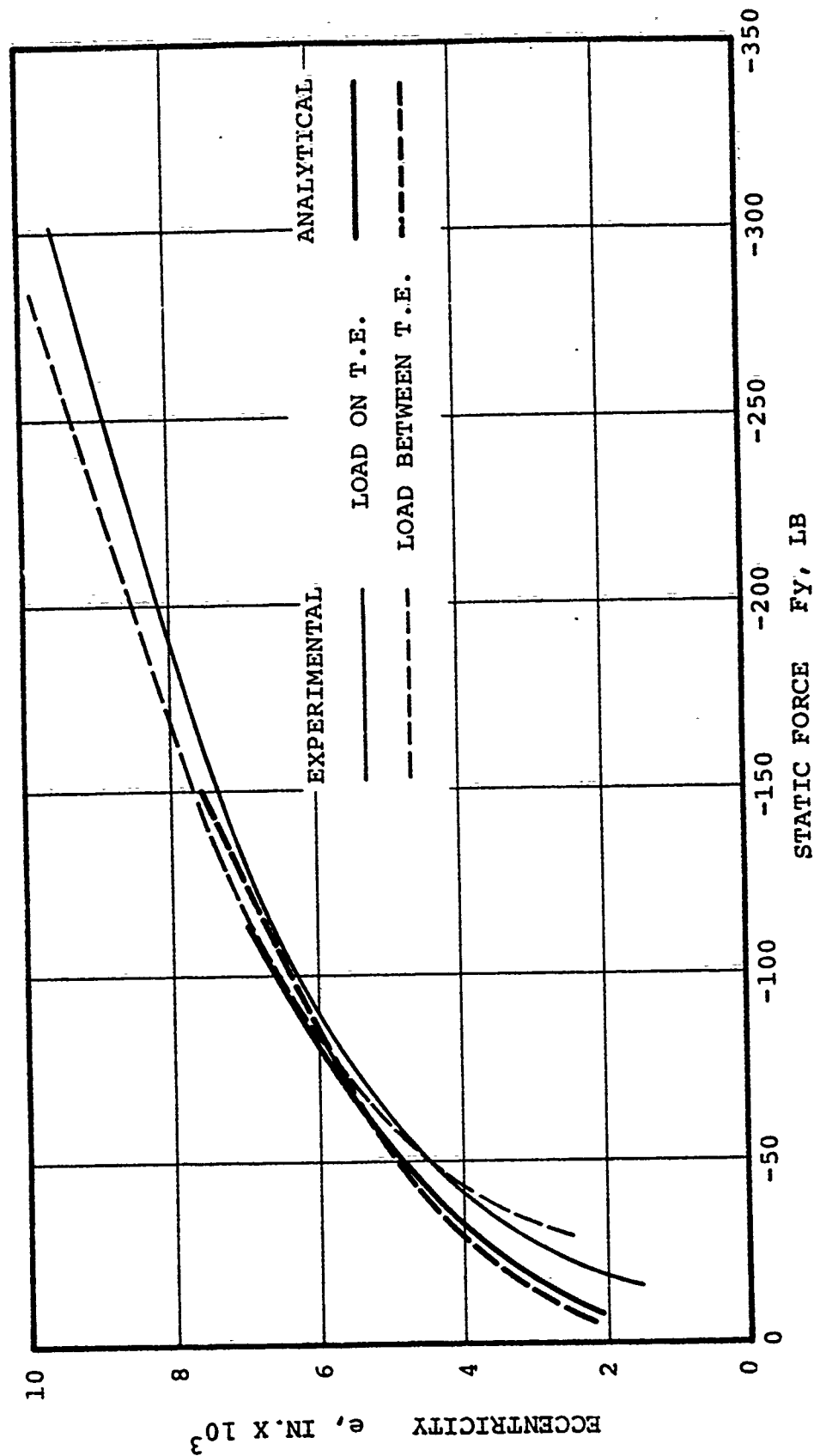


Figure 60. Twelve-Segment Foil Effect of Load Direction

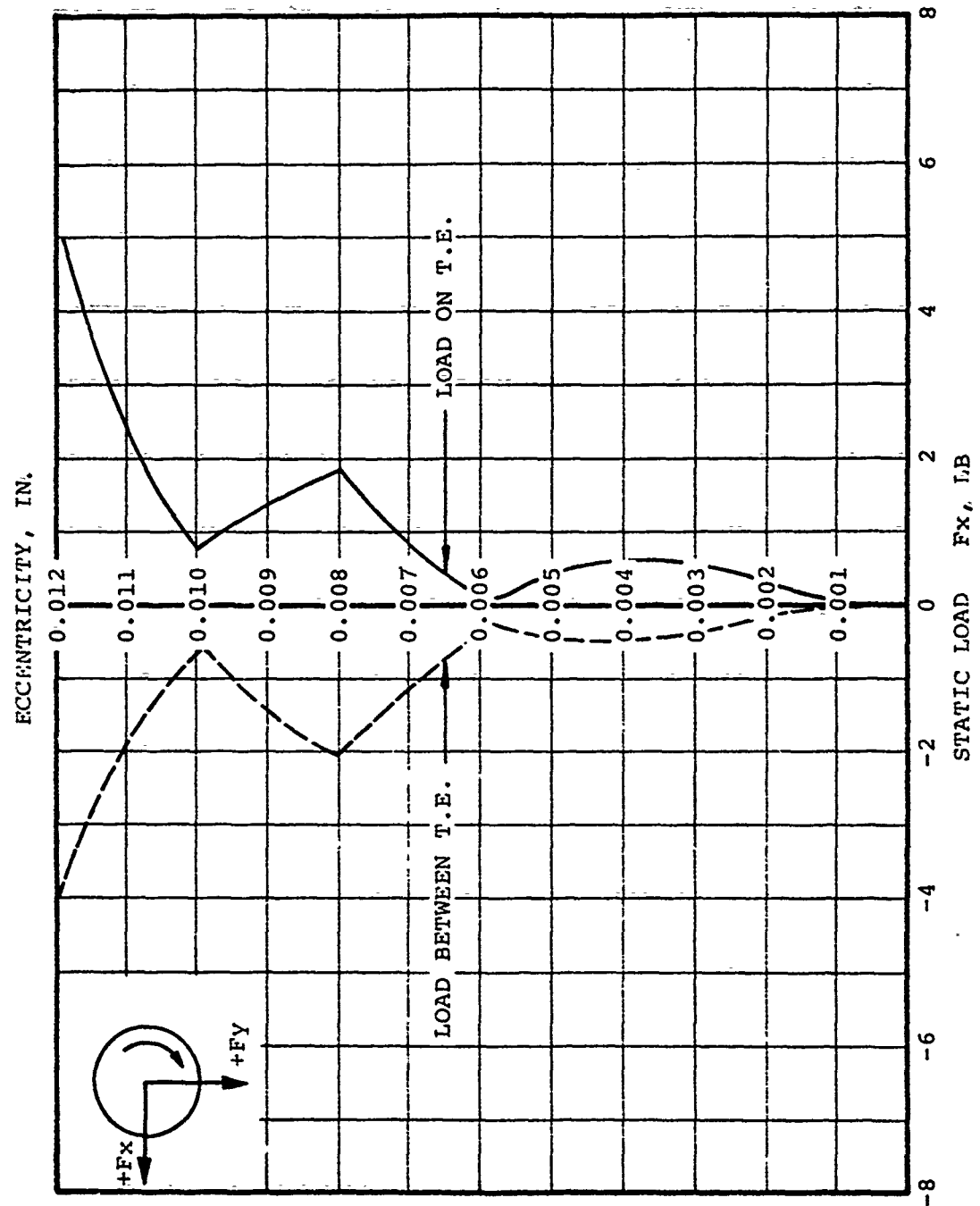


Figure 61. Twelve-Segment Foil Orthogonal Loading

- o Figure 62 is a 12-segment design analytic study of the effect of foil length on static stiffness. The solid line represents a minimum foil length (0.010 in. less than nominal) or a foil overlap of 47.2 percent. The "stiffer" dashed curve illustrates the load versus deflection data for a maximum foil length (0.010 in. greater than nominal) or an overlap of 47.7 percent (the nominal foil overlap is 47.5 percent).

#### 3.3.2.5 Foil Bearing Analytical Program Preliminary Results

Preliminary results of the nonlinear elasto-hydrodynamics program provided solutions that converged to an acceptable elasticity configuration, as well as an acceptable hydrodynamics solution.

Figure 63 represents the symmetric pressure profile for the zero eccentricity case of an 8-segment foil bearing. The computer solution verified the no-load configuration and the symmetry of pressure distribution.

Figure 64 is the same 8-segment configuration with an eccentricity of 0.004 in. The nonsymmetric pressure profile illustrates the pressure loading to oppose eccentricity.

#### 3.4 Materials Development

The foil bearing concept is based upon a rotating component supported on a thin film of air (or other gas), using compliant foils as the mating surface (a minimum speed is required to develop an adequate film). This behavior allows non-contact conditions to exist during most of the bearing operation. However, contact does occur when the shaft rotational speed is below that required

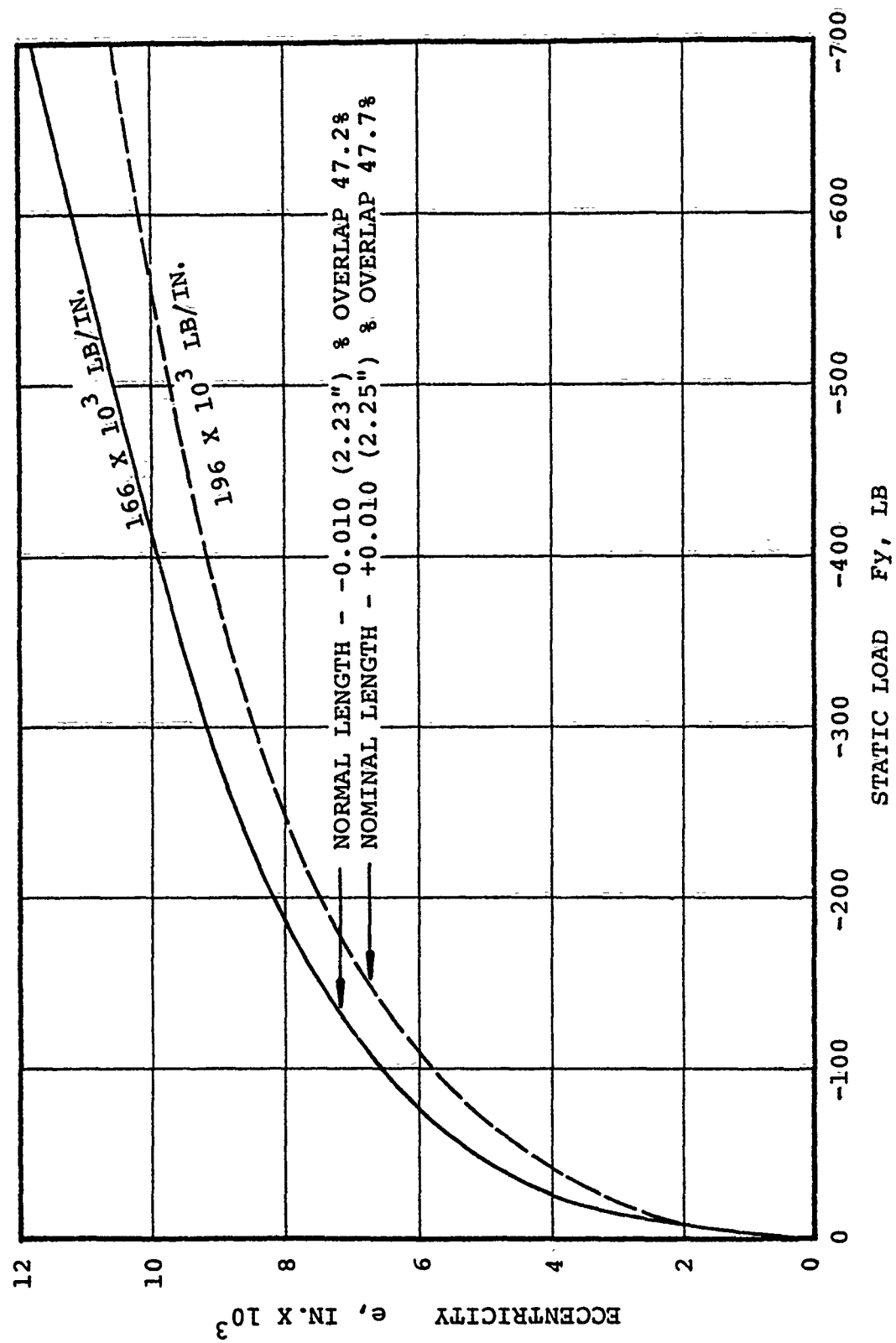


Figure 62. Twelve-Segment Foil Effect of Length

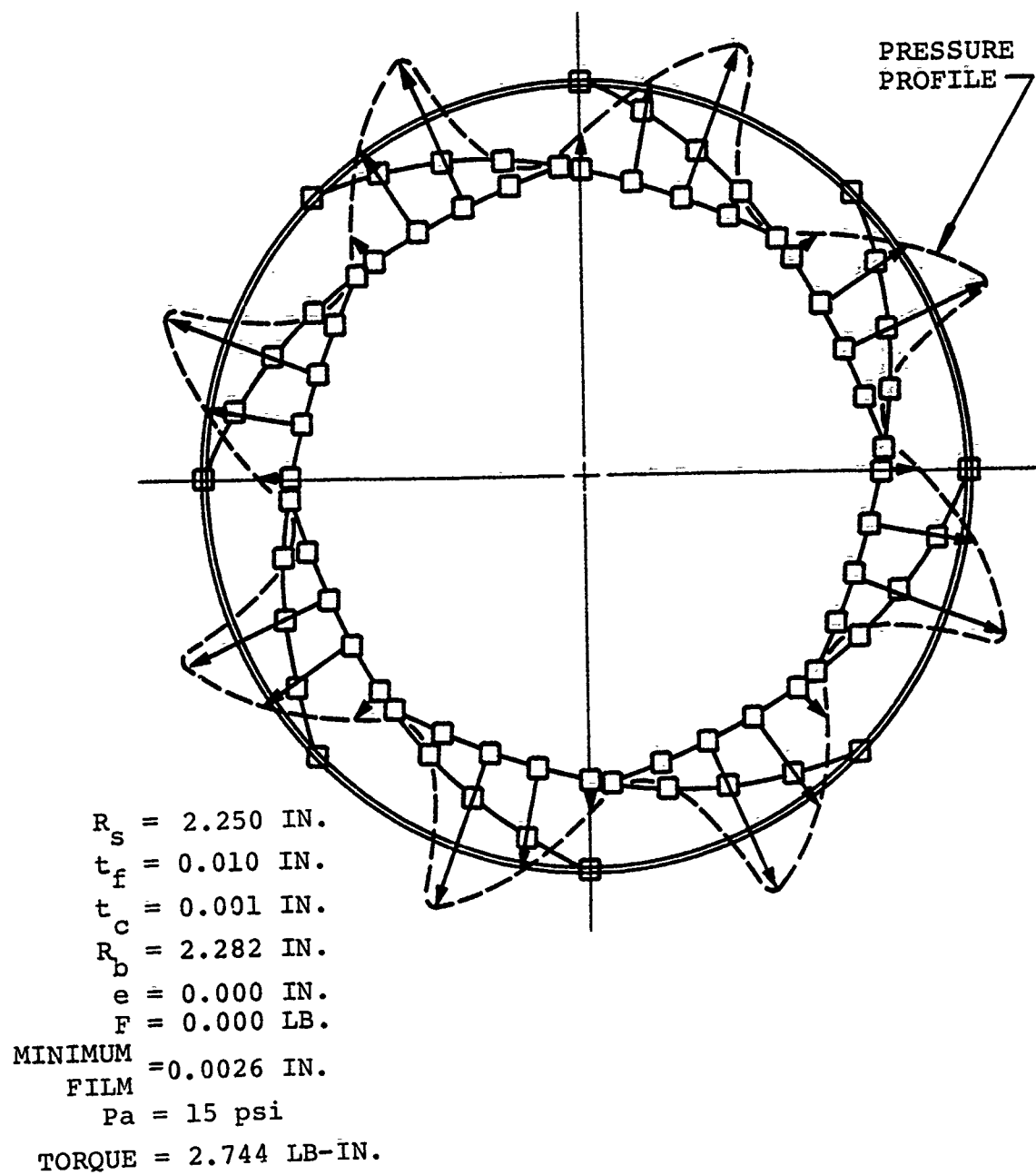


Figure 63. Eight-Segment Foil Center Plane Pressure Distribution

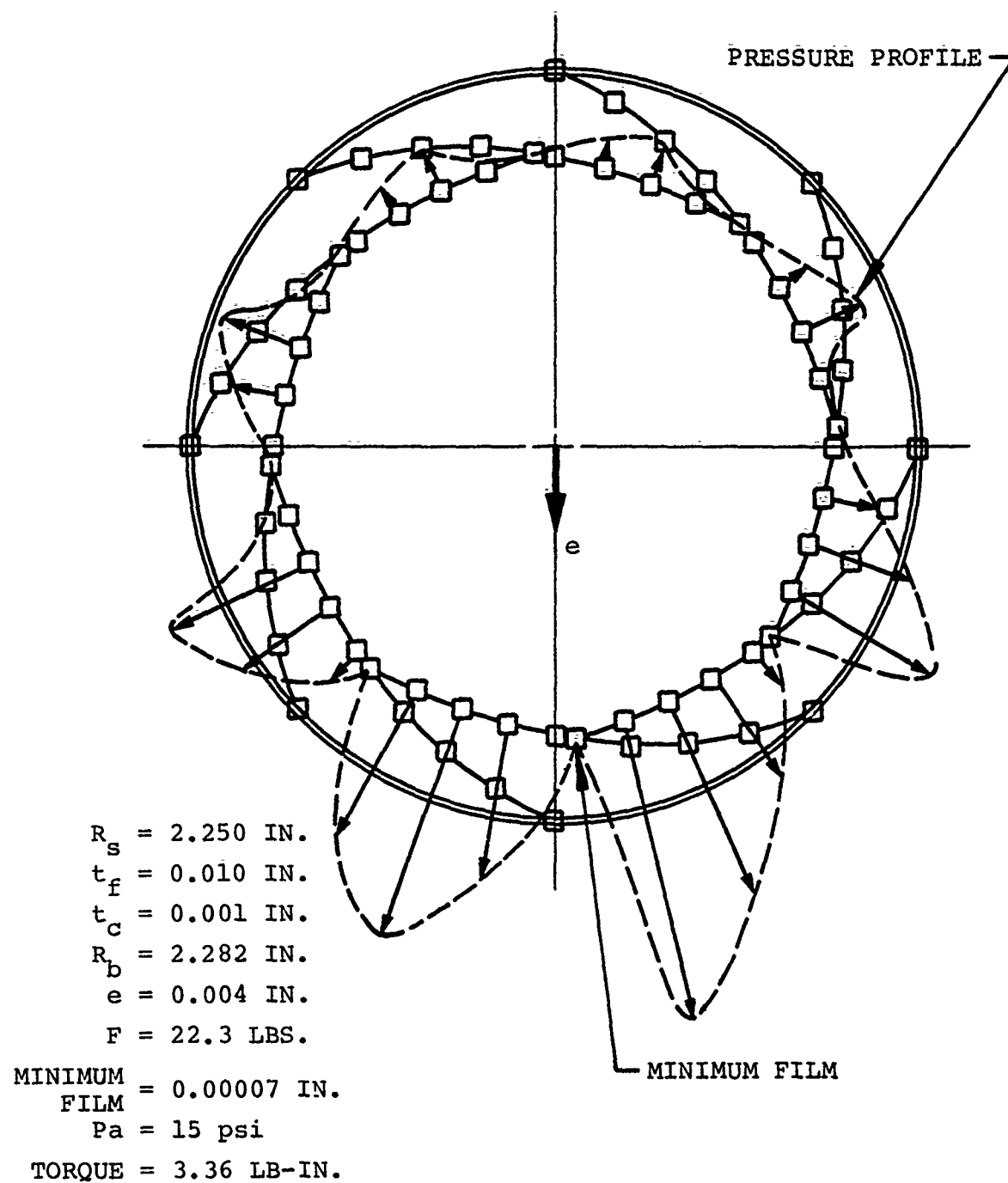


Figure 64. Eight-Segment Foil Center Plane Pressure Distribution

to develop a supporting hydrodynamic film, i.e., during turbomachine start-up or shut-down. At this time bearing surface lubrication becomes important and is provided in the form of a solid coating having optimum low friction, wear resistance, and a tolerance for ingested particulate contaminants, as well as acceptable properties in the temperature range from -65 to 1200°F.

In addition to coatings, it was necessary to specify substrate alloys, for rotating shafts and bearing foils, that were compatible with coatings and also capable of extended service at temperatures to 1200°F. Materials development activities culminated in selecting appropriate coatings and substrate alloys for use in thrust and journal foil bearing test rigs at elevated temperatures. Material development goals were as follows:

- (a) Identify and evaluate candidate foil coating materials for temperature capability to 1200°F.
- (b) Evaluate foil materials that show promise of a minimum loss in strength and elastic modulus from room temperature through the maximum operating temperature (1200°F).
- (c) Select the most appropriate coatings and alloys to provide the best combination of properties for operation in bearing test rigs.
- (d) Demonstrate survivability under simulated engine operating conditions (bearing test rigs)

Within the framework of these goals a materials development program was conducted as described in the following section.



### 3.4.1 Approach

To determine temperature requirements for substrate and coating materials, the following bearing temperature requirements were established:

- (a) A maximum inlet air temperature of 564°F (compressor discharge).
- (b) An additional temperature increment to provide adequate heat sink capability of the inlet air to cool the bearing (bearing therefore will operate 200-300°F above inlet air temperature).
- (c) An additional temperature increment due to frictional heating during bearing contact periods (approximately 100° to 200°F).
- (d) An additional temperature increment of approximately 100 to 200°F due to thermal soak back from a hot turbine (occurs when the engine is restarted soon after shutdown).

These define a requirement of up to 864°F for continuous bearing operation. Allowing for frictional heating, thermal soakback and a small safety margin, 1200°F was selected as the maximum temperature capability goal for bearing materials.

The above requirements led to organizing the materials development program into two general activities, described below:

Preliminary Materials Screening - Included a review of the literature to define candidate coatings and substrate alloys for evaluation in the program. Metallurgical evaluations were conducted on a variety of coatings and substrate alloys to define appropriate materials for wear rig testing.

Wear Rig Evaluations - Selected coatings were applied to bearing surfaces and evaluated for friction and wear at temperatures to 1200°F in a foil bearing materials test rig. Other evaluations of coating performance such as friction measurement and coating appearance were also conducted.

A materials development logic diagram is provided in Figure 65, showing the sequence of events leading to identification of the best materials (coatings and alloys) for use in the thrust and journal bearing test rigs. Final materials selection for bearing rigs was made using information gained throughout the program, and included fabrication and processing factors as well as oxidation behavior and wear rig performance.

#### 3.4.2 Materials Survey

Candidate coating and substrate alloy materials that appeared capable of meeting program goals, and selection rationale are discussed in the following paragraphs:

##### 3.4.2.1 Substrate Alloys

A previous AiResearch funded activity utilized several shaft construction alloys: Inconel 718, Inconel X-750, AF2-1DA, Haynes 25 (HS-25), and AMS 6250. Of these, Inconel 718 and X-750 and Haynes 25 are the best choices when considering fabricability, availability, and mechanical properties at 1200°F. These considerations led to selection of Inconel 718 for the wear test rig and the journal bearing rig shaft components. Inconel 718 also demonstrated compatibility with several coatings ( $\text{Cr}_2\text{O}_3$ ,  $\text{Al}_2\text{O}_3$ , Chromium, and AFSL 28) in the above activity.

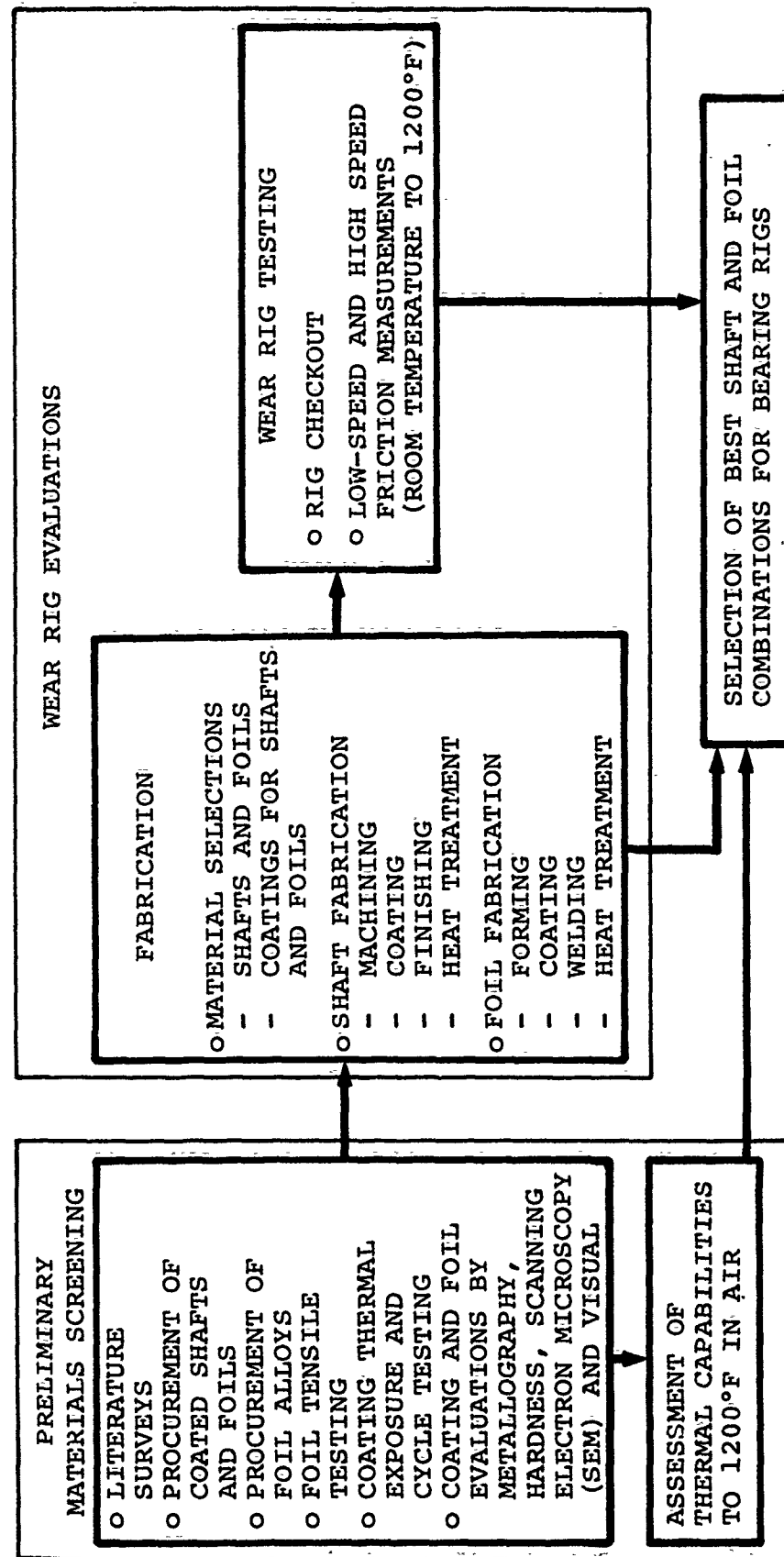


Figure 65. Materials Development Logic Diagram

Selecting alloys for foil construction was more difficult because of the higher temperatures generated at the coating surface during turbomachine start-up or shutdown. Several superalloys were considered, as well as the more available stainless steels. Candidate alloys are presented in Table 6 with several properties that would influence foil performance during coating as well as use in a bearing. Observations of this and other data establish the following:

- (a) Strength is generally acceptable in the temperature range 800°-1200°F.
- (b) Thermal expansion of these alloys is typically quite high compared to organic or ceramic materials that would be considered for coatings (presents fabrication and performance difficulties).
- (c) Thermal conductivity of these alloys is generally quite low, thus limiting the ability of the foil to conduct heat away from the coating during rubbing.
- (d) Data for long term exposures at 1200°F was generally not available in the literature and no assessment could be defined quantitatively (metallurgical stability or oxidation resistance).

Stainless steels and other iron base alloys were eliminated from consideration due to lower strength and elastic modulus and to anticipated poor oxidation resistance at elevated temperatures. The best alloys for foils were the nickel base alloys of the gamma-prime strengthening type (Inconel 718, X-750, and 706) from a standpoint of strength, oxidation resistance, and modulus. Cobalt base alloys have good oxidation resistance but their strength and elastic modulus are lower than the above nickel alloys. Therefore, the following alloys were selected as initial candidates for foil materials:

TABLE 6  
FOIL CANDIDATE ALLOYS AND PROPERTIES

ALLOY	NOMINAL COMPOSITION	CONDITION	TENSILE PROPERTIES				PHYSICAL PROPERTIES*				USUAL MAX. SERV. TEMP. (°F)
			TEMP. (°F)	UTS (ksi)	YTS (ksi)	EL. (%)	TEMP. (°F)	$E_m$ (psi x 10 <sup>6</sup> )	CTE** (°F x 10 <sup>-6</sup> )	CTC BTU-in ft <sup>2</sup> -hr-°F	
304	68Fe, 19Cr, 10Ni, 0.08C	Annealed	RT 1200	85 45	35 16	50 --	RT 1200	(28.6) 21.1	8.6 10.4	95 165	750
446	72Fe, 25Cr, 0.25M max, 0.2C max	Annealed (1400-1600°F)	RT 1000	80 40	50 --	25 --	RT --	29 --	5.8 --	145 --	750
17-4 PH	76Fe, 16Cr, 43Ni, 3.3Cu, 0.3Cb, 0.04C	1900°F (1/4 hr) AC + 1025°F (4 hr) AC	RT 1000	170 105	165 100	15 15	RT 1000	(38.5) (22.0)	(6.2) (6.9)	(113) (160)	900
17-7 PH	74Fe, 17Cr, 7Ni, 1Al, 1Mn, 0.09C	Mill anneal (1900) + Fabricate +1400 (1 1/2 hr) Air Cool +1050 (1 1/2 hr) Air Cool (TH-1050)	RT 900	193 124	192 100	10 10	RT 900	29.0 --	5.6 (6.7)	(110) 146	900
PH15-7 MO	73Fe, 15Cr, 7Ni, 2.5Mo, 1Al, 0.09C	Mill Anneal (1950) + Fabricate +1400°F (1 1/2 hr) AC +1050°F (1 1/2 hr) AC (TH-1050)	RT 1000	212 115	205 105	7 19	RT 1000	29.0 --	6.1 6.6	104 158	--
AMCO 21-6-9	65Fe, 21Cr, 6.5Ni, 9Mo, .08 or .04C	Annealed 1950°F, AC	RT 1100	110 68	64 28	42 30	RT 1000	28.5 --	9.3 10.6	(90) 156	--
A-286	56Fe, 25Ni, 15Cr, 2Ti, 1.3Mo, .15Al, 0.3V, 1.5Mn, .05C	1650°F (2 hr) OQ + 1300°F (16 hr) AC	RT 1200	195 (110)	102 (90)	28 10	RT 1200	29.1 22.2	9.2 9.9	88 172	1200
Hastelloy S	69Ni, 15.5Cr, 14.5Mo, 1Fe, .02C	1950°F, AC	RT 1200	116 85	49 28	65 72	RT 1200	30.8 25.2	6.4 7.5	97 163	--
Hastelloy X	48Ni, 22Cr, 9Mo, 18.5Fe, 0.8Al, 1.5Co, 0.1C	2150°F, RAC	RT 1200	114 83	52 40	43 37	RT 1200	28.5 22.3	7.7 8.6	(63) (151)	2000
INCO 706	43Ni, 34Fe, 16Cr, 3Cb+Ta, 2Ti, 0.4Al, 1Co max., 0.06C max.	1850°F, AC + 1550°F (3 hrs) AC + 1325 (8 hrs) FC to 1150°F for total of 18 hrs (Cond. A)	RT 1200	186 134	148 116	20 18	RT 1200	30.4 24.7	7.8 (8.8)	87 (158)	--
INCO 617	54Ni, 22Cr, 12.5Co, 9 Mo, 1Al, 0.07C	2150°F, Cooled and Cold Rolled	RT 1200	112 85	47 30	53 60	RT 1200	-- --	6.4 8.0	94 161	--
INCO 718	53Ni, 19Fe, 18Cr, 5Cb 3Mo, 1Ti, 0.5Al, 0.05C	1800°F + 1325°F (8 hr) FC to 1150°F (18 hrs) AC	RT 1200	180 140	150 115	12 5	RT 1200	29.0 23.7	7.2 8.6	77 148	1100
INCO X-750	74Ni, 15Cr, 7Fe, 2.5Ti, 0.85Cb, 0.8Al, 0.04C	Cold rolled + 1300°F (20 hrs) AC	RT 1200	177 123	122 105	27 6	RT 1200	31.0 25.5	7.0 8.4	83 143	1200
HS-25	52Co, 20Cr, 15W, 10Ni, 3Fe, 0.10C	2150°F, Rapid Air Cool	RT 1200	135 103	65 35	60 35	RT 1200	(32.6) (25.6)	6.8 8.24	(64.9) (150)	1800
Haynes 188	40Co, 22Cr, 22Ni, 14W, 1.5Fe, 0.06Al, 0.08C	2150°F, Spray Quench	RT 1200	130 93	65 38	69 70	RT 1200	33.5 26.9	6.0 8.5	76 156	1800
Rend 41	50Ni, 19Cr, 11Co, 10Mo, 5Fe, 3Ti, 1.4Al, 0.08C, 0.0068	1975°F, WQ + 1950°F (0.5 hr) AC + 1400°F (16 hr) AC	RT 1200	195 171	155 135	14 8	RT 1200	31.6 25.9	7.8	80 146	1400
Waspaloy	58Ni, 19Cr, 13Co, 4Mo, 3Ti, 2.0Fe, 1.4Al, 0.10C max.	1825°F (4 hr) AC + 1550°F (4 hr) AC + 1400°F (16 hr) AC (Cond. B)	RT 1200	165 150	117 99	29 23	RT 1200	30.2 25.5	6.8 8.0	72 140	1400

\* $E_m$  = Youngs Modulus, CTC = Mean Coefficient of Thermal Expansion, CTC = Coefficient of Thermal Conductivity  
 \*\*Room Temperature CTE is 70-200°F Mean Value. Other values are mean of 70° to indicated temperature.  
 ( ) Values in parentheses are estimated or interpolated.

- (a) PH 15-7Mo or 17-7PH, 304L and 446 stainless steels.
- (b) A-286 iron base superalloy.
- (c) Nickel base superalloys Inconel X-750, Inconel 718, Hastelloy X and Rene' 41.
- (d) Haynes 25 or 188 cobalt base superalloys.

These alloys were chosen primarily to provide a wide range of compositions to evaluate coating adherence and oxidation behavior. As indicated in Table 6, several alloys are of lower strength and could be considered only for applications below 1000°F.

#### 3.4.2.2 Coatings

One of the more critical factors affecting the successful application of gas lubricated foil bearings to gas turbine engines deals with the selection of a solid lubricant for bearing surfaces. The current program requires bearing operation at temperatures to 1200°F and demands a solid film lubricant which is advanced beyond current commercially available lubricants such as Teflon, molybdenum-sulfide ( $\text{MoS}_2$ ), graphite, or graphite-fluoride. Materials that may therefore be considered for solid film lubricants must display the following properties at room and 1200°F operating temperatures.

- o Lubricative qualities or high hardness
- o Satisfactory wear life
- o Adequate oxidation resistance and bonding
- o Compatibility with substrate materials

- o High temperature stability (will not form deleterious compounds upon long term exposures)
- o Adequate strength and ductility
- o Satisfactory tolerance for ingested materials

These requirements eliminate organic materials as well as many other coating compounds due to the temperature environment. Finding a single compound that meets all of the requirements also is quite difficult and therefore, the use of composite materials such as NiCr (metal) +  $\text{Cr}_3\text{C}_2$  (ceramic) or the possible use of one type coating on the rotating component and another coating on the stationary portion of the bearing were also considered. The literature provided guidelines for selecting appropriate materials as well as, in some cases, providing material choices and evaluations for the anticipated temperature range. Table 7 lists materials tested, based upon data in the literature, or selections based upon desirable physical and mechanical properties such as high hardness, oxidation resistance, high melting point, low friction coefficient, desirable crystal structure (hexagonal, close-packed), thermal expansion and thermal conductivity. Several materials<sup>(2,3)</sup> indicated survival of high speed overload, large number of start/stop cycles, and good performance over the entire temperature range.

The literature recommended  $\text{Cr}_3\text{C}_2$ ,  $\text{Cr}_2\text{O}_3$ , variations,<sup>(4)</sup>  $\text{CaF}_2$  or  $\text{BaF}_2$  compositions<sup>(5,6,7)</sup>, Ag-Re<sup>(8)</sup>, or  $\text{B}_4\text{C}$ <sup>(9)</sup> as the more promising high temperature materials. Comments relating to the value of other materials such as ceramic oxides and cobalt-containing metallics<sup>(10)</sup> influenced the selection of other materials listed in Table 7. Many materials qualified as candidates for coatings and therefore selections for screening efforts were representative of various classes of materials.

(2,3) Superscripts refer to the list of references at the back of this report.

TABLE 7  
COATING MATERIALS SELECTED FOR PROGRAM EVALUATION

COATING	VENDOR	BASIS FOR EVALUATION
<u>Plasma Spray or "D-gun"</u>		
WC-9Co	Union Carbide Corp.	Shaft coating; hard bindered carbide
WC-(W,Cr)C-NiCr		Shaft coating; carbide plus nichrome
(W,Ti)C-15Ni	LW-5	Shaft coating; mixed carbides
Cr <sub>3</sub> C <sub>2</sub> -20NiCr	WT-1	Shaft coating; carbide plus nichrome
Cr <sub>2</sub> O <sub>3</sub> -40Cr	LC-1C	Shaft coating; oxide plus binder
Co-28Mo-8Cr-2Si	LC-9	Shaft coating; hard phase in Co matrix
Co-25Cr-10Ni-7W	Dupont Corp. (Tribaloy-400)	Shaft coating; improved oxidation resistance
	Metco (45VF)	
<u>Slurry Application</u>		
SiO <sub>2</sub> -Cr <sub>2</sub> O <sub>3</sub> -Al <sub>2</sub> O <sub>3</sub>	Kaman Sciences (SCA)	Shaft coating; mixed oxides with Cr <sub>2</sub> O <sub>3</sub>
Cr <sub>2</sub> O <sub>3</sub>	Kaman Sciences (DES)	Foil coating; Cr <sub>2</sub> O <sub>3</sub>
(Ba,Ca)F <sub>2</sub>	NASA	Foil coating; mixed fluorides with glass
(Ba,Ca)F <sub>2</sub>	National Process Ind.	
	Mrionite 2500	Foil coating; mixed fluorides
<u>Sputtered</u>		
Cr <sub>2</sub> O <sub>3</sub>	Vacuum Tech Assoc (sputtered)	Foil coating; Cr <sub>2</sub> O <sub>3</sub>
Cr <sub>3</sub> C <sub>2</sub>		Foil coating; Cr <sub>3</sub> O <sub>2</sub>
Cr <sub>2</sub> O <sub>3</sub> +Al <sub>2</sub> O <sub>3</sub>		Foil coating; mixed oxides
B <sub>4</sub> C		Foil coating; carbide
TiC	Vacuum Tech Assoc (sputtered)	Foil coating; carbide
TiB <sub>2</sub>		Foil coating; boride
TiB <sub>2</sub> +Au overcoat		Foil coating; gold overcoat on boride
TiB <sub>2</sub> +CaF <sub>2</sub> overcoat		Foil coating; CaF <sub>2</sub> overcoat on boride
Tribaloy-400	Vacuum Tech Assoc (sputtered)	Foil coating; metallic
Si <sub>3</sub> N <sub>4</sub>		Foil coating; nitride
TiN		Foil coating; nitride
Cr <sub>2</sub> O <sub>3</sub> +Au opposite side		Foil coating; gold for heat dissipation
<u>Other</u>		
NiCo	AiResearch-electroplated	On both shaft & foil, Cobalt-oxide
Co-20Cr-15W-10Ni	AiResearch (Haynes 25 metal)	On both shaft & foil, Cobalt-oxide
Teflon-S	Thermtech Engr.	Foil coating, baseline material



Generally, the metallic type coatings were placed on the rotating component of the bearing as suggested by Murray<sup>(3)</sup> to reduce metal transfer. The following coatings were placed on both shaft and foil: NiCo, Kaman Cr<sub>2</sub>O<sub>3</sub> (DES and SCA), Tribaloy-400 and HS-25 (not a coating, typically used as an oxidized metal). Most, but not all of the coatings (Table 7) were evaluated in the materials screening activity (Paragraph 3.4.3). Some were selected after screening activity was concluded, and integrated into wear rig testing. These included NiCo, Teflon-S and Mrionite-2500. Discussions of these test activities as well as other materials evaluations are contained in following paragraphs.

#### 3.4.2.3 Fabrication and Process Considerations

The application of materials to foil bearings required additional considerations beyond their physical and mechanical properties. Matching a coating with substrate demands consideration of fabrication methods, repair techniques and integration with test rig design requirements. Chemical compatibility between coating and substrate, as well as coated surface-to-coated surface also was of concern.

##### 3.4.2.3.1 Chemical Compatibility

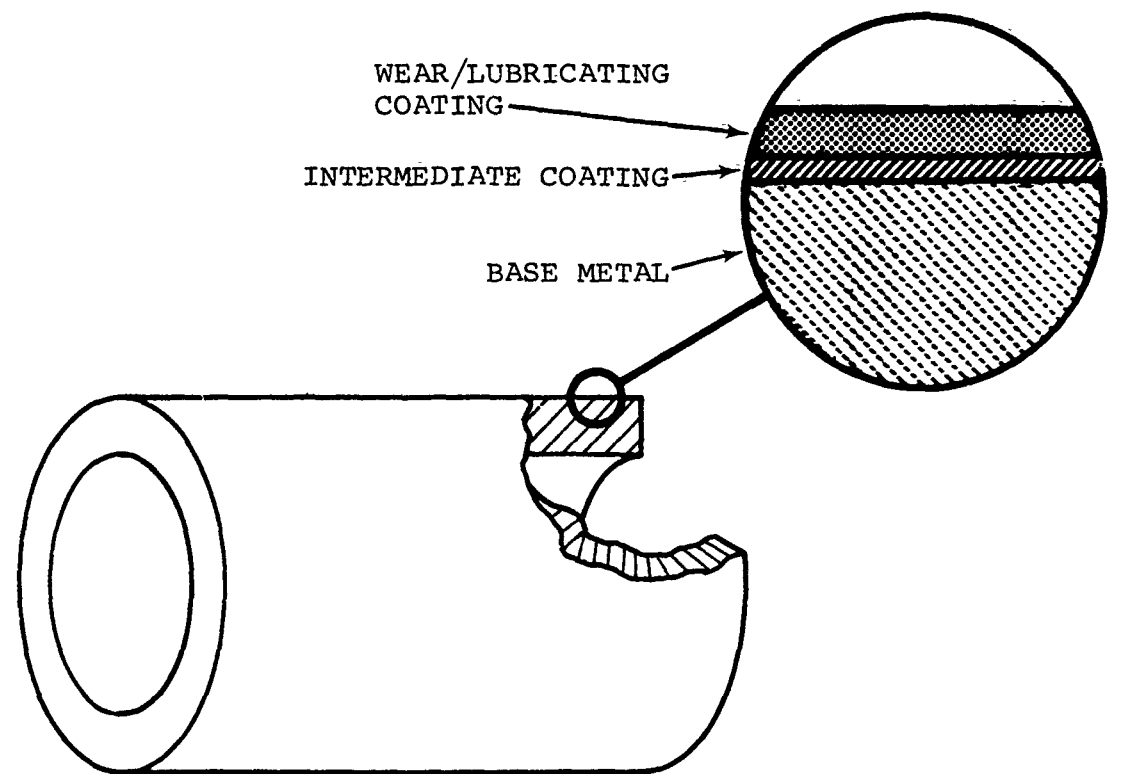
Chemical reactions can occur between materials at high temperatures that are not observed at ambient temperatures. Compatibility of the coating/substrate combinations served as one of the selection criteria and defined a need for stable materials. Only a few alloys and coatings evaluated in the program were expected to present compatibility problems, and included the iron base alloys and the fluoride coatings.

#### 3.4.2.3.2 Fabrication Requirements

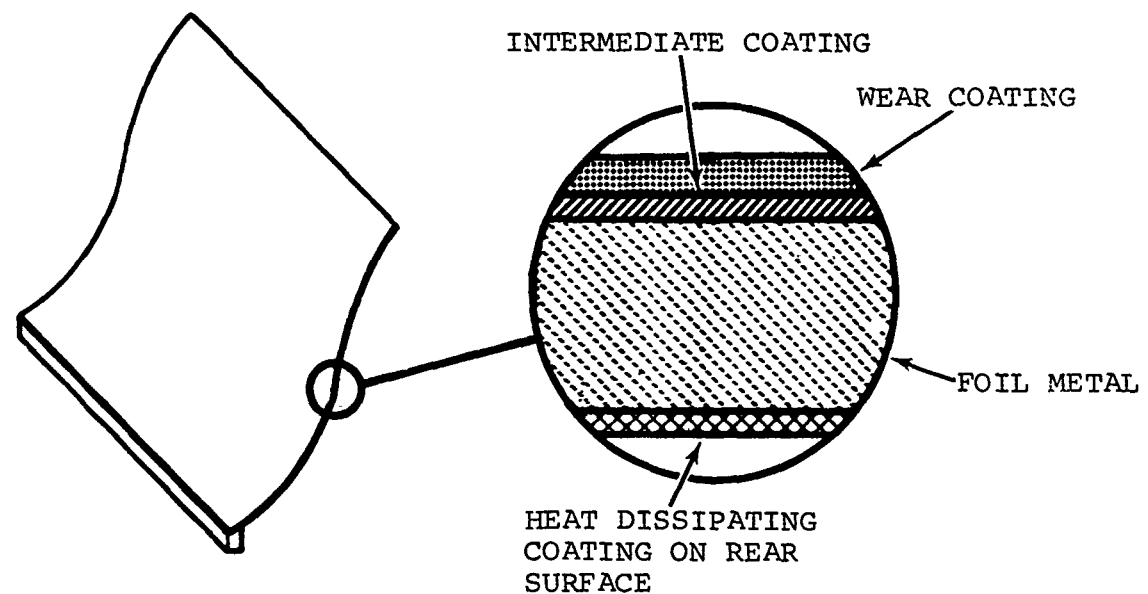
Fabrication procedures for coated shafts and foils were defined by comparing the individual heat treatment requirements of the coating and alloy, and by the appropriate manufacturing sequence including cleaning, forming, machining and quality control inspections. The typical configuration of coated components is illustrated in Figure 66, where more than one coating is used to obtain optimum performance. Intermediate coatings were used to gain desirable wear properties or improved bonding between the outer coating and the alloy substrate. An outer lubricative layer could be used over an intermediate coating which had good hardness or wear resistance. These are some of the coating approaches used during the program and will be defined (Paragraph 3.4.3) in detail for each of the coated components.

Wear resistant and/or lubricative coatings were considered for both foils and shafts. A shaft can accept a wide variety of coatings, especially very hard and/or thick ones if required. The foils, however, require a relatively thin coating (less than 0.001-in. thick), with some degree of flexibility. A wide variety of techniques may be used to apply coatings to metal substrates, as follows:

1. Dipping, spraying, or brushing followed by a thermal cure
2. Plasma spraying
3. Electrophoresis
4. Electrodeposition
5. Vacuum deposition
6. Sputtering
7. Ion Plating
8. Chemical diffusion (such as gas sulfiding or seleniding)



COATED SHAFT CONFIGURATION



COATED FOIL CONFIGURATION

Figure 66. Typical Coated Shaft and Foil Configurations

Since temperature requirements of the program preclude using organic and other low temperature coatings, only coatings with a temperature capability greater than 750°F were considered. Limited testing was also conducted with Teflon-S as a baseline bearing coating.

Coated component fabrication was therefore based upon many factors and varied from coating to coating. Generally, fabrication procedures for shafts differed somewhat from foils. Shaft outside diameters were achieved by one of two approaches. In the first, the shaft was machined to final dimension with a high quality finish, which would accommodate very thin 0.00004-in. (10,000 angstroms) sputtered coating. The second approach involved machining to approximately 2-6 mils undersize on the outside diameter with a rough finish, to accommodate thick coatings (1-3 mils) applied by bulk techniques such as dipping or plasma spraying, then machining back to final size and finish.

Foil fabrication involved the use of 0.006-in. thick alloy stock which presented a variety of problems during processing. Foils had the tendency to distort during heat treatment and roll forming as well as during the coating process itself. Foil fabrication typically involved a series of operations requiring, for each coating under consideration, definition of the proper foil forming, heat treatment, and coating application sequence.

Most coating activities were performed by commercial vendors while fabrication and heat treatment were primarily done at AiResearch. Foil curvature was performed on a two-roll bending device by compressing the foil between a large diameter (6-in.) rubber roll and a small diameter steel roll (1/2-in. diameter). Compression severity defined the foil curvature radius.

Process control requirements for coated shaft and foil fabrication typically included the following:

### Shafts and Foils

- (a) Composition - AMS specifications
- (b) Heat treatment - AMS or AiResearch specifications
- (c) Cleaning - AiResearch specifications
- (d) Surface finish - appropriate for particular situation

### Coatings

- (a) Composition - vendor or AiResearch specifications or specialized program requirements
- (b) Heat treatment - compatible with coating and alloy
- (c) Thickness - varied from angstrom range to several mils
- (d) Surface finish - desired at 4-8 rms or as feasible
- (e) Application - best method for situation

### 3.4.3 Materials Screening

The initial portion of the materials development program was devoted to screening alloys for substrates (shaft and foil) and coatings, for 1200°F operation in air. Material screening was performed by various metallurgical examinations such as tensile and bend testing, hardness, metallography and thermal exposures to evaluate oxidation and/or thermal stability. Results of these evaluations led to the selection of coatings and alloys for wear rig tests to evaluate friction and wear.

#### 3.4.3.1 Substrate Alloys

Six alloys were selected for shafts or foils and metallurgical evaluations conducted to define the appropriate alloy(s). Haynes 25, Inconel 718 and X-750 were considered for shaft

construction while 304L and 446 stainless, Inconel 718 and X-750, Haynes 25, and Hastelloy X were evaluated for foil construction.

#### 3.4.3.1.1 Alloy Thermal Exposures

Six alloys (0.006-in. foils) were exposed to 1200°F air for periods of 20, 168 and 550 hours in order to evaluate oxidation behavior, microstructural changes and hardness. All alloys displayed acceptable oxidation resistance, with 304L providing the poorest performance due to formation of 0.0002 inch of oxide after 500 hours of exposure.

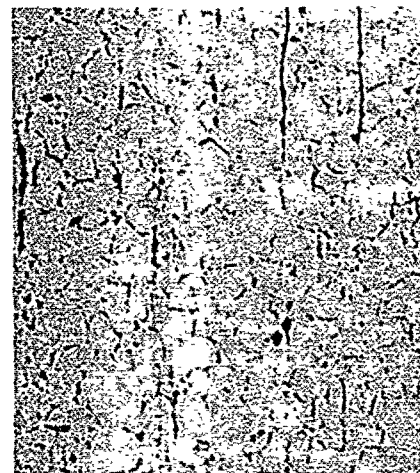
Microstructures of each alloy are shown in Figures 67 and 68 for the as-received samples and those exposed to 1200°F 550 hours. The 446 stainless, Inconel 718 and Inconel X-750 alloys appeared the least affected by thermal exposure. All other alloys show grain boundary precipitation. The Haynes 25 showed this precipitation after an exposure in excess of 20 hours while the 304L stainless and Hastelloy X developed it with exposures of less than 20 hours. Microstructures indicate 446SS, Inconel 718 (aged) and Inconel X-750, solution-treated or aged, would be the preferred alloys for use in the 1200°F range.

Measurements indicated negligible change in microhardness for Hastelloy X, aged Inconel X-750 and possibly 446 stainless steel. Minor hardness increases followed by decreases were observed for 304L stainless and solutioned Inconel X-750, while Inconel 718 and Haynes 25 decreased in hardness upon increased thermal exposure. Alloys Hastelloy X and Inconel X-750 (aged) maintained hardness through the several exposures and would be considered stable and therefore desirable alloys for long-term operation.

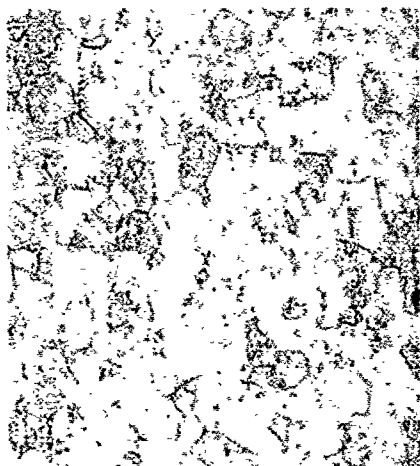
Based upon thermal stability, alloys 446SS, Inconel 718 and X-750 were considered good candidates for shaft construction,



AS-RECEIVED



EXPOSED  
304L STAINLESS



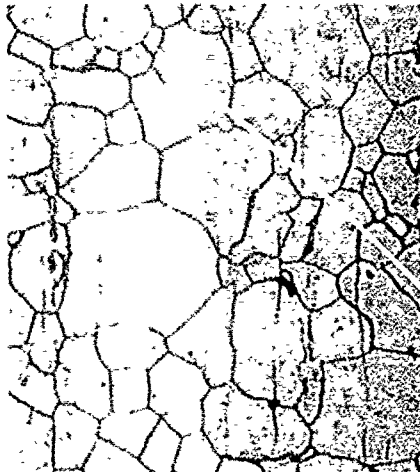
AS-RECEIVED



EXPOSED  
446 STAINLESS

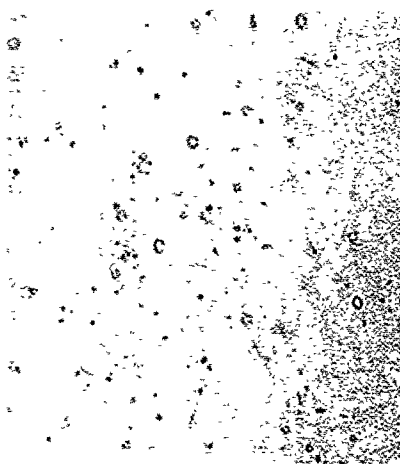


AS-RECEIVED

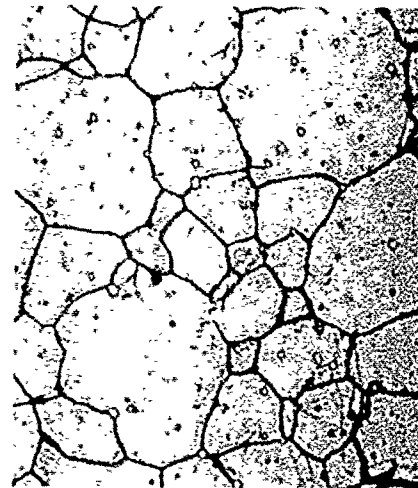


EXPOSED  
HASTELLOY X

Etched-500X  
Figure 67. Influence of Thermal Exposure on the Microstructure of Three Alloys



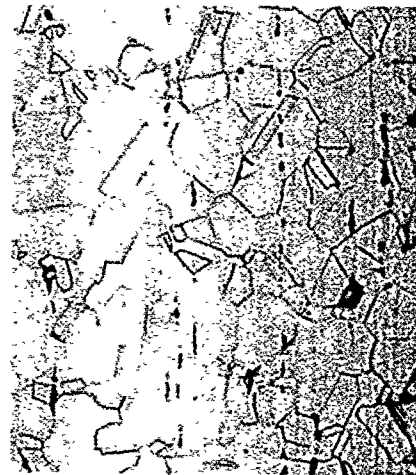
AS-RECEIVED



EXPOSED  
HAYNES 25



AS-RECEIVED



EXPOSED  
INCONEL 718



AS-RECEIVED



EXPOSED  
INCONEL X-750 (SOLUTIONED)

Figure 68. Influence of Thermal Exposure on the Microstructure of Three Alloys Etched-500X



while Inconel X-750 was the preferred material for foils. Use of 446SS was not recommended unless additional testing would verify its capability in the 800° to 1000°F range. The distinction in material selection here was based upon the need for 1200°F capability for foils but somewhat lower temperatures for shaft materials due to its cooler operation.

#### 3.4.3.1.2 Foil Alloy Tensile Properties

Three candidate high temperature foil alloys were evaluated for tensile properties at several temperatures and also after long term thermal exposures (Table 8). Strength properties of the three alloys are decreased at test temperatures above 1000°F as would be expected. The 1315°F/484-hour exposure promoted mixed results among the alloys, the most critical being ductility reductions. Low ductility for Inconel 718 and X-750 at temperatures above 1000°F would cause problems under high stress or fatigue situations. The long term exposure improved the ductility of Inconel 718 at 1300°F.

Tensile properties generally showed all three alloys to have various deficiencies and that no single alloy could be chosen above the others, the Inconels displaying high strength but very low ductility, while the Haynes 25 showed low strength but good ductility at high test temperatures. The Haynes 25 showed a high tendency for microstructural instability in the 1200°F range and would be expected to show further degradation with additional thermal exposure. Inconel alloys appeared adequate, based upon the best combination of strength and ductility at high temperatures.

TABLE 8  
COMPILATION OF TENSILE PROPERTIES FOR FOIL ALLOYS

Alloy	Condition (1)	Test Temp. (°F)	Foil Tensile Properties		Literature Tensile Properties	
			UTS (ksi)	YTS (ksi) (2)	YTS (ksi) (2)	Elong. (%)
Inconel 718	Aged	70	167	107	180	12
		1000	142	94	150	12
		1200	148	104	140	5
		1300	120	107	115	5
	Aged and exposed	70	183	126		
		1000	160	115		
Inconel X-750	Aged	70	162	97	177	27
		1000	130	86	154	26
		1200	> 34	(4)	123	6
		1300	> 17	(4)	110	3
	Aged and exposed	70	169	110		
		1000	144	101		
Haynes 25	Annealed	70	156	69	135	60
		1000	100	35	103	35
		1200				
		1300				
	Annealed and exposed	70	138	91		
		200	103	62		

(1) Aged Inconel 718 treated with the standard 1325°F/1150°F schedule.  
Aged Inconel X-750 treated with the standard 1300°F for 20 hours schedule.  
Exposed alloys treated at 1315°F for 484 hours in air.

(2) 0.2 percent offset.

(3) One sample displayed less than 2 percent.

(4) Specimens broke before yielding.

#### 3.4.3.1.3 Compatibility with Coatings

Limited thermal exposure tests were performed on the only two coatings [NASA fluoride and Kaman  $\text{Cr}_2\text{O}_3$  (DES)] expected to display possible chemical incompatibilities with substrate alloys. These results (presented later in Section 3.4.3.2) indicated an incompatibility of the fluoride coating with the stainless steels and HS-25 but not with the Inconel alloys.

#### 3.4.3.1.4 Selection of Final Alloys

For shaft applications (both wear rig and full scale journal and thrust bearing rigs) Inconel 718 was the primary selection with Inconel X-750 and HS-25 as acceptable substitutes. Inconel X-750 was specified for foils, and Inconel 718 and HS-25 were adequate substitutes.

#### 3.4.3.2 Coatings

Various coatings were applied to substrate alloys and evaluated for resistance to long term thermal exposure. Selected coatings were all expected to show good wear and/or lubrication qualities but their thermal behavior remained to be established. Behavior of the selected coatings in the 1200°F temperature range was evaluated by the tendency to spall, oxidize or deteriorate in static thermal exposure tests. Other criteria used to accept or reject coatings were integrity and surface finish.

The selected coatings are tabulated in Paragraph 3.4.2.2. All candidate shaft coatings were applied to Inconel 718 bar stock, ground to final diameter and finish, inspected, and subjected to thermal tests. Foil coatings were applied to several foil alloys, inspected, and subjected to thermal testing.

#### 3.4.3.2.1 Inspection of Coated Materials

Three groups of coated foils and/or shafts received from Union Carbide Corporation, NASA Lewis Research Center and Kaman Sciences were visually examined. The five UCAR coatings appeared well bonded and adequate for thermal testing. NASA  $(\text{Ba,Ca})\text{F}_2$  coating appeared to be well bonded to all alloys but considerable foil distortion was observed. Kaman coatings (Figure 69) also were well bonded and the foils with thin coatings (nominal 0.5 mils) exhibited only slight distortion, whereas the thicker coating (nominal 2.0 mils) promoted considerable distortion. Of these three groups of coatings, the Kaman coatings appeared the best, although they were expected to be subject to some cracking and spalling due to coating thickness.

A supply of sputter-coated Inconel X-750 foil was procured (Figures 70 and 71) to provide one set of bearings of each of 12 coatings for materials wear rig testing. Additional material also was available for preliminary laboratory evaluations (thermal exposure, bend tests, adherence tests and high resolution microscopy). Most of the sputter coatings had good adherence except for  $\text{TiN}$ ,  $\text{Si}_3\text{N}_4$ , and gold overcoat on the  $\text{TiB}_2$ . A variety of defects was observed among the sputtered coatings including evidence of poor cleaning of the foil prior to coating (Figure 70A), lack of coating adherence (Figure 70B), and target imprint image (Figure 71, A and B).

#### 3.4.3.2.2 Thermal Exposure Testing

Several coated foil and bar samples were exposed to 1200°F air for a period of 514 hours and then to approximately 100 cycles of alternate heating and cooling between 300°F and 1200°F (rapid rates). Coatings evaluated were:

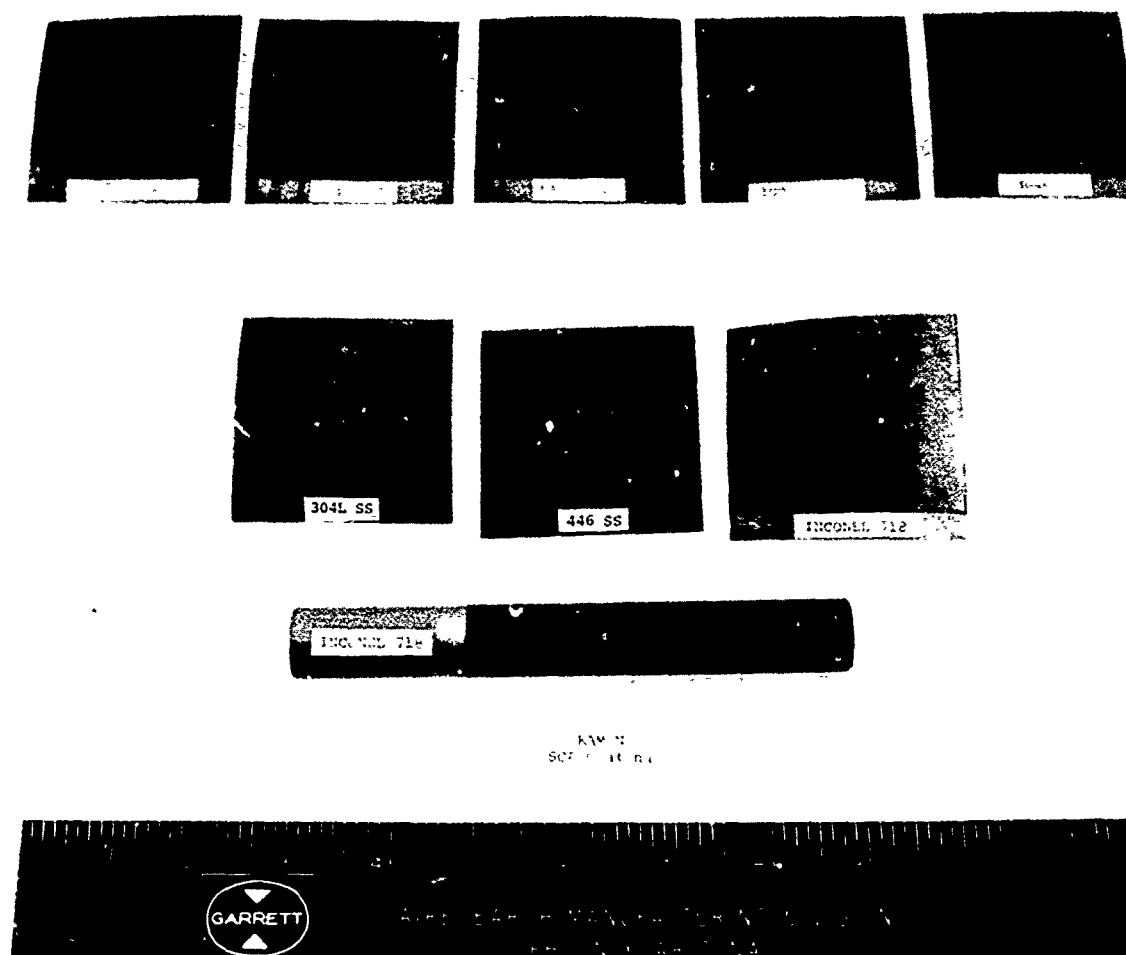


Figure 69. Kaman Sciences Corporation Ceramic Coated Samples. Foils at the Top Were Coated with DES Coating (Pure  $\text{Cr}_2\text{O}_3$ ), Thickness: 0.5-Mil. Bottom Foils and Bar Were Coated with SCA Coating ( $\text{Cr}_2\text{O}_3\text{-Al}_2\text{O}_3\text{-SiO}_2$ ), Thickness: 2-Mils.

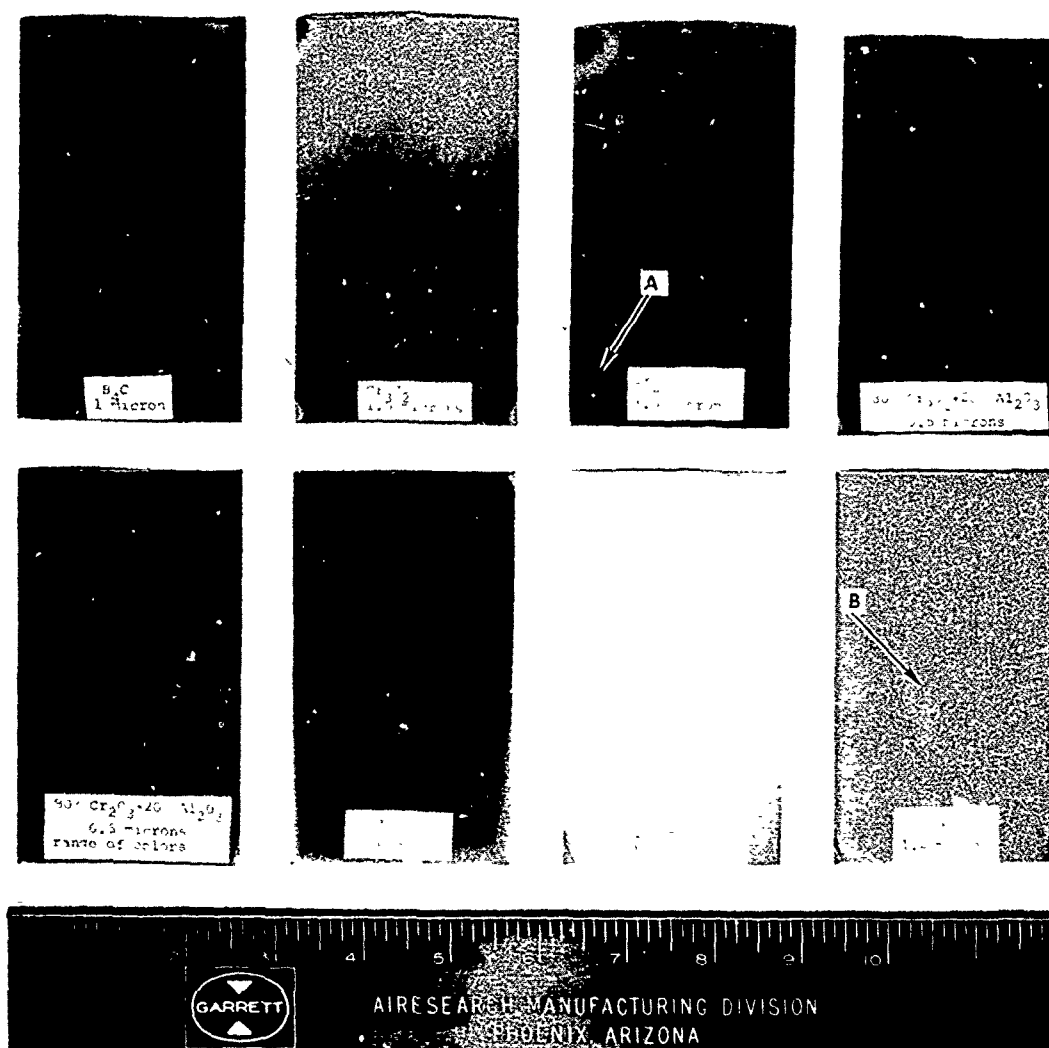


Figure 70. Sputter Coatings Applied to Inconel X-750 Foil ( $B_4C$ ,  $Cr_3C_2$ ,  $Cr_2O_3$ ,  $Cr_2O_3 + Al_2O_3$ ,  $Cr_2O_3$  One Side and Au on Reverse Side, and  $Si_3N_4$ ).

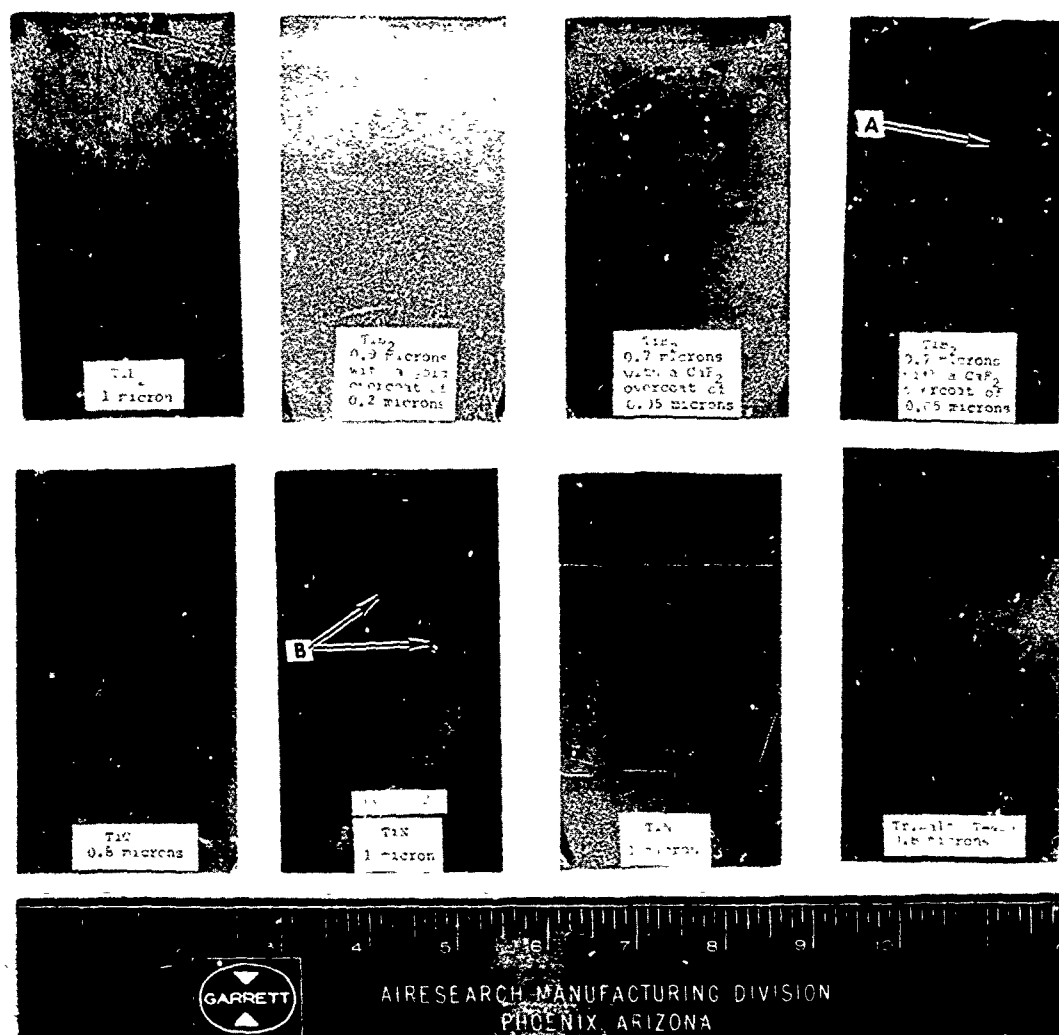


Figure 71. Sputtered Coatings Applied to Inconel X-750 Foil (TiB<sub>2</sub>, TiB<sub>2</sub> with Au Overcoat, TiB<sub>2</sub> with CaF<sub>2</sub> Overcoat, TiC, TiN, and Tribaloy T-400). Defect Patterns at Arrows Caused by Target Imprint Image Occurring During Sputtering.

- (a) Thick coatings (1 to 5 mils) on Inconel 718 bar;  
Tribaloy-400, Metco 45VF, Kaman SCA, UCAR LC-9,  
UCAR LC-1C, UCAR WT-1, UCAR LW-5, UCAR LW-1,  
NASA (Ba,Ca)F<sub>2</sub>, Co and NiCo Electroplate.
- (b) Kaman DES (thin coating) and NASA (Ba,Ca)F<sub>2</sub> (thick  
coating) on several foil alloys; 304L and 446  
stainless, Inconel 718 and X-750 and Haynes 25.
- (c) Control alloys; included Inconel 718 bar and the  
alloys listed in (b).

Results of thermal exposure in 1200°F air for 500 hours are shown in Figure 72 and indicate that three coatings (UCAR WT-1, LW-1, and LC-9) should not be used. Thermal cycle tests indicated that UCAR WT-1 and LC-9 coatings did not perform well (Figure 73). Visual examination of all samples showed spalling for the LW-1, LC-9, and LC-1C coatings and oxidation of the NASA (Ba,Ca)F<sub>2</sub> composition. The remaining coatings were all considered acceptable for long term 1200°F use in foil bearing applications.

The Kaman and UCAR coatings all showed good bonding after exposure and no indication of detrimental coating-to-substrate interactions (Figure 74). However, the (Ba,Ca)F<sub>2</sub> coating did show interactions with substrate alloys, particularly the stainless steels and Haynes 25. Metallographic examination indicated two phenomena occur with thermal exposures of increasing time; (1) the (Ba,Ca)F<sub>2</sub> coating increases in thickness (0.3 mils to 0.8 mils) and (2) the base metal develops an increasing reaction zone (Figure 75). This reaction was considerably reduced when the coating was applied to Inconel alloys, which were therefore the preferred choice for use with fluoride coatings.



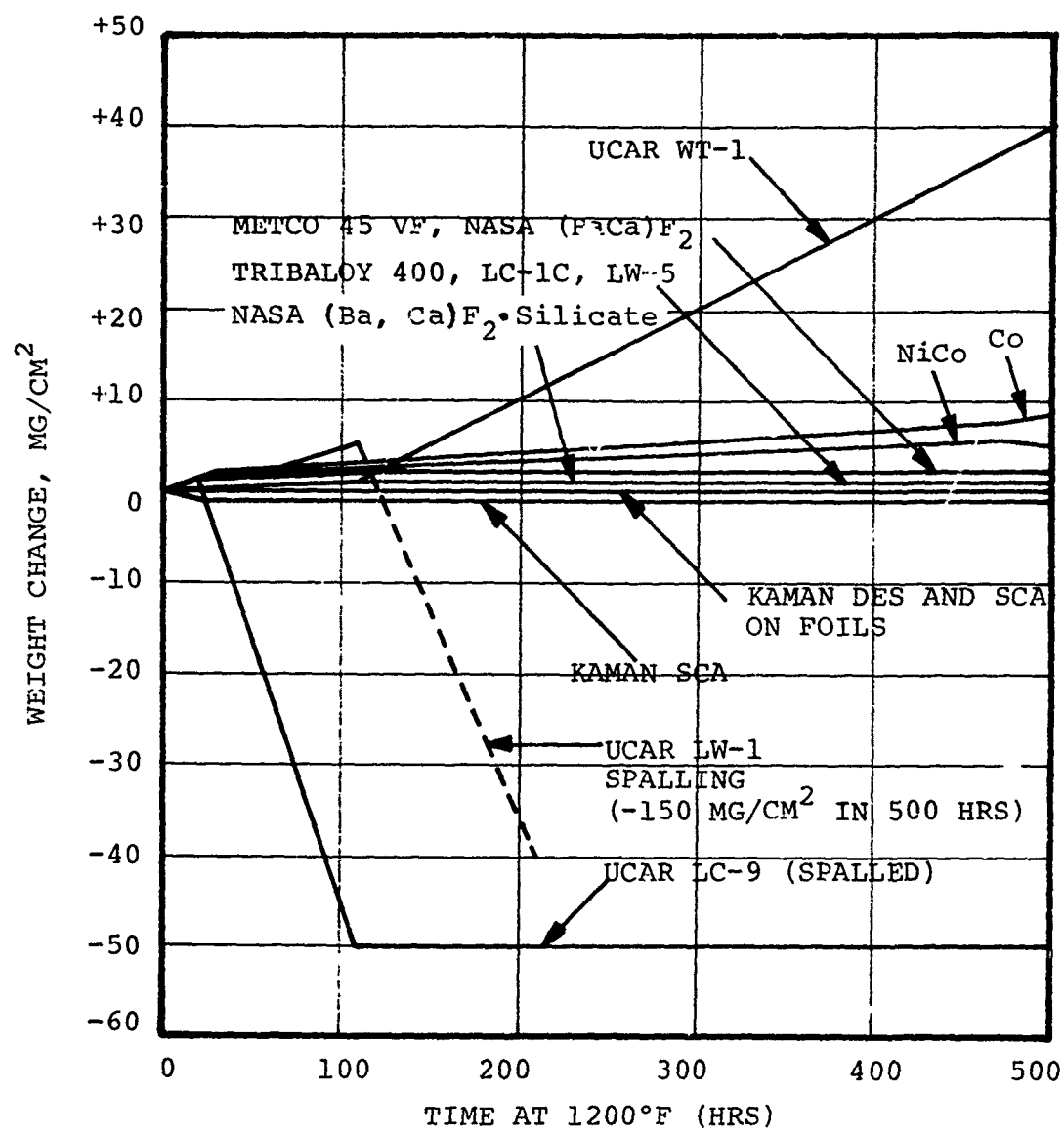


Figure 72. Influence of Thermal Exposure at 1200°F on Weight of Several Coated Samples

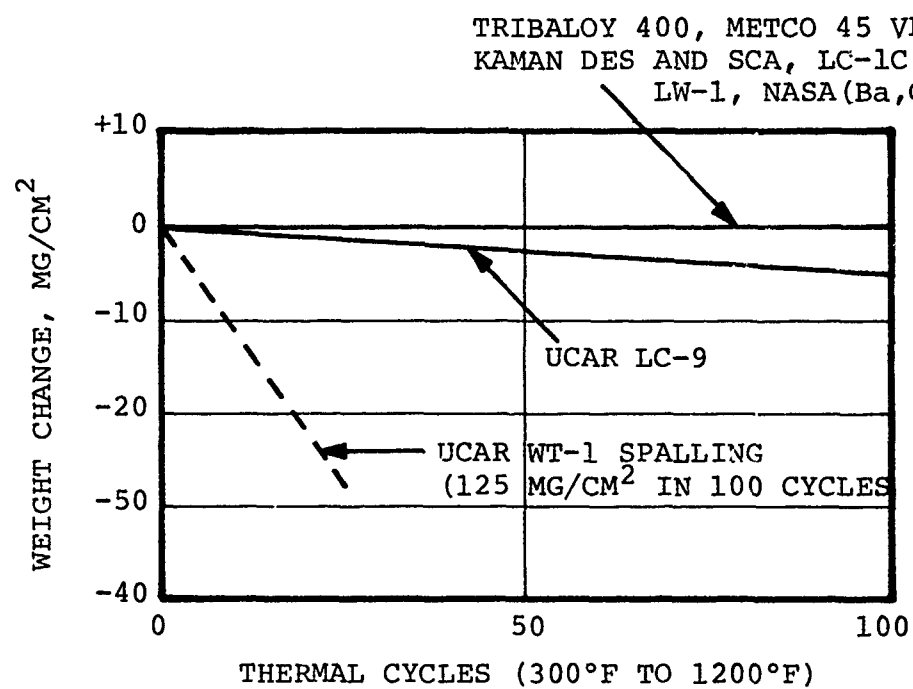
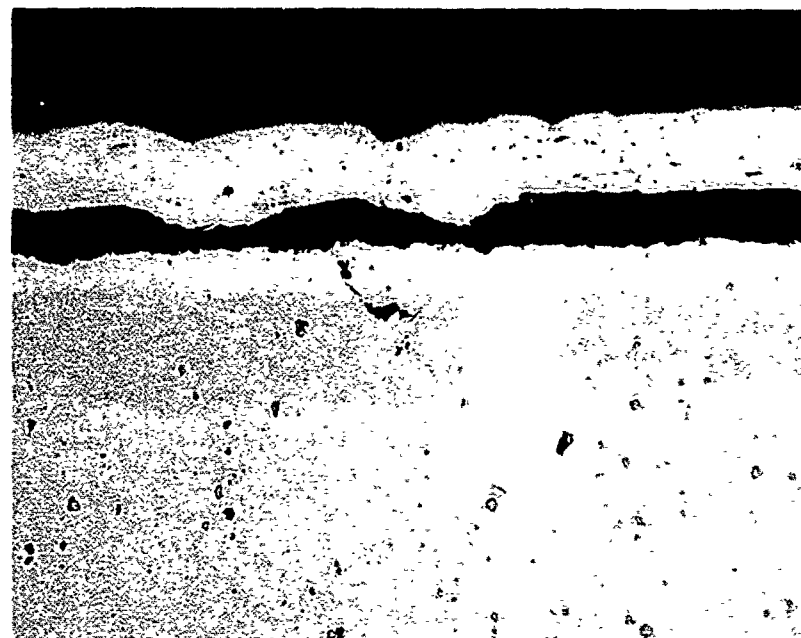


Figure 73. Influence of Thermal Cycling on Weight of Several Coated Samples



METALLOGRAPHIC  
NICKEL PLATE

COATING

INCONEL 718

(a)

100X



METALLOGRAPHIC  
NICKEL PLATE

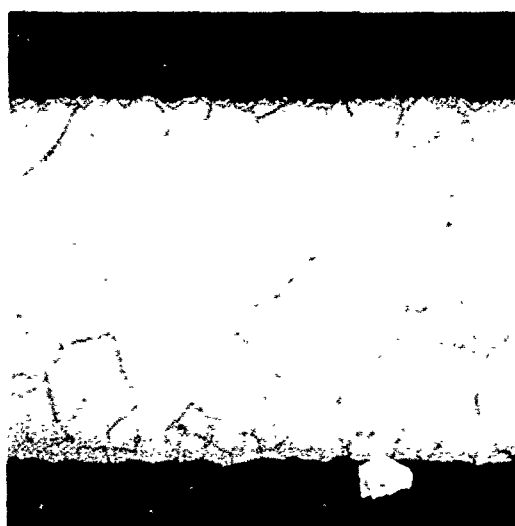
COATING

INCONEL 718

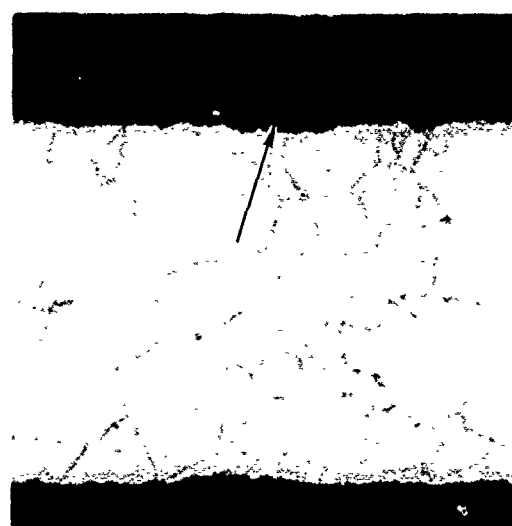
(b)

500X

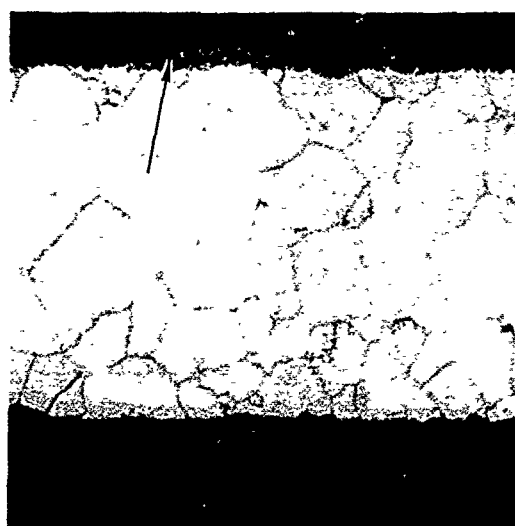
Figure 74. Typical Appearance of Coatings After Long Term Exposure (800 Hours) and Thermal Cycling (100 Cycles) at 1200°F. Coating is Kaman SCA.



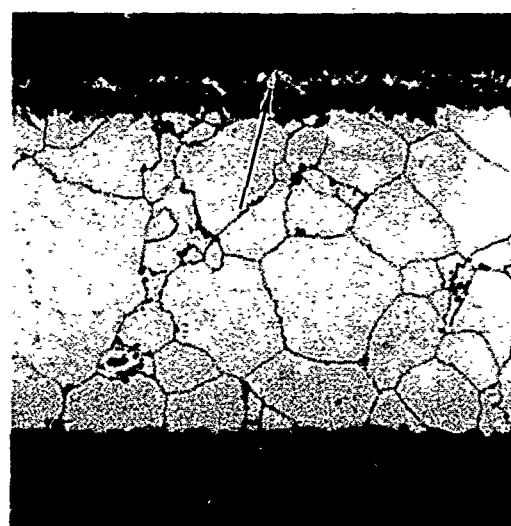
(A) UNEXPOSED



(B) 1295°F/21 HOURS



(C) 1225°F/100 HOURS



(D) 1260°F/503 HOURS

ETCHED-500X

Figure 75.  $(\text{Ba,Ca})\text{F}_2$  Coated Haynes 25 Alloy Foil.

#### 3.4.3.2.3 Coating Surface Evaluation

Several coatings were evaluated by scanning electron microscopy (SEM) for surface degradation subsequent to heat treatment at 1200°F for 260 hours and after deformation by bending about a 1/8-in. diameter mandrel. Most of the coatings were sputtered materials (Table 9) but two thick coatings also were evaluated (NASA Fluoride and Kaman DES). The primary objective was to evaluate cracking severity in various coatings, and how it was influenced by heat treatment in order to anticipate difficulties during fabrication of foils for wear rig testing.

All coatings cracked after the severe deformation bend as typically shown by Figure 76 (illustrations of the other examined coatings are compiled in Appendix A). The crack interval (average distance between cracks) for each coating in the as-coated and in the heat treated conditions (Figure 77) indicated several trends:

- o Most coatings showed improved ductility after heat treatment, the exceptions being  $\text{TiB}_2$ ,  $\text{TiN}$  and  $\text{Si}_3\text{N}_4$ .
- o The best ductility coatings were  $(\text{Ba,Ca})\text{F}_2$ ,  $\text{TiB}_2$ ,  $\text{Cr}_2\text{O}_3$ ,  $\text{B}_4\text{C}$ , and Tribaloy-400.
- o When coating thickness was considered, the fluoride was extremely ductile and the Kaman DES became equivalent to the best sputtered thin coatings.
- o Two coatings,  $\text{TiN}$  and  $\text{Si}_3\text{N}_4$  visually showed spalling associated with sputtering difficulties and therefore were not excluded from future consideration.

TABLE 9  
EVALUATION OF COATED FOIL SURFACES BY SCANNING ELECTRON MICROSCOPY

Coating	Type	Code	Appearance of Surface*		
			As-Coated	Heat Treated (1200°F/260 Hours)	Bend Area (D)
			Undeformed (A)	Undeformed (C)	Bend Area (D)
Uncoated Inconel X-750	---	I-X750		Some debris on surface, metal grain boundaries visible	No metal cracking, some cracking of debris
(Ba,Ca)F <sub>2</sub>	Slurry	DA91	Two-Phase, Rough	Cracking, with 0.7-mil interval	Cracking, 1.2-mil interval.
Cr <sub>2</sub> O <sub>3</sub>	Slurry, KAMAN DfS	DA3D1	Smooth, minimum debris	Cracking, 0.09-mil interval; no spalling	Smooth; spherical second phase lower occurrence; grain boundaries more evident; crack interval is 0.11 mil; no spalling
Cr <sub>3</sub> C <sub>2</sub>	Sputtered	VTA-3	Medium smoothness, some defects	Cracking, 0.21-mil interval, no spalling, jagged cracks	Cracking 0.26-mil interval, no spalling, smooth cracks
Cr <sub>2</sub> O <sub>3</sub>	Sputtered	VTA-150	Medium smoothness, some defects	Cracking, 0.52-mil interval, slight spalling	Cracking, 0.63-mil interval, heavy spalling
80% Cr <sub>2</sub> O <sub>3</sub> / 20% Al <sub>2</sub> O <sub>3</sub>	Sputtered	VTA-44	Medium smoothness	Cracking, 0.097-mil interval; no spalling	Cracking, 0.13-mil interval, surface crystallization; no spalling
B <sub>4</sub> C	Sputtered	VTA-101	Medium smoothness	Cracking, 0.17-mil interval, may be two-layer coating; spalling	Cracking, 0.52-mil interval, no spalling
TiC	Sputtered	VTA-21	Medium smoothness, some anomalies	Cracking, 0.12-mil interval, jagged crack path	Cracking, 0.22-mil interval, smooth crack path, some spalling

\*Coated foils and coated plus heat treated foils deformed by bending about a 1/8-in. mandrel to an angle of 90°.

TABLE 9  
(CONTD)

Coating	Type	Code	Appearance of Surface*			
			As-Coated Undeformed (A)	Bend Area (B)	Heat Treated Undeformed (C)	Bend Area (D)
TiB <sub>2</sub>	Sputtered	VTA-88	Medium smoothness, pebblegrain surface	Cracking, 0.83-mil interval; spalling; semi-jagged crack path	Maybe smoother than (A) but also may be affected by higher electrical insula- tive nature	Cracking 0.46-mil interval; spalling; smooth crack path
Au over TiB <sub>2</sub>	Sputtered	VTA-164	Medium rough	Cracking, 0.61-mil interval; light spalling; smooth crack path	Light whisker growth, medium rough	Cracking, 0.62-mil interval; light spal- ling, smooth crack path
CaF <sub>2</sub> over TiB <sub>2</sub>	Sputtered	VTA-178	Smooth but with some apparent shadow anomalies	Cracking, 0.31-mil interval, no spal- ling, semi-jagged crack path	Cracking and sepa- ration of CaF <sub>2</sub> layer from TiB <sub>2</sub> layer. Rough surface	Cracking, 0.73-mil (?) interval, spalling and CaF <sub>2</sub> separation from TiB <sub>2</sub>
TiN	Sputtered	VTA-224	Medium smoothness	Cracking, 0.16-mil interval, slight spalling, jagged crack path	Whisker growth	Cracking, 0.10-mil interval, no spalling, whisker growth, smooth crack path
Si <sub>3</sub> N <sub>4</sub>	Sputtered	VTA-234	Smooth but maybe a higher electrical insulator	Cracking, 0.34-mil interval; spalling; jagged cracking	Slight roughening compared to (A)	Cracking, 0.24-mil interval; light spal- ling, smooth crack path
Tribaloy T-400	Sputtered	VTA-67	Medium rough	Cracking, 0.15-mil interval, jagged crack path, no spal- ling	Surface effect, pebblegrain appear- ance	Cracking, 0.52-mil interval, semi-smooth crack path; spalling

\*Coated foils and coated plus heat treated foils deformed by bending about a 1/8-in. mandrel to an angle of 90°.

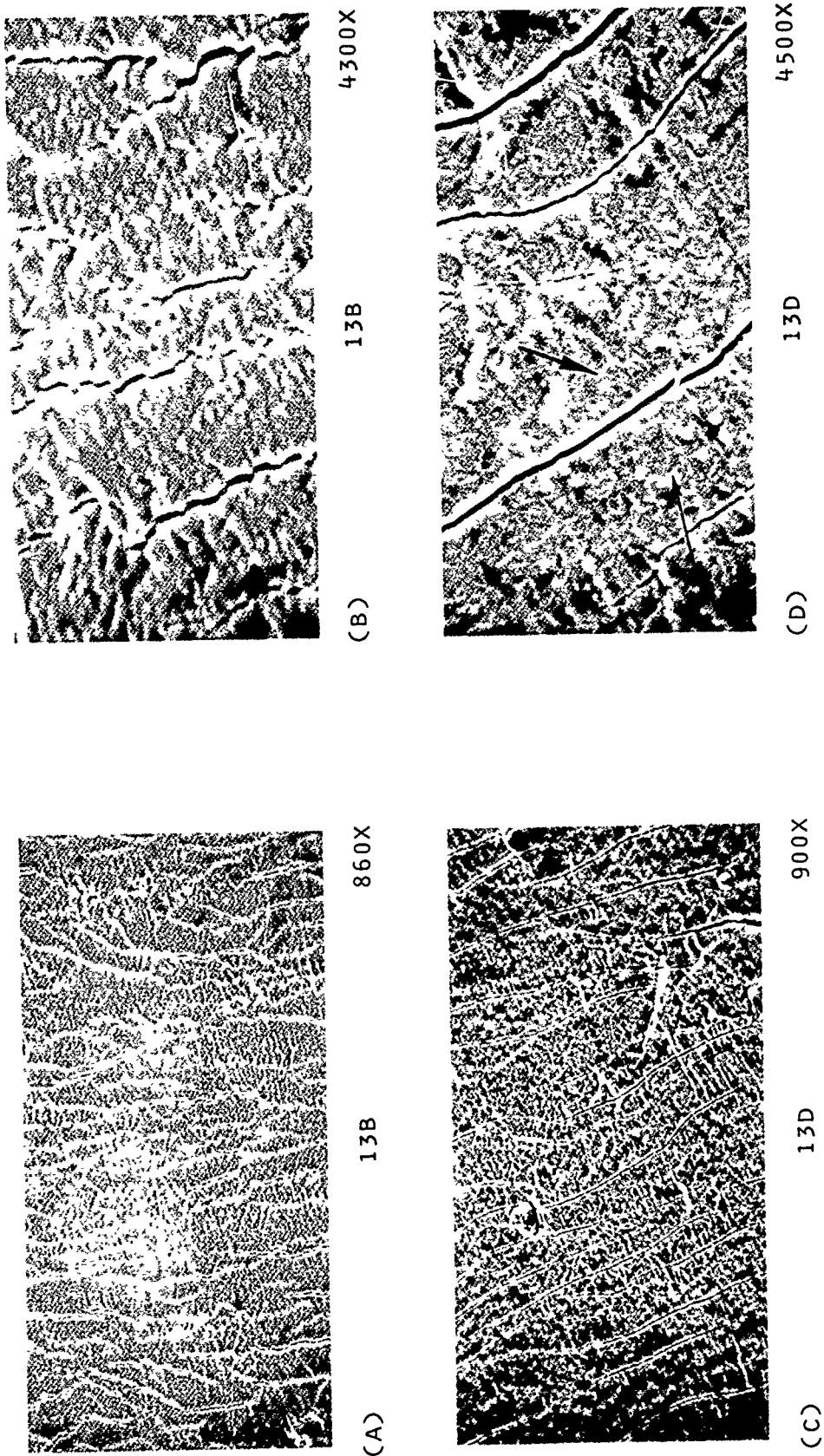


Figure 76. Typical SEM Appearances of Sputtered Coatings That Have Been Deformed. As-Received Coatings in (A) and (B) and the Same Coating After 1200°F/260-Hr Exposure in Air (Deformed After Exposure). This Sample is Chromium Carbide Sputtered to Thickness of 1.5 Microns.



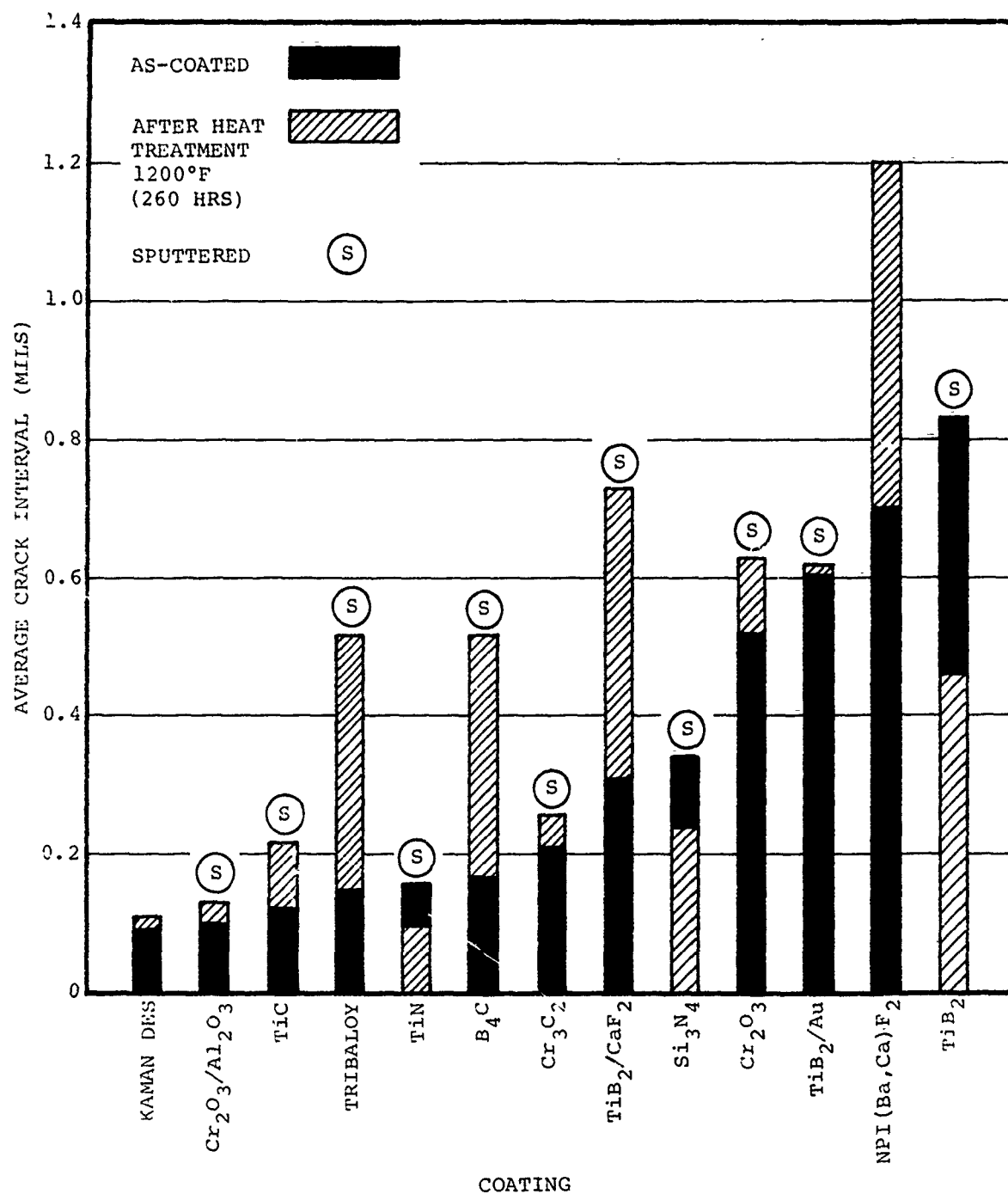


FIGURE 77. Comparison of Cracking For Various Coatings on 0.006-In. Thick INCONEL X-250 Foil Bent Around A 1/8-In. Diameter Mandrel. Highest Bars Indicate Best Ductility Coatings.

Several coatings also showed surface structural changes independent of cracking as a result of thermal exposure (Figure 76). These changes included grain growth, crystallization (Figure 76, arrows), coating homogenization and surface roughening, resulting from relatively high temperature and long time exposure, and would be much less for short time rig tested foils.

Coatings that did not form deleterious surface growths (Appendix A) and therefore are considered stable for long term use included:

- (a)  $\text{TiB}_2$
- (b)  $\text{TiC}$
- (c)  $\text{B}_4\text{C}$
- (d)  $\text{Si}_3\text{N}_4$
- (e)  $\text{CrO}_3$  (sputtered or Kaman DES)
- (f) Tribaloy-400

Surface roughening may degrade friction and wear behavior, and therefore may serve as criteria for rejecting the following coatings:

- (a)  $\text{Cr}_2\text{O}_3 + \text{Al}_2\text{O}_3$
- (b)  $\text{TiN}$
- (c)  $\text{Cr}_3\text{C}_2$
- (d)  $\text{CaF}_2$  overcoat on  $\text{TiB}_2$
- (e) Gold overcoat on  $\text{TiB}_2$

#### 3.4.3.3 Selection of Materials for Wear Rig Evaluation

The more promising materials for further testing in the wear rig are listed in Table 10 and show a wide range of promising qualities for high temperature wear resistance and lubrication.

TABLE 10  
MATERIAL SELECTIONS FOR WEAR RIG TESTING

<u>Component</u>	<u>Material</u>	<u>Est. Max. Temp. Capability (°F)</u>	<u>Coating Application Method</u>
<u>Shafts</u>	Inconel 718	1200	--
	HS-25	1200	--
<u>Foils</u>	Inconel X-750	1200	--
	HS-25	1200	--
<u>Shaft Coatings</u>	HS-25, Oxidized, not coated	>1200	--
	NiCo (60 to 80% Co), ox.	~1200	Electroplate
	Tribaloy-400, oxidized	~1200	Plasma Spray
	UCAR LW-5, (W,Cr)C-NiCr	>1200	"D-gun"
	Kaman SCA, SiO <sub>2</sub> + Cr <sub>2</sub> O <sub>3</sub> + Al <sub>2</sub> O <sub>3</sub>	>1300	Sintered slurry
<u>Foil Coatings</u>	HS-25, oxidized, not coated	>1200	--
	NiCo, oxidized	~1200	Electroplate
	Kaman DES, Cr <sub>2</sub> O <sub>3</sub>	>1300	Sintered slurry
	(Ba,Ca)F <sub>2</sub> , NPI	<1200	Sintered slurry
	(Ba,Ca)F <sub>2</sub> -silicate NASA	~1200	Sintered slurry
	Teflon-S	~550	Baked slurry
	Tribaloy 400	~1200	sputtered
	TiB <sub>2</sub>	>1200	Sputtered
	TiB <sub>2</sub> +Au overcoat	<1200	Sputtered
	TiB <sub>2</sub> +CaF <sub>2</sub> overcoat	<1200	Sputtered
	Cr <sub>2</sub> O <sub>3</sub>	<1200	Sputtered
	Cr <sub>2</sub> O <sub>3</sub> +Al <sub>2</sub> O <sub>3</sub>	<1200	Sputtered
	TiC	>1200	Sputtered
	B <sub>4</sub> C	>1200	Sputtered
	Cr <sub>3</sub> C <sub>2</sub>	<1200	Sputtered

All materials that had displayed reasonable temperature capabilities (greater than 800°F) are included, as well as Teflon-S, which was the baseline coating material. Several materials were eliminated from further study:

- (a) UCAR coatings LW-1, WT-1 and LC-9 dropped due to inadequate 1200°F temperature capability.
- (b) UCAR coating LC-1C dropped due to 1200°F degradation of surface of the similar sputtered  $\text{Cr}_3\text{C}_2$  coating, which is the hard constituent of the LC-1C coating.
- (c) Metco 45VF dropped due to poor surface finish that may be related to plasma spray technique rather than the coating composition.
- (d) Sputtered TiN and  $\text{Si}_3\text{N}_4$  were not tested due to spalling of the coating. TiN also showed surface growth structures.

Spalling of item (d) coatings was associated with the sputtering technique, and improvements could be made. On this basis it would be recommended that  $\text{Si}_3\text{N}_4$  be considered for future testing as a high temperature wear coating.

#### 3.4.3.4 Materials Screening Summary

Metallurgical evaluations were conducted on several alloys for use either as rotating shafts or journal foils and on coatings for use on both bearing components. Shaft alloy selection was limited to three alloys (Inconel 718, Inconel X-750, and Haynes 25) with Inconel 718 selected for wear rig shafts. Foil alloy candidates were selected from a variety of stainless steels (300, 400 and precipitation hardening grades) and superalloys (Ni, Co and Fe base). Tensile testing (to 1300°F) and long term

thermal exposure tests (at 1200°F) selected Inconel X-750 for wear rig foil fabrication with Inconel 718 and Haynes 25 acceptable substitutes.

Twenty-four materials were evaluated for use as wear/lubricative coatings on shafts and foils. Sixteen coatings were chosen for further wear rig testing on the basis of resistance to oxidation at 1200°F, fracture characteristics upon bending, surface finish, bonding quality, and fabrication requirements. The better coatings, having desirable qualities in the above categories, included Kaman DES and SCA,  $TiB_2$ ,  $TiC$  and  $B_4C$ .

#### 3.4.4 Materials Wear Rig

##### 3.4.4.1 Wear Rig Design

A high temperature materials wear test rig previously used for company funded foil bearing studies, was modified to increase and improve its capabilities for this program. The modified rig, shown schematically in Figure 78, included the following pertinent features:

- (a) Inertia Capability - An inertia section was added to the drive train to simulate engine start-up and shut-down behavior. The section could be varied from an inertia of the normal rotating parts (no inertia weight added) through two intermediate values to a maximum inertia nearly double the expected engine value ( $I_p = 0.35 \text{ in-sec}^2$ ).
- (b) Power Turbine - A larger power turbine was incorporated in order to obtain sufficient acceleration of the bearing shaft and inertia weight. High accelerations were required in order to ensure foil lift-off before excessive frictional heating occurred.

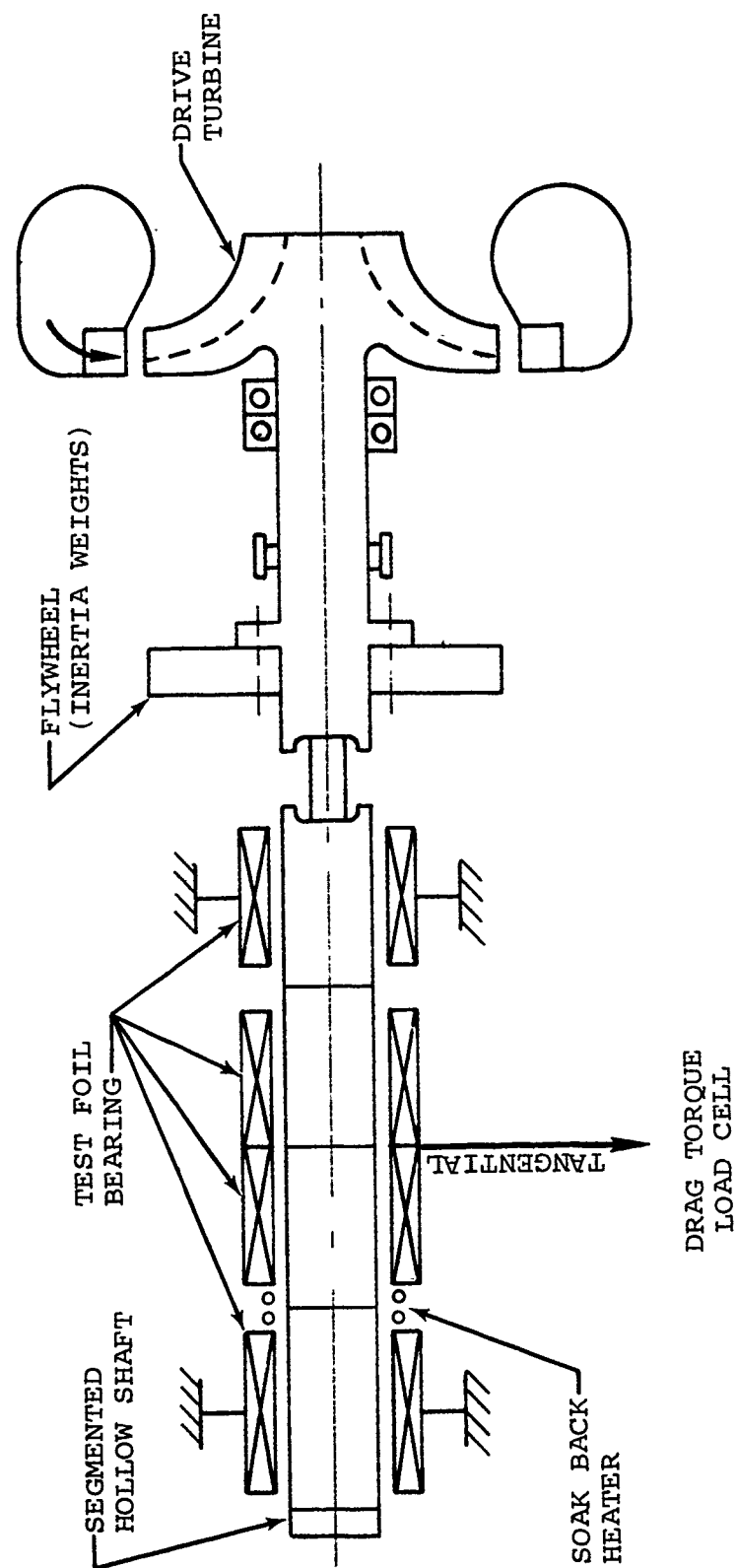


Figure 78. Schematic of Foil Bearing Materials Wear Test Rig

- (c) Torque Sensing - The torque sensing system was modified to gain better sensitivity. A low speed motor (100-200 rpm) was incorporated to allow constant contact conditions for evaluation of friction from torque data under reproducible conditions.
- (d) Shaft Design - A four-segment hollow shaft replaced a single solid shaft. This allowed thermal conditions approximating a hollow engine shaft. The segmented design was incorporated in order to replace a single section when it became unusable, without replacing the entire shaft assembly.
- (e) Soak Back Heater - An electrical resistive coil heater surrounding the shaft in one location was incorporated to simulate turbine heat soak back and its influence on bearing performance. The heater was placed between the two bearings on the end opposite the turbine drive.

The wear rig, installed in a high temperature oven, is shown in Figure 79 with the slow speed motor engaged with the high speed turbine. Component placement is illustrated in Figure 80. Drag torque measurements were made during all rig tests by sensing the frictional force exerted on the bearing carrier housing by the rotating shaft.

Bearing assembly temperatures were measured at end capscrew locations on two of the bearing housings (Figure 80). This location nearly 1/4-inch away from foils, was the most appropriate since anchoring thermocouples directly to the foils was detrimental to foil performance. As a result, no direct temperature measurements were made on foils where peak temperatures would occur as a result of frictional heating.

#### 3.4.4.2 Fabrication of Wear Rig Foil Bearings

Wear rig bearing components fabrication followed the schedule described in Paragraph 3.4.2.3.2. Some components, however,

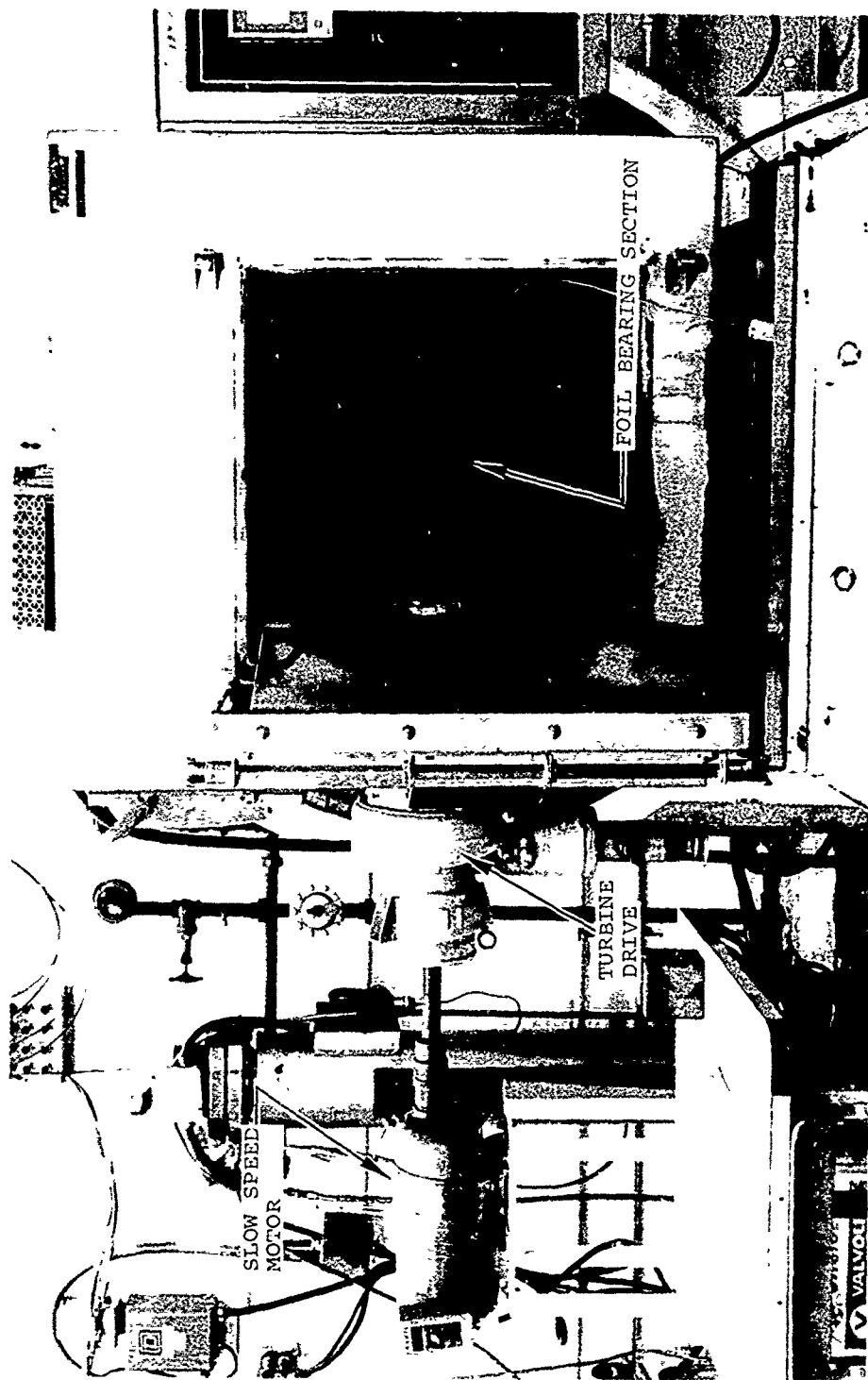


Figure 79. Materials Wear Test Rig Installed in High-Temperature Oven.



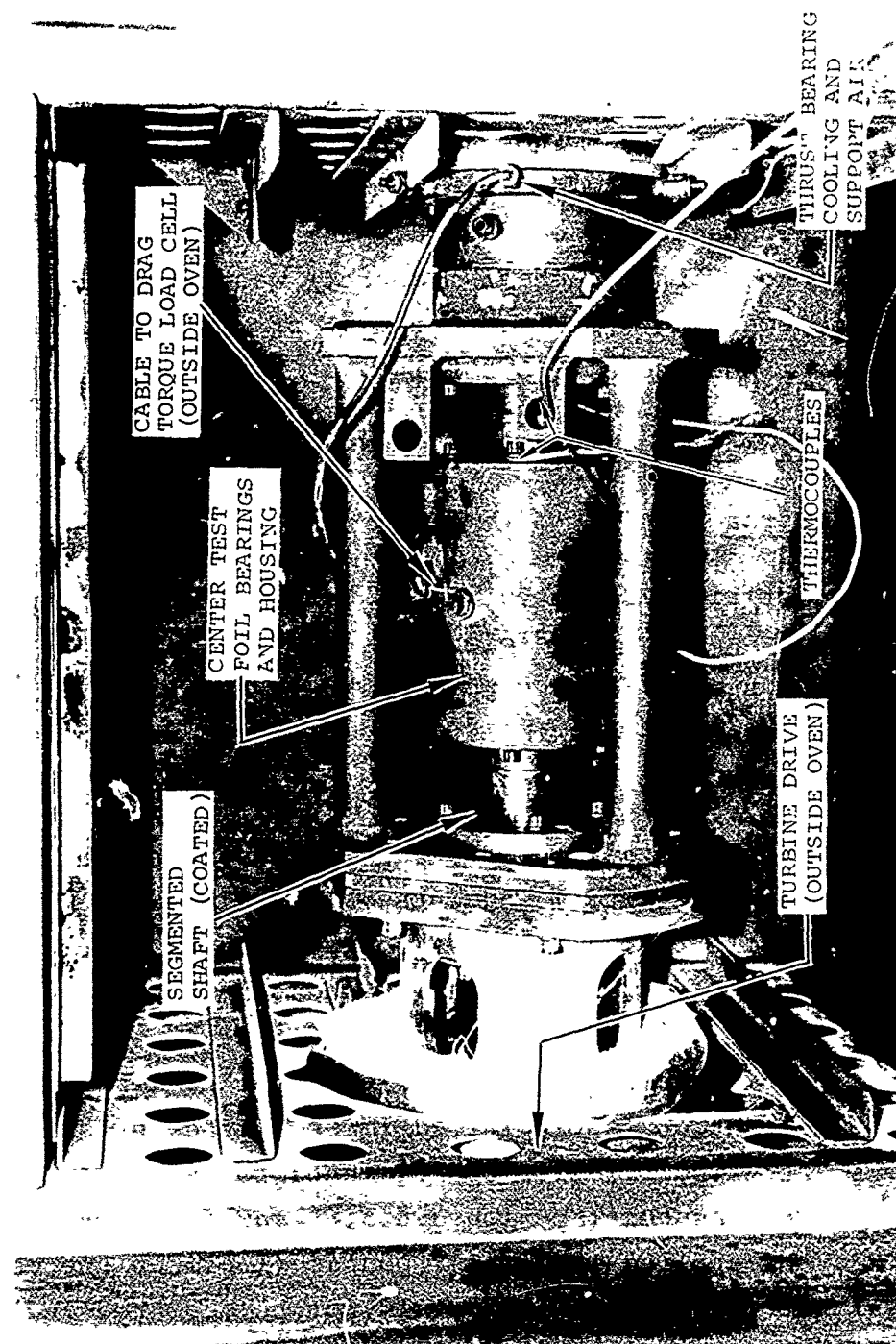


Figure 80. Materials Wear Test Rig Foil Bearing Section.

required special processing because of the coating applied and the compatibility of the thermal treatments given the coating and the alloy substrate. These special processes are described in Table 11.

Foil bearings tested in the wear rig were of the same configuration, but smaller than those for the large journal bearing rigs. Wear rig shafts were 2.0-in diameter and foils were formed to a  $1.45 \pm 0.05$ -in radius of curvature. The sway space (measured diametral clearance with the shaft inserted) was typically 0.010-in. but varied depending upon the thickness of foil coatings which ranged from near zero to 0.002-in.

#### 3.4.5 Materials Wear Rig Testing

##### 3.4.5.1 Test Approach

The wear test rig (Figure 79) was capable of being turned by hand, driven by a slow speed electric motor (157 rpm), or accelerated to high speeds (20,000 rpm or above) by an air turbine. This provided the desired flexibility to monitor bearing wear and torque response from test to test.

The shaft, with its appropriate coating was supported in four foil bearings (eight foil segments each), also with coated surfaces. The middle two bearings were contained within a housing, connected by cable to a load cell to measure bearing friction torque. This torque was a function of the friction coefficient between shaft coating and foil coating, the applied load on the bearings and the contact (spring) load imposed by each foil against the shaft. The friction coefficients for several coating combinations were measured (Section 3.4.5.6) and found between 0.08 and 0.23, the applied load was 8 pounds (1 psi on the center two bearings) but the contact load could not be measured and therefore the actual load of the foil against the shaft could not be determined. The load cell signal was transmitted to a chart recorder calibrated in inch-pounds of torque. The amount of friction torque developed between foils and the rotating shaft

TABLE 11

## SPECIAL FABRICATION OF WEAR RIG BEARING COMPONENTS

<u>Component</u>	<u>Coating</u>	<u>Processing</u>
<u>Shafts</u>	HS-25 Tribaloy-400	Machine coated surface final and then oxidize at 1000°F/2 hrs
<u>Shaft</u>	NiCo	Lap coated surface and then oxidize at 800°F/2 hrs
<u>Foils</u>	HS-25	Oxidize at 1000°F/2 hrs
	NiCo	Do not oxidize due to distortion
	(Ba,Ca)F <sub>2</sub>	Lap lightly with 600 grit or finer after coating
	(Ba,Ca)F <sub>2</sub> - Silicate	Lap lightly with 600 grit or finer after coating

could be measured at all times whether the rig was turbine-driven or hand-turned (or at elevated temperature.) Torque served as the primary measurement to evaluate coating performance over the 70°-1200°F temperature range. Visual and microscopic examinations were used to evaluate wear behavior.

The initial approach used for testing coated foils against coated shafts was later modified due to wear rig performance problems (discussed in Paragraph 3.4.5.2). The initial sequence of events for slow speed tests was as outlined below:

- (a) Build bearing section with set of four coated shaft segments and four sets of coated foils.
- (b) Measure sway space in bearing section.
- (c) Assemble rig and install in oven.
- (d) Make room temperature torque measurement while rotating shaft by hand. A torque wrench was used, which would read torque of all four bearings while the load cell indicated torque only on the center two bearings.
- (e) Rotate shaft at 157 rpm for 10 minutes at each test temperature (room temperature, 400°F, 800°F, 1000°F, and in some cases, 1080° or 1200°F). Center bearing torque and temperature were monitored continuously.
- (f) Hand torque measurements also were taken after each elevated temperature run as well as at room temperature after the final run.

The above approach was later modified (after Test 15) to run for less than 10-minute periods, due to test rig difficulties, (described in Section 3.4.5.2). Test temperatures above 1000°F also were abandoned because of these difficulties.

High speed testing approach was very similar as outlined below:

- (a) Bearing section build with coated components
- (b) Sway space not measured but was calculated
- (c) Install bearing section in rig and oven.
- (d) Make room temperature, hand-driven torque measurement.
- (e) Run shaft, using turbine drive to reach foil lift off. Lift off occurs when hydrodynamic forces separate foils from the rotating shaft. Torque therefore starts high and as speed approaches lift off, torque gradually drops to a low level.
- (f) Shut down turbine drive air supply and allow shaft to decelerate, touch the foils, and stop. Torque again will rise upon touchdown.
- (g) Repeat Steps (e) and (f) to give desired number of start/stop cycles to complete test.
- (h) Hand-driven torque measurements taken at conclusion of testing.

The above procedures allowed real-time monitoring of bearing coating performance or degradation. As a result, teardown inspections of bearings after each test condition change were eventually discontinued and testing proceeded much faster and with less influence from teardown damage.

#### 3.4.5.2 Wear Rig Performance Difficulty

Premature wear of foils and higher than normal torque values indicated changes in wear rig performance, especially at temperatures near 600°F and above. This prompted a re-evaluation of rig dimensional integrity, which indicated a localized 50 percent reduction of sway space (0.006 inch) at room temperature. The increased torque values were therefore attributed to distortion of the bearing housing and components caused by thermal cycling particularly due to a test at 1200°F (Test 13). This distortion appeared to increase with higher temperature (>600°F), resulting in higher than actual torque values at elevated temperature. Therefore, torque values for tests conducted after Test 13 are believed to be higher than actual, reflecting the influence of rig misalignment. This condition was not fully realized until after Test 26, whereupon test durations of ten minutes were reduced to near 10 seconds to minimize bearing wear.

#### 3.4.5.3 Wear Rig Low Speed Test Results

Thirty-nine slow speed tests were conducted with a summary of torque values compiled in Appendix A. Real-time torque measurements were obtained at various temperatures for the foil vs shaft coatings indicated in Table 10. Five shaft coatings were evaluated by running against Teflon-S coated foils. Data is summarized in Table 12 according to best performance at the end of a 10-minute run at room temperature. Of the five shaft coatings, NiCo (oxidized or unoxidized), HS-25 (oxidized), Tribaloy-400 (oxidized), and Kaman SCA appeared satisfactory. NiCo (oxidized) and Tribaloy-400 (oxidized) were the best when 400°F torque values were considered. This data also indicated Tribaloy-400 friction characteristics were improved by heat treatment to form an oxide surface layer (Tests 3b and 3a) whereas NiCo did not benefit by oxidation of the surface (Tests 2c and 2b).

TABLE 12  
TORQUE MEASUREMENTS FOR VARIOUS SHAFT COATINGS RUN AGAINST  
RUN AGAINST TEFLON-S COATED FOILS\*

Bearing Torque (in.-lb)  
at 157 rpm\*\*

Test No.	Shaft Coating	Room Temperature		400°F	
		At Start	After 10 min	At Start	After 10 min
2c	NiCo (not oxidized)	11	14	3	9
2b	NiCo (oxidized)	13	15	6	5
1	HS-25 (oxidized)	13	15	11	14
3b	Tribaloy-400 (oxidized)	12	17	4	5
8	Kaman SCA	13	20	12	9
9	NiCo (oxidized)***	30	21	25	11
7	UCAR LW-5 + gold overplate	23	34	17	16
4a	UCAR LW-5	24	42	--	--
3a	Tribaloy-400 (not oxidized)	70	--	--	--

\*Ranked according to room temperature torque after 10-min run.

\*\*Torque values corrected for wear of Teflon over 11 tests.

\*\*\*The NiCo coated shaft had been run a total of 60 min prior to this test, shows effect of wear on torque (compare to Test 2b).

Only the UCAR LW-5 shaft coating was rejected by this testing (Test 4a) and efforts to improve its performance by applying an electroplated gold layer promoted only a modest decrease in torque.

Foil coatings were evaluated by running against one of three coated shafts, Kaman SCA, NiCo and Tribaloy-400. Results of these wear rig tests are plotted in Figure 81 with the better coatings shown first. These foil coatings are classified according to lowest torque values at all temperatures, as follows:

<u>Best</u>	<u>Moderate</u>	<u>Poor</u>
Kaman DES	$C_3C_2$	$(Ba,Ca)F_2$
$Cr_2O_3 + Al_2O_3$	$TiB_2 + Au$ overcoat	Tribaloy-400
$TiB_2$	$Cr_2O_3$	HS-25 (oxidized)
TiC	$B_4C$	$(Ba,Ca)F_2$ .Silicate

Several coatings were not evaluated in the wear rig as planned due to a variety of problems. These included the electroplated NiCo (coating too thick for rig tolerances) and sputtered  $TiB_2$  with  $CaF_2$  overcoat (used as a partial setup in another test that degraded the foils).

Visual examination of foils and shafts (Figure 82) subsequent to wear rig tests provided only a crude appraisal of relative wear resistance since a wide range of test times and conditions were used. Tests were divided into three categories: long term (greater than 20 minutes total running time from all temperatures), medium time (3 to 6 minutes total running time) and short time (0.1 to 1.1 minutes total time). Coatings were ranked according to wear appearance (wear appearance rank categories are shown in Figure 83 and Table 13). A limited assessment may be made by comparing coatings within the test time categories but due to the varied test times and rig misalignment difficulties



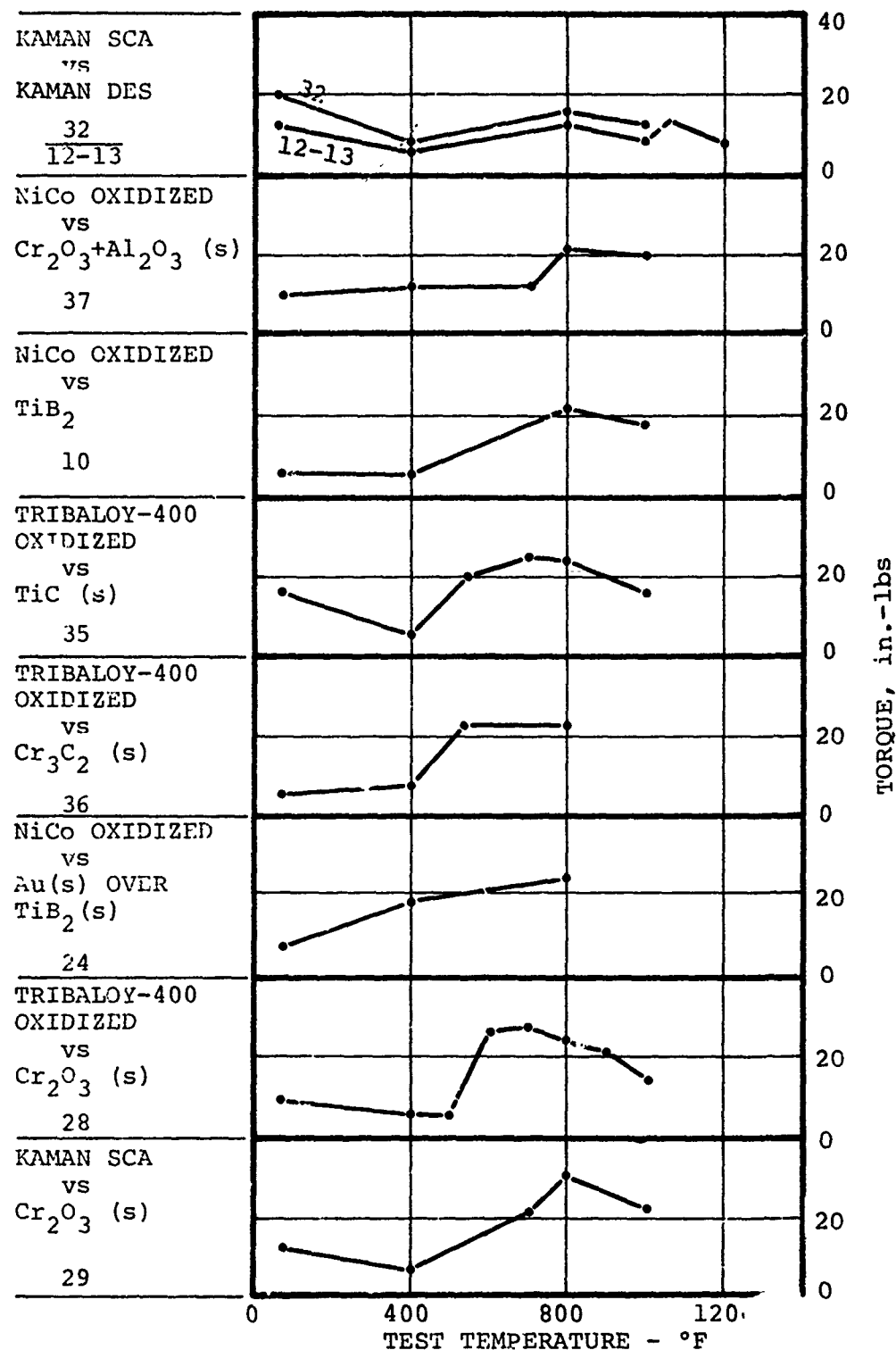


Figure 81. Torque Measurements (Vertical Axis) for Various Coating Combinations Tested in the Materials Wear Test Rig. (Numbers in Caption Block Refer to Test Number. The First Coating Listed was Applied to Shaft and the Second Coating Listed was Applied to Foils).

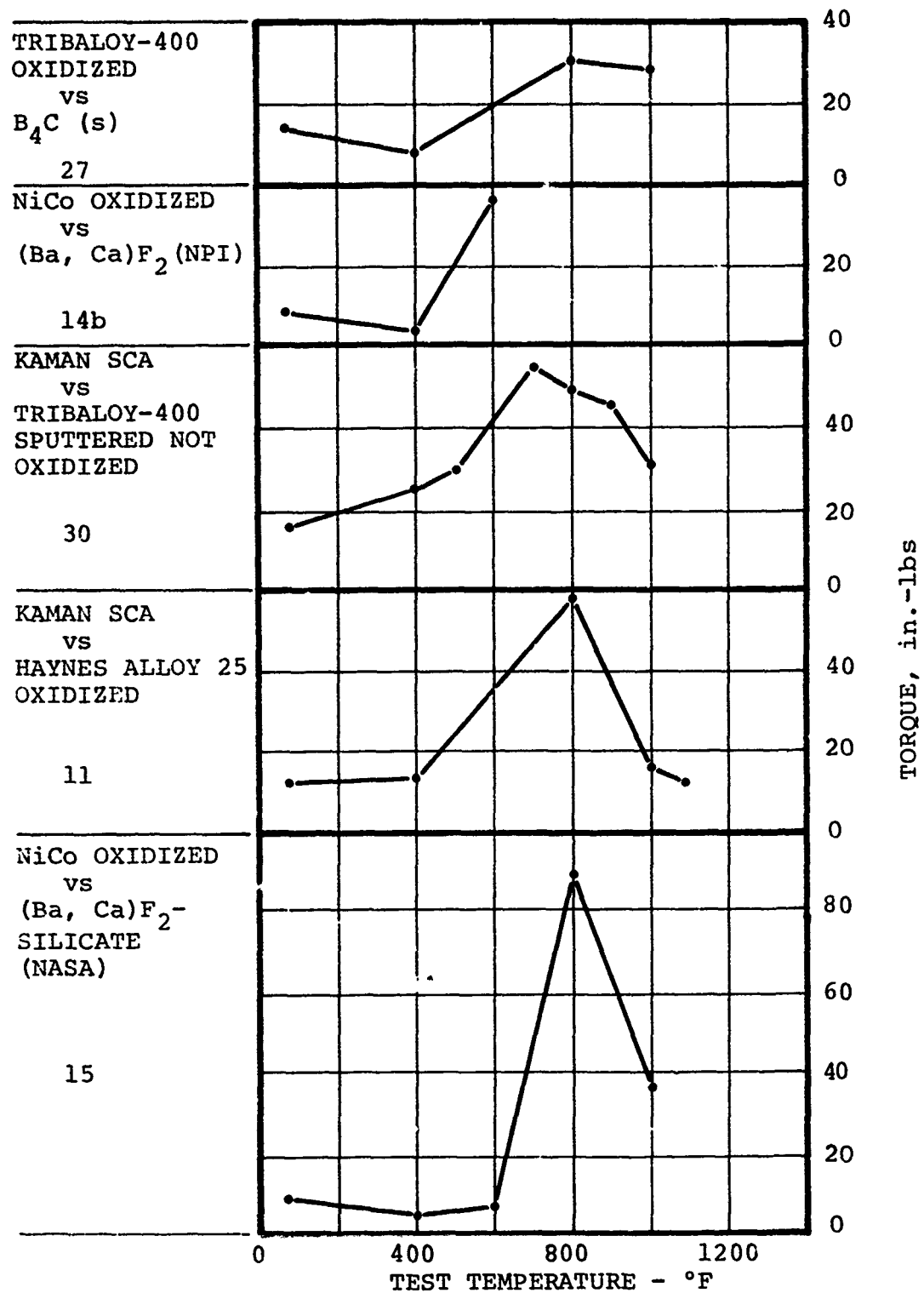
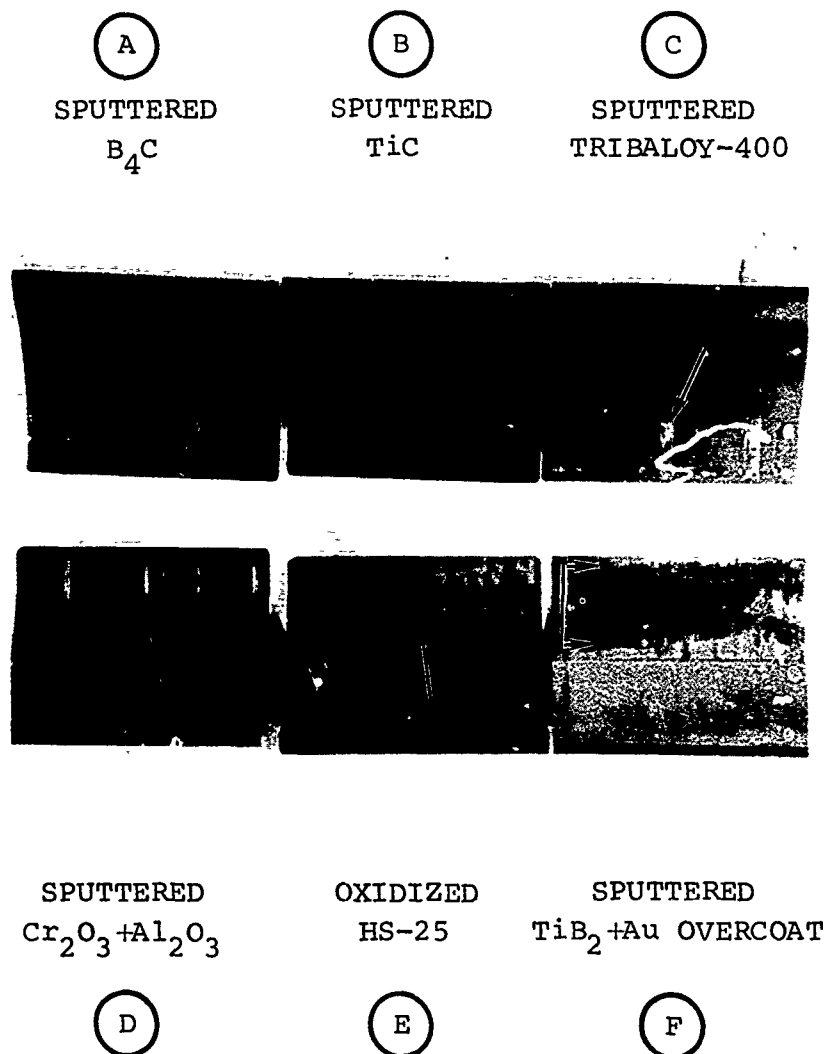


Figure 81. (Continued)



Figure 82. Typical Appearance of Wear Rig Shaft and Foils After Testing. Center Two Bearing Groups Were Evaluated for Wear Appearance. B<sub>4</sub>C Coating on Foils and Tribaloy-400 Coated Shaft Segments (Test 27).



WEAR APPEARANCE RANKING SCALE: "A" RANK  
IS BEST WITH LOWEST WEAR, "F" IS WORST.  
NOTE WEAR SCARS AT ARROWS.

Figure 83. Foil Bearing Wear Categories.

TABLE 13

WEAR APPEARANCE OF COATED FOILS EVALUATED  
IN WEAR RIG TESTS

Foil Coating	Test No.	Total Test Time (min)	Shaft Coating (s)	Visual Wear on Center Two Bearing Foils	Rank*
<u>Long Time</u>					
(Ba,Ca)F <sub>2</sub>	23	49	NiCo, Kaman	Light to moderate	.
TiB <sub>2</sub>	10	24	NiCo	Moderate	C
(Ba,Ca)F <sub>2</sub> · Silicate	15	23	NiCo	Moderate	C
Kaman DES	19	65	Kaman, Tribaloy	Poor	D
HS-25 (ox)	11	40	Kaman, Tribaloy	Poor	E
TiB <sub>2</sub> + Au	24	17	NiCo	Severe	F
<u>Medium Time</u>					
TiB <sub>2</sub> + CaF <sub>2</sub>	21	6	Kaman SCA	Moderate	C
Cr <sub>2</sub> O <sub>3</sub>	25	3.5	Tribaloy	Moderate	C
<u>Short Time</u>					
B <sub>4</sub> C	27	0.4	Tribaloy	Light	A
Cr <sub>3</sub> C <sub>2</sub>	36	<0.1	Tribaloy	Light	A
TiC	35	0.4	Tribaloy	Light to moderate	B
Kaman DES	32	0.6	Kaman SCA	Light to moderate	C
Tribaloy	30	0.1	Kaman SCA	Light to moderate	C
Cr <sub>2</sub> O <sub>3</sub>	29	1.1	Tribaloy, Kaman	Poor	D
Cr <sub>2</sub> O <sub>3</sub> +Al <sub>2</sub> O <sub>3</sub>	37	0.3	NiCo	Poor	D

\*Rank according to A, B, C, D, E, and F levels with A the best and the only wear level that could be considered acceptable in a production situation.

described earlier, comparisons between groups could not be made. In other words, the poorest short time coating ( $\text{Cr}_2\text{O}_3 + \text{Al}_2\text{O}_3$ ) may be a better coating than the best high time coating  $[(\text{Ba,Ca})\text{F}_2]$  due to rig misalignment imposing locally concentrated loads (this situation would be valid when comparing Tests 1-12 with Tests 13 through 37). Additional metallurgical evaluations of tested shafts and foils are contained in Paragraph 3.4.5.5.

Within each time category, the best wear resistant coatings appear to be  $(\text{Ba,Ca})\text{F}_2$ ,  $\text{TiB}_2$ , and  $\text{B}_4\text{C}$ . However, this appraisal had only a minor influence on selection of coatings for the journal and thrust rigs and on definition of the best program coatings.

#### 3.4.5.4 Wear Rig High Speed Test Results

The better coatings from low speed testing were to have been subjected to high speed wear rig testing. In part, this was done as shown in Table 14, Test 19, where Kaman DES was run against Kaman SCA for several start/stop cycles at room temperature with no sign of degradation. This performance was extremely encouraging but the test was performed only to check out high speed operation of the rig and was not continued for estimates of higher temperature performance or endurance as were eventually contemplated. Test 20 was run using the Teflon-S baseline foil coating for comparison to the Kaman coating and Teflon-S showed, as expected, superior low torque behavior. Foil lift-off from the shaft (observed by the torque dropping to zero) was near 11,000 rpm for both test setups. Only minor temperature rises ( $5^\circ\text{F}$ ) were observed at the foil housing position compared to  $10^\circ$  to  $15^\circ\text{F}$  temperature gains observed during low speed, constant contact tests.

Near the end of the test program, only a limited number of coated foils were in acceptable condition for additional high

# COATING PERFORMANCE FOR HIGH SPEED WEAR RIG TESTS

TEST NO.	DATE	SHAFT COATING	FOIL COATING	BEARING TORQUE AT LIFT-OFF AND TOUCH-DOWN (IN.-LBS) *											
				ROOM TEMPERATURE											
				AT START	AT END	AT START	AT END	AT START	AT END	AT START	AT END	AT START	AT END		
19	4-13-76	Kaman SCA	Kaman DES	21	36	Air Turbine Run - 13 Cycles									
20	4-19-76	Kaman SCA	Teflon-S	11	21	Air Turbine Run - 3 Cycles									
34	6-29-76	Kaman SCA	Teflon-S	8	21	Air Turbine Run - 1 Cycle (failed)									
38	7-19-76	NiCo (Oxidized)	Cr <sub>2</sub> O <sub>3</sub> +Al <sub>2</sub> O <sub>3</sub> (Sputtered)	18	37	Air Turbine Run - 1 Cycle (failed)									

173

speed testing. These were incorporated into Tests 34 and 38 (Table 14) and results were extremely poor as foils were capable of only one start/stop cycle due to severe wear (Figure 84). The high wear is not, however, attributed to the material selections but was caused by rig misalignment (Paragraph 3.4.5.2) imposing high local stresses as well as longer rubbing in local areas, evidenced by torque not falling to a low level until speeds near 13,000-20,000 rpm were attained.

Early high speed wear rig tests demonstrated that the selected materials were capable of surviving several cycles of high speed contact with only minor wear and friction increases. The final wear rig test (No. 38) resulted in damage to the test rig that would have required time consuming repairs. Since only one set of foils (Kaman DES) was available for testing and because additional high speed testing results would not alter materials selection for thrust and journal rigs, further high speed testing was not undertaken.

#### 3.4.5.5 Metallurgical Evaluation of Wear Rig Materials

Several specific materials and problems associated with wear rig testing were investigated and are described in the following paragraphs.

##### 3.4.5.5.1 National Process Industries (NPI) Fluoride Coating Evaluation

As a result of apparent high torque measurements for the NPI fluoride coating  $[(Ba,Ca)F_2]$ , several areas of a coated foil subjected to wear rig testing (Test 23) were examined by scanning electron microscopy (SEM). The NPI coating showed erratic surface wear patterns, and several polished and rough areas, as shown in



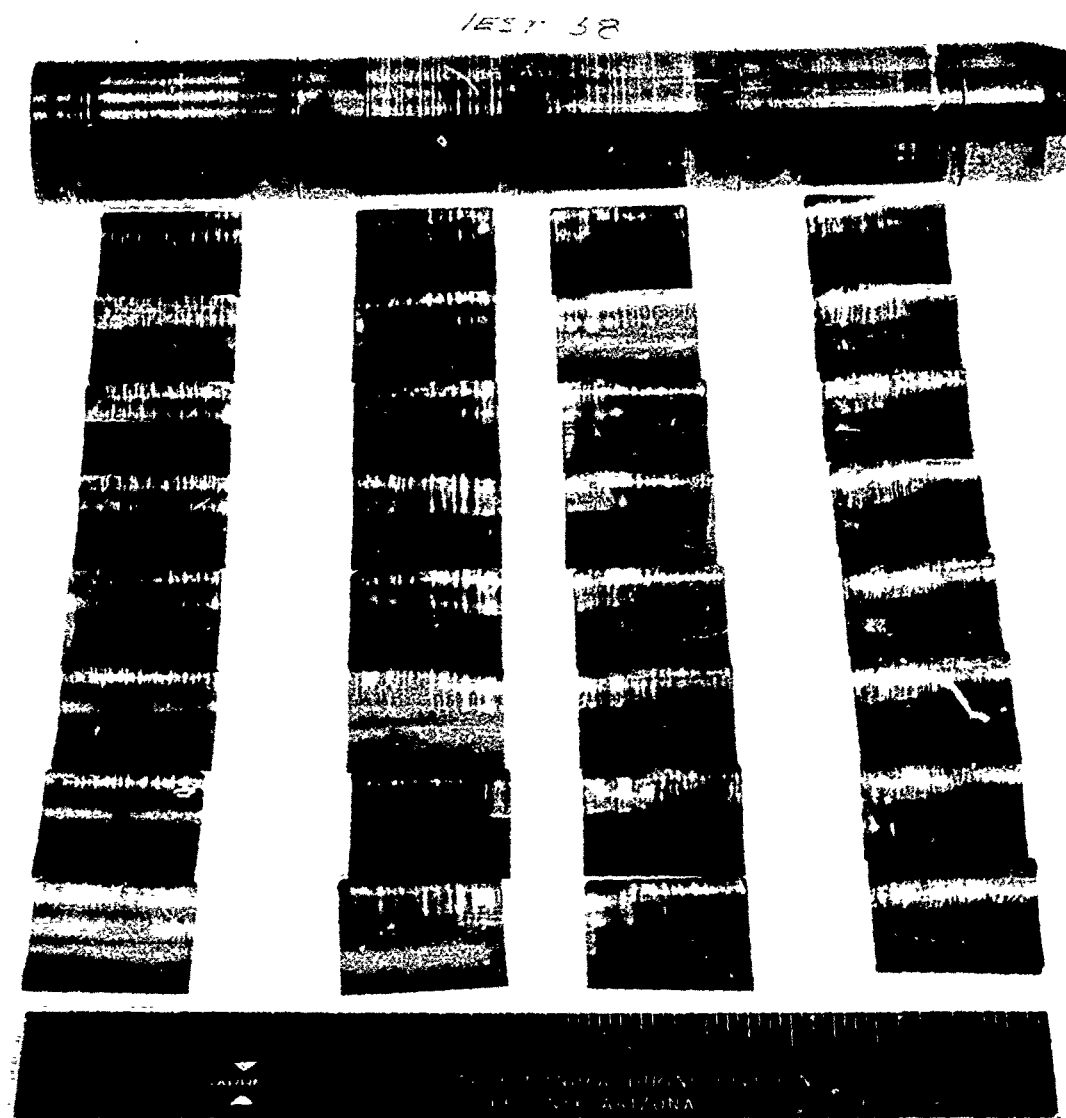


Figure 84. Coated Shaft (NiCo) and Foils (Sputtered  $\text{Cr}_2\text{O}_3 + \text{Al}_2\text{O}_3$ ) After High Speed Test 38.

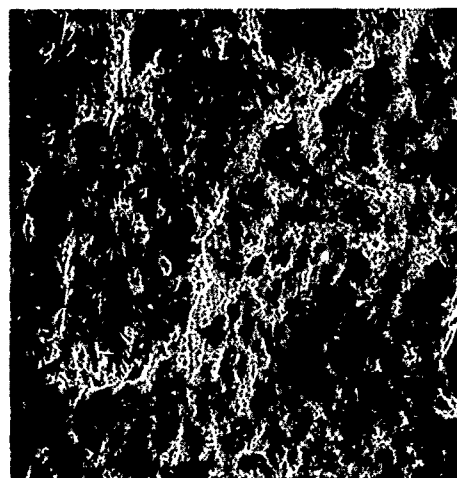
Figure 85. Unworn areas were typified by varied surface contours, small voids, and some cracking (Figure 85, a and b). Smooth wear areas (c and d) showed a high percentage of smooth surface, while rough wear areas indicated only intermittent occurrence of surface smoothing (f, arrow). The presence of both smooth and rough coating wear areas on the same foils was attributed to wear rig characteristics rather than compositional or surface contour differences in the coating.

Several microstructural features shown at the arrows in Figure 85(d) were electron probed to determine elemental constituents. Analytical results are summarized in Table 15 and indicate the light colored areas are primarily Ba, while the dark areas contain high amounts of Ca. There were local concentrations of these areas in the microstructure but these could not be correlated to wear patterns. No abnormal areas believed to be deleterious to wear or friction behavior were observed, other than some that would benefit by an improvement in surface finish.

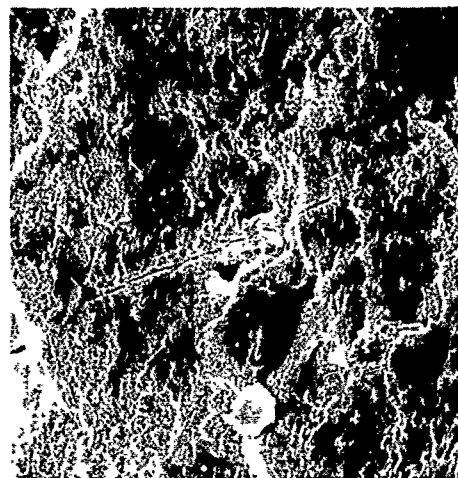
#### 3.4.5.5.2 NASA Fluoride Coating Evaluation

The NASA fluoride coatings (Figure 86) appeared rougher than NPI coatings (Figure 85), and SEM examination indicated this roughness was due primarily to nodular appearing growth formations on the surface (Figure 86; a, c, and e) during the coating process. These nodular growths appear resistant to smoothing during bearing operation.

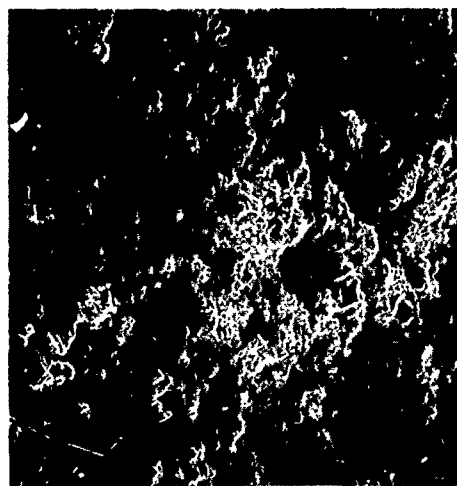
The NASA coating was subjected to a long term thermal exposure (1200°F-1300 hours) and also examined by SEM. Structures shown in Figure 87 suggest that surface features are altered (to a possible damaged condition) by this thermal exposure.



(a) 300X



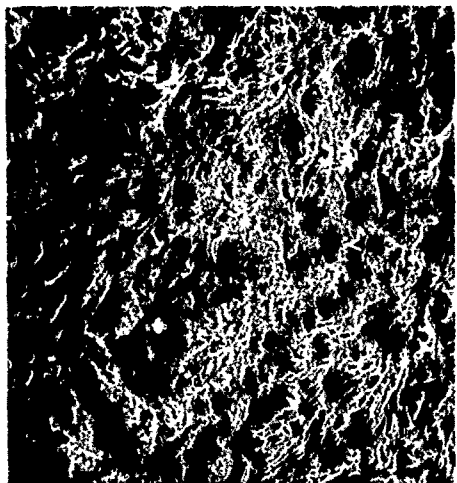
(b) 1500X  
NON-WEAR AREA



(c) 300X



(d) 1500X  
SMOOTH WEAR AREA



(e) 300X



(f) 1500X  
ROUGH WEAR AREA

Figure 85. Typical Appearance (SEM) of National Process Industries (Ba,Ca)F<sub>2</sub> Coating Surface.

TABLE 15

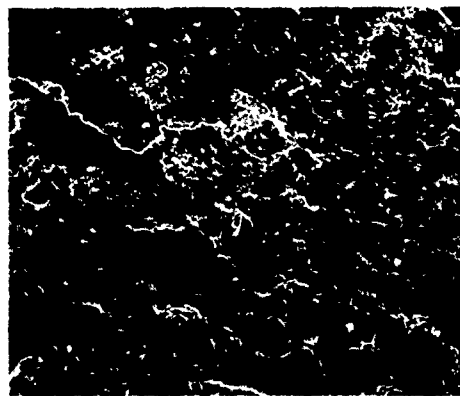
SUMMARY OF ELECTRON PROBE MICROANALYSIS  
OF NPI AND NASA FLUORIDE COATINGS

<u>Coating*</u>	<u>Description</u>	<u>Composition</u>
NPI-S1	Smooth Dark Area	Major Ca; Minor Ba and Si
NPI-S2	Smooth Light Area	Major Ba; Minor Ca, Si and Mg
NPI-S3	Smooth area Eutectic, Dark Phase	Major Ca and Ba (Ca:Ba/2:1); Minor Si and Mg
NPI-S4	Smooth area Eutectic, Light Phase	Major Ba; Minor Ca; Trace Si
NASA-S5	Oxidized**, Blocky Particle	Major Ca, Ti and Cr; Minor Ni; Trace Fe, Al and Si
NASA-S6	Oxidized**, Round Particle	Major Ca, Ba, and Cr; Minor Si, Ni and Fe
NASA-S7	Oxidized **, General Coating	Major Ca and Ba; Minor Cr, Si, Ni, Fe and Al

\*NPI -  $(\text{Ba}, \text{Ca})\text{F}_2$ ; NASA -  $(\text{Ba}, \text{Ca})\text{F}_2 \cdot \text{CaSiO}_3 \cdot \text{CaO}$

\*\*1200°F for 1300 hours in air.

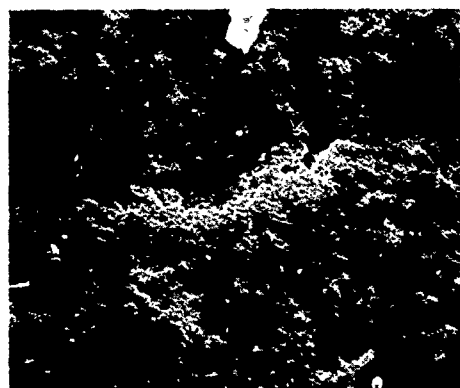
SMOOTH LIGHT COATING (Sample d)



(a) UNWORN AREA 300X

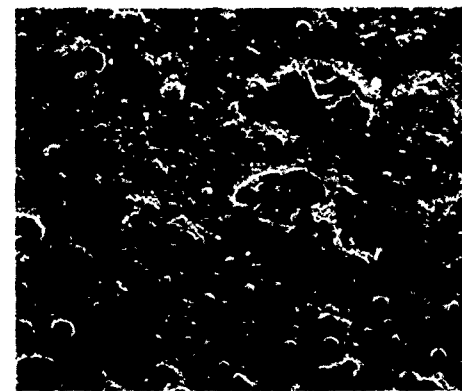


(b) WEAR AREA 300X

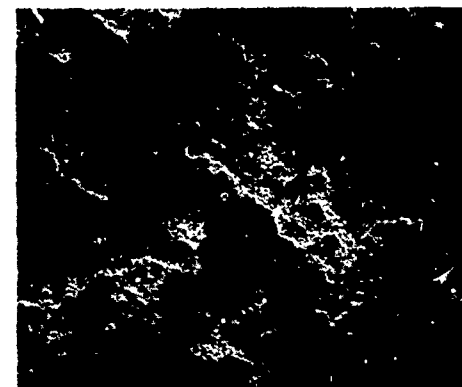


(c) WEAR AREA 1500X

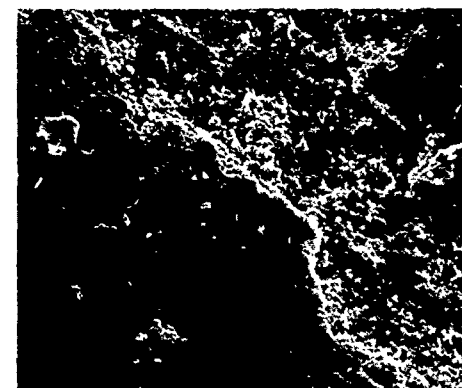
ROUGH DARK COATING (Sample e)



(d) UNWORN AREA 300X



(e) WEAR AREA 300X



(f) WEAR AREA 1500X

Figure 86. Typical Appearance (SEM) of NASA Fluoride Coating  $[(Ba,Ca)F_2 \cdot CaSiO_3 \cdot CaO]$  in Smooth and Rough Areas.

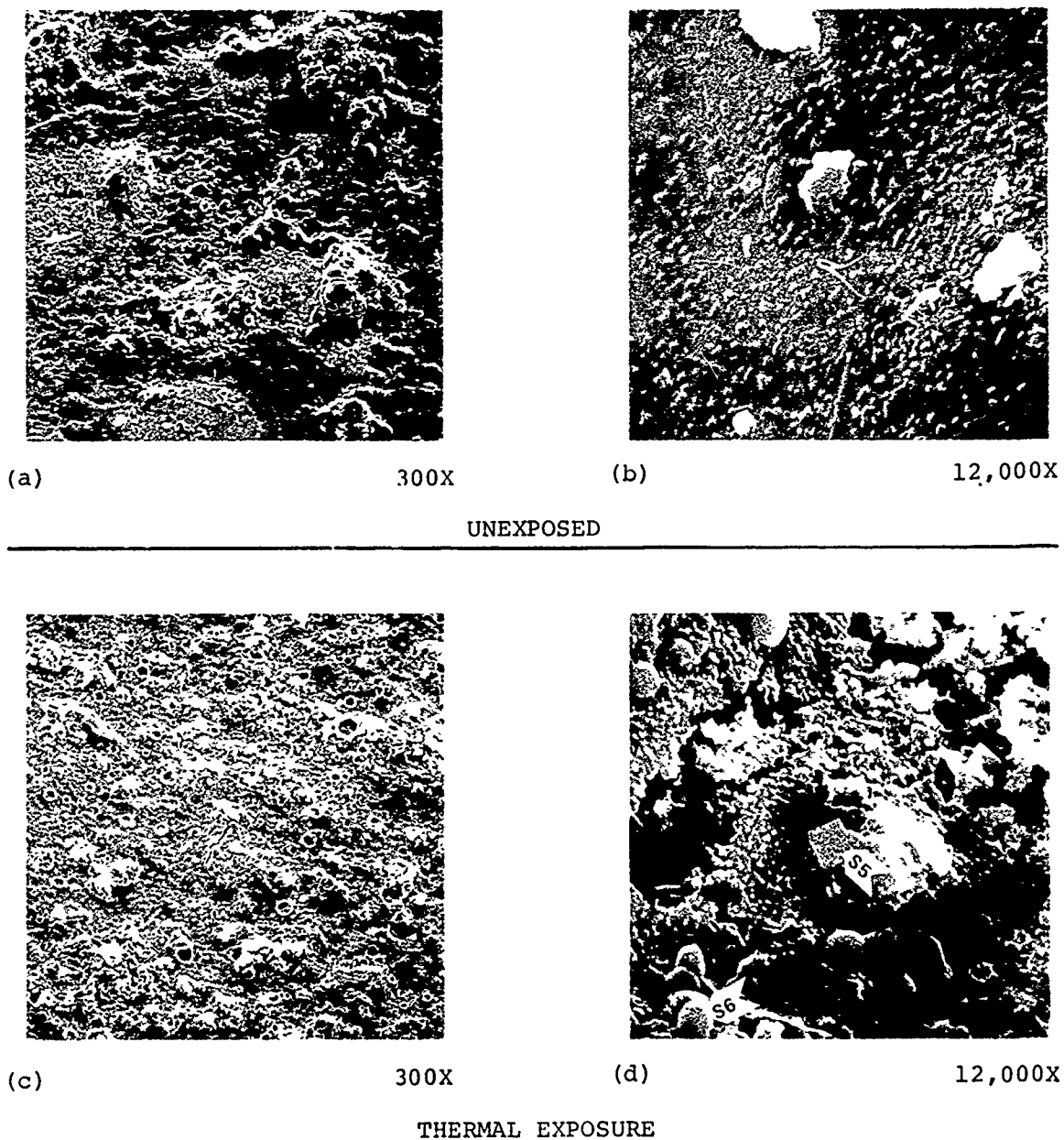


Figure 87. Appearance of NASA  $\text{CaSiO}_3$  Modified Fluoride Coating Before (a and b) and After (c and d) Thermal Exposure at 1200°F for 1300 Hours.

Two specific microstructural features, as well as the general thermal exposed material (Figure 87d, arrows), were electron probed for composition as summarized in Table 15. Of particular interest is the presence of titanium in the block-type particles (analysis S5). Chromium is also high, but is suspected as a contaminant vaporized from the Inconel-718 support tray used to contain the thermal exposure samples. Several other elements appear in the analyses (Ni, Fe, and Al) that are not primary constituents of the coating, but their influence on friction and wear was not assessed.

#### 3.4.5.5.3 Blister Formation on Tribaloy-400 Coated Shafts

Wear rig shafts coated with plasma-sprayed Tribaloy-400 displayed surface blistering after repeated thermal cycling and rig operations to 1000°F (Figure 88). Discussions with the vendor (Plasma Technology Inc.) and scanning electron microscope (SEM) evaluations indicate blistering was related to Ti, Al and/or Ca contamination, which may have occurred from the grit blasting operation used on the substrate alloy surface. Figure 89 illustrates the appearance of the blister fracture surface as viewed by SEM. The dark area (bottom arrow) was analyzed and found to contain alloy constituents (Co, Cr, Mo, and Si) and Fe present as a typical impurity.

The light "fluffy" appearing area (top arrow) showed the presence of Ti and Al contamination in addition to the above. Precautions to eliminate contamination were therefore implemented by the vendor for coating the full scale journal rig shaft.

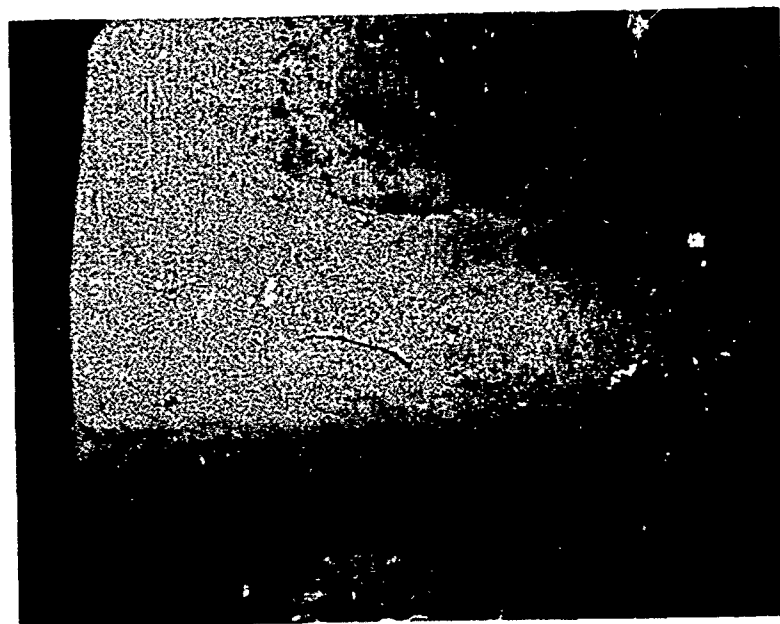
#### 3.4.5.5.4 Generation of Oxide Coating on NiCo Coating

Samples of electroplated NiCo alloy (60 percent Co - 40 percent Ni) were subjected to a series of thermal exposures in air to determine what temperature was required to form metal



(a)

1.1X

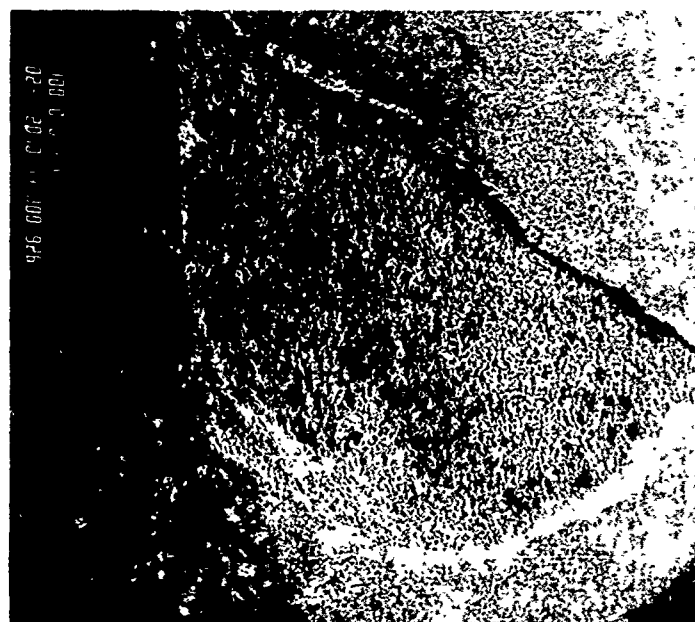


(b)

6.5X

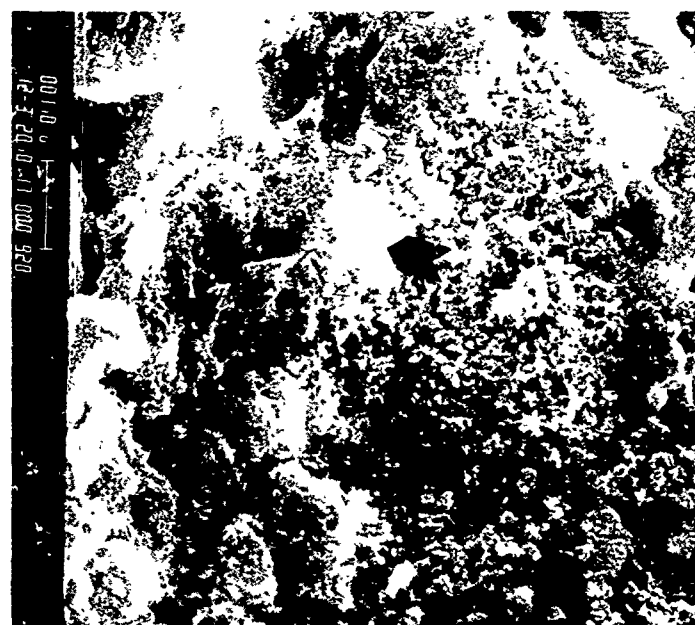
Figure 88. Typical Appearance of Blisters on Surface of Plasma Sprayed Tribaloy 400 Wear Rig Shaft Segment





(a)

20X



(b)

12,000 X

Figure 89. Appearance of Blister Area (a) and Area of Ti and Al Contamination (b)

oxides and what composition those oxides were. Exposures were made at 200°F, 400°F, 500°F, 600°F, 800°F and 1000°F for one hour in static air. X-ray diffraction patterns of these samples were obtained, as well as an unexposed NiCo sample. This analysis indicated:

- o Detectable Ni and Co oxide surface layers were formed at temperatures between 600-800°F and above.
- o Free nickel and cobalt metal appears to be decreasing at temperatures of 600-800°F and above, coincident with oxide formation.

Cobalt-containing coatings, which depend upon the formation of cobalt-oxide for some lubricity and wear resistance (NiCo, HS-25 and Tribaloy-400) require 800°F or higher temperatures for either preoxidation or oxidation during operation.

#### 3.4.5.6 Friction Measurements

Measurements of the coefficient of friction were made for several coating combinations using the experimental set-up shown in Figure 90. Coefficients are summarized in Table 16 in order of the lowest to the highest. Most coefficients were near that of Teflon (0.13) and therefore indicate these coating combinations may be equivalent from that aspect (realizing that this test was conducted under ideal conditions at very low surface speeds, and not at elevated temperatures). Significant observations from this Table as well as other data not presented are as follows:

- (a) Several coating combinations were superior to Teflon or Kaman DES coatings ( $\text{TiB}_2$  or  $\text{B}_4\text{C}$ ).

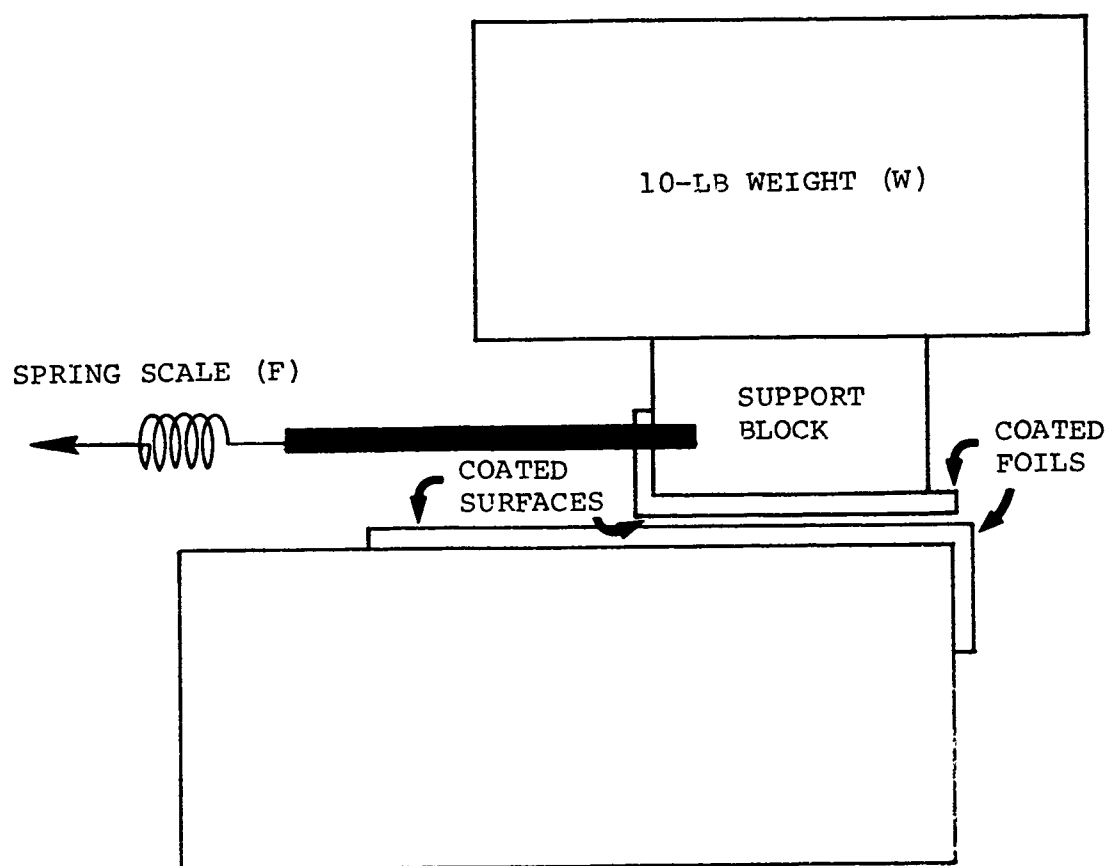


Figure 90. Experimental Setup for Coefficient of Friction ( $C_f$ ) Measurements ( $C_f = F/W$ )

TABLE 16  
MEASURED SLIDING COEFFICIENT OF FRICTION

STATIONARY MATERIAL COATING	SLIDING MATERIAL COATING	COEFFICIENT OF FRICTION (10# LOAD)	
		BREAKAWAY	SLIDING
B <sub>4</sub> C	B <sub>4</sub> C	0.08	0.08
TiB <sub>2</sub>	B <sub>4</sub> C	0.09	0.09
B <sub>4</sub> C	TiB <sub>2</sub>	0.09	0.09
TiB <sub>2</sub>	Gold	0.10	0.10
B <sub>4</sub> C	Gold	0.11	0.11
TiN	Teflon	0.20	0.13
Cr <sub>2</sub> O <sub>3</sub>	Teflon	0.18	0.13
Gold	Kaman (DES)	0.13	0.13
Teflon	Kaman (DES)	0.13	0.13
Teflon	Teflon	0.18	0.13
Kaman (DES)	Teflon	0.18	0.15
B <sub>4</sub> C	Teflon	0.19	0.17
B <sub>4</sub> C	Kaman (DES)	0.18	0.18
Gold	Teflon	0.26	0.18
TiB <sub>2</sub>	Kaman (DES)	0.18	0.18
Cr <sub>2</sub> O <sub>3</sub>	Kaman (DES)	0.18	0.18
TiB <sub>2</sub>	Teflon	0.23	0.19
TiN	Kaman (DES)	0.23	0.20
TiC	Kaman (DES)	0.22	0.22
Kaman (DES)	Kaman (DES)	0.22	0.22
TiC	Teflon	Grabs and Slips	

- o Accuracy of measurements:  $C_f = \pm 0.03$
- o Sputtered coatings show slight dependency on thickness (thinner coating has higher  $C_f$ )
- o Some coatings exhibit break-in  $C_f$  reduction

- (b) Sputtered coatings appeared to show lower friction coefficients than thicker coatings.
- (c) Some coatings exhibited decreased friction coefficients after a "break-in" period.
- (d) Load did not significantly influence friction coefficients until it was great enough to cause degradation of the coating.

#### 3.4.6 Materials Selections for Journal and Thrust Rigs

Several coatings for dry film lubrication at high temperatures (800-1200°F) were evaluated. Specification of appropriate coatings for the full scale journal and thrust foil bearing rigs was based upon 1200°F oxidation resistance, wear rig dynamic torque measurements of friction over the temperature range 70°-1000°F, wear appearance, and sliding friction values.

This data indicated three coatings were acceptable for the rotating component, with NiCo the best based upon drag torque measurements against Teflon-S (peak values at room temperature) as follows:

- o NiCo (14 in.-lbs.)
- o Tribaloy-400 (19 in.-lbs.)
- o Kaman SCA (25 in.-lbs.)

All the above coatings were specified and used for the thrust runner in the thrust bearing test rig. One high temperature coating (Tribaloy-400) was specified for the journal bearing test rig shaft.

Evaluations also indicated several foil coatings were acceptable on the basis of oxidation resistance and friction behavior:

- o  $B_4C$  - Sputtered
- o  $TiB_2$  - Sputtered
- o  $Cr_2O_3$  - Sputtered
- o  $TiC$  - Sputtered
- o Kaman DES - Slurry dip and fired
- o NiCo - Electroplated

While the above coatings are listed in preferred order with respect to oxidation resistance and friction behavior, Kaman DES and NiCo were selected as foil coatings for both full scale rigs. The sputter coatings were not selected due to low thickness, lack of production experience, and high fabrication lead times.

Long term wear resistance was not considered in the above foil coating selections because material evaluation did not provide adequate data on that aspect. However, all of the above foil and shaft coatings displayed the required high temperature and frictional characteristics necessary for foil bearing applications. Additional work should be directed toward improving manufacturing and processing procedures for foil bearing applications.

### 3.5 Bearing Development and Testing

#### 3.5.1 Foil Journal Bearing Development Tests

##### 3.5.1.1 General

The journal bearing development testing can be characterized as three general, sequential phases of activity. Each phase was oriented toward the solution of a particular observable problem with either test rig operation or bearing characteristics. Phase A, which included Configurations 1-10 (refer to Configuration

sheets included as Appendix B), was a sequence of tests designed to eliminate a subsynchronous excitation situation that resulted in several bearing failures. Phase B was initiated with the testing of Configuration 11, the first to eliminate the previous causes of failure. This phase continued through Configuration 18, in attempts to successfully operate the test rig at the design speed of 33,000 rpm. Conclusions reached from this test phase were that the third critical speed (i.e., shaft bending mode) was being excited at the higher operating speeds and that major rig modifications would be required to proceed further. No failures occurred during this phase and Configurations 11 through 18 were all tested with the same bearing foils. The journal bearing test rig was then reworked to shorten the bearing span by 6.0 inches and thus drive the bending frequency so far beyond the maximum operating speed that it could not be excited by bearing dynamics. Phase C, therefore, represented the foil journal bearing development program on the shortened test rig, with the sole intent of developing a bearing with target load carrying capacity.

#### 3.5.1.2 Phase A - Journal Bearing Development Tests

##### 3.5.1.2.1 Eight-Segment Bearing Configurations

The eight-segment bearing configurations represented a direct scale of the DC-10 ECS cooling turbine production bearing configuration from a 2.0 inch journal diameter to the 4.5 inch journal diameter size. Bearing arc length was set to achieve a 47.5 percent overlap based on journal diameter. Bearing foil arc length as a function of overlap is determined from the following relationship:

$$L = \frac{\pi D}{N \left( 1 - \frac{\% \text{ O.I.}}{100} \right)}$$

Where:

L = foil length in inches  
D = shaft diameter in inches  
N = number of foil segments  
% O.L. = percentage overlap

Variation in overlap for a given geometry bearing affects the unlapped length of the foil. Unlapped length and overlap are depicted schematically in Figure 91, which shows the journal fully bottomed in the bearing. (Note: Figure 91 illustrates a theoretical condition only.)

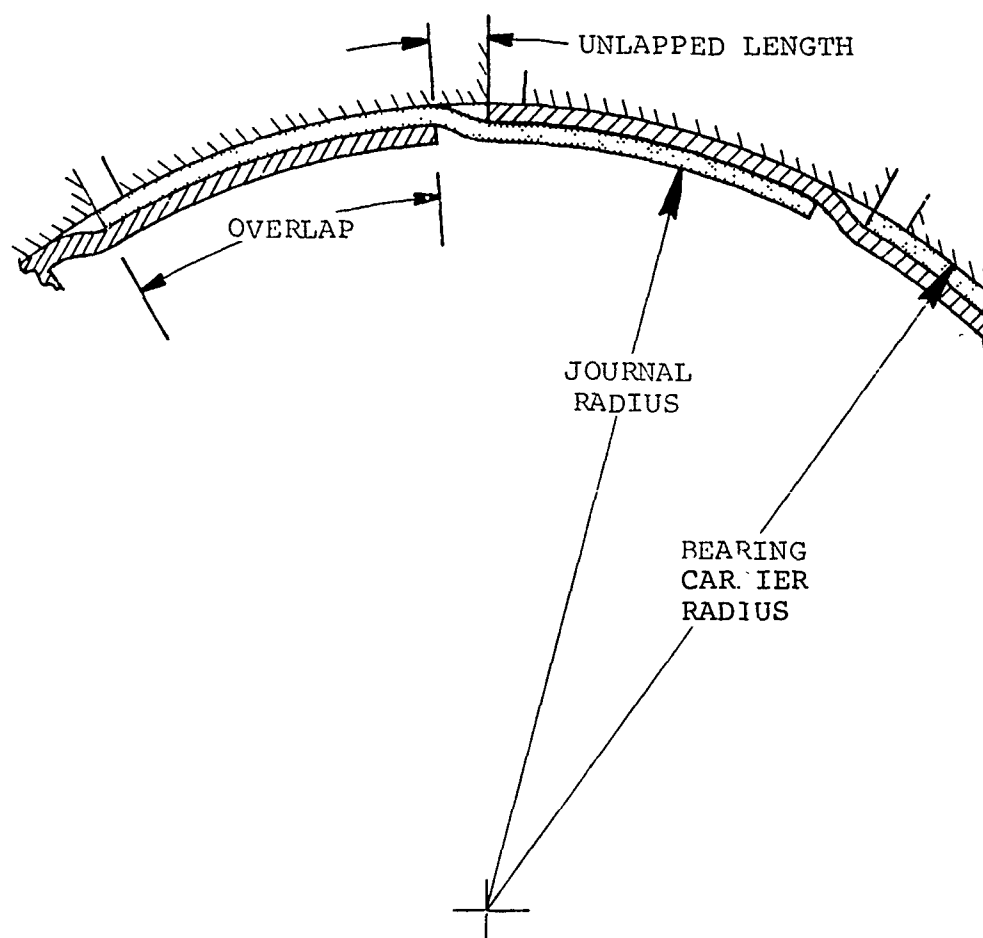


Figure 91. Theoretical Foil Journal Bearing Overlap Schematic.



For a given foil thickness, reducing unlapped length increases the foil bending strain required to achieve a fully bottomed journal, thus increasing the final spring rate (i.e., spring rate at maximum load of the bearing). Figure 92 shows how percent overlap can be varied to obtain a desired unlapped length, given various numbers of bearing segments. Thus a bearing configuration in which the number of foils is selected for bearing stability, can have a desired final spring rate by proper selection of overlap.

Foil coating material used for initial test configurations was OBD26-20, a derivative of Teflon-S, with approximately 75°F higher temperature capability. The journal surfaces were originally plated with thin dense chrome, which on the turbine end journal, was replaced by LW-1N-30 after an early failure. Balancing was achieved by machine balancing the shaft, thrust runner, and drive turbine individually. Match marks on these three components insured constant assembly orientation. Bearing geometry for the first three configurations included 0.010 inch thick foils with a 3.0 inch preform radius and 0.016 inch calculated sway space. Calculated sway space (CSS) is defined as:

$$CSS = BD - JD - 4t$$

where:

BD = bearing diameter in inches

JD = journal diameter in inches

t = total foil thickness (including coating)  
in inches

and is a measure of the total available diametral clearance space. Bearing length-versus-diameter ratio (L/D) for all early test configurations was 1.33. The parachute loader was installed for the initial test work and three failures occurred. It was not possible to obtain design operating speed due to increases in the

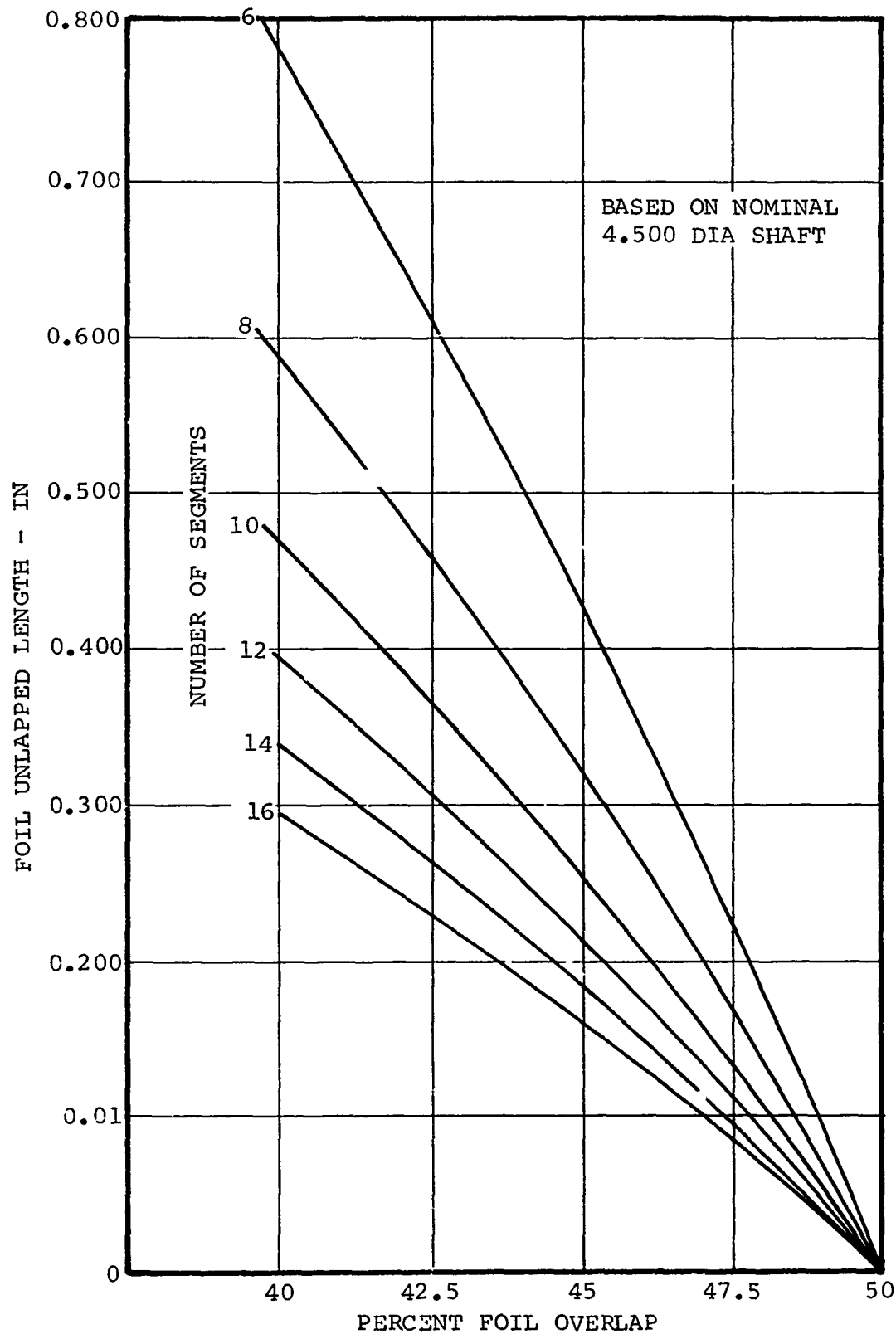
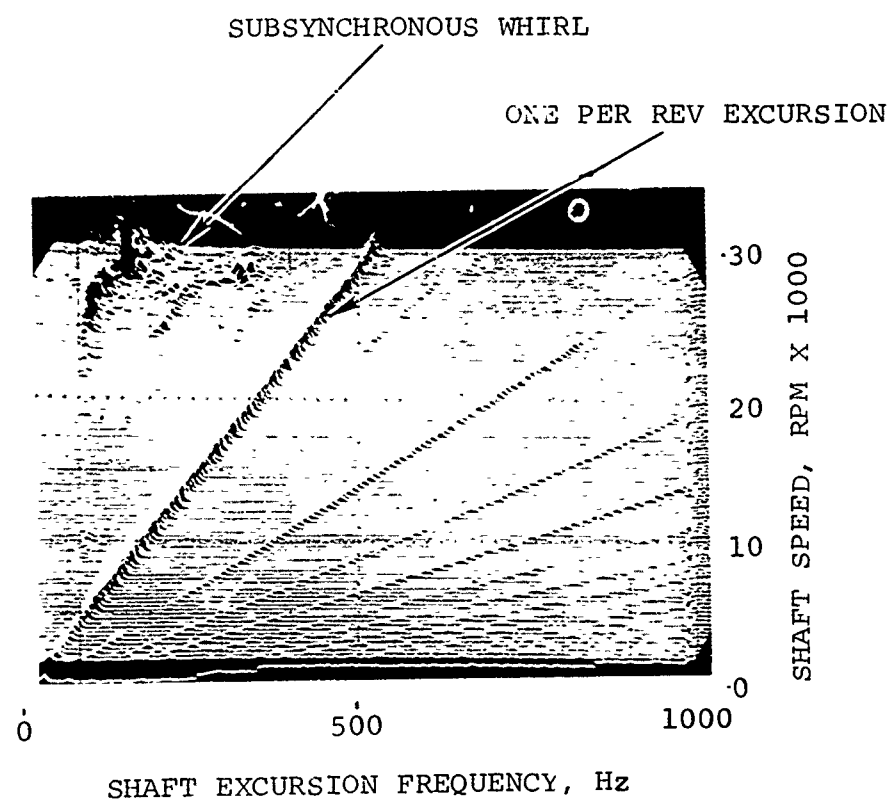


Figure 92. Foil Journal Bearings Overlap vs Unlapped Length

amplitude of subsynchronous shaft excursions with speed, until either failure occurred or testing was terminated. Figure 93 describes the Configuration 3 failure. Configuration 1 incurred a failure while decelerating from an unsuccessful attempt to reach operating speed. Failure was attributed to unacceptable growth of the second critical speed orbital amplitude.

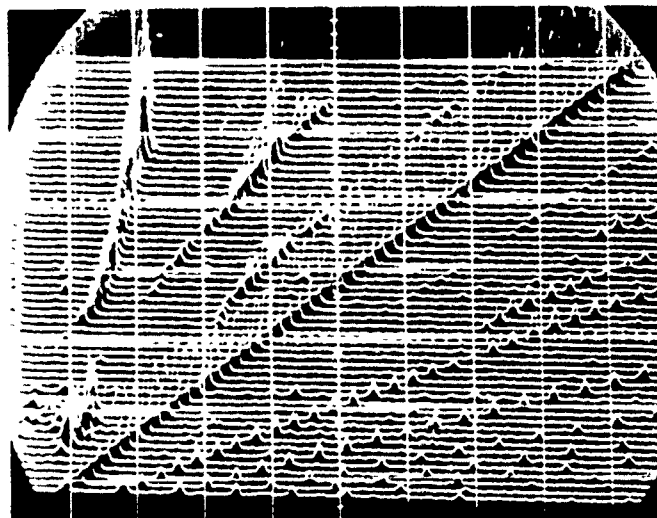
As part of the normal development and diagnostic procedures for this program, nonsynchronous whirl measurements, both subsynchronous and supersynchronous, have been made. Frequency decomposition of signals obtained from Bently probes, CEC vibration pickups, accelerometers and strain gauges were obtained from a Spectral Dynamics 330A spectrum analyzer. By passing the signal through a series of narrow-band filters, input decomposition can be achieved for a specified operational speed.

The so-called "mountain range" shown in Figures 93 and 94 is generated by a series of frequency decompositions at specified speeds. As speed is increased, the frequency decomposition is displaced vertically and produces the frequency spectrum analyses for the entire speed range. Figure 94 is a mountain range acceleration pattern observed on the GTCP36-50 APU rotor dynamics rig. The pronounced diagonal line extending from the lower left to the upper right in both photographs represents imbalance (one-per-rev) response. To the left of this line is the subsynchronous excitation, whereas the supersynchronous excitations are viewed to the right of the imbalance response line. The top photograph was obtained from signal conditioning of a proximity probe located over the compressor. The bottom photograph is an overlay of the top photo and the modes determined by analysis. As shown, the excitation of the first forward and backward modes proved most sensitive. Difficulty in reaching maximum speed was encountered on some occasions. For this example, a squeeze-film mount, located over the compressor bearing was successfully used to reduce nonsynchronous effects as well as to reduce bearing loads on the GTCP36-50 APU.



CONFIGURATION 3  
Figure 93. Shaft Excursion Characteristics

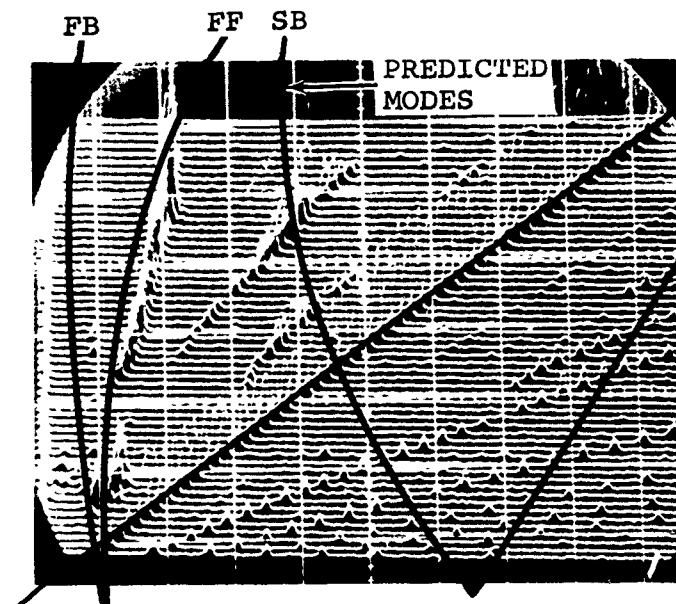
ROTATIONAL SPEED, 8000 RPM/CM



1 PER REV

WHIRL FREQUENCY, 100 CPS/CM

ROTATIONAL SPEED, 8000 RPM/CM



1 PER REV

SF

WHIRL FREQUENCY, 100 CPS/CM

FB - FIRST BACKWARD MODE  
FF - FIRST FORWARD MODE

SB - SECOND BACKWARD MODE  
SF - SECOND FORWARD MODE

Figure 94. Mountain Ranges Obtained From the GTCP36-50 APU Rotor Dynamics Rig.

A final configuration was run without the parachute loader installed and was trim balanced to minimize the high speed unbalance effects. It was not possible to reach design speed with this test.

Five eight-segment bearings were tested in this first test sequence with three bearing failures occurring. The maximum speed attained was 32,500 rpm, with all configurations exhibiting shaft excursions at frequencies below the 1/rev. excitation.

#### 3.5.1.2.2 Six-Segment Bearing Configurations

Configuration 4 was established with a six-segment bearing, 0.010 inch thick foils coated with OBD26-20. The objective was to increase bearing compliancy through the use of longer foils. Subsynchronous activity was again observed in this test, with a calculated sway space (CSS) of 0.021 inch. The next configuration, with CSS reduced to 0.013 inch, resulted in a test bearing failure. Attempting to improve performance through high speed trim balancing produced no better results, nor did the addition of a 9.0 pound mass at the test end of the shaft, intended to symmetricize the bearing loading by simulating the mass of the turbine. The final six-segment bearing test was an attempt to multi-plane balance the shaft. Although balancing was accomplished, another failure occurred, again characterized by subsynchronous excursions. All six-segment bearing tests were run without the parachute loader installed, to avoid loader complicity in the test results.

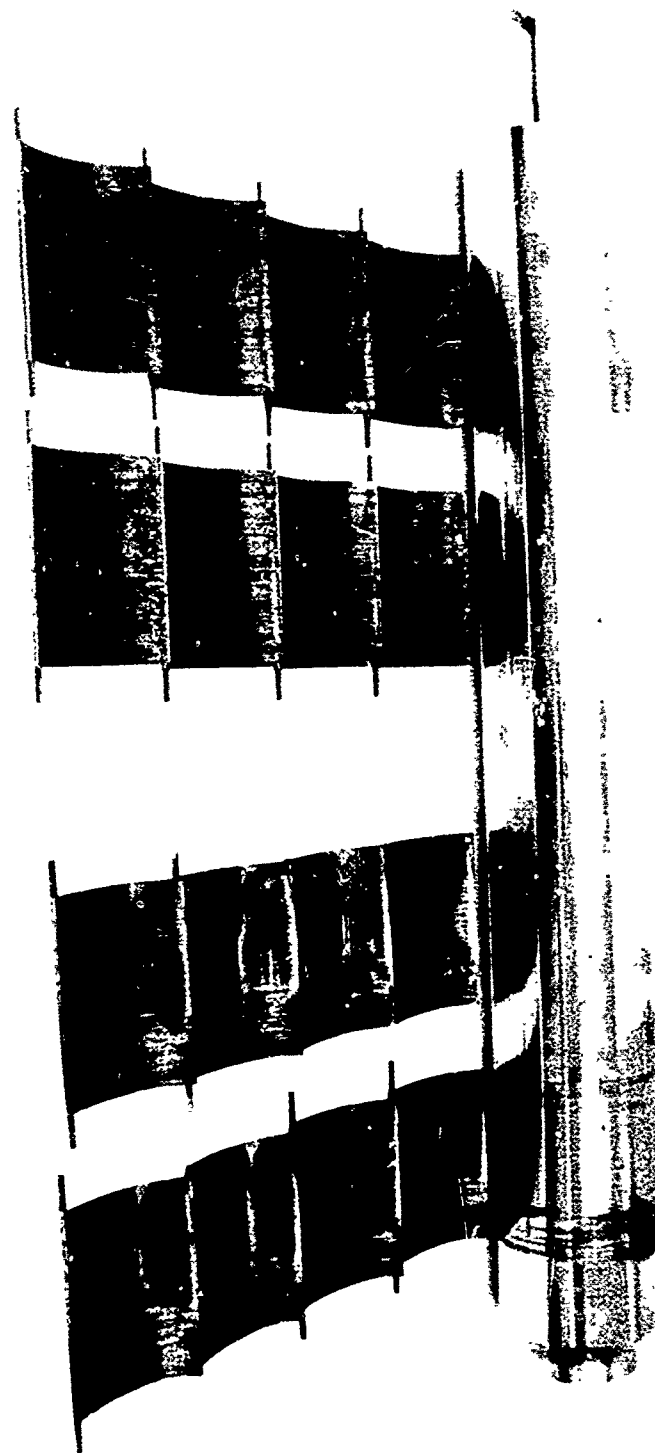
Five configurations were tested during this test sequence, with various amounts of sway space and machine, trim, and multi-plane balancing. Tests resulted in attaining maximum speed of 30,000 rpm, two failures and a continuation of the subsynchronous phenomenon.

### 3.5.1.2.3 L/D = 1. Bearing Configurations

Several failures earlier in the testing were characterized by bearing rubs in the center of the foils. It was therefore theorized that the air film might have been pumped away from the bearing midspan, starving that area and allowing the foils to contact the shaft. Shortening the bearing length, while obviously limiting bearing maximum load capacity, was thought to ameliorate this presumed problem.

Configuration 9 was tested as an eight-segment bearing with 0.012 inch thick foils and 3.4 inch preform radius. Foil coating was OBD 26-5 and shaft coating was electroless nickel. Both thickness and preform increases were intended to increase bearing stiffness to compensate for the reduced bearing length. The result was a very tight bearing as measured by breakaway torque (determined by slowly rotating the shaft with a torque wrench). This tightness, together with the surface characteristics of the shaft resulted in almost instantaneous deterioration of the OBD coating upon initial starting, and thus failure. This failure terminated further use of electroless nickel as a shaft material, and upon reviewing poor performance, also terminated the use of the OBD type foil coatings. These coatings, while providing an increase in operating temperature relative to Teflon-S, had demonstrated a lack of tolerance to small rubs and a tendency to ball up upon failure and thus increase the resulting damage level. The failure of Configuration 9 is shown in Figure 95.

Because of the nature of the previous failure, another  $L/D = 1.0$  configuration was established. This test was unique in that strain gages were attached to the back of two of the eight foils to determine if foil flutter (aeroelastic instability) was exciting the continually observable subsynchronous excursions.



CONFIGURATION 9

Figure 95. Test Journal Bearing and Shaft



The strain gage installation is shown in Figure 96. The stainless steel shim stock attached to the back of the foil was used to avoid local bumps caused by the gages, and to reduce the bearing sway space for these 0.010 inch thick foils. Testing again revealed dangerous subsynchronous activity levels. Strain gages indicated that foil flutter was neither a driving force for the low frequency nor a consequence of that activity. No flutter of any kind was noted.

#### 3.5.1.2.4 Test Rig and Bearing Investigations

While it was believed that the problems experienced to date had been a result of bearing operational characteristics, several investigations of test rig assembly and operation were made. Dimensional checks were made on the shaft-to-turbine pilot diameters, orthogonality of the thrust runner, and airflow distribution within the test rig. Figure 97 indicates the general coolant through-flow characteristics of a static journal bearing. In order to obtain this data the test rig was modified to provide bearing inlet and exit pressure information. Subsequent to this modification, bearing pressure ratio was used instead of the coolant supply line metering orifice to set coolant flow rate. Additionally, the effect of the hydrostatically supported dynamometer upon bearing characteristics was investigated. Several tests were run either with the dynamometer physically locked or with no hydrostatic air supply. Results showed that the bearing radial freedom permitted by the hydrostatic support did not contribute to the observed problem, nor did this support assist by acting as a squeeze film damping mechanism.

Having ascertained that the rig could not be the cause of the observed problems, the bearing characteristics exclusive of the rig were investigated. Using a dummy shaft, a test setup as



Figure 96. Foil Journal Bearing Strain Gage Installation

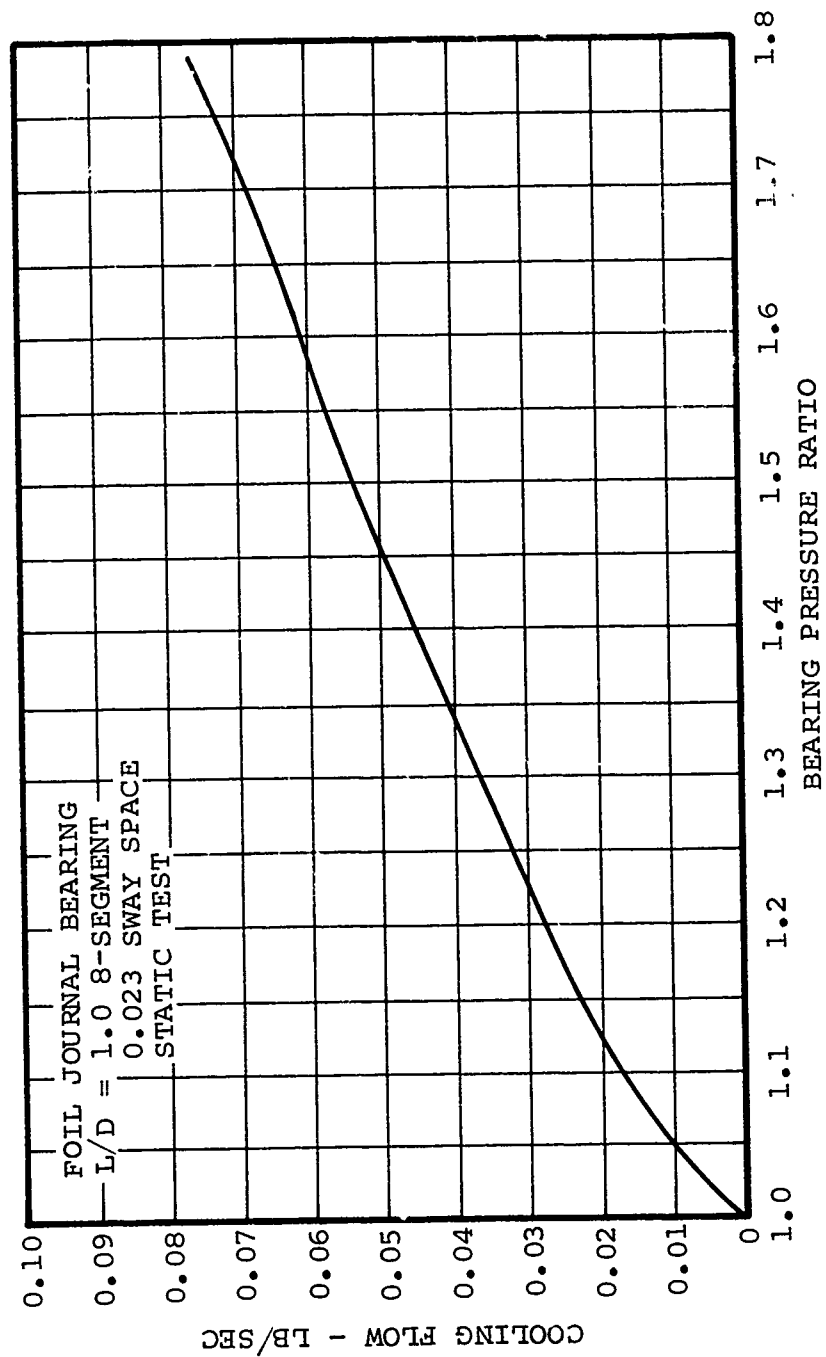


Figure 97. 8-Segment Bearing Static Cooling Flow Test

shown in Figure 98 permitted determining the load-deflection characteristics of the various journal bearing configurations. Figure 99 shows typical load/deflection data, in this case the Configuration 27 bearing. Bearing test results are indicated in Table 17.

In order to operate successfully, i.e., without subsynchronous shaft activity, it appears that certain bearing characteristics must be present. The data on the original eight-segment bearing indicates a relatively stiff bearing at 1 g, one which would not deflect appreciably under typical 1/rev unbalance conditions. The unsuccessful six-segment bearings display this same phenomena to a more extreme degree. Since stiffness prevents the bearing from accommodating small excursions, intermittent rubbing of the journal on the foils could take place during operation. Instability experienced by hydrodynamic bearings during rub is primarily subsynchronous in nature, which was observed during the eight- and six-segment bearing tests. Thus bearing stiffness may likely have been the cause of the failures.

As indicated, the 12- and 10-segment bearing configurations exhibit a more modest spring rate, thus better accommodate the 1/rev unbalance. Operation of these configurations was without subsynchronous activity. The 16-segment configuration, while exhibiting an apparently acceptable spring rate, experienced a large deflection. This bearing, designed to permit entry of film air into the center of the bearing, is shown in Figure 100. This configuration therefore appeared to be a risk, either because of the initial softness or because of the large initial deflection, leaving little remaining operating sway space.

It should not be construed that static spring rate of a given bearing geometry is the sole determinant of operational stability.

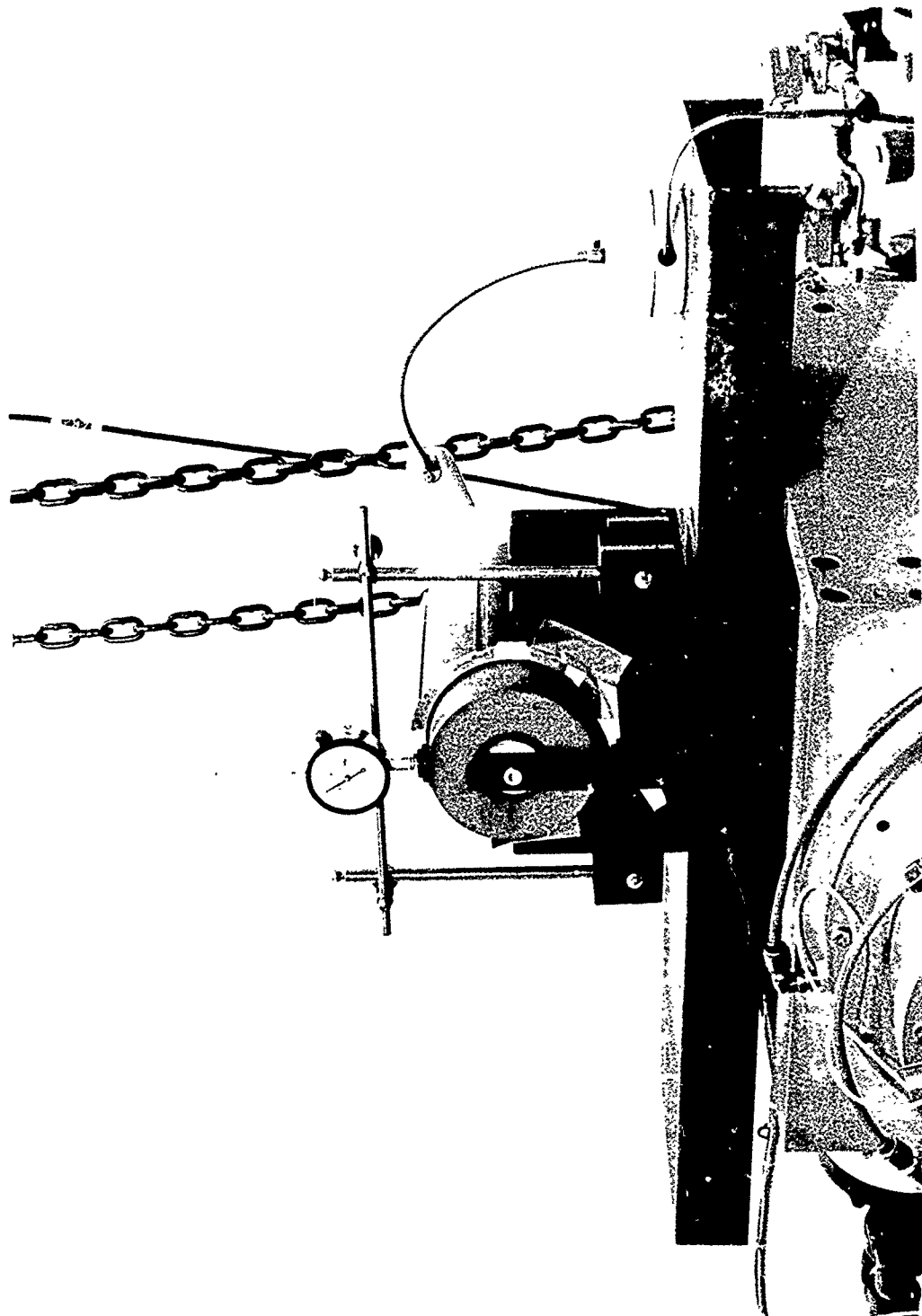


Figure 98. Journal Bearing Spring Rate Measurement Test Set-up

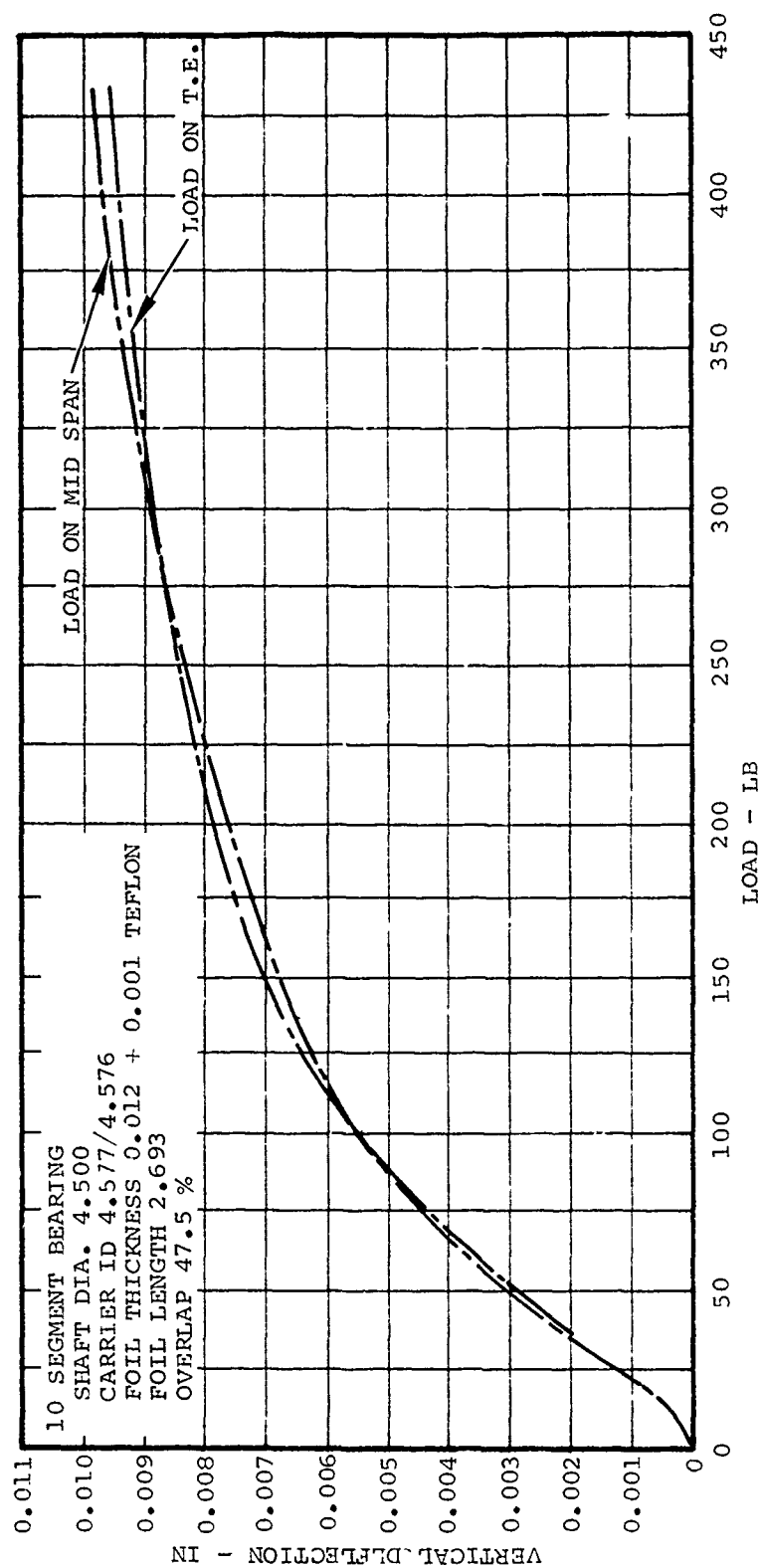


Figure 99. Load/Deflection, 10-Segment Journal Bearing

TABLE 17  
JOURNAL BEARING SPRING RATE SUMMARY

SEGMENTS	CONFIGURATION FOIL THICKNESS	% OVERLAP	1G LOAD 28 LB		450 LB LOAD	
			DEFLECTION MILS	SPRING RATE LB/IN	DEFLECTION MILS	SPRING RATE LB/IN
6	0.012 + 0.001	42.5	1.0	27500	11.2	174,400
6	0.012 + 0.001	48.5	.5	86700	9.5	89,500
8	0.010 + 0.001	47.5	3.1	18000	N/A	N/A
8	0.010 + --	47.6	8.8	17050	13.8	220,700
10	0.012 + 0.001	47.5	2.2	13130	9.7	305,900
12	0.012 + 0.001	47.5	3.1	9700	11.2	116,000
12	0.012 + 0.001	47.5	3.4	10600	9.0	264,000
16	0.085 + 0.001	47.5	6.3	12600	10.2	700,000

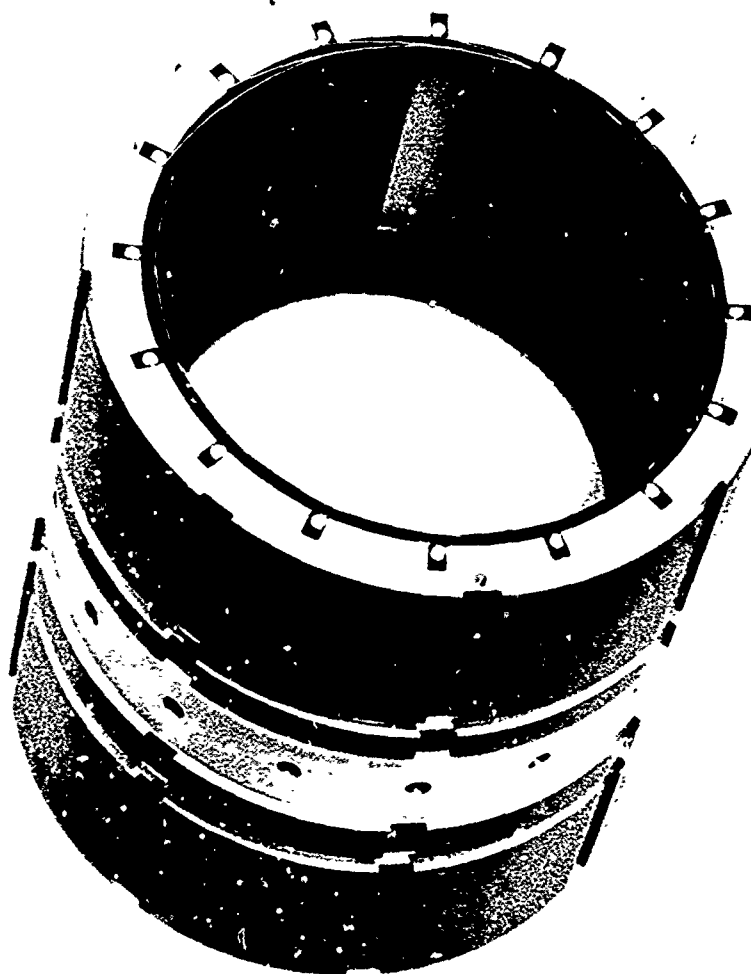


Figure 100. 16-Segment Bearing Design



The test provides no information about resiliency of the supporting air film once the shaft has lifted off. Nor does it yield any data about dynamic damping, a necessary parameter for shaft stability, which does not appear to be substantial in air bearings, despite some foil-to-foil coulomb interaction. And finally, bearing geometries that have exhibited acceptable spring rate characteristics have shown subsynchronous instability until sway space was reduced by adding shims. The relationship between stability and sway space for a constant spring rate bearing has not been established.

### 3.5.1.3 Phase B - Journal Bearing Development Tests

#### 3.5.1.3.1 12-Segment Bearing Initial Tests

Configuration 11 was the first bearing assembly using a 12-segment foil geometry. Foil thickness was 0.012 inch with a 0.001 inch thick Teflon-S coating. Foil L/D was 1.33 with preform radius of 2.9 inches. Calculated sway space was 0.023 inches with the actual sway space measured at approximately 0.015 inch. Test bearing journal coating was thin dense chrome with turbine bearing journal coating of LW-1N-30. Several starts were made without any incidents of subsynchronous activity, but as shaft speed increased, orbital amplitude excursions increased to 0.00325 inches at 30,000 rpm at the test bearing. It was felt that the combination of low operational sway space and some shaft unbalance was contributory to the high excursions, so the bearing carriers were slightly machined and the shaft trim balanced (one speed, one plane). Measured sway space increased to approximately 0.020 inches but this configuration (Configuration 12) exhibited orbits of 0.006 inch at 30,900 rpm. Bearing performance comparisons of the 6, 8, and 12 segment bearing including shaft whirl amplitude, for those configurations where it was available, did not give any insight to the reason for the test rigs inability to operate at full speed. However, the 12 segment bearing being the stiffest of the three was able to operate without failure and thus permit an intensive investigation as to the cause of the previous bearing failures.

#### 3.5.1.3.2 Aerodynamic Investigations

It was surmised that the problem preventing attainment of design speed could be related to aerodynamic phenomena, specifically Reynolds number effect on turbulence. Configurations 13, 14, and 15 were tested using carbon dioxide (CO<sub>2</sub>), hot air, and helium as coolants, respectively, in order to significantly change coolant kinematic viscosity. No improvement was noted; in fact, the pressure pulse transmitted to the bearing, upon opening the high pressure helium bottle regulator, appeared to trigger some short duration subsynchronous instability.

Configuration 16 was run with increased drive turbine clearances to investigate the possibility that drive turbine vibratory excitation was causing the bearing problems. Additionally, because the parachute loader was observed to have significant vibratory response, both aural and visual, it was coated with 0.010 thick viscoelastic damping material. Several runs, with and without the loader, and with loader side stiffener plates installed, provided no improvement.

#### 3.5.1.3.3 Shaft Bending Investigations

One of the most important technical considerations in designing reliable, high speed rotating machinery is the rotor dynamics. All rotating equipment produces loading on its bearings and support structure due to the centrifugal loads encountered by the rotating mass. These loads are generated due to centrifugal effects because the center of gravity of the rotor is not coincident with the geometric centerline of the bearings. Although balancing may reduce the centrifugal loading, when rotation occurs, a periodic excitation develops at a frequency equal to the rotor spin. If the excitation frequency is equal to a natural frequency of

the system, then a "critical" speed is encountered and large excursions may be expected. Therefore, the severity of this particular critical speed is solely dependent upon damping and unbalance, as the former can control the excursion limit at a natural frequency.

It is noteworthy that if the rotational speed equals the natural frequency of the system, it may or may not be a critical speed. To clarify, it is necessary to provide some definitions. First, as the deformed geometric centerline of the rotor precesses (whirls) about the undeformed bearing centerline, a whirl speed is defined. Second, spin speed is the circular frequency of the rotation of the mass center about the geometric deformed centerline. If the natural frequency produces a whirl in the same direction as the spin, it is said to be a forward mode. A backward mode is obtained when the whirl is in an opposite direction from the spin. A critical speed occurs by definition, when the unbalance excitation (spin speed) is equal in magnitude and direction to the natural frequency or when the rotational speed intersects a forward mode. When the rotational speed intersects a backward mode a natural frequency is encountered, but it is not a critical speed as it is difficult to excite by unbalance. The mechanisms that provide for the existence of both forward and backward precessional modes are gyroscopic effects and specialized bearing characteristics. Backward modes, although not easily excited, may be severe and also produce substantial shaft excursions.

Therefore, further investigations (Configurations 17 and 18) incorporated orthogonal proximity probes in the center of the shaft normally occupied by the parachute loader. The installation is shown in Figure 101. By obtaining data from the existing two sets and these additional probes, speed deformation characteristics (Figure 102) were identified. As illustrated, shaft bending

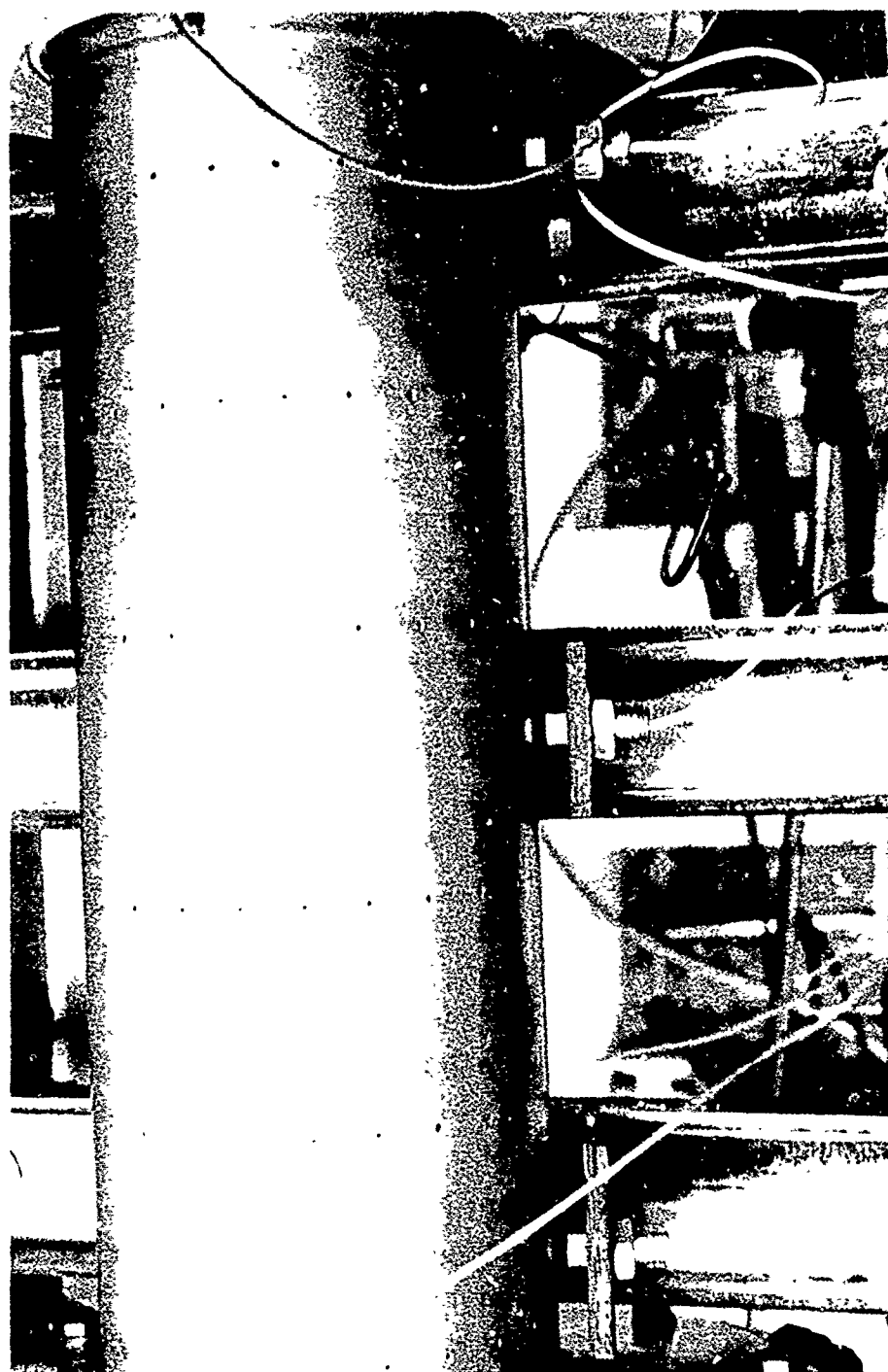


Figure 101. Center 3 of 5 Plane Clearance Probes Used to Determine Shaft Bending in Configuration 18

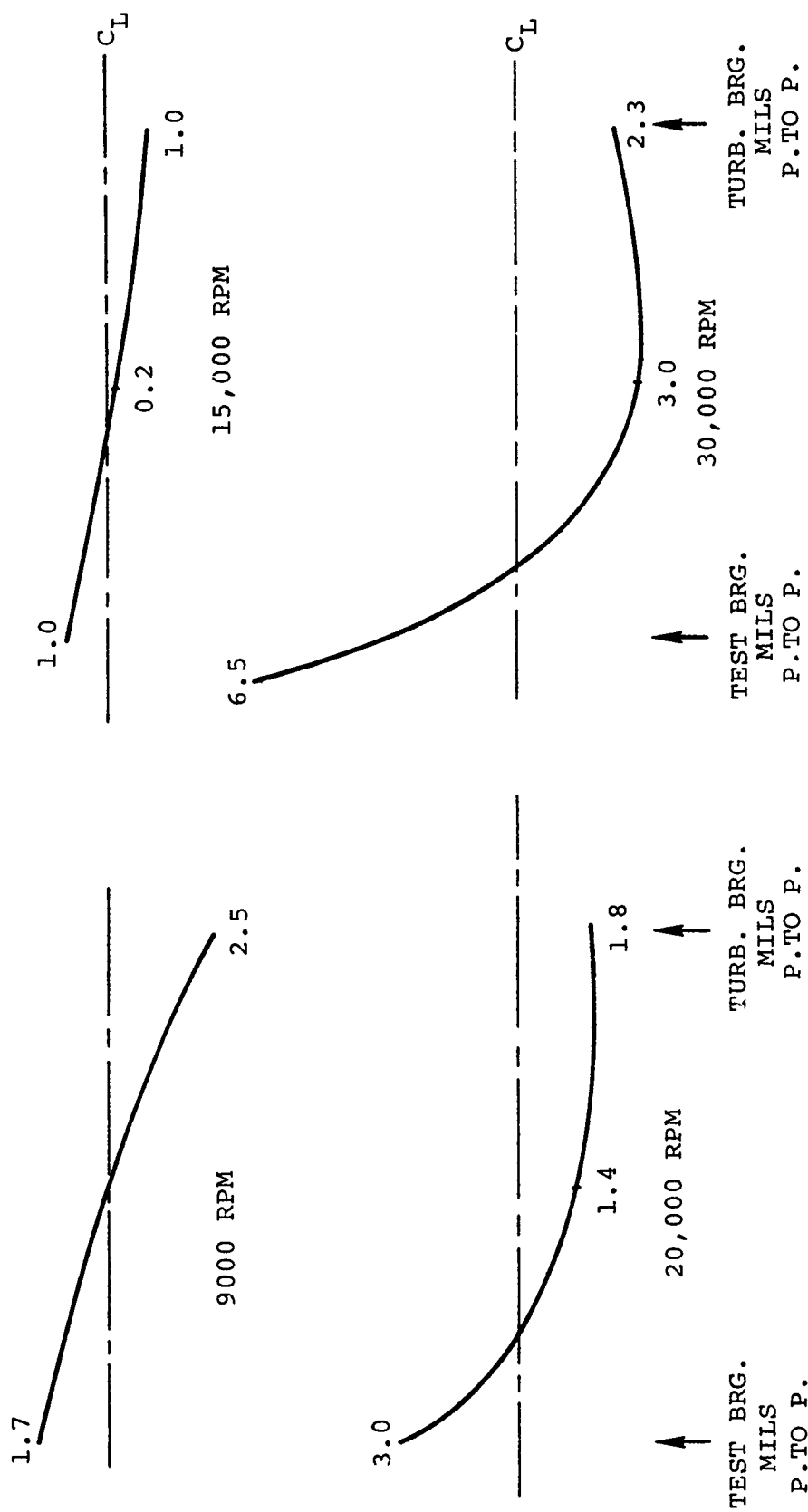
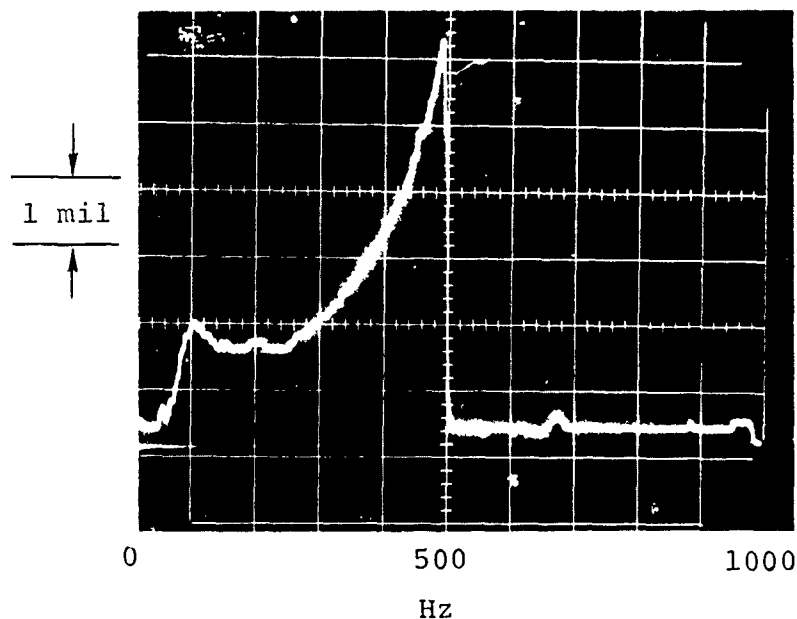


Figure 102. Measured Shaft Bending at Speed.

began at approximately 20,000 rpm, and became more pronounced at 30,000 rpm. The rate of amplitude increased with speed as shown by the roll-down of the test bearing 1/rev amplitude from approximately 30,000 rpm below:



Data reduction confirmed that the system was operating in a forward precession mode (precession and shaft rotation in the same direction).

A rotor dynamics analysis review performed on this rig (Figure 103) showed that predicted critical speeds were acceptable for operation at 33,000 rpm. To substantiate the analytic model, a comparison was made of the experimentally determined free-free modes, to those predicted by the rotor dynamics model. The results are shown in Figure 104, which demonstrates excellent analytical/experimental correlation. Also, the two rigid body criticals location confirmed by observation of rig low speed performance, indicates two low-frequency modes at 60 to 70 Hz, and are the first and second natural modes of this system (Figure 105.)

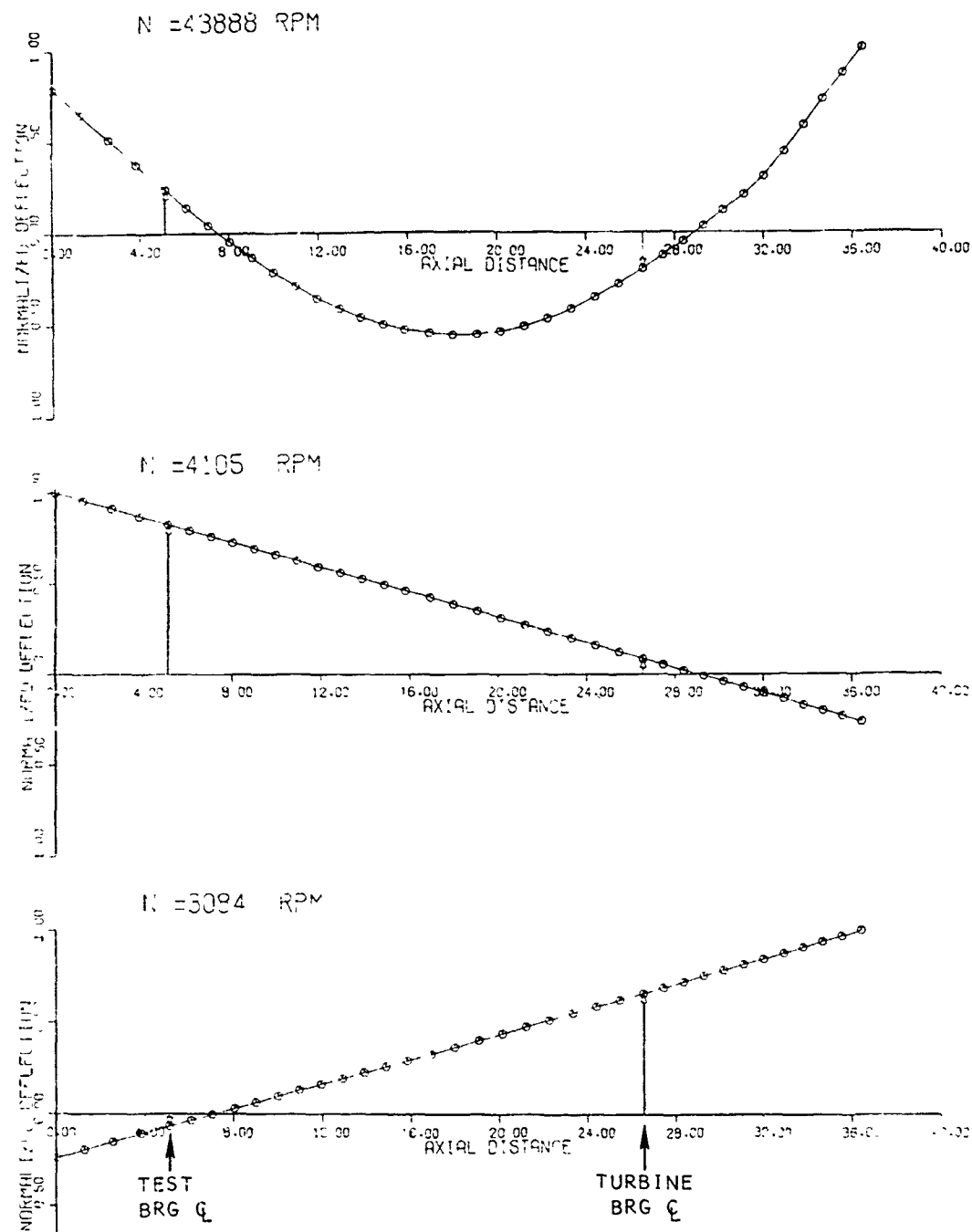


Figure 103. Normalized Mode Shapes, TJE331 Foil Journal  
Bearing Rig - Bearing Spring Rate = 10,000 LB/IN.

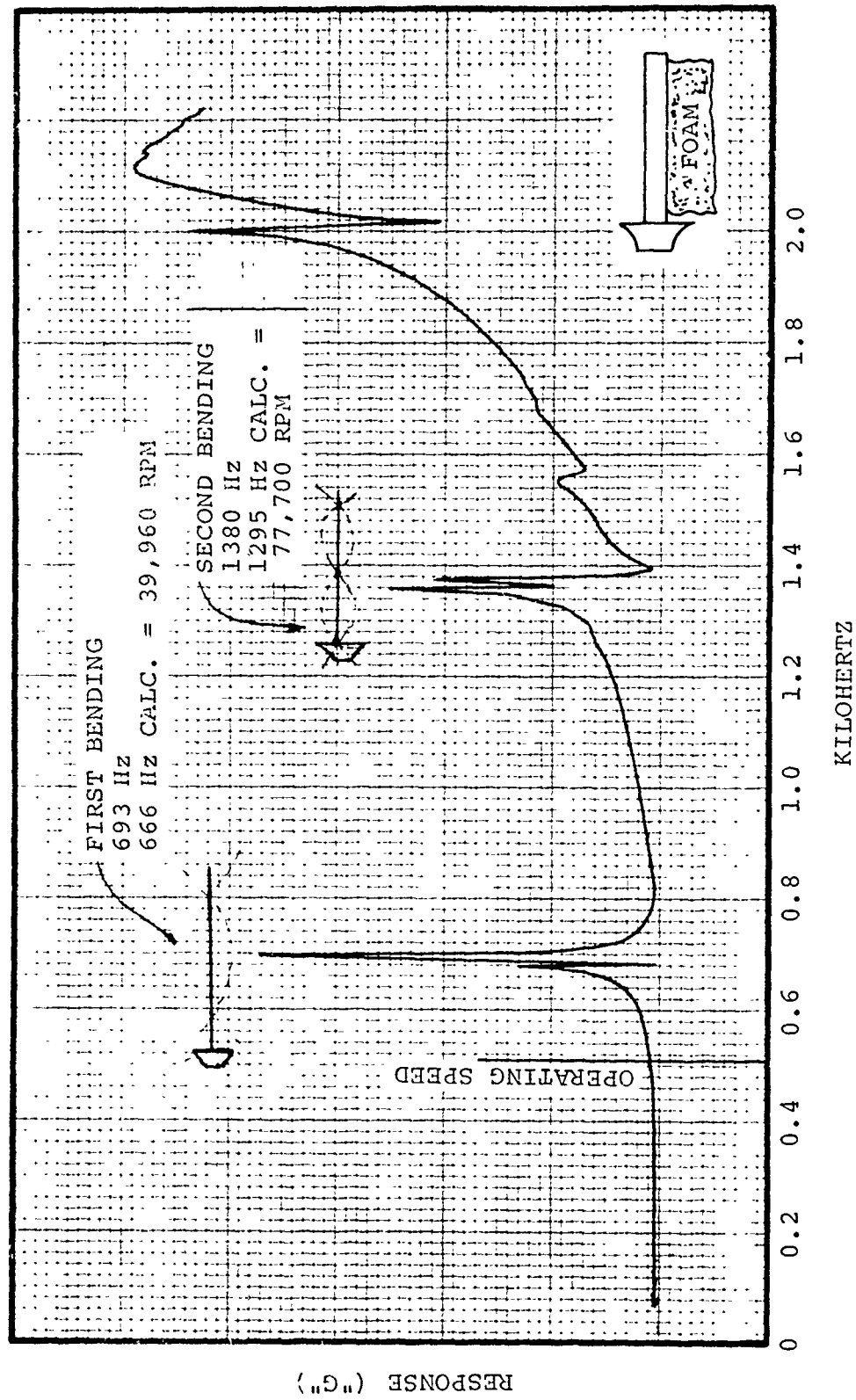


Figure 104. Free-Free Shaft Excitation



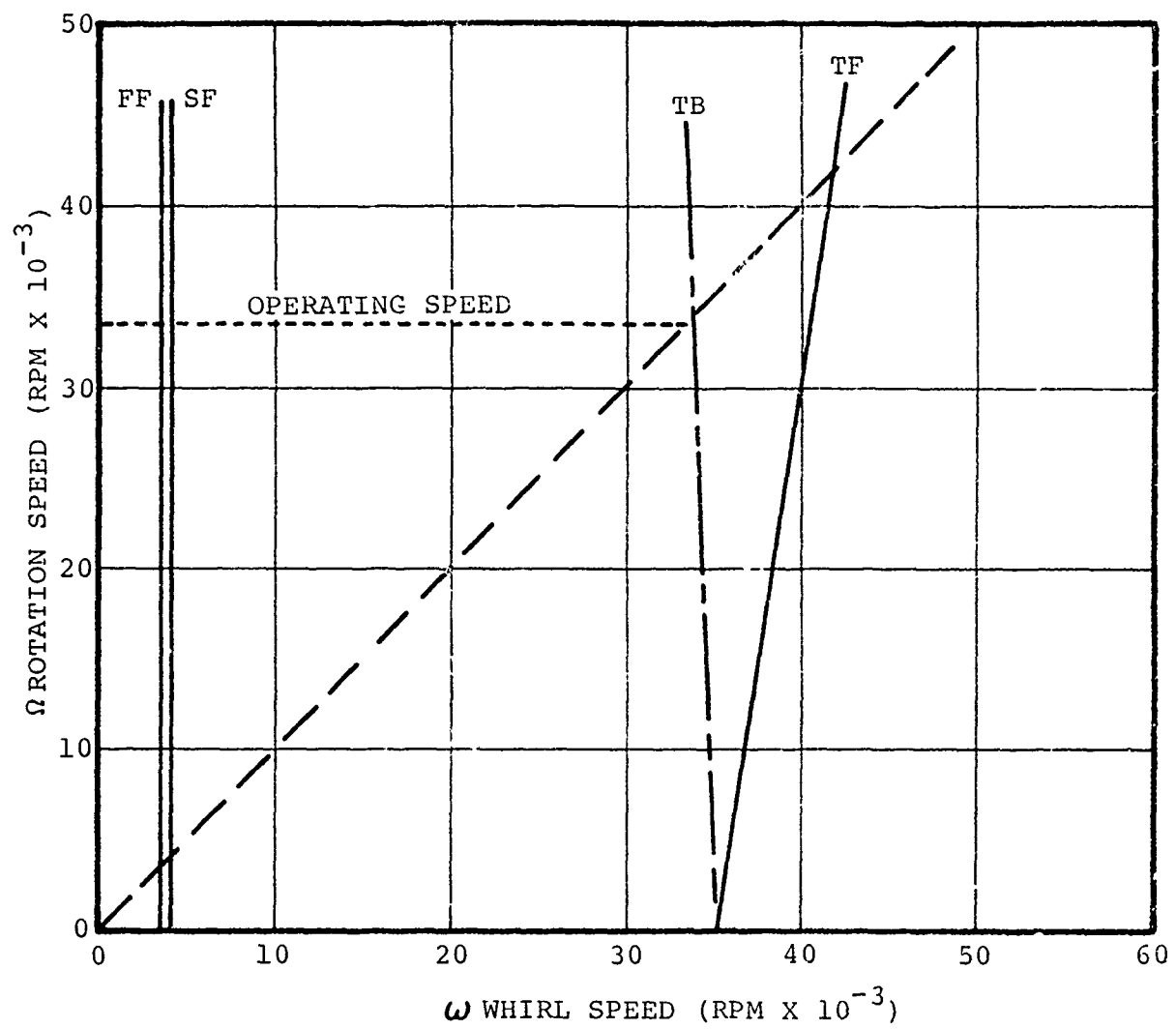


Figure 105. Shaft Whirl Influence on Critical Speeds.

The most attractive method available to drive the onset of bending well above operating speed was to shorten the bearing span, thus increasing the bending rigidity of the shaft. The influence of span on critical speed is shown in Figure 106. Shortening the shaft by six inches was selected to provide 140 percent operating margin above the third backward bending critical speed.

It must be pointed out that the interrelationship between the foil journal bearing operation and the shaft system rotor dynamics is not completely understood. The apparent lack of substantial bearing damping capability may contribute to higher shaft orbital excursions than would be present with other types of bearing systems.

#### 3.5.1.4 Phase C - Journal Bearing, Development Tests

##### 3.5.1.4.1 Twelve-Segment Bearing Configuration

The test rig was shortened six inches by remachining the side plate mounting holes and the shaft was shortened by removing six inches from the test end. The test bearing now covered three rows of holes previously used to supply air to the parachute loader. These holes were plug welded. A new parachute loader was designed to accommodate the shortened rig, and incorporated changes both to increase its stiffness and to facilitate installation. In addition to these changes, three proximity probes were installed in the turbine end bearing carrier to observe relative changes in foil position.

Configuration 19 was assembled using the same 12-segment bearing foils as had been used throughout Phase B. Because of several reworks required to provide a good thin dense chrome journal surface over the weld-repaired holes, the test bearing

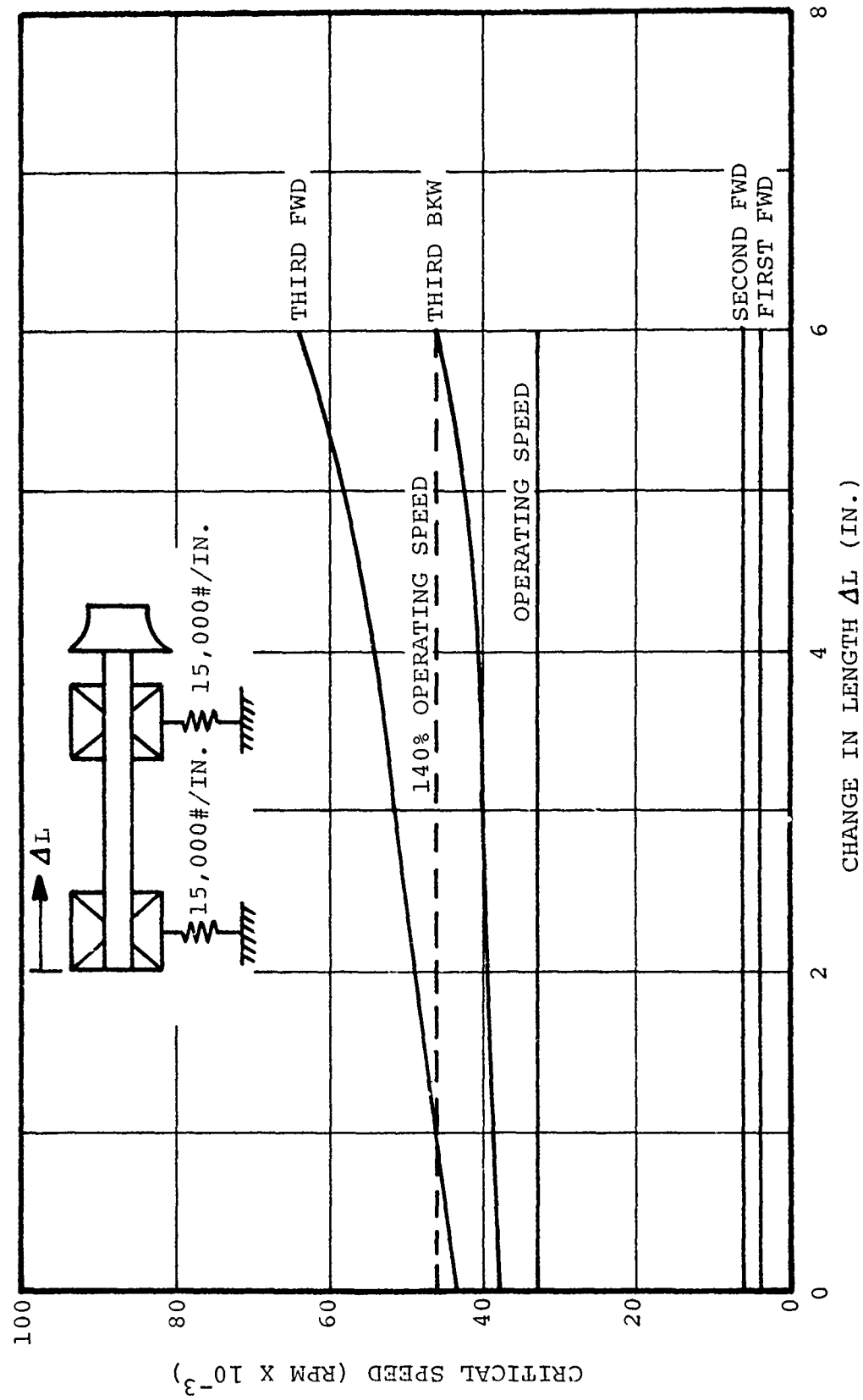


Figure 106. Shaft Shortening Influence on Critical Speeds.

calculated sway space was 0.0295 inch. Initial tests showed continued subsynchronous activity, which was modified somewhat when the parachute loader was installed. Vibration in the parachute loader was minimized by aluminum viscoelastic damping tape. Midplane probes confirmed that the bending phenomenon had been eliminated. Shims were used to reduce the Configuration 20 test end calculated sway space to 0.0215 inch and the rig was run to a maximum speed of 34,000 rpm with no subsynchronous activity or shaft bending noted.

Configuration 21 represented the development of the parachute loader. It had been observed that viscoelastic damping tape modified loader vibration but sufficient vibratory energy was present either to separate the adhesive bond or fatigue-fail the aluminum. The final loader configuration is shown in Figure 107. The stainless steel wrap shown is used to maintain the damping material in contact with the loader.

To ensure successful loader operation, the journal bearing shaft was multi-speed/multi-plane balanced. This technique was used to limit the shaft excursions in the area of the parachute loader without major bearing orbits at 33,000 rpm, and to minimize the second critical frequency effect during start and stop. Configuration 23, using the shimmed 12-segment bearing with the balanced shaft and optimized parachute loader, experienced a failure at a bearing load of 6.549 psi. Results of this failure are shown in Figures 108 and 109.

The Configuration 23 failure represents the first instance of reaching bearing ultimate capacity at design rpm. The bearing load of 6.549 psi, while considerably below bearing target load of 16.4 psi, represents a supported weight of 176.8 lb per bearing, equivalent to a 6+ g maneuver.

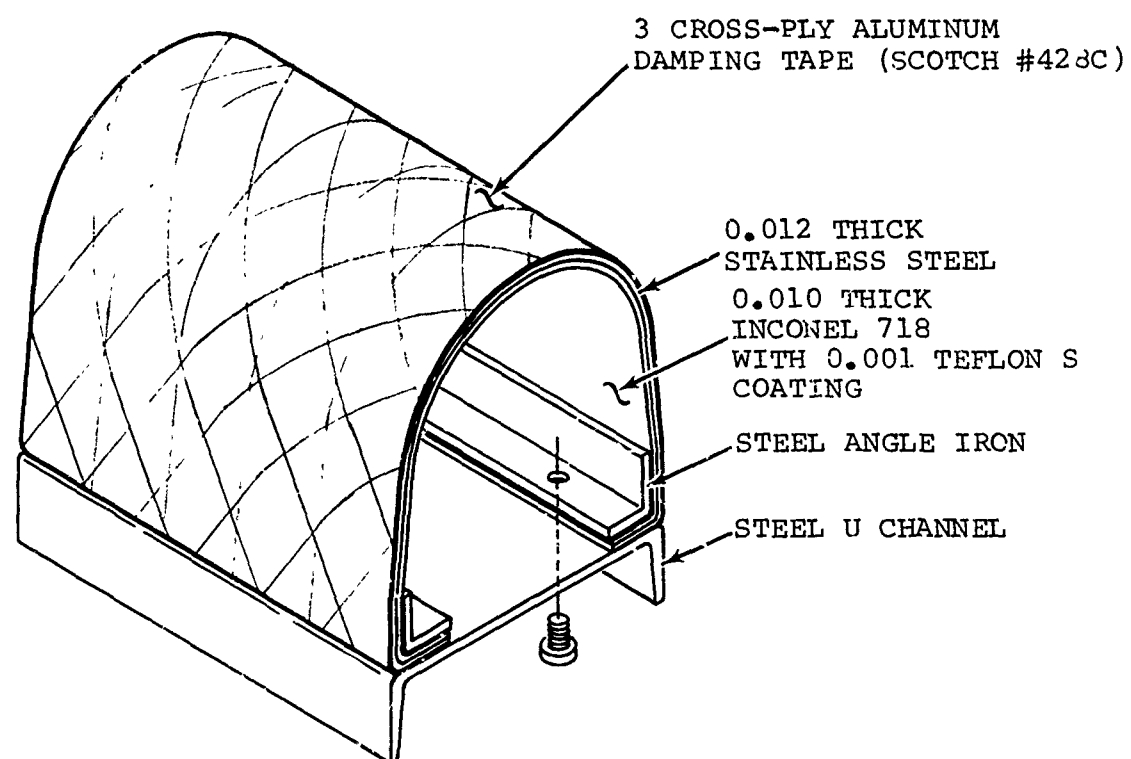
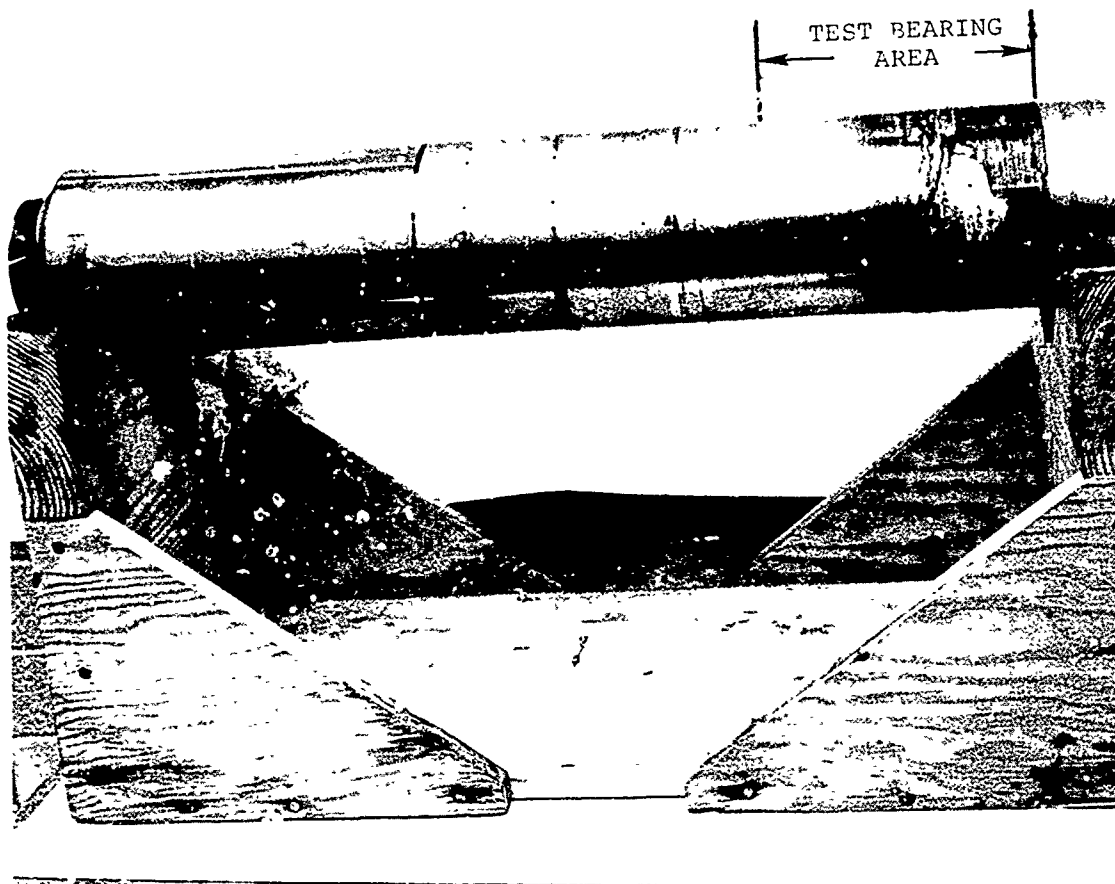


Figure 107. Parachute Loader Final Configuration



CONFIGURATION 23

Figure 108. Journal Bearing Test Pig Shaft After Bearing Failure  
at 6.5 psi and 33,000 rpm



CONFIGURATION 23

Figure 109. 12-Segment Journal Bearing Foils After Bearing Failure at 6.5 psi and 33,000 rpm

It should be noted that this failed configuration utilized the same foils that were installed at the start of Phase B. While Teflon-S does not possess the temperature capacity required for the intended end item application, it does provide a durable and forgiving foil coating for use during development testing. As shown in Figure 110, these bearings experienced 72 start-stop cycles and accumulated nearly 32 hours of run time before the failure occurred.

After repairing and rebalancing the shaft, configuration 24 was assembled with new 12 segment bearings. Because of the under-size repaired shaft, the calculated bearing swayspace was increased by 0.0047 inches. Loaded runs were made at reduced speeds to minimize risk. Since maximum load capacity has been determined to be only a weak function of speed, the low speed runs were felt to provide additional insight into bearing performance. Initial tests ran to 3.14 and 4.42 bearing psi at 20,000 and 25,000 rpm respectively. Further testing demonstrated 5.1 bearing psi at 23,000 rpm but the onset of bearing instability, as noted by changes in the synchronous orbit, was observed at 4.8 bearing psi at 28,000 rpm. Disassembly revealed the bearing wear pattern was too close to the foil trailing edge. Configuration 25 was therefore run with foil overlap reduced from 47.5 percent to 46.3 percent (foil length reduced by approximately 0.050 inch). Operation of this configuration was characterized by the recurrence of subsynchronous shaft excursions. This again points out the fact that subtle changes made to enhance bearing performance can have significant impact on the rotor dynamics of the entire system. Since the foil cutback had increased the measured sway space from 0.0175 to 0.0215 inch, shims again were used to reduce this value to 0.017 inch for Configuration 26. Testing was repeated at 23,000 and 28,000 rpm for this configuration. Bearing limit, evidenced by the onset of half frequency whirl, was reached at 3.737 bearing psi at 23,000 rpm. The bearing was gradually loaded to 5.4 psi at 28,000 rpm (Time 0 shown on Figure 111), when



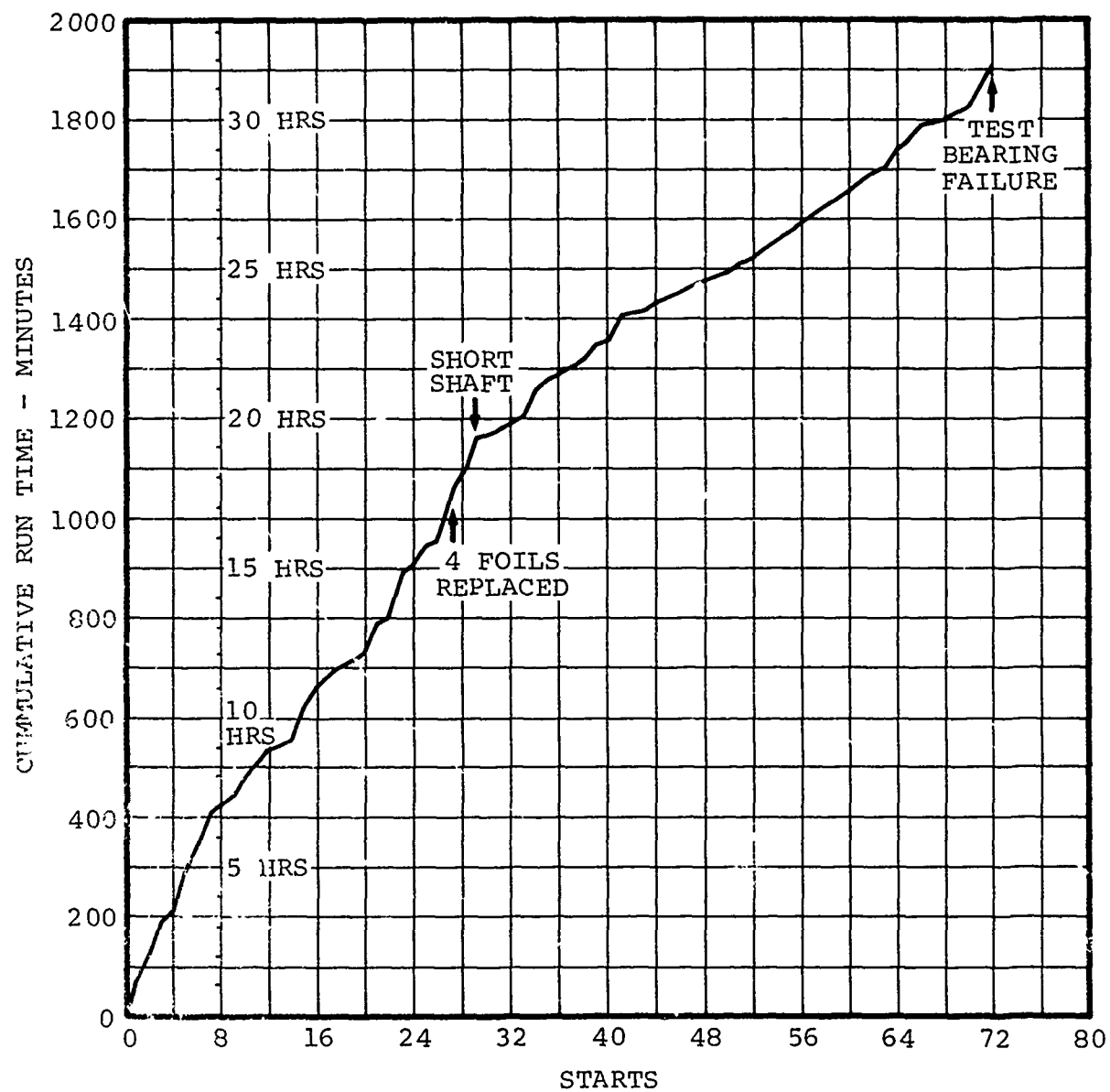
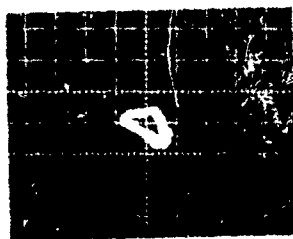


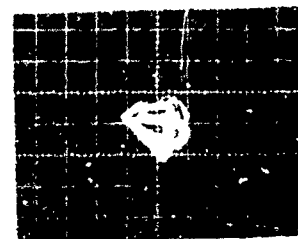
Figure 110. Run History, 12-Segment Teflon-S Journal Bearing

ORBIT

001 IN



001 IN



TEST BE

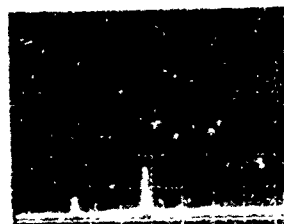
REAL TIME  
ANALYZER

001 IN



0 - 1000 Hz

T1 = 0.0 SECONDS



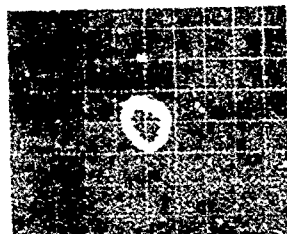
T2 = 3.0



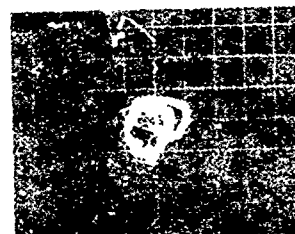
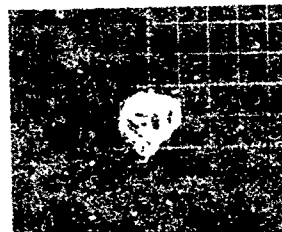
T3 = 4.5

ORBIT

001 IN



001 IN



TURBINE

REAL TIME  
ANALYZER

001 IN



0 - 1000 Hz

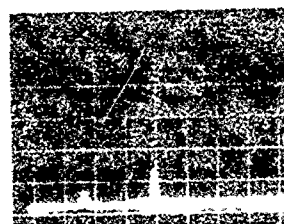
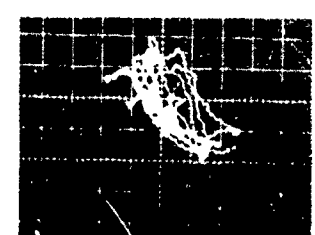
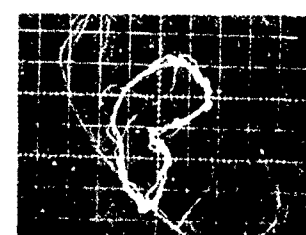
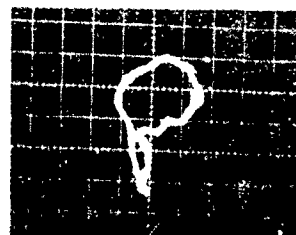
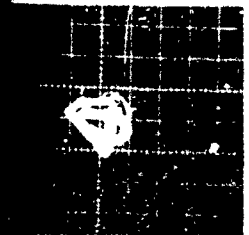
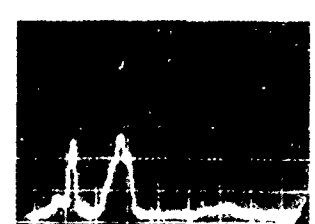
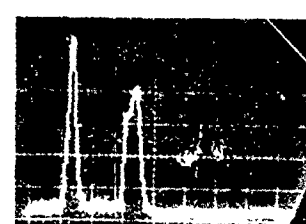
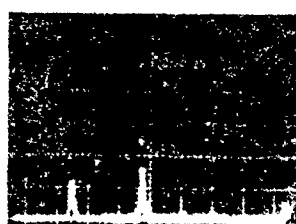


Figure 111. 12-Segment Foil Journal Bearing Failure Development--28,000

NOT.  
Preceding Page BLANK - FILMED



TEST BEARING

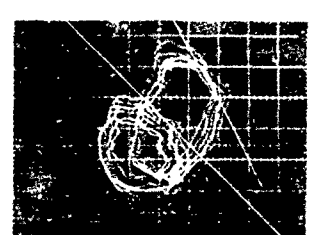
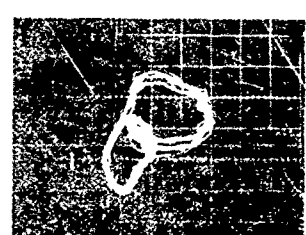
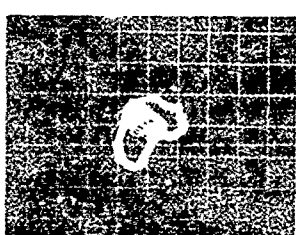


T3 = 4.5

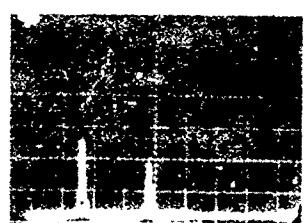
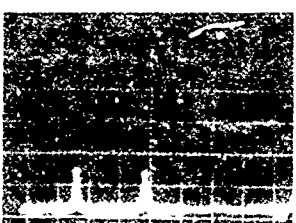
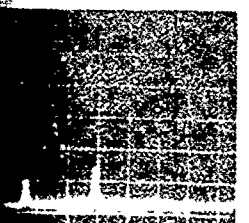
T4 = 5.0

T5 = 5.5

T6 = 6.0 SECONDS



TURBINE BEARING



BINE

28,00

development--28,000 rpm, 5.5 psi Bearing Load

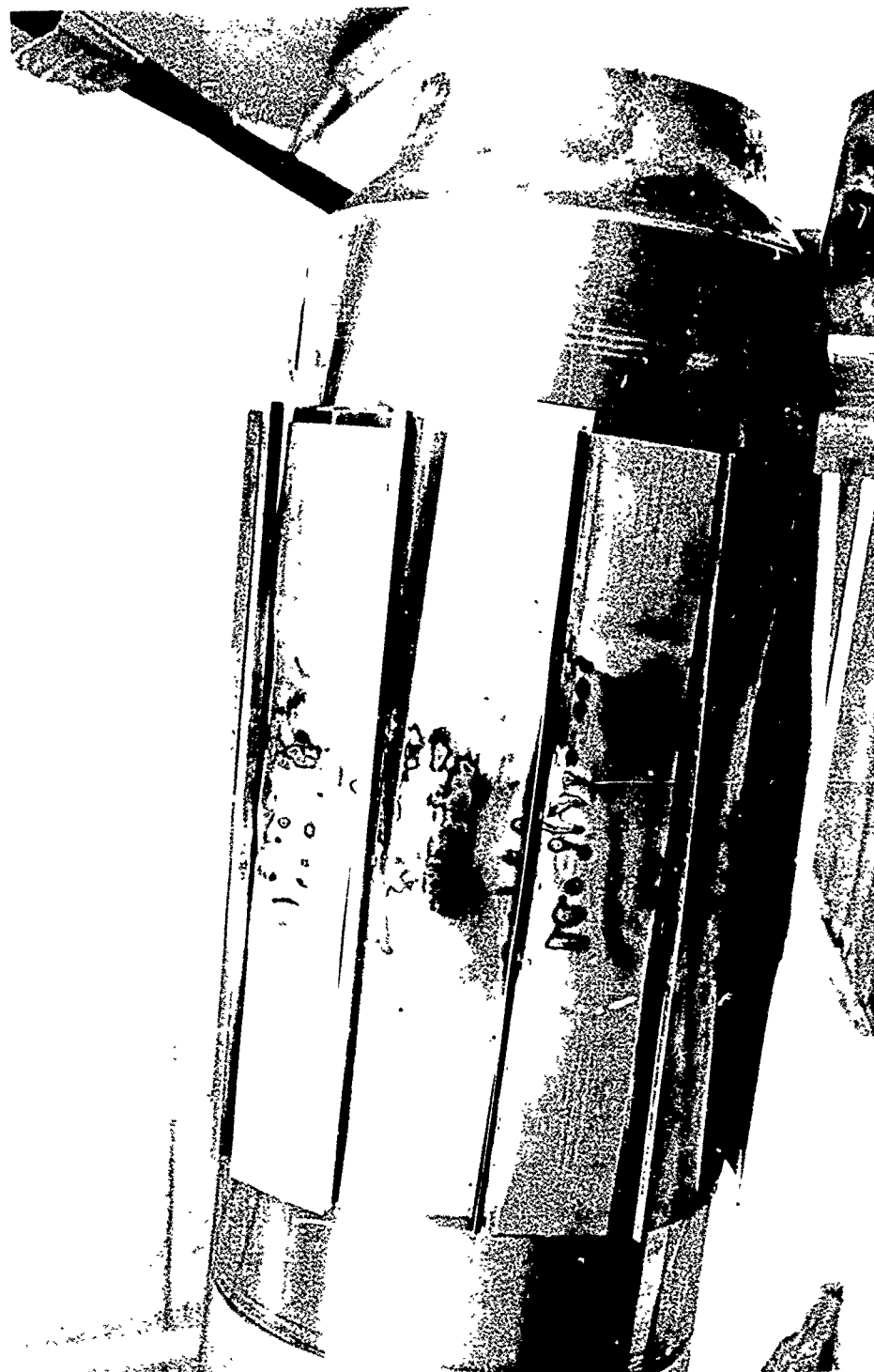
2

a half frequency excitation condition developed, which is shown on Time 3 seconds on Figure 111. At this point, the load was reduced to zero. The excursions continued to grow to the point of failure with a nearly instantaneous speed reduction to zero rpm and a total elapsed time of 6 seconds. The turbine-end bearing had welded itself to the shaft as shown in the sequence of photos (Figures 112, 113, and 114.) As shown in Figure 115, this test data can be extrapolated to approximately 7.5 bearing psi at design speed. The half-frequency excitation could be attributed to a sub-harmonic arising from shaft rub on the foils.

Conclusions reached after extensive testing of 12-segment bearings utilizing 0.012 inch foil material is that the available compliancy of this configuration limits bearing capacity to the 6 psi range. When 0.012 inch thick material for overlapping foils is used, too much of the arc length has a thick low pressure film thus limiting the overall capacity of the bearing. This bearing geometry, however, did exhibit a degree of stability unmatched by any of the six-or eight-segment bearings tested in this program.

Configuration 27, the preplanned high temperature test configuration, was assembled. This configuration consisted of a stainless steel bearing carrier (previously aluminum) for the high temperature air, machined for a 10-segment bearing. Foils were available with Kaman DES coating, but the initial test run of this configuration was with Teflon-S for the multi-plane multi-speed balancing operation. The test shaft was the shortened Inconel 718 shaft with Tribaloy-400 coating on the journal surfaces. When the test rig was operated to 22,000 rpm, the high ellipticity of the orbit indicated the possible approach of a backward precession mode, which produced a mid-plane excursion of 12 mils that could not be corrected by multi-speed/multi-plane balancing. Shaft excursions with speed are shown in Figure 116.

A contributory cause of the lowered speed at which the backward mode develops is currently considered to be the lack of a foil



CONFIGURATION 26

Figure 112. Turbine-end Bearing and Shaft Before Disassembly



CONFIGURATION 26

Figure 113. Shaft After Bearing Removal



CONFIGURATION 26  
Figure 114. Bearing Segments

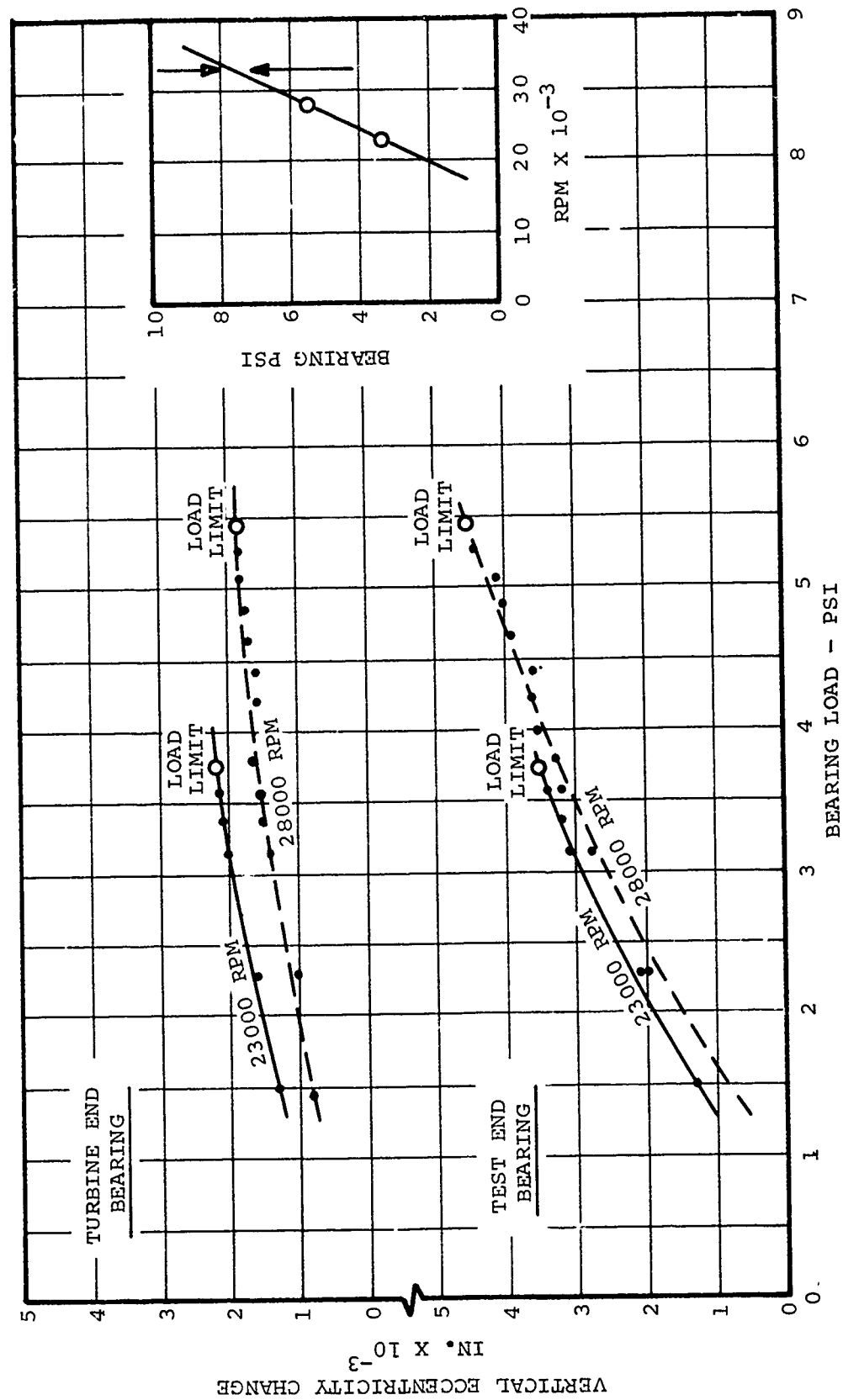


Figure 115. Configuration 26 Foil Journal Bearing Test.



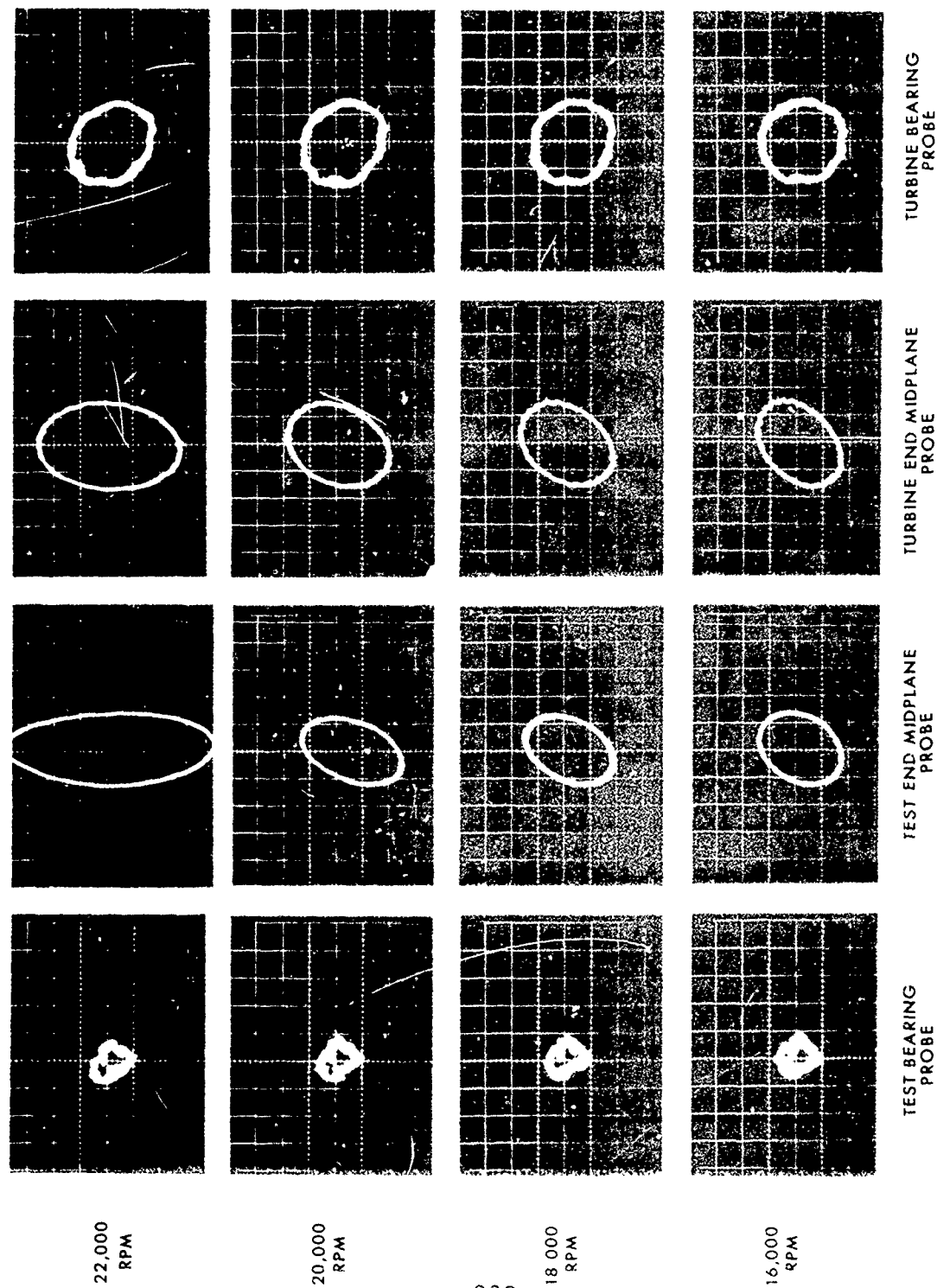


Figure 116. Shaft Excursion Versus Speed. (Configuration 27-10 Segment Bearing)

at the 90° circumferential position, (i.e., lack of perpendicular symmetry) to resist the cross-coupling forces observed in the journal bearing static elasticity analysis. As a result, high temperature testing was performed at 20,000 rpm. The material combination of Kaman DES on the foils and oxidized Tribaloy-400 on the journal is acceptable for operation at temperatures far in excess of Teflon-S allowable limits. Test conditions achieved during run 1 of Configuration 28 at 1 g were 385°F and 440°F coolant inlet temperature, respectively, at the test bearing and turbine bearing. The temperature differences are a result of different amounts of dilution of the high temperature coolant due to secondary rig air flows, which are different at both ends. The test bearing end of the rig has cold air sources from the hydrostatically supported dynamometer and from the parachute loader hydrostatic support air (used to provide a small amount of shaft ID cooling flow.)

The second run with this configuration was a 50-start foil durability test. The sequence of testing was 10 room temperature starts followed by 10 starts at 500°F coolant temperature, then repeat room temperature tests followed by 10 starts at 300°F and a final 10 at 500°F. This plan was incorporated to investigate whether the high temperature would regenerate any beneficial journal coating oxide which might have been removed during the low temperature starts. Test results are shown in Figure 117. The left hand scale represents the peak torque recorded during start at the initiation of shaft breakaway. The breakaway torque values indicated in the right margin represent recorded values obtained by rotation of the shaft with a torque wrench at very slow speed. The only anomaly noted after disassembly was the presence of scratches apparently caused by some foreign particles. Conclusions reached from this test are that: (1) the coating has sufficient durability to be a candidate for further bearing programs; (2) some coating deterioration takes place during the start-stop cycle; (3) operation at temperatures typical of engine compressor exit temperature will not significantly regenerate journal oxide coating and therefore will not restore friction coefficients to new part levels.

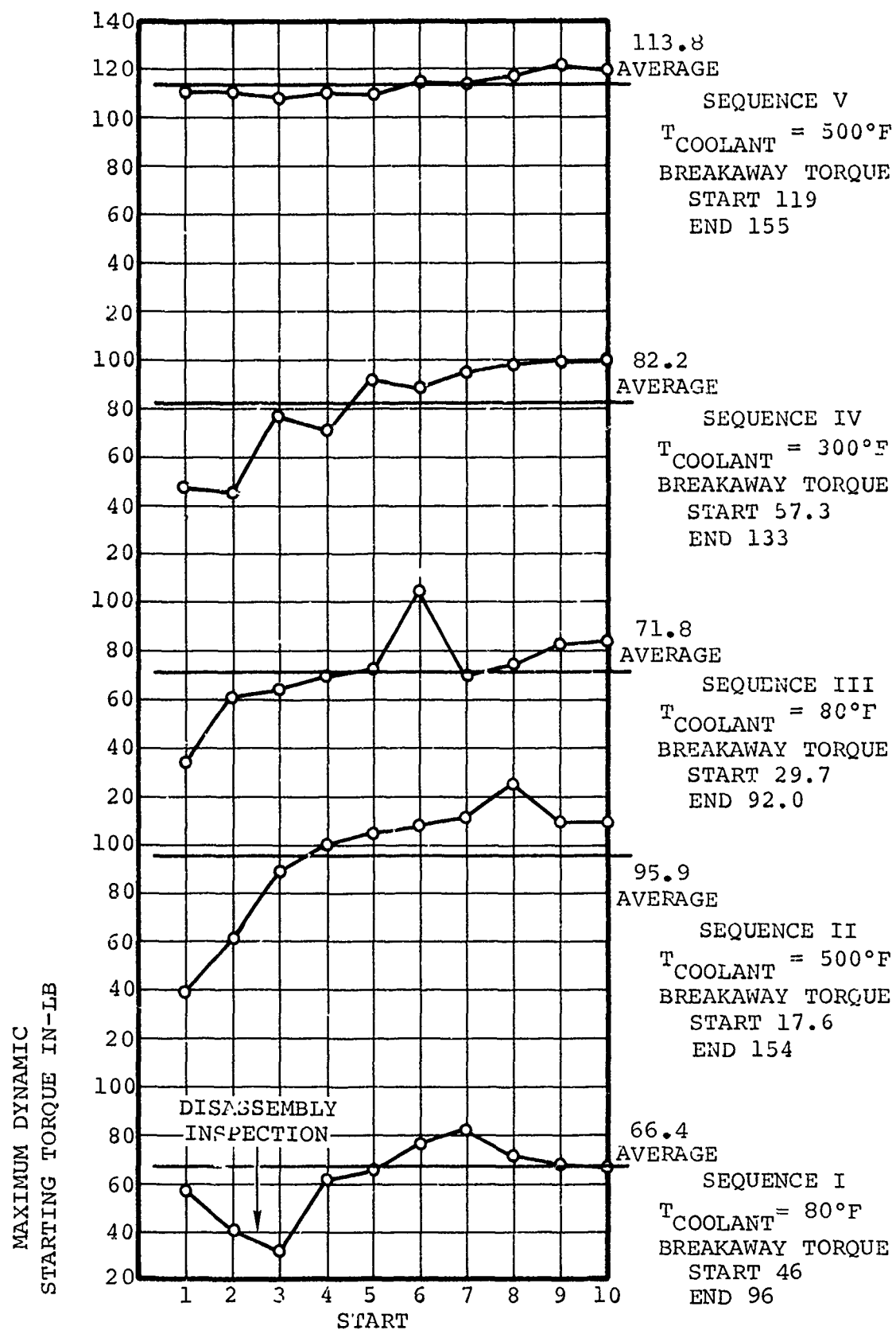


Figure 117. Configuration 28, Run 2-Start Cycles

The final run using this bearing configuration was an attempt to simulate bearing coolant pressure and temperature conditions representative of engine operation. However the large radial clearance of the test bearing fore and aft labyrinth seals, needed to accommodate the required sway space, permitted high pressure coolant to leak into the rig end cavity and create a rig thrust unbalance that exceeded the capacity of the thrust bearings. This was the only thrust bearing failure experienced on the journal bearing test rig. Note in Figure 118 that the inboard bearing failed at the OD while the outboard bearing, which absorbed the thrust unbalance, failed at the ID, indicating that some dishing of the thrust runner had occurred.

For Configuration 30, the test rig was modified to perform the dynamic simulation test within the limits of the 12-segment bearing capacity. Twelve-segment bearings with Teflon-S were installed at the turbine end and NiCo coated foils installed at the test bearing end. An initial checkout run was made and all parameters were considered acceptable to 25,000 rpm. The rig was then modified to misalign the test bearing equivalent to the misalignment developed under a 3.5 radian/second yaw condition (0.05 degree) and the parachute loader was added to apply the radial load to the bearing. The test bearing seized at 21,200 rpm during the first acceleration. Disassembly of the bearing revealed that only the outboard edges of the bearing had rubbed the shaft hard enough to cause the seizure.

The outboard wear was partially the consequence of insufficient bearing air film (because of the edge leakage) until speeds above the nominal foil lift-off speeds are reached. It is felt that the factors of low speed bearing end leakage, the thin film foil coating, and the axial bending rigidity of the 0.012 thick preformed foils, contributed to the seizure. This axial rigidity limits the variation in axial foil compliancy that is required to accommodate the misaligned condition.

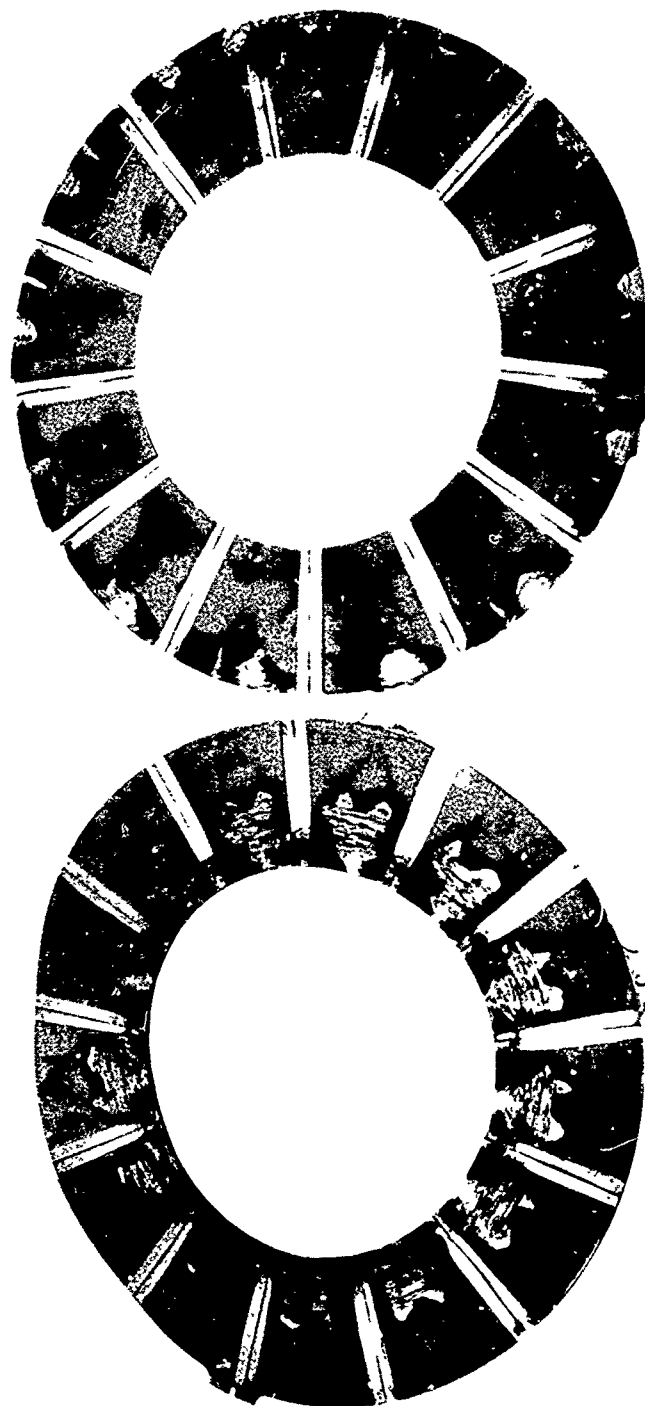


Figure 118. Journal Bearing Test Rig Thrust Bearing Failure.

### 3.5.2 Foil Thrust Bearing Development Tests

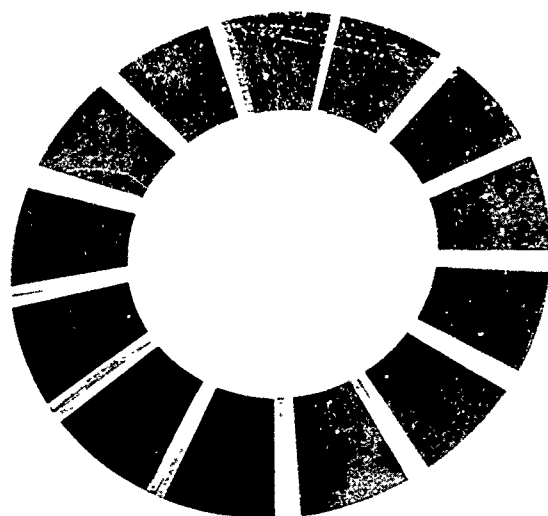
#### 3.5.2.1 Baseline Bearing

The baseline foil thrust bearing was a previously proven design scaled to the size required for this application. The bearing is a three-part assembly in the form of an annulus, 6.15 inches OD and 3.5 inches ID. The bearing is made of 13 0.006 inch thick Inconel X-750 foils welded to a base of 0.010 inch Inconel. The foils are coated with 0.001 inch thick Teflon-S. The teflon coated area represents 89.5 percent of the projected annulus area which is capable of carrying a thrust load. These foils, welded on one side only, are free to conform to the required shape to support the load carrying air film. The spring assembly consists of 13 Inconel springs as shown in Figure 119, welded to a 0.012 inch thick Inconel base. An intermediate stiffener between the bearing and spring assembly provides additional stiffness as required. The spring centerline orientation is approximately 17° beyond the leading edge of the foil.

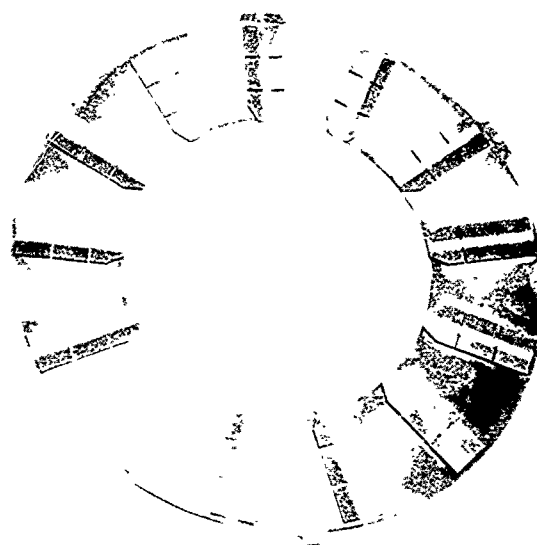
Initial testing during test rig checkout showed heavy bearing wear at the foil ID. This problem was eliminated by providing spring assemblies with gradually increasing spring height from ID to OD. Several tests were made on this baseline configuration with maximum demonstrated capacity at about 300 lb load. Wear patterns similar to that shown in Figure 120 are indicative of maximum bearing capacity levels.

#### 3.5.2.2 Dual Spring Design

Analytical prediction of maximum baseline bearing capacity closely agreed with test results. To provide an increased area of support for the high pressure air film, a spring assembly using two springs was designed. This spring configuration is shown schematically in Figure 121. During test the air film was lost at a low load of 200 pounds at 33,000 rpm, resulting in foil melting



BEARING  
ASSEMBLY



SPRING  
ASSEMBLY

Figure 119. Thrust Bearing.

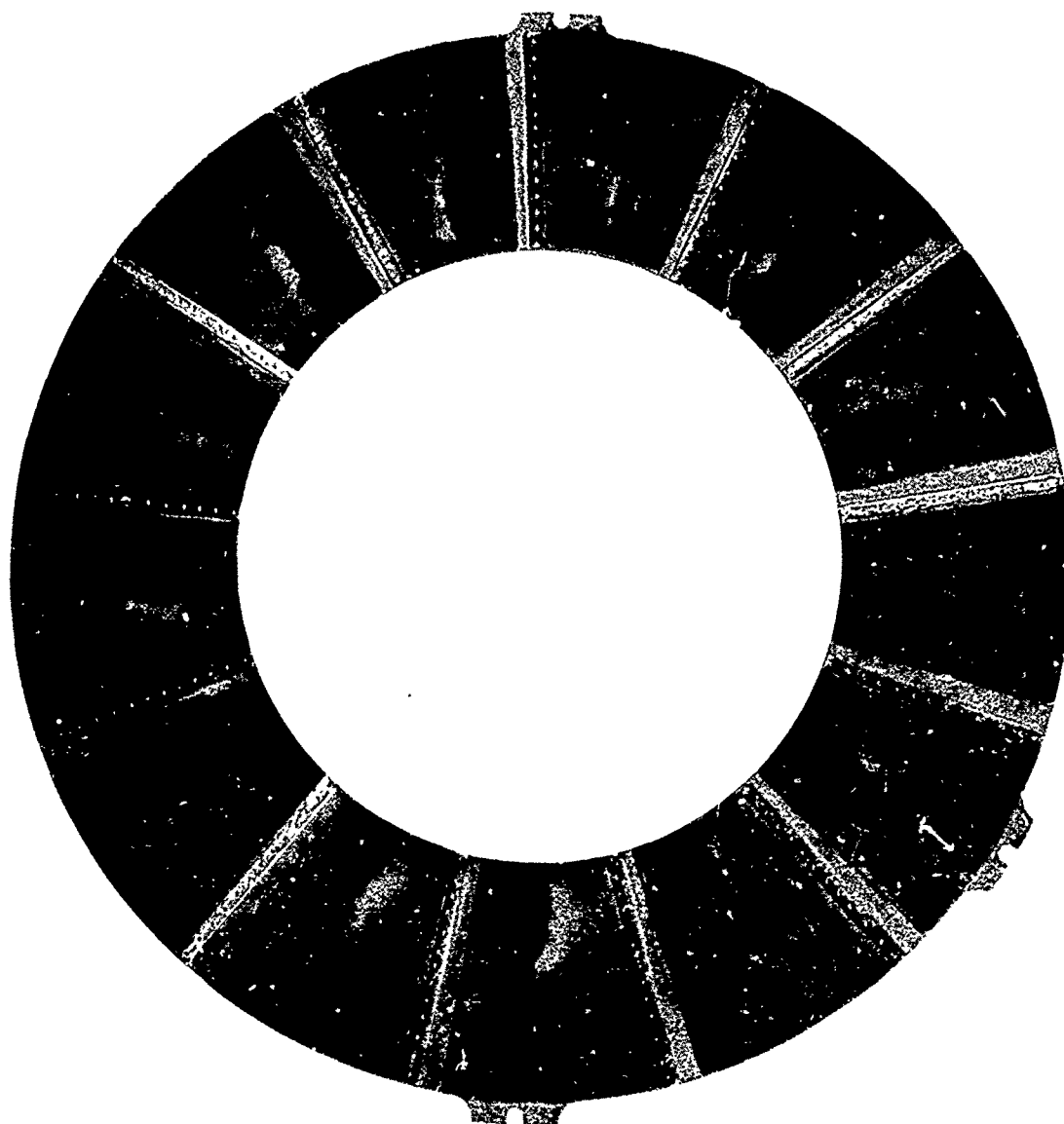


Figure 120. Thrust Bearing Load Pattern 304  
Pounds Applied at 23,000 RPM.



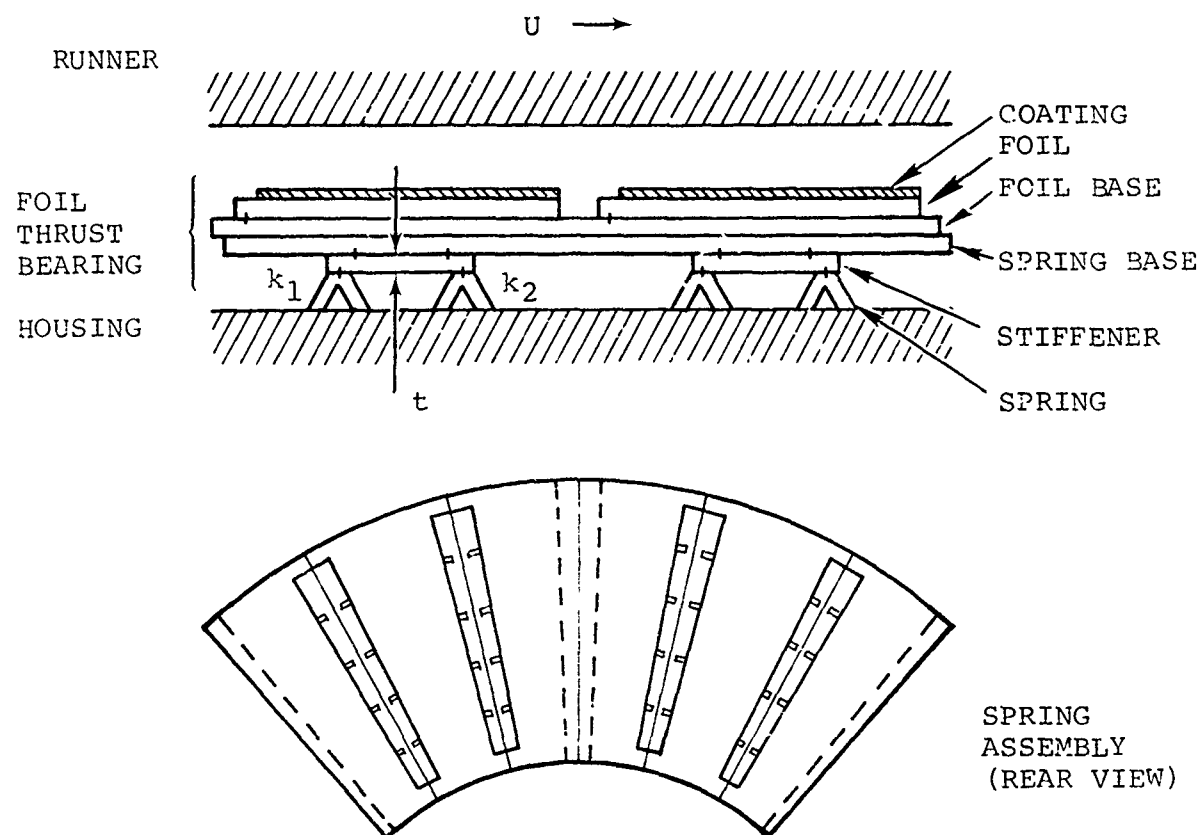


Figure 121. Dual Spring Foil Thrust Bearing Schematic.

as shown in Figure 122. The air film loss was attributed to spring height relationship between two pad springs. Although the individual springs have a manufacturing tolerance, a relative tolerance must be applied after assembly that can be met only by machining each spring. The leading spring, which has the lower spring rate, has the lower height, therefore making a natural built-in wedge to initially develop a load carrying film.

With considerable difficulty, a dual spring assembly was fabricated with proper spring height relationships, i.e., an increase in spring height from foil leading to trailing edge and an increase from ID to OD. Results of test were no better than before, nor were better results achieved with further modifications reducing the leading edge spring length. Maximum load capacity of this spring configuration remained at 200 lb.

#### 3.5.2.3 Partial Pad Stiffener

The partial pad stiffener spring design, shown schematically in Figure 123, evolved as a means to accomplish pad stiffening of the dual spring assembly and to eliminate manufacturing difficulties previously experienced. Initial test sequence involved direct comparison tests of the three designs developed to that date. All configurations used a Teflon-coated foil but with variations in the spring and stiffener assemblies. These variations included combinations of the baseline spring assembly, modified dual spring assembly, partial pad stiffener spring assembly, and the 0.010 or 0.012 inch thick intermediate stiffener. Data from this test series were used as an instrument to analyze friction torque and cooling characteristics, as a function of bearing load. Some data resulted in a typical plot (Figure 124), which shows the specific torque-versus-torque for three configurations of interest. Configuration 10 (modified dual spring) is near capacity limit because the specific torque (torque per unit load) is increasing. The curve also shows that the

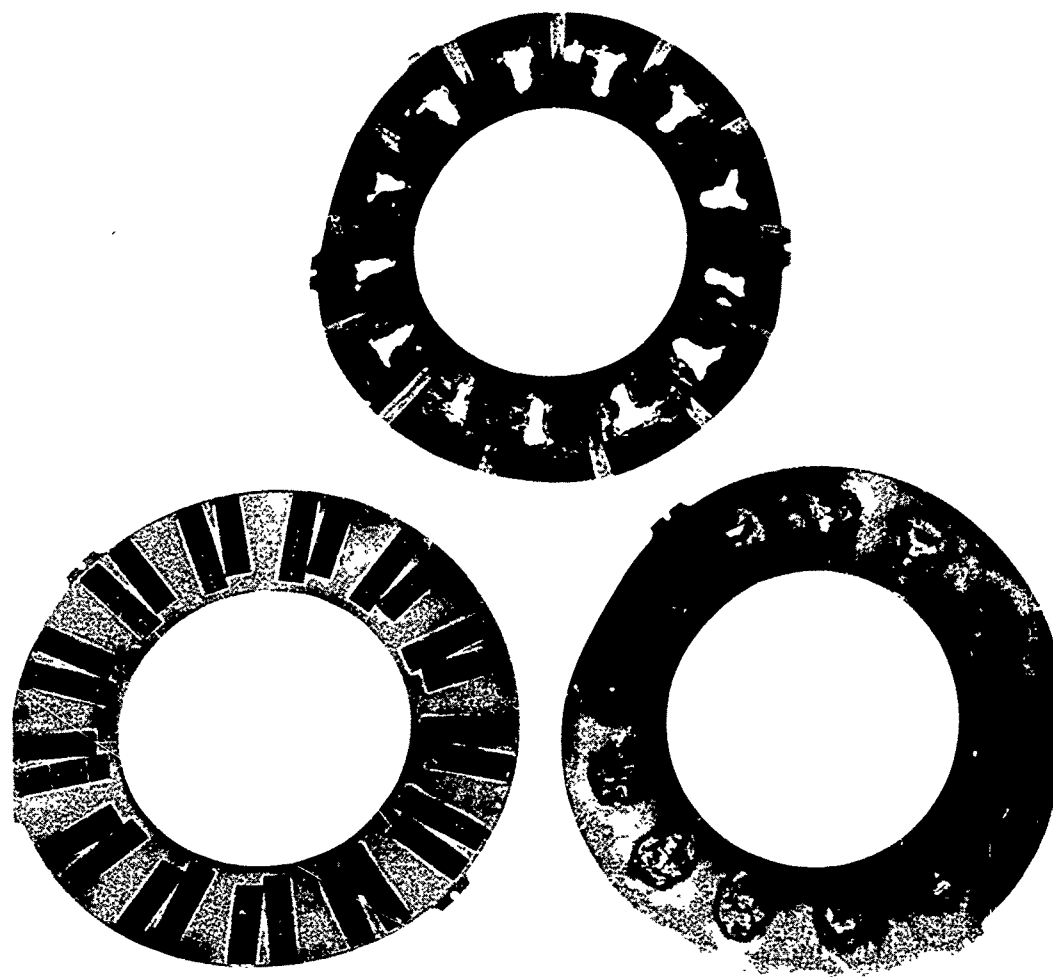


Figure 122. Dual Spring Thrust Bearing Deterioration.

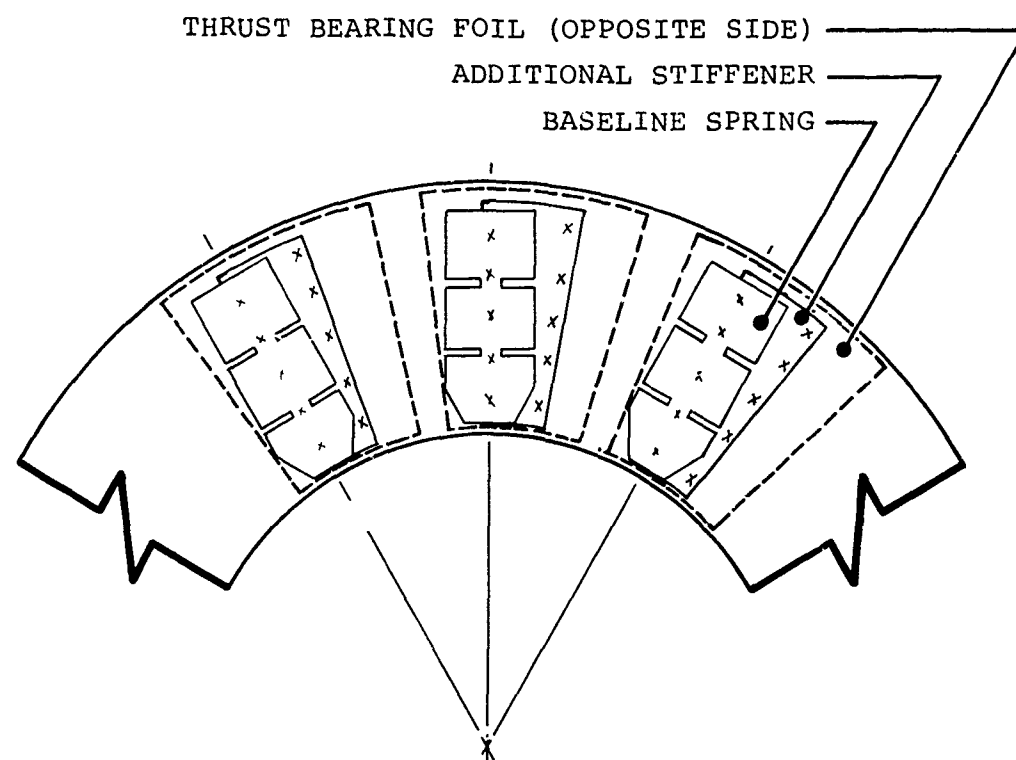


Figure 123. Baseline Spring With Partial Pad Stiffener.

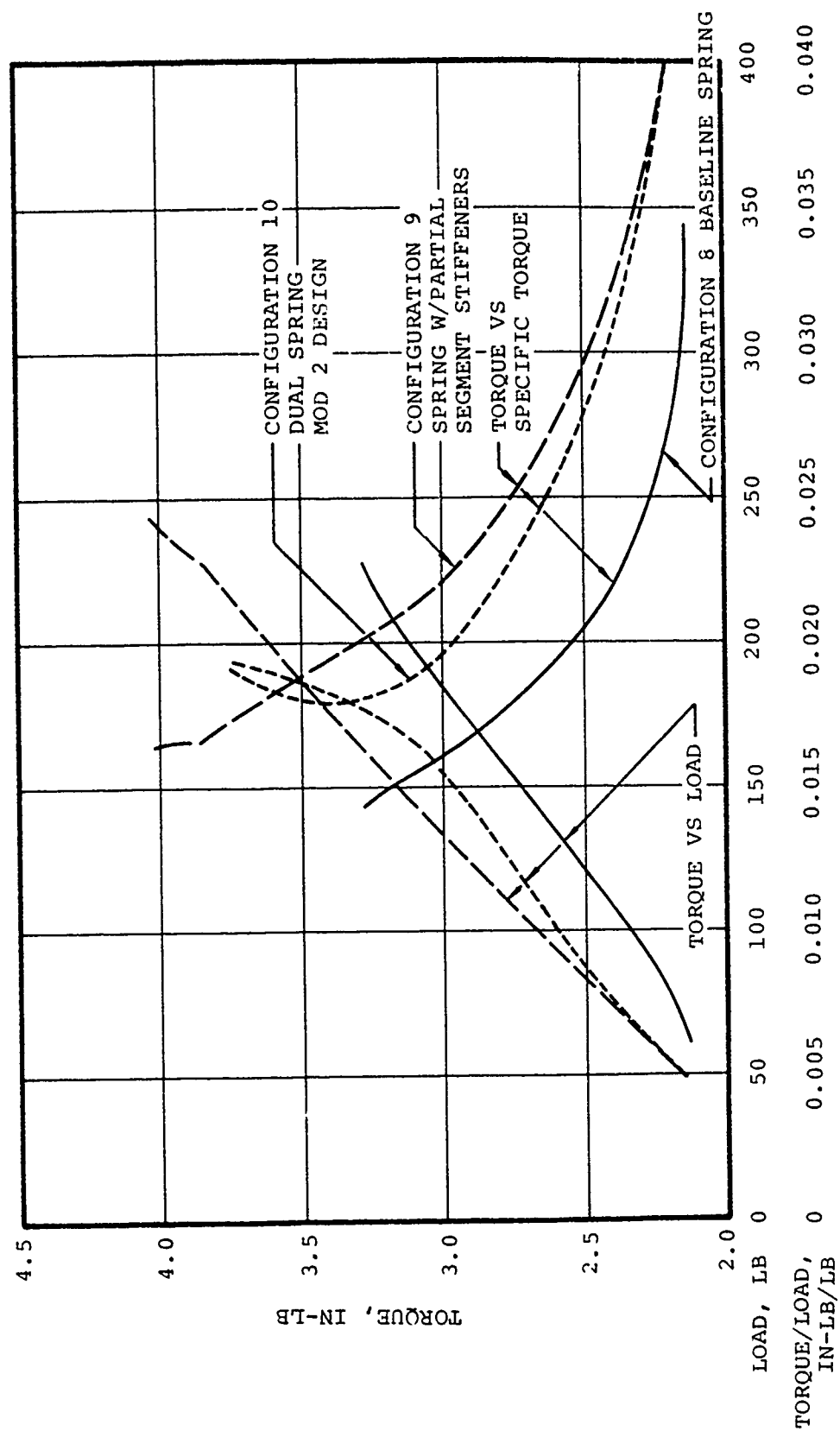


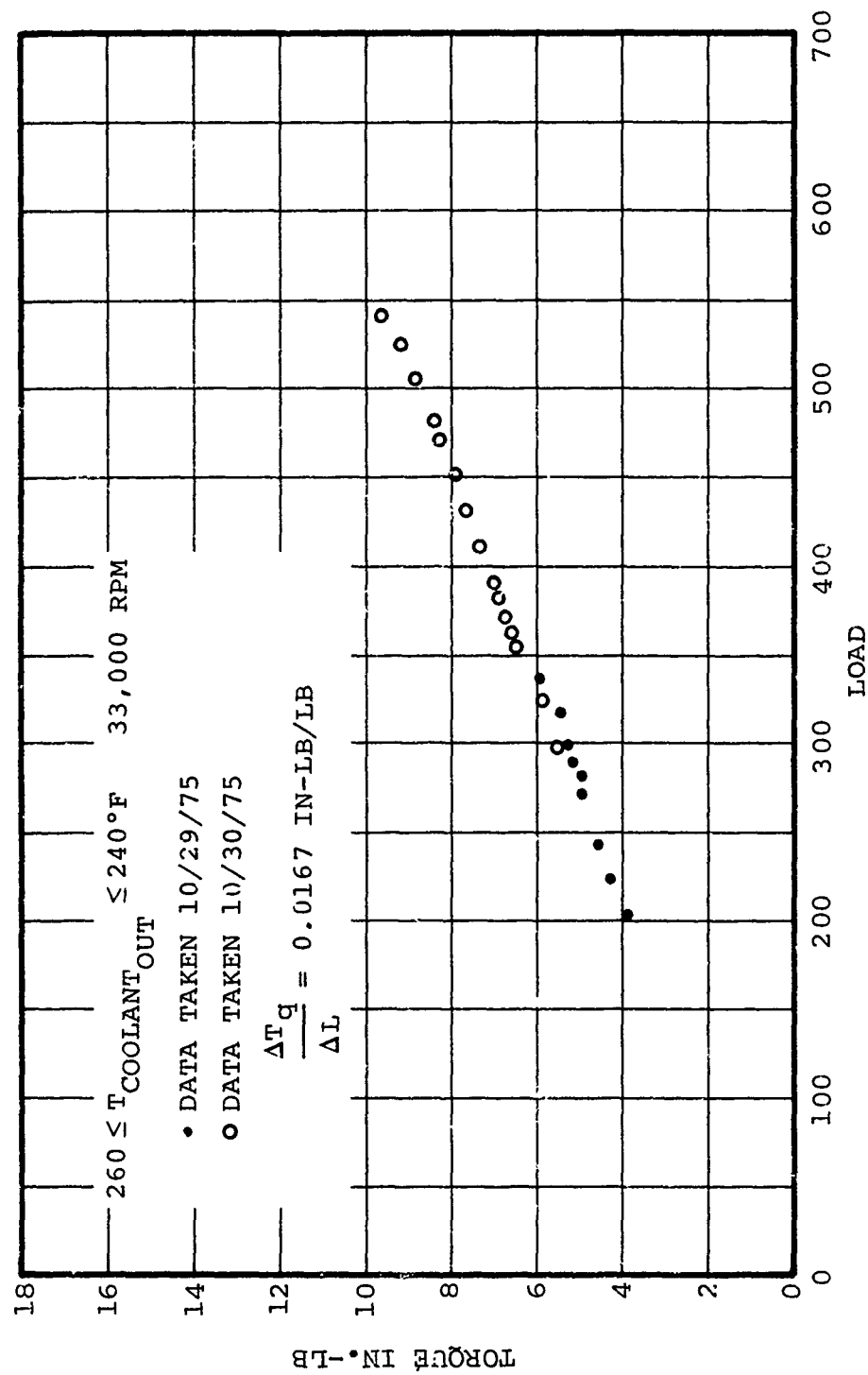
Figure 124. Foil Thrust Bearing Data Torque Versus Specific Torque.

baseline spring assembly and partial pad stiffener spring assembly have not reached capacity limit for the loads shown.

However, it was felt that continued testing with the partial pad stiffener design offered more opportunity to achieve higher load capacity, based on the correlation between analytical predictions and previous tests.

In reviewing data from previous failures, it appeared that foil operating temperature could have been a contributory factor. Operational temperature limits for Teflon-S are about 550°F but measuring actual foil temperature had proven to be extremely difficult. Previous attempts to attach thermocouples to the foils or intermediate stiffeners had always resulted in failures due to local protrusions or the inability of the thermocouple lead wires to conform to the bearing operational geometry. Since the only reliable temperature obtainable was that of the cooling air leaving the bearing, and data revealed that bearing failures had occurred when this temperature reached 300°F, a test was run using increasing amounts of cooling air to maintain a constant discharge air temperature as load increased. This testing required a larger quantity of cooling air at higher loads, and resulted in maintaining the bearing coating temperature while subjecting the bearing to a previously unachieved 540-pound load (27 psi), shown in Figure 125. The test was terminated at this load due to test instrumentation limits and not by the achievement of maximum bearing load capacity.

A spring rate test also was conducted on the spring assembly utilizing the partial pad stiffener and baseline spring. Since the baseline spring was not designed for these high loads, the test purpose was to determine maximum spring capability. Subsequent bearing testing with this spring assembly indicated a rotor instability, which was traced to uneven heights of the 13 springs, indicating spring material yielding during the spring



CONFIGURATION 13

Figure 125. Constant Discharge Air Temperature Test.

rate test. A spring stress analysis showed that the material could have yielded when the total load exceeded 600 pounds. Therefore, a thrust bearing pad spring, capable of supporting the target thrust bearing loads, was designed. The spring material was changed from Inconel X-750 to Inconel 718, which permitted a spring design with higher stress levels. Material thickness was increased from 0.014 to 0.020 inch, and the spring width from 0.46 to 0.64 inch.

Thrust bearing foils of 0.006 inch thick Inconel X-750 for higher temperature use were coated with molybdenum disulphide ( $\text{MoS}_2$ ) and another group of foils was cut from 0.004 inch thick Haynes 25, and oxidized.

The test that incorporated both the redesigned springs and the  $\text{MoS}_2$  coated foils resulted in failure at the low load of 40 lb (See Figure 126). Since this failure could have been due either to the spring assembly, the foil coating, or a foil weld failure, subsequent tests were used to evaluate the individual changes.

A 200 lb load demonstration was made with a Teflon-S bearing and the original partial pad stiffener spring assembly, which verified rig operation. The next test, using the same bearing but the Inconel 718 spring assembly, resulted in failure below 200 lb load, indicating the spring design was too stiff to provide required foil compliancy characteristics.

In order to better evaluate the individual spring assembly components, a fixture that permitted testing individual springs was obtained. The test procedure was to measure the spring deflection upon application of 20 pound and 50 pound loads. This represented a total bearing load level of 260 and 650 pounds respectively. Approximately 15 samples of each type of spring were tested. In addition, one spring was repeatedly tested for 15 trials at 50 pounds load, to assess test accuracy. Results



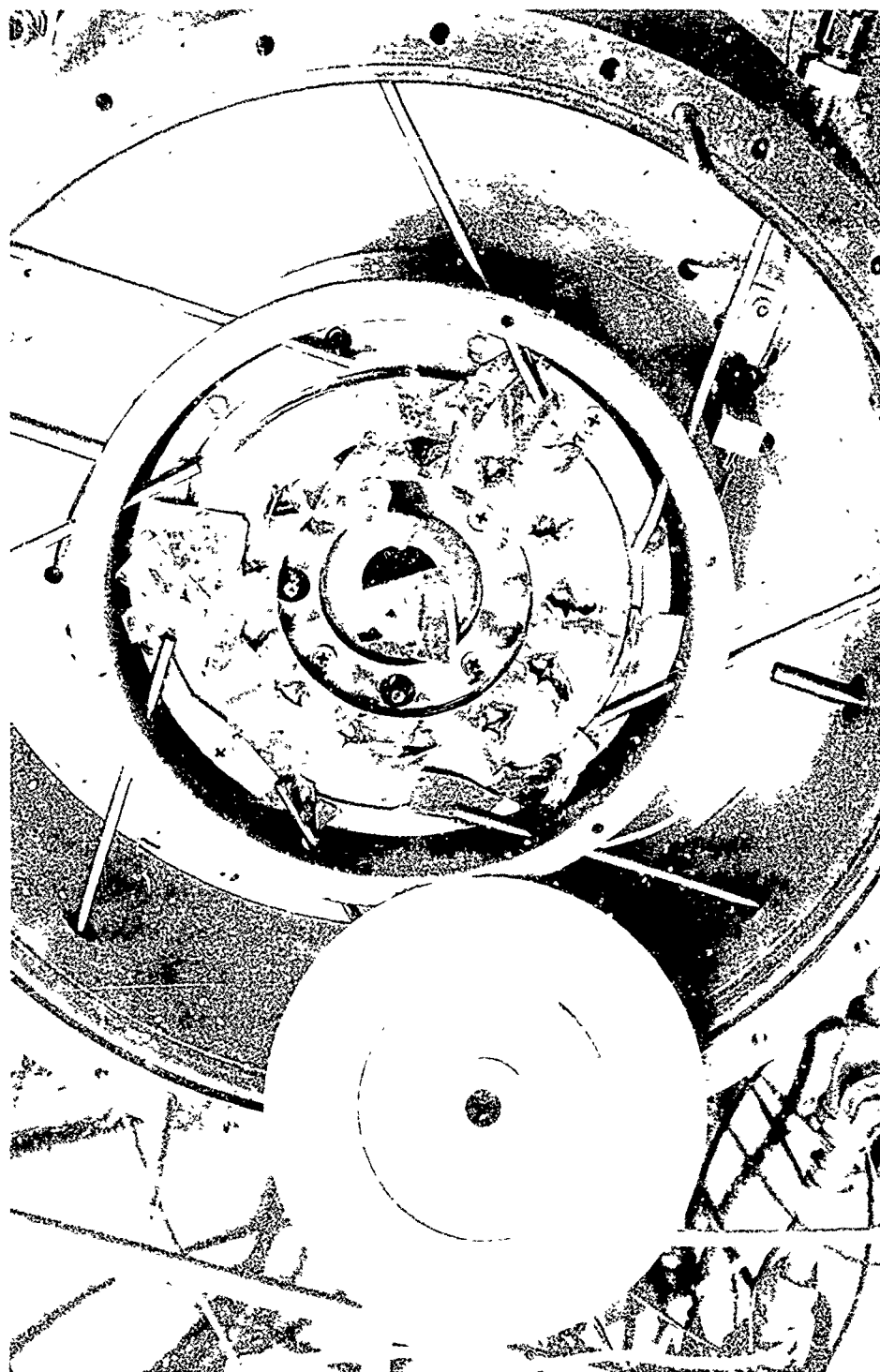


Figure 126. Failed Thrust Bearing, 40 lb Load.

are indicated in Table 18. As shown, the accuracy of the test is very high, but in all cases at the higher loads the Inconel 718 springs experience less deflection. These higher stiffness values imply that bearing compliance is reduced as load increases, although the 0.014 thick Inconel 718 springs nearly duplicate the X-750 spring performance. The high standard deviation of these springs would have to be reduced significantly through manufacturing process improvements to minimize circumferential variations in bearing compliance.

Further insight into the spring geometry problem is provided in Figure 127. The "as assembled" data shows the variation in both circumferential and radial spring height of a just completed spring assembly. The "after adjustment" data shows a more uniform assembly. Data in the right margin indicates the mean height, maximum and minimum variation from the mean, and circumferential standard deviation, for the three radial portions of the spring. Note the achievement, after adjustment, of a slight height increase from ID to OD. Obtaining this type of data requires a measurement at 39 locations, followed by hand adjustment, as required, and remeasurement.

Verification of spring yielding was obtained from single spring test data. Figure 128 shows a comparison of the original Inconel X-750 spring (-3) with the 0.020 thick Inconel 718 type (-4). The net deformation after relaxation, shows considerable yielding at bearing loads of 700 lb and above for the Inconel X-750 type. The Inconel 718 spring shows no yielding whatsoever, making the spring assembly height adjustment quite difficult. It is anticipated that further manufacturing development would be required to alleviate this situation.

Upon resumption of bearing tests, a standard spring assembly with a  $\text{MoS}_2$  coated bearing was tested. The bearing coating (0.0007 inch thick) showed considerable wear after a maximum load of 100 pounds. After a test of another bearing to assure the rig was not misaligned it was concluded that the thin  $\text{MoS}_2$  coating was not a good wear resistant coating.

TABLE 18  
DEFLECTION CHARACTERISTICS OF THRUST BEARING SPRINGS

Configuration	20 Pound Load Deflection		50 Pound Load Deflection	
	Sample Mean In X $10^{-3}$	Sample Standard Deviation In X $10^{-3}$	Sample Mean In X $10^{-3}$	Sample Standard Deviation In X $10^{-3}$
Test Accuracy 0.020 Thick Inconel 718 Spring			9.59	0.16
Baseline Spring 0.014 Thick Inconel X	5.32	0.27	12.02	0.74
0.020 Thick Inconel 718 Spring	4.84	0.30	9.53	0.90
0.020 Thick Inconel 718 Spring Chem milled to 0.018	5.64	0.41	9.15	0.45
0.014 Thick Inconel 718 Spring	5.41	1.12	10.43	1.53

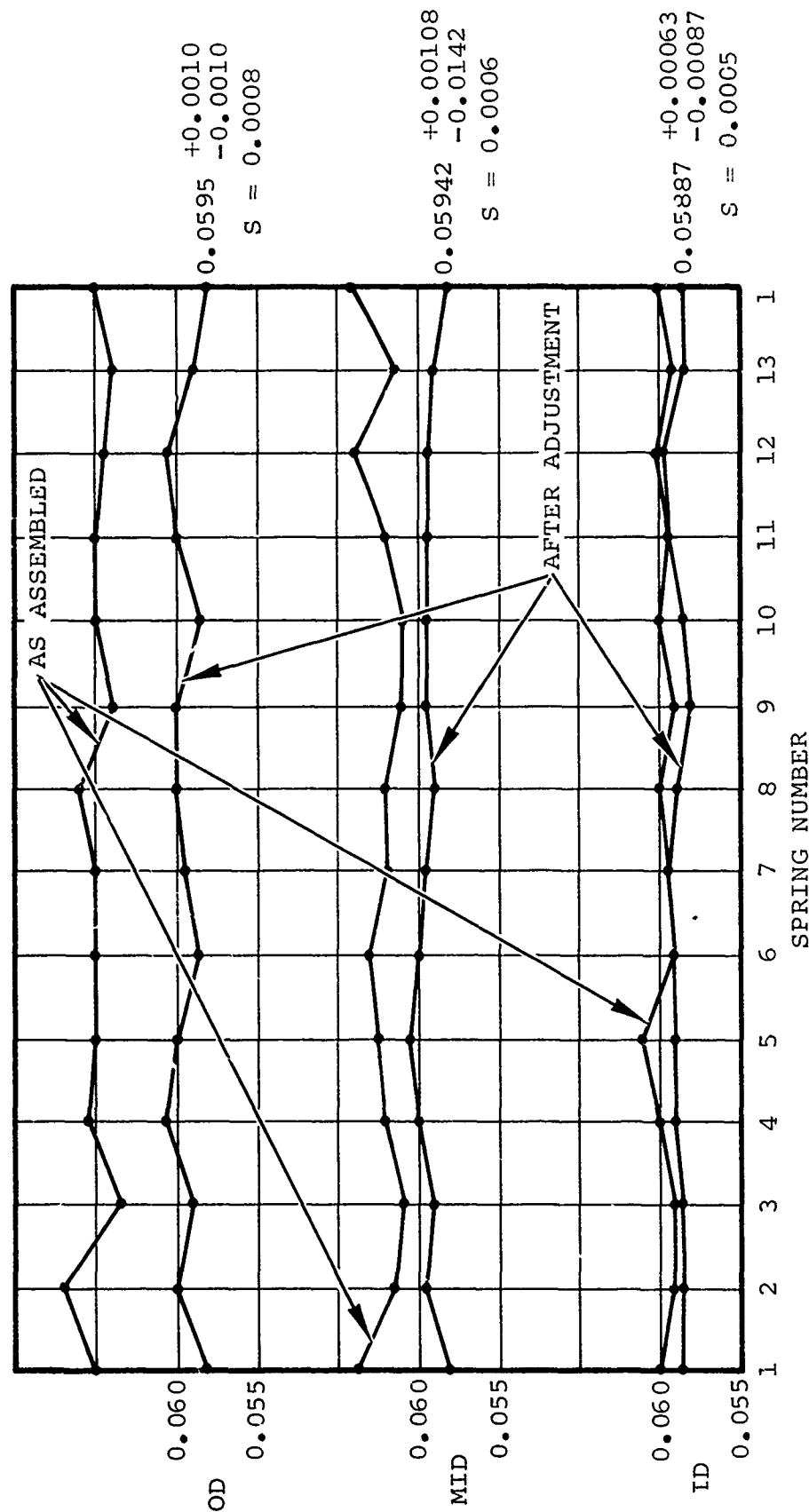


Figure 127. Thrust Bearing Spring Heights Before and After Adjusting.

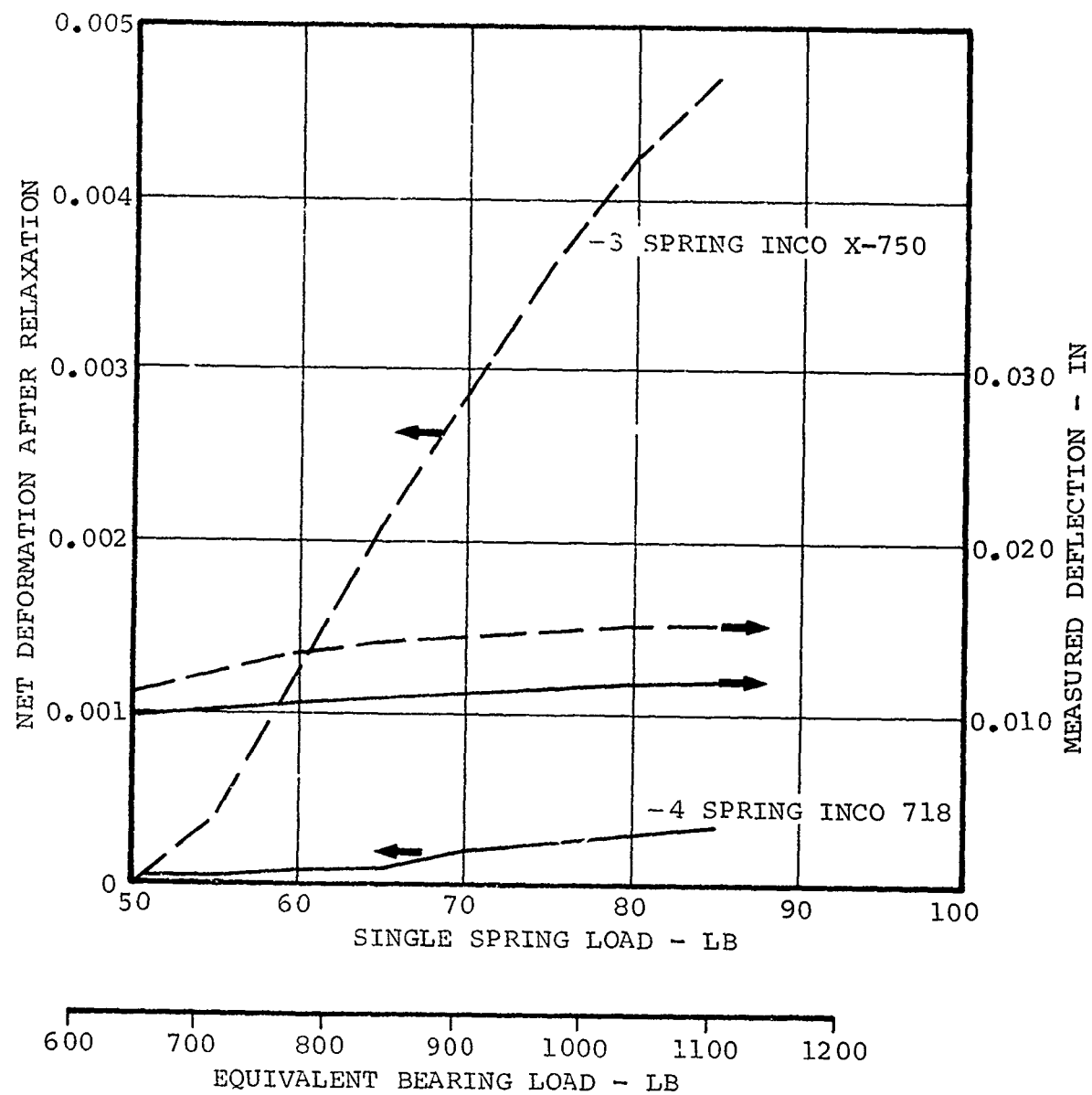


Figure 128. Single Thrust Bearing Spring Yield Point.

It was felt that increasing bearing pad area would increase load capacity, so a wide pad bearing was defined, in which the coated surface was increased to 94.1 percent of the total projected area. When tested, this pad assembly (Configuration 20) achieved a load of 342 lb before prefailure indications appeared. Upon examination, the pad wear patterns indicated that the trailing portion of this larger pad was not being effectively utilized. This same bearing assembly was modified by repositioning the locating slots, which rotated the spring assembly centerline  $2.2^\circ$  toward foil pad trailing edge. This resulted in a 30 percent increase in load capacity to 441 pounds and, as shown in Figure 129, the area of Teflon discoloration at the minimum film, maximum temperature point, had been relocated as intended. Another test was performed with  $\text{MoS}_2$  on wide pad foils, which again demonstrated inadequate performance, achieving a maximum capacity of 180 pounds. The reason for failure is considered to be the effect of a thin foil coating as it affects the development of the load carrying film, which is discussed later in the report.

The conclusion reached as a result of test configurations described above relates to high film temperature reached at the point of minimum film thickness. The Inconel foil materials used to date have had a low thermal conductivity factor, and therefore retain heat at the point of generation, which may cause foil distortion. Therefore, materials with a higher rate of thermal conductance were investigated for suitability to foil bearing fabrication. An alternate method of conducting heat from the "hot spot" is to increase foil thickness. Configurations 25 and 29 explore this concept of conducting heat from the minimum film space, as discussed later in this report.

Configuration 23 was fabricated and assembled with Kaman SCA coating on the thrust runner and Kaman DES coating on the foils. Difficulty was experienced in photo-etching the foil shapes, as the etching agent attacked the coating, thereby rendering the foils unusable. As a result, the individual foils were hand cut.

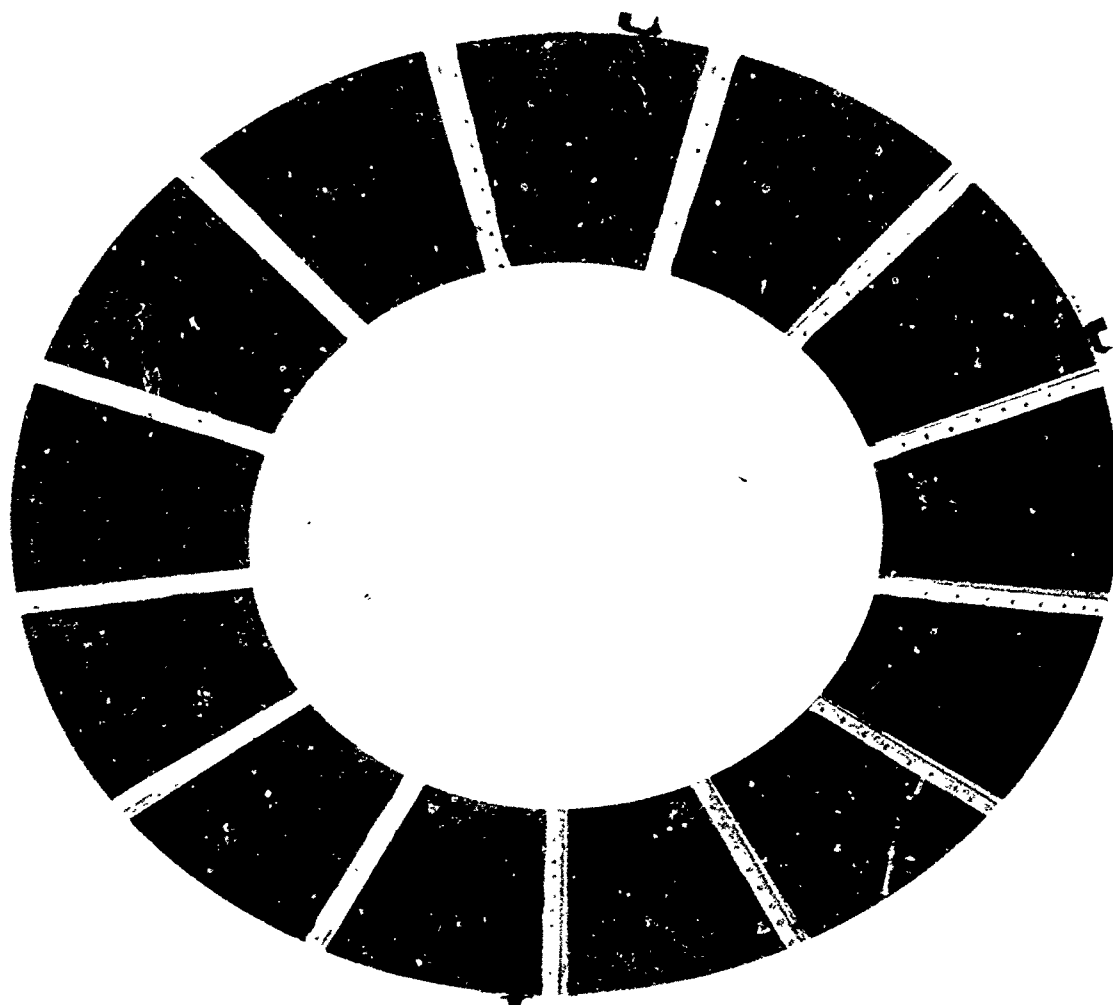


Figure 129. Bearing Assembly With Repositioned Locating Slots.

Since this represented the initial high temperature run of this material combination, which had proven successful in the wear test rig, the bearing was inspected after several revolutions of hand turning. The foil coating had worn through at several high points because of three contributing factors as follows:

- o The torque table had hung up on a chamfer and, therefore, was at an angle to the thrust runner.
- o One foil was not flat.
- o The foil coating in this case was 0.0001 inch thick, whereas the wear test rig foil coatings were 0.0003 inch thick. The reason for the thinner coating was to keep the foils flat, as the application process for Kaman DES curls the 0.006 inch thick foils.

Therefore, this combination of Kaman coating does not appear to be acceptable for thrust bearings, but may be for the thicker journal bearings.

Configuration 24 was fabricated with a rectangular shaped partial stiffener welded between the spring and circumferential stiffener, and wide pad Teflon-S coated foils. This stiffener geometry is intended to additionally stiffen the ID of the bearing and thus transfer some load to the OD. A foreign particle, less than 0.005 inches thick, under one foil caused termination of testing at 225 lb load.

Configuration 25 was fabricated with 0.0085 inch thick wide pad foils (normally 0.006 inch thick) for the purpose of providing a larger heat sink for heat generated at the point of minimum film thickness. The remainder of the configuration was identical to the earlier configuration that was experiencing shaft instability. Load capacity achieved was 324 pounds. Teflon scorching was also evident at disassembly. Two reasons are cited for this

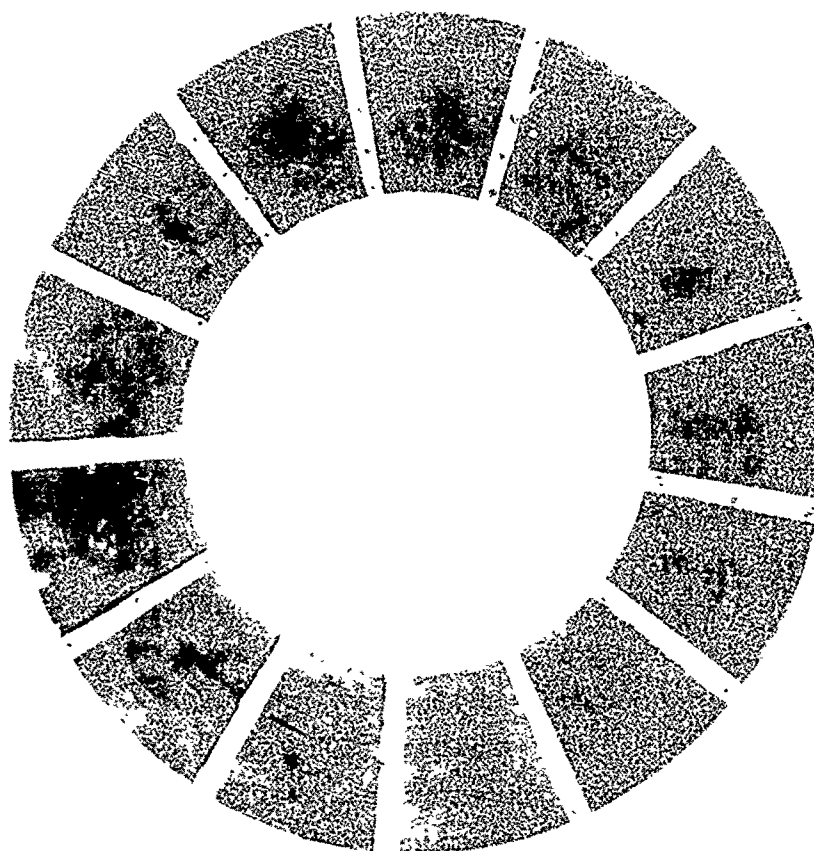


bearing's inability to carry a higher load; the thicker foils lack of compliancy, and the materials thermal conductivity is more important than thickness for heat sink considerations.

Retesting of the wide pad bearing with the rectangular shaped partial stiffener (Configuration 27) was considerably more successful. This configuration was loaded to 397 pounds. The wider thrust pad had previously been tested with the partial pad stiffener to a load of 342 pounds. This indicates a load capacity increase of 55 pounds for the rectangular stiffener. Comparing this test data with results of previous configuration tests indicates (although it cannot positively be concluded) that the wider thrust pad slightly reduces the thrust bearing capacity.

The second test configuration (28) was the same as Configuration 27 except for a 2.2 degree rotation of the spring toward the trailing edge of the pad. This increased the bearing capacity by 89 pounds, to 486 pounds. The spring rotation on a previous bearing configuration increased the capacity by 100 pounds, which substantiates the credibility of this design technique.

Configuration 29 was fabricated with Teflon-S coated 0.006 inch thick beryllium copper wide pad foils. The spring assembly was the same as Configuration 20, which demonstrated a 342 pound capacity. This test was terminated after a 469 pound load was applied to the bearing. Although the bearing capacity had not been reached, the foils were no longer flat, resulting in localized wear-through of the Teflon-S (Figure 130). The test demonstrated that, with a high thermal conductance, beryllium copper conducted the heat from the minimum film space, where the highest temperatures occur within the bearing. This is shown in Figure 130 by the broader area of discoloration in the Teflon-S. The reduced temperature in the minimum film space permitted the bearing to operate at a higher load before overtemperaturing the



CONFIGURATION 29

Figure 130. Beryllium Copper Foils With Teflon-S Coating After 469-lb Load.

Teflon coating. Using a bearing material possessing high thermal conductance is a desirable design technique for almost any coating. Beryllium copper is not considered an acceptable material for this program's final bearing, but it has been demonstrated that maximized bearing performance can be achieved by optimizing a bearing material's thermal conductance.

Test configuration number 30 consisted of 0.0001 inch thick Kaman DES on Inconel X-750 foils, and a spring assembly with the modified rectangular partial stiffener rotated 2.2° from basic, which is considered the highest capacity configuration tested to date. Purpose of the test was to note the bearing's performance at full engine thrust (i.e., 200 pounds on the engine thrust bearing) while supplying cooling air to the bearing in temperature increments up to that experienced in the engine. The test data plotted in Figure 131 show no unusual bearing performance. The condition of the bearing after the test (Figure 132) did not indicate any distress as a result of the bearing operating temperature, but did show that the coating, which was only 0.0001 thick, was not very tolerant of the starts and stops or the small foreign particles existing in the bearing after fabrication. The thicker Teflon coatings have demonstrated a degree of tolerance for these conditions. Thicker Kaman DES coatings need further investigation and development, having previously shown that the base foil distorts during the coating application. The thrust bearing wear characteristic was not exhibited in the journal bearing wear test rig because the journal bearing has a different contact characteristic. Therefore, a higher level of confidence can be placed in Kaman-coated journal bearing tests.

Configuration 31 consisted of Teflon-S coated beryllium copper foils with the Configuration 30 spring assembly. Purpose of the test was to subject the bearing to conditions of misalignment and note changes in bearing performance. This test was performed in thrust bearing load increments up to the full power thrust load on the rotating group, approximately 200 pounds. Misalignment

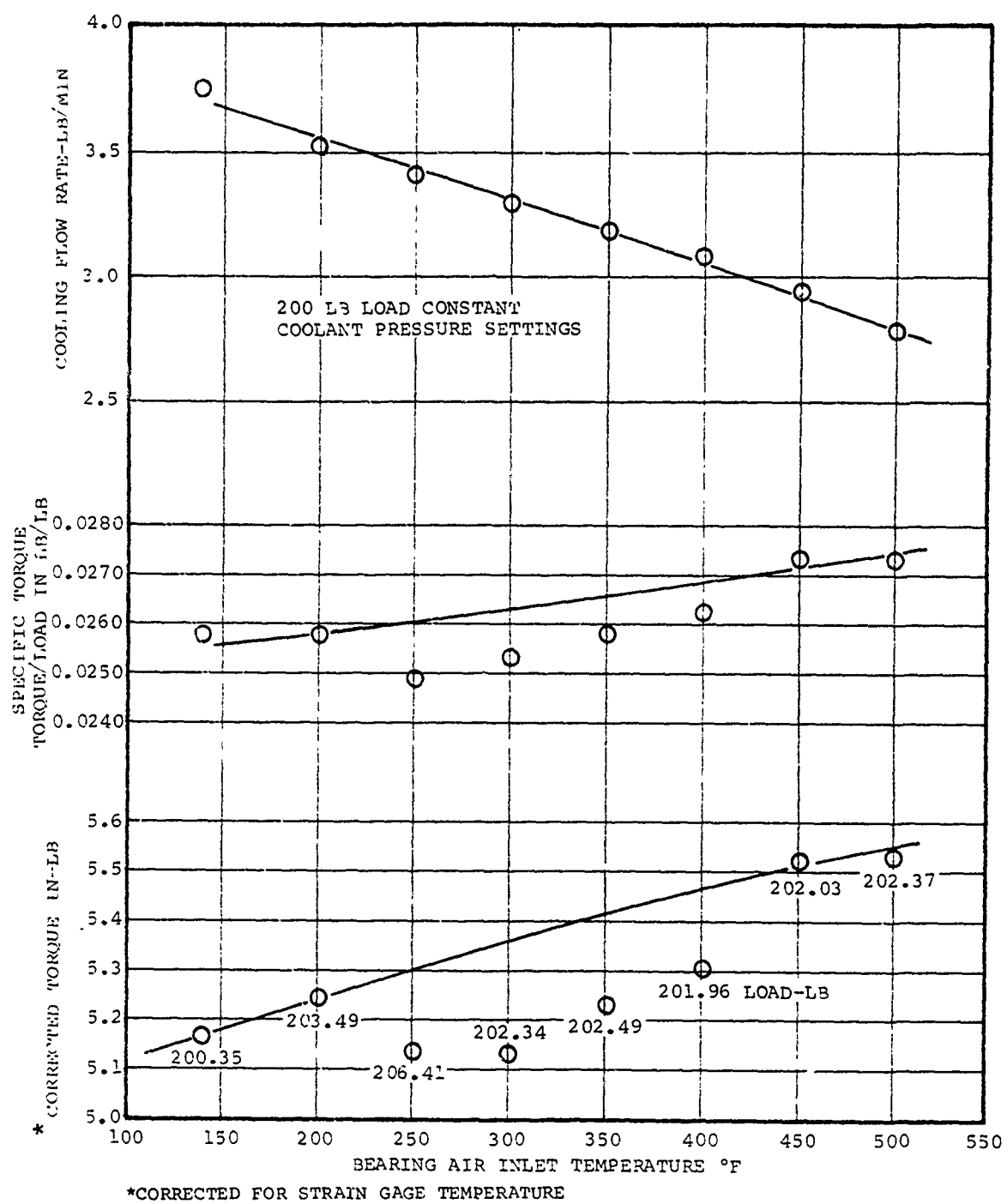
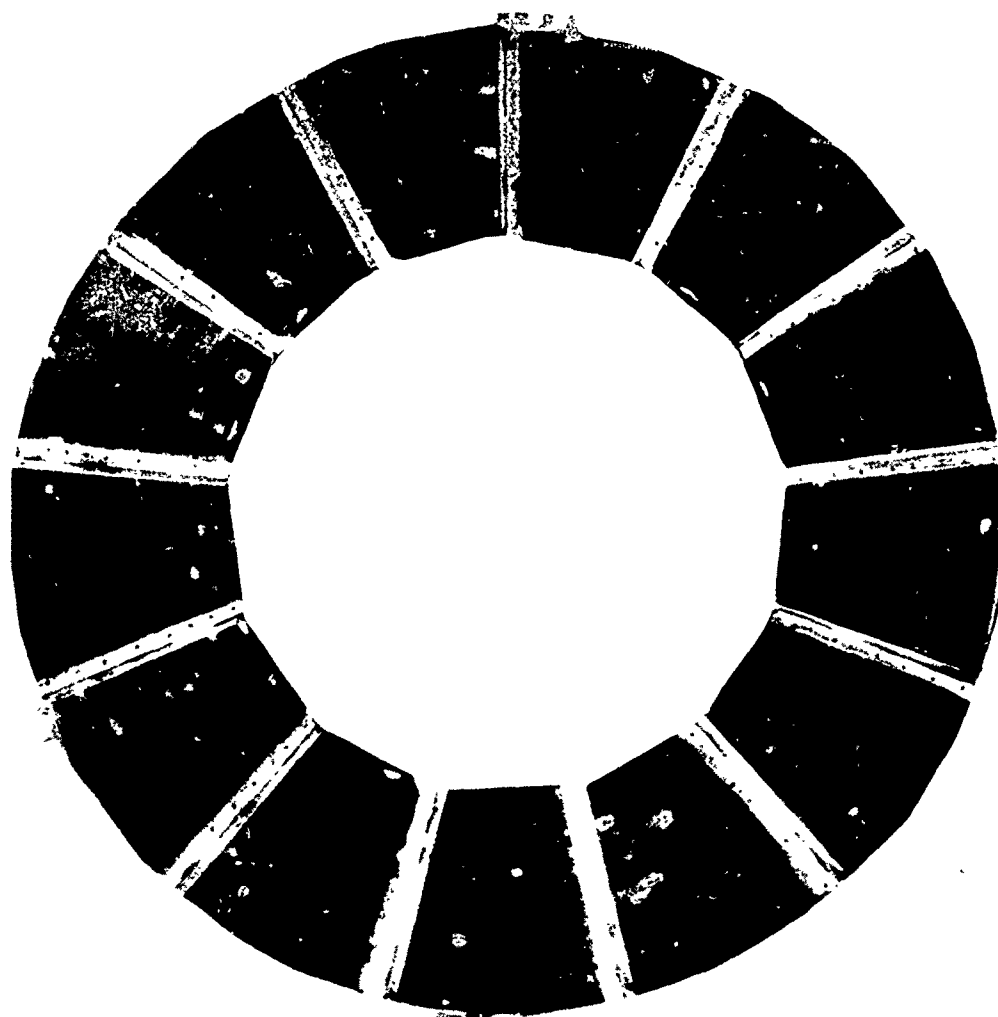


Figure 131. Test Results-Foil Thrust Bearing Configuration  
30-High Temperature Test.



CONFIGURATION 30

Figure 132. Kaman DES on Inconel X-750  
Foils After Full (200 lbs)  
Engine Thrust Test at  
Operating Temperature.

conditions up to 0.006 inch diametral were tested. The only bearing characteristic affected to any degree was the bearing torque, which decreased with increased misalignment (Figure 133). The cause of this phenomenon is currently unknown. However, the thrust bearing has demonstrated the ability to operate at the maximum misalignment conditions expected in the engine application.

The final foil thrust bearing development program test sequence was a dynamic load test, intended to simulate more realistically arrested landing loads and other short duration maneuver conditions. For this test, an alternative material with high temperature capability was selected, due to the relatively poor performance demonstrated by the Kaman coating. A nickel cobalt tank plating process was selected, but it was found that during the plating process, stresses were induced in the base material, causing it to distort or peel the coating from base material. Material was coated by the "Selectron Process" and was mechanically rolled to produce flat foil stock. Configuration 32 was fabricated using this pad coating on wide pad foils with the rectangular partial stiffener and 2.2° rotation. The test was run with Kaman SCA coated thrust runner, but failure occurred prior to reaching the nominal 200 pound load rating point.

The spring assembly survived the failure and the final test configuration was assembled using the beryllium copper bearing that had performed the misalignment tests and a nickel cobalt coated runner. Load was applied dynamically at a rate of 63 lb/sec, starting from the 200 lb load level. The test history is shown in Figure 134. The bearing successfully achieved a transient load level of 630 lb. Upon the final load application, a failure occurred at a load of 682 lb. This failure could have resulted either by reaching maximum bearing capacity or due to yielding of the Inconel X-750 springs.

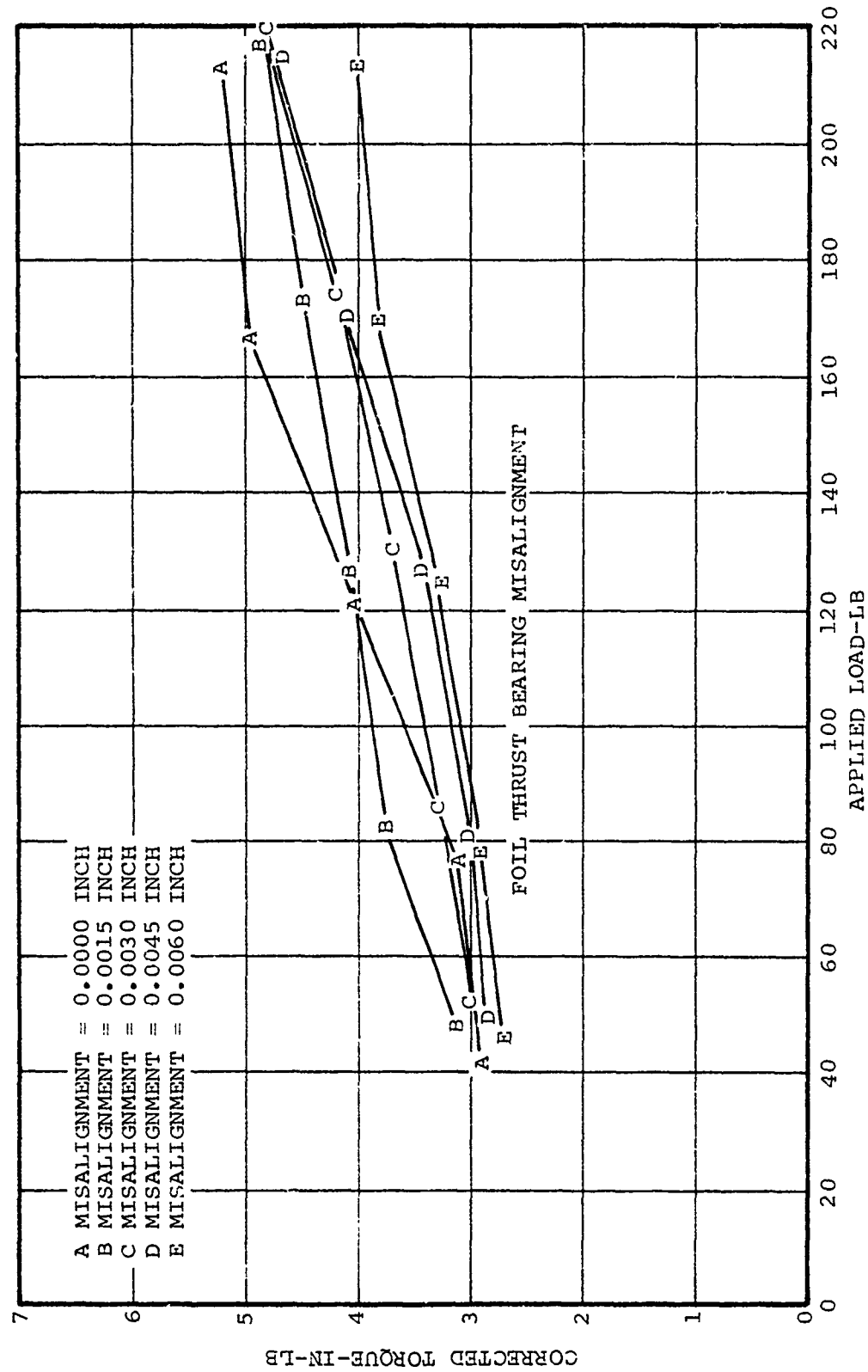
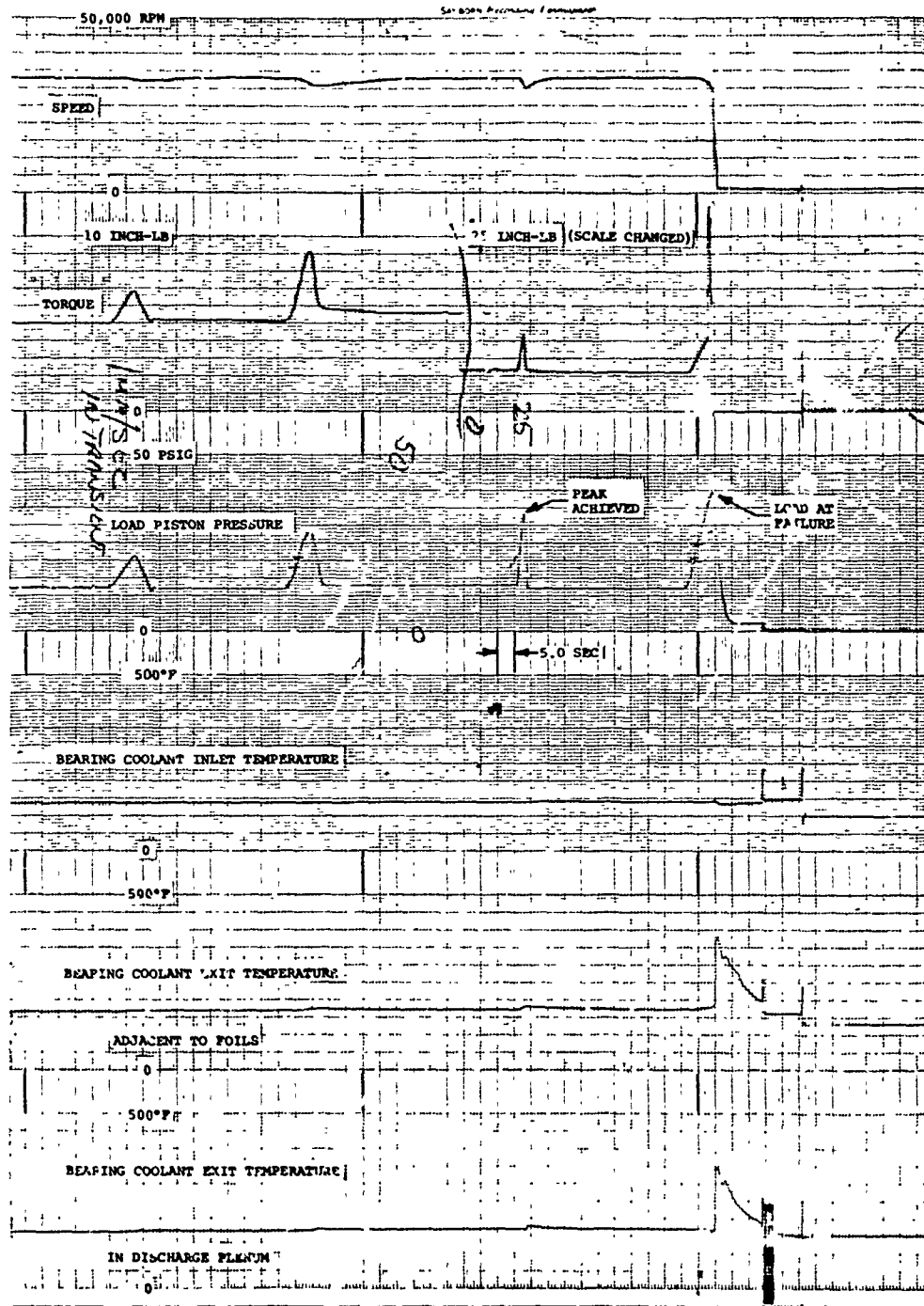


Figure 133. Foil Thrust Bearing Misalignment Test-Configuration 31.



CONFIGURATION 33

Figure 13.. Dynamic Loading Test Results



#### 4.0 CONCLUSIONS AND RECOMMENDATIONS

##### 4.1 Analytical Program

###### 4.1.1 Analytical Tools - Conclusions

The elasto-hydrodynamic thrust bearing analytical program has proved to be a valuable design tool in predicting foil thrust bearing performance. In addition, this computer program has permitted critical examination of the baseline bearing deficiencies and yielded viable design alternatives that have proved successful in improved thrust bearing load capacity. The optimization study and subsequent testing demonstrates that much improved load capacities can be achieved.

The journal bearing analytical computer simulation was a most valuable tool in assessing foil elasticity for rotor stability and critical speed design of the journal bearing rig. This complex multi-foil non-linear elasto-hydrodynamics program has successfully analyzed foil journal bearing performance. However, the current journal bearing program has limitations with respect to convergence at eccentricities greater than 0.002 to 0.005 inches as was demonstrated in this test program with a journal bearing capacity of 6.5 psi.

###### 4.1.2 Analytical Tools - Recommendations

###### 4.1.2.1 Bearings

It is apparent from the success of the analytical efforts that foil bearing performance can be significantly improved by proper utilization of these computer simulations. However, these design tools, and in particular the journal bearing computer program, are only a first step in achieving full design capability. The journal bearing program should be upgraded to permit a finite element representation of foil elasticity as in the thrust bearing program. This extension will permit examination of axial effects such as anti-clastic curvature, which may affect overall bearing

performance. Specialized foil contours such as tapered foils could be handled more efficiently with a finite-element representation.

#### 4.1.2.2 Foil Journal Bearing/Rotor Dynamic Analysis

It should be recognized that rotor stability has played a dominant role in the journal bearing test rig program. Load capacity alone does not guarantee a-priori that a rotor system is stable. Rotor inertia and elasticity must be coupled with support properties to permit full stability evaluation of rotor systems. Extending the foil bearing analytic programs to provide dynamic stiffness and damping coefficients that can be utilized in rotor stability analysis is required.

#### 4.1.3 Thermal Analysis Conclusions

Thermal analytical activity results clearly indicated foil bearing operating temperature trends to the degree that operation at a 50,000 ft altitude will exceed the foil materials and coating capability. The validity of this analysis must be checked by actual foil temperature measurement in the future. Where unacceptably high temperatures exist they can be reduced by internal rotor cooling schemes.

#### 4.1.4 Thermal Analysis Recommendations

Actual measurement of the foil bearing component temperatures should be obtained to determine the validity of the analyses accomplished in this program. Some of the temperatures are difficult to obtain but when bearing operating temperatures approach base materials and coatings limits, measurement of bearing component actual temperatures become extremely important.

## 4.2 Materials Development

### 4.2.1 Conclusions

Conclusions resulting from materials development activities are as follows:

- (a) Three alloys were established for shaft and foil substrate materials. Inconel X-750, Inconel 718 and Haynes 25 are capable of meeting foil bearing strength, modulus of elasticity, and oxidation resistance requirements, to temperatures of 1200°F.
- (b) Several low friction, oxidation resistant coatings were acceptable for use to temperatures of 1200°F and were as follows in their order of preference:
  - o  $B_4C$
  - o  $TiB_2$
  - o  $Cr_2O_3$
  - o  $TiC$
  - o Kaman DES or SCA ( $Cr_2O_3$  containing)
  - o NiCo electroplate (60-80 percent Cobalt)
  - o Tribaloy-400

Full scale rig testing indicated Kaman DES is an acceptable journal foil coating but this material exhibits a variable friction coefficient. As a thrust foil coating, Kaman DES must be thicker for adequate life and conformity.

Tests with NiCo used as the foil coating, in both full scale test rigs, were unsuccessful for geometric reasons. Because of successful tests in the high temperature wear test rig, NiCo is still considered an acceptable coating.

(c) Processing or application of the above coatings was not optimized but the following parameters were established:

- o Adequate surface finish, less than 12  $\mu$ -inch
- o Adequate thickness, 0.0002 inch minimum.
- o Sufficient ductility in thin layers to allow post-coating fabrication (bend about a 1-inch diameter mandrel without microscopic cracking).

#### 4.2.2 Recommendations

Recommendations for future materials work are as follows:

- (a) The best coatings evaluated in the program (Item b, conclusions) should be optimized with respect to application parameters and then tested to meaningful estimates of wear performance at temperatures to 1200°F. This also may include multiple coating layers of different materials.
- (b) The test plan for these coatings should include tests to determine the influence of brief contacts of bearings at high speeds as well as start/stop cyclic endurance.
- (c) Re-evaluate several of the less promising coatings using wear test rig and possibly lower test temperatures (1000°F) to establish merit for further consideration. These would include  $(B_a, Ca)F_2$  type coatings,  $Si_3N_4$ ,  $Cr_2O_3$  and  $Cr_3C_2$ .

### 4.3 Bearing Tests and Development Program

#### 4.3.1 Thrust Bearing - Conclusions

##### 4.3.1.1 Bearing Configuration

Table 19 summarizes the major steps in the development of a high load capacity thrust bearing. As indicated, all of these configurations are capable of continuous duty at 200 lb load, which represents the static bearing thrust for a Phase II engine. However, it is concluded that the wide pad bearing with the rotated orientation, using a rectangular spring stiffener has the highest probability of reaching maximum dynamic load capacity.

With the help of the analytical program the thrust bearing load capacity was increased from 300 pounds to 540 pounds under steady-state conditions, and up to 680 pounds under transient conditions, which approximate applicable MIL-E-5007 maneuver loads. This is 8 percent short of the goal to meet the arrested landing load requirement.

Achieving the goal is well within the reach of further development through spring design refinement and foil coating improvements.

##### 4.3.1.2 Foil Coatings

Conclusions drawn from the test program are that high temperature coatings, which are characterized as relatively thin and hard surfaced, are not able to sustain a high load capacity. While some of these coatings, specifically Kaman DES, have demonstrated the ability to operate at nominal (200 lb) loads at high temperatures, failure of these coatings have been extremely

TABLE 19

## PERFORMANCE COMPARISONS - COMPLIANT FOIL THRUST BEARING GEOMETRIES

Configuration No.	Bearing Geometry			Coating Thickness, in.	Bearing Orientation	Spring Geometry	Load Capacity, lb
	Pad Thickness, in.	Pad Size	Pad Coating			Spring Material Stiffener	
13	0.006	Standard	Teflon S	0.001	Standard	X-750 Partial Pad	540+
20	0.006	Wide	Teflon S	0.001	Standard	X-750 Partial Pad	342
21	0.006	Wide	Teflon S	0.001	2.2° T.E.	X-750 Partial Pad	442
25	0.0085	Wide	Teflon S	0.001	Standard	X-750 Partial Pad	325
27	0.006	Wide	Teflon S	0.001	Standard	X-750 Rectangular	397
28	0.006	Wide	Teflon S	0.001	2.2° T.E.	X-750 Pectangular	486
29	0.006*	Wide	Teflon S	0.001	Standard	X-750 Partial Pad	469+
33	0.006*	Wide	Teflon S	0.001	2.2° T.E.	X-750 Rectangular	682 (Dynamic)

All bearing base 0.010 inches  
 All intermediate stiffeners 0.010 inches  
 All spring bases 0.012 inches  
 \*BeCu Foil Pads

abrupt and totally without warning. These coatings are not able to deform plastically and provide warnings of imminent failure as the Teflon-S coated bearings consistently have done.

It is felt that the load limitation is due in part to the geometry effect of the thin coatings. With Teflon-S the bearing pad has a geometry as shown in Figure 135A. The step up to the Teflon is felt to enhance the formation of the load carrying wedge film. The high temperature coatings in Figure 135B do not provide this presumably favorable situation.

#### 4.3.2 Thrust Bearing - Recommendations

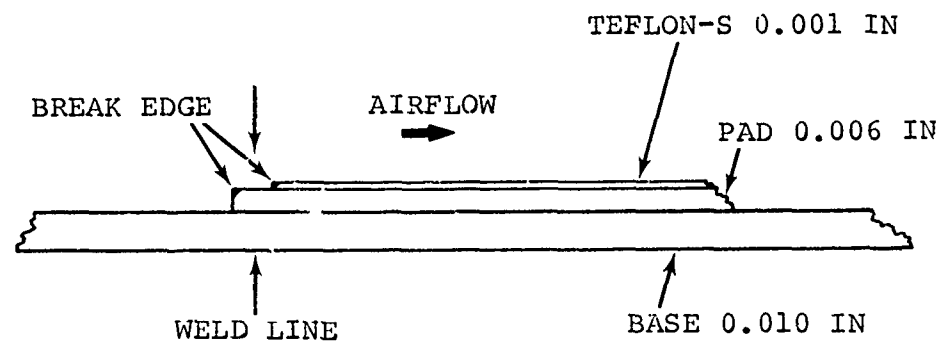
It is recommended that foil thrust bearing tests and development be continued as follows:

- (a) Select and test a pad material with the highest possible thermal conductivity to avoid pad thermal distortion at the highest film temperature location within the bearing.
- (b) Develop a spring design with the strength capability of Inconel 718 but continuing the adjustability features demonstrated with the Inconel X-750 designs.
- (c) Increase the load carrying ability of high temperature material coated foils.

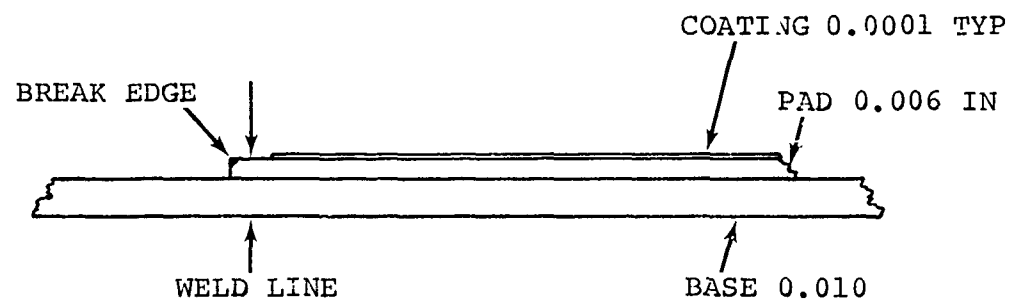
#### 4.3.3 Journal Bearing - Conclusions

##### 4.3.3.1 Bearing Configuration

The journal bearing capacity improvement program was hampered by the initially undetermined premature bending of the test shaft in the journal bearing test rig. Considerable effort



(A) TEFLON-S FOIL COATING



(B) HIGH TEMPERATURE COATING TYPICAL

APPROXIMATELY 20 x SIZE

Figure 135. Foil Thrust Bearing Geometry



was spent before the problem was determined and the test shaft shortened 6 inches so the test rig could be brought up to full speed without a bearing failure. This permitted a limited amount of testing with a 12-segment bearing but did not permit extensive 10-segment bearing testing. It is now obvious that more analytical study is required in the area of the dynamic interrelationship of foil bearings and shaft dynamics. The lack of test success with the 10 segment bearing compared to the 12 segment indicates that if a bearing other than the 12 segment bearing is required to accept the full maneuver loads of MIL-E-5007 the dynamic interrelationship must be readdressed to assure successful engine operation.

Therefore, the conclusion reached in this program is that the journal bearing that can best meet engine demonstration needs for Phase II consists of the 12-segment bearing using 0.012 in. thick Inconel foils, with a measured sway space range of 0.016 - 0.020 in. for a 4.50 in. diameter journal. This bearing can adequately handle the dynamics situation described above, and still have a demonstrated capacity of 6.5 psi and an extrapolated capacity (of another configuration extrapolated for speed and effect of engine bearing cavity pressure) of 8.6 psi. Even though the shortened test rig was used to demonstrate the 12 foil design, it should be noted that the shortened rig dynamics better approximate the engine dynamics than the original rig design. This fact is based upon a recognition that the engine rotor principal bending mode (Figure 11) is at 57,255 rpm and the redesigned rig's rotor bending mode is at 63,000 rpm. The mode illustrated in Figure 11 at 51,500 rpm is a tiebolt mode with little rotor bending activity. Thus the original rig design had a rotor bending mode at 76 percent of the engine rotor bending mode, whereas the 6-inch shorter rig has a bending mode at 110 percent of the engine bending mode.

The bearing diameter selected for the test engine, coupled with engine shaft speed results in a peripheral velocity of 39,000 feet/minute, which is approximately 50 percent higher than known successful cantilevered-leaf foil bearing applications.

The development of these characteristics of foil journal bearing demonstrates the need for additional analytical and test work to further expand their range of usefulness and meet the full maneuver loads of the intended application.

Testing revealed that a certain combination of bearing spring rate and operating sway space must be present to obtain satisfactory system rotor dynamics. Satisfactory rotor dynamics must be obtained because small values of bearing damping will permit shaft excursions to grow to unacceptable levels if excitation occurs. It is not understood why an otherwise acceptable system should incur problems if foils are cut back slightly or sway space increases. Testing these systems must be done with extreme care as the rotational energy absorbed at failure results in significant damage to journal surfaces. It has also been observed that the bearing geometry must have both a vertical and horizontal symmetry to preclude what has been identified as backward precession.

#### 4.3.2.2 Foil Coatings

Testing indicated that Kaman DES coated foils and oxidized Tribaloy-400 coated journals can provide sufficient capacity for the Phase II engine test program. Further work will be required to provide materials with the long term durability required by the applications of high temperature foil bearings to existing or advanced turbomachines.

#### 4.3.3 Journal Bearing - Recommendations

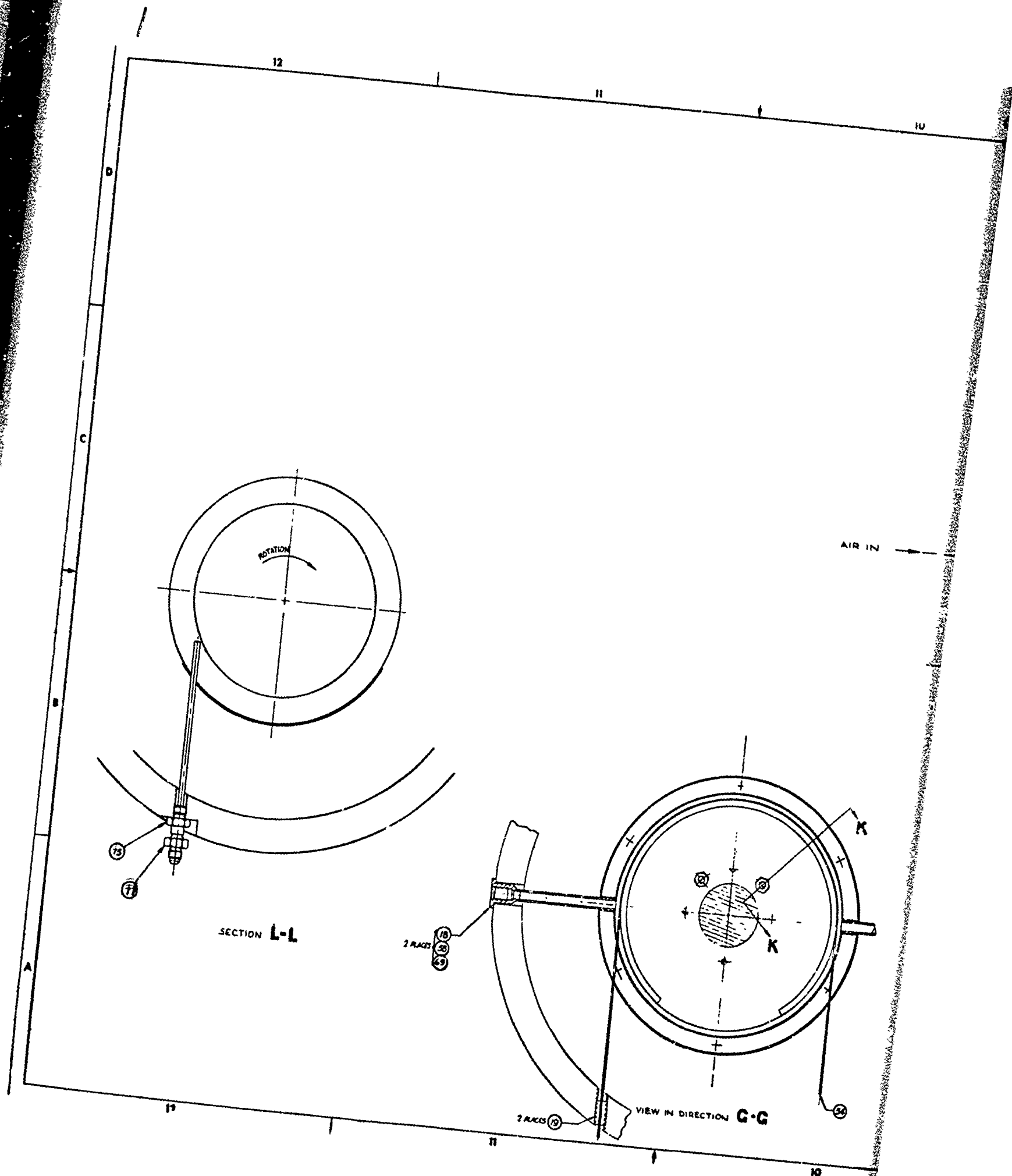
It is recommended that foil journal bearing tests and development be continued as follows:

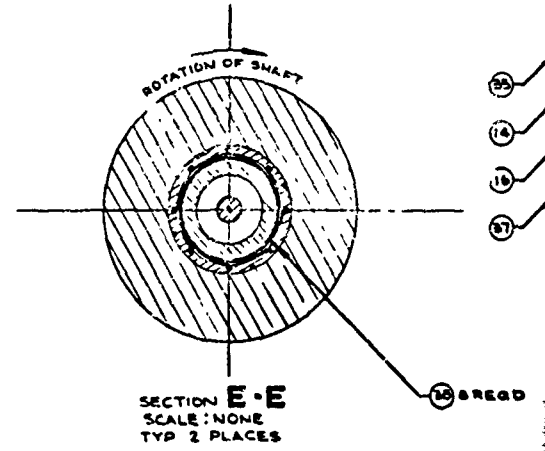
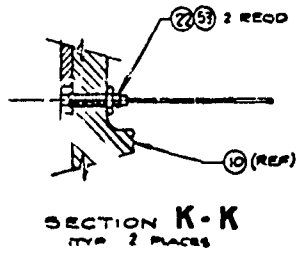
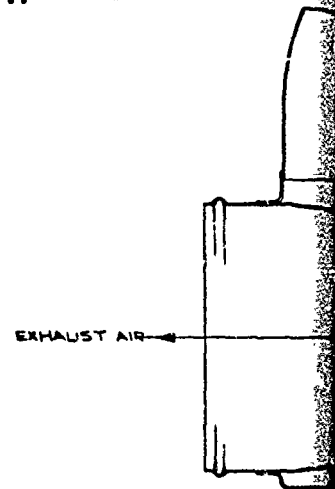
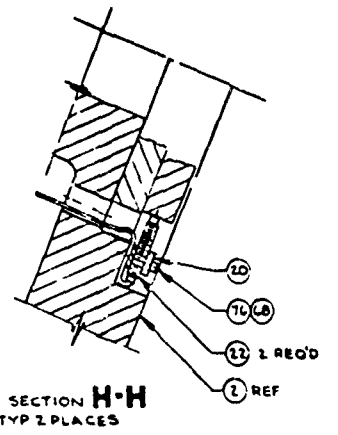
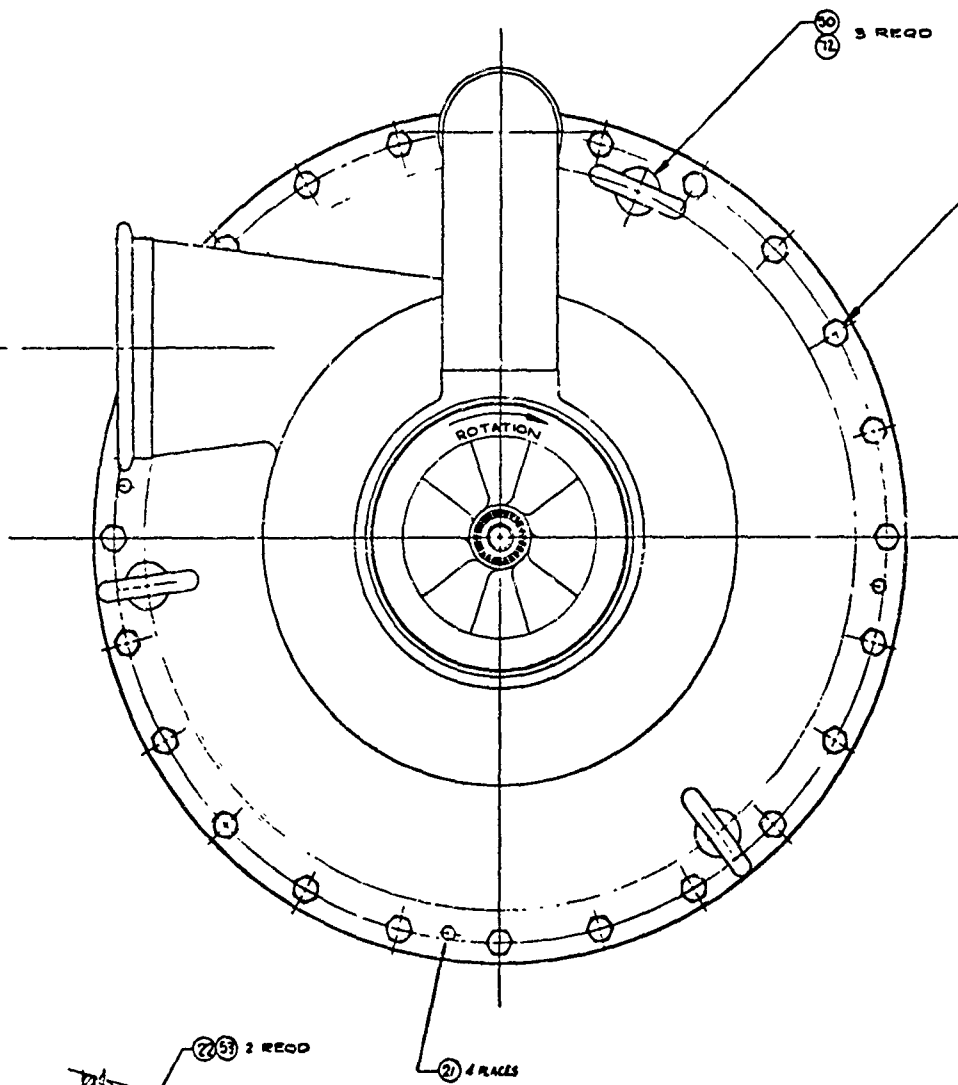
- (a) Further analytical study of the foil journal bearings as well as shaft dynamics relationship.
- (b) Continue foil journal bearing testing with the support of the analytical program, to increase its load carrying capacity.
- (c) Continue efforts to provide coating materials with long term durability.

#### 4.4 Overall Conclusions and Recommendations

The in-depth study of foil bearing characteristics and analytical tools developed and demonstrated during this program have significantly advanced techniques to improve foil bearing capacity for turbomachine applications.

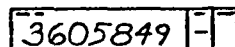
The foil bearings developed in the study exceed the requirements for a static, sea level propulsion engine demonstration. Therefore, it is recommended that this demonstration program be undertaken.





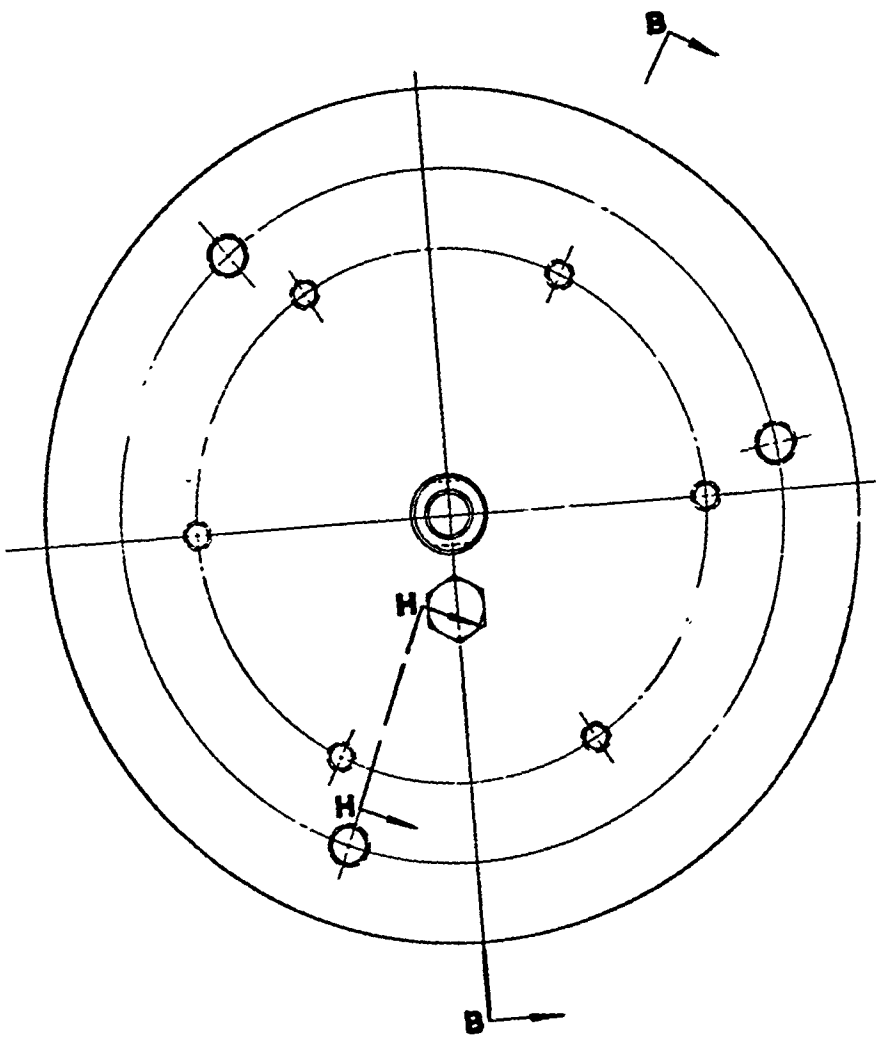
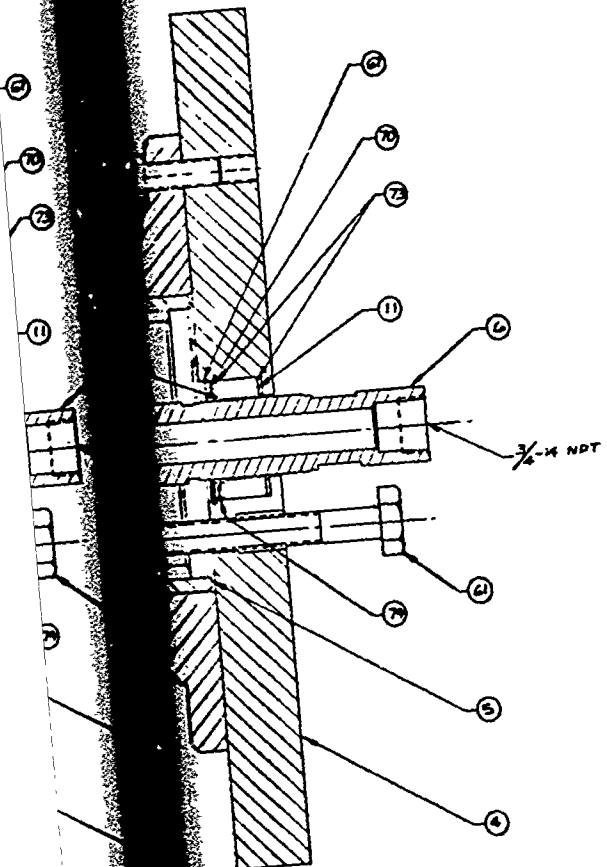
3605849

4



4.

PART NUMBER



2 ROTATING ASSY TO BE BALANCED BEFORE FINAL ASSY  
 SHIM TO OBTAIN .010-.014 GAP BETWEEN TURBINE  
 WHEEL ITEM 35 REF & NOZZLE ITEM 37 REF WHEN  
 FLYWHEEL ITEM 11 REF IS AGAINST ORIFICE PLATE ITEM  
 13 REF & A 70 LB LOAD IS APPLIED TO SHAFT IN  
 THE DIRECTION OF THE TURBINE WHEEL.

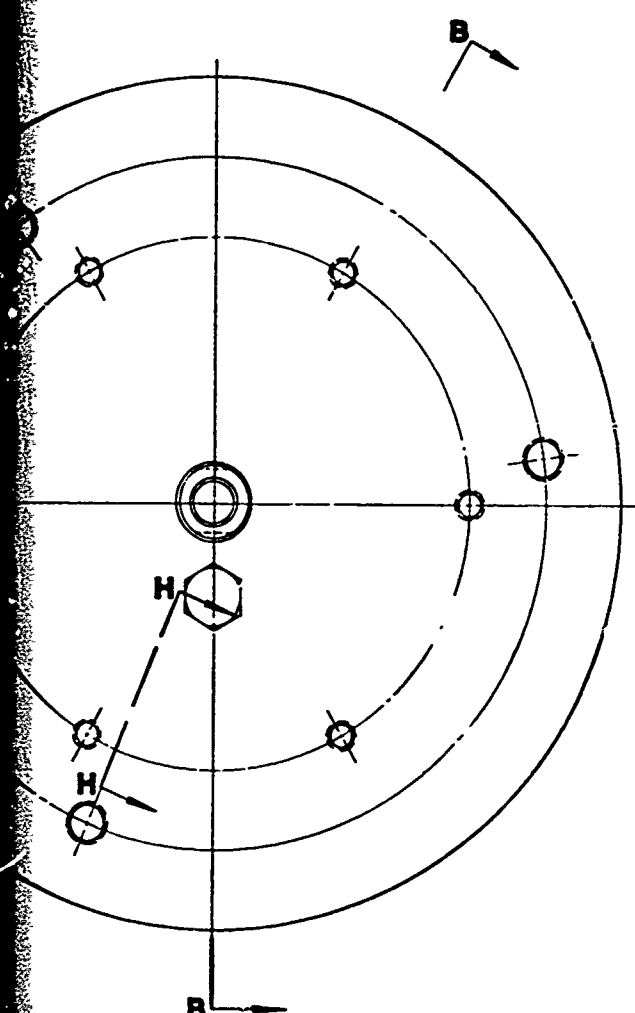
UNLESS OTHERWISE SPECIFIED

275

2

5

REVISIONS			
NO.	DATE	DESCRIPTION	BY



110	MS 4996-24	SCREW CAP	6
111	MS 4996-24	NOZZLE	6
112	MS 4996-24	SCREW CAP	7
113	MS 4996-24	NOZZLE	7
114	MS 4996-24	SCREW CAP	7
115	MS 4996-24	NOZZLE	7
116	MS 4996-24	SCREW CAP	7
117	MS 4996-24	NOZZLE	7
118	MS 4996-24	SCREW CAP	7
119	MS 4996-24	NOZZLE	7
120	MS 4996-24	SCREW CAP	7
121	MS 4996-24	NOZZLE	7
122	MS 4996-24	SCREW CAP	7
123	MS 4996-24	NOZZLE	7
124	MS 4996-24	SCREW CAP	7
125	MS 4996-24	NOZZLE	7
126	MS 4996-24	SCREW CAP	7
127	MS 4996-24	NOZZLE	7
128	MS 4996-24	SCREW CAP	7
129	MS 4996-24	NOZZLE	7
130	MS 4996-24	SCREW CAP	7
131	MS 4996-24	NOZZLE	7
132	MS 4996-24	SCREW CAP	7
133	MS 4996-24	NOZZLE	7
134	MS 4996-24	SCREW CAP	7
135	MS 4996-24	NOZZLE	7
136	MS 4996-24	SCREW CAP	7
137	MS 4996-24	NOZZLE	7
138	MS 4996-24	SCREW CAP	7
139	MS 4996-24	NOZZLE	7
140	MS 4996-24	SCREW CAP	7
141	MS 4996-24	NOZZLE	7
142	MS 4996-24	SCREW CAP	7
143	MS 4996-24	NOZZLE	7
144	MS 4996-24	SCREW CAP	7
145	MS 4996-24	NOZZLE	7
146	MS 4996-24	SCREW CAP	7
147	MS 4996-24	NOZZLE	7
148	MS 4996-24	SCREW CAP	7
149	MS 4996-24	NOZZLE	7
150	MS 4996-24	SCREW CAP	7
151	MS 4996-24	NOZZLE	7
152	MS 4996-24	SCREW CAP	7
153	MS 4996-24	NOZZLE	7
154	MS 4996-24	SCREW CAP	7
155	MS 4996-24	NOZZLE	7
156	MS 4996-24	SCREW CAP	7
157	MS 4996-24	NOZZLE	7
158	MS 4996-24	SCREW CAP	7
159	MS 4996-24	NOZZLE	7
160	MS 4996-24	SCREW CAP	7
161	MS 4996-24	NOZZLE	7
162	MS 4996-24	SCREW CAP	7
163	MS 4996-24	NOZZLE	7
164	MS 4996-24	SCREW CAP	7
165	MS 4996-24	NOZZLE	7
166	MS 4996-24	SCREW CAP	7
167	MS 4996-24	NOZZLE	7
168	MS 4996-24	SCREW CAP	7
169	MS 4996-24	NOZZLE	7
170	MS 4996-24	SCREW CAP	7
171	MS 4996-24	NOZZLE	7
172	MS 4996-24	SCREW CAP	7
173	MS 4996-24	NOZZLE	7
174	MS 4996-24	SCREW CAP	7
175	MS 4996-24	NOZZLE	7
176	MS 4996-24	SCREW CAP	7
177	MS 4996-24	NOZZLE	7
178	MS 4996-24	SCREW CAP	7
179	MS 4996-24	NOZZLE	7
180	MS 4996-24	SCREW CAP	7
181	MS 4996-24	NOZZLE	7
182	MS 4996-24	SCREW CAP	7
183	MS 4996-24	NOZZLE	7
184	MS 4996-24	SCREW CAP	7
185	MS 4996-24	NOZZLE	7
186	MS 4996-24	SCREW CAP	7
187	MS 4996-24	NOZZLE	7
188	MS 4996-24	SCREW CAP	7
189	MS 4996-24	NOZZLE	7
190	MS 4996-24	SCREW CAP	7
191	MS 4996-24	NOZZLE	7
192	MS 4996-24	SCREW CAP	7
193	MS 4996-24	NOZZLE	7
194	MS 4996-24	SCREW CAP	7
195	MS 4996-24	NOZZLE	7
196	MS 4996-24	SCREW CAP	7
197	MS 4996-24	NOZZLE	7
198	MS 4996-24	SCREW CAP	7
199	MS 4996-24	NOZZLE	7
200	MS 4996-24	SCREW CAP	7
201	MS 4996-24	NOZZLE	7
202	MS 4996-24	SCREW CAP	7
203	MS 4996-24	NOZZLE	7
204	MS 4996-24	SCREW CAP	7
205	MS 4996-24	NOZZLE	7
206	MS 4996-24	SCREW CAP	7
207	MS 4996-24	NOZZLE	7
208	MS 4996-24	SCREW CAP	7
209	MS 4996-24	NOZZLE	7
210	MS 4996-24	SCREW CAP	7
211	MS 4996-24	NOZZLE	7
212	MS 4996-24	SCREW CAP	7
213	MS 4996-24	NOZZLE	7
214	MS 4996-24	SCREW CAP	7
215	MS 4996-24	NOZZLE	7
216	MS 4996-24	SCREW CAP	7
217	MS 4996-24	NOZZLE	7
218	MS 4996-24	SCREW CAP	7
219	MS 4996-24	NOZZLE	7
220	MS 4996-24	SCREW CAP	7
221	MS 4996-24	NOZZLE	7
222	MS 4996-24	SCREW CAP	7
223	MS 4996-24	NOZZLE	7
224	MS 4996-24	SCREW CAP	7
225	MS 4996-24	NOZZLE	7
226	MS 4996-24	SCREW CAP	7
227	MS 4996-24	NOZZLE	7
228	MS 4996-24	SCREW CAP	7
229	MS 4996-24	NOZZLE	7
230	MS 4996-24	SCREW CAP	7
231	MS 4996-24	NOZZLE	7
232	MS 4996-24	SCREW CAP	7
233	MS 4996-24	NOZZLE	7
234	MS 4996-24	SCREW CAP	7
235	MS 4996-24	NOZZLE	7
236	MS 4996-24	SCREW CAP	7
237	MS 4996-24	NOZZLE	7
238	MS 4996-24	SCREW CAP	7
239	MS 4996-24	NOZZLE	7
240	MS 4996-24	SCREW CAP	7
241	MS 4996-24	NOZZLE	7
242	MS 4996-24	SCREW CAP	7
243	MS 4996-24	NOZZLE	7
244	MS 4996-24	SCREW CAP	7
245	MS 4996-24	NOZZLE	7
246	MS 4996-24	SCREW CAP	7
247	MS 4996-24	NOZZLE	7
248	MS 4996-24	SCREW CAP	7
249	MS 4996-24	NOZZLE	7
250	MS 4996-24	SCREW CAP	7
251	MS 4996-24	NOZZLE	7
252	MS 4996-24	SCREW CAP	7
253	MS 4996-24	NOZZLE	7
254	MS 4996-24	SCREW CAP	7
255	MS 4996-24	NOZZLE	7
256	MS 4996-24	SCREW CAP	7
257	MS 4996-24	NOZZLE	7
258	MS 4996-24	SCREW CAP	7
259	MS 4996-24	NOZZLE	7
260	MS 4996-24	SCREW CAP	7
261	MS 4996-24	NOZZLE	7
262	MS 4996-24	SCREW CAP	7
263	MS 4996-24	NOZZLE	7
264	MS 4996-24	SCREW CAP	7
265	MS 4996-24	NOZZLE	7
266	MS 4996-24	SCREW CAP	7
267	MS 4996-24	NOZZLE	7
268	MS 4996-24	SCREW CAP	7
269	MS 4996-24	NOZZLE	7
270	MS 4996-24	SCREW CAP	7
271	MS 4996-24	NOZZLE	7
272	MS 4996-24	SCREW CAP	7
273	MS 4996-24	NOZZLE	7
274	MS 4996-24	SCREW CAP	7
275	MS 4996-24	NOZZLE	7

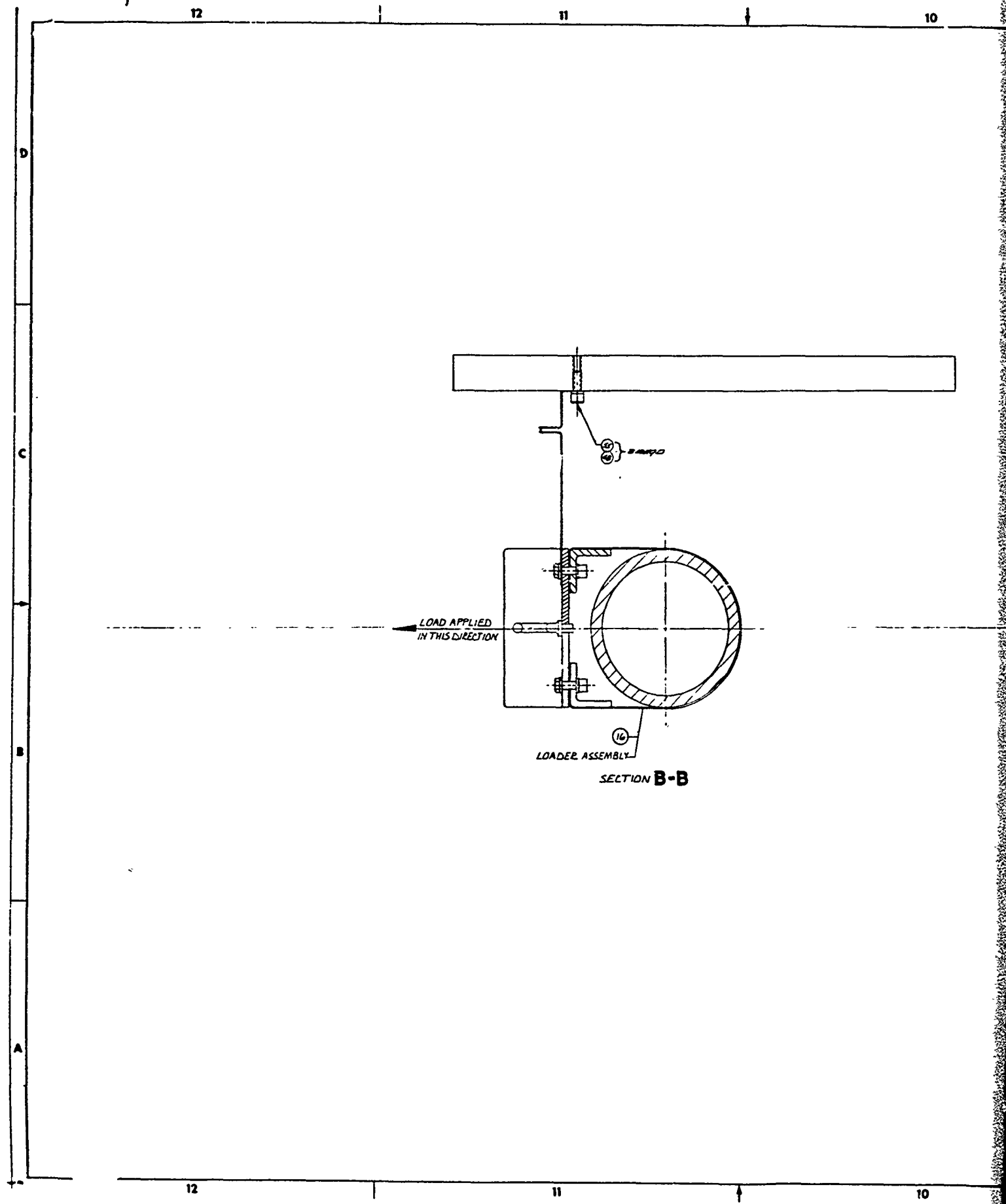
2 ROTATING ASSY TO BE BALANCED BEFORE FINAL ASSY  
 SHIM TO OBTAIN .010-.014 GAP BETWEEN TURBINE WHEEL ITEM 35 REF & NOZZLE ITEM 37 REF WHEN FLYWHEEL ITEM 11 REF IS AGAINST ORIFICE PLATE ITEM 13 REF & A TOLB LOAD IS APPLIED TO SHAFT IN THE DIRECTION OF THE TURBINE WHEEL.

NOTES: UNLESS OTHERWISE SPECIFIED

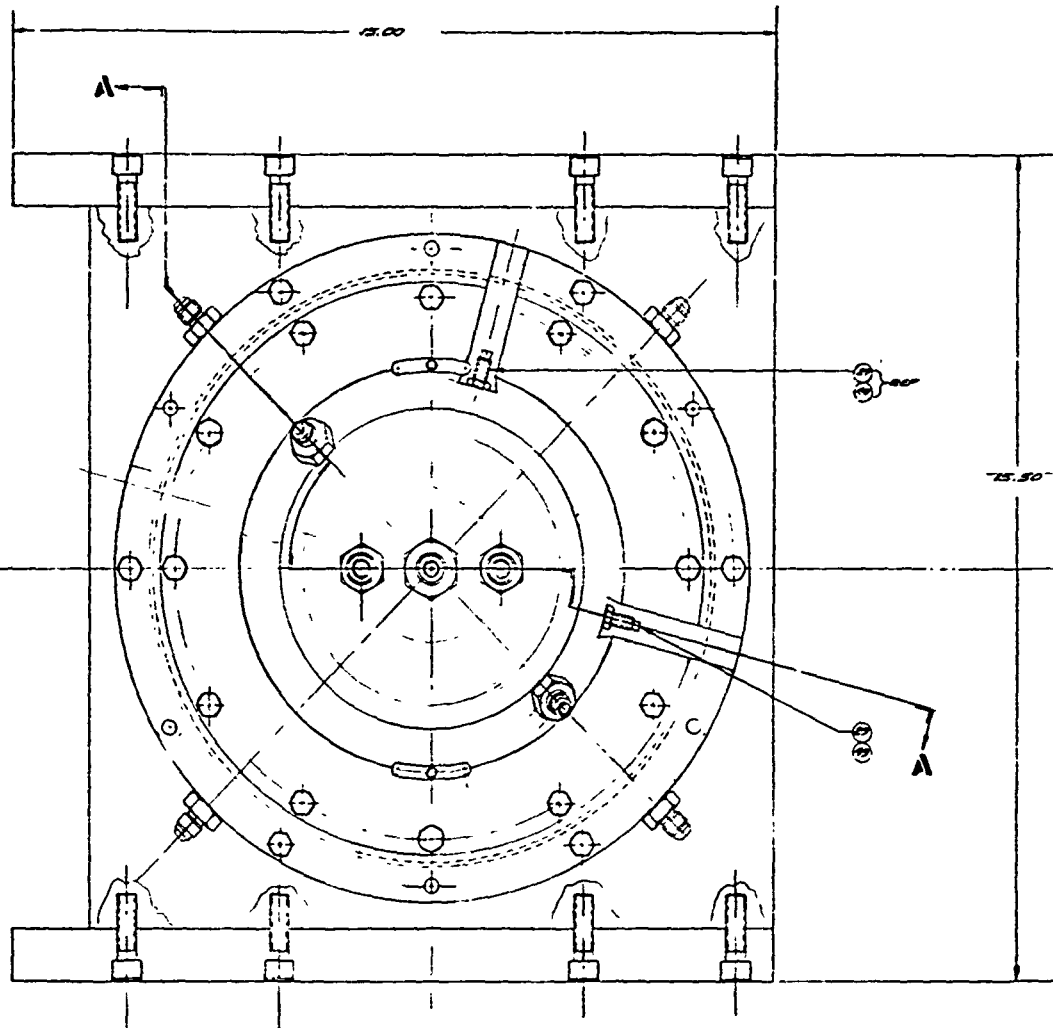
275

QUANTITY UNIT PART NO. DESCRIPTION MATERIAL FINISH TOLERANCE DIMENSIONS WEIGHT APPLICATION		PARTS LIST TEST FIXTURE ASSY, GEN THRUST BRG. 1 99/93 3605849 SCALE 1/1 SHEET 1 OF 1	
---	--	---	--



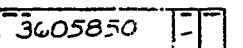


2



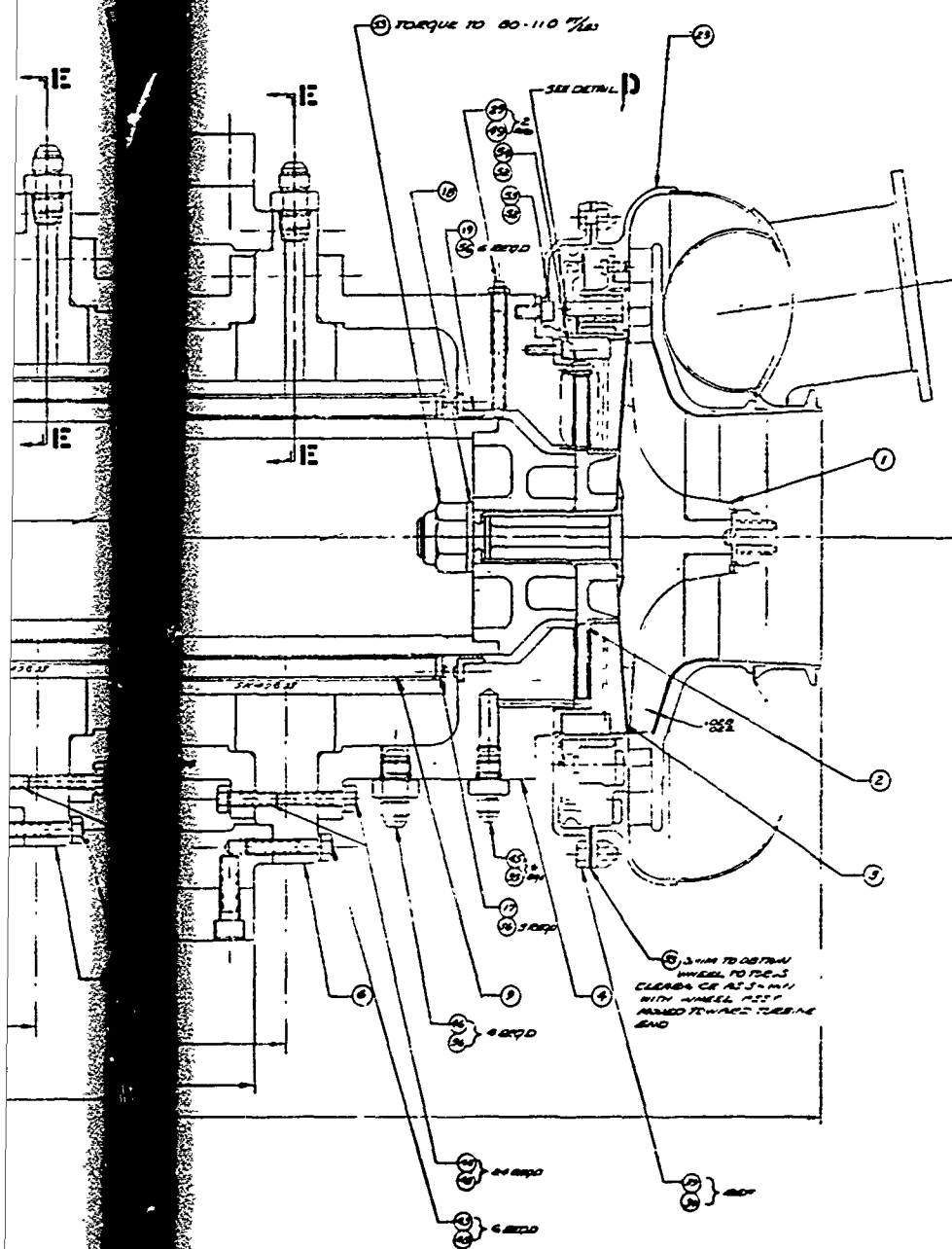
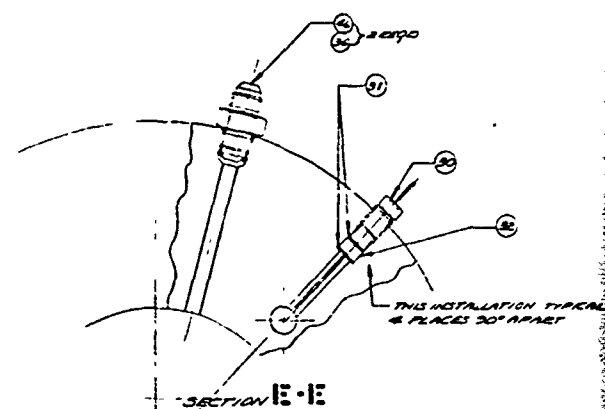
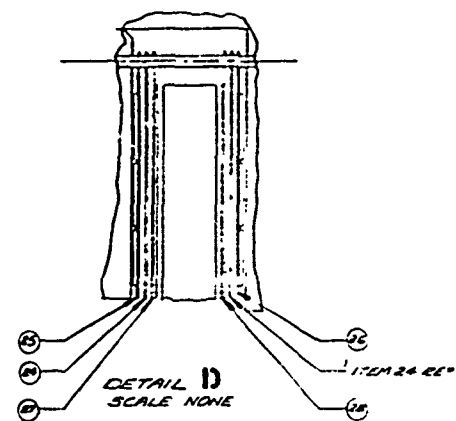
3605850

4



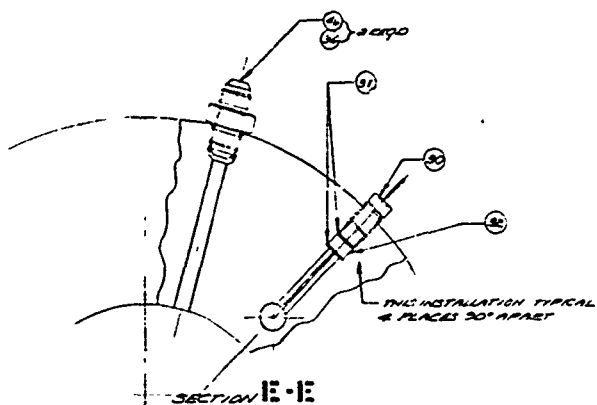
4

4



1. APPLY LOCKWASH PER MS 33540  
2. USE WASH WHEEL SET

277



REVISIONS				
FILE NO.	DESCRIPTION	DATE	APPROVED	

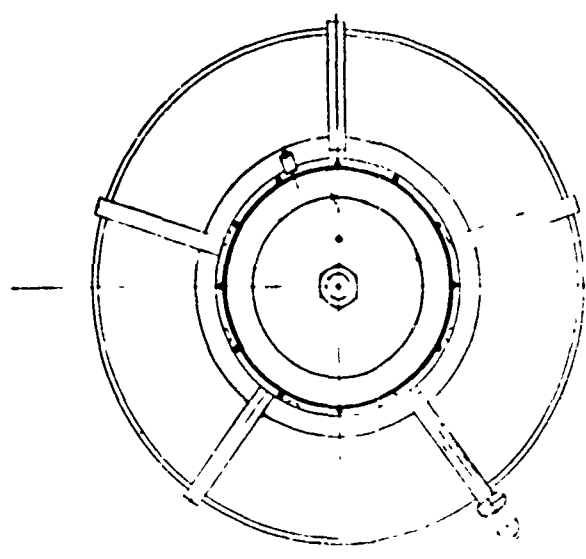
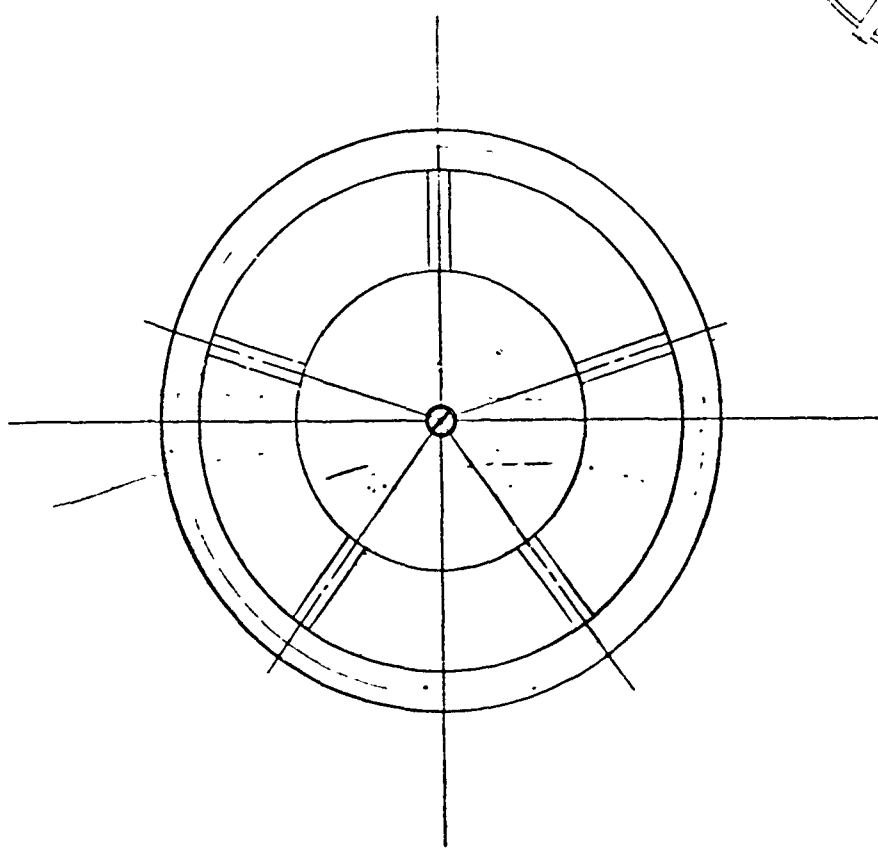
557	AN350-12A	SCREEN 5.32 30.00 AWING	7
556	AN350-26	SCREEN 6.40 12.00 AWING	7
553	AN350-70	SCREEN 18.38 16.00 SK HD	4
554	AN350-70	SCREEN 18.38 30.00	4
553	AN350-16	V-T 5.16 16.00 E. ROCKING	3
552	AN350-30	LOGE WEE	3
549	AN356-5	HOT	4
540	AN360-46L	NAS-EE	7
147	AN35-5	JN-11	4
546	AN35-6	JN-11	7
545	AN35-4	UNLX	7
543	AN4-12A	R-2 16.23 11.42	2
542	AN4-11A	R-2 16.23 11.42	2
541	AN4-10A	R-2 16.23 11.42	7
540	AN4-7A	R-2 16.23 11.42	4
539	AN4-5A	R-2 16.23 11.42	4
137	AN5195-0	AN5195-0	7
536	AN5195-0	AN5195-0	7
535	AN5195-1	AN5195-1	7
534	AN5195-2	AN5195-2	7
533	AN5195-3	AN5195-3	7
532	AN5195-4	AN5195-4	7
531	AN5195-5	AN5195-5	7
530	AN5195-6	AN5195-6	7
529	AN5195-7	AN5195-7	7
528	AN5195-8	AN5195-8	7
527	AN5195-9	AN5195-9	7
526	AN5195-10	AN5195-10	7
525	AN5195-11	AN5195-11	7
524	AN5195-12	AN5195-12	7
523	AN5195-13	AN5195-13	7
522	AN5195-14	AN5195-14	7
521	AN5195-15	AN5195-15	7
520	AN5195-16	AN5195-16	7
519	AN5195-17	AN5195-17	7
518	AN5195-18	AN5195-18	7
517	AN5195-19	AN5195-19	7
516	AN5195-20	AN5195-20	7
515	AN5195-21	AN5195-21	7
514	AN5195-22	AN5195-22	7
513	AN5195-23	AN5195-23	7
512	AN5195-24	AN5195-24	7
511	AN5195-25	AN5195-25	7
510	AN5195-26	AN5195-26	7
509	AN5195-27	AN5195-27	7
508	AN5195-28	AN5195-28	7
507	AN5195-29	AN5195-29	7
506	AN5195-30	AN5195-30	7
505	AN5195-31	AN5195-31	7
504	AN5195-32	AN5195-32	7
503	AN5195-33	AN5195-33	7
502	AN5195-34	AN5195-34	7
501	AN5195-35	AN5195-35	7
500	AN5195-36	AN5195-36	7
499	AN5195-37	AN5195-37	7
498	AN5195-38	AN5195-38	7
497	AN5195-39	AN5195-39	7
496	AN5195-40	AN5195-40	7
495	AN5195-41	AN5195-41	7
494	AN5195-42	AN5195-42	7
493	AN5195-43	AN5195-43	7
492	AN5195-44	AN5195-44	7
491	AN5195-45	AN5195-45	7
490	AN5195-46	AN5195-46	7
489	AN5195-47	AN5195-47	7
488	AN5195-48	AN5195-48	7
487	AN5195-49	AN5195-49	7
486	AN5195-50	AN5195-50	7
485	AN5195-51	AN5195-51	7
484	AN5195-52	AN5195-52	7
483	AN5195-53	AN5195-53	7
482	AN5195-54	AN5195-54	7
481	AN5195-55	AN5195-55	7
480	AN5195-56	AN5195-56	7
479	AN5195-57	AN5195-57	7
478	AN5195-58	AN5195-58	7
477	AN5195-59	AN5195-59	7
476	AN5195-60	AN5195-60	7
475	AN5195-61	AN5195-61	7
474	AN5195-62	AN5195-62	7
473	AN5195-63	AN5195-63	7
472	AN5195-64	AN5195-64	7
471	AN5195-65	AN5195-65	7
470	AN5195-66	AN5195-66	7
469	AN5195-67	AN5195-67	7
468	AN5195-68	AN5195-68	7
467	AN5195-69	AN5195-69	7
466	AN5195-70	AN5195-70	7
465	AN5195-71	AN5195-71	7
464	AN5195-72	AN5195-72	7
463	AN5195-73	AN5195-73	7
462	AN5195-74	AN5195-74	7
461	AN5195-75	AN5195-75	7
460	AN5195-76	AN5195-76	7
459	AN5195-77	AN5195-77	7
458	AN5195-78	AN5195-78	7
457	AN5195-79	AN5195-79	7
456	AN5195-80	AN5195-80	7
455	AN5195-81	AN5195-81	7
454	AN5195-82	AN5195-82	7
453	AN5195-83	AN5195-83	7
452	AN5195-84	AN5195-84	7
451	AN5195-85	AN5195-85	7
450	AN5195-86	AN5195-86	7
449	AN5195-87	AN5195-87	7
448	AN5195-88	AN5195-88	7
447	AN5195-89	AN5195-89	7
446	AN5195-90	AN5195-90	7
445	AN5195-91	AN5195-91	7
444	AN5195-92	AN5195-92	7
443	AN5195-93	AN5195-93	7
442	AN5195-94	AN5195-94	7
441	AN5195-95	AN5195-95	7
440	AN5195-96	AN5195-96	7
439	AN5195-97	AN5195-97	7
438	AN5195-98	AN5195-98	7
437	AN5195-99	AN5195-99	7
436	AN5195-100	AN5195-100	7
435	AN5195-101	AN5195-101	7
434	AN5195-102	AN5195-102	7
433	AN5195-103	AN5195-103	7
432	AN5195-104	AN5195-104	7
431	AN5195-105	AN5195-105	7
430	AN5195-106	AN5195-106	7
429	AN5195-107	AN5195-107	7
428	AN5195-108	AN5195-108	7
427	AN5195-109	AN5195-109	7
426	AN5195-110	AN5195-110	7
425	AN5195-111	AN5195-111	7
424	AN5195-112	AN5195-112	7
423	AN5195-113	AN5195-113	7
422	AN5195-114	AN5195-114	7
421	AN5195-115	AN5195-115	7
420	AN5195-116	AN5195-116	7
419	AN5195-117	AN5195-117	7
418	AN5195-118	AN5195-118	7
417	AN5195-119	AN5195-119	7
416	AN5195-120	AN5195-120	7
415	AN5195-121	AN5195-121	7
414	AN5195-122	AN5195-122	7
413	AN5195-123	AN5195-123	7
412	AN5195-124	AN5195-124	7
411	AN5195-125	AN5195-125	7
410	AN5195-126	AN5195-126	7
409	AN5195-127	AN5195-127	7
408	AN5195-128	AN5195-128	7
407	AN5195-129	AN5195-129	7
406	AN5195-130	AN5195-130	7
405	AN5195-131	AN5195-131	7
404	AN5195-132	AN5195-132	7
403	AN5195-133	AN5195-133	7
402	AN5195-134	AN5195-134	7
401	AN5195-135	AN5195-135	7
400	AN5195-136	AN5195-136	7
399	AN5195-137	AN5195-137	7
398	AN5195-138	AN5195-138	7
397	AN5195-139	AN5195-139	7
396	AN5195-140	AN5195-140	7
395	AN5195-141	AN5195-141	7
394	AN5195-142	AN5195-142	7
393	AN5195-143	AN5195-143	7
392	AN5195-144	AN5195-144	7
391	AN5195-145	AN5195-145	7
390	AN5195-146	AN5195-146	7
389	AN5195-147	AN5195-147	7
388	AN5195-148	AN5195-148	7
387	AN5195-149	AN5195-149	7
386	AN5195-150	AN5195-150	7
385	AN5195-151	AN5195-151	7
384	AN5195-152	AN5195-152	7
383	AN5195-153	AN5195-153	7
382	AN5195-154	AN5195-154	7
381	AN5195-155	AN5195-155	7
380	AN5195-156	AN5195-156	7
379	AN5195-157	AN5195-157	7
378	AN5195-158	AN5195-158	7
377	AN5195-159	AN5195-159	7
376	AN5195-160	AN5195-160	7
375	AN5195-161	AN5195-161	7
374	AN5195-162	AN5195-162	7
373	AN5195-163	AN5195-163	7
372	AN5195-164	AN5195-164	7
371	AN5195-165	AN5195-165	7
370	AN5195-166	AN5195-166	7
369	AN5195-167	AN5195-167	7
368	AN5195-168	AN5195-168	7
367	AN5195-169	AN5195-169	7
366	AN5195-170	AN5195-170	7
365	AN5195-171	AN5195-171	7
364	AN5195-172	AN5195-172	7
363	AN5195-173	AN5195-173	7
362	AN5195-174	AN5195-174	7
361	AN5195-175	AN5195-175	7
360	AN5195-176	AN5195-176	7
359	AN5195-177	AN5195-177	7
358	AN5195-178	AN5195-178	7
357	AN5195-179	AN5195-179	7
356	AN5195-180	AN5195-180	7
355	AN5195-181	AN5195-181	7
354	AN5195-182	AN5195-182	7
353	AN5195-183	AN5195-183	7
352	AN5195-184	AN5195-184	7
351	AN5195-185	AN5195-185	7
350	AN5195-186	AN5195-186	7
349	AN5195-187	AN5195-187	7
348	AN5195-188	AN5195-188	7
347	AN5195-189	AN5195-189	7
346	AN5195-190	AN5195-190	7
345	AN5195-191	AN5195-191	7
344	AN5195-192	AN5195-192	7
343	AN5195-193	AN5195-193	7
342	AN5195-194	AN5195-194	7
341	AN5195-195	AN5195-195	7
340	AN5195-196	AN5195-196	7
339	AN5195-197	AN5195-197	7
338	AN5195-198	AN5195-198	7
337	AN5195-199	AN5195-199	7
336	AN5195-200	AN5195-200	7
335	AN5195-201	AN5195-201	7
334	AN5195-202	AN5195-202	7
333	AN5195-203	AN5195-203	7
332	AN5195-204	AN5195-204	7
331	AN5195-205	AN5195-205	7
330	AN5195-206	AN5195-206	7
329	AN5195-207	AN5195-207	7
328	AN5195-208	AN5195-208	7
327	AN5195-209	AN5195-209	7
326	AN5195-210	AN5195-210	7
325	AN5195-211	AN5195-211	7
324	AN5195-212	AN5195-212	7
323	AN5195-213	AN5195-213	7
322	AN5195-214	AN5195-214	7
321	AN5195-215	AN5195-215	7
320	AN5195-216	AN5195-216	7
319	AN5195-217	AN5195-217	7
318	AN5195-218	AN5195-218	7
317	AN5195-219	AN5195-219	7
316	AN5195-220	AN5195-220	7
315	AN5195-221	AN5195-221	7
314	AN5195-222	AN5195-222	7
313	AN5195-223	AN5195-223	7
312	AN5195-224	AN5195-224	7
311	AN5195-225	AN5195-225	7
310	AN5195-226	AN5195-226	7
309	AN5195-227	AN5195-227	7
308	AN5195-228	AN5195-228	7
307	AN5195-229	AN5195-229	7
306	AN5195-230	AN5195-230	7
305	AN5195-231	AN5195-231	7
304	AN5195-232	AN5195-232	7
303	AN5195-233	AN5195-233	7
302	AN5195-234	AN5195-234	7
301	AN5195-235	AN5195-235	7
300	AN5195-236	AN5195-236	7
299	AN5195-237	AN5195-237	7
298	AN5195-238	AN5195-238	7
297	AN5195-239	AN5195-239	7
296	AN5195-240	AN5195-240	7
295	AN5195-241	AN5195-241	7
294	AN5195-242	AN5195-242	7
293	AN5195-243	AN5195-243	7
292	AN5195-244	AN5195-244	7
291	AN5195-245	AN5195-245	7
290	AN5195-246	AN5195-246	7
289	AN5195-247	AN5195-247	7
288	AN5195-248	AN5195-248	7
287	AN5195-249	AN5195-249	7
286	AN5195-250	AN5195-250	7
285	AN5195-251	AN5195-251	7
284	AN5195-252	AN5195-252	7
283	AN5195-253	AN5195-253	7
282	AN5195-254	AN5195-254	7
281	AN5195-255	AN5195-255	7
280	AN5195-256	AN5195-256	7
279	AN5195-257	AN51	

[illegible]

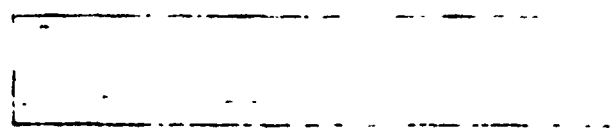
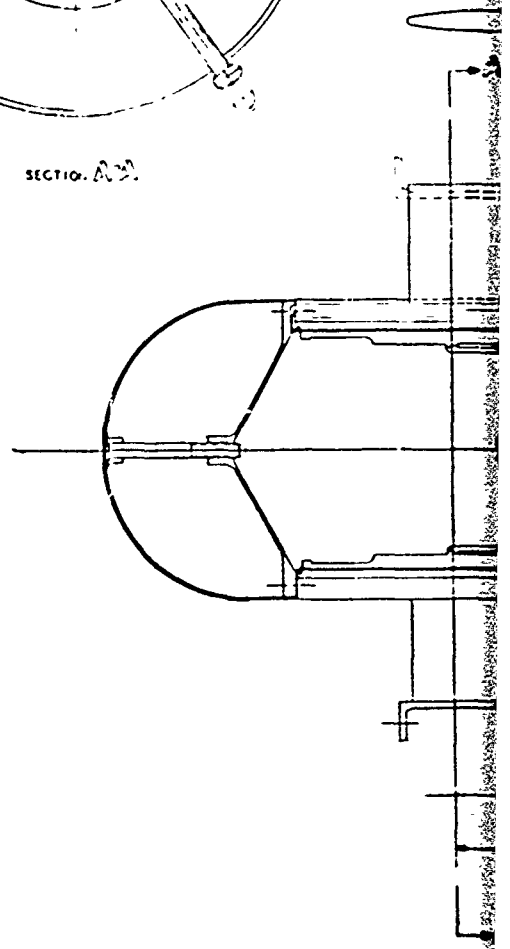
5

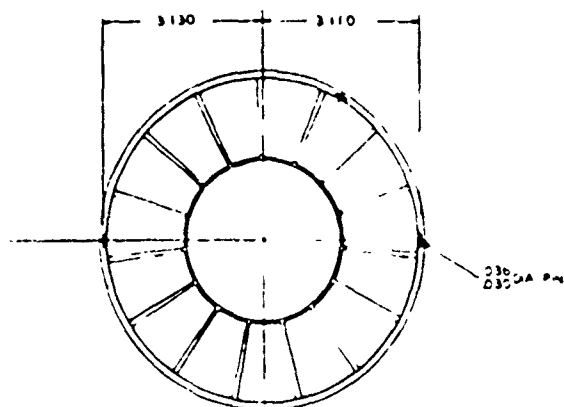
1

2



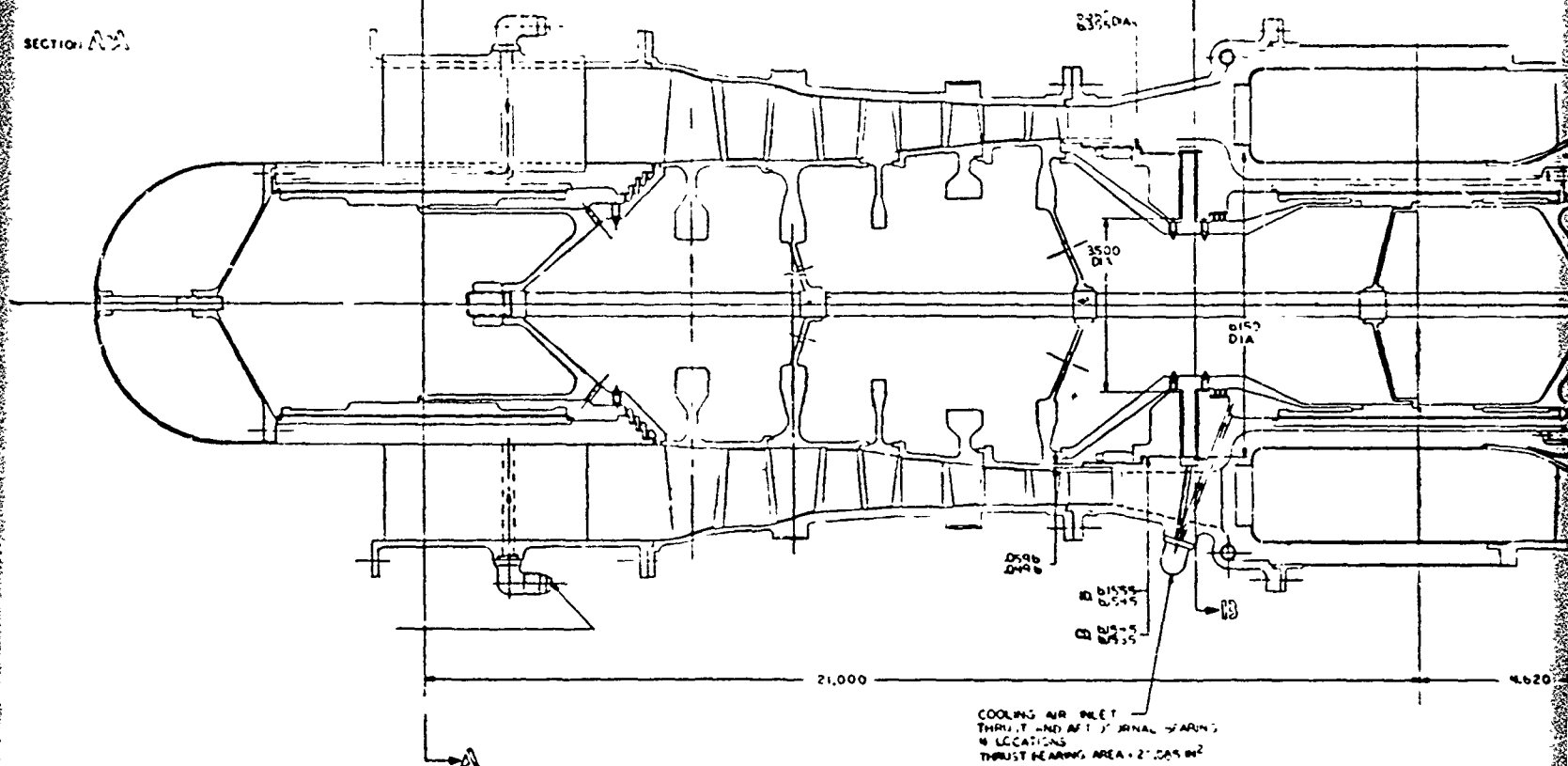
SECTION A-A





SECTION 5.3

8335 DA



COOLING AIR BLEET  
THRU. T AND A1 JOURNAL BEARING;  
4 LOCATIONS  
THRUST BEARING AREA = 2" DIA IN2





3

APPENDIX A

Scanning Electron Microscopy Photographs (14 Pages)

Table A-1. Coating Performance for Low Speed  
Wear Rig Tests (2 Pages)

PRECEDING PAGE BLANK - <sup>N</sup>FIL

AS-COATED



(A)

810X

HEAT TREATED (1200°F/260 HRS)



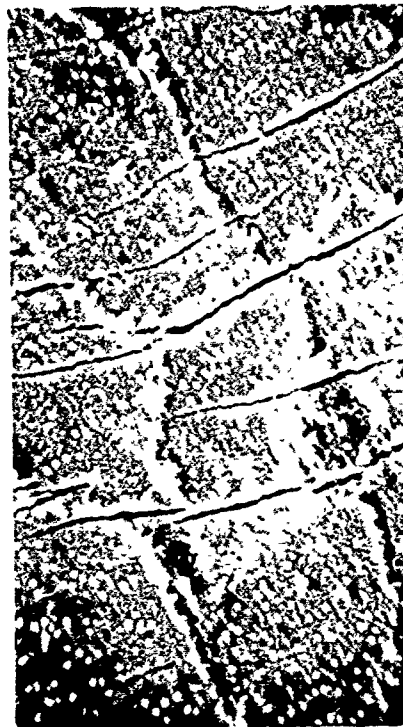
(C)

525X



(B)

4000X

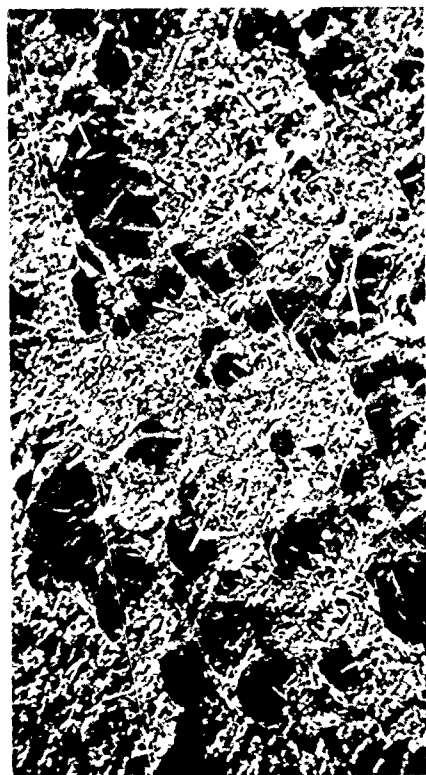


(D)

5200X

Figure A-1. Typical SEM Appearance of Surface of Kaman DES Coating on Inconel X-750 Foil After Bending About a 1/8-In. Diameter Mandrel (After Heat Treatment). Coating Thickness: 6.4 Microns.

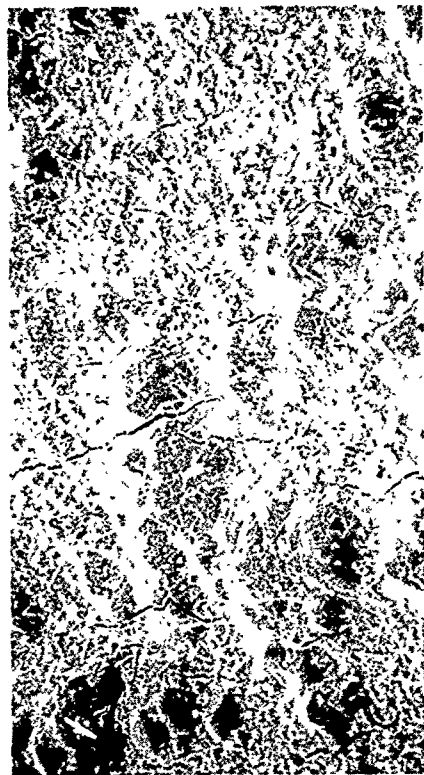
AS-COATED



(A)

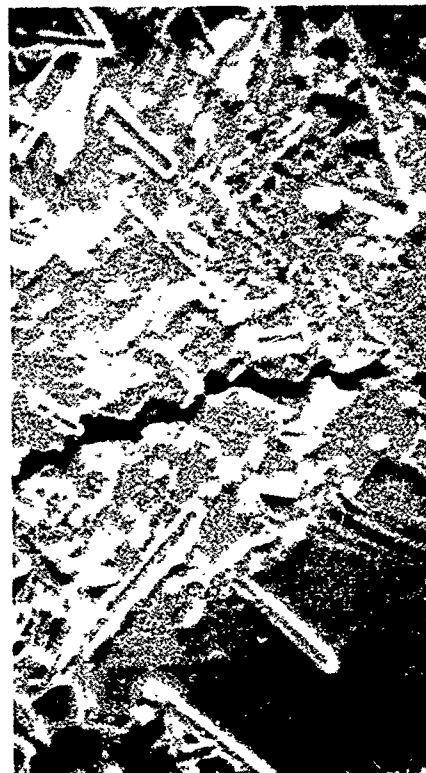
520X

HEAT TREATED (1200°F/260 HRS)



(C)

500X



(B)

5200X



(D)

5000X

Figure A-2. Typical SEM Appearance of Surface of (Ba,Ca)F<sub>2</sub> Coating on Inconel X-750 Foil After Bending About a 1/8-In. Diameter Mandrel (After Heat Treatment). Coating Thickness 20.3 Microns.

AS-COATED

HEAT TREATED (1200°F/260 HRS)



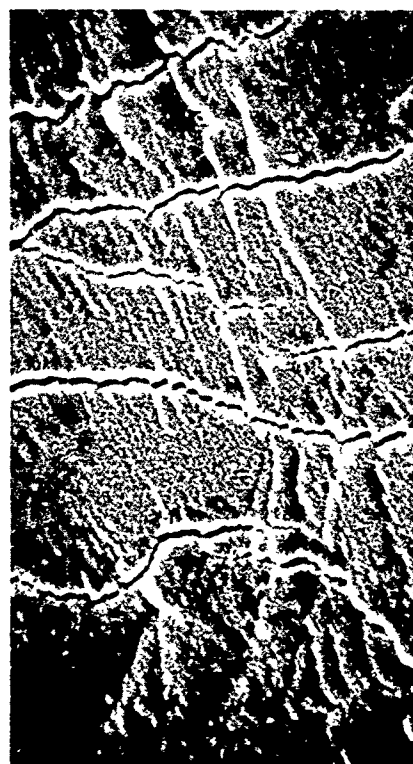
(A)

490X



(C)

180X



(B)

4900X

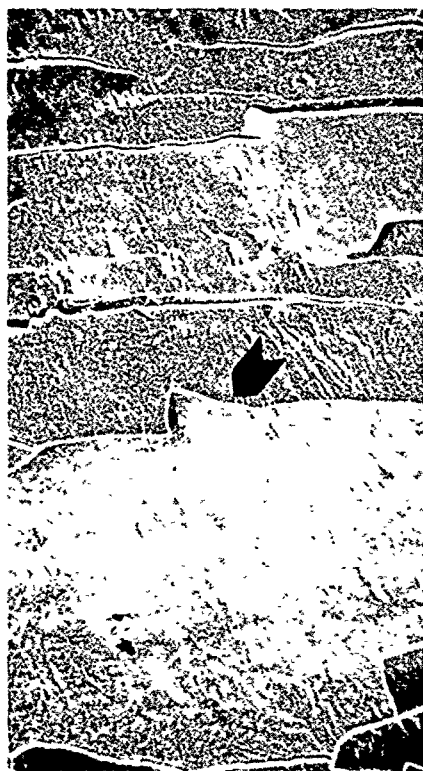


(D)

4600X

Figure A-3. Typical SEM Appearance of Surface of Sputtered Tribaloy-400 Coating on Inconel X-750 Foil After Bending About a 1/8-in. Diameter Mandrel (After Heat Treatment). Coating Thickness: 0.8 Micron.

AS-COATED



(A)

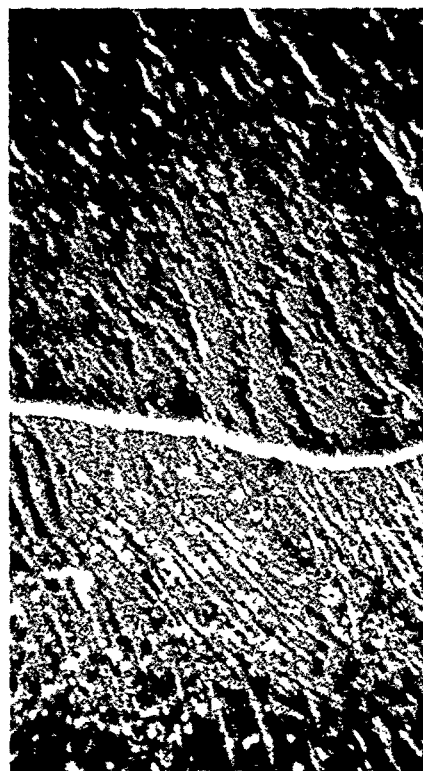
520X

HEAT TREATED (1200°F/260 HRS)



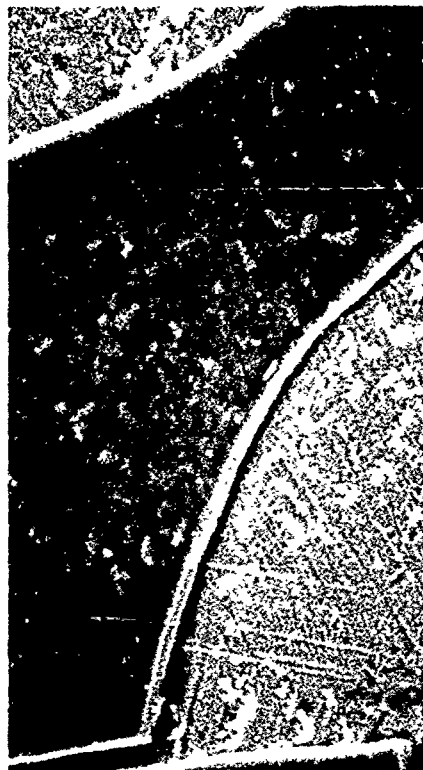
(C)

350X



(B)

5200X



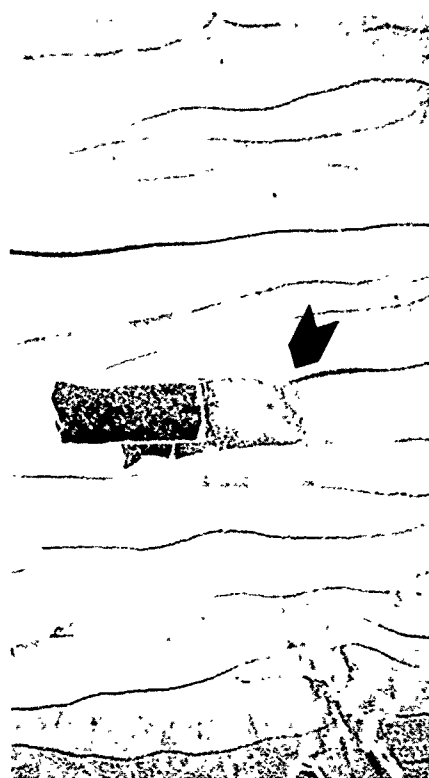
(D)

5200X

Figure A-4. Typical SEM Appearance of Surface of Sputtered TiB<sub>2</sub> Coating on Inconel X-750 Foil After Bending About a 1/8-In. Diameter Mandrel (After Heat Treatment). Coating Thickness: 1.0 Microns.

AS-COATED

HEAT TREATED (1200°F/260 HRS)



(A)

550X



(C)

350X



(B)

5500X



(D)

3500X

Figure A-5. Typical SEM Appearance of Surface of Sputtered Au Over Sputtered TiB<sub>2</sub> Coating on Inconel X-750 Foil After Bending About a 1/8-In. Diameter Mandrel (After Heat Treatment). Coating Thickness: 1.1 Microns.



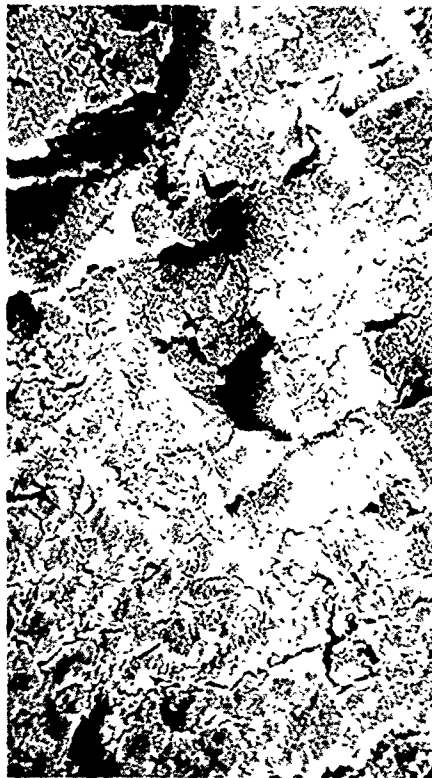
AS-COATED



(A)

720X

HEAT TREATED (1200°F/260 HRS)



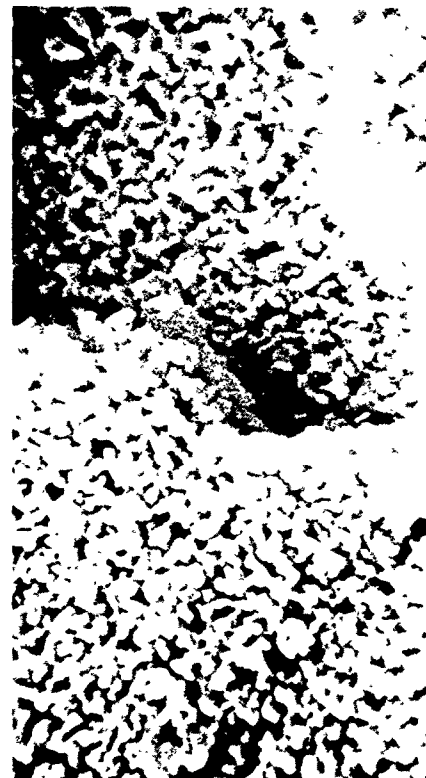
(C)

520X



(B)

3600X



(D)

5200X

Figure A-6. Typical SEM Appearance of Surface of Sputtered  $\text{CaF}_2$  Over Sputtered  $\text{TiB}_2$  Coating on Inconel X-750 Foil After Heat Treatment). Coating Thickness: 0.7 Micron.

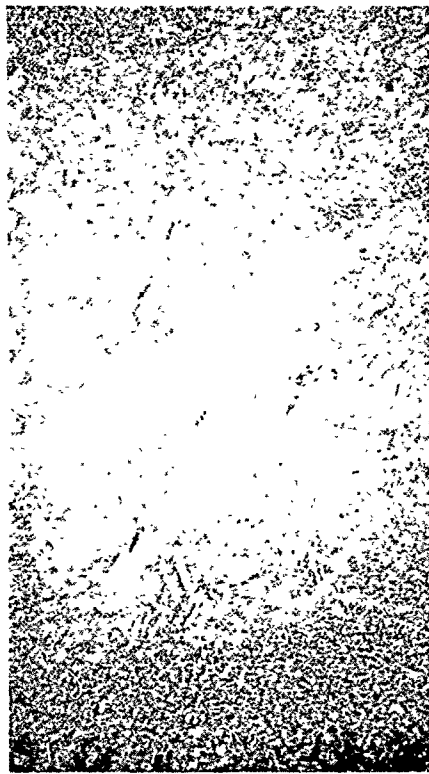
AS-COATED



(A)

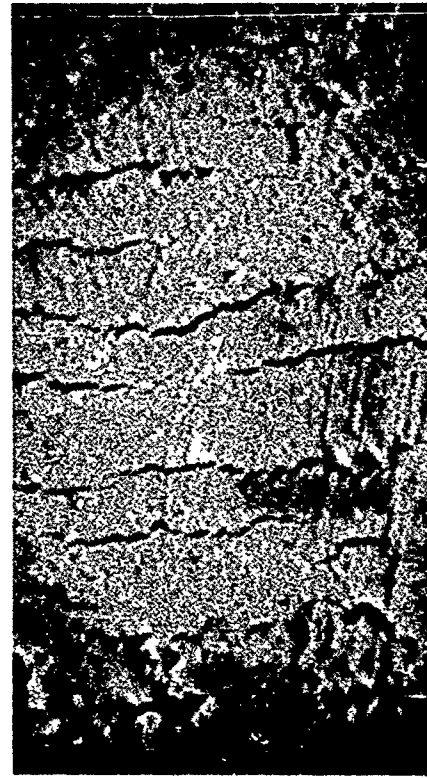
450X

HEAT TREATED (1200°F/260 HRS)



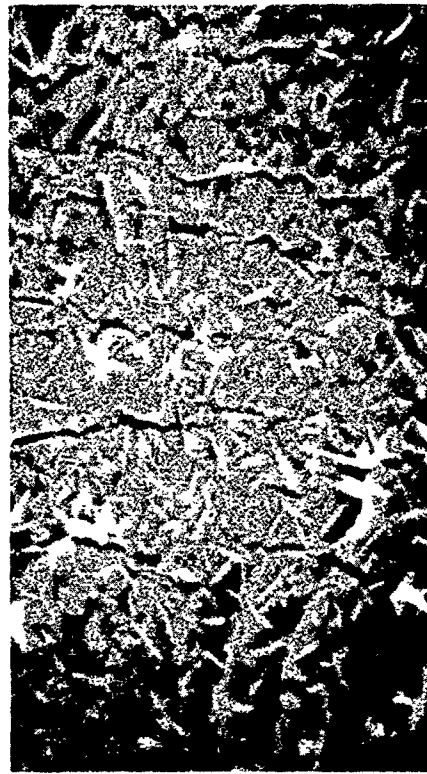
(C)

450X



(B)

4500X



(D)

4500X

Figure A-7. Typical SEM Appearance of Surface of Sputtered  $\text{Cr}_2\text{O}_3+\text{Al}_2\text{O}_3$  Coating on Inconel X-750 Foil After Bending About a 1/8-In. Diameter Mandrel (After Heat Treatment). Coating Thickness: 0.5 Micron.



AS-COATED



(A)

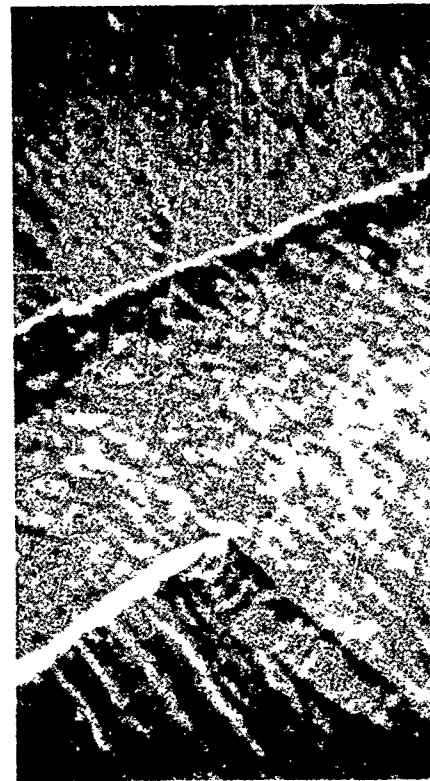
500X

HEAT TREATED (1200°F/260 HRS)



(C)

500X



(B)

4800X



(D)

5000X

Figure A-8. Typical SEM Appearance of Surface of Sputtered  $\text{Cr}_2\text{O}_3$  Coating on Inconel X-750 Foil After Bending About a 1/8-In. Diameter Mandrel (After Heat Treatment). Coating Thickness: 1.3 Microns.

AS-COATED



(A)

470X

HEAT TREATED (1200°F/260 HRS)



(C)

450X



(B)

470X



(D)

450X

Figure A-9. Typical SEM Appearance of Surface of Sputtered TiC Coating on Inconel X-750 Foil After Bending About a 1/8-In. Diameter Mandrel (After Heat Treatment). Coating Thickness: 0.8 Micron.

AS-COATED



(A)

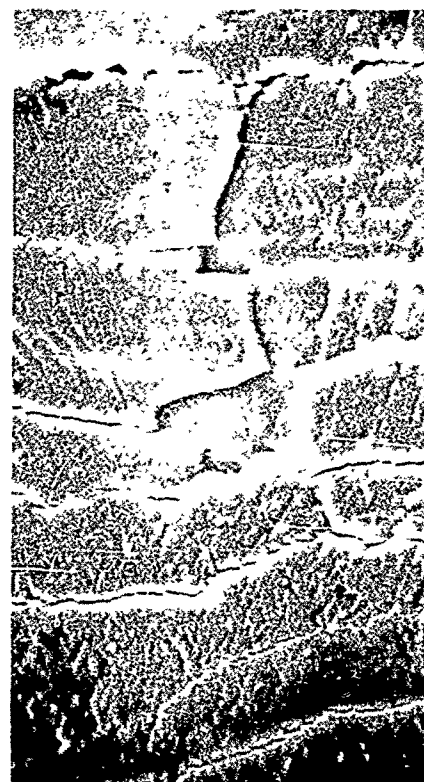
760X

HEAT TREATED (1200°F/260 HRS)



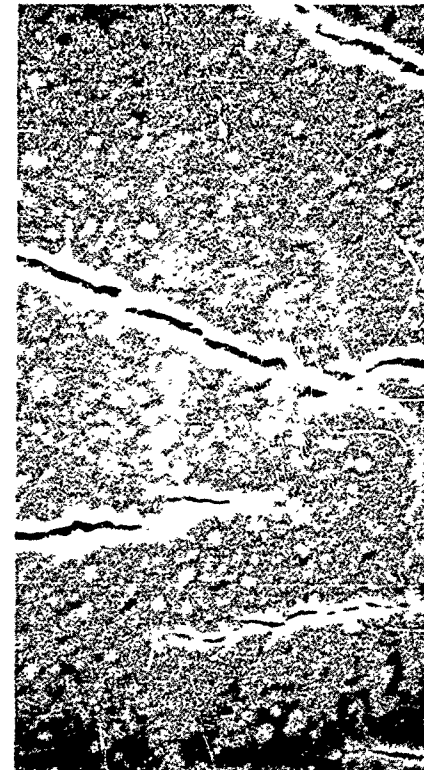
(C)

950X



(B)

3800X

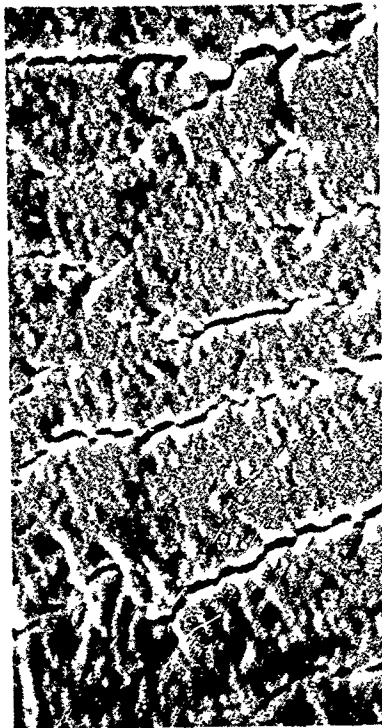


(D)

4700X

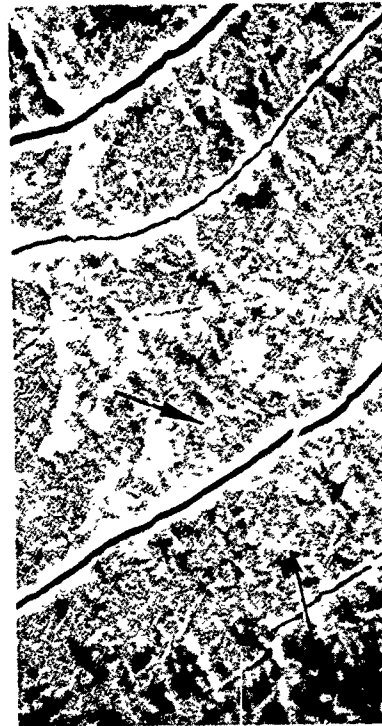
Figure A-10. Typical SEM Appearance of Surface of Sputtered B<sub>4</sub>C Coating on Inconel X-750 Foil After Bending About a 1/8-In. Diameter Mandrel (After Heat Treatment). Coating Thickness: 1.0 microns.

HEAT TREATED (1200°F/260 HRS)



4300X

(C)



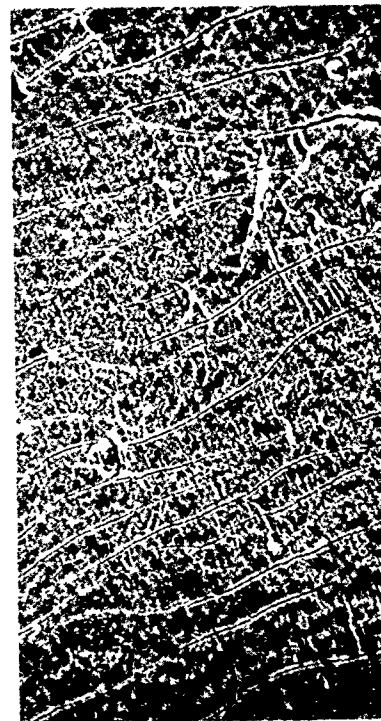
4500X

AS-COATED



860X

(A)



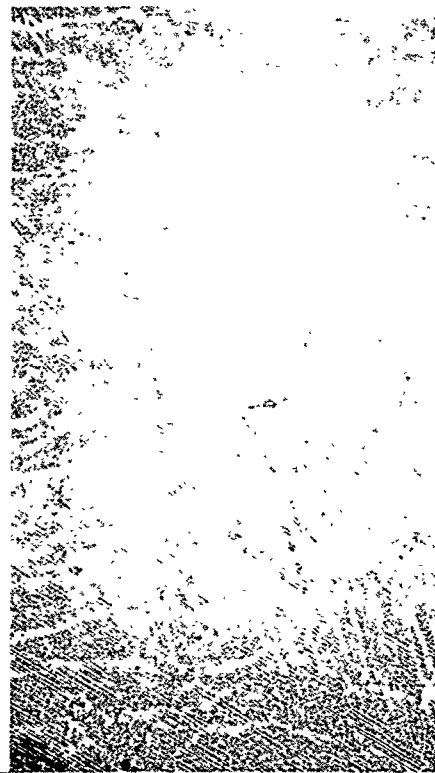
900X

(D)

Figure A-11. Typical SEM Appearances of Sputtered Coatings Which Have Been Deformed. As-Received Coating in (A) and (B) and the Same Coating After 1200°F/260-Hr Exposure in air (Deformed After Exposure). This Sample is Chromium Carbide Sputtered to Thickness of 1.5 Microns.



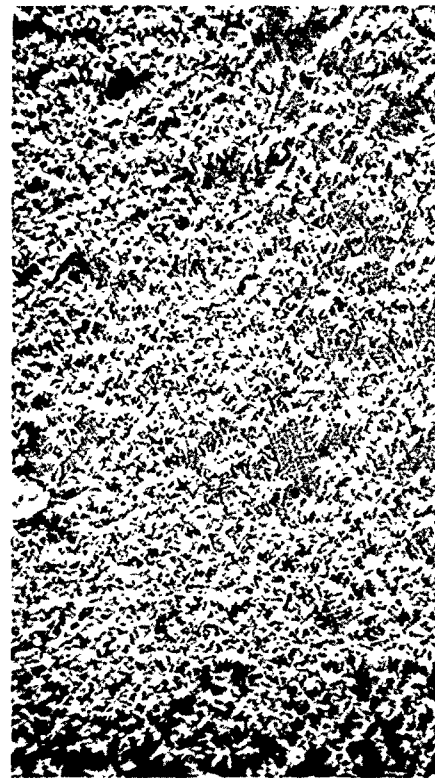
AS-COATED



(A)

1000X

HEAT TREATED (1200°F/260 HRS)



(C)

700X



(B)

5000X



(D)

3600X

Figure A-12. Typical SEM Appearance of Surface of Sputtered TiN Coating on Inconel X-750 Foil After Bending About a 1/8-In. Diameter Mandrel (After Heat Treatment). Coating Thickness: 1.0 Micron.

AS-COATED



(A)

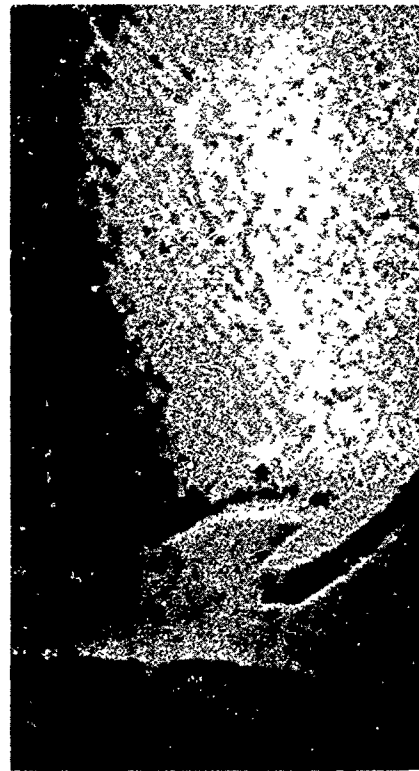
1000X

HEAT TREATED (1200°F/260 HRS)



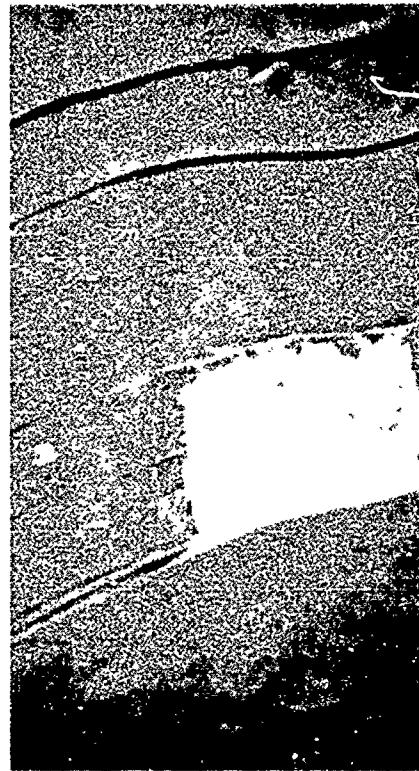
(B)

400X



(C)

5000X



(D)

4000X

Figure A-13. Typical SEM Appearance of Surface of Sputtered  $\text{Si}_3\text{N}_4$  Coating on Inconel X-750 Foil After Bending About a 1/8-In. Diameter Mandrel (After Heat Treatment). Coating Thickness: 1.2 Microns.

AS-COATED



(A)

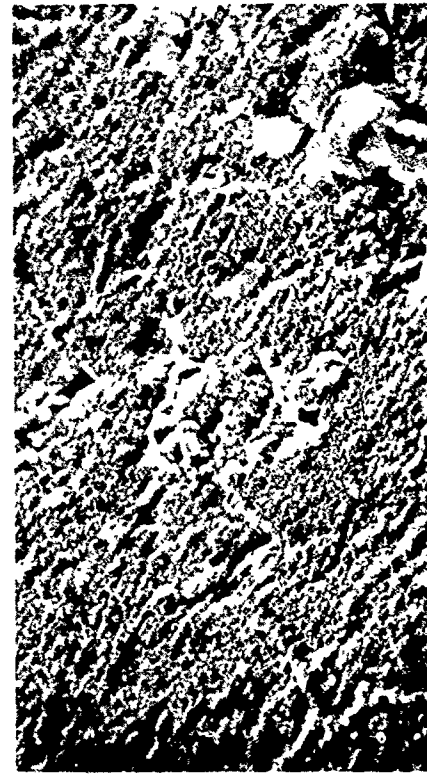
410X

HEAT TREATED (1200°F/260 HRS)



(C)

800X



(B)

4100X



(D)

4100X

Figure A-14. Typical SEM Appearance of Surface of Inconel X-750 Foil After Bending About a 1/8-In. Diameter Mandrel (After Heat Treatment).

TABLE A-1. COATING PERFORMANCE FOR LOW SPEED WEAR RIG TESTS

TEST NO.	DATE	SHAFT COATING	FOIL COATING	ROOM TEMP.		BEARING TORQUE AT 157 RPM (IN.-LBS) *											
				AT START	AT END	400°F		800°F		1000°F		1080°F		1200°F			
						AT START	AT END	AT START	AT END	AT START	AT END	AT START	AT END	AT START	AT END		
1	6-10-75	HS-25 (Oxidized)	Teflon-S	13.0	15	11	14	--	--	--	--	--	--	--	--		
2a**	6-23-75	NiCo (Oxidized)	Teflon-S	10	18	--	--	--	--	--	--	--	--	--	--		
2b	6-23-75	NiCo (Oxidized)	Teflon-S	13	15	6	5	--	--	--	--	--	--	--	--		
2c	8-4-75	NiCo (Not oxidized)	Teflon-S	11	14	3	9	--	--	--	--	--	--	--	--		
2d	10-21-75	NiCo (Oxidized)	Teflon-S	7	14	4	4	--	--	--	--	--	--	--	--		
3a	8-25-75	Tribaloy 400	Teflon-S	70	--	--	--	--	--	--	--	--	--	--	--		
3b	10-23-75	Tribaloy 400 (Oxidized)	Teflon-S	14	19	6	7	--	--	--	--	--	--	--	--		
4a	10-17-75	UCAR LW-5	Teflon-S	28	46	--	--	--	--	--	--	--	--	--	--		
5	10-31-75	Tribaloy 400 (Oxidized)	HS-25	8	13	9	27	--	--	--	--	--	--	--	--		
6	11-5-75	Tribaloy 400 (Oxidized)	Kaman DES (Cr <sub>2</sub> O <sub>3</sub> )	11	25***	--	--	--	--	--	--	--	--	--	--		
7	11-12-75	LW-5, Gold Plated	Teflon-S	27	38	21	20	--	--	--	--	--	--	--	--		
8	11-25-75	Kaman SCA	Teflon-S	18	25	17	14	--	--	--	--	--	--	--	--		
9	12-1-75	NiCo (Oxidized)	Teflon-S	30	21	25	11	--	--	--	--	--	--	--	--		
10	1-7-76	NiCo (Oxidized)	TiB <sub>2</sub> (Sputtered)	6	9	5	15	23	21(2)	18	18(2)	--	--	--	--		
11	1-14-76	Kaman SCA	HS-25 (Oxidized)	13	13	14	32(1)	60	60(1)	16	15(5)	13	13(1)	--	--		
12	1-30-76	Kaman SCA	Kaman DES	12	15(1)	6	7(1)	12	11(1)	9	10(1)	--	--	--	--		
13	3-9-76	Kaman SCA	Kaman DES	11	16	--	--	--	--	13	12	8	8	--	--		
14a	3-24-76	NiCo (Oxidized)	Nat'l Proc. Ind. (Ba,Ca)F <sub>2</sub>	16	50	--	--	--	--	--	--	--	--	--	--		
14b**	3-25-76	NiCo (Oxidized)	Nat'l Proc. Ind. (Ba,Ca)F <sub>2</sub> ***	9	15	5	4	40 @ >540°F	--	--	--	--	--	--	--		
15	3-29-76	NiCo (Oxidized)	NASA (Ba,Ca)F <sub>2</sub> + CaSiO <sub>3</sub> +CaO	9	10	5	7	90	115(3)	37	125(1)	--	--	--	--		



TABLE A-1. (CONTD)

TEST NO.	DATE	SHAFT COATING	FOIL COATING	ROOM TEMP.				400°F				800°F				1000°F				1080°F			
				AT	START	END	AT	START	END	AT	START	END	AT	START	END	AT	START	END	AT	START	END	AT	END
16	4-1-76	Kaman SCA	NPI	12	53(9)	15	26(3)	2	>600°F	>70	--	--	--	--	--	--	--	--	--	--	--	--	--
17	4-5-76	Kaman SCA	Kaman DLS	32	52(1)	39	49(2)	22	28(6)	--	--	--	--	--	--	--	--	--	--	--	--	--	--
18	4-7-76	Kaman SCA	Kaman DLS	12	10	4.5	15	--	--	--	--	--	--	--	--	--	--	--	--	--	--	--	--
21	4-21-76	Kaman SCA	NPI	19	26(6)	--	--	--	--	--	--	--	--	--	--	--	--	--	--	--	--	--	--
22	4-21-76	Kaman SCA	NPI	19	22(0.1)	--	--	--	--	--	--	--	--	--	--	--	--	--	--	--	--	--	--
23	4-22-76	Kaman SCA (New coating)	NPI	24	26(1)	--	--	--	--	--	--	--	--	--	--	--	--	--	--	--	--	--	--
24	4-30-76	NiCo (Oxidized)	TiB <sub>2</sub> plus Au overcoat (Sputtered)	7	31	18	29(5)	24	44(2)	--	--	--	--	--	--	--	--	--	--	--	--	--	--
25	5-5-76	Tribaloy-400 (Oxidized)	Cr <sub>2</sub> O <sub>3</sub> (Sputtered)	9	47(3.5)	--	--	--	--	--	--	--	--	--	--	--	--	--	--	--	--	--	--
26	5-11-76	Tribaloy-400 (Oxidized)	Teflon-S	18	27(9.5)	--	--	--	--	--	--	--	--	--	--	--	--	--	--	--	--	--	--
27	6-3-76	Tribaloy-400 (Oxidized)	B <sub>4</sub> C (Sputtered)	14	14(0.2)	8	9(0.2)	31	--	--	29	--	--	--	--	--	--	--	--	--	--	--	--
28	6-8-76	Tribaloy-400 (Oxidized)	Cr <sub>2</sub> O <sub>3</sub> /Au Opp. side(Sputtered)	9	8.5(0.2)	5.5	8(0.2)	24	--	--	14	13.5(0.1)	--	--	--	--	--	--	--	--	--	--	--
29	6-11-76	Kaman SCA	Cr <sub>2</sub> O <sub>3</sub> /Au Opp. side(Sputtered)	13.5	15(0.2)	8	8(0.2)	31	42(0.2)	23	24(0.2)	--	--	--	--	--	--	--	--	--	--	--	--
30	6-15-76	Kaman SCA	Tribaloy-400 (Sput.-not ox.)	16	29(0.1)	25	--	50	--	--	31	--	--	--	--	--	--	--	--	--	--	--	--
31	6-17-76	Kaman SCA	NiCo	Est. 90	--	--	(Foil too thick, insufficient sway space)																
32	6-18-76	Kaman SCA	Kaman DLS (Group 2-new)	20	30(0.2)	8	--	16	25(0.2)	13	14(0.2)	--	--	--	--	--	--	--	--	--	--	--	--
33	6-23-76	Kaman SCA	Teflon-S (Old)	Est. 16	--	--	--	--	--	--	--	--	--	--	--	--	--	--	--	--	--	--	--
35	7-2-76	Tribaloy-400 (Oxidized)	TiC (Sputtered)	16	13(0.2)	6.3	--	24	--	--	16	16.5(0.3)	--	--	--	--	--	--	--	--	--	--	--
36	7-7-76	Tribaloy-400 (Oxidized)	Cr <sub>2</sub> O <sub>3</sub> (Sputtered)	6	--	8	--	23	--	--	200 (seized)	--	--	--	--	--	--	--	--	--	--	--	--
37	7-16-76	NiCo (Oxidized)	Cr <sub>2</sub> O <sub>3</sub> +Al <sub>2</sub> O <sub>3</sub>	10	.2(0.2)	12	--	21	--	--	20	16.5(0.2)	--	--	--	--	--	--	--	--	--	--	--

\*Materials wear rig testing: 2-in. diameter coated shaft, 0.006-in. thick coated foils (Haynes-25 foils are 0.004-in. thick) 1-lb/in.<sup>2</sup> load, constant contact. Run time if not 10-minutes is indicated in parentheses next to the torque value in the AT END columns.

\*\*Load cell failure which terminated torque measurement capability

\*\*\*Torque after 3-minutes; torque continued to rise and test terminated.

\*\*\*\*Bearings 1 and 4 replaced with Kaman DLS coated foils to reduce torque. Center bearings 2 and 3 replaced with best of the (Ba,Ca)F<sub>2</sub> coated foils for a re-run.

APPENDIX B

Table B-1. Thrust Bearing Configurations Tested (1 Page)

Table B-2. Journal Bearing Configurations Tested (1 Page)

Thrust Bearing Test Configuration Sheets (37 Pages)

Journal Bearing Test Configuration Sheets (30 Pages)

*Preceding Page BLANK*

TABLE B-1

## THRUST BEARING CONFIGURATIONS TESTED

CONFIG. NO.	NUMBER OF FOILS	FOIL THICKNESS	FOIL COATING	PREFORM RADIUS	CALC. SWAY SPACE	TEST COMMENTS
0	8	0.010	OBD 26-20	3.0	0.016	Turbine bearing failure at 20K rpm
00						Bearing instability noted
1			OBD 26-20			Rebalance, turbine bearing failure decel. from 26.5K rpm
2			OBD 26-5			Rebalance, turbine bearing failure at 32.5K rpm
3	8		OBD 26-5		0.016	Trim balance at 22.3K rpm, bearing, instability
4	6	0.010	OBD 26-20		0.021	Bearing instability
5		0.012			0.013	Test bearing failure at 21K rpm
6		0.010			0.019	Trim balance at 25K rpm, bearing instability
7		0.010			0.019	Test bearing weight added, bearing instability
8	6	0.012	OBD 26-20	3.0	0.021	Multiplane balance, turbine bearing failure at 30K rpm
9	8 (L/D=1)	0.012	OBD 26-5	3.4	0.023	Electroless nickel shaft coating failure at 21K rpm
10	8 (L/D=1)	0.010	Teflon-S	3.0	0.023	Strain-gaged foil. No flutter detected
11	12	0.012		2.9		Excursions OK to 30K rpm
12						Sway space mod., 30.9K rpm
13						CO <sub>2</sub> bearing film media; 19K rpm
14						Hot air bearing film media; 30K rpm
15						Helium bearing film media; 26.7K rpm
16						Turbine clearance incr. 28.5K rpm
17						Mid-plane probe shows shaft bending
18					0.023	2 additional probe planes confirm bending
19					0.029	First run with short shaft, high subsynch.
20					0.022	Decreased sway space, run to 34K rpm
21						Special carrier I.D. profile to incr. actual sway space
22						Multi-plane-speed balance
23				2.9	0.022	6.5 psi load, failure at 33K rpm
24				3.1	0.026	4.8 psi load, instability at 28K rpm
25					0.026	46.3% overlap, incr. instability
26	12				0.022	46.3% overlap, 5.44 psi at 23K rpm, turbine bearing failure
27	10		Teflon-S	3.1	0.024	Backward precession at 22K rpm
28	10		Kaman DES	3.2	0.028	500°f air in to 20K rpm, 50 starts and stops, altitude test attempt with rig failure
29	12		NiCo	3.1	0.024	Rebuild checkout run OK to 25K rpm
30	12	0.012	NiCo	3.1	0.024	Dynamic simulation; 21K rpm failure

TABLE B-2

## JOURNAL BEARING CONFIGURATIONS TESTED

CONFIG. NO.	FOIL MATERIAL	FOIL COATING	FOIL THICKNESS	STIFFENER THICKNESS	SPRING ASSEMBLY CONFIGURATION	TEST AT LOAD LIMIT	REMARKS
1	INCO X-750	Teflon-S	0.006	0.012	Baseline		175 lb
2					0.007 tapered baseline		200 lb
3					0.004 tapered baseline		300 lb
4				0.012	Dual spring	Yes	200 lb, failure
5				0.010	0.001 tapered dual spring		Thrust runner rub
6		Teflon-S		0.010	0.001 tapered dual spring 2/3 leading edge spring		Thrust runner rub
7		OBD-26		0.012	Same as 6		Continue failure
8		Teflon-S			Baseline		R1, seal failure, 220 lb
9					Baseline with 0.012 PS stiffener		224 lb
10					Dual spring		195 lb
11					Same as 9	Yes	No lift-off, failure
12				0.012	Same as 9		197 lb
13		Teflon-S		0.010	Same as 9		540 lb
14		MoS <sub>2</sub>			Same as 9		Rig bearing failure
15		MoS <sub>2</sub>			INCO 718 wide spring PS stiffener	yes	40 lb, failure
16		Teflon-S			Baseline spring PS stiffener		208 lb
17		Teflon-S		0.010	INCO 718 wide spring PS stiffener	yes	162 lb, failure
18		MoS <sub>2</sub>		0.012	Baseline spring PS stiffener		97 lb, coat worn out
19		Teflon-S		0.010	Baseline spring PS stiffener		200 lb
20					Baseline spring PS stiffener	Yes	342 lb
21		Teflon-S			2.2° Rot. Baseline spring PS stiffener	Yes	441 lb
22		MoS <sub>2</sub>			Baseline spring PS stiffener	yes	180 lb, failure
23		Kaman DES			Baseline spring PS stiffener		Low speed test coating worn through
24		Teflon-S	0.006		Baseline spring Rect. stiffener	yes	225 lb
25			0.0085		Baseline spring PS stiffener	yes	324 lb
26			0.006		Baseline spring Rect. stiffener		Thrust runner failure
27					Baseline spring Rect. stiffener	Yes	397.2 lb
28	INCO X-750				2.2° Rot. Baseline spring Rect. stiffener	yes	156.4 lb failure
29	BeCu	Teflon-S			PS stiffener Baseline spring	Yes	469.5 lb
30	INCO X-750	Kaman DES			Baseline spring Rect. stiffener 2.2° Rot.		500°F at 200 lb
31	BeCu	Teflon-S		0.010	Baseline spring Rect. stiffener 2.2° Rot.		Misalignment, 200 lb
32	INCO X-750	NiCo		0.012	Baseline spring Rect. stiffener 2.2° Rot.		Dyn. loading, coating failure
33	BeCu	Teflon-S	0.006	0.010	Baseline spring Rect. stiffener 2.2° Rot.	yes	Dyn. loading, 152 lb failure

Note. PS = Partial Segment

DATE 13 MAR 75  
PREPARED BY W. KOLMSE  
CHECKED BY \_\_\_\_\_

CALC NO \_\_\_\_\_  
MODEL \_\_\_\_\_  
PART NO. \_\_\_\_\_

THRUST BEARING TEST CONFIGURATION N° 1

FOIL: ASSY P/N SK40423-2  
NUMBER 13  
THICKNESS .006  
COATING TEFLON S  
BASE THKNESS .010  
SPECIAL CONFIG. ~

STIFFENER: P/N SK40421-2  
THICKNESS .012  
SPEC. CONF. ~

SPRING ASSY: P/N SK40422-2  
BASE THKNESS .012  
SPEC. CONFIG. ~

BREAK-AWAY TORQUE: TOTAL RIG 35 in. lbs.  
TEST BRG. \_\_\_\_\_ in. lbs.

RUNNING TORQUE: AT 33 Krpm, 200 lbs 3.48 in. lbs.  
AT 33 Krpm, max load 3.55 in. lbs.

MAX. LOAD 275 lbs.  
MAX. SPEED 33,200 lbs.  
LIFT-OFF SPEED \_\_\_\_\_ rpm  
TOUCH DOWN SPEED \_\_\_\_\_ rpm

DATA POINT N° 0 TO 15

REMARKS: BASELINE BEARING CONFIGURATION

*Preceding Page BLANK - F*

DATE 4 APR 75  
PREPARED BY W F KOEPEL  
CHECKED BY \_\_\_\_\_

CALC. NO. \_\_\_\_\_  
MODEL \_\_\_\_\_  
PART NO. \_\_\_\_\_

**THRUST BEARING TEST CONFIGURATION N° 2**

FOIL: ASS'Y P/N SK40423-2  
NUMBER 13  
THICKNESS .006  
COATING TEFLON 5  
BASE THKNESS .010  
SPECIAL CONFIG. ~

STIFFENER: P/N SK40421-2  
THICKNESS .012  
SPEC. CONF. ~

SPRING ASS'Y : P/N SK40422-2  
BASE THKNES .012  
SPEC. CONFIG. .007 thicker at O.D than I.D.

BREAK-AWAY TORQUE : TOTAL RIG 30 in. lbs.  
TEST BRG. \_\_\_\_\_ in. lbs.

RUNNING TORQUE : AT 33 Krpm, 200 lbs 3.3 in. lbs.  
AT 33 Krpm, max load 3.3 in. lbs.

MAX. LOAD 200 lbs.  
MAX. SPEED 33,000 lbs.  
LIFT-OFF SPEED \_\_\_\_\_ rpm  
TOUCH DOWN SPEED \_\_\_\_\_ rpm

DATA POINT N° 16 THRU 19

REMARKS:

REPORT

PAGE 1 OF 1

AIRESEARCH MANUFACTURING COMPANY

DATE 7 MAY 75  
 PREPARED BY W F KOERSEL  
 CHECKED BY \_\_\_\_\_

CALC. NO. \_\_\_\_\_  
 MODEL \_\_\_\_\_  
 PART NO. \_\_\_\_\_

**THRUST BEARING TEST CONFIGURATION N° 3**

FOIL: Ass'y P/N SK40423-2  
 NUMBER 13  
 THICKNESS .006  
 COATING TEFLON S  
 BASE THKNESS .010  
 SPECIAL CONFIG. ~

STIFFENER: P/N SK40421-2  
 THICKNESS .012  
 SPEC. CONF. ~

SPRING ASSY: P/N SK40422-2  
 BASE THKNES .012  
 SPEC. CONFIG. .004 Δh f(r)

BREAK-AWAY TORQUE: TOTAL RIG 32 in. lbs.  
 TEST BRG. \_\_\_\_\_ in. lbs.

RUNNING TORQUE: AT 33 Krpm, 200 lbs ~ in. lbs.  
 AT 33 Krpm, max load 3.99 in. lbs.

MAX. LOAD 300 lbs.  
 MAX. SPEED 33,000 lbs.  
 LIFT-OFF SPEED \_\_\_\_\_ rpm  
 TOUCH DOWN SPEED \_\_\_\_\_ rpm

DATA POINT N° 20421

REMARKS:

AIRESEARCH MANUFACTURING COMPANY

DATE 7 MAY 75  
 PREPARED BY M. F. Kuepfer  
 CHECKED BY \_\_\_\_\_

CALC. NO. \_\_\_\_\_  
 MODEL \_\_\_\_\_  
 PART NO. \_\_\_\_\_

THRUST BEARING TEST CONFIGURATION N° 4

FOIL: Ass'y P/N SK40423-2  
 NUMBER 13  
 THICKNESS .006  
 COATING TEFLON F  
 BASE THKNESS .010  
 SPECIAL CONFIG. ~

STIFFENER: P/N SK40422-2  
 THICKNESS .012  
 SPEC. CONF. ~

SPRING ASS'Y: P/N 3604730-1  
 BASE THKNESS .012  
 SPEC. CONFIG. 2 SPRINGS PER FOIL

BREAK-AWAY TORQUE: TOTAL RIG 32 in. lbs.  
 TEST BRG. \_\_\_\_\_ in. lbs.

RUNNING TORQUE: AT 33 Krpm, 200 lbs N/A in. lbs.  
 AT 33 Krpm, max load N/A in. lbs.

MAX. LOAD 200 lbs.  
 MAX. SPEED 33,000 lbs.  
 LIFT-OFF SPEED \_\_\_\_\_ rpm  
 TOUCH DOWN SPEED \_\_\_\_\_ rpm

DATA POINT N° 22, 23, 24

REMARKS: FIRST ATTEMPT AT DUAL SPRING CONFIG.  
 BEARING MELTED AS 200 lb LOAD WAS ACHIEVED.  
 CAUSE OF FAILURE WAS THE LEADING EDGE  
 SPRING HAVING BEEN HIGHER THAN TRAILING SPRING  
 SINCE NO ATTEMPT WAS MADE TO CONTROL IT

REPORT  
 PAGE 1 OF 1



DATE 28 Jul 75  
PREPARED BY W.F. Noel 1361  
CHECKED BY \_\_\_\_\_

CALC. NO. \_\_\_\_\_  
MODEL \_\_\_\_\_  
PART NO. \_\_\_\_\_

THRUST BEARING TEST CONFIGURATION N° 5

FOIL: Ass'y P/N SK40423-7  
NUMBER 13  
THICKNESS .006  
COATING TERWU 5  
BASE THKNESS .010  
SPECIAL CONFIG. THERMOCOUPLES WELDED ON BACK OF FOILS (2)

STIFFENER: P/N SK40421-1  
THICKNESS .010  
SPEC. CONF. ~

SPRING ASSY: P/N 3604730- MP  
BASE THKNES .012  
SPEC. CONFIG. .008/.012 .001 SH PER 1 AWING

BREAK-AWAY TORQUE: TOTAL RIG 33 in. lbs.  
TEST BRG. 17.4 in. lbs.

RUNNING TORQUE: AT 33 Krpm, 200 lbs \_\_\_\_\_ in. lbs.  
AT 33 Krpm, max load \_\_\_\_\_ in. lbs.

MAX. LOAD \_\_\_\_\_ lbs.  
MAX. SPEED \_\_\_\_\_ lbs.  
LIFT-OFF SPEED 15,000 rpm  
TOUCH DOWN SPEED 7,000 rpm

DATA POINT N° \_\_\_\_\_

REMARKS: ROB AT T/C WIELD

AIRESEARCH MANUFACTURING COMPANY

DATE 7/31/75  
 PREPARED BY 1210016  
 CHECKED BY \_\_\_\_\_

CALC. NO. \_\_\_\_\_  
 MODEL \_\_\_\_\_  
 PART NO. \_\_\_\_\_

THRUST BEARING TEST CONFIGURATION N° 6

FOIL: Ass'y P/N SK40423-2  
 NUMBER 12  
 THICKNESS .006  
 COATING TEFLON S  
 BASE THKNESS .010  
 SPECIAL CONFIG. TC on back of foil plate - removed lower  
tab of higher R spring

STIFFENER: P/N SK40421-1  
 THICKNESS .010  
 SPEC. CONF. S

SPRING ASSY: P/N 3604730 - Mod 1  
 BASE THKNES .012  
 SPEC. CONFIG. .008/.012 .001 in per lapping

BREAK-AWAY TORQUE: TOTAL RIG 30.0 in. lbs.  
 TEST BRG. 17.3 in. lbs.

RUNNING TORQUE: AT 33 Krpm, 200 lbs \_\_\_\_\_ in. lbs.  
 AT 33 Krpm, max load \_\_\_\_\_ in. lbs.

MAX. LOAD \_\_\_\_\_ lbs.  
 MAX. SPEED \_\_\_\_\_ lbs.  
 LIFT-OFF SPEED 15,000 rpm  
 TOUCH DOWN SPEED 6,000 rpm

DATA POINT N° \_\_\_\_\_

REMARKS:

ROB AT 1/C WELD

REPORT

PAGE 1 OF

DATE 15-1-55  
 PREPARED BY W. F. [unclear]  
 CHECKED BY [unclear]

CALC NO. [unclear]  
 MODEL [unclear]  
 PART NO. [unclear]

# THRUST BEARING TEST CONFIGURATION N° 7

FOIL: ASSY P/N SK40423-2  
 NUMBER 13  
 THICKNESS .006  
 COATING OPD 26  
 BASE THKNESS .010  
 SPECIAL CONFIG. ~

STIFFENER: P/N SK40421-2  
 THICKNESS .012  
 SPEC. CONF. T/C AT SPRING &

SPRING ASSY: P/N 3604730-M00 2  
 BASE THKNES .012  
 SPEC. CONFIG. INNER THIRD OF LEAF'S TENDS  
 BROKEN OFF

BREAK-AWAY TORQUE: TOTAL RIG 40 in. lbs.  
 TEST BRG. 20 in. lbs.

RUNNING TORQUE: AT 33 Krpm, 200 lbs [unclear] in. lbs.  
 AT 33 Krpm, max load [unclear] in. lbs.

MAX. LOAD 11.5 lbs.  
 MAX. SPEED 21,000 lbs.  
 LIFT-OFF SPEED 20,000 rpm  
 TOUCH DOWN SPEED 8,000 rpm

DATA POINT N° 12

REMARKS: COATING RUBBED AND TENDS TO BRUISE during  
 lift + start.

DATE 18 Sep 15  
 PREPARED BY J. Koepf  
 CHECKED BY \_\_\_\_\_

CALC NO \_\_\_\_\_  
 MODEL \_\_\_\_\_  
 PART NO. \_\_\_\_\_

# THRUST BEARING TEST CONFIGURATION N° 8

FOIL: ASSY P/N SK40423-2  
 NUMBER 13  
 THICKNESS .006  
 COATING TEFLON  
 BASE THKNESS .010  
 SPECIAL CONFIG. ~

STIFFENER: P/N SK40421-2  
 THICKNESS .012  
 SPEC. CONF. ~

SPRING ASSY: P/N SK40422-2  
 BASE THKNESS .012  
 SPEC. CONFIG. ~

New TECHNIQUE  
 2004 5" Hc Thrust Aeron

BREAK-AWAY TORQUE: TOTAL RIG 40/20 in. lbs.  
 TEST BRG. 10.2 in. lbs.

RUNNING TORQUE: AT 33 Krpm, 200 lbs \_\_\_\_\_ in. lbs.  
 AT 33 Krpm, max load \_\_\_\_\_ in. lbs.

MAX. LOAD \_\_\_\_\_ lbs.  
 MAX. SPEED \_\_\_\_\_ lbs.  
 LIFT-OFF SPEED 10,000 rpm  
 TOUCH DOWN SPEED 2,000 rpm

DATA POINT N° \_\_\_\_\_

REMARKS: A. TEFLON SHEARED DURING FIRST START WHICH WAS IMMEDIATELY FOLLOWED BY A STOPPER LIFT-OFF. THE SAME HAPPENED IN CONF #7. THIS PRACTICE WILL BE STOPPED.

B. THE HYDROSTATIC SEAL KUBBLD REQUIRING REWORK OF SEAL

C (30 Sep 75) ADDED 1 LINE SPRING TO SEAL PLATE AND PUT 5 SMALL HOLES ON RIM FOR SPEED SIGNAL AT BEVEL PROBE.

REPORT

PAGE 1 OF

AIRESEARCH MANUFACTURING COMPANY

DATE Oct 8 1975  
 PREPARED BY S. M. N. W.  
 CHECKED BY \_\_\_\_\_

CALC. NO. \_\_\_\_\_  
 MODEL \_\_\_\_\_  
 PART NO. \_\_\_\_\_

THRUST BEARING TEST CONFIGURATION N° 8

RETEST

FOIL: ASSY P/N SK40423-2  
 NUMBER 13  
 THICKNESS .006  
 COATING T6F10W S  
 BASE THKNESS .010  
 SPECIAL CONFIG. ~

STIFFENER: P/N SK40421-2  
 THICKNESS .012  
 SPEC. CONF. \_\_\_\_\_

SPRING ASSY: P/N SK40422-2  
 BASE THKNESS .012  
 SPEC. CONFIG. \_\_\_\_\_

BREAK-AWAY TORQUE: TOTAL RIG 35 / 5.7 <sup>1</sup>/<sub>2</sub> in. lbs.  
 TEST BRG. 13.7 in. lbs.

RUNNING TORQUE: AT 33 Krpm, 200 lbs 3.13 @ 202.1 <sup>\*</sup> in. lbs.  
 AT 33 Krpm, max load \_\_\_\_\_ in. lbs.

MAX. LOAD 228 lbs.  
 MAX. SPEED 33,000 lbs.  
 LIFT-OFF SPEED 10,000 rpm  
 TOUCH DOWN SPEED 6,000 rpm

DATA POINT N° 46-52

REMARKS: Torque vs Load UPTO 228.3 LB  
 ABOVE 228.3 COULDN'T GET INCREASE T  
 ROTOR WORKING SEEN ON BENTLEY PLOTTER

AIRESEARCH MANUFACTURING COMPANY

DATE 8 001 1975  
 PREPARED BY SPINIE  
 CHECKED BY \_\_\_\_\_

CALC. NO. \_\_\_\_\_  
 MODEL \_\_\_\_\_  
 PART NO. \_\_\_\_\_

THRUST BEARING TEST CONFIGURATION N° 9

REBUILD

FOIL: ASSY P/N SK40423-2  
 NUMBER 13  
 THICKNESS .006  
 COATING TETRA S  
 BASE THKNESS .010  
 SPECIAL CONFIG. -

STIFFENER: P/N SK40421-2  
 THICKNESS .012  
 SPEC. CONF. -

SPRING ASSY: P/N \_\_\_\_\_  
 BASE THKNESS .012  
 SPEC. CONFIG. PARTIAL SEGMENT STIFFENER

BREAK-AWAY TORQUE: TOTAL RIG 35 in. lbs.  
 TEST BRG. 17.15 in. lbs.

RUNNING TORQUE: AT 33 Krpm, 200 lbs 3.66 @ 204.5 in. lbs.  
 AT 33 Krpm, max load \_\_\_\_\_ in. lbs.

MAX. LOAD 220 lbs.  
 MAX. SPEED 33,000 lbs.  
 LIFT-OFF SPEED 18,000 rpm  
 TOUCH DOWN SPEED 7000 rpm

DATA POINT N° 53-65

REMARKS: 1. Torque Vs Torque / LOAD  
 2. Torque Fluctuations noted ABOVE 220 LB LOAD

DATE 8/9 OCT 1975  
PREPARED BY S. M. TWIK  
CHECKED BY \_\_\_\_\_

CALC. NO. \_\_\_\_\_  
MODEL \_\_\_\_\_  
PART NO. \_\_\_\_\_

## THRUST BEARING TEST CONFIGURATION N° 10

FOIL: ASSY P/N SK40423-2  
NUMBER 13  
THICKNESS .006  
COATING TEFLON S  
BASE THKNESS .010  
SPECIAL CONFIG. ~

STIFFENER: P/N SK410421-2  
THICKNESS .012  
SPEC. CONF. \_\_\_\_\_

SPRING ASSY: P/N 3604730-Mod 2  
BASE THKNES .012  
SPEC. CONFIG. DUAL SPRINGS

BREAK-AWAY TORQUE: TOTAL RIG 30-35 in. lbs.  
TEST BRG. 15.08 in. lbs.

RUNNING TORQUE: AT 33Krpm, 200 lbs \_\_\_\_\_ in. lbs.  
AT 33Krpm, max load \_\_\_\_\_ in. lbs.

MAX. LOAD 195 lbs.  
MAX. SPEED 33,000 lbs.  
LIFT-OFF SPEED 10000 rpm  
TOUCH DOWN SPEED 6000 rpm

DATA POINT N° \_\_\_\_\_

REMARKS: 1 DUAL SPRINGS TORQUE VS SPECIFIC TORQUES  
2. TORQUE SPIKE TO 7 #IN ON TRAVEL TO  
195# LOAD - STABLE POINT AT 195  
BUT NO REPEATABILITY ON PREVIOUS  
POINTS

DATE 9 OCT 1975PREPARED BY S. MITCHELL

CHECKED BY \_\_\_\_\_

CALC NO \_\_\_\_\_

MODEL \_\_\_\_\_

PART NO. \_\_\_\_\_

THRUST BEARING TEST CONFIGURATION N° 11

FOIL: ASSY P/N SK40423-2  
NUMBER 13  
THICKNESS .006  
COATING TEFLON 3  
BASE THKNESS .010  
SPECIAL CONFIG. \_\_\_\_\_

STIFFENER: P/N SK40421-2  
THICKNESS .012  
SPEC. CONF. 2 T/C INSTALLED

SPRING ASSY: P/N 3604730-3  
BASE THKNESS .012  
SPEC. CONFIG. PARTIAL SEGMENT STIFFER

BREAK-AWAY TORQUE: TOTAL RIG 30-35 in. lbs.  
TEST BRG. 13.67 in. lbs.

RUNNING TORQUE: AT 33 Krpm, 200 lbs \_\_\_\_\_ in. lbs.  
AT 33 Krpm, max load \_\_\_\_\_ in. lbs.

MAX. LOAD \_\_\_\_\_ 105.  
MAX. SPEED \_\_\_\_\_ 105.  
LIFT-OFF SPEED \_\_\_\_\_ rpm  
TOUCH DOWN SPEED \_\_\_\_\_ rpm

DATA POINT N° \_\_\_\_\_

REMARKS: 1. TORQUE vs LOAD  
2. BEARING FAILED ON INITIAL STARTUP  
NO LIFT OFF



AIRSEARCH MANUFACTURING COMPANY

DATE 10-15-75  
 PREPARED BY S. M. NIE  
 CHECKED BY \_\_\_\_\_

CALC NO. \_\_\_\_\_  
 MODEL \_\_\_\_\_  
 PART NO. \_\_\_\_\_

THRUST BEARING TEST CONFIGURATION N° 12

FOIL: ASSY P/N SK40423-2  
 NUMBER 13  
 THICKNESS .006  
 COATING TEFLON S  
 BASE THKNESS .010  
 SPECIAL CONFIG. REWORKED 3 FOIL SEGMENTS REPLACED

STIFFENER: P/N SK40421-2  
 THICKNESS .012  
 SPEC. CONF. -

SPRING ASSY: P/N 3604730-3  
 BASE THKNESS .012  
 SPEC. CONFIG. PARTIAL SEGMENT STIFFENER

BREAK-AWAY TORQUE: TOTAL RIG 34-35 in. lbs.  
 TEST BRG. 15.5 in. lbs.

RUNNING TORQUE: AT 33 Krpm, 200 lbs 396 @ 19736 in. lbs.  
 AT 33 Krpm, max load \_\_\_\_\_ in. lbs.

MAX. LOAD 197.36 lbs.

MAX. SPEED 33,000 lbs.

LIFT-OFF SPEED 10000 rpm

TOUCH DOWN SPEED 7000 rpm

DATA POINT N° \_\_\_\_\_

REMARKS: • THRUST RUNNER IS SK65965-2 - NiCo PLATED

• REPLANT OF TESTING DONE IN CONFIG 9

• FIRST RUN DATA PTS #73-81 HIGH TORQUE

FOUND W/ 1/2 IN OF NEW FOILS - CLEANED

• RETURN DATA PTS 82 - 88

AIRESEARCH MANUFACTURING COMPANY

DATE 10-15-75

PREPARED BY S.M. FINE

CHECKED BY \_\_\_\_\_

CALC. NO. \_\_\_\_\_

MODEL \_\_\_\_\_

PART NO. \_\_\_\_\_

THRUST BEARING TEST CONFIGURATION N° 13

FOIL: ASS'Y P/N SK40423-2  
 NUMBER 13  
 THICKNESS .006  
 COATING TEFLON 5  
 BASE THKNESS .010  
 SPECIAL CONFIG. REWORKED 3 SEGMENTS REPLACED

STIFFENER: P/N SK40421-1  
 THICKNESS .010  
 SPEC. CONF. \_\_\_\_\_

SPRING ASS'Y: P/N 3604730-3  
 BASE THKNESS .012  
 SPEC. CONFIG. PARTIAL SEGMENT STIFFENER

BREAK-AWAY TORQUE: TOTAL RIG 325 in. lbs.  
 TEST BRG. 162 in. lbs.

RUNNING TORQUE: AT 33 Krpm, 200 lbs 365 @ 197.36 in. lbs.  
 AT 33 Krpm, max load 4.42 @ 276.48 in. lbs.

MAX. LOAD 276.48 lbs.  
 MAX. SPEED 33,000 lbs.  
 LIFT-OFF SPEED 10,000 rpm  
 TOUCH DOWN SPEED 9,000 rpm

DATA POINT N° 89 - 104

REMARKS: . RETEST OF CON FIG 12 WITH DIFFERENT STIFFENER  
 . SAME FOIL ASS'Y  
 . TERMINATED @ 275°F TOUT

AIRESEARCH MANUFACTURING COMPANY

DATE 10-16-75  
 PREPARED BY S. MIMIK  
 CHECKED BY \_\_\_\_\_

CALC NO. \_\_\_\_\_  
 MODEL \_\_\_\_\_  
 PART NO. \_\_\_\_\_

THRUST BEARING TEST CONFIGURATION N° 12

FOIL: ASSY P/N SK40423-2  
 NUMBER 13  
 THICKNESS .006  
 COATING TEFLON S  
 BASE THKNESS .010  
 SPECIAL CONFIG. PGW001K00

STIFFENER: P/N SK40421-2  
 THICKNESS .012  
 SPEC. CONF. \_\_\_\_\_

SPRING ASSY: P/N 3604730-3  
 BASE THKNES .012  
 SPEC. CONFIG. PARTIAL SEGMENT STIFFENER

BREAK-AWAY TORQUE: TOTAL RIG 34-35 in. lbs.  
 TEST BRG. 19.4 in. lbs.

RUNNING TORQUE: AT 33 Krpm, 200 lbs \_\_\_\_\_ in. lbs.  
 AT 33 Krpm, max load \_\_\_\_\_ in. lbs.

MAX. LOAD \_\_\_\_\_ lbs.  
 MAX. SPEED 33,000 lbs.  
 LIFT-OFF SPEED 10000 rpm  
 TOUCH DOWN SPEED 9600 rpm

DATA POINT N° 105-119

REMARKS: RETEST OF 10-15-75 CONFIG  
 BRG SHOWS SOME HYSTERESIS NOT SEEN  
 W/ CONFIG 13

AIRESEARCH MANUFACTURING COMPANY

DATE 10/17/  
 PREPARED BY M. J. J. K.  
 CHECKED BY \_\_\_\_\_

CALC. NO. \_\_\_\_\_  
 MODEL \_\_\_\_\_  
 PART NO. \_\_\_\_\_

THRUST BEARING TEST CONFIGURATION N° 13

FOIL: ASSY P/N SK4423-2  
 NUMBER 13  
 THICKNESS .006  
 COATING TERRA-S  
 BASE THKNESS .010  
 SPECIAL CONFIG. REWORKED 3 SEGMENTS REDUCED

STIFFENER: P/N SK4621-1  
 THICKNESS .010  
 SPEC. CONF. \_\_\_\_\_

SPRING ASSY: P/N 3604730-3  
 BASE THKNESS .012  
 SPEC. CONFIG. PARTIAL SEGMENT

BREAK-AWAY TORQUE: TOTAL RIG \_\_\_\_\_ in. lbs.  
 TEST BRG. \_\_\_\_\_ in. lbs.

RUNNING TORQUE: AT 33Krpm, 200 lbs \_\_\_\_\_ in. lbs.  
 AT 33Krpm, max load \_\_\_\_\_ in. lbs.

MAX. LOAD \_\_\_\_\_ lbs.  
 MAX. SPEED \_\_\_\_\_ lbs.  
 LIFT-OFF SPEED \_\_\_\_\_ rpm  
 TOUCH DOWN SPEED \_\_\_\_\_ rpm

DATA POINT N° 10-124

REMARKS: INVESTIGATION OF COOLING FLOW EFFECT

AIRSEARCH MANUFACTURING COMPANY

DATE 10/28/75 11/4/75  
 PREPARED BY MINIK  
 CHECKED BY \_\_\_\_\_

CALC. NO. \_\_\_\_\_  
 MODEL \_\_\_\_\_  
 PART NO. \_\_\_\_\_

THRUST BEARING TEST CONFIGURATION N° 13

FOIL: ASSY P/N SK40423-2  
 NUMBER 13  
 THICKNESS .006  
 COATING TFLON 5  
 BASE THKNESS .010  
 SPECIAL CONFIG. 7 WORKED 3 SEGMENTS

STIFFENER: P/N SK40421-1  
 THICKNESS .010  
 SPEC. CONF. \_\_\_\_\_

SPRING ASSY: P/N 3704730-3  
 BASE THKNESS .312  
 SPEC. CONFIG. PARTIAL SEGMENT STIFFENER

BREAK-AWAY TORQUE: TOTAL RIG 39 in. lbs.  
 TEST BRG. 23.6 in. lbs.

RUNNING TORQUE: AT 33 Krpm, 200 lbs 5.90 in. lbs.  
 AT 33 Krpm, max load 9.60 in. lbs.

MAX. LOAD 540 lbs.  
 MAX. SPEED 33,000 lbs.  
 LIFT-OFF SPEED 10000 rpm  
 TOUCH DOWN SPEED 6000 rpm

DATA POINT N° 25-133 10/29  
134-148 10/30

REMARKS: ① RUN AT CONST  $T_{OUT}$   $T_{OUT} = 275^{\circ}F$

②  $T_{OUT}$  CON-PULLS B. INCREASE 240 - 260°F

③ TEST RUN USAF DEMO 11/4/75 - PROXIMITY PROBE  
 INSTABILITY (APPROXIMATELY LOAD DEPENDENT) AT ~350#  
 TEST TERMINATED

FOUND THAT SPRING RATE TEST DAMAGED ASSY

DATE 1-7-76  
 PREPARED BY MITNIK  
 CHECKED BY \_\_\_\_\_

CALC. NO. \_\_\_\_\_  
 MODEL \_\_\_\_\_  
 PART NO. \_\_\_\_\_

# THRUST BEARING TEST CONFIGURATION N° 14

FOIL: ASSY P/N SK40423-2  
 NUMBER 13  
 THICKNESS .006  
 COATING MgS<sub>2</sub> .0007 "THK  
 BASE THKNESS .010  
 SPECIAL CONFIG. NEW-HANDMADE

STIFFENER: P/N SK40421-1  
 THICKNESS .010  
 SPEC. CONF. \_\_\_\_\_

SPRING ASSY: P/N 3704730-3  
 BASE THKNESS .012  
 SPEC. CONFIG. PARTIAL SEGMENT STIFFENER

BREAK-AWAY TORQUE: TOTAL RIG 30 26.0 in. lbs. @ 5 PSI  
 TEST BRG. 11.80 10.04 in. lbs. 13.9 PISTON PRESSURE

RUNNING TORQUE: AT 33 Krpm, 200 lbs \_\_\_\_\_ in. lbs.  
 AT 33 Krpm, max load \_\_\_\_\_ in. lbs.

MAX. LOAD \_\_\_\_\_ lbs.  
 MAX. SPEED \_\_\_\_\_ lbs.  
 LIFT-OFF SPEED \_\_\_\_\_ rpm  
 TOUCH DOWN SPEED \_\_\_\_\_ rpm

DATA POINT N° 149-

REMARKS: 1. COATING PERL E MS 52402 ~~7~~ 5.2.7  
 2. HYDROSTATIC THRUST BRG FAILURE.

AIRESEARCH MANUFACTURING COMPANY

DATE 2-23-76  
 PREPARED BY MITNIK  
 CHECKED BY \_\_\_\_\_

CALC. NO. \_\_\_\_\_  
 MODEL \_\_\_\_\_  
 PART NO. \_\_\_\_\_

THRUST BEARING TEST CONFIGURATION N° 15

FOIL: ASSY P/N SK40423-2  
 NUMBER 13  
 THICKNESS .006  
 COATING MOS<sub>2</sub> .0007"  
 BASE THKNESS .010  
 SPECIAL CONFIG. NEW HANDMADE / RESPRAYED

STIFFENER: P/N SK40421-1  
 THICKNESS .010  
 SPEC. CONF. \_\_\_\_\_

SPRING ASSY: P/N 3604730-4  
 BASE THKNESS .012  
 SPEC. CONFIG. 719 SPRING WITH PARTIAL SEGMENT  
 STIFFENING

BREAK-AWAY TORQUE: TOTAL RIG 22 2/24 in. lbs. @ 5.0" Hg  
 TEST BRG. 10.8 13 Y in. lbs.

RUNNING TORQUE: AT 33 Krpm, 200 lbs \_\_\_\_\_ in. lbs.  
 AT 33 Krpm, max load \_\_\_\_\_ in. lbs.

MAX. LOAD 40 lbs.  
 MAX. SPEED 33000 lbs.  
 LIFT-OFF SPEED 4000 rpm  
 TOUCH DOWN SPEED \_\_\_\_\_ rpm

DATA POINT N° 150 -

REMARKS: FAILURE RESULTING IN COMPLETE DESTRUCTION @ 40<sup>#</sup> LOAD  
 SUSPECT PAD CAME OFF BRG

AIRESEARCH MANUFACTURING COMPANY

DATE 3-11-76

PREPARED BY \_\_\_\_\_

CHECKED BY \_\_\_\_\_

CALC. NO. \_\_\_\_\_

MODEL \_\_\_\_\_

PART NO. \_\_\_\_\_

THRUST BEARING TEST CONFIGURATION N<sup>o</sup> 16

FOIL: ASSY P/N SK 40423-2  
 NUMBER 13  
 THICKNESS .006  
 COATING TEFLON S  
 BASE THKNESS .010  
 SPECIAL CONFIG. \_\_\_\_\_

STIFFENER: P/N SK 40421-1  
 THICKNESS .010  
 SPEC. CONF. \_\_\_\_\_

SPRING ASSY: P/N 3704730-3  
 BASE THKNES .012  
 SPEC. CONFIG. PARTIAL SEGMENT 3" TAIL

BREAK-AWAY TORQUE: TOTAL RIG 25 in. lbs. @ 5"  $\Delta$   
 TEST BRG. 99 in. lbs.

RUNNING TORQUE: AT 33 Krpm, 200 lbs 4.2 in. lbs.  
 AT 33 Krpm, max load 208/4.2 in. lbs.

MAX. LOAD 208 lbs.  
 MAX. SPEED 33000 RPM  
 LIFT-OFF SPEED 11000 rpm  
 TOUCH DOWN SPEED 4000 rpm

DATA POINT N<sup>o</sup> 151-154

REMARKS: RETEST OF CONFIG 13 TO CHECKOUT RIG AFTER  
 PROBLEMS WITH CONFIG 14:15  
 TRIBOLGY 400 RUNNIN  
 CHECK OUT OK

REPORT

PAGE 1 OF



AIRESEARCH MANUFACTURING COMPANY

DATE 3-11-76

PREPARED BY \_\_\_\_\_

CHECKED BY \_\_\_\_\_

CALC. NO. \_\_\_\_\_

MODEL \_\_\_\_\_

PART NO. \_\_\_\_\_

THRUST BEARING TEST CONFIGURATION N<sup>o</sup> 17

FOIL: ASSY P/N SK40423-2  
 NUMBER 13  
 THICKNESS .006  
 COATING TEFLON S  
 BASE THKNESS .010  
 SPECIAL CONFIG. \_\_\_\_\_

TRIBALLOY 400 RUNNING

STIFFENER: P/N SK40421-1  
 THICKNESS .010  
 SPEC. CONF. \_\_\_\_\_

SPRING ASSY: P/N 3704730-4  
 BASE THKNESS .012  
 SPEC. CONFIG. INCO 718 SPRING WITH PARTIAL  
SEGMENT STIFFENER

BREAK-AWAY TORQUE: TOTAL RIG 22 in. lbs. @ 5.0" Hg.  
 TEST BRG. 9.3 in. lbs.

RUNNING TORQUE: AT 33 Krpm, 200 lbs \_\_\_\_\_ in. lbs.  
 AT 33 Krpm, max load \_\_\_\_\_ in. lbs.

MAX. LOAD See Remark. lbs.  
 MAX. SPEED 22,000 RPM  
 LIFT-OFF SPEED 15500 rpm  
 TOUCH DOWN SPEED \_\_\_\_\_ rpm

DATA POINT N<sup>o</sup> 155-157

REMARKS: CHECKOUT TEST OF SPRING ASSY WITH TEFLON BRG  
 FAILED BETWEEN 162 & 200 #

DATE 3-25-76

PREPARED BY \_\_\_\_\_

CHECKED BY \_\_\_\_\_

CALC. NO. \_\_\_\_\_

MODEL \_\_\_\_\_

PART NO. \_\_\_\_\_

THRUST BEARING TEST CONFIGURATION N° 18

FOIL: Assy P/N SK40432-2  
 NUMBER 13  
 THICKNESS .006  
 COATING MoS<sub>2</sub> .0007"  
 BASE THKNESS .010  
 SPECIAL CONFIG. REWORKED (NEW COATING) UNUSED TFE BRG

STIFFENER: P/N SK40421-1  
 THICKNESS .010  
 SPEC. CONF. \_\_\_\_\_

SPRING ASSY: P/N 3704730-3  
 BASE THKNESS .012  
 SPEC. CONFIG. \_\_\_\_\_

BREAK-AWAY TORQUE: TOTAL RIG 40 in. lbs.  
 TEST BRG. 10.0 in. lbs.

RUNNING TORQUE: AT 33 Krpm, 200 lbs \_\_\_\_\_ in. lbs.  
 AT 33 Krpm, max load \_\_\_\_\_ in. lbs.

MAX. LOAD 9737 lbs.  
 MAX. SPEED 33000 RPM  
 LIFT-OFF SPEED \* rpm  
 TOUCH DOWN SPEED 8500  $\pm$  1 rpm

\* N/A DUE TO LOCK OF  
 SPEED SIGNAL

DATA POINT N° 155-164 RUN #1

REMARKS: 1. HS25 NiCo PLATED

2. TEST TO DETERMINE BRG CHARACTERISTICS WITH THIN FILM COATINGS.

3. TERMINATED TEST FOUND COATING WORN THRU IN SPOTS FOR ABOUT 50% CIRCUM. - APPEARED TO BE FAILURE DUE TO MISALIGNMENT - INSPECTION OF RIG DID NOT REVEAL ANY MISALIGNED HOWE

DATE 4-8-76

PREPARED BY \_\_\_\_\_

CHECKED BY \_\_\_\_\_

CALC. NO. \_\_\_\_\_

MODEL \_\_\_\_\_

PART NO. \_\_\_\_\_

THRUST BEARING TEST CONFIGURATION N<sup>o</sup> 19

FOIL: ASSY P/N SK40432-2  
 NUMBER 13  
 THICKNESS .006  
 COATING TEFLON S  
 BASE THKNESS .010  
 SPECIAL CONFIG. NEW

STIFFENER: P/N SK40421-1  
 THICKNESS .010  
 SPEC. CONF. \_\_\_\_\_

SPRING ASSY: P/N 3704730-3  
 BASE THKNESS .012  
 SPEC. CONFIG. \_\_\_\_\_

BREAK-AWAY TORQUE: TOTAL RIG 31 in. lbs.  
 TEST BRG. 10.7 in. lbs.

RUNNING TORQUE: AT 33 Krpm, 200 lbs 3.9 in. lbs.  
 AT 33 Krpm, max load \_\_\_\_\_ in. lbs.

MAX. LOAD 205.9 lbs.  
 MAX. SPEED 33000 RPM  
 LIFT-OFF SPEED N/A rpm  
 TOUCH DOWN SPEED 10500 rpm

DATA POINT N<sup>o</sup> 165-169

REMARKS: HS25 THRUST RUNNER - BASELINE CHECKOUT  
SIMILAR TO CONFIG 16  
CHECKOUT OK TO 200 # LOAD

DATE 12 4-8-76  
 PREPARED BY \_\_\_\_\_  
 CHECKED BY \_\_\_\_\_

CALC. NO. \_\_\_\_\_  
 MODEL \_\_\_\_\_  
 PART NO. \_\_\_\_\_

# THRUST BEARING TEST CONFIGURATION N<sup>o</sup> 20

FOIL: ASS'Y P/N SK40432-2  
 NUMBER 13  
 THICKNESS .006  
 COATING TaFLUWS  
 BASE THKNESS .010  
 SPECIAL CONFIG. NEW

STIFFENER: P/N SK40421-1  
 THICKNESS .010  
 SPEC. CONF. \_\_\_\_\_

SPRING ASS'Y: P/N 3704730-3  
 BASE THKNES .012  
 SPEC. CONFIG. \_\_\_\_\_

Run 1 Run 2

BREAK-AWAY TORQUE: TOTAL RIG 28 28 in. lbs.  
 TEST BRG. 9.7 9.6 in. lbs.

RUNNING TORQUE: AT 33 Krpm, 200 lbs 4.0 in. lbs.  
 AT 33 Krpm, max load 7 in. lbs.

MAX. LOAD 341 lbs.  
 MAX. SPEED 33k RPM  
 LIFT-OFF SPEED 6000 7000 rpm  
 TOUCH DOWN SPEED 8000 4500 rpm  
 Run 1 Run 2

DATA POINT N<sup>o</sup> \_\_\_\_\_

## REMARKS: COMPARISON RUN OF WIDE PAD BEARING

Run #1 300 LB @ 5.6 IN LB DATA PT 170-179  
 Run #2 341.5 7.0 180-183

Run 2 TERMINATED ON NOTING TORQUE SPIKE - SHUTDOWN  
 ACCOMPLISHED W/O FAILURE - 10% AREA WORN IN CENTRAL  
 OF EACH PAD

REPORT

PAGE 1 OF

DATE 4-13-76

PREPARED BY \_\_\_\_\_

CHECKED BY \_\_\_\_\_

CALC NO \_\_\_\_\_

MODEL \_\_\_\_\_

PART NO. \_\_\_\_\_

THRUST BEARING TEST CONFIGURATION N° 21

FOIL: ASSY P/N SK40432-3  
NUMBER 13  
THICKNESS .006  
COATING TiFLOX S .001"  
BASE THKNESS .010  
SPECIAL CONFIG. RELOCATED PAD RELATIVE TO SPRING  
BEARING ROTATED CCW 2.2° (.120")

STIFFENER: P/N SK40421-1  
THICKNESS .010  
SPEC. CONF. \_\_\_\_\_

SPRING ASSY: P/N 3704730-3  
BASE THKNES .012  
SPEC. CONFIG. \_\_\_\_\_

BREAK-AWAY TORQUE: TOTAL RIG 28 in. lbs.  
TEST BRG. 9.9 in. lbs.

RUNNING TORQUE: AT 33 Krpm, 200 lbs 3.9/4.0 in. lbs.  
AT 33 Krpm, max load 7.1 in. lbs.

MAX. LOAD 441.5 lbs.  
MAX. SPEED 33000 RPM  
LIFT-OFF SPEED 2500 rpm  
TOUCH DOWN SPEED 6000 rpm

DATA POINT N° 184-197

REMARKS: 1. SAME FOR ASSY AS USED FOR CONFIG 20  
2. NOTED TORQUE FLUCTUATION - TERMINATED - LITERUS  
WEAR PATTERN NOTED, ROTATED AFT ON PAD

DATE 4-15-76

PREPARED BY \_\_\_\_\_

CHECKED BY \_\_\_\_\_

CALC. NO. \_\_\_\_\_

MODEL \_\_\_\_\_

PART NO. \_\_\_\_\_

THRUST BEARING TEST CONFIGURATION N<sup>o</sup> 22

FOIL: Assy P/N SK40432-3  
NUMBER 13  
THICKNESS .006  
COATING MoS<sub>2</sub> .0007"  
BASE THKNESS .010  
SPECIAL CONFIG. \_\_\_\_\_

STIFFENER: P/N SK40421-1  
THICKNESS .010  
SPEC. CONF. \_\_\_\_\_

SPRING ASSY: P/N 3704730-3  
BASE THKNES .012  
SPEC. CONFIG. \_\_\_\_\_

BREAK-AWAY TORQUE: TOTAL RIG 30 in. lbs.  
TEST BRG. 9.1 in. lbs.

RUNNING TORQUE: AT 33Krpm, 200 lbs \_\_\_\_\_ in. lbs.  
AT 33Krpm, max load \_\_\_\_\_ in. lbs.

MAX. LOAD 180 lbs.  
MAX. SPEED 33K RPM  
LIFT-OFF SPEED 12000 rpm  
TOUCH DOWN SPEED \_\_\_\_\_ rpm

DATA POINT N<sup>o</sup> 198-201REMARKS: MoS<sub>2</sub> WIDE PAD BRG.

FAILED @ ~180 lb LOAD - INSTANTANEOUS FAILURE WITH  
NO WARNING

REPORT

PAGE 1 OF

DATE 7-19-76

PREPARED BY \_\_\_\_\_

CHECKED BY \_\_\_\_\_

CALC. NO. \_\_\_\_\_

MODEL \_\_\_\_\_

PART NO. \_\_\_\_\_

THRUST BEARING TEST CONFIGURATION N<sup>o</sup> 23

FOIL: ASSY P/N SK40432-3  
 NUMBER 13  
 THICKNESS .006  
 COATING KAMAN DES .0001" THICK  
 BASE THKNESS .010  
 SPECIAL CONFIG. \_\_\_\_\_

STIFFENER: P/N SK40421-1  
 THICKNESS .010  
 SPEC. CONF. \_\_\_\_\_

SPRING ASSY: P/N 3704730-3  
 BASE THKNES .012  
 SPEC. CONFIG. \_\_\_\_\_

BREAK-AWAY TORQUE: TOTAL RIG <sup>45/60</sup> \_\_\_\_\_ in. lbs.  
 TEST BRG. <sup>30</sup> \_\_\_\_\_ in. lbs.

RUNNING TORQUE: AT 33 Krpm, 200 lbs \_\_\_\_\_ in. lbs.  
 AT 33 Krpm, max load \_\_\_\_\_ in. lbs.

MAX. LOAD \_\_\_\_\_ lbs.  
 MAX. SPEED \_\_\_\_\_ RPM  
 LIFT-OFF SPEED \_\_\_\_\_ rpm  
 TOUCH DOWN SPEED \_\_\_\_\_ rpm

DATA POINT N<sup>o</sup> \_\_\_\_\_

## REMARKS:

INCO 713 THRUST RUNNER COATED WITH KAMAN SCA  
 THRUST RUNNER P/N SK65965-4

RIG ROTATED WITH WRENCH APPROX / 202 REVS — COATING  
 WORN THROUGH — NO HIGH SPEED RUN ATTEMPTED

REPORT

PAGE 1 OF

DATE 5-27-76PREPARED BY MITNIK

CHECKED BY \_\_\_\_\_

CALC NO \_\_\_\_\_

MODEL \_\_\_\_\_

PART NO \_\_\_\_\_

THRUST BEARING TEST CONFIGURATION N° 24

FOIL: ASSY P/N

SK40432-3

NUMBER

13

THICKNESS

.006

COATING

TEFLON S

BASE THKNESS

.010

SPECIAL CONFIG. \_\_\_\_\_

NOTE: SAME BRG

AS WAS USED

IN CONFIGS 20 &amp; 21

HS 25 RUNNER WITH

OXIDIZED NiCo

STIFFENER: P/N

SK40421-1

THICKNESS

.010

SPEC. CONF. \_\_\_\_\_

SPRING ASSY: P/N

3704730-3

BASE THKNESS

.012SPEC. CONFIG. MODIFIED 77

BREAK-AWAY TORQUE: TOTAL RIG

24

in. lbs.

TEST BRG.

11.4

in. lbs.

RUNNING TORQUE: AT 33 Krpm, 200 lbs

in. lbs.

AT 33 Krpm, max load

in. lbs.

MAX. LOAD ~225 lbs.MAX. SPEED 33 K RPMLIFT-OFF SPEED 7500 rpmTOUCH DOWN SPEED 7500 rpmDATA POINT N° 202-204

REMARKS:

TORQUE INDICATION - SUSPECT  
DUE TO LOW TORQUE ON 1 PAD

REPORT

PAGE 1 OF



DATE 5/27/76PREPARED BY MITNIK

CHECKED BY \_\_\_\_\_

CALC NO \_\_\_\_\_

MODEL \_\_\_\_\_

PART NO \_\_\_\_\_

THRUST BEARING TEST CONFIGURATION N° 25

FOIL: ASSY P/N  
 NUMBER  
 THICKNESS  
 COATING  
 BASE THKNESS  
 SPECIAL CONFIG.

SK40432-3  
.013  
.0085  
TEFLONS  
.010

COMPARISON TEST  
 TO CONFIG 20  
 .006" PADS TO  
 .0085" PADS

STIFFENER: P/N  
 THICKNESS  
 SPEC. CONF.

SK40421-1  
.010

SPRING ASSY: P/N  
 BASE THKNESS  
 SPEC. CONFIG.

3704730-3  
.012

BREAK-AWAY TORQUE: TOTAL RIG 21.5 25 in. lbs.  
 TEST BRG. 10.6 10.8 in. lbs.

RUNNING TORQUE: AT 33Krpm, 200 lbs 4.2 in. lbs.  
 AT 33Krpm, max load 5.94 in. lbs.

MAX. LOAD 324.5 lbs.

MAX. SPEED 33000 RPM

LIFT-OFF SPEED 14600 15000 rpm

TOUCH DOWN SPEED 10300 9300 rpm

DATA POINT N° 205-

REMARKS: RUN 1 TO 206<sup>+</sup> SHUT DOWN FOR CHECKOUT

RUN 2 - TORQUE INDICATION - SHUT DOWN - RUB THEN TO  
 METAL - FOIL ONLY APPROX 1" DIA

REPORT

PAGE 1 OF

DATE 6-8-76PREPARED BY MITNIK

CHECKED BY \_\_\_\_\_

CALC NO \_\_\_\_\_

MODEL \_\_\_\_\_

PART NO. \_\_\_\_\_

**THRUST BEARING TEST CONFIGURATION N° 26**

FOIL: ASSY P/N SK40432 HS25 RUNNER  
 NUMBER .013 W/ OXIDIZED Ni Co  
 THICKNESS .006  
 COATING TITANUS  
 BASE THKNESS .010  
 SPECIAL CONFIG. \_\_\_\_\_

STIFFENER: P/N SK40421-1  
 THICKNESS .010  
 SPEC. CONF. \_\_\_\_\_

SPRING ASSY: P/N 3704730-3  
 BASE THKNESS .012  
 SPEC. CONFIG. PARTIAL SEMIWIT STIFFENER

BREAK-AWAY TORQUE: TOTAL RIG 26 in. lbs.  
 TEST BRG. 10.1 in. lbs.

RUNNING TORQUE: AT 33 Krpm, 200 lbs \_\_\_\_\_ in. lbs.  
 AT 33 Krpm, max load \_\_\_\_\_ in. lbs.

MAX. LOAD \_\_\_\_\_ lbs.  
 MAX. SPEED \_\_\_\_\_ RPM  
 LIFT-OFF SPEED \_\_\_\_\_ rpm  
 TOUCH DOWN SPEED \_\_\_\_\_ rpm

DATA POINT N° \_\_\_\_\_

REMARKS: THRUST RUNNER CAME APART AT 4000 RPM -  
 SEVERE UNBALANCE FAILED JOURNAL BRGS - WILL RERUN  
 THIS CONFIG

DATE 7-7-76  
 PREPARED BY MITNIK  
 CHECKED BY \_\_\_\_\_

CALC NO \_\_\_\_\_  
 MODEL \_\_\_\_\_  
 PART NO. \_\_\_\_\_

# THRUST BEARING TEST CONFIGURATION N° 27

FOIL: ASSY P/N SK40432 TRIBALLOY 400 RUNNER  
 NUMBER 13  
 THICKNESS .006  
 COATING TEFLONS  
 BASE THKNESS .010  
 SPECIAL CONFIG. \_\_\_\_\_  
 REPERT TEST FOR.  
 CONFIG 26

STIFFENER: P/N SK40421-1  
 THICKNESS .010  
 SPEC. CONF. \_\_\_\_\_

SPRING ASSY: P/N 3704730-3  
 BASE THKNES .012  
 SPEC. CONFIG. PARTIAL SEGMENT STIFFENER

BREAK-AWAY TORQUE: TOTAL RIG 26 in. lbs.  
 TEST BRG. .0 in. lbs.

RUNNING TORQUE: AT 33 Krpm, 200 lbs 4.3 in. lbs.  
 AT 33 Krpm, max load 7.0 in. lbs.

MAX. LOAD 397.2 lbs.  
 MAX. SPEED 3300 RPM  
 LIFT-OFF SPEED 7000 rpm  
 TOUCH DOWN SPEED 4000 rpm

DATA POINT N° 215-228

## REMARKS:

Run 1 max load 215 FLOW DOWN IN THE SIGNAL  
 Run 2 max load 227  
 Run 3 7/9/76 BREAK, 11 6/44

REPORT  
 PAGE 1 OF

DATE 1-9-76  
 PREPARED BY MIRNIK  
 CHECKED BY \_\_\_\_\_

CALC NO \_\_\_\_\_  
 MODEL \_\_\_\_\_  
 PART NO \_\_\_\_\_

# THRUST BEARING TEST CONFIGURATION N° 28

FOIL: ASSY P/N SK42432 TRISALLOY 400 RUNNER  
 NUMBER 13 SAME BRG AS  
 THICKNESS .006 CONF K- 29  
 COATING TETRASS  
 BASE THKNESS .010  
 SPECIAL CONFIG. LOCATED 90° RELATIVE TO SPRING  
12° POST CFW 2.2°

STIFFENER: P/N SK40421-1  
 THICKNESS .010  
 SPEC. CONF. \_\_\_\_\_

SPRING ASSY: P/N 3704730-3  
 BASE THKNESS .012  
 SPEC. CONFIG. PARTIAL SEGMENT STIFFENER

BREAK-AWAY TORQUE: TOTAL RIG \_\_\_\_\_ 39 in. lbs.  
 TEST BRG. \_\_\_\_\_ 10.4 in. lbs.

RUNNING TORQUE: AT 33 Krpm, 200 lbs \_\_\_\_\_ in. lbs.  
 AT 33 Krpm, max load 8.2 in. lbs.

MAX. LOAD 486.4 lbs.  
 MAX. SPEED 33 K RPM  
 LIFT-OFF SPEED 7000 rpm  
 TOUCH DOWN SPEED \_\_\_\_\_ rpm

DATA POINT N° 22a

REMARKS: FAILED AT LOAD

DATE \_\_\_\_\_  
 PREPARED BY MITNIE  
 CHECKED BY \_\_\_\_\_

CALC NO \_\_\_\_\_  
 MODEL \_\_\_\_\_  
 PART NO \_\_\_\_\_

# THRUST BEARING TEST CONFIGURATION N° 29

FOIL: ASSY P/N SK40432 COMPARISON  
 NUMBER 13 TEST OF  
 THICKNESS .006 INCONEL  
 COATING TEFLON S BE CU  
 BASE THKNESS .010  
 SPECIAL CONFIG. BE CU FOIL MATL COMPARE TO  
 CONFIG 20

STIFFENER: P/N SK40421-1  
 THICKNESS .010  
 SPEC. CONF. \_\_\_\_\_

SPRING ASSY: P/N 3764730-3  
 BASE THKNES .012  
 SPEC. CONFIG. PARTIAL SEGMENT STIFFENER

BREAK-AWAY TORQUE: TOTAL RIG 38 in. lbs.  
 TEST BRG. 10 in. lbs.

RUNNING TORQUE: AT 33 Krpm, 200 lbs 39 in. lbs.  
 AT 33 Krpm, max load 7.7 in. lbs.

MAX. LOAD <sup>Row 1</sup> 469.5 lbs.  
 MAX. SPEED 3016 RPM  
 LIFT-OFF SPEED 12000 16000 rpm  
 TOUCH DOWN SPEED 11300 rpm

DATA POINT N° <sup>Row 1</sup> 242-255

REMARKS:

DATE 8-11-74PREPARED BY MITNIK

CHECKED BY \_\_\_\_\_

CALC NO \_\_\_\_\_

MODEL \_\_\_\_\_

PART NO. \_\_\_\_\_

THRUST BEARING TEST CONFIGURATION N° 30

FOIL: ASSY P/N SK40432-3  
 NUMBER 13  
 THICKNESS .006  
 COATING KAMAN DES .0001 THICK  
 BASE THKNESS .010  
 SPECIAL CONFIG. BRG ROTATED 2.2° CCW  
RELATIVE TO SPRING

STIFFENER: P/N SK40421-1  
 THICKNESS .010  
 SPEC. CONF. \_\_\_\_\_

SPRING ASSY: P/N 3704730-3  
 BASE THKNES .012  
 SPEC. CONFIG. MODIFIED, RECTANGULAR STIFFENER

BREAK-AWAY TORQUE: TOTAL RIG 37 in. lbs.  
 TEST BRG. 10.2 in. lbs.

RUNNING TORQUE: AT 33 Krpm, 200 lbs \_\_\_\_\_ in. lbs.  
 AT 33 Krpm, max load 30 in. lbs.

MAX. LOAD 200 lbs.  
 MAX. SPEED 33000 RPM  
 LIFT-OFF SPEED 20K rpm  
 TOUCH DOWN SPEED 12K rpm

DATA POINT N° 256-264

REMARKS: HS25 THRUST RUNNER W/OXIDIZED NiCo

HIGH TEMP TESTS @ 200 # LOAD

~~COOLING FLOW CONTINUOUS TO 12.5 LBS/HR~~DEL. TEMP. = 500° T<sub>10</sub>

REPORT

PAGE 1 OF

DATE 8/13 / 8/14 / 76PREPARED BY MITCHELL

CHECKED BY \_\_\_\_\_

CALC NO \_\_\_\_\_

MODEL \_\_\_\_\_

PART NO. \_\_\_\_\_

THRUST BEARING TEST CONFIGURATION N° 31

FOIL: Ass'y P/N SK40482-3  
 NUMBER 13  
 THICKNESS .006  
 COATING Teflon S .001  
 BASE THKNESS .010  
 SPECIAL CONFIG. BrCu Foils  
2.2° CCW Rotation

MS25  
 Running  
 w/ N<sub>2</sub> Co

STIFFENER: P/N SK40421-1  
 THICKNESS .010  
 SPEC. CONF. \_\_\_\_\_

SPRING ASSY: P/N 3704730-3  
 BASE THKNESS .012  
 SPEC. CONFIG. MODIFIED RECTANGULAR  
STIFFENER

BREAK-AWAY TORQUE: TOTAL RIG SUE DATA in. lbs.  
 TEST BRG. SILETS in. lbs.

RUNNING TORQUE: AT 33Krpm, 200 lbs \_\_\_\_\_ in. lbs.  
 AT 33Krpm, max load \_\_\_\_\_ in. lbs.

MAX. LOAD \_\_\_\_\_ lbs.  
 MAX. SPEED 33K RPM  
 LIFT-OFF SPEED 565 rpm  
 TOUCH DOWN SPEED DATA rpm

DATA POINT N° 265-789

REMARKS: MISALIGNMENT TESTING TO  
 200<sup>+</sup> MAX LOAD

SAME BRG CONFIG AS TEST CONFIG # 29

SAME SPRING ASSY AS USED FOR TEST CONFIG # 30

DATE 10-15-76PREPARED BY Mitnik

CHECKED BY \_\_\_\_\_

CALC NO. \_\_\_\_\_

MODEL \_\_\_\_\_

PART NO. \_\_\_\_\_

**THRUST BEARING TEST CONFIGURATION N° 32**

FOIL: ASSY P/N SK40432-2  
 NUMBER 13  
 THICKNESS .006  
 COATING NiCo .0005  
 BASE THKNESS .010  
 SPECIAL CONFIG. LOW ROTATION

Inconel  
 Runner  
 w/  
 KAMAN ~~DEF~~  
 SCA

STIFFENER: P/N SK40421-2  
 THICKNESS .010 .012  
 SPEC. CONF. \_\_\_\_\_

SPRING ASSY: P/N 3704730-3  
 BASE THKNESS .012  
 SPEC. CONFIG. RECTANGULAR STIFFENER

BREAK-AWAY TORQUE: TOTAL RIG 10.7 in. lbs.  
 TEST BRG. 43.0 in. lbs.

RUNNING TORQUE: AT 33 Krpm, 200 lbs \_\_\_\_\_ in. lbs.  
 AT 33 Krpm, max load \_\_\_\_\_ in. lbs.

MAX. LOAD \_\_\_\_\_ lbs.  
 MAX. SPEED 35500 RPM  
 LIFT-OFF SPEED N/A rpm  
 TOUCH DOWN SPEED \_\_\_\_\_ rpm

DATA POINT N° \_\_\_\_\_

REMARKS: **DYNAMIC LOADING TEST - AMBIENT COOLING**  
 FAILED UPON INITIAL LOAD APPLICATION <sup>Air</sup>



DATE 10-15-76PREPARED BY Mitnik

CHECKED BY \_\_\_\_\_

CALC NO \_\_\_\_\_

MODEL \_\_\_\_\_

PART NO. \_\_\_\_\_

THRUST BEARING TEST CONFIGURATION N° 33

FOIL: ASSY P/N

SK40432-3HS 25 RUNNER  
W/ NICONUMBER 13THICKNESS .006COATING TEFLON S.001BASE THKNESS .010SPECIAL CONFIG. BE Cu PADSSAME BRG AS  
CONFIG 31GRAPHITE  
~~W/~~ SPRAY APPLIED

STIFFENER: P/N

SK40421-1THICKNESS .010

SPEC. CONF. \_\_\_\_\_

SPRING ASSY: P/N

3704730-3BASE THKNES .012SPEC. CONFIG. RECTANGULAR STIFFENER

BREAK-AWAY TORQUE: TOTAL RIG

39.0

in. lbs.

TEST BRG.

4.5

in. lbs.

RUNNING TORQUE: AT 33 Krpm, 200 lbs

in. lbs.

AT 33 Krpm, max load

in. lbs.

MAX. LOAD 630 DYNAMIC lbs.MAX. SPEED 33 K RPMLIFT-OFF SPEED N/A rpm

TOUCH DOWN SPEED \_\_\_\_\_ rpm

DATA POINT N° \_\_\_\_\_

REMARKS: REPEAT TRY DYNAMIC LOADING TEST

FAILED AT 682.1 LB LOAD RATE OF 63 LB/SEC

DATE 5/18/75  
 PREPARED BY W.F. KOPPEL  
 CHECKED BY \_\_\_\_\_

CALC. NO. \_\_\_\_\_  
 MODEL \_\_\_\_\_  
 PART NO. \_\_\_\_\_

## JOURNAL BEARING TEST CONFIGURATION # 1

	TEST BRG.	TURB. BRG.
CARRIER: I.D.	4.5594/4.5603	4.5592/4.5602
SHAFT : O.D. COATING	4.4997/4.4998 THIN DENSE CHROM.	4.4997/4.4998 THIN DENSE CHROM.
FOIL : BASE THKNS BASE MAT'L COATING MAT'L TOTAL THKNS LENGTH BEND RADIUS NUMBER OF FOILS SPECIAL CONFIGURATION	.010 INCONEL X 750 OBD 26-20 .011 6" 3" 8 ~	.010 INCONEL X 750 OBD 26-20 .011 6" 3" 8 ~
SWAY SPACE: C-S-4F ASSEMBLY MEAS.	.0161 N/A	.0159 N/A
BREAK-AWAY TORQUE lb.-in. RUNNING TORQUE (1G, 33K rpm) lb.-in.	65 TOTAL & 2.0 @ 13,700 rpm	~ ~
LIFT-OFF SPEED TOUCH DOWN SPEED	10,000 rpm 6,000 rpm	~ ~
SHAFT DISPL: STATIC RUNNING & LOADED	N/A N/A	N/A N/A

## REMARKS:

DATA POINT # ~MAX. SPEED 26,500MAX. LOAD 46 lb + 55 TARE ÷ 54 in<sup>2</sup> = 1.67 psi (BRG)4.6 in<sup>2</sup> PISTON

Turbine and ball bearings all shut down. PH-70 P52499-1 thru 9  
 Shaft surface finish is .06 deep

Preceding Page BLANK -

DATE 21 MAY 75  
PREPARED BY W.F. KOWAL  
CHECKED BY \_\_\_\_\_

CALC. NO. \_\_\_\_\_  
MODEL \_\_\_\_\_  
PART NO. \_\_\_\_\_

	TEST BRG.	TURB. BRG.
CARRIER: I.D.	4.5594/4.5603	4.5592/4.5602
SHAFT : O.D. COATING	4.4997/4.4998 THIN DENSE CHROM.	4.5002 LW-1N30
FOIL : BASE THKNSS BASE MAT'L COATING MAT'L TOTAL THKNSS LENGTH BEND RADIUS NUMBER of FOILS SPECIAL CONFIGURATION	.010 INCOSEL X 750 CRO 2G-5 .011 6" 3" 8 RE COATED FOILS	.010 CRO 2G-5 .011 6" 3" 8 RE COATED FOILS
SWAY SPACE: C-S-4F ASSEMBLY MEAS.	.0161 N/A	.0155 N/A
BREAK-AWAY TORQUE lb.-in. RUNNING TORQUE (1G, 33K rpm) lb.in.	10,57. TOTAL 4-- ~	~
LIFT-OFF SPEED TOUCH DOWN SPEED	10,000. rpm 6,000 rpm	~ ~
SHAFT DISPL: STATIC RUNNING & LOADED	N/A N/A	N/A N/A

REMARKS:  
DATA POINT # 1, 2, 3, 4  
MAX. SPEED 25.007 in.  
MAX. LOAD 112 lbs  $(112 + 54) \div 27 = 6.15 \text{ psi}$

TURBINE BRG FAILURE DURING RAPID START to 32,000 RPM  
SHAFT CLEANED UP OK w/FAIR  
SEE MOUNTAIN RANGE PHOTO'S IN 24th. Tail - 1st RT

DATE 27 MAR 75  
 PREPARED BY W F KOEDEL  
 CHECKED BY \_\_\_\_\_

CALC NO \_\_\_\_\_  
 MODEL \_\_\_\_\_  
 PART NO. \_\_\_\_\_

# JOURNAL BEARING TEST CONFIGURATION # 3

	TEST BRG.	TURB. BRG.
CARRIER: I.D.	4.5574/4.5603	4.5592/4.5602
SHAFT : O.D. COATING	4.4997/4.4778 THIN DENSE CHROM	4.5002 LW-IN30
FOIL : BASE THKNS BASE MAT'L COATING MAT'L TOTAL THKNS LENGTH BEND RADIUS NUMBER OF FOILS SPECIAL CONFIGURATION	.010 INCOEL X-750 OBD-26-5 .011 6" 3" 8 RECOATED FOILS	.010 INCOEL X 750 TEFLON S .011 6" 3" 8 NEW
SWAY SPACE : C-S-4F ASSEMBLY MEAS.	.0161 N/A	.0155 N/A
BREAK-AWAY TORQUE lb.-in. RUNNING TORQUE (1G, 33K $\mu$ m) lb.in.	8750 lb.in. ~	~
LIFT-OFF SPEED TOUCH DOWN SPEED	8250 rpm 6000 rpm	~ ~
SHAFT DISPL: STATIC RUNNING & LOADED	N/A N/A	N/A N/A

REMARKS:  
 DATA POINT # TRIM BALANCE TEST  
 MAX. SPEED 22,300  
 MAX. LOAD W/O PARACHUTE LOADS

1 on AF Demo loads w/parachute loader to 12,000 ft.

CALC. NO. \_\_\_\_\_  
MODEL \_\_\_\_\_  
PART NO. \_\_\_\_\_

CARRIER : I.D.

SHAFT : O.D.  
COATING

FOIL : BASE THKNSS  
BASE MAT'L  
COATING MAT'L  
TOTAL THKNSS  
LENGTH  
BEND RADIUS  
NUMBER of FOILS  
SPECIAL CONFIGURATION

SWAY SPACE: C-S-4F  
ASSEMBLY MEAS.

BREAK-AWAY TORQUE 1b.-in.  
RUNNING TORQUE (1G, 33K $\mu$ m) 1b. in.

LIFT-OFF SPEED  
TOUCH DOWN SPEED

SHAFT DISPL: STATIC (Below  $\phi$ )  
RUNNING & LOADED

REMARKS:

DATA POINT #	None
MAX. SPEED	27,000
MAX. LOAD	1 G.

Subsynchronous critical test: starts at 25 Kipm at the test bearing end and at 27 Kipm at the turbine end.

TEST BRG.	TURB. BRG.
4.5655	4.5664/4.5648
4.4997/4.4998	4.5002
TAIN DENSE CHROM	6W-1N30
.010	.010
INCONEL X 750	INCONEL X 750
0BD 26-20	0BD 26-20
.011	.011
6"	6"
3'	3"
6	6
NEW	NEW
.02175	.0214
.0173	.0167
14.6	~
3 in lbs at 27K	~
8500 rpm	~
6500 rpm	~
~	.0065
	~

AIRSEARCH MANUFACTURING COMPANY

DATE 6-11-66  
 PREPARED BY W.F. KOSAR  
 CHECKED BY \_\_\_\_\_

CALC NO. \_\_\_\_\_  
 MODEL \_\_\_\_\_  
 PART NO. \_\_\_\_\_

JOURNAL BEARING TEST CONFIGURATION # 5

CARRIER: I.D.  
 SHAFT : O.D.  
 COATING  
 FOIL : BASE THKNSS  
 BASE MAT'L  
 COATING MAT'L  
 TOTAL THKNSS  
 LENGTH  
 BEND RADIUS  
 NUMBER OF FOILS  
 SPECIAL CONFIGURATION  
 SWAY SPACE: C-S-4F  
 ASSEMBLY MEAS.  
 BREAK-AWAY TORQUE lb.-in.  
 RUNNING TORQUE (1G, 33Krpm) lb. in.  
 LIFT-OFF SPEED  
 TOUCH DOWN SPEED  
 SHAFT DISPL: STATIC  
 RUNNING & LOADED

TEST BRG.	TURB. BRG.
4.5655	4.5667/4.5648
4.4997/4.4998	4.5000
Time: 0.0001 Galkob	LW-1030
.012	.012
100.1750	100.1750
080 26-20	080 26-20
.013	.013
6"	6"
30"	30"
6	6
1000	1000
.01375	.01375
.010	.010
53	115
	~
	~
	~

W/OK

REMARKS:  
 DATA POINT # \_\_\_\_\_  
 MAX. SPEED 20,000  
 MAX. LOAD 1G

Sub synchronous whirl test: Test bearing end excursions continued to grow at 20,000rpm to failure. Shaft scoring is reproducible and foils are recontable. Cause of failure is 1. OBD 26-20 balled or 2. Conical shaft whirl.

REPORT  
 PAGE OF

AIRSEARCH MANUFACTURING COMPANY

DATE 10/14/10  
 PREPARED BY W. K. KOSMILL  
 CHECKED BY \_\_\_\_\_

CALC. NO. \_\_\_\_\_  
 MODEL \_\_\_\_\_  
 PART NO. \_\_\_\_\_

JOURNAL BEARING TEST CONFIGURATION # 6

	TEST BRG.	TURB. BRG.
CARRIER: I.D.	4.5635	4.5661/4.5648
SHAFT : O.D. COATING	4.4177/4.4718 THIN DENSE CHR.	4.5002 LW IN 30
FOIL : BASE THKNSS	.010	.010
BASE MAT'L	INC 7 150	INC 7 150
COATING MAT'L	010 26-20	010 26 20
TOTAL THKNSS	.011	.011
LENGTH	6	6
BEND RADIUS	3.0	3.0
NUMBER OF FOILS	6	6
SPECIAL CONFIGURATION	.003 BACK FOIL	.003 BACK FOIL
SWAY SPACE : C-S-4F	.0175	.01740
ASSEMBLY MEAS.	.012	.0125
BREAK-AWAY TORQUE lb.-in.	23	TOTAL 58 w/o PARA
RUNNING TORQUE (16,33Krpm) lb.in.		~
LIFT-OFF SPEED	10,000	~
TOUCH DOWN SPEED	9000	~
SHAFT DISPL: STATIC		
RUNNING & LOADED		

REMARKS:  
 DATA POINT # \_\_\_\_\_  
 MAX. SPEED \_\_\_\_\_  
 MAX. LOAD No Fat.

AIRESEARCH MANUFACTURING COMPANY

DATE 13 Aug 75  
 PREPARED BY C. R. Jones/jwk  
 CHECKED BY \_\_\_\_\_

CALC. NO. \_\_\_\_\_  
 MODEL \_\_\_\_\_  
 PART NO. \_\_\_\_\_

JOURNAL BEARING TEST CONFIGURATION # 7

CARRIER: I.D.

SHAFT : O.D.  
 COATING

FOIL : BASE THKNS  
 BASE MAT'L  
 COATING MAT'L  
 TOTAL THKNS  
 LENGTH  
 BEND RADIUS  
 NUMBER OF FOILS  
 SPECIAL CONFIGURATION

SWAY SPACE : C-S-4F  
 ASSEMBLY MEAS.

BREAK-AWAY TORQUE lb.-in.  
 RUNNING TORQUE (16,33Krpm) lb.-in.

LIFT-OFF SPEED  
 TOUCH DOWN SPEED

SHAFT DISPL: STATIC  
 RUNNING & LOADED

REMARKS:  
 DATA POINT # \_\_\_\_\_  
 MAX. SPEED 25406  
 MAX. LOAD No PARA

TRIM BALANCED SHAFT

EXCURSIONS STILL EXIST SOME AT SPEED 25Krpm

TEST BRG.	TURB. BRG.
<p>9# WL ADDED</p> <p>34</p>	<p>CONC 46</p> <p>~</p> <p>~</p> <p>~</p>



AIRSEARCH MANUFACTURING COMPANY

DATE 3-24-75  
 PREPARED BY J. W. Koeppel  
 CHECKED BY \_\_\_\_\_

CALC NO. \_\_\_\_\_  
 MODEL \_\_\_\_\_  
 PART NO. \_\_\_\_\_

JOURNAL BEARING TEST CONFIGURATION # 8

	TEST BRG.	TURB. BRG.
CARRIER: I.D.	4.5655	4.5614/4.5648
SHAFT : O.D. COATING	4.4977/4.4998 THIN DENSE CH	4.5002 CWN IN 30
FOIL : BASE THKNSS	.010	.010
BASE MAT'L	INCY 750	INCY 750
COATING MAT'L	2500 G 10	2500 G 10
TOTAL THKNSS	.011	.011
LENGTH	6	6
BEND RADIUS	3.38	3.38
NUMBER OF FOILS	6	6
SPECIAL CONFIGURATION		
SWAY SPACE : C-S-4F	.0115	.0114
ASSEMBLY MEAS.	.0155	.015
BREAK-AWAY TORQUE lb.-in.	27	75 TOTAL U/6 PARA
RUNNING TORQUE (1G, 33Krpm) lb.-in.		~
LIFT-OFF SPEED	6000 rpm	~
TOUCH DOWN SPEED	6000 rpm	~
SHAFT DISPL: STATIC		
RUNNING & LOADED		

REMARKS:  
 DATA POINT # 1  
 MAX. SPEED 30,000  
 MAX. LOAD U/LAKE

TEST POINT 27.5 ANALYZED FOR INCREASED SWAY SPACE. A  
 HAVE BEEN RE-EXAMINED

TEST RESULTS: EXCURSION EXCEEDED 2 TIMES AT 30,000 RPM. NO LUBRICATION  
 BALANCE WAS DONE ON THE TEST RIG

SUCCESSFUL OPERATION AT 30,000 RPM. NO SOLIDIFICATION. LUBRICANT

FAILED AT 30,000 RPM UNDER 10% OF FULL PLANE BEARING CONDITION

SHOULD NEED REPAIR. BEARING FAILED IN CENTER

REPORT

PAGE OF

DATE: 10 Dec 75  
 PREPARED BY: SWIMINIL  
 CHECKED BY: \_\_\_\_\_

CALC. NO. \_\_\_\_\_  
 MODEL \_\_\_\_\_  
 PART NO. \_\_\_\_\_

JOURNAL BEARING TEST CONFIGURATION # 9

	TEST BRG.	TURB. BRG.
CARRIER: I.D.	<del>4.565</del> 4.5795/4.5747	<del>4.5664/4.5648</del> 4.5751/4.5762
SHAFT : O.D. COATING	4.4985/4.4990 ELECTROLESS Ni	4.4990 ELECTROLESS Ni
FOIL : BASE THKNS BASE MAT'L COATING MAT'L TOTAL THKNS LENGTH BEND RADIUS NUMBER OF FOILS SPECIAL CONFIGURATION	.012 INC 750 OBD26-5 .0135/.0140 4.5 3.375 8	.012 INC 750 OBD26-5 0135/.0140 4.5 3.375 8
SWAY SPACE : C-S-4F ASSEMBLY MEAS.	.0227 .0189 .0262/.0185 .01950	.0231-.0207 .0212/.0211 .01435
BREAK-AWAY TORQUE lb.-in. RUNNING TORQUE (1G, 33Krpm) lb.in.	630	175 TOTAL
LIFT-OFF SPEED	7000	~
TOUCH DOWN SPEED	FAILURE	~
SHAFT DISPL: STATIC RUNNING & LOADED		

## REMARKS:

DATA POINT # \_\_\_\_\_  
 MAX. SPEED 21,000  
 MAX. LOAD 1G

FAILURE AT TURBINE END BRG - MAX SPEED  $\approx$  20000 RPM  
 SHAFT COATING FAILURE AT TEST BRG.

AIRESEARCH MANUFACTURING COMPANY

DATE 12-3-75

PREPARED BY MITNIK

CHECKED BY \_\_\_\_\_

CALC. NO. \_\_\_\_\_

MODEL \_\_\_\_\_

PART NO. \_\_\_\_\_

JOURNAL BEARING TEST CONFIGURATION # 10

	TEST BRG.	TURB. BRG.
CARRIER: I.D.	4.57458 AVE	4.57608 AVE
SHAFT : O.D.	4.501	4.500
COATING	THIN DENSE CHR	LW 1-N 30
FOIL : BASE THKNSS in.	.010	.010
BASE MAT'L	x750	x750
COATING MAT'L	TEFLON S	TEFLONS
TOTAL THKNSS in.	.011	.011
LENGTH in.	4.50	4.50
BEND RADIUS in.	3.0	3.0
NUMBER OF FOILS	8	8
SPECIAL CONFIGURATION		2 STRAIN GAGES EACH ON 2 FOILS
SWAY SPACE: C-S-4F ASSEMBLY MEAS.	.023	.023
BREAK-AWAY TORQUE lb.-in.	9.5 BRG SS TOTAL	~
RUNNING TORQUE (16,33K $\mu$ m) lb.-in.		~
LIFT-OFF SPEED rpm		~
TOUCH DOWN SPEED rpm		~
SHAFT DISPL: STATIC in.		
RUNNING & LOADED in.		

REMARKS:

DATA POINT # \_\_\_\_\_  
 MAX. SPEED \_\_\_\_\_ rpm  
 MAX. LOAD CELL  $\frac{.051 \times 4.6 \text{ in}^2}{.54 \text{ in}^2} =$

NOTE .004 SHIM ADDED TO ACHIEVE .023 CALC SWAY SPACE  
 INITIAL TEST TO BE AT .05 LB/SEC COOLING BOTH BRG  
 CHLCHOUT RUNS ONLY 12-2-75  
 SUBSYNC WHIRL AT 15000 RPM  $\frac{1}{2}$  BELOW - TEST TERMINATED

REPORT

PAGE OF

AIRESEARCH MANUFACTURING COMPANY

DATE 12-16-75  
 PREPARED BY MITNIK  
 CHECKED BY \_\_\_\_\_

CALC. NO. \_\_\_\_\_  
 MODEL \_\_\_\_\_  
 PART NO. \_\_\_\_\_

JOURNAL BEARING TEST CONFIGURATION # 11

	TEST BRG.	TURB. BRG.
CARRIER: I.D.	$\frac{4.5745}{4.5735}$	$\frac{4.5774}{4.5741}$
SHAFT : O.D. COATING	4501 THIN DENSE CHR	4500 LW / N30
FOIL : BASE THKNS in.	.012	.012
BASE MAT'L	718	718
COATING MAT'L	TEFLON S	TEFLON S
TOTAL THKNS in.	.013	.013
LENGTH in.	6.0	6.0
BEND RADIUS in	2.9	2.9
NUMBER OF FOILS	12	12
SPECIAL CONFIGURATION		
SWAY SPACE: C-S-4F ASSEMBLY MEAS.	.023 .0152/.0149	.023 .0164/.0157
BREAK-AWAY TORQUE lb.-in.	75 TOTAL RIG	
RUNNING TORQUE (16,33K $\mu$ m) lb.in.	71 78	~
LIFT-OFF SPEED rpm		~
TOUCH DOWN SPEED rpm	5500	~
SHAFT DISPL: STATIC in.		
RUNNING & LOADED in.		
ASSEMBLED BRG FOIL DIA.	4.325	4.325

REMARKS:

DATA POINT # \_\_\_\_\_  
 MAX. SPEED \_\_\_\_\_ rpm  
 MAX. LOAD  $\frac{CELL}{PSI} \times 4.6in^2 \div 54in^2 =$

1. 12-16 TEST WITH DYNO LOCKED
2. 12-17 CHECKOUT RUNS TO 25000 RPM, TEST END AMPLITUDE TO 3MR.
3. 12-18 CHECKOUT RUN TO 30000 TEST END AMPLITUDE TO 3-3.25 MMS  
NO FAILURE

REPORT

PAGE OF

AIRESEARCH MANUFACTURING COMPANY

DATE 1-26-76  
 PREPARED BY MITNIK  
 CHECKED BY \_\_\_\_\_

CALC. NO. \_\_\_\_\_  
 MODEL \_\_\_\_\_  
 PART NO. \_\_\_\_\_

JOURNAL BEARING TEST CONFIGURATION # 12

	TEST BRG.	TURB. BRG.
CARRIER: I.D.	4.5715 / 4.5735 *	4.5714 / 4.5711 *
SHAFT : O.D. COATING	4.501 THIN DOUBLE CR.	4.500 LW-1N30
FOIL : BASE THKNSS in.	.012	.012
BASE MAT'L	718	718
COATING MAT'L	TEFLON S	TEFLON S
TOTAL THKNSS in.	.013	.013
LENGTH in.	60	60
BEND RADIUS in.	2.9	2.9
NUMBER OF FOILS	12	12
SPECIAL CONFIGURATION		
SWAY SPACE : C-S-4F ASSEMBLY MEAS.	.023 .0496	.023 .0218
BREAK-AWAY TORQUE lb.-in. RUNNING TORQUE (16,33Kipm) lb.in.	75 RIG <del>40</del> TEST BRG	~
LIFT-OFF SPEED rpm	5000	~
TOUCH DOWN SPEED rpm	4500	~
SHAFT DISPL: STATIC in. RUNNING & LOADED in.		
ASSEMBLED BRG FOIL DIA	4.288 / 4.324	

REMARKS:

DATA POINT # \_\_\_\_\_

MAX. SPEED 30,900 rpm

MAX. LOAD CELL  $\text{psi} \times 4.6 \text{ in}^2 \div 54 \text{ in}^2 =$

\* CARRIERS MODIFIED TO INCREASE ACTUAL SWAY SPACE WITHOUT INCR. CSS  
 1-26-76 TEST TO 30500 RPM - 3.5 MIN TEST BRG END  
 SUSPECT CALIBRATION ERROR

REPORT

PAGE OF

AIRESEARCH MANUFACTURING COMPANY

DATE 2-5-76  
 PREPARED BY MITNIE  
 CHECKED BY \_\_\_\_\_

CALC. NO. \_\_\_\_\_  
 MODEL \_\_\_\_\_  
 PART NO. \_\_\_\_\_

JOURNAL BEARING TEST CONFIGURATION # 13

	TEST BRG.	TURB. BRG.
CARRIER: I.D.	4.5745 / 4.5735 *	4.5774 / 4.5771 *
SHAFT : O.D. COATING	4.501 THIN DENSE CHR	4.500 LI: IN-30
FOIL : BASE THKNSS in. BASE MAT'L COATING MAT'L TOTAL THKNSS in. LENGTH in. BEND RADIUS in. NUMBER OF FOILS SPECIAL CONFIGURATION	.012 INCO 718 TEFLONS .013 6.0 2.9 12 —	.012 INCO 718 TEFLONS .013 6.0 2.9 12 —
SWAY SPACE: C-S-4F ASSEMBLY MEAS.	.023 .0196	.023 .0218
BREAK-AWAY TORQUE lb.-in. RUNNING TORQUE (16,33K $\mu$ m) lb.in.	77 TOTAL	26 BRG ~
LIFT-OFF SPEED rpm TOUCH DOWN SPEED rpm		~ ~
SHAFT DISPL: STATIC in. RUNNING & LOADED in.		

REMARKS:  
 DATA POINT # \_\_\_\_\_  
 MAX. SPEED 19000 rpm  
 MAX. LOAD CELL  $\text{psi} \times 4.6 \text{ in}^2 \div 54 \text{ in}^2 =$

\* CARRIERS MODIFIED

1. TEST RUN WITH  $\text{CO}_2$  AS COOLANT
2. FIRST TEST TO 18000 RPM
3. RUN WITH LOADER TO 19000 RPM / 10<sup>5</sup> LOAD

AIRESEARCH MANUFACTURING COMPANY

DATE 2-6-1949  
 PREPARED BY MTNHC  
 CHECKED BY \_\_\_\_\_

CALC. NO. \_\_\_\_\_  
 MODEL \_\_\_\_\_  
 PART NO. \_\_\_\_\_

JOURNAL BEARING TEST CONFIGURATION # 14

	TEST BRG.	TURB. BRG.
CARRIER: I.D.		
SHAFT : O.D. COATING	SAME AS	
FOIL : BASE THKNSS in. BASE MAT'L COATING MAT'L TOTAL THKNSS in. LENGTH in. BEND RADIUS in. NUMBER OF FOILS SPECIAL CONFIGURATION		#13
SWAY SPACE: C-S-4F ASSEMBLY MEAS.		
BREAK-AWAY TORQUE lb.-in. RUNNING TORQUE (16,33Kipm) lb.in.	90 RIG 28.5 BRG	~
LIFT-OFF SPEED rpm TOUCH DOWN SPEED rpm		~ ~
SHAFT DISPL: STATIC in. RUNNING & LOADED in.		

REMARKS:

DATA POINT # \_\_\_\_\_  
 MAX. SPEED 30,000 rpm  
 MAX. LOAD CELL  $\text{psi} \times 4.6 \text{ in}^2 \div 54 \text{ in}^2 =$

1. TEST WITH HOT AIR COOLANT
2. LOADER OFF RUN TO 25000 WITH 280°F INLET AIR
3. MAX TO 30000 ON 2-9

AIRESEARCH MANUFACTURING COMPANY

DATE 9-76

PREPARED BY WILLIAM

CHECKED BY \_\_\_\_\_

CALC. NO. \_\_\_\_\_

MODEL \_\_\_\_\_

PART NO. \_\_\_\_\_

JOURNAL BEARING TEST CONFIGURATION # 15

	TEST BRG.	TURB. BRG.
CARRIER: I.D.		
SHAFT : O.D. COATING	SAME	
FOIL : BASE THKNS in. BASE MAT'L COATING MAT'L TOTAL THKNS in. LENGTH in. BEND RADIUS in. NUMBER OF FOILS SPECIAL CONFIGURATION		-3
SWAY SPACE: C-S-4F ASSEMBLY MEAS.		
BREAK-AWAY TORQUE lb.-in. RUNNING TORQUE (16,33Kipm) lb.in.	86-39.2 BRG	~
LIFT-OFF SPEED rpm TOUCH DOWN SPEED rpm		~
SHAFT DISPL: STATIC in. RUNNING & LOADED in.		

REMARKS:

DATA POINT # \_\_\_\_\_

MAX. SPEED \_\_\_\_\_ rpm

MAX. LOAD CELL  $\text{PSI} \times 4.6 \text{ in}^2 \div 54 \text{ in}^2 =$

1. TEST WITH HELIUM AS COOLANT
2. STARVATION OF COOLANT AT 26700 ACCOMPANIED BY SUBSYNC ACTIVITY - SHUT DOWN
3. 2-20 PM TEST WITH LOADER



AIRESEARCH MANUFACTURING COMPANY

DATE 3-3-76  
 PREPARED BY MITNIK  
 CHECKED BY \_\_\_\_\_

CALC. NO. \_\_\_\_\_  
 MODEL \_\_\_\_\_  
 PART NO. \_\_\_\_\_

JOURNAL BEARING TEST CONFIGURATION # 16

	TEST BRG.	TURB. BRG.
CARRIER: I.D.		
SHAFT : O.D. COATING	same	
FOIL : BASE THKNSS in. BASE MAT'L COATING MAT'L TOTAL THKNSS in. LENGTH in. BEND RADIUS in. NUMBER of FOILS SPECIAL CONFIGURATION		#13
SWAY SPACE: C-S-4F ASSEMBLY MEAS.		
BREAK-AWAY TORQUE lb.-in. RUNNING TORQUE (16,33K $\mu$ m) lb.in.	49.2 BRG 930	RIG
LIFT-OFF SPEED rpm TOUCH DOWN SPEED rpm	6000 4000	~ ~
SHAFT DISPL: STATIC in. RUNNING + LOADED in.		

REMARKS:

- DATA POINT # \_\_\_\_\_  
 MAX. SPEED 28500 rpm  
 MAX. LOAD CELL  $0.51 \times 4.6 \text{ in}^2 \div 54 \text{ in}^2 = 30 \text{ LB}$
1. DRIVE TURBINE CLEARANCES INCREASED .040 DIAMETERICALLY
  2. PARACHUTE LOADER COATED W/ VISCO ELASTIC MAT'L ~.010 THK
  - 3 RUN W/O LOADOR NO SIGNIFICANT CHANGE
  4. LOADER REINSTALLED WITH SIDE PLATE STIFFENERS

AIRESEARCH MANUFACTURING COMPANY

DATE 3-5-76

PREPARED BY MITOIK

CHECKED BY \_\_\_\_\_

CALC. NO. \_\_\_\_\_

MODEL \_\_\_\_\_

PART NO. \_\_\_\_\_

JOURNAL BEARING TEST CONFIGURATION # 17

	TEST BRG.	TURB. BRG.
CARRIER: I.D.		
SHAFT : O.D. COATING		
FOIL : BASE THKNSS in. BASE MAT'L COATING MAT'L TOTAL THKNSS in. LENGTH in. BEND RADIUS in. NUMBER of FOILS SPECIAL CONFIGURATION		
SWAY SPACE : C-S-4F ASSEMBLY MEAS.		
BREAK-AWAY TORQUE lb.-in. RUNNING TORQUE (1G, 33K $\mu$ m) lb.in.	55.8 TEST 88	TOTAL ~
LIFT-OFF SPEED rpm TOUCH DOWN SPEED rpm	5000 5500	~ ~
SHAFT DISPL: STATIC in. RUNNING & LOADED in.		

REMARKS:

DATA POINT # \_\_\_\_\_  
MAX. SPEED 30700 rpm  
MAX. LOAD CELL  $\text{psi} \times 4.6 \text{ in}^2 \div 54 \text{ in}^2 = 0$

1. MID PLANE PROBES INSTALLED LOADER REMOVED
2. NOMINAL DRIVE TURBINE AXIAL CLEARANCE
3. TEST INDICATED SHAFT OPERATING IN BENDING MODE ABOVE 15K RPM. TEST AMPLITUDE > 6 MIL AT 30.7K RPM & CLIMBING. SEE PHOTO ATTACHED REVERSE SIDE

DATE 3-17-76

PREPARED BY \_\_\_\_\_

CHECKED BY \_\_\_\_\_

CALC. NO. \_\_\_\_\_

MODEL \_\_\_\_\_

PART NO. \_\_\_\_\_

JOURNAL BEARING TEST CONFIGURATION # 18

	TEST BRG.	TURB. BRG.
CARRIER: I.D.		
SHAFT : O.D. COATING		
FOIL : BASE THKNSS in. BASE MAT'L COATING MAT'L TOTAL THKNSS in. LENGTH in. BEND RADIUS in. NUMBER OF FOILS SPECIAL CONFIGURATION	SAME	15 * 13 *
SWAY SPACE: C-S-4F ASSEMBLY MEAS.		
BREAK-AWAY TORQUE lb.-in. RUNNING TORQUE (1G, 33Krpm) lb. in.	54.5 TEST 86	RIG ~
LIFT-OFF SPEED rpm TOUCH DOWN SPEED rpm	7000 6000	~ ~
SHAFT DISPL: STATIC in. RUNNING & LOADED in.		

## REMARKS:

DATA POINT # \_\_\_\_\_

MAX. SPEED \_\_\_\_\_ rpm

MAX. LOAD  $\frac{\text{CELL PSI} \times 4.6 \text{ in}^2}{54 \text{ in}^2} =$ \* 2 FOILS TEST END + 2 FOILS TURBINE END REPLACED FROM  
CONFIG 17 TEST

PROBES INSTALLED TO READ 5 PLANES OF DEFLECTION

SHAFT BENDING IN FWD MODE CONFIRMED

DATE June 2, 1976

PREPARED BY \_\_\_\_\_

CHECKED BY \_\_\_\_\_

CALC. NO. \_\_\_\_\_

MODEL \_\_\_\_\_

PART NO. \_\_\_\_\_

# JOURNAL BEARING TEST CONFIGURATION # 19

	TEST BRG.	TURB. BRG.
CARRIER: I.D.	4.5745 4.5735 *	4.5774 4.5771 *
SHAFT : O.D. COATING	4.492/4.493 Thin Dense CR	4.500 LW-IN-30
FOIL : BASE THKNS in. BASE MAT'L COATING MAT'L TOTAL THKNS in. LENGTH in. BEND RADIUS in. NUMBER OF FOILS SPECIAL CONFIGURATION	012 718 TEFLON S 013 6.0 2.9 12 SAME SET AS	012 718 TEFLON S .013 6.0 2.9 12 PROBES INST CONFIG 18
SWAY SPACE: C-S-4F ASSEMBLY MEAS.	0295	.023
BREAK-AWAY TORQUE lb.-in. RUNNING TORQUE (16,33Krpm) lb.in.	26.8 TEST 90 37.5 TEST	RIG ~
LIFT-OFF SPEED rpm TOUCH DOWN SPEED rpm	5500	~ ~
SHAFT DISPL: STATIC in. RUNNING & LOADED in.		

## REMARKS:

\* MODIFIED PER DAP106703

DATA POINT # \_\_\_\_\_

MAX. SPEED \_\_\_\_\_ rpm

MAX. LOAD  $CELL \frac{0.51 \times 4.6 \text{ in}^2}{\div 54 \text{ in}^2} =$

SHORTER SHAF - 1.3" TEST - PROX. BY PROBES IN

TO ONE END BRG. LOOKING AT FOILS

2 IN. PLANE BEVELY PROBES

RUN 1 HIGH SUBSYNCH ACTIVITY INTO .015 ORBIT AT 29K DYNO AIR ON & OFF  
BETTER OFF BUT NOT SIGNIF.

RUN 2 LOADER INSTALLED - NOISE & VIB AT 15K

RUN 3 LOADER WITH VISCO TAPE - NOISE GONE - SPEED TO 20K - LOAD TO 5 PSI PRESS

RUN 4 MORE VISCO TAPE - SAME RESULTS

REPORT

PAGE OF

DATE JUNE 3 1976

CALC. NO. \_\_\_\_\_

PREPARED BY \_\_\_\_\_

MODEL \_\_\_\_\_

CHECKED BY \_\_\_\_\_

PART NO. \_\_\_\_\_

JOURNAL BEARING TEST CONFIGURATION # 20

	TEST BRG.	TURB. BRG.
CARRIER: I.D.	4.5745 * 4.5735	4.5774 * 4.5771 *
SHAFT : O.D. COATING	4.492 / 4.493 THIN DENSE CHR.	4.500 LW-IN-30
FOIL : BASE THKNSS in. BASE MAT'L COATING MAT'L TOTAL THKNSS in. LENGTH in. BEND RADIUS in. NUMBER OF FOILS SPECIAL CONFIGURATION	.012 718 TEFLONS .013 1 6.0 2.9 12	.012 718 TEFLONS .013 6.0 2.9 12
SWAY SPACE : C-S-4F ASSEMBLY MEAS.	SEE BELOW .0215	.023
BREAK-AWAY TORQUE lb.-in. RUNNING TORQUE (15,33Krpm) lb.in.	38.5 / 98 5.0	~ ~
LIFT-OFF SPEED rpm TOUCH DOWN SPEED rpm	9000 6500	~ ~
SHAFT DISPL: STATIC in. RUNNING & LOADED in.		

## REMARKS:

DATA POINT # \_\_\_\_\_

MAX. SPEED 34000 rpmMAX. LOAD CELL  $\frac{251 \times 4.6 \text{ in}^2}{54 \text{ in}^2} =$ 

## SHORT SHAFT

1 SAME FOILS AS CONFIG 19 TEST END WITH .004 SS SHIM  
TACKED TO BACK

MID PLATE PROBES INSTALLED

DATE JUNE 4 1976

CALC NO. \_\_\_\_\_

PREPARED BY \_\_\_\_\_

MODEL \_\_\_\_\_

CHECKED BY \_\_\_\_\_

PART NO. \_\_\_\_\_

JOURNAL BEARING TEST CONFIGURATION # 21

	TEST BRG. 1	TURB. BRG. 1
CARRIER: I.D.	4.5745/4.5735	4.5774/4.5771
SHAFT : O.D.	4.492/4.493	4.500
COATING	Thin Dense Chr	LW-IN-30
FOIL : BASE THKNS	.012	.012
BASE MAT'L	INCO 718	INCO 718
COATING MAT'L	TEFLONS	TEFLONS
TOTAL THKNS	.013	.013
LENGTH	6.0	6.0
BEND RADIUS	2.9	2.9
NUMBER OF FOILS	12	12
SPECIAL CONFIGURATION	SHORT	SHAFT
SWAY SPACE: C-S-4F		023
ASSEMBLY MEAS.		
BREAK-AWAY TORQUE lb.-in.	460 BRG 100 RIG	
RUNNING TORQUE (16,33Krpm) lb.-in.		~
LIFT-OFF SPEED rpm	9000	~
TOUCH DOWN SPEED rpm	4200	~
SHAFT DISPL: STATIC		
RUNNING & LOADED in.		

## REMARKS:

DATA POINT # \_\_\_\_\_

MAX. SPEED \_\_\_\_\_ rpm

MAX. LOAD \_\_\_\_\_  $\text{psi} \times 4.4 \text{ in}^2 = 54 \text{ in}^2$ 

1 CARRIERS MODIFIED PER PAID 106703

2 .004 SS SHIM INSTALLED ON FOIL BACK

RUN 2 CHECKOUT HARD MOUNT LOADER - SPEED TO 228K

RUN 3 LOADER MODIFIED RUN TO 20K VIBRATION PERESISIS

RUN 4 MORE VISCO TAPE ON LOADER

RUN 5 ACCELEROMETER ON LOADER - FELL OFF - MAX LOAD TO 14 PSI @ 1000 PRESSURE

REPORT

PAGE OF

DATE JUNE 16, 1976

PREPARED BY \_\_\_\_\_

CHECKED BY \_\_\_\_\_

CALC. NO. \_\_\_\_\_

MODEL \_\_\_\_\_

PART NO. \_\_\_\_\_

JOURNAL BEARING TEST CONFIGURATION # 22

	TEST BRG. 4	TURB. BRG. 1
CARRIER: I.D.	4.5745/4.5735	4.5774/ 4.5771
SHAFT : O.D. COATING	4.492/4.493 TIN DYNAL-CH	4.500 LW-IN-30
FOIL : BASE THKNS in. BASE MAT'L COATING MAT'L TOTAL THKNS in. LENGTH in. BEND RADIUS in. NUMBER OF FOILS SPECIAL CONFIGURATION	012 Inco 718 TEFLONS .013 <sup>2</sup> 6.6 2.9 12	012 Inco 718 TEFLONS .013 6.0 2.9 12
SWAY SPACE: C-S-4F ASSEMBLY MEAS.		
BREAK-AWAY TORQUE lb.-in. RUNNING TORQUE (15,33Krpm) lb.in.	53.4/115	~
LIFT-OFF SPEED rpm TOUCH DOWN SPEED rpm	5100 3250	~ ~
SHAFT DISPL: STATIC in. RUNNING & LOADED in.		

## REMARKS:

DATA POINT # \_\_\_\_\_

MAX. SPEED \_\_\_\_\_ rpm

MAX. LOAD CELL  $\text{PSI} \times 4.6 \text{ in}^2 \div 54 \text{ in}^2 =$ 

1 0.004 SS SHIP INST

2 0.004 SS SHIP INST

TIRM BALANCE TEST - MID PLANE PROBES INST  
MULTI PLANE / MULTI SPEED

REPORT

PAGE 05

**BALANCED SHAFT**DATE **6-24-76**

PREPARED BY \_\_\_\_\_

CHECKED BY \_\_\_\_\_

CALC NO. \_\_\_\_\_

MODEL \_\_\_\_\_

PART NO. \_\_\_\_\_

**JOURNAL BEARING TEST CONFIGURATION # 23**

	TEST BRG.	TURB. BRG.
CARRIER: I.D.	4.5745/4.5735	4.5774/4.5771
SHAFT : O.D.	4.492/4.493	4.500
COATING	Thin Dens Cr	LU-IN-30
FOIL : BASE THKNS	.012 *	.012
BASE MAT'L	718	718
COATING MAT'L	TEFLON S	TEFLON S
TOTAL THKNS	.013	.013
LENGTH	6.0	6.0
BEND RADIUS	2.9	2.9
NUMBER OF FOILS	12	12
SPECIAL CONFIGURATION		WAYNE KERR PAGES IN CARRIER
SWAY SPACE: C-S-4F	.0215 (245)	.02525
ASSEMBLY MEAS.		
BREAK-AWAY TORQUE lb.-in.	89 lb-in / 140	~
RUNNING TORQUE (16,33K rpm) lb.-in.		~
LIFT-OFF SPEED rpm	4400	~
TOUCH DOWN SPEED rpm		~
SHAFT DISPL: STATIC		
RUNNING & LOADED in.		

**REMARKS:**

DATA POINT # \_\_\_\_\_

MAX. SPEED \_\_\_\_\_ rpm

MAX. LOAD \_\_\_\_\_

DINING AVE 4602" <sup>2</sup>**\*.004 SS SHIM ON FOIL BACKS**

MAX LOAD RUN 1 30 PSI LONG PRESS 2556 PSI BRG 1219 LB

RUN 2 6-28- Break away 33,3 BL/100 RIG

RUN 3 6-29 456/99 DATA POINTS 6-12 60 PSI 51 PSI BRG END

RUN 4 6-30 TEST BRG FAILURE AT 6.549 BRG PSI 33000 RPM



DATE 9/6/76PREPARED BY M. J. NIK

CHECKED BY \_\_\_\_\_

CALC NO \_\_\_\_\_

MODEL \_\_\_\_\_

PART NO \_\_\_\_\_

JOURNAL BEARING TEST CONFIGURATION # 24

	TEST BRG.	TURB. BRG.
CARRIER: I.D.	<u>4.5643/4.5233</u>	<u>4.5774/4.5771</u>
SHAFT : O.D.	<u>4.4860/4.5852</u>	<u>4.500</u>
COATING	<u>Thin Dense GR</u>	<u>Ln -1N-30</u>
FOIL : BASE THKNSS in.	<u>.012</u>	<u>.012</u>
BASE MAT'L	<u>Inco 718</u>	<u>Inco 718</u>
COATING MAT'L	<u>TEFLON S</u>	<u>TEFLON S</u>
TOTAL THKNSS in.	<u>.013</u>	<u>.013</u>
LENGTH in.	<u>6.0</u>	<u>6.0</u>
BEND RADIUS in.	<u>3.1</u>	<u>3.1</u>
NUMBER of FOILS	<u>12</u>	<u>12</u>
SPECIAL CONFIGURATION		
SWAY SPACE : C-S-4F	<u>.0262</u>	<u>.02525</u>
ASSEMBLY MEAS.	<u>.0175</u>	<u>.0175</u>
BREAK-AWAY TORQUE lb.-in.	<u>285/32.5</u>	<u>100/120</u>
RUNNING TORQUE (1G, 33K RPM) lb.-in.		<u>~</u>
LIFT-OFF SPEED rpm	<u>10600</u>	<u>~</u>
TOUCH DOWN SPEED rpm	<u>7000</u>	<u>~</u>
SHAFT DISPL: STATIC in.		
RUNNING & LOADED in.		

## REMARKS:

DATA POINT # \_\_\_\_\_

MAX. SPEED 33000 rpmMAX. LOAD 5.1 PSI @ 33000 rpm

RUN 1 - SUBSYNCH BOTH ENDS 28.9K - ORBIT DATA TAKEN AT 28.5 ± 10K

RUN 2 - OK TO 33K 9/7/76

RUN 3 - MULTI SPEED MULTI PLANE BALANCING 9/8/76

RUN 4 - LOADER CHECKOUT 3.141 ORG PSI @ 20K 9/9/76  
4.419 @ 25KRUN 5 - 5.1 ORG PSI @ 23K 9/10/76  
4.8 @ 28K - INSTABILITY NOTED - SHUTDOWN NO FAILURE

DATE 9-18-76

PREPARED BY \_\_\_\_\_

CHECKED BY \_\_\_\_\_

CALC. NO. \_\_\_\_\_

MODEL \_\_\_\_\_

PART NO. \_\_\_\_\_

JOURNAL BEARING TEST CONFIGURATION # 25

	TEST BRG.	TURB. BRG.
CARRIER: I.D.	4.5643/4.5633	4.5774/4.5771
SHAFT : O.D. COATING	4.4860/4.5852 THIN DENSE CHR.	4.500 LW-IN-30
FOIL : BASE THKNESS in.	.012	.012
BASE MAT'L	INCO 718	INCO 718
COATING MAT'L	TEFLON S	TEFLON S
TOTAL THKNESS in.	.013	.013
LENGTH in.	6.0	6.0
BEND RADIUS in.	3.1	3.1
NUMBER OF FOILS	12	12
SPECIAL CONFIGURATION	46.3% OVERLAP	46.3%
SWAY SPACE: C-S-4F ASSEMBLY MEAS.	.0262 .0215	.02525 .021
BREAK-AWAY TORQUE lb.-in.	39.7	98 RB
RUNNING TORQUE (16,33Krpm) lb.in.		~
LIFT-OFF SPEED rpm	10000	~
TOUCH DOWN SPEED rpm		~
SHAFT DISPL: STATIC in.		
RUNNING & LOADED in.		

## REMARKS:

DATA POINT # \_\_\_\_\_

MAX. SPEED \_\_\_\_\_ rpm

MAX. LOAD \_\_\_\_\_

1. RECHAMFERED PARACHUTE LOADER HOLES IN SHAFT

PRONOUNCED SUBSYNCHRONOUS ACTIVITY

DATE 9.15  
 PREPARED BY \_\_\_\_\_  
 CHECKED BY \_\_\_\_\_

CALC. NO. \_\_\_\_\_  
 MODEL \_\_\_\_\_  
 PART NO. \_\_\_\_\_

# JOURNAL BEARING TEST CONFIGURATION # 26

	TEST BRG.	TURB. BRG.
CARRIER: I.D.	4.5643 / 4.5633	4.5774 / 4.5771
SHAFT : O.D.	4.4860 / 4.5852	4.500
COATING	Thin Dense Coat	LW-IN-30
FOIL : BASE THKNSS in.	.012	.012
BASE MAT'L	Inco 718	Inco 718
COATING MAT'L	TEFLON S	TEFLON S
TOTAL THKNSS in.	.013	.013
LENGTH in.	6.0	6.0
BEND RADIUS in.	3.1	3.1
NUMBER OF FOILS	12	12
SPECIAL CONFIGURATION *	46.3% overlap	46.3% overlap
SWAY SPACE: C-S-4F	.0222	.02125
ASSEMBLY MEAS.	.018	.017
BREAK-AWAY TORQUE lb.-in.	~ 49.5	140 RIC
RUNNING TORQUE (16,33Krpm) lb.in.	~	~
LIFT-OFF SPEED rpm	~	~
TOUCH DOWN SPEED rpm	~	~
SHAFT DISPL: STATIC in.		
RUNNING & LOADED in		

## REMARKS:

DATA POINT # \_\_\_\_\_  
 MAX. SPEED \_\_\_\_\_ rpm  
 MAX. LOAD \_\_\_\_\_ psia @ \_\_\_\_\_ rpm

\* .002 SS. SHIM STOCK ADDED TO FOIL BACK

FAILURE AT 5.44 BRG PSI @ 28000 RPM TURBINE END FAILURE

DATE 9-27-76

CALC NO. \_\_\_\_\_

PREPARED BY \_\_\_\_\_

MODEL \_\_\_\_\_

CHECKED BY \_\_\_\_\_

PART NO. \_\_\_\_\_

JOURNAL BEARING TEST CONFIGURATION # 27

	TEST BRG.	TURB. BRG.
CARRIER: I.D.	4.577/4.576	4.577/4.576
SHAFT : O.D.	4.500	4.500
COATING	TRIMALLOY 400	TRIMALLOY 400
INCONEL SHAFT - SHORTENED	OXIDIZED	OXIDIZED
FOIL : BASE THKNS in.	.012	.012
BASE MAT'L	INCO 718	INCO 718
COATING MAT'L	TEFLON S	TEFLON S
TOTAL THKNS in.	.013	.013
LENGTH in.	6.0	6.0
BEND RADIUS in.	3.1	3.1
NUMBER OF FOILS	10	10
SPECIAL CONFIGURATION		
SWAY SPACE : C-S-4F	.0245	.0245
ASSEMBLY MEAS.	.019	.021
BREAK-AWAY TORQUE lb.-in.	59.8 $\pm$ 5%	95 $\pm$ 10%
RUNNING TORQUE (16,33Krpm) lb.-in.		~
LIFT-OFF SPEED rpm	6000	~
TOUCH DOWN SPEED rpm	10400	~
SHAFT DISPL: STATIC in.		
RUNNING & LOADED in.		

## REMARKS:

DATA POINT # \_\_\_\_\_

MAX. SPEED \_\_\_\_\_ rpm

MAX. LOAD  $\frac{CELL \times 4.5in^2}{54in^2} =$ 

Run 1 - MULTIPLANE BALANCING - INCLAMP OVAL MODAL  
ORBITS AT 2210 - SUSPECT INST.

2 - INSTR MODIFIED - SAME RESULTS IN PROPER PERSPECTIVE

3 9/27 MULTI SPEED MULTI PLANE BALANCE

4 9/28 BAL W/ INST 69/115 TORQ PERIOD

DATE 10/1

CALC. NO. \_\_\_\_\_

PREPARED BY \_\_\_\_\_

MODEL \_\_\_\_\_

CHECKED BY \_\_\_\_\_

PART NO. \_\_\_\_\_

JOURNAL BEARING TEST CONFIGURATION # 28

	TEST BRG.	TURB. BRG.
CARRIER: I.D.	4.577/4.576	4.577/4.576
SHAFT : O.D. <u>Inconel 718</u> COATING	4.570 TRIBALOY 400 OXIDIZED	4.500
FOIL : BASE THKNS <u>in.</u> BASE MAT'L COATING MAT'L TOTAL THKNS <u>in.</u> LENGTH <u>in.</u> BEND RADIUS <u>in.</u> NUMBER OF FOILS SPECIAL CONFIGURATION	.012 Inco 718 KAMAN DES 0122 6.0 3.2 10	.012 Inco 718 KAMAN DES 0122 6.0 3.2 10
SWAY SPACE : C-S-4F ASSEMBLY MEAS.	.277	.277
BREAK-AWAY TORQUE <u>lb.-in.</u> RUNNING TORQUE (1G, 33K $\mu$ m) <u>lb. in.</u>	35 ARC	70 RIG
LIFT-OFF SPEED <u>rpm</u> TOUCH DOWN SPEED <u>rpm</u>		~ ~
SHAFT DISPL: STATIC <u>in.</u> RUNNING & LOADED <u>in.</u>		

## REMARKS:

DATA POINT # \_\_\_\_\_  
 MAX. SPEED \_\_\_\_\_ rpm  
 MAX. LOAD \_\_\_\_\_

Run 1 HIGH TEMP TEST @ 1G AT LOW SPEED

Run 2 Start/Stop Tests

Run 3 ALTITUDE SIMULATION - FAILED THRUST BEARING

DATE 10-21

PREPARED BY \_\_\_\_\_

CHECKED BY \_\_\_\_\_

CALC. NO. \_\_\_\_\_

MODEL \_\_\_\_\_

PART NO. \_\_\_\_\_

JOURNAL BEARING TEST CONFIGURATION # 20

	TEST BRG.	TURB. BRG.
CARRIER: I.D.	4.5734/4.5710	4.5682/4.5639
SHAFT : O.D. COATING	4.5001/ 4.4999 <del>TOTAL 900 0.0012</del>	4.5004/ 4.5000
FOIL : BASE THKNS in.	.010	.012
BASE MAT'L	INCO 718	INCO 718
COATING MAT'L	NiCo TANK PLATE	TAFLONS
TOTAL THKNS in.	.012	.013
LENGTH in.	6	6
BEND RADIUS in.	3.1	3.1
NUMBER OF FOILS	12	12
SPECIAL CONFIGURATION	46.8% OVERLAP	
SWAY SPACE: C-S-4F	<del>0.024</del> .0242	.024
ASSEMBLY MEAS.	.0190	.0190
BREAK-AWAY TORQUE lb.-in.	56.7 / 275	RIG
RUNNING TORQUE (15,33K $\mu$ m) lb.in.		
LIFT-OFF SPEED rpm		~
TOUCH DOWN SPEED rpm		~
SHAFT DISPL: STATIC in.		
RUNNING & LOADED in.		

## REMARKS:

DATA POINT # \_\_\_\_\_

MAX. SPEED 25000 rpmMAX. LOAD CELL  $\text{psi} \times 4.6 \text{ in}^2 \div 54 \text{ in}^2 =$ CHECKOUT RUN - NO LOADS - TEST END BALANCE  
RETURNED TO ORIGINAL VALUE

NEW T BRGS

1/REV SMALL, 2/REV MORE DOMINANT

AIRESEARCH MANUFACTURING COMPANY

DATE 10-22

PREPARED BY \_\_\_\_\_

CHECKED BY \_\_\_\_\_

CALC. NO. \_\_\_\_\_

MODEL \_\_\_\_\_

PART NO. \_\_\_\_\_

JOURNAL BEARING TEST CONFIGURATION

30

	TEST BRG.	TURB. BRG.
CARRIER: I.D.	4.5734/4.5710	4.5682/4.5639
SHAFT : O.D.	4.5001/4.4999	4.5004/4.5000
COATING	TRIBOLLOY	400 OXIDIZED
FOIL : BASE THKNS	.010	.012
BASE MAT'L	INCO 718	INCO 718
COATING MAT'L	MC6 TRAK PLATE	TRILONS
TOTAL THKNS	.012	.013
LENGTH	6	6
BEND RADIUS	3.1	3.1
NUMBER OF FOILS	12	12
SPECIAL CONFIGURATION	46.3% OVERLAP	
SWAY SPACE : C-S-4F	.0187 .0242	.021
ASSEMBLY MEAS.	.0180	.0190
BREAK-AWAY TORQUE lb.-in.	41.9 BRG 290	RIG
RUNNING TORQUE (16,33Kxpm) lb.in.		~
LIFT-OFF SPEED rpm	11000	~
TOUCH DOWN SPEED rpm		~
SHAFT DISPL: STATIC in.		
RUNNING & LOADED in.		

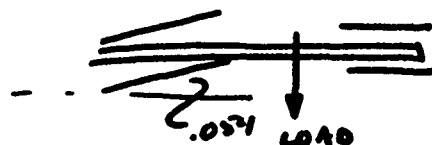
REMARKS:

DATA POINT # \_\_\_\_\_

MAX. SPEED \_\_\_\_\_ rpm

MAX. LOAD  $\frac{CELL \times 4.6in^2}{.54in^2} =$

DYNAMIC SIMULATION - TEST BRG MISALIGNED .054°  
AS FOLLOWS



FAILED AT 21000  
TEST END  
UNBOUNDED INCR IN  
1/REV NO OTHER  
INDICATIONS

## REFERENCES

1. Six, L.D., F.W. Lewis, and C.S. Stone, Low Cost, Limited Life Turbine Engine Analysis, AFAPL-TR-71-102, January 19, 1972.
2. Gray, S., Applying Resilient Foil Air Bearings to Turbomachinery Techniques and Challenges, Society of Automotive Engineers, National Aerospace Engineering and Manufacturing Meeting, Culver City, November 1975
3. S. F. Murray, Material Combinations for Hydrodynamic Inert Gas-Lubricated Bearings, Journal of Lubrication Technology, January, 1968.
4. Waldron, W. D., W. E. Young and P. W. Curwen, An Investigation of Air Bearings for Gas Turbine Engines, USAAMRDL Technical Report 71-59, December 1971.
5. Walowit, J., S. F. Murray, J. McCabe, E. B. Arwas, T. Moyer, Gas Lubricated Foil Bearing Technology Development for Propulsion and Power Systems, AFAPL-TR-73-92, December 1973.
6. Sliney, H. E., An Investigation of Oxidation Resistant Solid Lubricant Materials, ASLE Trans., V. 15, N. 3, July 1972.
7. Sliney, H. E., Self-Lubricating Plasma-Sprayed Composites for Sliding-Contact Bearings to 900°C, NASA Technical Note, NASA-TN-D-7556, February 1974
8. E. W. Turns and R. D. Krienke, Alloy Electrodeposition of Silver Matrix Solid Film Lubricants, Proceedings American Electroplaters Society Annual Meeting, July 1965.
9. Borik, F., Using Tests to Define the Influence of Metallurgical Variables on Abrasion, Metals Engineering Quarterly, May 1972.
10. Fen, E. K., G. A. Boukun, and V. V. Polotai, Strength and Wear Resistance of Oxides of the Transition Metals, Poroshkovaya Metallurgiya, No. 1 (145), pp 94-98, January 1975, Translation, A76-13574.
11. Dupont Technical Bulletin, Tribaloy, Bulletin No. 1, July 1973.